

INTER - International Network on Timber Engineering Research

2014 the International Network on Timber Engineering Research (INTER) was founded.

Scope

Presentation, discussion and documentation of research results in timber engineering and development of application rules for timber design codes or standards related to timber engineering.

Approach

Annual meetings in different countries/places hosted by meeting participants

Presentation and discussion of papers

Peer review of the abstracts before the meeting and of the papers during the meeting

Decision of the acceptance of the abstracts before the meeting by a well-defined review process

Decision of the acceptance of the papers for the proceedings during the meeting

Publication of the papers and the discussion in proceedings

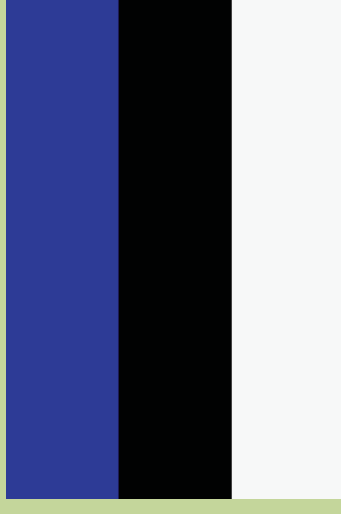
Rules

All decisions including the appointment of the chairperson or the location of annual meetings are made by the participants attending a meeting.

Membership

Persons contributing to or being interested in research related to timber engineering.

INTER PROCEEDINGS MEETING FIFTY-ONE 2018



MEETING FIFTY-ONE

TALLINN, ESTONIA

AUGUST 2018

INTER

International Network on Timber Engineering Research

Proceedings

Meeting 51

13 - 16 August 2018

Tallinn, Estonia

Edited by Rainer Görlacher

Timber Scientific Publishing
KIT Holzbau und Baukonstruktionen
Karlsruhe, Germany
2018

Publisher:

Timber Scientific Publishing
KIT Holzbau und Baukonstruktionen
Reinhard-Baumeister-Platz 1
76131 Karlsruhe
Germany
2018

ISSN 2199-9740

Table of Contents

1	List of Participants	1
2	Minutes of the Meeting	5
3	INTER Papers, Tallinn, Estonia 2018	27
51 - 6 - 1	Modelling the Variation of Mechanical Properties along Oak Boards - C Tapia, S Aicher	31
51 - 7 - 1	Deviations Between Planned and Actual Position of Wood Screws - Consequences for their Spacing - M Frese, M Jordan	49
51 - 7 - 2	Analytical Method to Derive Overstrength of Dowel-Type Connections - L-M Ottenhaus, Minghao Li, T Smith	65
51 - 7 - 3	Pinching-free Timber Connection - P Quenneville, N Chan, P Zarnani	79
51 - 7 - 4	In-plane Shear Connection for CLT Diaphragms - T Schmidt, H J Blaß	95
51 - 7 - 5	Seismic Response of Connections with Glued-in Steel Rods - J Ogrizovic, R Jockwer, A Frangi	109
51 - 7 - 6	Cyclic Performance of a Full-scale Timber Column Equipped with Resilient Slip Friction Joints - A Valadbeigi, P Zarnani, P Quenneville	125
51 - 7 - 7	Load-Deformation Behaviour and Stiffness of Lateral Connections with Multiple Dowel Type Fasteners - R Jockwer, A Jorissen	141
51 - 7 - 8	Design Parameters of Notched Connections for TCC Structures as Part of Eurocode 5 - U Kuhlmann, S Mönch	161
51 - 7 - 9	Bond Performance of Glued-in CFRP and GFRP Rods in Timber - E Toumpanaki, M H Ramage	177
51 - 7 - 10	Multiple Shear Plane Timber Connections with Slotted-in Steel Plates and Dowel-type Fasteners: a Study of the Brittle Failure Mode in the Parallel-to-grain Direction - M Yurrita, J M Cabrero, P Quenneville	195
51 - 7 - 11	Group-Effect of Self-Tapping Screws in CLT Shear Connections - A Hossain, M Popovski, T Tannert	211

51 - 7 - 12	Performance of the Different Models for Brittle Failure in the Parallel-to-Grain Direction for Connections with Dowel-Type Fasteners - J M Cabrero, M Yurrita	225
51 - 7 - 13	Beam-on-Foundation (BOF) Modelling as an Alternative Design Method for Timber Joints with Dowel-Type Fasteners – Part 1: Strength and Stiffness per Shear Plane of Single-Fastener Joints - R Lemaître, J-F Bocquet, M Schweigler, T K Bader	241
51 - 10 - 1	Formulaic Design Methods for TCC Floors - A Smith, J Schänzlin, M Piazza, A Lawrence, O Bell	257
51 - 11 - 1	Adaptation of Eurocode 5 Standard to French Hardwoods - Proposal of New Hygroscopic Equilibrium Charts - M Varinier, N Sauvat, C Montero, F Dubois, J Gril	273
51 - 12 - 1	CLT under In-Plane Loads: Investigation on Stress Distribution and Creep - M Gräfe, P Dietsch, S Winter	289
51 - 12 - 2	Tensile and Compression Strength of Small Cross Section Beech (Fagus s.) Glulam Members - M Westermayr, P Stapel, J W G van de Kuilen	307
51 - 12 - 3	Behaviour of Glulam and LVL Beams Loaded Perpendicular to the Grain - L Windeck, H J Blaß	323
51 - 12 - 4	Mechanical Properties of European Beech Glued Laminated Timber - T Ehrhart, R Steiger, P Palma, A Frangi	343
51 - 12 - 5	Cross Laminated Timber at in-plane Beam Loading – New Analytical Model Predictions and Relation to EC5 - M Jeleč, H Danielsson, E Serrano, V Rajčić	361
51 - 15 - 1	Seismic Resilient CLT buildings Using Resilient Slip Friction Joints (RSFJs) with Collapse Prevention Mechanism: Ductility, Behaviour Factor, Design Methods and Numerical Validation - A Hashemi, P Zarnani, F M Darani, S M M Yousef-Beik, P Quenneville	379
51 - 16 - 1	An Improved Design Model for Fire Exposed Cross Laminated Timber Floors- J Schmid, M Klippel, R Fahrni, A Frangi, N Werther, A Just	395
51 - 18 - 1	Press Glued Connections - Research Results for Discussion and Standardization - S Franke, M Schiere, B Franke	413

51 - 20 - 1	A New Design Method for Timber Floors – Peak Acceleration Approach - Wen-Shao Chang, T Goldsmith, R Harris	429
51 - 20 - 2	Development of a Floor Vibration Design Method for Eurocode 5 - I K Abeysekera, P Hamm, T Toratti, A Lawrence	445
4	INTER Notes, Tallinn, Estonia 2018	461
	Criteria for Evaluating the Simplification of Design Values for Dowel Type Fasteners - R Jockwer, T Uibel, M Kleiber	
5	Peer Review of Papers for the INTER Proceedings	467
6	Meeting and List of CIB-W18 and INTER Papers	469

1 List of participants

AUSTRALIA

K Crews	University of Technology Sydney
R Shrestha	University of Technology Sydney

BELGIUM

G Goossens	BuildSoft, Merelbeke
D Sonck	BuildSoft, Merelbeke

CANADA

F Lam	University of British Columbia, Vancouver
T Tannert	UNBC Prince George

CHINA

Minjuan He	Tongji University
Zheng Li	Tongji University

CROATIA

M Jeleč	University of Osijek
---------	----------------------

ESTONIA

G Ayansola	Tallinn University of Technology
A Just	Tallinn University of Technology
J Liblik	Tallinn University of Technology
K N Mäger	Tallinn University of Technology
M Tiso	Tallinn University of Technology
E Tuhkanen	Tallinn University of Technology

FINLAND

J Hakkarainen	Eurofins Expert Services Ltd
T Toratti	Federation of the Finnish woodworking industries, Helsinki

FRANCE

F Dubois
R Lemaître

University of Limoges
University of Lorraine, LERMAB

GERMANY

S Aicher
H J Blaß
P Dietsch
M Frese
R Görlacher
M Gräfe
U Kuhlmann
M Loebijnski
T Schmidt
P Stapel
C Tapia Camu
N Werther
M Westermayr
L Windeck
S Winter

MPA University Stuttgart
Karlsruhe Institute of Technology (KIT)
Technical University of Munich
Karlsruhe Institute of Technology (KIT)
Karlsruhe Institute of Technology (KIT)
Technical University of Munich
University of Stuttgart
Brandenburg University of Technology
Blass&Eberhart, Karlsruhe
Technical University of Munich
MPA University Stuttgart
Technical University of Munich
Technical University of Munich
Karlsruhe Institute of Technology (KIT)
Technical University of Munich

JAPAN

K Kobayashi
T Nagashima
H Nakashima
M Yasumura

Shizuoka University
Sumitomo Forestry CO.,LTD., Tsukuba
Sumitomo Forestry CO.,LTD., Tsukuba
Tokyo

NEW ZEALAND

L-M Ottenhaus
P Quenneville

University of Canterbury
University of Auckland

SOUTH KOREA

Gi Young Jeong
Jung-kwon Oh

Chonnam National University
Seoul National University

SPAIN

J M Cabrero
M Yurrita

Universidad de Navarra, Pamplona
Universidad de Navarra, Pamplona

SWEDEN

R Atashipour	Chalmers University of Technology
H Danielsson	Lund University
K Forsman	Lund University
T Persson	Masonite Beams, Rundvik
E Serrano	Lund University

SWITZERLAND

T Ehrhart	IBK-ETH Zürich
A Frangi	IBK-ETH Zürich
S Franke	Berner Fachhochschule, Biel
R Jockwer	IBK-ETH Zürich
J Ogrizovic	IBK-ETH Zürich
S Schilling	IBK-ETH Zürich
J Schmid	IBK-ETH Zürich
C Sigrist	Berner Fachhochschule, Biel

UNITED KINGDOM

I Abeysekera	Arup, London
R Harris	Time for Timber Ltd, Bath
A Lawrence	Arup, London
A Smith	Arup, London
E Toumpankai	University of Cambridge

USA

B Yeh	APA - The Engineered Wood Association, Tacoma
-------	---

2 Minutes of the Meeting

by F Lam, Canada

CHAIRMAN'S INTRODUCTION

Prof. Hans Blass welcomed the delegates to the 5th International Network of Timber Engineering Research (INTER) which constitutes the 51st meeting of the group including the series of former CIB-W18 meetings. INTER continues the tradition of yearly meetings to discuss research results related to timber structures with the aim of transferring them into practical applications. The attendance of the yearly meetings is a clear indication of the high interest in the work of the group.

The chair thanked A Just and his team J Liblik, K N Mäger and E Tuhkanen from Tallinn University of Technology for hosting the meeting.

There were 26 papers accepted for this meeting. The papers were selected based on a review process for the abstracts with 4 acceptance criteria (state of the art, originality, assumed content, and relation to standards or codes).

Papers brought directly to the meeting were not accepted for presentation, discussions, or publication. Same rule applied to papers where none of the authors was present or papers which were not defended by one of the authors. The presentations were limited to 20 minutes each, allowing time for meaningful discussions after each presentation. The Chair asked the presenters to conclude the presentation with a general proposal or statement concerning the impact of the research results on existing or future potential applications and development in codes and standards.

The topics covered in this meeting were: Serviceability (2), Glued Joints (1), Fire (1), Structural Stability (1), Laminated Members (5), Environmental Conditions (1), Timber Beams (1), Timber Joints and Fasteners (13), Stresses for Solid Timber (1). Numbers in parentheses are the number of papers presented in each topic based on initial allocation.

The participants could present notes towards the end of the technical session. R Görlacher brought a list of intended note presentations. Participants intending to present notes that were not on the list would need to notify R Görlacher accordingly.

An address list of the participants was circulated for verification of accuracy.

J Kurnitski Head of Dept. of Civil Engineering and Architecture of Tallinn University of Technology gave a welcoming address. A Just welcomed the participants and made housekeeping announcements.

GENERAL TOPICS

C Sigrist provided information about CEN revision of EN 408 and amendment of A1:2012 under WG1/TC124. H Blass commented that including engineering wood products would be a good idea. C Sigrist clarified that the table of contents already included compression perpendicular to grain test method. S Winter commented that these test standards are important to provide information for design standards and appreciated the work of the working group. F Lam received confirmation that the standard deals only with test methods. The test standard can however reference other relevant standards in establishing sample size and number of replicates. H Blass asked about N. American approach whether the number of replicates are also given in test standards. F Lam responded that some N. American test standards contain such information. L-M Ottenhaus and C Sigrist discussed about test methods for material properties on for example tensile strength for CLT. P Dietsch and C Sigrist discussed the importance and practicability of keeping one part or having two parts especially for consideration of new products.

STRESSES FOR SOLID TIMBER

51 - 6 - 1 Modelling the Variation of Mechanical Properties along Oak Boards - C Tapia, S Aicher

Presented by C Tapia

F Lam commented about non stationarity of material property along the length of the member which is aligned along the length of the tree. F Lam said that this was observed in MOE data for 5 m long members. C Tapia said that their specimens are short and not likely be an issue. F Lam asked about verification of the model. C Tapia said that the statistical parameters are checked. F Lam commented that there is a need to verify the model more fully with independent data sets.

T Ehrhart asked about the density variation. C Tapia said this have not been done and will check. T Ehrhart commented that the KAR R^2 is influenced by a single data point at the high range of the data.

BJ Yeh asked about potential damage accumulation from tensile testing same board multiple times. C Tapia said that the sequential test is always higher than past test on the same board even though damage accumulation could underestimate the real strength. S Aicher discussed the relative strength charts and said that in few cases where the second strength is close to the first strength some damage accumulation could be present.

S Franke said that MOE measurement with 30 kN load level was used while some boards failed at 40 kN. He questioned how accurate were the MOE measurements at these load levels. C Tapia showed information of about 1% error for MOE measurements.

P Stapel questioned about the gauge length used in the study and stated that the gauge length may influence the results. The information is needed on free length of the second and subsequent test. S Aicher said that information on the free length of sequential tests is irrelevant. This is because one is interested in the local strength and its relationship with MOE. H Blass commented that material grade may be different in the subsequent tests..

TIMBER JOINTS AND FASTENERS

51 - 7 - 1 Deviations between Planned and Actual Position of Wood Screws -
Consequences for their Spacing - M Frese, M Jordan

Presented by M Frese

A Smith asked if it is too conservative to assume the screws always bend towards each other. M Frese agreed that the cone model is conservative and commented about Modes 2 and 3 where annual rings are curved.

P Dietsch commented about the predrill rod case with the assumption of the tendency of the rods go towards the fibre direction. Their experience indicates the drill followed the path of lesser stiffness direction which is opposite to the fibre direction. He suggested future work to consider the predrill case.

E Serrano discussed the tendency of screws to follow the grain direction. He asked if this is evident in results of placement 1. M Frese provided more detailed information of the interpretation of placement 1 case and further confirmed such tendency in placement 3 cases.

S Aicher asked about the outliers as to whether they are affected by large knots. He recommended also to look at influence beside grain direction. M Frese agreed and showed a scan that indicates knots have an effect.

R Jockwer asked whether the screw installers were skilled carpenter. M Frese responded that they were unskilled at the beginning of the study but became very skilled quickly.

R Jockwer asked about unsymmetrical screw tips and whether different types of screw tips were tried. M Frese said that they only tried two types of screw in this

paper but would like to extend the work to considered different types of screw and screw tips.

L-M Ottenhaus commented about issues related to drilling through CLT where the screw direction can deviate as it travels into the cross layer.

51 - 7 - 2 Analytical Method to Derive Overstrength of Dowel-Type Connections - L-M Ottenhaus, Minghao Li, T Smith

Presented by L-M Ottenhaus

U Kuhlmann commented additional thoughts are needed about realistic resistance of the dowel as all steel connections are typically directed towards the tensile strength of the steel. H Blass said that there are lots of results available confirming that bending strength of steel is 90 to 100% of its tensile strength. U Kuhlmann further commented that the steel community has a valuable data bank containing the strength properties of steel for their code. One should get more information from the steel community for this work. L-M Ottenhaus agreed and responded that in plastic design one designs to the yield point and not the ultimate strength.

A Frangi referred to slide 13 and asked how to achieve ductile failure when minimum distances are needed. L-M Ottenhaus agreed and said that a lot of time brittle failures were experienced and this depends also on connection layup. There is a need to consider fastener distances to ensure ductile failure mode.

H Blass disagreed with the statement that EYM is pretty accurate. He said that rope effect in dowels can appear and is ignored in EYM. This can compromise the approach as the EYM equations were made for static design and not for overstrength issues in seismic design.

C Sigrist and L-M Ottenhaus discussed comparisons between full scale experimental results and the model.

51 - 7 - 3 Pinching-free Timber Connection - P Quenneville, N Chan, P Zarnani

Presented by P Quenneville

H Blass commented that this system is not for changing force directions. P Quenneville agreed.

L-M Ottenhaus commented that in a shear wall application at 2.5% drift a lot of deflection is needed to mobilize the ductility. P Quenneville agreed and commented that in some cases with high stiffness and capacity even with more ductility maybe

less deflection is possible. He said that after an earthquake, reset of the fasteners can be done; however, it is not a damage connection system.

A Frangi commented that in CLT one can crush the timber without splitting; however, in glulam one would cause splitting. P Quenneville agreed and said that one would need to prevent wood brittle failure. In this case one does not want too many bolts and using bigger dowels rather than more bolts is the key.

L-M Ottenhaus commented that splitting can be reinforced by screws. P Quenneville said that in cross banded LVL splitting is not an issue.

M Frese asked about the need for maintenance work to ensure moveable gadget for the life of the structure. P Quenneville agreed and would like to verify the concept.

51- 7 - 4 In-plane Shear Connection for CLT Diaphragms - T Schmidt, H J Blaß

Presented by T Schmidt

R Harris stated that they studied oak dowel joints and FRP joints where compatibility between shear connector and wood and FRP connection behaviour are the key issues. Wedges were created to lock in the joint as resistance to initial horizontal movement is weak. He asked how to hold the joint together.

T Schmidt responded that it is not a problem in the test setup as compression is activated. In real structure, one needs a chord member to hold the system together.

F Lam commented that in Canada the Seismic design community suggests that diaphragms need to behave linear-elastically so that ductile energy dissipation happens in the prime lateral resistant elements. Here very large forces would need to be transmitted linear-elastically in the diaphragm splines. This is particularly true for concrete wood hybrid system. H Blass asked how would the nail spline work in the UBC Brock Commons building. F Lam said that it would not as this thinking was initiated after the building was built. In addition there exists a concrete layer which could help provide the shear transfer in the plan of the diaphragm.

P Quenneville said that this system can also be used in shear walls.

A Frangi asked about the possible initial slip from humidity effects and asked if there was initial slip in test which may be different from field application. T Schmidt and H Blass said that the ETA has conical shape of connector to provide good contact.

A Frangi and T Schmidt discussed about the depth of the shear key elements versus the depth of the panels as an issues that can be optimized.

C Sigrist asked how to get the tolerance in the building site. H Blass responded that the first shear key will align the member as CNC production can meet the 0.5 mm precision.

E Serrano and H Blass discussed the width of the CLT laminae may create a gap at the end of the shear key. H Blass said that tension test perpendicular to grain is created within the full board in cases without gaps. In cases with gaps (i.e. without a full board) different stress distribution would result but should not affect the load slip behaviour.

BJ Yeh asked about loading horizontally which could cause the diaphragm to open up. H Blass said that the diaphragm needs chord which will keep the diaphragm from opening up.

F Lam received confirmation that full scale diaphragm tests were performed.

51 - 7 - 5 Seismic Response of Connections with Glued-in Steel Rods - J Ogrizovic, R Jockwer, A Frangi

Presented by J Ogrizovic

H Blass asked why unbonded length was used. J Ogrizovic responded that the intent is for the steel to yield at the unbonded zone. H Blass said that even if you have unbonded length you have brittle failures.

P Quenneville said that transverse reinforcement was not used. Since the dowels may not be perfectly in line with loading direction, transverse reinforcement would help to prevent brittle failures. J Ogrizovic said that the connections were made with CNC machine so alignment should not be a problem. R Jockwer commented that this is not a problem; even buckling happens at high loads.

S Winter received confirmation about splitting occurring with unbonded length. He commented that their experience is that splitting can be avoided with unbonded area. He asked about the elongation of the glued in rod. J Ogrizovic responded that sensors were mounted at the steel plate. The stiffness values compare reasonably well with published information.

E Toumpanaki received clarification on the deformation measurement system.

S Aicher commented that results indicate spruce has little ductility while ash has much better ductility. So the spruce specimens may be able to handle a few more cycles. He wondered where does the ductility come from. It could come from the steel yielding but the failure mode is brittle. He said one should decouple the two modes and overdesign for the brittle behaviour so that ductile behaviour is achieved. A Frangi said that these connections, especially Ash, have good ductility in spite of final failure mode being brittle.

H Blass said that the results are only valid for the edge distances used in the test; otherwise, results are unsafe. J Ogrizovic said that a minimum edge distance of 2 to 2.5 d can be used for these connections.

51 - 7 - 6 Cyclic Performance of a Full-scale Timber Column Equipped with Resilient Slip Friction Joints - A Valadbeigi, P Zarnani, P Quenneville

Presented by P Quenneville

A Frangi asked when the column is out of plane is there no vertical force and do you have concerns about P-Delta effect? P Quenneville responded that the max deflection is 2.5% and the engineers want to demonstrate that the out of plane movement did not cause damage. This was achieved. A Frangi asked what is the function for placing the device at the top section of the column. P Quenneville said that the engineers wanted to have the top section remain more or less as a rigid body hence the introduction of a mid-column device.

H Blass asked how did you determine the embedment strength of the 100 mm diameter dowel as equations are only valid for dowel diameter up to 30 mm. P Quenneville said it was based on judgement and the design of the engineer.

T Tannert received clarification that the apparent crack line of the LVL was the lamination of the veneer joint and not failure.

S Franke asked why different number of washers were used in one device. P Quenneville said that the connection needed more rigidity in the out of the plane direction and needed more washers to counter the prying forces; there are also dummy washers in the connection.

A Smith asked whether a bow tie profile can be used. P Quenneville answered yes and discussed the advantages of current approach.

51 - 7 - 7 Load-Deformation Behaviour and Stiffness of Lateral Connections With Multiple Dowel Type Fasteners - R Jockwer, A Jorissen

Presented by R Jockwer

Z Li said that this area of study is important for structural analysis. He asked if this can be applied to beam to column connections. R Jockwer said that most studies has parallel to grain information. It may be possible to do more research. There are works in Växjö Sweden on the topic.

L-M Ottenhaus commented about the 95th percentile and the 5th percentile curve and CLT. H Blass confirmed there may be a factor of up to 10.

C Sigrist commented that large connections may have higher stiffness. In some large connections very small deformation was observed without ductile behaviour. R Jockwer agreed and there are many more possibilities that need to be studied.

51 - 7 - 8 Design Parameters of Notched Connections for TCC Structures as Part of Eurocode 5 - U Kuhlmann, S Mönch

Presented by U Kuhlmann

S Winter received confirmation that screws in front of notch mean at the loaded edge and screws in the notch did not play a role.

A Frangi agrees with the results. He said screws in the notch did not play a role because the crack was developed above the screw and anchoring it in the compression zone would work.

51 - 7 - 9 Bond Performance of Glued-in CFRP and GFRP Rods in Timber - E Toumpanaki, M H Ramage

Presented by E Toumpanaki

A Frangi commented that this could be a good solution. He commented that push out and pull out results are not compared. E Toumpanaki said results of different test methods can be compared with this data. H Blass said that if you want to use it as a tensile member you should test it as a tensile member.

A Smith asked why GFRP has higher bond stiffness. E Toumpanaki responded that it may be related to how the loads are transferred.

E Serrano received confirmation that one should expect better performance with compression pull through test because compression stresses are developed. He further commented that this may be different in larger specimens. F Lam commented the supporting plate in the compression pull through test may restrain the specimen from developing splitting failure mode; hence over estimation of capacity will result from this test set up besides the presence of compression stresses.

P Dietsch commented about the statement that FRP is more durable compared to steel. In service class 3 wood would be the problem. P Dietsch and E Toumpanaki discussed the potential difference in results if service class 3 condition rather than service class 1 was considered in the test.

S Aicher commented that there are significant outliers with low strength properties. One should focus on these. The difference in strength results are very low between

the groups given the variability expected in wood. S Aicher and E Toumpanaki discussed the difference in stiffness is one the other hand very high. This may be attributed to the bond characteristics between the adhesive and the rod which is also related to the outliers.

51 - 7 - 10 Multiple Shear Plane Timber Connections with Slotted-in Steel Plates and Dowel-type Fasteners: a Study of the Brittle Failure Mode in the Parallel-to-grain Direction - M Yurrita, J M Cabrero, PQuenneville

Presented by M Yurrita

F Lam asked and received clarification about the reason why R^2 value greater than 1 and being negative was fitting the regression through the origin. F Lam commented that the brittle strength in the model is stressed volume dependent hence model should capture this aspect to be more generally applicable. H Blass agreed and said that the tensile strength failure mode is an example where failure always occurs in the same location hence stressed volume effect should indicate the tensile strength value in the model can be increased.

R Jockwer commented about the conversion of characteristic strength properties to mean values needing assumption of COV. This assumption needs to be checked as the assumed COV may be low. M Yurrita will look into this.

S Winter commented that if you are doing tests and comparing to model predictions, you should use real strength values from tests rather than conversion of properties from other references.

51 - 7 - 11 Group-Effect of Self-Tapping Screws in CLT Shear Connections - A Hossain, M Popovski, T Tannert

Presented by T Tannert

F Lam asked about the R^2 or standard error of the regression fits. T Tannert said it was not done but they would be low. He said the intent is to provide guidance to code committee that group effect is not as severe as indicated in these connections while providing recommendation for a new conservative group effect. F Lam further received confirmation that only 8 mm screws were used. He commented that given the low R^2 values and limited screw diameters and screw type considered, it will be difficult to convince code committee to accept the results.

L-M Ottenhaus commented about the low cycle fatigue type failures with the ISO protocol. She said it is not sure that one can rely on the joint to dissipate energy with

brittle failure mode. She said also high overstrength factor can result if you are too conservative with group effect. T Tannert agreed with the over strength factor issue. He said part of the problem is that the prototype may not be based on earthquake response. He wants to develop loading protocol for this types of screws. F Lam said that the CUREE protocol was developed by H Krawinkler with consideration of the earthquake response of light wood frame systems.

51 - 7 - 12 Performance of the Different Models for Brittle Failure in the Parallel-to-Grain Direction for Connections with Dowel-Type Fasteners - J M Cabrero, M Yurrita

Presented by J M Cabrero

LM Ottenhaus received clarification that LVL, glulam and lumber were considered also the characteristic value of the material from standards were used to convert into mean values for evaluation of performance in the study.

A Frangi and JM Cabrero discussed the assessment of Eurocode for differentiation of brittle and ductile failure mode and effective number of fasteners. A Frangi said that Eurocode works quite well for the failure mode that it intends for. However it does not work well to distinguish between the brittle and ductile failures. They also discussed about the intent of the code to discourage the practitioners to design for brittle failure.

T Tannert commented that existing model seem to be less reliable about high capacity joints. Do they over or underestimate these cases. JM Cabrero agreed and said that they tend to overpredict the capacity in most cases.

L-M Ottenhaus commented that in seismic design it is important not to predict ductile failure if it is actually brittle. JM Cabrero agreed.

I Abeysekera asked what happens if you use all the values rather than just the mean value. JM Cabrero said that the model cannot do this now.

P Quenneville said that the moment the engineers know that there is a possibility of brittle failure mode, they will need to control it.

R Jockwer commented that it would be useful to give information with minimum spacing and distances to avoid brittle mode. JM Cabrero agreed but it is not yet available. P Quenneville disagreed as there is no one solution because there are too many variables.

P Dietsch, A Frangi and JM Cabrero discussed the role of reinforcements, practicality issues and the need for good and reliable model.

51 - 7 - 13 Beam-on-Foundation (BOF) Modelling as an Alternative Design Method for Timber Joints with Dowel-Type Fasteners – Part 1: Strength and Stiffness per Shear Plane of Single-Fastener Joints - R Lemaître, J-F Bocquet, M Schweigler, T K Bader

Presented by R Lemaître

A Frangi stated that one needs to compare to test results rather than just comparisons with other models. R Lemaître showed some additional test results showing relatively good agreement between model and test results. A Frangi commented that one is designing for connection rather than a single connector. One will need simple equation for design. He asked about rope effect. R Lemaître showed additional information on the subject to be presented in a WCTE paper in Seoul.

R Jockwer stated that there are additional parameters such as gaps. Also there is more information that can be obtained from test results rather than a single point of capacity. R Lemaître said that the gap issue can be handled by the model.

S Winter asked about the basis for the foundation spring properties. R Lemaître said this comes from the load slip curve of the dowel embedment strength tests of different material.

H Blass commented that the model can potentially be used to give information for dowels in multiple shear plane connection.

P Dietsch elaborated on the background of the COST action for this type of work and outlook for the next step.

TIMBER BEAMS

51 - 10 - 1 Formulaic Design Methods for TCC Floors - A Smith, J Schänzlin, M Piazza, A Lawrence, O Bell

Presented by A Smith

A Frangi suggested that more simplification should be considered for technical specification. The suggested model is too complicated for technical specification even though it is broader in scope compared to the gamma approach. The simple gamma approach should be extended and reformulated for cracked concrete considerations. A Smith responded that issues related to the complexities in the proposed method may be important for design consideration.

H Blass commented that inclined screws rely on withdrawal capacity from concrete which need to be tested with the cracked concrete case.

R Jockwer suggested that sensitivity studies should be considered to reevaluate the impact of some of the parameters on design. A Smith responded that such sensitivities studies may have already be initiated.

R Harris commented that there were much discussions in past years on this topic. Balance between simple code provisions versus more generalized approach is a topic of discussion. He suggested the interested parties should form a group to look in this issue.

A Frangi, I Abeysekera and A Smith further discussed the need for balance between simplification in design and a more generalized approach to cover more cases.

ENVIRONMENTAL CONDITIONS

51 - 11 - 1 Adaptation of Eurocode 5 Standard to French Hardwoods - Proposal of New Hygroscopic Equilibrium Charts - M Varinier, N Sauvat, C Montero, F Dubois, J Gril

Presented by F Dubois

C Sigrist asked if the theory can be applied to fibreboard or other material. F Dubois answered that the model cannot be applied to material such as fibreboard but can be applied to heavy timber.

F Lam received confirmation that the 3D FEM model can be used to model moisture gradient and moisture movement in the timber subjected to changing relative humidity and temperature conditions.

S Franke asked since the model only deals with mean timber material properties, how can it deal with variability of material properties. F Dubois answered the model can use different material properties if they are known.

S Franke raised issues related to equilibrium and time as Service Class 2 has to deal with issues related to wind and sunshine. F Dubois said that the model and data do not take these issues into account.

H Blass asked if the model can be applied to the timber drying case. F Dubois answered that it can be extended to free water case.

S Winter commented that the model is a good start. More work is needed to cover the code related issues in Eurocode 5.

LAMINATED MEMBERS

51 - 12 - 1 CLT under In-Plane Loads: Investigation on Stress Distribution and Creep -
M Gräfe, P Dietsch, S Winter

Presented by M Gräfe

H Blass commented that the steel tendon is used to pre-stress and creep is defined as deformation under continuous load. He questioned whether the loading can be considered continuous. M Gräfe agreed that they do not have continuous loading.

S Aicher discussed the use of steel supporting rail and asked how the buckling load was determined under such loading condition. M Gräfe responded that an average load at mid height was used.

H Blass and M Gräfe discussed the meaning of buckling of the CLT whether it is bending stiffness based or compression failure based.

S Aicher asked which width of the load distribution is considered. M Gräfe answered that it is the load corresponding to the width at mid height of the CLT panel. He also said that some FEM studies on 2D elements has been performed which show high capacity compared to individual columns.

A Frangi asked what happens when the load is not applied at the middle. M Gräfe said that the situation is not the same and will be different. He said that it will be a good future topic. A Frangi received confirmation that the beams were end sealed.

H Blass asked about the effective width for buckling design. M Gräfe explained that it is based on the load distribution angle to establish the width at mid height. H Blass said that if you have continuous load versus concentrated load and you cut out a strip, it would be too conservative. You could use a large effective width from the remaining part of the member which takes some loads.

U Kuhlmann commented that the load distribution needs to be examined carefully. There is a big different between parallel to face grain and perpendicular to face grain loading and the angle should be bounded to stiffness. M Gräfe responded that this is already considered based on the percentage of cross layers in the panel.

I Abeysekera asked how conservative is the proposed method compared to the length of effective width approach. I Abeysekera and M Gräfe discussed about the load distribution angle always between 20 to 30 degrees.

51 - 12 - 2 Tensile and Compression Strength of Small Cross Section Beech (Fagus s.)
Glulam Members - M Westermayr, P Stapel, J W G van de Kuilen

Presented by M Westermayr

H Blass commented that the conclusion about the performance of combined glulam built up depends on the built up used. M Westermayr agreed and said that it may be considered in a later study.

F Lam commented that in N. America tension test of glulam is rarely done with its characteristic strength taken as a percentage of the bending strength. He asked whether there are plans to do some bending tests as a benchmark. M Westermayr answered no plans at this time.

S Franke commented that connection values are also important. M Westermayr said that they are working on screw values.

S Aicher commented that build up is important and depends on the number of laminates. Also tension strength of the laminae is important and will provide important information. M Westermayr responded that there are concerns about the dimensional stability of the laminae hence testing on members was studied. P Stapel added that there was previous test data on the strength properties of the low quality laminae and increase of sample size will not change the results.

A Frangi and M Westermayr discussed the merit of the concept of using beech as structural material and the continuing going after low quality laminae to achieve high strength. H Blass said that Beech LVL is a good example of high strength product made of low quality material.

T Ehrhart commented that EN 408 requires clear specimens for compression testing. M Westermayr said that with this quality of wood it is not always possible to find clear specimen easily. H Blass commented that as a research project one should look at the weakest part of glulam material.

T Ehrhart also discussed issues regarding material with reject grade which could be upgraded by cutting out the defects and finger joining.

M Frese commented that the size of the members in the material approval being different from the size of material considered in the testing and direct comparison should not be made.

51 - 12 - 3 Behaviour of Glulam and LVL Beams Loaded Perpendicular to the Grain - L Windeck, H J Blaß

Presented by L Windeck

C Sigrist and L Windeck discussed the method of checking for stiffness.

J Hakkarainen and L Windeck discussed cross lamination effects and the difference in performance between spruce and pine.

P Quenneville asked for comments on load distribution angle theory in relation paper 51-12-1. L Windeck responded that for serviceability performance the approach in this paper works and is more appropriate.

A Frangi stated that one should try to convince engineers to avoid compression perpendicular to grain. Especially if you apply this work to taller buildings, it will not work. H Blass agreed and said this work shows compression perpendicular to grain is okay for three stories and commented that this type of issue are no different from issues related to tension perpendicular to grain.

51 - 12 - 4 Mechanical Properties of European Beech Glued Laminated Timber - T Ehrhart, R Steiger, P Palma, A Frangi

Presented by T Ehrhart

S Aicher commented that finger joint strength information is missing and shear strength comparison with ASTM test method is missing. T Ehrhart agreed that finger joint strength information is important. He explained that the shear test is intended for load configuration similar to one encounters in practice with multiple spans.

BJ Yeh discussed four point bending test method in terms of the reactions and double curvature of the member under load. He asked why failure occurred in the end section where there were low shear stresses. T Ehrhart said that secondary failure occurred in the end section and initial failure occurred in the interior section.

BJ Yeh said that the reaction force can stop the propagation of shear failure. T Ehrhart responded that the initial failure was independent of the presence of glued-in-rod or screw reinforcements.

P Dietsch commented that the assumption of shear crack not being influenced by the reinforcing screws was ok. He commented that industry may not follow the 8% moisture content rule and reinforcement may create confinement and promote crack development. T Ehrhart said that the intent is to create shear failures in multiple span beam structures which is a practical issue.

F Lam commented that 7 replicates is low based on experience in Canada on glulam testing. T Ehrhart responded that this database is intended for use to verify a model with more attention paid to testing of laminae properties. F Lam said this was also the approach taken in Canada but with a large number of replicates especially for the reference depth. F Lam further commented that the three-point bending with an I-section is simpler compared to the multiple span four point tests with fewer issues related to the interpretation of the results.

S Aicher and T Ehrhart discussed issues related to beam width in shear and volume effect versus depth effect and the need for simplification of design rules for practicing engineers.

S Winter received confirmation that effect of laminae thickness was not considered. Also issues related to influence of failure mode on compression perpendicular to grain were discussed. S Winter commented that field experience indicates that even in stable environment beech glulam suffers cracks. Production at 8% MC and testing at 8% MC is idealized. Testing with moisture content variation is needed.

51 - 12 - 5 Cross Laminated Timber at in-plane Beam Loading – New Analytical Model Predictions and Relation to EC5 - M Jeleč, H Danielsson, E Serrano, V Rajčić

Presented by M Jeleč

H Blass commented that constant shear distribution across the beam width was not considered in earlier work as only one layup was studied. M Jeleč agreed. H Danielsson discussed previous work when this was also assumed.

STRUCTURAL STABILITY

51 - 15 - 1 Seismic Resilient CLT buildings Using Resilient Slip Friction Joints (RSFJs) with Collapse Prevention Mechanism: Ductility, Design Methods and Numerical Validation - A Hashemi, P Zarnani, P Quenneville

Presented by P Quenneville

H Blass stated running non-linear time history analysis with different earthquakes will influence the ductility factor and asked how did you decide the ductility factor of 3.4. P Quenneville received confirmation from A Hashemi that 3.4 was the average value of the ductility ratios for all of the different seismic analysis.

Z Li commented that the capacities of these connections are high and how much restoring forces can these connectors produce. P Quenneville said angles less than 15 degrees will allow restoring forces to be developed which is approximately 1/3 of the ultimate capacity. Z Li commented that in pseudo dynamic tests good results can be obtained and the real dynamic behaviour of structures may be different. P Quenneville agreed and said that snap back test was done and good results were obtained.

I Abeysekera asked about the cost. P Quenneville stated that the economics must be considered especially for high importance building.

L-M Ottenhaus asked for comments on overstrength forces in the hold down which must be resisted by the CLT. P Quenneville responded that there are reinforcement methods or other connection methods that can be employed to take the required loads. He added that the performance of these connectors is reliable therefore a lower overstrength factor of 1.25 is recommended. L-M Ottenhaus and P Quenneville further discussed how to achieve the high post tension forces in the system.

M Yasumura asked whether these systems need to be installed at every floor or just at the base of the panels. P Quenneville said that the position and placement of these connectors depend on the building shape and building height but they will not be placed at every story.

F Lam commented that the recommendation from NZ engineering community to demolish timber buildings with residual drift of ½% seems harsh especially for light wood frame structures.

FIRE

51 - 16 - 1 An Improved Design Model for Fire Exposed Cross Laminated Timber Floors- J Schmid, M Klippel, R Fahrni, A Frangi, N Werther, A Just

Presented by J Schmid

S Aicher asked how does one account for the non-edge glued CLT with variable gap sizes and whether the model only accounts for edge glued CLT. J Schmid discussed the 6 mm gap allowance for CLT which is deemed to be inappropriate. He added that in European research 2 mm gaps will not allow heat to go into the gap as the wood chars. Also most CLT producers using vacuum press has a gap limit of 2 mm which is deemed acceptable. H Blass added that the 6 mm gap size was fixed at the earlier stage of CLT production. Nowadays the gap value is much smaller.

GLUED JOINTS

51 - 18 - 1 Press Glued Connections - Research Results for Discussion and Standardization - S Franke, M Schiere, B Franke

Presented by S Franke

P Quenneville asked about the cost effectiveness for so many screws being used. S Franke responded that this depends on individual companies. Some firms feel that it could be economically effective. P Quenneville received confirmation that the screws can be removed after curing if one desires.

S Aicher commented that one should make sure about the 0.1 MPa pressure requirement as this is currently not certified for structural use in Europe. He questioned whether the screws are used just to achieve the required pressure of 0.1 MPa. He stated that one component PU is not allowed for screw gluing in structural use for a range of reasons. He also stated that in principle gluing does not require pressure; however, pressure at 0.6 MPa and 1.0 MPa are needed to bring the two gluing surfaces together. Furthermore, in CLT rolling shear dominates so shear strength of the board and glue bond may not be critical. Finally the performance of the glue bond should be measured in terms of glue line thickness which dominate glue bond strength. S Franke agreed in general and commented that washer head screws may not be desirable to some companies as they are more visible. S Aicher added that nail bonding is not under consideration in Eurocode now and bond thickness is decisive. There is a need to consider dry-wet type testing. S Winter agreed with S Aicher and commented that the system of glue performance considered should be delamination tests with the screws removed. S Franke said that they are doing tests. S Aicher commented that for serviceability requirements the 0.1 MPa level may be okay but not for strength considerations.

SERVICEABILITY

51 - 20 - 1 A New Design Method for Timber Floors – Peak Acceleration Approach -
Wen-Shao Chang, T Goldsmith, R Harris

Presented by R Harris

T Toratti commented that the response factor method deals with square of the acceleration and asked why the proposed acceleration based method would be different.

R Harris responded that timber floors are more responsive than concrete floors even though timber floors still have good performance. In the proposed method the whole sequence of event is taken into consideration. If you measure a sequence of event, the timber floor is less responsive compared to the response factor method.

I Abeysekera asked how one can predict the number of events that will occur within a certain period. He asked what would happen to floors built with other materials using the proposed method. R Harris answered that the proposed method is material

independent and there is no special criterion for timber floors. Further details to the questions need to be addressed with W-S Chang.

Discussion took place about the applicability of VDV to floors built with other materials which could lead to equal improved predicted response and increase of their spans. I Abeysekera pointed out that the VDV is not used by the industry. A Smith discussed the value of adopting a consistent approach for all materials. R Harris agreed that it would be desirable but there is an inconsistency with wood being penalized.

51 - 20 - 2 Development of a Floor Vibration Design Method for Eurocode 5 - I Abeysekera, P Hamm, T Toratti, A Lawrence

Presented by I Abeysekera

R Harris commented that it is important to measure acceptable floors to check against the criteria so that the design procedures are not too penalizing. I Abeysekera responded that a range of limits is set to allow different levels of performance to be accepted. K Crews commented that there is always a dilemma that the floor vibration design method being either un-conservative or too conservative. The different levels of performance approach is interesting.

U Kuhlmann stated that Europe attempted to apply a criterion for all materials. She suggested that may be flexible long span timber floor can be accepted by clients recognizing that such timber floors are more flexible compared to concrete floors. However this type of criterion should be material independent.

P Dietsch questioned whether it is desirable to standardize values in tables where floors are deemed unacceptable. I Abeysekera stated that this should not be a problem. Floors can be engineered and clients can choose their criteria based on the desired performance level.

S Winter commented that methods to evaluate floor performance are needed. However people in practice may not be too skilled to use these methods. There are other publications that can help fill the gap.

NOTES

R Jockwer presented a note on Criteria for evaluating the simplification of design values for dowel type fasteners by R Jockwer T Uibel and M Kleiber

VENUE AND PROGRAMME FOR NEXT MEETING

BJ Yeh presented an invitation and information about the 2019 meeting in Seattle, August 26 to 29, 2019.

Planned future meeting locations are: 2020 Chile to coordinate with WCTE, 2021 München Germany, 2022 Biel Switzerland, 2023 Shanghai China, 2024 Padova Italy.

CLOSE

H Blass thanked F Lam for his contribution to the CIB W18 and Inter meetings.

H Blass thanked R Görlacher's organizational support and for the production of proceedings.

H Blass thanked P Dietsch for taking over the Chairmanship and reiterated the goals for this meeting are to improve researchers to become better researchers and to apply the latest research in Timber Engineering towards practice.

H Blass thanked the host from TUT for organization of a wonderful meeting.

3 INTER Papers, Tallinn, Estonia 2018

- 51 - 6 - 1 Modelling the Variation of Mechanical Properties along Oak Boards - C Tapia, S Aicher
- 51 - 7 - 1 Deviations Between Planned and Actual Position of Wood Screws - Consequences for their Spacing - M Frese, M Jordan
- 51 - 7 - 2 Analytical Method to Derive Overstrength of Dowel-Type Connections - L-M Ottenhaus, Minghao Li, T Smith
- 51 - 7 - 3 Pinching-free Timber Connection - P Quenneville, N Chan, P Zarnani
- 51 - 7 - 4 In-plane Shear Connection for CLT Diaphragms - T Schmidt, H J Blaß
- 51 - 7 - 5 Seismic Response of Connections with Glued-in Steel Rods - J Ogrizovic, R Jockwer, A Frangi
- 51 - 7 - 6 Cyclic Performance of a Full-scale Timber Column Equipped with Resilient Slip Friction Joints - A Valadbeigi, P Zarnani, P Quenneville
- 51 - 7 - 7 Load-Deformation Behaviour and Stiffness of Lateral Connections with Multiple Dowel Type Fasteners - R Jockwer, A Jorissen
- 51 - 7 - 8 Design Parameters of Notched Connections for TCC Structures as Part of Eurocode 5 - U Kuhlmann, S Mönch
- 51 - 7 - 9 Bond Performance of Glued-in CFRP and GFRP Rods in Timber - E Toumpanaki, M H Ramage
- 51 - 7 - 10 Multiple Shear Plane Timber Connections with Slotted-in Steel Plates and Dowel-type Fasteners: a Study of the Brittle Failure Mode in the Parallel-to-grain Direction - M Yurrita, J M Cabrero, P Quenneville
- 51 - 7 - 11 Group-Effect of Self-Tapping Screws in CLT Shear Connections - A Hossain, M Popovski, T Tannert
- 51 - 7 - 12 Performance of the Different Models for Brittle Failure in the Parallel-to-Grain Direction for Connections with Dowel-Type Fasteners - J M Cabrero, M Yurrita
- 51 - 7 - 13 Beam-on-Foundation (BOF) Modelling as an Alternative Design Method for Timber Joints with Dowel-Type Fasteners – Part 1: Strength and Stiffness

- per Shear Plane of Single-Fastener Joints - R Lemaître, J-F Bocquet, M Schweigler, T K Bader
- 51 - 10 - 1 Formulaic Design Methods for TCC Floors - A Smith, J Schänzlin, M Piazza, A Lawrence, O Bell
- 51 - 11 - 1 Adaptation of Eurocode 5 Standard to French Hardwoods - Proposal of New Hygroscopic Equilibrium Charts - M Varinier, N Sauvat, C Montero, F Dubois, J Gril
- 51 - 12 - 1 CLT under In-Plane Loads: Investigation on Stress Distribution and Creep - M Gräfe, P Dietsch, S Winter
- 51 - 12 - 2 Tensile and Compression Strength of Small Cross Section Beech (Fagus s.) Glulam Members - M Westermayr, P Stapel, J W G van de Kuilen
- 51 - 12 - 3 Behaviour of Glulam and LVL Beams Loaded Perpendicular to the Grain - L Windeck, H J Blaß
- 51 - 12 - 4 Mechanical Properties of European Beech Glued Laminated Timber - T Ehrhart, R Steiger, P Palma, A Frangi
- 51 - 12 - 5 Cross Laminated Timber at in-plane Beam Loading – New Analytical Model Predictions and Relation to EC5 - M Jeleč, H Danielsson, E Serrano, V Rajčić
- 51 - 15 - 1 Seismic Resilient CLT buildings Using Resilient Slip Friction Joints (RSFJs) with Collapse Prevention Mechanism: Ductility, Behaviour Factor, Design Methods and Numerical Validation - A Hashemi, P Zarnani, F M Darani, S M M Yousef-Beik, P Quenneville
- 51 - 16 - 1 An Improved Design Model for Fire Exposed Cross Laminated Timber Floors- J Schmid, M Klippel, R Fahrni, A Frangi, N Werther, A Just
- 51 - 18 - 1 Press Glued Connections - Research Results for Discussion and Standardization - S Franke, M Schiere, B Franke
- 51 - 20 - 1 A New Design Method for Timber Floors – Peak Acceleration Approach - Wen-Shao Chang, T Goldsmith, R Harris
- 51 - 20 - 2 Development of a Floor Vibration Design Method for Eurocode 5 - I K Abeysekera, P Hamm, T Toratti, A Lawrence

Modelling the variation of mechanical properties along oak boards

Cristóbal Tapia Camú, Materials Testing Institute, University of Stuttgart

Simon Aicher, Materials Testing Institute, University of Stuttgart

Keywords: timber variability, stochastic modelling, autoregressive model

1 Introduction

The study of the variation of the mechanical properties along structural lumber has been a recurring subject in the field of timber engineering for the past four decades. The results can be used straight forward in the analysis of size effects in laminations subjected e.g. to pure tension loading (*Showalter et al.*, 1987; *Lam and Varoglu*, 1991; *Taylor and Bender*, 1991; *Isaksson*, 1999), but, most importantly, the study of the length-wise variation of the material properties serves as a corner stone in the development of complex numerical strength models for glued laminated timber (GLT) beams (*Ehlbeck and Colling*, 1987; *Blaß et al.*, 2009; *Frese et al.*, 2010; *Fink*, 2014). Here, it sets the necessary underlying stochastic variability model for the laminations, which, together with the properties of the finger-joints, determines the strength characteristics of GLT beams.

Mainly two types of models are used for the simulation of the variation of properties within the boards. One comprises the use of a set of fitted linear regressions comprising a set of correlated variables, like knot area ratio (KAR), modulus of elasticity (MOE) and density (ρ). This is used by *Ehlbeck and Colling* (1987), *Isaksson* (1999) and *Blaß et al.* (2009) in their respective models. Alternatively, the variability can be described as an autoregressive (AR) process of different orders, where the serial correlation and cross-correlation coefficients are considered. This approach used by *Kline et al.* (1986) for the MOE variation, and *Taylor and Bender* (1991) regarding MOE and f_t variation, with AR models of order 2 and 3, respectively. Similar to the latter approach, *Lam and Varoglu* (1991) used a moving average (MA) model of order 3 for the tensile strength. The model used by Lam and Varoglu differs from an AR model by the fact that in a MA process the previous innovation values, typically representing white noise, are weighted instead of the previous computed values.

The latter type of models were calibrated by *Kline et al.* (1986), *Taylor and Bender* (1991) and *Lam and Varoglu* (1991) with data obtained from tensile tests, where window lengths between 610 mm and 762 mm were used for the measurement of MOE and/or strengths. These measurement lengths are fairly large when compared to the windows of 150 mm used to obtain the *KAR* and densities values used in the former models by *Ehlbeck and Colling* (1987). This is especially true, when the length of the boards used in some currently produced oak GLT beams can be in the same length range of around 600 mm (see e.g. ETA-13/0642 (2013)). Another problem with the models of *Kline et al.* (1986), *Lam and Varoglu* (1991) and *Taylor and Bender* (1991) consists in the explicit disregard of stiffness and strength indicators such as the *KAR* and density. These indicators, especially the *KAR* value, can be useful in a further refinement of the model.

This paper presents the first state of a newly developed stochastic model for the simulation of the variation of MOE and tensile strength along oak lumber boards. In a first part, experiments made on a total of 47 oak boards of 2.5 m length will be presented, where the MOE variation was measured over a length of 1.5 m in windows of 100 mm, giving a total of 15 measurements per board. Further, the maximum possible number of tensile strength values for each board was obtained, by successively testing the pieces not damaged after the initial failure. In the second part, an autoregressive model for the MOE and tensile strength is developed.

2 Experimental campaign with oak boards

2.1 Material

The variation of the modulus of elasticity was measured in a batch of oak boards (*Quercus robur*), originating from France, delivered by the company Scierie Mutelet, Rahon, France. The batch consisted of a total of 47 boards and contained a mixture of appearance grades QF2 and QF3, according to EN 975-1 (2009), which were classified in a follow-up grading at the MPA, University of Stuttgart, according to the LS strength grading classes described in DIN 4074-5 (2008). The different appearance grades enable a variable degree of *knotiness* and grain deviation in the sample, which leads to different amounts of variation in the MOE measurements of each board. The nominal dimensions of the specimens were 2500 mm × 175 mm × 24 mm (length × width × thickness) and the moisture content (measured with a pin-type resistance meter) was 10.2 % (COV = 4.6 %).

2.2 MOE and tensile strength measurements

An experimental campaign was set-up to measure the variation of the modulus of elasticity along the board and fiber direction for oak boards. A total of 47 boards were tested in tension in a servo-hydraulic universal testing machine (max. load 600 kN). The

boards were placed in the testing machine as shown in Fig. 1. The free length between the grips was about 1700 mm, providing approx. 350 mm of clamping length at both ends.

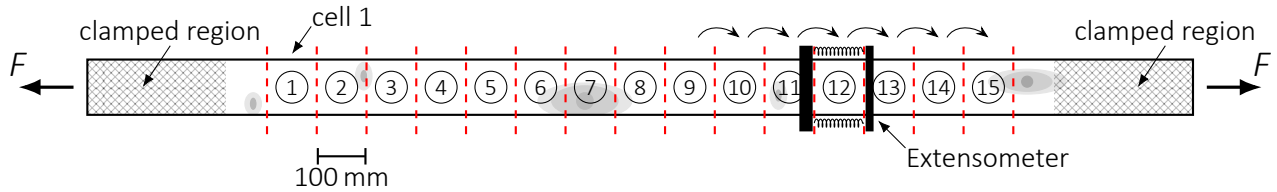


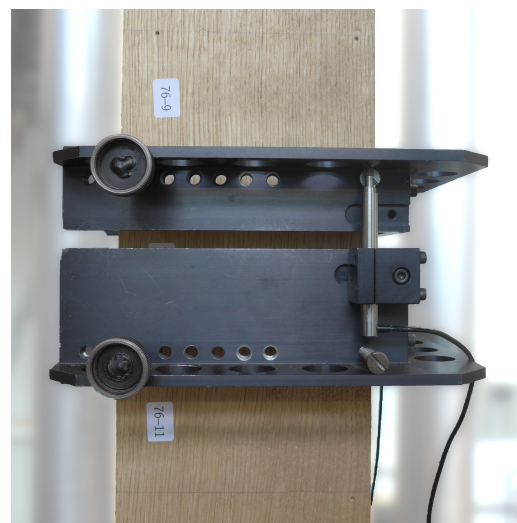
Figure 1. Used test set-up for the determination of the variation of the elastic modulus along the boards.

The free length of each board was divided into 15 *cells* (windows) of length 100 mm, and the (mean) elongation was measured for every cell by means of a specific extensometer, as shown in Fig. 1. The extensometer consists of two U-shaped steel frames, attached to the board by means of special screws, with two linear variable displacement transducers (LVDTs) placed at diagonally opposite sides of the board cross-section for the measurement of the axial deformations (see Figs. 2a,b). The respective tests started with a displacement-controlled loading of the board at a stroke rate of 0.04 mm/min and were stopped once a tensile load of 30 kN was reached. Then, the specimens were unloaded at a rate of 5 kN/s until zero load. After this, the extensometer was shifted to the next cell and the described sequence of loading and displacement measurement was repeated. The process described was performed for each cell within the free length.

In a subsequent step, the global MOE was measured over a length of 1500 mm, equal to the summed-up length of all the investigated cells in the board. This serves the purpose of checking the overall quality of the measurements at the individual cells. (Note: if the local measurements are correct, then the difference between the measured global MOE



(a)



(b)

Figure 2. Extensometer used for the measurement of the deformations in the 100 mm long cells. (a) rear-side view; (b) lateral view. The used LVDTs can be seen in both figures.

and the global MOE computed with the local measurements (cell data) should be small in relative terms.)

Finally, the boards were tested in tension until failure occurred. The position (number of the cell) where the board failed was recorded, in order to obtain a correlation between tensile strength and MOE. If the remaining pieces of the board were not damaged, another tensile test was performed on each one of the remaining parts, which allowed to gather additional information regarding the distribution of the tensile strength along the board. Due to the nature of some of the observed failures, a rigorous assignment of the *weak cell* was not always possible. Nevertheless, a careful observation during and after the test leads, in general, to the onset of the crack initiation, which most of the times can be associated with a knot or extreme fiber deviation.

2.3 Measurement of knot-related variables and grain deviation

The position and dimensions of each knot larger than 5 mm was recorded using a digital caliper gauge. For each knot, three dimensions were measured: the minimum and the maximum diameter of the assumed ellipse, and the width taken perpendicular to the principal axis of the board. These three variables allow for the later determination of the rotation angle of the knot, which is represented by an ellipse. Knots (areas) at different faces of the board, corresponding to the same knot volume, are marked with a unique number. This information is used to digitally reconstruct the geometry of the knots in each board and compute the *KAR* values for each cell, and globally, for the grading according to DIN 4074-5 (2008).

The maximum grain deviation was manually measured for each board by means of a special scriber. The determination of the grain deviation throughout the board is out of the scope of this paper, but would certainly give additional, relevant information for the MOE-tensile strength model.

3 Analysis of the experimental results

3.1 Modulus of elasticity

The longitudinal deformation measurements of each cell were used to compute the MOE values, for which the mean value of both LVDTs was taken. In the evaluation, only the data-points starting from 10 kN were considered, which helps to avoid possible non-linearities produced by slip-movements of the boards in the clamping areas at the beginning of the loading regime. The analysis of the data showed, that all measurements were within the linear range, which was proven by computed squared correlation coefficients, R^2 , almost equal to unity.

Similarly, the global MOE values ($E_{\text{glob,test}}$), measured with a gauge length spanning all cells, were measured for each board and were then compared to the global MOE values

($E_{\text{glob,cells}}$) computed directly from the local MOEs. The MOE $E_{\text{glob,cells}}$ is obtained from the known equation for springs connected in series, given by

$$\frac{L_{\text{glob}}}{E_{\text{glob,cells}} \cdot A} = \sum_i \frac{\ell_{i,\text{cell}}}{E_{i,\text{cell}} \cdot A} \quad , \quad (1)$$

where L_{glob} is the reference length (1500 mm) over all 15 cells, $E_{i,\text{cell}}$ are the MOEs measured for each cell and $\ell_{i,\text{cell}}$ is the cell length (100 mm). The value A corresponds to the cross-section area and it is only shown for completeness, since it cancels out in Eq. (1). The comparison of the measured MOE with the computed global MOE showed a good agreement $E_{\text{glob,test}}/E_{\text{glob,cells}} = 1.01 \pm 0.01$.

3.2 Knot-related variables

The gathered data for the position and dimensions of the knots on the surface of the boards is processed and plotted, in order to determine pairs of knots corresponding to the same volume entity. This process was performed manually. With the data relating the pairs of knots, a 3D model of each board with its knots was produced using the python library python-occ (Paviot, 2018). Fig. 3 shows an example of one of these 3D models, where the knots and the respective clear wood area of each studied cell can be observed. The latter is used to compute the *clear wood area ratio* (CWAR), which is the complement of the KAR value.

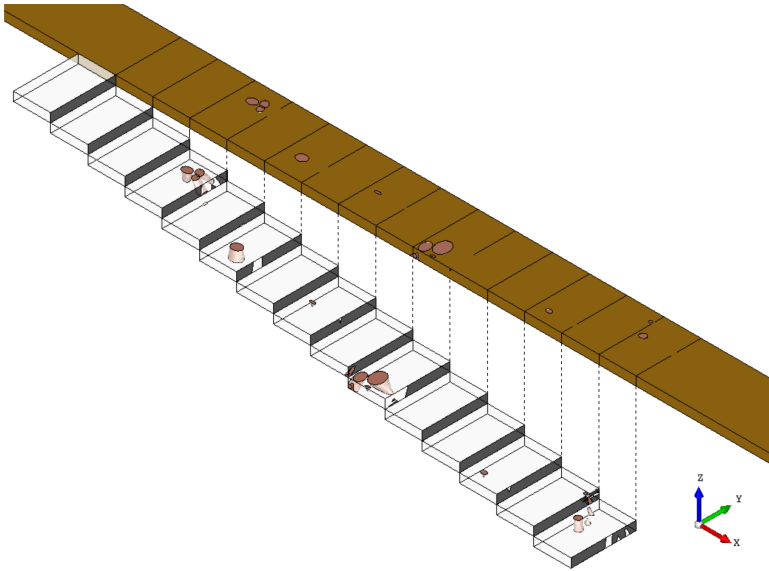


Figure 3. Post-processing of the gathered knot data, exemplary shown for board No. 50. The black areas in front of each one of the cells correspond to the respective clear wood area ratio.

3.3 Relationship between modulus of elasticity, tensile strength and CWAR

The post-processed data obtained for MOE, tensile strength and CWAR allows for an analysis of the relationships between them. Three specific relations were analyzed: (a) the one between the MOE variation and the CWAR; (b) the correlation between

tensile strength and MOE; (c) and the correlation between tensile strength and CWAR. Figs. 4a–d show the MOE and CWAR-value variation for four different tested specimens, as well as the position of the weakest sections (cells observed to be responsible of the global failure for each board). The chosen examples depict typical situations with different observed coefficients of variation (COV) for the MOEs and different CWAR variations throughout the boards.

From the information depicted in Figs. 4a–d (and from all the other boards studied) it can be clearly seen that, as expected, most of the time the boards failed in regions containing knots, which also exhibit relatively lower MOE values. It can also be seen, that large variations of MOE can be observed in absence of knots, too (see Fig. 4c), and that also in these situations the board will probably fail in this position. This indicates

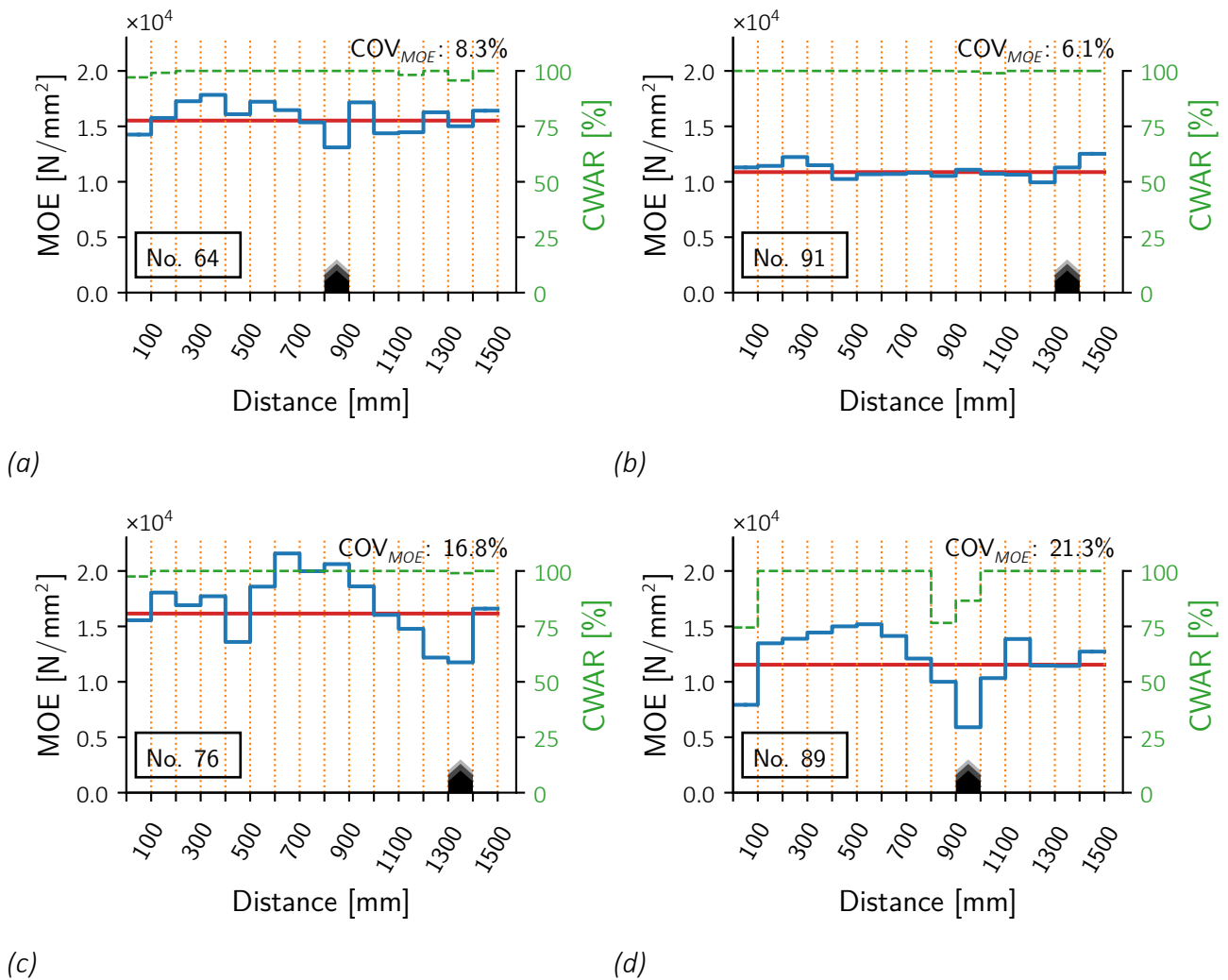


Figure 4. Variation of the measured MOE and CWAR (dashed line), weak sections and tensile strengths for different specimens. The weakest sections are marked by a black wedge at the bottom of each axis for every specimen; the red, straight line denotes the measured global MOE of all the 15 cells together ($E_{glob,test}$). (a) Specimen 64 is characterized by a relatively large COV for the MOE and a rather small correlation with CWAR values; (b) Specimen 91 shows a small COV for the MOE with no presence of knots; (c) Specimen 76 presents a high COV for the MOE which is not explained by a high knotiness; (d) Specimen 89 shows a high COV for the MOE with a very good correlation with CWAR values.

a probable correlation between the MOE and strength values at the weakest section of the board.

The correlation between global MOE of a board and its tensile strength has been shown to be low, and this was also the case in this study ($R^2 = 0.213$, see Fig. 5a). It is therefore of much interest to notice that a positive correlation between the MOE of the weakest section and the tensile strength occurring frequently in the same region is observed, reflected by a squared correlation coefficient of $R^2 = 0.509$ (see Fig. 5b).

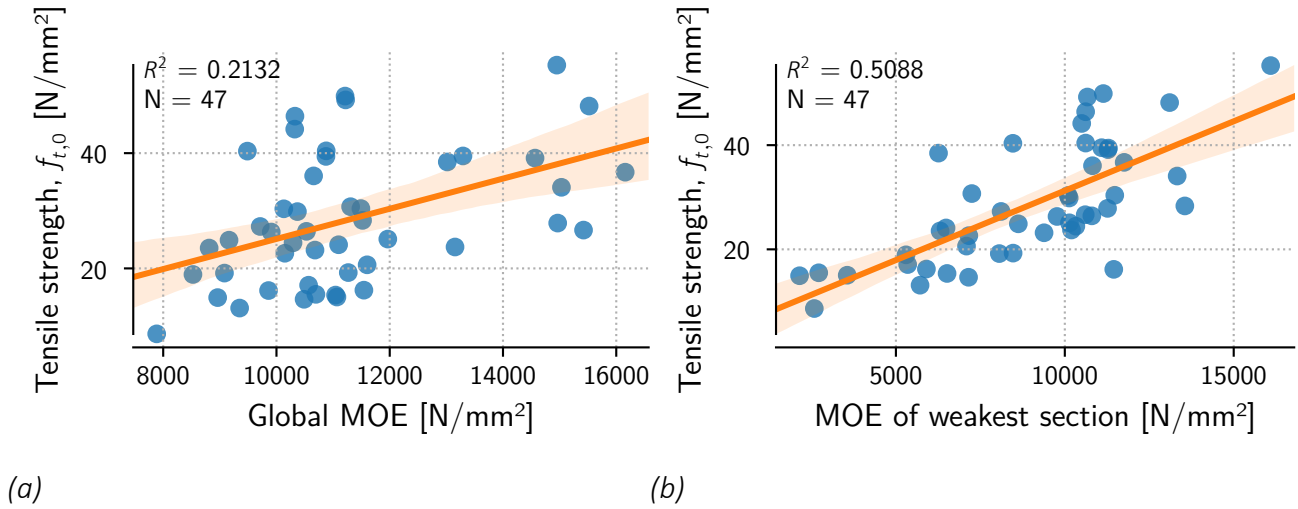


Figure 5. Correlations between MOE and tensile strength. (a) Correlation between the global MOE vs. $f_{t,0}$; (b) local MOE measured at the weakest cell and its corresponding tensile strength.

3.4 Variation of the modulus of elasticity

As it was shown in the previous section, the MOE can present a relatively high fluctuation with respect to its *global* value. A large portion of the fluctuation can be directly attributed to the presence of knots (see e.g. Fig. 4d). However, a high variation of the measured MOE throughout the board was observed in *knot-free* regions, too (see e.g. Fig 4c). For the purpose of this paper, this variation in the *knot-free* region is considered as a *base* variation of the MOE. A deeper analysis of the *knot-free* segments would reveal the statistical characteristics of this base fluctuation, giving relevant information for the development of a model for the simulation of the MOE variation.

For the following analysis, the concept of the serial *lag-k* correlation is used, which captures the correlation between each element of a vector and the corresponding k -shifted element of the same vector. The serial *lag-k* correlation coefficients are computed for the MOE variation of each board, similar as done by Showalter et al. (1987), Taylor and Bender (1991) and Lam and Varoglu (1991). In order to capture the information concerning the base variation of the MOE, only long enough clear-wood segments are considered. These segments are defined as a minimum of 7 contiguous cells (i.e. 700 mm) in each board with a KAR-value below 2 %. This small accepted KAR-value allows for a few extra boards to be chosen for the computation of the serial correlations.

An important aspect of the method used for the computation of the serial correlations comprises the *normalization* of the MOE data of each board, so that they can all be analyzed together. This process uses the same concept presented by *Taylor and Bender* (1988) to map random variates belonging to one distribution to another one. In this case, the MOE values of each board are fitted to a normal distribution and then *mapped* into a $\mathcal{N}(0, 1)$ distribution. This process brings the MOE data from different boards to a common base level, which allows for a simultaneous analysis. It is also important to notice that the tuples (E_n, E_{n+k}) , used for the computation of each *lag-k* correlation, always belong to a same board, i.e. the MOE values of the different boards are *not* concatenated into a single vector to perform the correlation. Putting all the data into a single vector would be a mistake, since cells of different boards would be mixed when computing the serial correlations.

Figs. 6a–c show the computation of the first three serial correlations for the previously defined clear wood segments. It can be noticed, that the serial correlation beyond *lag-1* is practically non-existent (see Fig. 6d) and that even for the first lag the serial correlation

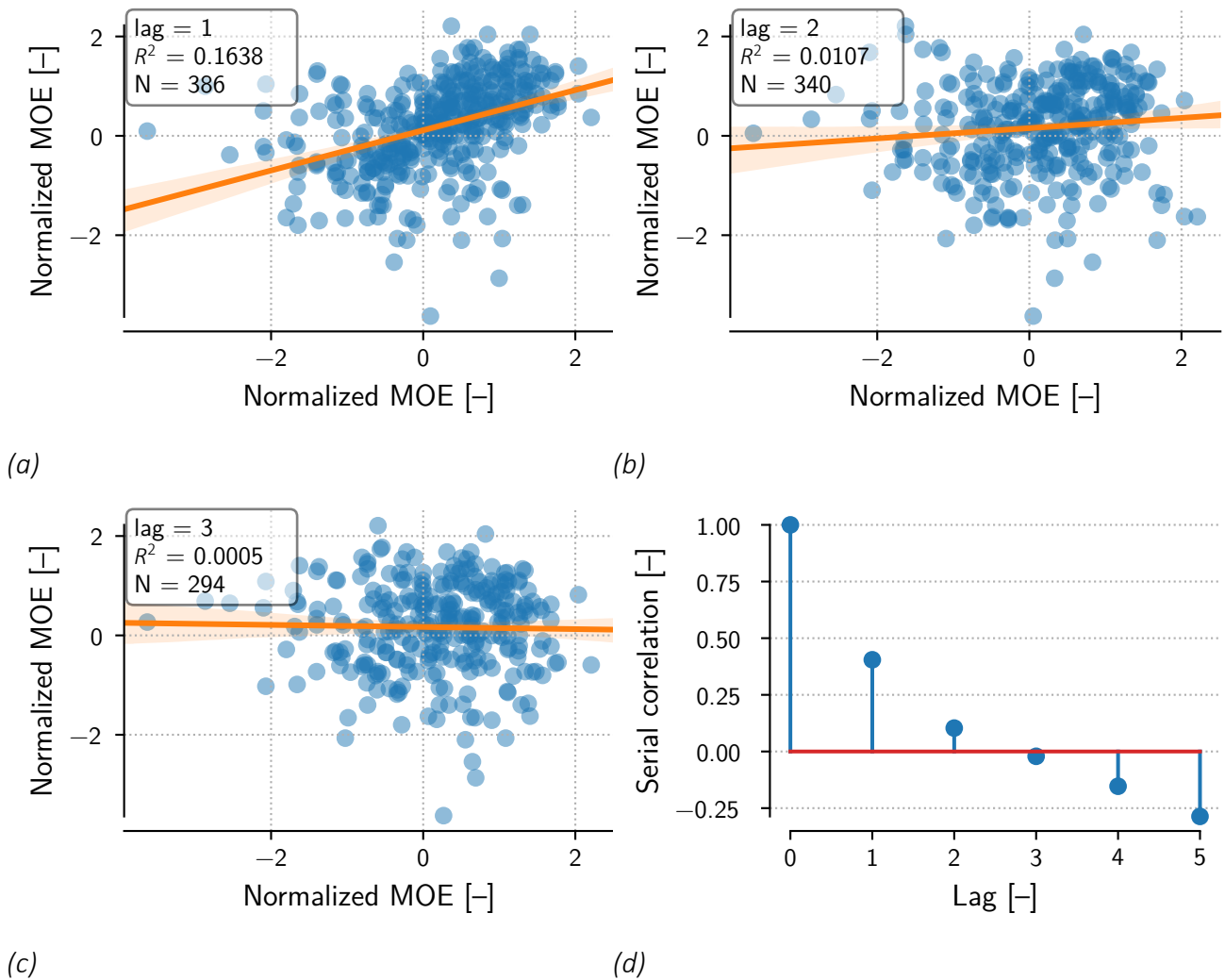


Figure 6. Linear regression used to compute the first three lags of the serial correlation (Figs. (a), (b) and (c)) and calculated serial correlations (d)

it is rather weak ($R = 0.405$). The values for the serial correlations can be taken from Table 1, where, additionally to the mentioned clear wood segments, the serial correlation coefficients for all the boards are presented (i.e. the serial correlations computed for the whole dataset, without additional filtering). From here it can be seen, that the process of filtering out the segments containing knots helps to improve the obtained serial correlation values (from $R = 0.330$ to $R = 0.405$ for the first lag).

Table 1. First five serial correlation values computed for the clear wood segments and for all the segments without making any additional filtering

	<i>lag-1</i>	<i>lag-2</i>	<i>lag-3</i>	<i>lag-4</i>	<i>lag-5</i>
clear wood ¹	0.405	0.103	-0.021	-0.153	-0.286
all segments ²	0.330	0.000	-0.092	-0.170	-0.220

¹ Segments containing a minimum of 7 contiguous cells in each board with a KAR-value below 2 %.

² Every cell of each board is used for the analysis.

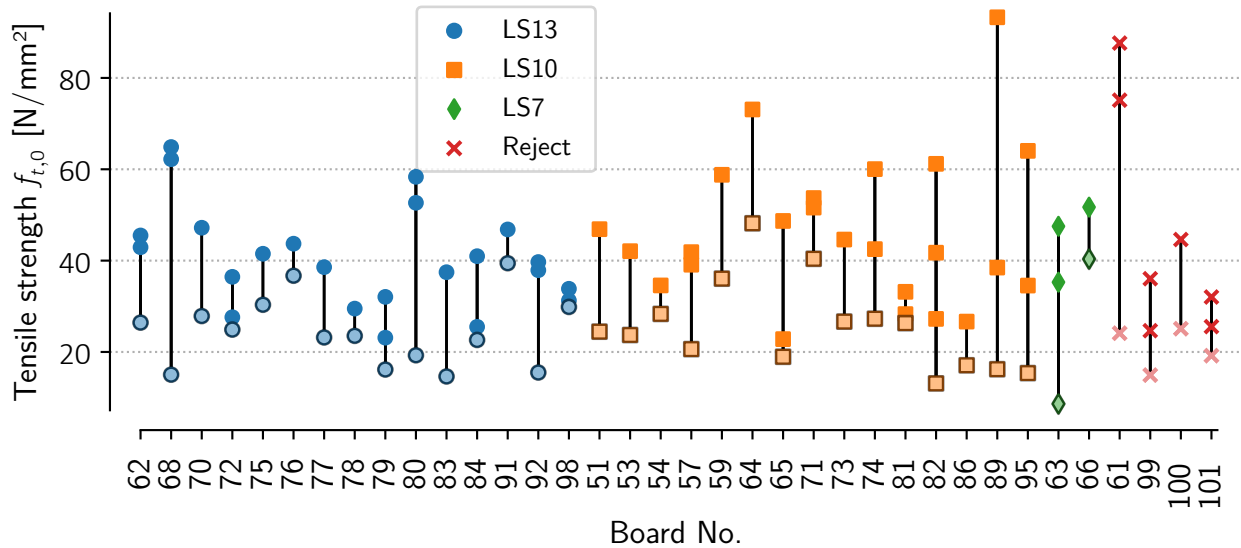
3.5 Variation of tensile strength

The estimation of the tensile strength variation along a single board presents some apparent difficulties. The most evident of which is presented by the impossibility of taking measurements in two short, consecutive regions, such as the basic units of 100 mm studied here. The second problem results from the different failure modes that can occur. In some cases cracks propagate throughout the whole board after the first failure, leaving no long enough undamaged section to be tested again.

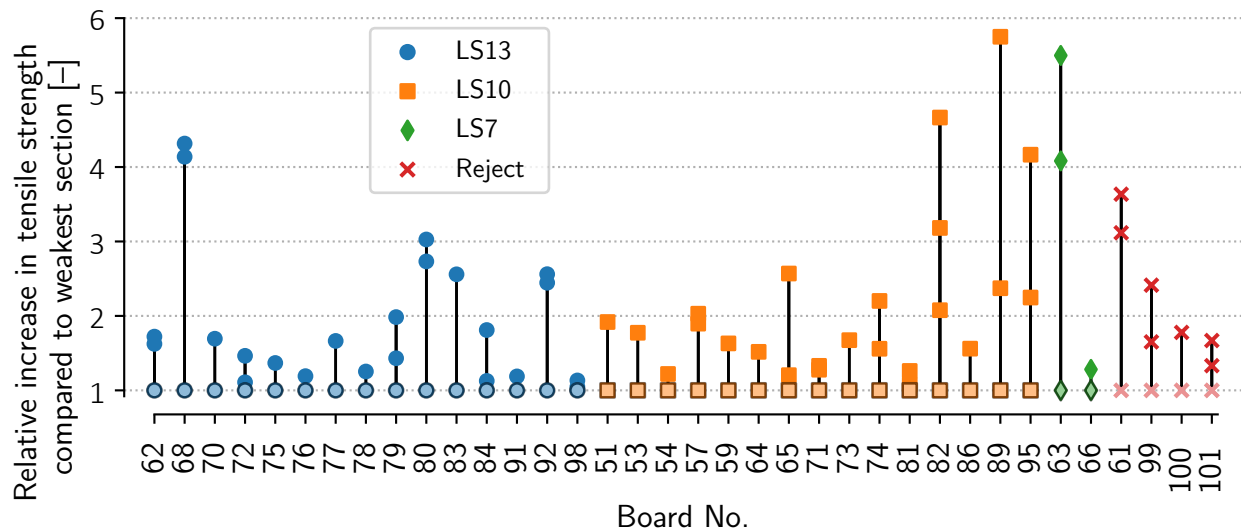
The tests performed on the oak boards exhibited a large amount of blunt failures, which allowed to take the remaining parts and test them up to three times (only in one case four tensile strengths were obtained). The results of this process can be seen in Fig. 7a, where the boards tested in tension more than one time are presented, separated by the assigned LS-grade.

It becomes evident that the variation of the tensile strength within a single board can be extremely large. The relative increase between the strength of the weakest section and the strength(s) of other (clear wood) sections can reach the order of six (see Fig. 7b). A slight distinction is observed in this regard for the different LS grades, where grades LS10 and LS7 show larger relative differences between the strength of the weakest cell (first failure of the full board length) and the strengths obtained by testing the fractured parts. This is also somewhat expected, since a rather “good” board, denoted by a smaller size of defects, will probably have high tensile strength values throughout its length, making the variation less pronounced.

Since the weakest spots mostly coincide with the position of a knot, this information can be used to quantify the effect of knots of different sizes (or more precisely, sections with different KAR-values) with respect to the clear wood properties of the board. This can be



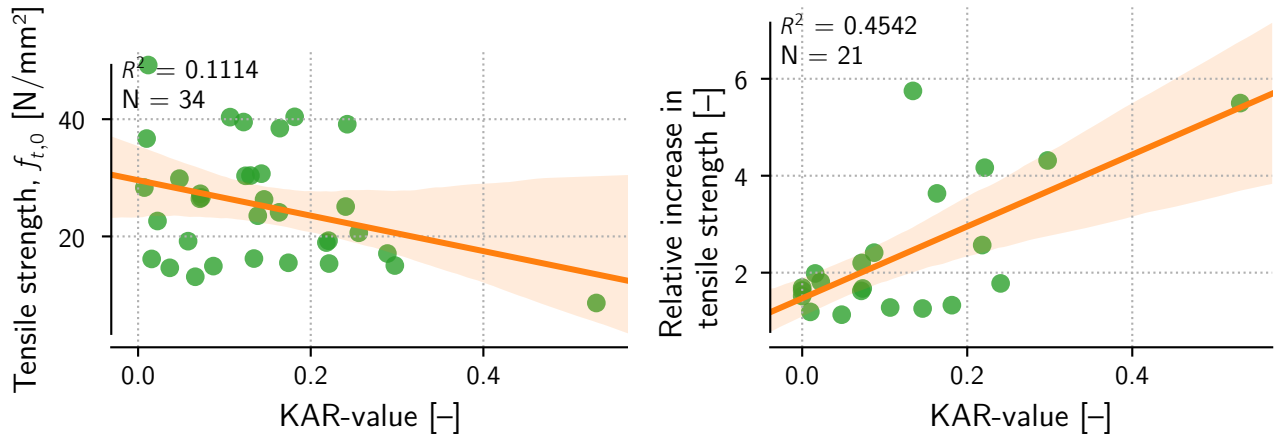
(a)



(b)

Figure 7. Variation of the tensile strength between and along individual oak boards. (a) absolute values; (b) values relative to the global failure. The results are divided into four different groups according to the classification in LS-grades (DIN 4074-5, 2008). Global failures are marked with a black edge and lighter color (always the lowest value for each board).

analyzed from different angles. Fig. 8a compares the tensile strength against the *KAR*-value. It can be seen, that no correlation is obtained. This is so, because all strengths measurements are treated equally, when they actually should be studied relative to the other strengths in the same board (each board would have a different *base* tensile strength). Another manner of observing the effect of the *knotiness* of a section is to compare this value against the relative increase observed in the maximum value of the other tested sections of the same board. Fig. 8b depicts this methodology and shows that a moderate correlation can be obtained ($R^2 = 0.454$).



(a)

(b)

Figure 8. (a) Correlations between KAR-values at the weakest cells and their tensile strength; (b) Correlation between KAR-values at the weakest cells and the maximum relative increase in strength for the other tested parts of the same board. Only weakest sections with $KAR > 0$ ($N=34$) were used and additional failures occurring in clear wood ($N=21$).

The rather moderate correlation is bound to the fact that knots do not represent the exclusive property that determines the decrease in tensile strength along the board, but interacts with other (defect) characteristics like grain deviation and density. Furthermore, as already mentioned, it is not always possible to determine the exact region where the failure began with sufficient certainty (although much care was taken to do so), which introduces an additional error to the data.

However, the shown experimental results reveal the magnitude of the variation of the tensile strength along oak boards, and their correlation with the elastic modulus and knot area ratio. This information is of high usefulness in the further development of a model to simulate the variation of both MOE and tensile strength within a board.

4 Simulation of mechanical properties along single boards

The gathered experimental data provide relevant information about the variation of the mechanical properties (MOE and $f_{t,0}$) along the studied oak boards. The next logical step consists in using this information in the development of a stochastic model to simulate this intra-board variation. In the following, it is shown how these data can be used to this end, based on the concept of an autoregressive model.

4.1 Autoregressive model applied to the simulation of MOE data

For the simulation of the MOE along the board, the approach used by *Kline et al.* (1986) and *Taylor and Bender* (1991) was implemented, which represents the variation of the MOE and tensile strength along each board as an autoregressive model. In its general form, an autoregressive model for a variable X_t (MOE or $f_{t,0}$) of order p has the form

$$X_t = C + \sum_{i=1}^p \varphi_i X_{t-i} + \varepsilon_t, \quad (2)$$

where the values φ_i are the parameters of the model, C is a constant and ε_t is white noise. According to the experimental results, an AR(1) model (order: 1) should be enough to reproduce the observed variability of the MOE along the board. In such case, the only parameter of the model, φ_1 , takes the same value as the obtained *lag-1*-correlation, i.e. $\varphi_1 = 0.405$. This model will generate data in a normal distribution $\mathcal{N}(0, 1)$, which then can be mapped into a distribution that represents the MOE values of a given board (*Taylor and Bender, 1988*). With this, the model is fully determined and can be used to simulate any number of oak segments.

However, the data generated by the model described in general do not delivers the global value assigned to the board—i.e. the global MOE computed from the single cells will not match the MOE assigned to the whole board—, which is a result of the stochastic nature of the method. A correction is, therefore, required. For the case of the MOE, this is done by simply shifting the data so that the resulting stiffness of the board, computed from the individual values of each cell, matches the assigned global stiffness. The resulting global MOE is computed by means of Eq. (1) and the difference between this value and the assigned global MOE is calculated. This difference is then added (summed) to the generated data. In order to obtain a small error between this two values, this process has to be repeated in an iterative way. In this case, five iterations were used, then resulting in a negligible error.

4.2 Cross-correlation applied to the generation of the strength data

For the generation of the strength data along the board, the concept of a vector autoregressive model (VAR) was applied, which is used to correlate different time-series-like variables. However, differently as in a typical VAR model, the generated data are based on the already generated (autocorrelated) X_t data for the MOE. For this, the *lag-0* cross-correlation between the MOE and $f_{t,0}$ is used. The model takes the following form:

$$Y_t = C + \psi_0 X_t + \varepsilon_t, \quad (3)$$

where Y_t are the data needed to be generated (tensile strength), X_t are the data (MOE) to be correlated to and ψ_0 is the model parameter corresponding to the lag-0 cross-correlation ($\psi_0 = 0.7$). C and ε_t have the same meaning as before. Now, the reason why the MOE data are generated in the $\mathcal{N}(0, 1)$ space becomes obvious: since the $f_{t,0}$ data have to be correlated to the MOE values by means of the coefficient ψ_0 , the fact that both variables correspond to the same distribution $\mathcal{N}(0, 1)$ spares the need to compute a scaling factor between two different distributions.

Similar as for the MOE-data, a correction is applied to the strength values, which consists of shifting the data so that the minimum value of each board equals the assigned strength of the board.

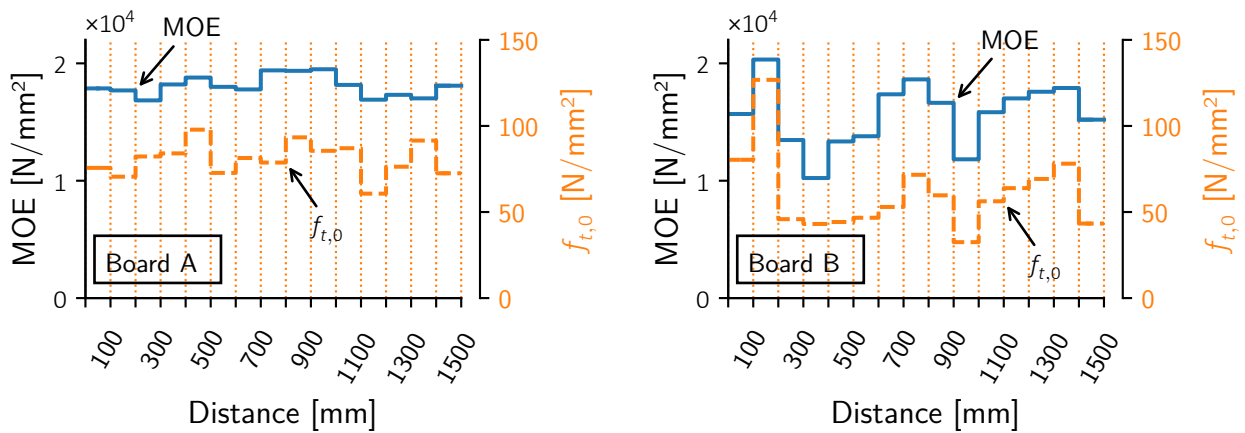
4.3 Application of the described simulation model

The model was applied to two different configurations of boards (A and B), which were assumed to have a different COVs for the variation in their elastic modulus and tensile strength. This COVs, together with the mean values for the MOE and minimum values for the $f_{t,0}$ are presented in Table 2. The statistical distributions used for the properties along the board correspond to *lognormal* distributions, since this ensures only positive values to be generated.

Table 2. Coefficients of variation used for the MOE and $f_{t,0}$ used for the simulations of boards A and B

	E_{mean} [N/mm ²]	$f_{t,0,\text{min}}$ [N/mm ²]	COV_{MOE} [%]	$COV_{f_{t,0}}$ [%]
Board A	18 000	60	5	15
Board B	15 000	30	15	40

Figs. 9a,b show the results of the simulations performed given the parameters from Table 2. From both figures the serial correlation in the MOE can be noticed, as well as the cross-correlation between the MOE and $f_{t,0}$. Although a setting of a high COV for the modulus of elasticity (Board B) could be used to simulate sudden decreases in the MOE, like the ones produced by the presence of knots (as seen in Fig. 9b), there might be a better option to do it. Namely, this could be preferably achieved by creating a low variability board (e.g. Board A, see Fig. 9a) and then include knots in a stochastic manner to reduce the properties accordingly. Nevertheless, the presented approach



(a)

(b)

Figure 9. Results of the simulations for the variation of MOE (continuous line) and $f_{t,0}$ (dashed line). (a) Board A: a board with low COV in the MOE (5 %) and $f_{t,0}$ (15 %); (b) Board B: a board with higher variation in its MOE (15 %) and in its $f_{t,0}$ (40 %).

shows that an autoregressive model can be used to model the stochastic variability of the mechanical properties along oak boards.

5 Conclusions

The variation of the mechanical properties (MOE and $f_{t,0}$) of oak boards was studied experimentally by means of a series of tensile tests. Measurements of the MOE over the short lengths of 100 mm allowed for the computation of serial correlation coefficients, which, for clear wood segments, yielded a *lag-1*-correlation of 0.4. Due to the low values obtained for the rest of the *lag-k* correlation coefficients, it can be assumed that a serial correlation of order larger than 1 has no relevance.

The analysis of the variation of the tensile strength within each board showed a large relative increases in the strength of the cells that failed in the secondary tensile tests. The magnitude of this increase was shown to have a relationship with the knot area ratio (*KAR*), expressed by a linear regression with a squared correlation coefficient of $R^2 = 0.45$.

Although a very low correlation between global MOE and tensile strength was observed ($R^2 = 0.21$), it could be observed that a higher correlation was obtained between the MOE of the weakest cell (the cell where the board failed) and the tensile strength ($R^2 = 0.51$).

The gathered statistical information was used for a model to simulate the variation of the MOE and tensile strength along the board. The model consists of two parts: the first part generates the MOE data by means of an autoregressive model, and the second part generates the strength values by means of a modified vector autoregressive model. Overall, the model can simulate the MOE data in a good manner, when compared to the experimental measurements, being able to replicate different COVs, depending on the type of board that is needed. A further improvement to the model would be the inclusion of a third variable accounting for the explicit location of knots along the board, which could be combined with the simulated MOE and $f_{t,0}$ values to produce more realistic results.

6 References

- Blaß, H. J., M. Frese, P. Glos, J. K. Denzler, P. Linsenmann, and A. Ranta-Maunus (2009). *Zuverlässigkeit von Fichten-Brettschichtholz mit modifiziertem Aufbau, Bd. 11*. Tech. Rep. Karlsruhe, Germany: Karlsruher Berichte zum Ingenieurholzbau. DOI: 10.5445/KSP/1000008462.
- DIN 4074-5 (2008). *Strength grading of wood – Part 5: Sawn hard wood*. Berlin, Germany: German Institute for Standardization.
- EN 975-1 (2009). *Sawn timber – Appearance grading of hardwoods – Part 1: Oak and beech*. Brussels, Belgium: European Committee for Standardization.

- Ehlbeck, J. and F. Colling (1987). *Biegefestigkeit von Brettschichtholz in Abhängigkeit von Rohdichte, Elastizitätsmodul, Ästigkeit und Keilzinkung der Lamellen, der Lage der Keilzinkung sowie von der Trägerhöhe*. Tech. Rep. Karlsruhe, Germany: Versuchsanstalt für Stahl, Holz und Steine, Universität Fridericiana Karlsruhe.
- ETA-13/0642 (2013). *European technical approval – Glued laminated timber of oak*. OIB, Vienna, Austria.
- Fink, G. (2014). “Influence of varying material properties on the load-bearing capacity of glued laminated timber”. PhD thesis. ETH Zürich. DOI: 10.3929/ethz-a-010294974.
- Frese, M., F. Hunger, H. J. Blaß, and P. Glos (2010). “Verifikation von Festigkeitsmodellen für die Brettschichtholz-Biegefestigkeit”. German. In: *European Journal of Wood and Wood Products* 68.1, pp. 99–108.
- Isaksson, T. (1999). “Modelling the Variability of Bending Strength in Structural Timber – Length and Load Configuration Effects”. PhD thesis. Lund Institute of Technology – Division of Structural Engineering.
- Kline, D., F. Woeste, and B. Bendtsen (1986). “Stochastic model for modulus of elasticity of lumber”. In: *Wood and Fiber Science* 18(2), pp. 228–238.
- Lam, F. and E. Varoglu (July 1991a). “Variation of tensile strength along the length of lumber – Part 1: Experimental”. In: *Wood Science and Technology* 25.5, pp. 351–359. DOI: 10.1007/BF00226174.
- (Sept. 1991b). “Variation of tensile strength along the length of lumber – Part 2: Model development and verification”. In: *Wood Science and Technology* 25.6, pp. 449–458. DOI: 10.1007/BF00225237.
- Paviot, T. (2018). *pythonOCC, 3D CAD/CAE/PLM development framework for the Python programming language, PythonOCC – 3D CAD Python*. (accessed May 10, 2018). URL: <http://www.pythonocc.org/>.
- Showalter, K., F. Woeste, and B. Bendtsen (1987). *Effect of Length on Tensile Strength in Structural Lumber*. Research Report FPL-RP-482. Madison, USA: U.S. Department of Agriculture, Forest Service, Forest Products Laboratory.
- Taylor, S. and D. Bender (1988). “Simulating Correlated Lumber Properties Using a Modified Multivariate Normal Approach”. In: *Trans. ASAE* 31 (1), pp. 182–186. DOI: 10.13031/2013.30685.
- (1991). “Stochastic model for localized tensile strength and modulus of elasticity in lumber”. In: *Wood and Fiber Science* 23(4), pp. 501–519.

Discussion

The paper was presented by C Tapia

F Lam commented about non stationarity of material property along the length of the member which is aligned along the length of the tree. F Lam said that this was observed in MOE data for 5 m long members. C Tapia said that their specimens are short and not likely be an issue. F Lam asked about verification of the model. C Tapia said that the statistical parameters are checked. F Lam commented that there is a need to verify the model more fully with independent data sets.

T Ehrhart asked about the density variation. C Tapia said this have not been done and will check. T Ehrhart commented that the KAR R^2 is influenced by a single data point at the high range of the data.

BJ Yeh asked about potential damage accumulation from tensile testing same board multiple times. C Tapia said that the sequential test is always higher than past test on the same board even though damage accumulation could underestimate the real strength. S Aicher discussed the relative strength charts and said that in few cases where the second strength is close to the first strength some damage accumulation could be present.

S Franke said that MOE measurement with 30 kN load level was used while some boards failed at 40 kN. He questioned how accurate were the MOE measurements at these load levels. C Tapia showed information of about 1% error for MOE measurements.

P Stapel questioned about the gauge length used in the study and stated that the gauge length may influence the results. The information is needed on free length of the second and subsequent test. S Aicher said that information on the free length of sequential tests is irrelevant. This is because one is interested in the local strength and its relationship with MOE. H Blass commented that material grade may be different in the subsequent tests.

Deviations between planned and actual position of wood screws- consequences for minimum spacing

Matthias Frese, Markus Jordan

Karlsruhe Institute of Technology, Timber Structures and Building Construction

Keywords: screw connection, inclined screws, crossed screw couple, position tolerance, damages to wood screws

1 Introduction and technical background

1.1 Motivation and aim

The insertion of self-tapping (self-threading) or self-drilling wood screws is usually accompanied by minor or major deviations between the planned screw axis and the actual one. The actual positions can be seen as a result of an individual insertion process influenced by a complex interaction between multiple parameters. A concise representation of this issue is for example given by Trautz and Koj 2015. They stress amongst others the necessity of sufficient spacing between adjacent screws to avoid contact problems.

Occasionally, screw connections comparable to those in Fig. 1 have shown harmful contact between narrow placed screws although minimum spacing was observed in design and execution. The minimum spacing between the represented crossed screw couples is usually given as a multiple (k) of the nominal screw diameter (d).

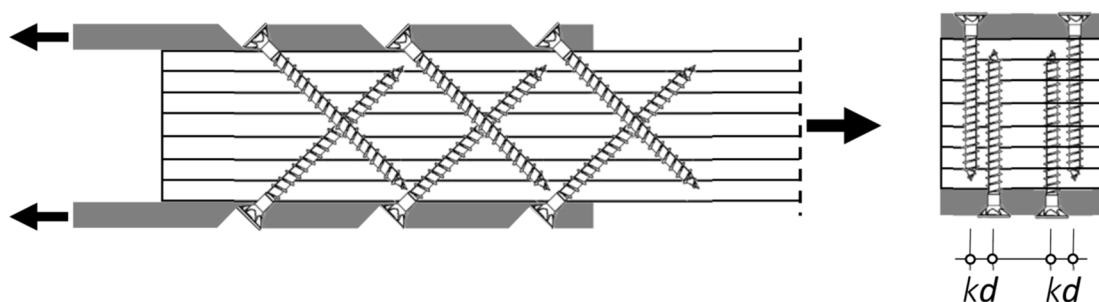


Figure 1. Crossed screw couples with hazard of contact in case of too narrow mutual spacing.

Several European technical assessments stipulate at least 1.5 for k . Eurocode 5 contains the general rules for minimum spacing rules being completed and extended by European technical assessments (ETAs).

Müller 2017 and Blaß 2017 recently reported contact problems with crossing screws. Furthermore, skilled carpenters, practitioners and designers have experienced such contact problems. Fig. 2 shows typical damages to screws of a crossed couple caused by contact. Even in reinforcement measures with long screws for shear and stresses perpendicular to the grain, critical deviations of the actual screw channel occur (Krüger 2010). Otherwise, reinforcing techniques based on controlled contact between screws and dowels require very accurate screw placements to ensure the intended load distribution between these components (e.g. Bejtka and Blaß 2005).

These aspects show the necessity to realistically estimate deviations between the planned and actual screw axis. For that purpose, about 350 insertion tests with wood screws were conducted and evaluated in a preliminary study (Jordan 2017). The aims of this study were 1. the identification of some crucial parameters influencing deviations, 2. the experimental determination of such deviations and 3. a proposal for a first tentative model predicting appropriate minimum spacing.

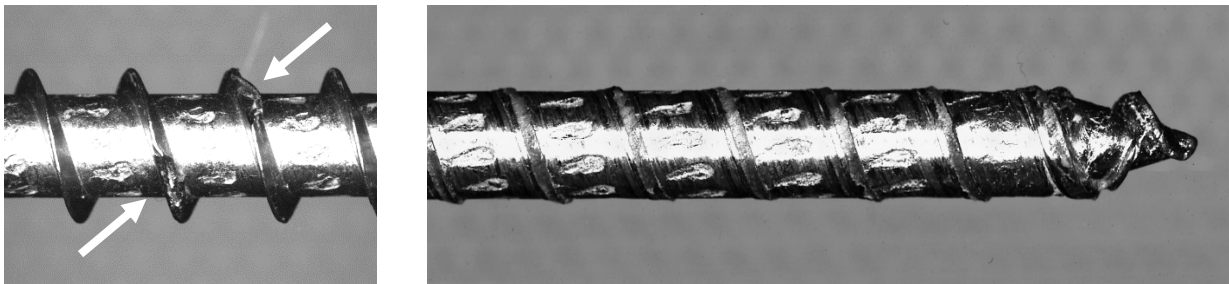


Figure 2. Damages to wood screws caused by mutual contact. Local damage to a firstly screwed-in screw (left) hit by a secondly screwed-in one (right) resulting in almost complete loss of the thread

1.2 Interaction between insertion and wood structure

Potential parameters influencing deviations between the planned and actual screw axis are amongst others (cf. Trautz and Koj 2015): the technical equipment, the way someone screws in, with/without pre-drilling, use of short pilot holes, insertion angle between screw axis and wood surface (β), shape of the screw tip, straightness of the screw, angle between screw axis and grain direction (α), natural growth characteristics along the screw channel, glue lines, insertion length (ℓ), wood species, physical wood properties, screw stiffness or even unintended contact with other screws crossing the actual screw channel.

The glulam cube in Fig. 3 exemplifies that a planned screw axis can be described by a vector \vec{a} in the spatial wood structure. Hence, the connection between the screw axis and the glulam structure is defined by a given orientation of the cube in the coordinate system and the coordinates a_x , a_y and a_z defining the screw axis. Using this system, the examined placements of screws in glulam are described below.

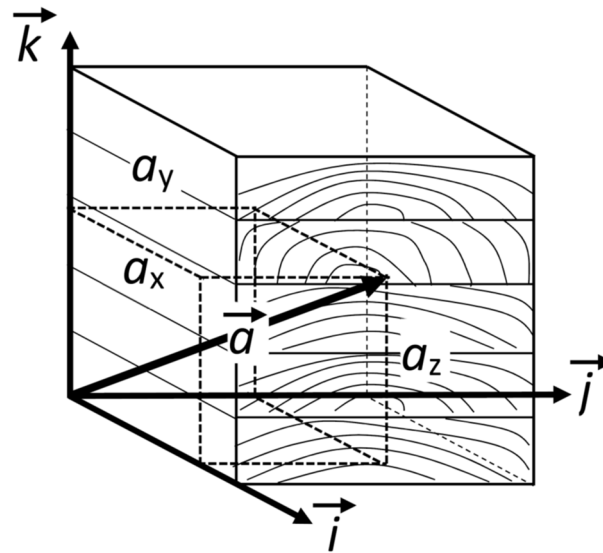


Figure 3. Direction of a planned screw axis by means of the vector \vec{a} .

2 Materials and methods

72 specimens for the insertion tests were made of spruce glulam GL24c. The specimens were realised from four glulam members, each 12 m in length, 180 mm in width and 200 mm in depth. The members consisted of five laminations. Where necessary, specimens were glued together to obtain sufficient dimensions for the intended insertion lengths. The density and the moisture content were measured by means of a cross-sectional slice at one third of the specimens. The results are compiled in Table 1. Table 2 contains the properties of the screws. Crucial variations refer to the screw length (to realise three different insertion lengths), the thread length and the tip shape. The nominal diameter was uniformly 8 mm.

Table 1. Density and moisture content of the glulam specimens.

Glulam property	N	Mean	SD	Min	Max
Density in kg/m ³	21	428	24	388	470
Moisture content in %	21	11.4	0.89	10.4	14.7

Table 2. Wood screws.

Drill tip	d mm	Screw length mm	Thread length mm	Insertion length mm	Tip shape
with	8	220	200	160	
		280	260	220	
		370	350	340	
without	8	220	100	160	
		260	100	220	
		380	100	340	

Four different screw placements (I, II, III and IV) were examined. The corresponding section planes, in which the planned screw axes lie, are visualised in Fig. 4. The vectors of the screw axes and the resulting angles (α) between screw axes and grain direction are quoted in Table 3. The screws were inserted by a single person using a hand-hold electric-powered screwdriver. The holes were neither pre-drilled nor pilot holes were provided. At the beginning of the insertion wedge-shaped screw guides equipped with grooves were used to ensure the intended insertion angle ($\beta = 45^\circ$ and 90°) between screw axis and surface as accurately as possible. Up to six screws were inserted in each specimen. Deviations between the planned exit points (E) and the actual ones were measured at the surface of the exit point. The coordinates $\Delta 1$ and $\Delta 2$ defined as orthogonal vectors originating from E were then computed by means of vector calculations. Fig. 4 in total represents the connection between the planned exit points, the actual ones and the positive directions of the computed coordinates $\Delta 1$ and $\Delta 2$.

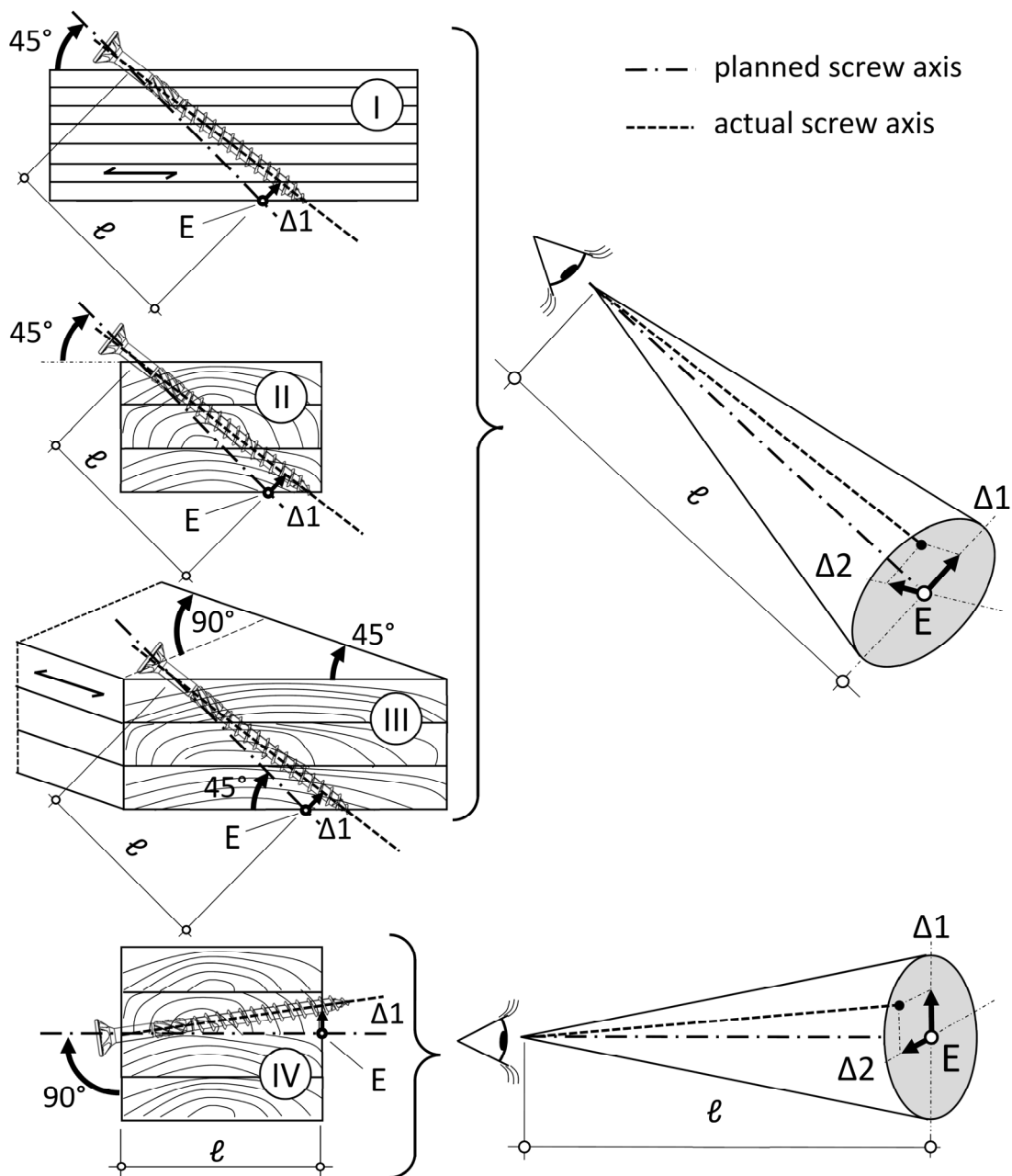


Figure 4. Examined placements

Table 3. Coordinates of the examined vectors \vec{a} .

Placement	a_x	a_y	a_z	\vec{a}	α	β	placement in the..
I	1	0	1	(1,0,1)	45°	45°	longitudinal section
I	1	1	0	(1,1,0)	45°	45°	longitudinal section
II	0	1	1	(0,1,1)	90°	45°	cross-section
III	0.71*	0.71*	1	(0.71,0.71,1)	60°	45°	diagonal section
IV	0	1	0	(0,1,1)	90°	90°	cross-section/glue line

*= $\sqrt{1/2}$

3 Results

3.1 Deviations $\Delta 1$ and $\Delta 2$

Fig. 6 shows the results for the placement imperfections I-IV. The four pairs of diagrams contain the deviations $\Delta 1$ and $\Delta 2$ differentiated by insertion length (top) and tip shape (bottom). Amongst others, these observations were made:

- **Placement I:** $\Delta 1$ is almost exclusively positive (Fig. 6-I); $\Delta 2$ is obviously higher for screws with drill tips compared to $\Delta 2$ for those without drill tips (Fig. 6-I bottom). Independent of the insertion length and tip shape, $\Delta 2$ is more or less symmetrically distributed around the vertical axis with $\Delta 2 = 0$.
- **Placement II:** $\Delta 1$ is almost exclusively positive except for the insertion length of 340 mm (Fig. 6-II top). The screws inserted with 340 mm having negative $\Delta 1$ values are equipped with a drill tip. Independent of the insertion length and tip shape, $\Delta 2$ is more or less symmetrically distributed around the vertical axis with $\Delta 2 = 0$.
- **Placement III:** $\Delta 1$ is exclusively positive; however, screws inserted with 220 mm exhibit also almost exclusively positive $\Delta 2$ values (Fig. 6-III top). The distribution of $\Delta 2$ is symmetrical.
- **Placement IV:** The scatter of $\Delta 1$ is larger than the one of $\Delta 2$ (Fig. 6-IV top). Independent of the insertion length and tip shape, both deviations are symmetrically distributed around their corresponding axes with $\Delta = 0$. Only three screws kept their screw channel exactly in the glue line.

3.2 Absolute deviation and cone model

Using equation (1) the absolute deviation denoted as radius r was computed. The radius r and the corresponding insertion length yield a deviation angle ε , see equation (2). Fig. 7 shows all relations between the radius r and the insertion lengths. The maximum of $\tan \varepsilon$ ($\max \tan \varepsilon$) is quoted in Table 4 for the four placements and the corresponding insertion lengths.

$$r = \sqrt{\Delta 1^2 + \Delta 2^2} \quad (1)$$

$$\tan \varepsilon = r / \ell \quad (2)$$

Table 4. Statistics of the absolute deviation.

Placement	Insertion length mm	N	$r = \sqrt{\Delta 1^2 + \Delta 2^2}$			max $\tan \varepsilon$
			Mean mm	CV %	Max mm	
I	160	41	8.02	33	13.5	0.084
	220	48	10.4	36	22.2	0.101
	340	37	23.8	32	37.1	0.109
II	160	37	5.24	31	8.82	0.055
	220	31	9.17	31	14.6	0.066
	340	30	10.3	50	20.7	0.061
III	160	19	10.7	41	19.3	0.121
	220	20	9.89	33	19.6	0.089
	340	21	13.5	40	26.1	0.077
IV	160	23	5.38	37	8.06	0.050
	220	20	6.09	38	11.4	0.052
	340	21	11.6	45	26.1	0.077
Total: 348 insertion tests						

The placements I/III and II/IV are grouped because of comparable placement conditions and similar magnitude of deviations. In doing so, the maximum angles given by $\tan \varepsilon$ are 0.121 and 0.077 for the placement groups I/III and II/IV, respectively.

Fig. 5 shows a general cone model. This model would basically be suitable to estimate the cone shaped clear space around a planned screw axis a screw¹ needs to be inserted without having contact with other screws. Based on the presently available data the space should be calculated with $\tan \varepsilon$ of about 0.12 (≈ 0.121) and 0.08 (> 0.077) for the groups I/III and II/IV, respectively. These proposed values for the tangent do not contradict deviations published by Trautz and Koj 2015.

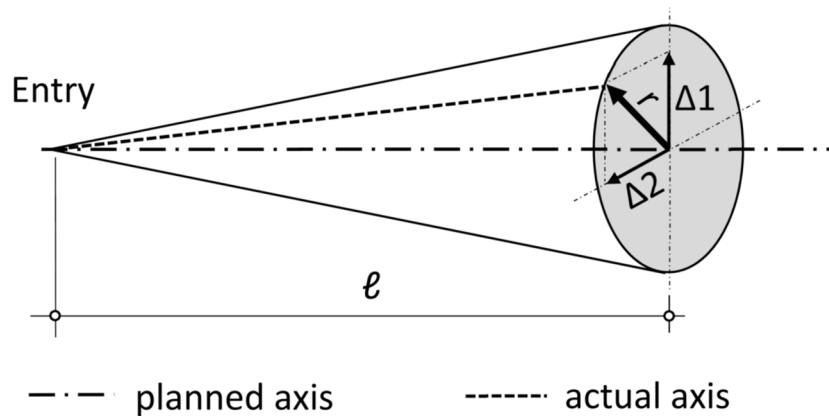


Figure 5. Visualised cone model.

¹ Nominal diameter here assumed as 0

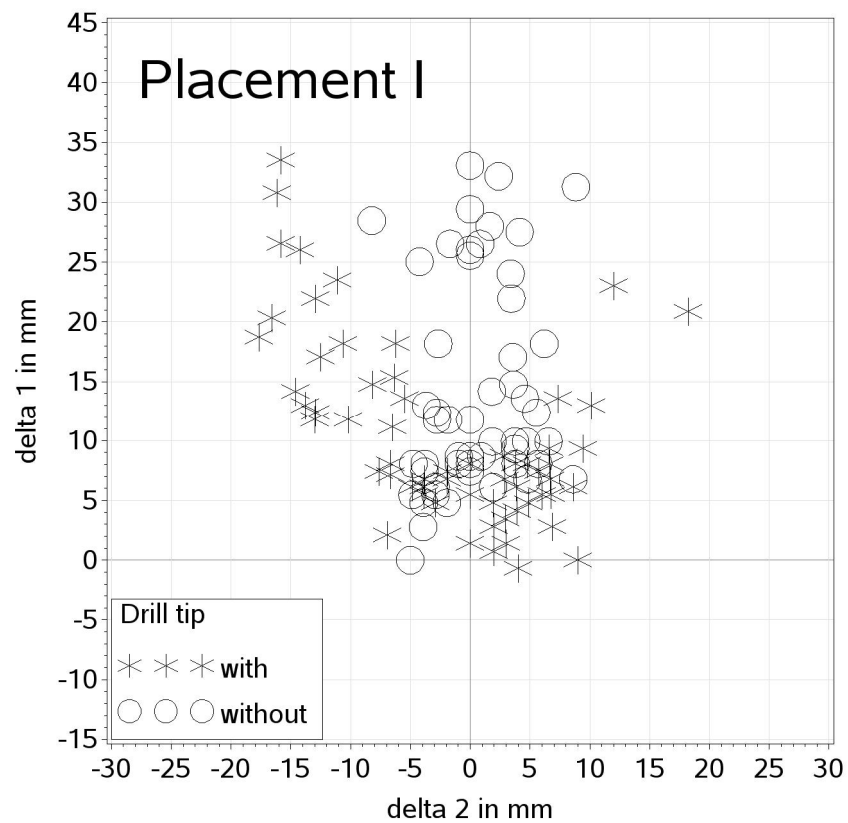
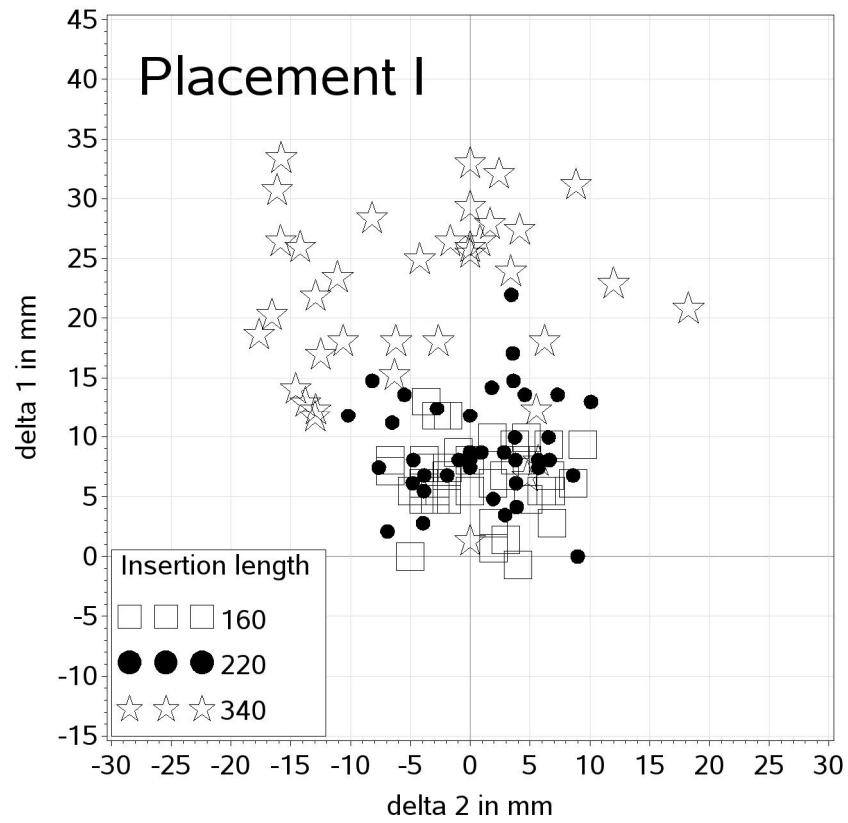


Figure 6-I. Placement I.

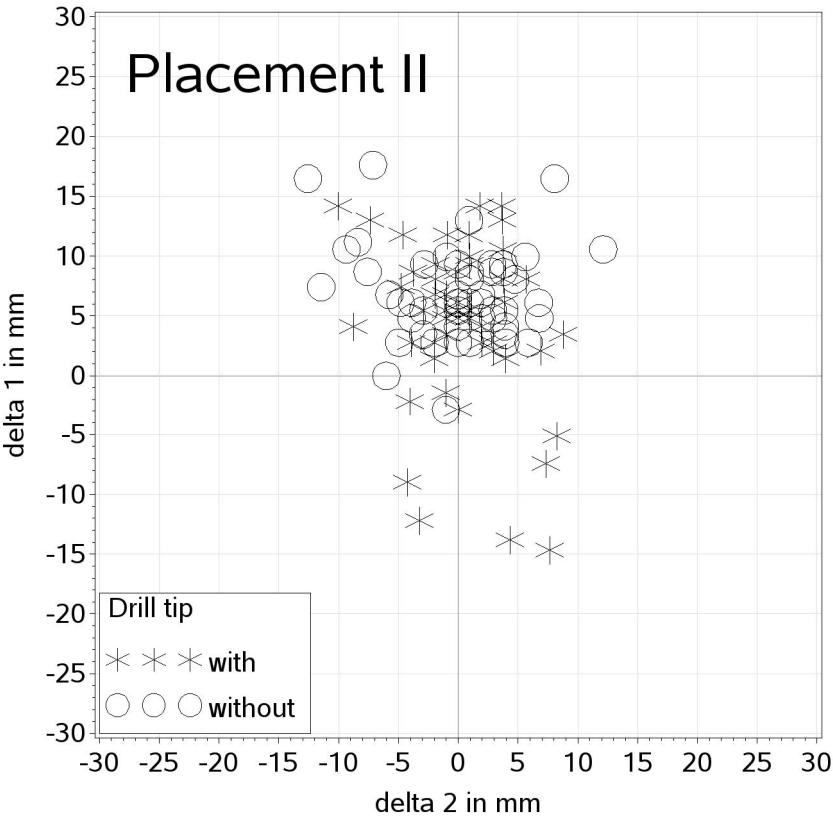
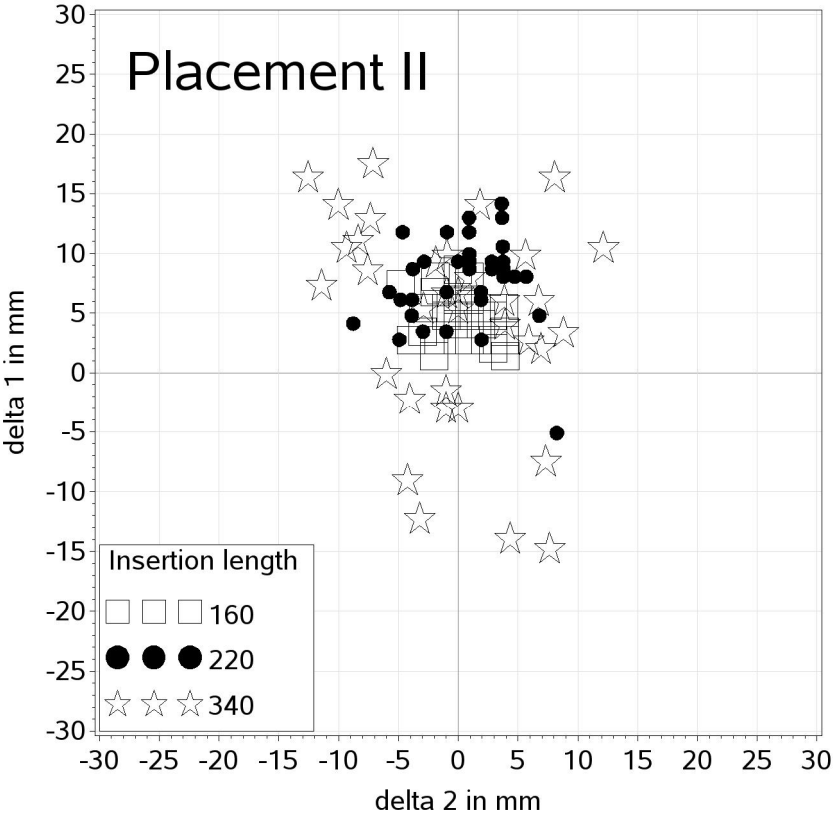


Figure 6-II. Placement II.

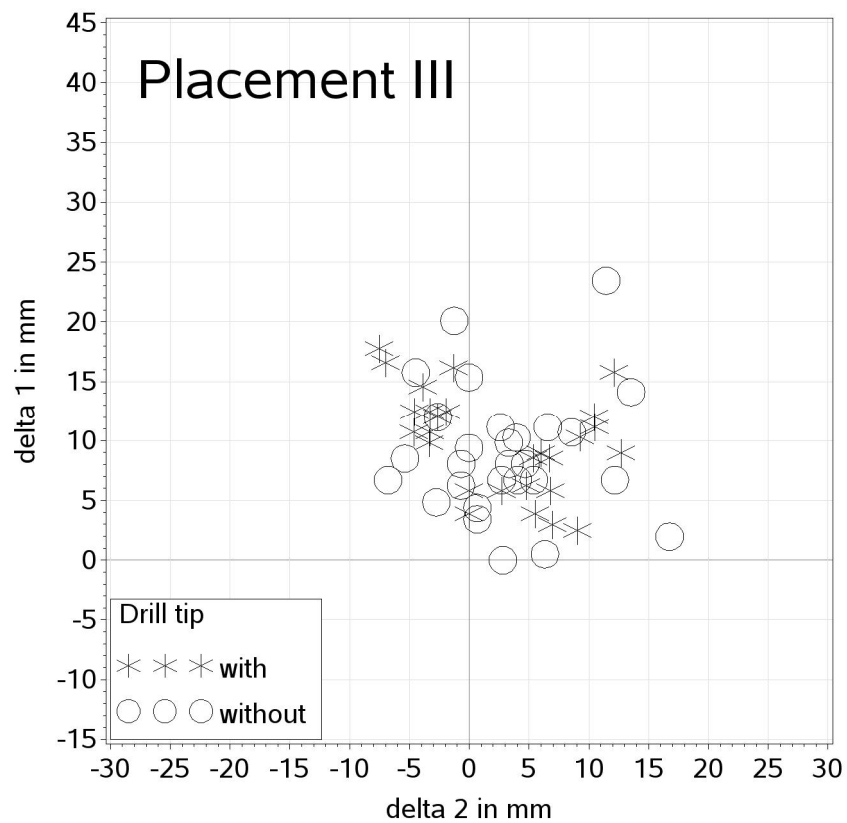
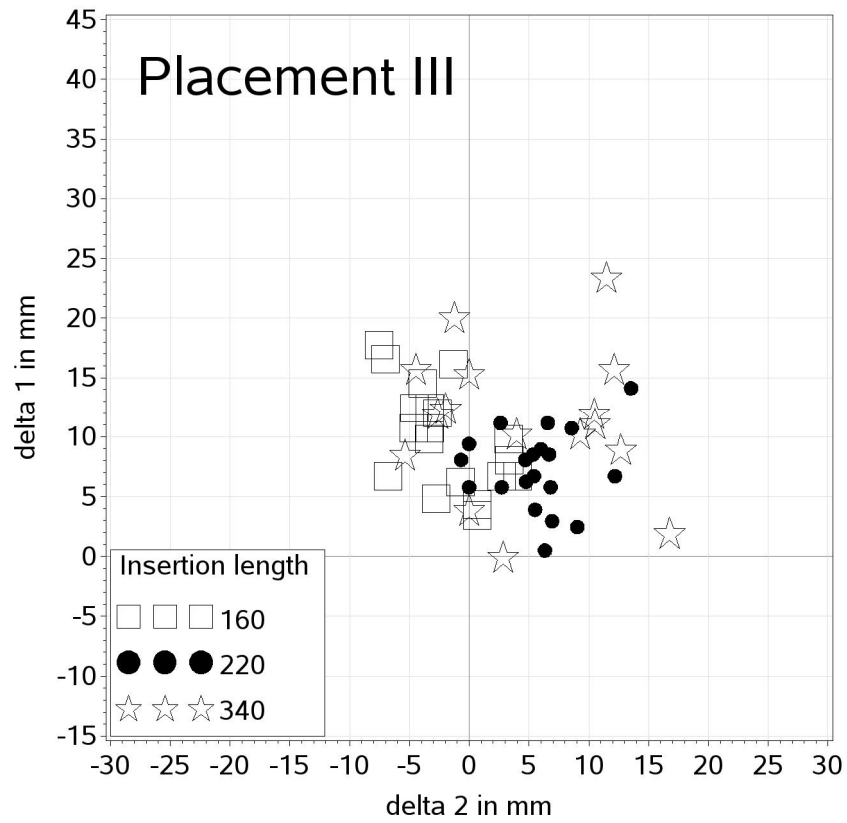


Figure 6-III. Placement III.

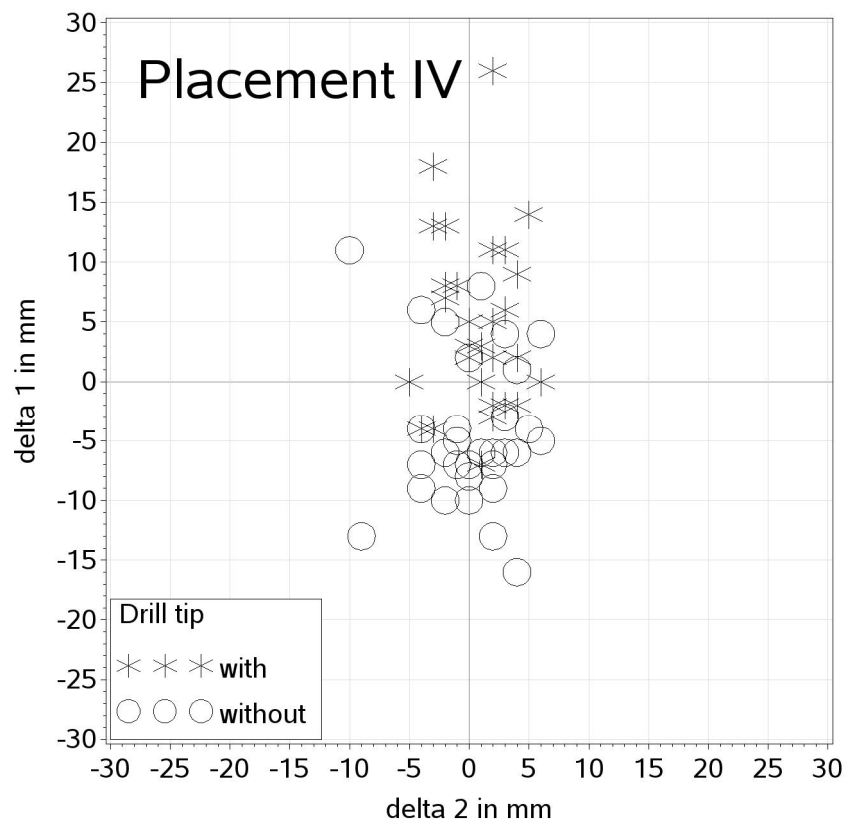
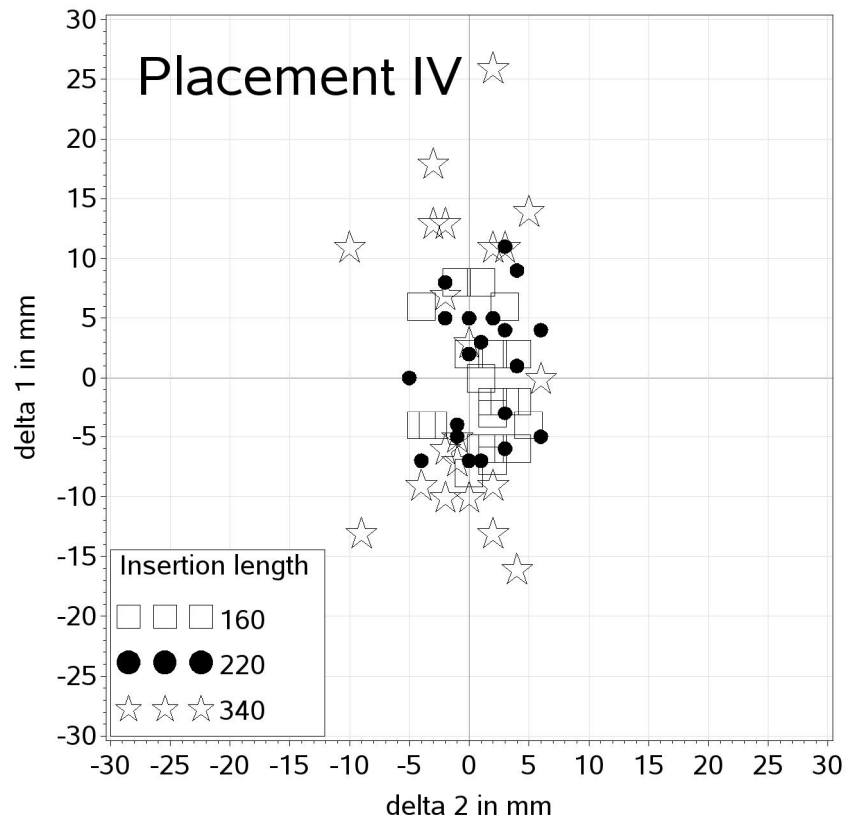


Figure 6-IV. Placement IV.

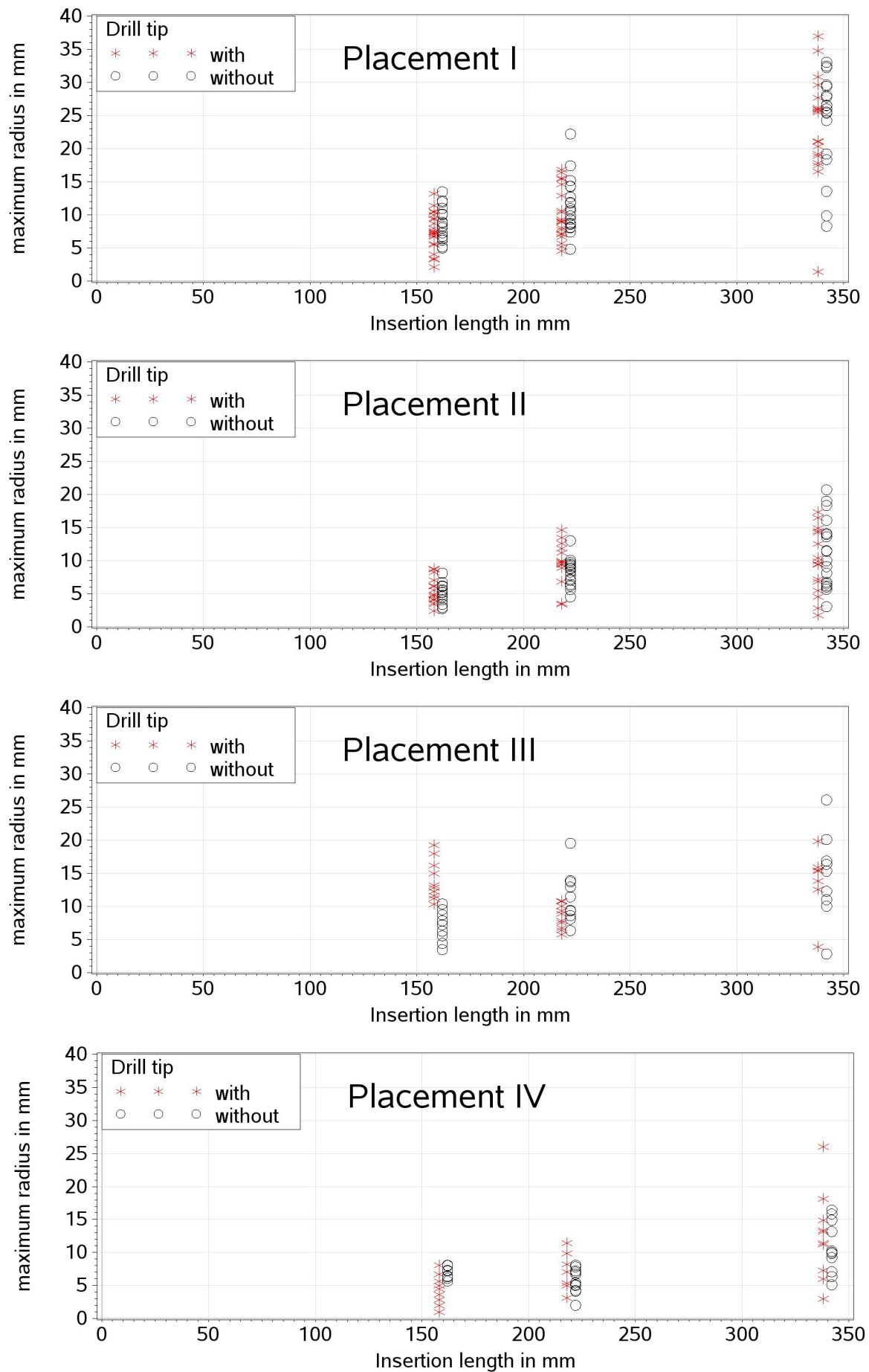


Figure 7. Maximum radius over insertion length.

3.3 Proposal for minimum screw spacing considering stochastic effects

The statistics in Table 5 show that significant differences exist between the upper percentiles of $\tan \varepsilon$ belonging to the corresponding placement groups.

Table 5. Statistics and upper percentiles of $\tan \varepsilon$.

Placement group	N	Mean	SD	95 %	99 %	Max
I/III	176	0.0542	0.0218	0.0950	0.112	0.121
II/IV	172	0.0339	0.0131	0.0543	0.0665	0.0767

Stochastic effects for group I/III and II/IV (values in brackets) are considered using the 95th percentile. Consequently, the exceedance probability of $\tan \varepsilon = 0.0950$ (0.0543) is less than 5 %. Hence, the probability that the unintended tangent of two independent adjacent screws exhibits 0.1 (0.06) is less than 0.25 %. Fig. 8 exemplifies that the actual probability of contact between two screws in the critical area is far lower than 0.25 % due to the circular distribution² of possible locations after a corresponding large insertion length ℓ_{crit} .

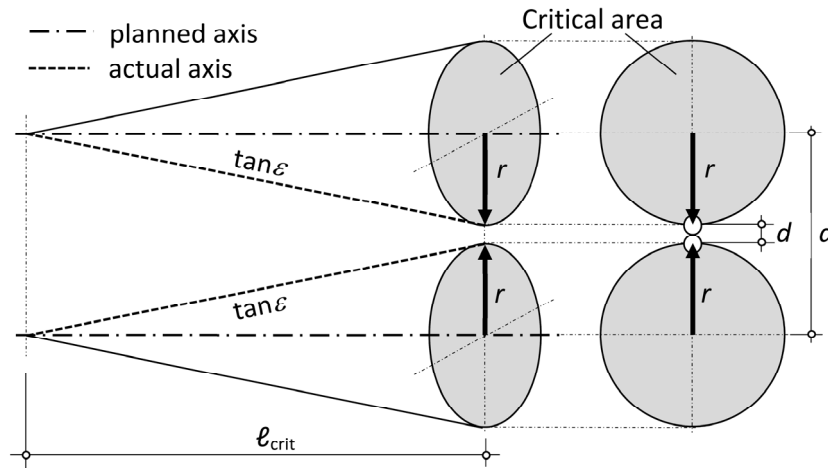


Figure 8. Spacing a between two planned screw axes based on $\tan \varepsilon$, ℓ_{crit} and d .

Equation (3) reflects these considerations. Inserting $\tan \varepsilon = 0.1$ and 0.06 for group I/III and II/IV, respectively, yield the mutual spacing a between two adjacent screws in a critical area.

$$a = 2\ell_{\text{crit}} \cdot \tan \varepsilon + d \quad (3)$$

Favourable effects of almost only positive $\Delta 1$ values in group I/III are not yet considered in equation (3), compare Fig. 6-I and 6-III. Furthermore, independence of adjacent screws is a strongly simplifying assumption owing to similar wood properties in the critical area and similar insertion geometry in case of parallel oriented adjacent screws.

² Uniform circular distribution of locations assumed for simplicity reasons

4 Conclusions and consequences

Based on insertion tests with 8 mm self-tapping and self-drilling wood screws in spruce glulam these conclusions are drawn:

- Deviations between the actual and planned screw axis depend on the insertion geometry. In unfavourable cases the magnitude amounts to 12 % related to the insertion length. This maximum is covered by tests without pre-drilling and with a maximum insertion length of 340 mm.
- If the intended angle between screw axis and grain direction is considerably less than 90°, the actual screw axis tends to follow the grain direction.
- The mainly positive $\Delta 1$ deviations in placement I and particularly in placement II and III are likely also caused by insertion angles systematically less than the intended 45°. The reason for this systematic inaccuracy is supposed to lie in the insertion procedure using the wedge-shaped screw guides (cf. Trautz et al. 2007, p. 67).
- If the entry point of the screw tip coincides with the glue line, it seems to be unlikely that the axis of screws remains in the glue line. This may be explained by the tendency of a screw to proceed in the lamination with lower density.
- Considering placement imperfections the necessary space for a single screw is cone-shaped. A cone model is therefore proposed in order to determine minimum screw spacing. Due to limited experimental data, the formulation of the model is in a tentative stage.

So far, consequences for screw spacing requirements are:

- Using the proposed cone model minimum screw spacing can be estimated such that harmful contact between adjacent screws is avoided. The model applies to four common insertion geometries. So far, its application is restricted to 8 mm wood screws, to spruce glulam and to an insertion length of approximately 400 mm.
- Screw spacing requirements should be discussed against the background of unintended deviations and harmful contact.
- Requirements in Eurocode 5 and technical assessments should at least be checked, amended where necessary or a general note should be made in provisions that deviations have to be taken into account.
- The results of the study are being used for a research proposal covering open questions. Several issues to be examined concern the use of screw guides and their influence on the actual screw axis, wood species, connection principles, insertion lengths exceeding 340 mm, the influence of the screw diameter and other than the examined insertion geometries.

5 References

- Trautz M, Koj C (2015): Laser-drilled guide holes for self-tapping screws - Installation and load bearing behaviour. Bautechnik 92, 403-411
- Trautz M et al. (2007): Mit Schrauben bewehren - Selbstbohrende Vollgewinde-schrauben als Verstärkung in Brettschichtholzträgern und zur Ausbildung von hochleistungsfähigen Verbindungen. Forschungsbericht 01/2007, Lehrstuhl für Tragkonstruktionen, RWTH Aachen
- EN 1995-1-1:2004 Eurocode 5: Design of timber structures – Part 1-1: General – Common rules and rules for buildings
- Müller V (2017): [...] Untersuchungen zu Fachwerkträgern mit [...] Zugdiagonalen aus BauBuche. Bachelorarbeit, KIT Holzbau und Baukonstruktionen (unpublished)
- Blaß HJ (2017): Selbstbohrende Schrauben und Systemverbinder - Stand der Technik und Herausforderungen. 23. Internationales Holzbau-Forum IHF
- Blaß HJ, Krüger O (2010): Schubverstärkung von Holz mit Holzschrauben und Gewindestangen. Bd. 15 Karlsruher Berichte zum Ingenieurholzbau, KIT Scientific Publishing
- Bejtka I, Blaß HJ (2015): Self-tapping screws as reinforcements in connections with dowel-type fasteners. CIB-W18/38-7-4
- Jordan M (2017): Entwicklung und Erprobung eines Untersuchungsverfahrens zur Ermittlung von Lagetoleranzen selbstbohrender Holzschrauben. Bachelorarbeit, KIT Holzbau und Baukonstruktionen (unpublished)

Discussion

The paper was presented by M Frese

A Smith asked if it is too conservative to assume the screws always bend towards each other. M Frese agreed that the cone model is conservative and commented about Modes 2 and 3 where annual rings are curved.

P Dietsch commented about the predrill rod case with the assumption of the tendency of the rods go towards the fibre direction. Their experience indicates the drill followed the path of lesser stiffness direction which is opposite to the fibre direction. He suggested future work to consider the predrill case.

E Serrano discussed the tendency of screws to follow the grain direction. He asked if this is evident in results of placement 1. M Frese provided more detailed information of the interpretation of placement 1 case and further confirmed such tendency in placement 3 cases.

S Aicher asked about the outliers as to whether they are affected by large knots. He recommended also to look at influence beside grain direction. M Frese agreed and showed a scan that indicates knots have an effect.

R Jockwer asked whether the screw installers were skilled carpenter. M Frese responded that they were unskilled at the beginning of the study but became very skilled quickly.

R Jockwer asked about unsymmetrical screw tips and whether different types of screw tips were tried. M Frese said that they only tried two types of screw in this paper but would like to extend the work to considered different types of screw and screw tips.

L-M Ottenhaus commented about issues related to drilling through CLT where the screw direction can deviate as it travels into the cross layer.

Analytical Method to Derive Overstrength of Dowel-Type Connections

Lisa-Mareike Ottenhaus, University of Canterbury, New Zealand

Minghao Li, University of Canterbury, New Zealand

Tobias Smith, PTL | Structural Consultants Ltd, New Zealand

Keywords:

Overstrength, dowel-type connections

1 Introduction

Currently, limited values are available for overstrength factors of timber connections in design standards. In capacity design of timber structures, the potential for connection overstrength needs to be taken into account to ensure ductile response of the system under seismic loading. However, overly conservative overstrength factors can lead to uneconomic design and increase building cost unnecessarily.

In the past, the overstrength factor, γ_{Rd} , has often been derived for a whole connection or structural system, although several authors have also identified individual overstrength components (Gavric et al. 2015, Vogt et al. 2014, Dickof et al. 2014, Brühl et al. 2014). Figure 1 shows the desired strength hierarchy and overstrength components modified from Jorissen and Fragiaco (2011):

$$\gamma_{Rd} * F_{Rd} = \gamma_M * \gamma_{an} * \gamma_{0.95} * F_{Rd} = \gamma_{an} * \gamma_{0.95} * F_{Rk} \leq F_{BRd} \quad (1)$$

where γ_M is the material safety factor, γ_{an} accounts for conservatism of analytical models, and $\gamma_{0.95}$ quantifies the difference between the 5th and 95th percentile of the strength distribution, ($F_{0.05}$ and $F_{0.95}$, respectively). F_{Rk} and F_{Rd} denote the connection's characteristic and design strength, and F_{BRd} is the design strength of the brittle member or connection failure mode. The individual components are calculated as:

$$\gamma_M = F_{Rk} / F_{Rd} \quad (2.1)$$

$$\gamma_{an} = F_{0.05} / F_{Rk} \quad (2.2)$$

$$\gamma_{0.95} = F_{0.95} / F_{0.05} \quad (2.2)$$

This paper presents a detailed procedure on how to analytically derive and quantify these individual overstrength components for dowel-type connections in the context of Eurocode 5.

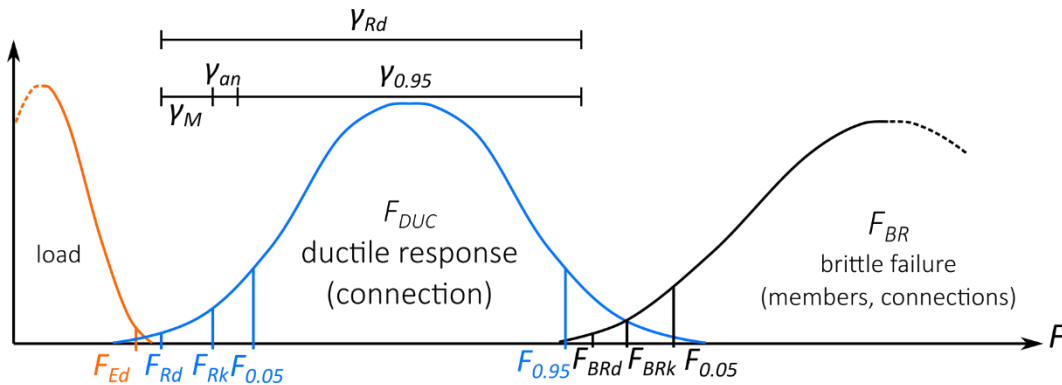


Figure 1. Overstrength concept (modified from Jorissen and Fragiaco 2011)

2 Overstrength components

The break-down of overstrength components is shown in Figure 2 and explained in the following paragraphs. The European Yield Model (EYM, based on the Johansen's Equations) presented in Eurocode 5 is based on timber material embedment strength, f_h , which is correlated to timber density, ρ , and the fastener yield moment, M_y , which in turn depends on the steel yield strength, f_y . Each overstrength component can thus be subdivided into a contribution from the timber and steel material.

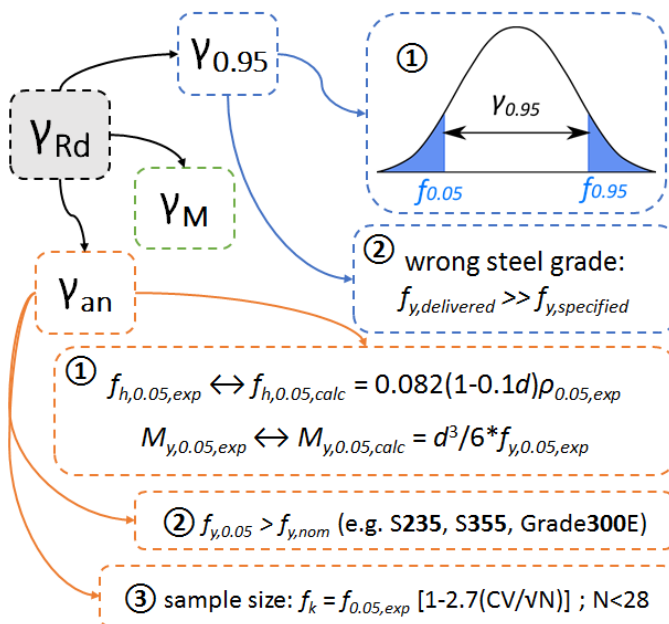


Figure 2. Overstrength components.

2.1 Material safety factor γ_M

The material safety factor, γ_M , is given as 1.30 in Eurocode 5 and therefore known to the designer.

2.2 Analytical model overstrength γ_{an}

Analytical model overstrength, γ_{an} , stems from the difference between the 5th percentile of material strength, $f_{0.05}$, and the calculated characteristic value, f_k . Generally speaking, analytical model overstrength is introduced by conservatism in semi-empirical formulas as shown in Figure 3. $F_{0.05}$ and F_{Rk} can be calculated by inserting the respective embedment strength values ($f_{h,0.05}$ and $f_{h,k}$) and yield moment values ($M_{y,0.05}$ and $M_{y,k}$) into the EYM.

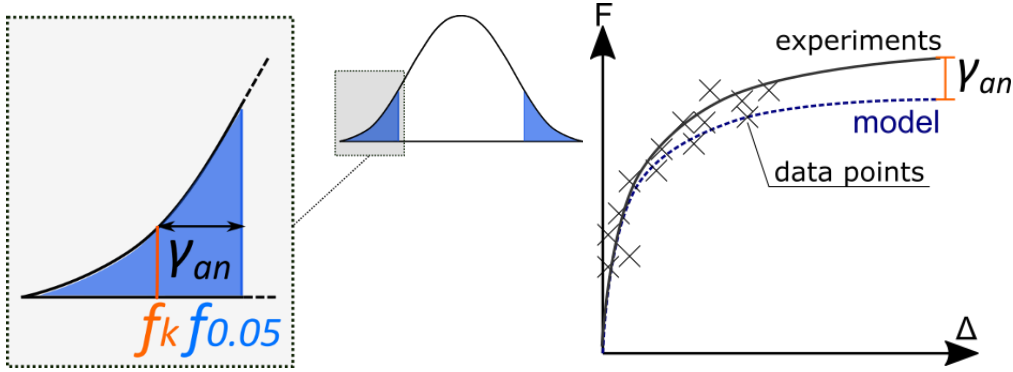


Figure 3. Analytical model overstrength.

2.2.1 Difference between semi-empirical model and data $\gamma_{an,1}$

Semi-empirical models are usually established by conservatively calibrating an analytical model to a dataset. As discussed in Ottenhaus et al. 2017, due to this calibration method the difference between calculated and experimental embedment strength is rather small which leads to small overstrength factors $\gamma_{an,fh}$:

$$\gamma_{an,fh} = F(f_{h,0.05,exp}) / F(f_{h,0.05}(\rho_{0.05,exp})) \approx 1.06 \quad (3)$$

$F(f_{h,0.05,exp})$ is obtained by inserting the experimentally established 5th percentile of embedment strength, $f_{h,0.05}$, into the EYM equations.

$F(f_{h,0.05}(\rho_{0.05,exp}))$ is obtained if the 5th percentile of the measured density, $\rho_{0.05,exp}$, is used to calculate the embedment strength $f_{h,0.05} = 0.082(1-0.1d)\rho_{0.05,exp}$ (Eurocode 5).

As discussed in Ottenhaus et al. 2016, little overstrength is introduced by the difference between $M_{y,exp}$ and $M_{y,calc}$:

$$\gamma_{an,My} \approx 1.0. \quad (4)$$

The total analytical overstrength factor, $\gamma_{an,1}$, is calculated as $\gamma_{an,1} = \gamma_{an,fh} * \gamma_{an,My}$.

2.2.2 Nominal values of steel grades $\gamma_{an,2}$

Karmazínová and Melcher (2012) conducted experiments on grade S235 and S355 steel (grades according to Eurocode 3). Their results for the mean value for yield strength, $f_{y,mean}$, coefficient of variation, CV, as well as sample size, N, are given in Table 1. Based on their findings, it is possible to calculate the 5th percentile, $f_{y,0.05}$, for a log-normal distribution with $f_{y,0.05} = f_{y,mean} * e^{-k*CV}$, where k depends on the sample size,

N, confidence interval (75%) and percentile (5th percentile). Table 1 shows that the 5th percentile of steel yield strength, $f_{y,0.05}$, was higher than the nominal strength, $f_{y,nom}$, which is used instead of a characteristic value and indicated by the grade's name (e.g. S235 with $f_{y,nom} = 235\text{MPa}$). This difference introduces overstrength:

$$\gamma_{an,2} = \gamma_{an,fy,nom} = F(f_{y,0.05}) / F(f_{y,nom}) \quad (5)$$

Furthermore, a New Zealand steel supplier made their tensile test data available for New Zealand steel grades Grade300 and Grade500 (AS/NZS 4671:2001), providing N, $f_{y,mean}$, $f_{y,0.05}$, and $f_{y,0.95}$.

Table 1. Overstrength from steel yield strength distribution (Karmazínová and Melcher 2012).

	$f_{y,nom}$ [MPa]	$f_{y,mean}$ [MPa]	CV	N	k	$f_{y,0.05}$ [MPa]	$\gamma_{an,fy,nom}^{(4)}$
S235	235	327 ⁽¹⁾	0.075 ⁽¹⁾	26 ⁽¹⁾	1.890 ⁽²⁾	284	1.10
S355	355	452 ⁽¹⁾	0.05 ⁽¹⁾	19 ⁽¹⁾	1.942 ⁽²⁾	410	1.08
Grade300	300	339		320		320	1.03
Grade500	500	554		230		523	1.02

⁽¹⁾ Karmazínová and Melcher (2012), ⁽²⁾ Guttman (1970), ⁽³⁾ tensile test data provided by Pacific Steel, ⁽⁴⁾ holds for $\rho \in [300,600] \text{ kg/m}^3$, $d \in [6,30] \text{ mm}$, $t/d \in [2,10]$

2.2.3 Sample size $\gamma_{an,3}$

The accuracy of a model is limited by the sample size and variability of the underlying dataset. Therefore, the characteristic strength value needs to take the sample size, N, and coefficient of variation, CV, of a dataset into account: $f_k = f_{mean} (1 - k \text{ CV})$. k is thus dependent on N, and $k = 1.645$ only holds for a normal distribution with $N \rightarrow \infty$.

Generally speaking, a dataset should consist of at least 28 samples in order to derive a characteristic value or 5th percentile with 75% confidence. However, this may not always be feasible or possible. For small sample sizes Leicester (1986) proposes:

$$F_k = F_{0.05,exp} [1 - 2.7(\text{CV}/\sqrt{N})]; \text{ for } 10 \leq N < 28 \quad (6.1)$$

$$F_k = F_{min} (N/27)^{\text{CV}} \text{ for } N < 10 \quad (6.2)$$

where $f_{0.05,exp}$ is estimated from the data (e.g. with linear interpolation and nearest rank method), and f_{min} is the minimum value of the sample. As Equation (6.1) delivers reasonably accurate results (Smith and Foliente 2002), an estimated overstrength can be computed for $10 \leq N < 28$ as

$$\gamma_{an,3} = \gamma_{an,sample} = F_{0.05,exp} / F_k = 1 / [1 - 2.7(\text{CV}/\sqrt{N})] \quad (7)$$

For sample sizes $N < 10$, γ_{an} should only be treated as a rough estimate.

2.3 Material Overstrength $\gamma_{0.95}$

This overstrength component is caused by the variability of material properties which can be expressed as the difference of the 95th and 5th percentile of the strength distribution ($f_{h,0.95}$ and $f_{h,0.05}$, respectively) as shown in Figure 4. However, it is also sometimes the case that steel suppliers deliver a stronger grade than specified, thinking that they act in the best interest of the client (Sandhaas and v. d. Kuilen 2017, Ottenhaus et al. 2018). This can lead to undesirable failure modes and impair seismic safety.

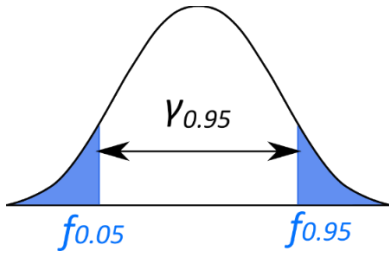


Figure 4. Material overstrength.

2.3.1 Difference between $F_{0.95}$ and $F_{0.05}$ ($\gamma_{0.95,1}$)

This overstrength component can be easily calculated if the mean value and coefficient of variation of the strength distribution are known. In many cases, the timber supplier can either provide data of the timber density distribution, or the material is stress-graded in which case the expected density range is defined by the strength grade given in the respective standard, e.g. EN338:2016.

For a given density distribution, the overstrength, $\gamma_{0.95,fh}$, can be calculated by inserting $\rho_{0.05}$ and $\rho_{0.95}$ into the embedment formula applicable for the timber material, and inserting the obtained values for f_h into the EYM:

$$\gamma_{0.95,fh} = F(f_{h,0.95}) / F(f_{h,0.05}) \quad (8)$$

As shown in Table 2, $\gamma_{0.95}$ decreases if the material is stress-graded or if the material is relatively homogenous as is the case with Laminated Veneer Lumber (LVL). This should encourage designers and suppliers to use stress-graded timber material with less variability.

Table 2. Overstrength from timber density distribution.

	$\rho_{0.05}$ [kg/m ³]	$\rho_{0.95}$ [kg/m ³]	$\gamma_{0.95,fh}^*$
NZ ungraded <i>radiata pine</i> ⁽¹⁾	402	608	1.51
LVL10 ⁽²⁾	470	558	1.19
LVL11 ⁽²⁾	480	564	1.18
LVL13 ⁽²⁾	500	585	1.17
C18 ⁽³⁾	320	440	1.38
C24 ⁽³⁾	350	490	1.40

⁽¹⁾ provided by XLam Ltd, ⁽²⁾ provided by Nelson Pine Industries Ltd grades according to AS/NZS 4357.0:2005,

⁽³⁾ EN336:2016 with assumed standard distribution * holds for $d \in [6,30]$ mm, $t/d \in [2,10]$

Although steel has relatively consistent material properties, there is still a certain variability in the yield strength distribution. An allowable range for f_y is given in AS/NZS 4671:2001 but not in Eurocode 3. For instance for Grade300 steel, the allowable range of 300-380 MPa leads to an overstrength factor of $\gamma_{0.95,fy} = 1.13$ (Ottenhaus et al. 2017). Additionally, experimental results were available for grade S235 and S355 (Karmazínová and Melcher 2012) and supplier tensile test data was provided for Grade300 and Grade500. The overstrength factor, $\gamma_{0.95,fy}$, was obtained with Equation (9) by inserting $f_{y,0.05}$ and $f_{y,0.95}$ into Equations 8.9 through 8.13 of Eurocode 5 Part 1-1:

$$\gamma_{0.95,fy} = F(f_{y,0.95}) / F(f_{y,0.05}) \quad (9)$$

The total material overstrength factor, $\gamma_{0.95,1}$, is calculated as $\gamma_{0.95,1} = \gamma_{0.95,fh} * \gamma_{0.95,fy}$.

Table 3. Overstrength from steel yield strength distribution and allowable range.

	$f_{y,0.05}$ [MPa]	$f_{y,0.95}$ [MPa]	$\gamma_{0.95,fy}^*$
S235 ⁽¹⁾	284	377	1.15
S355 ⁽¹⁾	410	498	1.10
Grade300 ⁽²⁾	320	358	1.06
Grade500 ⁽²⁾	523	584	1.06
Grade300 ⁽³⁾	300	380	1.13
Grade500 ⁽³⁾	500	600	1.10

* holds for $\rho \in [300,600]$ kg/m³, $d \in [6,30]$ mm, $t/d \in [2,10]$, ⁽¹⁾Karmazínová and Melcher 2012, ⁽²⁾tensile test data provided by Pacific Steel, ⁽³⁾allowable range AS/NZS 4671:2001

2.3.2 Unexpected overstrength due to delivery of stronger grade ($\gamma_{0.95,2}$)

Unexpected overstrength is introduced if the supplied steel grade is significantly stronger than the specified grade. Often, suppliers think that they are acting in the best interest of the client, as the material is stronger and thus “better”. In the case of recently conducted connection tests at the University of Canterbury, Grade500 steel dowels instead of Grade300 dowels (grades according to AS/NZS 4671:2011) were delivered which introduced additional overstrength of up to 1.50 (Ottenhaus et al. 2018). This issue was discovered during three-point bending and tensile yield tests. In practice, in-situ material testing is uncommon and hence this sort of mistake often goes unnoticed which likely leads to unsafe seismic design. Therefore, this issue needs to be addressed with suppliers, and if necessary material samples need to be strength tested.

As several timber material properties such as bending and embedment strength are correlated with density, delivery of a higher timber densities also causes unexpected overstrength and needs to be avoided. Shear strength and tensile splitting strength on the other hand are independent of the density of commonly used softwoods and brittle capacity remains unchanged for higher timber densities (Ranta-Maunus 2007).

3 Methodology to analytically derive overstrength

In order to design timber structures with Eurocode 5, designers need to know the characteristic material values. If the timber material is stress-graded, the characteristic timber density, ρ_k , is defined by the strength class and the nominal steel yield strength, $f_{y,nom}$, is defined by the steel grade (e.g. S235, S335, Grade300, Grade500). The connections can then be designed to withstand all load cases (including seismic loading) using the EYM as given in Eurocode 5 (Figure 5):

$$F_{Ed} \leq F_{Rd} = F_{Rk} / \gamma_M \quad (10)$$

where F_{Ed} designates the design demand, F_{Rd} is the connection's ductile design strength calculated with the EYM, γ_M is the material safety factor, and F_{Rk} is the connection's characteristic strength using ρ_k and $f_{y,nom}$.

The next step is to ensure that ductility can be achieved in the connection by protecting all brittle members and brittle connection failure modes from the connection's overstrength γ_{Rd} using Equation 1: $\gamma_{Rd} * F_{Rd} = \gamma_{an} * \gamma_{0.95} * F_{Rk} \leq F_{BR,d}$

The overstrength components can be calculated as follows:

- 1) Determine the 5th and 95th percentile of the density and yield strength distribution ($\rho_{0.05}$, $\rho_{0.95}$, $f_{y,0.05}$, and $f_{y,0.95}$). These can be obtained from the timber and steel supplier. Alternatively, acceptable limits for these values may be derived from the strength class definitions.
- 2) Calculate the yield moment and embedment strength $M_{y,0.95}$, $M_{y,0.05}$, $f_{h,0.95}$, $f_{h,0.05}$ for the given dowel diameter d . M_y should be calculated as $M_y = d^3/6 * f_y$ to avoid introducing analytical overstrength (Ottenhaus et al. 2017).
- 3) From the design, the governing EYM mode is known for F_{Rk} . Now calculate $F_{0.95}$ and $F_{0.05}$ for this mode.
- 4) The material overstrength can be calculated as $\gamma_{0.95} = F_{0.95} / F_{0.05}$
- 5) The model overstrength can now be calculated as $\gamma_{an} = F_{0.05} / F_{Rk}$
- 6) The entire overstrength is $\gamma_{Rd} = \gamma_M * \gamma_{an} * \gamma_{0.95}$ with $\gamma_M = 1.3$.

Calculation formulas for γ_{Rd} for dowel-type steel-to-timber connections are outlined in the following. The failure modes according to Eurocode 5 are depicted in Figure 5.

- (a) $F_R = 0.4 \cdot f_h \cdot t \cdot d \rightarrow \gamma_{Rd,a} = F_{0.95} / F_{Rd} = 1.3 \cdot f_{h,0.95} / f_{h,k}$
- (b) $F_R = 1.15 \sqrt{2M_y \cdot f_h \cdot d} + F_{ax}/4$
 $\rightarrow \gamma_{Rd,b} = 1.3 \cdot [\sqrt{2M_{y,0.95} \cdot f_{h,0.95} \cdot d} + F_{ax,0.95}/4.6] / [\sqrt{2M_{y,k} \cdot f_{h,k} \cdot d} + F_{ax,k}/4.6]$
- (c) $F_R = f_h \cdot t \cdot d \rightarrow \gamma_{Rd,c} = \gamma_{Rd,a} = 1.3 \cdot f_{h,0.95} / f_{h,k}$
- (d) $F_R = f_h \cdot t \cdot d [\sqrt{2+4M_y/(f_h \cdot d \cdot t^2)} - 1] + F_{ax}/4$
 $\rightarrow \gamma_{Rd,d} = 1.3 \cdot [f_{h,0.95} \cdot t \cdot d [\sqrt{2+4M_{y,0.95}/(f_{h,0.95} \cdot d \cdot t^2)} - 1] + F_{ax,0.95}/4] / [f_{h,k} \cdot t \cdot d [\sqrt{2+4M_{y,k}/(f_{h,k} \cdot d \cdot t^2)} - 1] + F_{ax,k}/4]$
- (e) $F_R = 2.3 \sqrt{2M_y \cdot f_h \cdot d} + F_{ax}/4$
 $\rightarrow \gamma_{Rd,e} = 1.3 \cdot [\sqrt{2M_{y,0.95} \cdot f_{h,0.95} \cdot d} + F_{ax,0.95}/9.2] / [\sqrt{2M_{y,k} \cdot f_{h,k} \cdot d} + F_{ax,k}/9.2]$
- (f) $F_R = f_h \cdot t \cdot d \rightarrow \gamma_{Rd,f} = \gamma_{Rd,a}$
- (g) $F_R = f_h \cdot t \cdot d [\sqrt{2+4M_y/(f_h \cdot d \cdot t^2)} - 1] + F_{ax}/4 \rightarrow \gamma_{Rd,g} = \gamma_{Rd,d}$
- (h) $F_R = 2.3 \sqrt{2M_y \cdot f_h \cdot d} + F_{ax}/4 \rightarrow \gamma_{Rd,h} = \gamma_{Rd,e}$
- (j) $F_R = 0.5 f_h \cdot t \cdot d \rightarrow \gamma_{Rd,j} = \gamma_{Rd,a}$
- (k) $F_R = 1.15 \sqrt{2M_y \cdot f_h \cdot d} + F_{ax}/4 \rightarrow \gamma_{Rd,k} = \gamma_{Rd,b}$
- (l) $F_R = 0.5 f_h \cdot t \cdot d \rightarrow \gamma_{Rd,l} = \gamma_{Rd,a}$
- (m) $F_R = 2.3 \sqrt{2M_y \cdot f_h \cdot d} + F_{ax}/4 \rightarrow \gamma_{Rd,m} = \gamma_{Rd,e}$

For dowelled steel-to-timber connections, the rope effect reduces to zero: $F_{ax}/4 = 0$. The overstrength factors can then be simplified as follows:

$$\gamma_{Rd,a} = \gamma_{Rd,c} = \gamma_{Rd,f} = \gamma_{Rd,j} = \gamma_{Rd,l} = 1.3 \cdot f_{h,0.95} / f_{h,k}$$

$$\gamma_{Rd,b} = \gamma_{Rd,e} = \gamma_{Rd,h} = \gamma_{Rd,k} = \gamma_{Rd,m} = 1.3 \cdot \sqrt{(M_{y,0.95} \cdot f_{h,0.95}) / (M_{y,k} \cdot f_{h,k})}$$

$$\gamma_{Rd,d} = \gamma_{Rd,g} = 1.3 \cdot (f_{h,0.95} [\sqrt{2+4M_{y,0.95}/(f_{h,0.95} \cdot d \cdot t^2)} - 1]) / (f_{h,k} [\sqrt{2+4M_{y,k}/(f_{h,k} \cdot d \cdot t^2)} - 1])$$

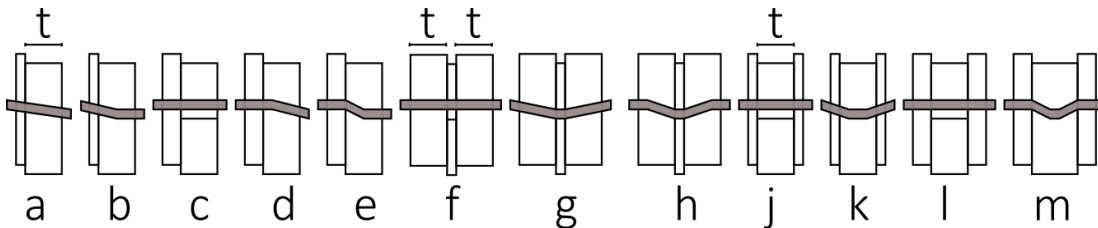


Figure 5. Failure modes for steel-to-timber connections (modified from Eurocode 5).

4 Example calculation

Let's consider a single-sided dowelled connection in ungraded sawn New Zealand *radiata pine* and New Zealand LVL11 under seismic loading. The connection is made of $d = 12$ mm Grade300 steel dowels with a thin steel plate and side member thickness of $t = 5.5d = 66$ mm. The connection is loaded parallel to the grain (dowel in shear) and the design load is $F_{Ed} = 52.0$ kN. The possible failure modes are mode (a) and (b) depicted in Figure 5.

For a single dowel in shear and a thin steel plate, Eurocode 5 gives the characteristic ductile strength as:

$$F_k = \min[0.4 \cdot f_{h,k} \cdot t \cdot d; 1.15 \sqrt{2M_{y,k} \cdot f_{h,k} \cdot d}] ; F_{ax,k} = 0 \text{ for dowels} \quad (11)$$

with $M_{y,k} = d^3/6 \cdot f_{y,nom}$ and $f_{h,k} = 0.082(1-0.1d)\rho_k$ for sawn timber. Note that different embedment formulas can be used in this step, e.g. Franke and Quenneville (2011) or Uibel and Blaß (2014).

Table 4 gives the material strength values. As timber grades in New Zealand are based on the Young's Modulus and no characteristic embedment strength values are available, $\rho_{0.05}$ is used to calculate $f_{h,0.05}$, and an overstrength factor, γ_{an} , is applied.

Table 4. Input values for example calculation.

	ρ_{sawn} [kg/m ³]	ρ_{LVL} [kg/m ³]	$f_{h,sawn}$ [MPa]	$f_{h,LVL}$ [MPa]	$f_{y,Grade300}$ [MPa]	$M_{y,Grade300}$ [Nmm]
$X_k (X_{nom})$					300	86 400
$X_{0.05}$	402 ⁽¹⁾	480 ⁽²⁾	29.01	34.66	320 ⁽³⁾	92 160
$X_{0.95}$	608 ⁽¹⁾	564 ⁽²⁾	43.87	40.73	358 ⁽³⁾	103 104

⁽¹⁾ provided by XLam Ltd, ⁽²⁾ provided by Nelson Pine Industries Ltd, ⁽³⁾ provided by Pacific Steel for Grade300 round bar

Inserted into Equation 11, we find that mode (b) is governing. Note that mode (a) relies solely on timber crushing for ductility and should therefore be avoided in seismic design. In order to satisfy Equation 10 ($F_{Ed} \leq F_{Rd}$), we require 8 dowels in sawn timber and 7 dowels in LVL:

$$F_{Rd,sawn} = F_{Rk,sawn} / \gamma_M = \min\{9.19, 8.92\} / 1.3 = 6.86 \text{ kN} \rightarrow 52.0 \text{ kN} < 8 \times 6.86 = 54.89 \text{ kN}$$

$$F_{Rd,LVL} = F_{k,LVL} / \gamma_M = \min\{10.98, 9.75\} / 1.3 = 7.50 \text{ kN} \rightarrow 52.0 \text{ kN} < 7 \times 7.50 = 52.50 \text{ kN}$$

Furthermore, we assume that the dowels are arranged in such a manner that their full capacity can be utilized ($n_{eff} = 1.0$).

Let's first consider the analytical model overstrength, γ_{an} . From Ottenhaus et al. (2017) it is known that $\gamma_{an,My} = 1.00$ and $\gamma_{an,fh} = 1.06$. The latter was derived as an upper bound for CLT and can serve as a conservative estimate for LVL. Furthermore, Table 1 gives $\gamma_{an,fy,nom} = 1.03$ for Grade300 which results in $\gamma_{an} = 1.00 \cdot 1.06 \cdot 1.03 = 1.09$.

As outlined above, $\gamma_{0.95}$ can be calculated as $\gamma_{0.95} = \sqrt{[(M_{y,0.95} \cdot f_{h,0.95}) / (M_{y,0.05} \cdot f_{h,0.05})]} = \{1.30 \text{ sawn}, 1.15 \text{ LVL}\}$.

The resulting overstrength can now be calculated:

$\gamma_{Rd,sawn} = \gamma_M * \gamma_{an} * \gamma_{0.95,sawn} = 1.3 * 1.09 * 1.30 = 1.85$ for ungraded sawn *radiata pine*
and $\gamma_{Rd,LVL} = \gamma_M * \gamma_{an} * \gamma_{0.95,LVL} = 1.3 * 1.09 * 1.15 = 1.63$ for LVL.

The resulting strength hierarchy is:

$$\begin{aligned} F_{Ed} = 52.0 \text{ kN} &\leq F_{Rd,sawn} = 8 \times 6.86 = 54.89 \text{ kN} \\ &\leq \gamma_{Rd,sawn} * F_{d,sawn} = 1.85 * 54.89 \text{ kN} = 101.61 \text{ kN} \\ &\leq F_{BR,d} \\ F_{Ed} = 52.0 \text{ kN} &\leq F_{Rd,LVL} = 7 \times 7.50 = 52.50 \text{ kN} \\ &\leq \gamma_{Rd,LVL} * F_{d,LVL} = 1.63 * 52.50 \text{ kN} = 85.66 \text{ kN} \\ &\leq F_{BR,d} \end{aligned}$$

This example illustrates how designers can estimate the expected overstrength, γ_{Rd} , of any timber material and connection layout with relatively high confidence by using a combination of stress-graded material, accurate material modelling, and the analytical overstrength derivation method presented in this paper.

5 Conclusions

- A simple procedure to analytically determine overstrength was presented.
- Analytical model overstrength is caused by conservative model assumptions and the difference between the nominal steel strength, $f_{y,nom}$, and the 5th percentile steel strength, $f_{y,0.05}$. As semi-empirical analytical models in design codes are calibrated on test data, γ_{an} is generally small. The overstrength factor was calculated for dowelled connections making use of timber materials with $\rho_k \in [300,600]$ kg/m³, dowel diameters $d \in [6,30]$ mm, and side-member thickness to dowel diameter ratios $t/d \in [2,10]$ as: $\gamma_{an,S235} = 1.10$, $\gamma_{an,S355} = 1.08$, $\gamma_{an,Grade300} = 1.03$, and $\gamma_{an,Grade500} = 1.02$ for S235, S355, Grade300 and Grade500 steel, respectively.
- Material overstrength factors for different steel grades were derived:
 $\gamma_{0.95,S235} = 1.15$, $\gamma_{0.95,S355} = 1.10$, $\gamma_{0.95,Grade300} = 1.13$, $\gamma_{0.95,Grade500} = 1.10$
While the value for Grade300 and Grade500 were based on an allowable range of f_y given in AS/NZS 4671:2001, the values for S235 and S355 are based on experimental data with small sample numbers (26 and 19, respectively). These should therefore be validated with larger sample sizes.
- The upper bound material overstrength factors for New Zealand ungraded sawn *radiata pine* and graded LVL were calculated based on the information provided by suppliers: $\gamma_{0.95,sawn} = 1.51$ and $\gamma_{0.95,LVL} = 1.17-1.19$. For European timber grades, the overstrength factors were calculated based on the density ranges given in EN 338:2016: $\gamma_{0.95,C20} = 1.36$ for C20 and $\gamma_{0.95,C24} = 1.24$ for C24.

It is apparent that timber strength grading results in lower variability in material strength and smaller overstrength factors.

- Significant unexpected overstrength can be introduced from delivery of material that is stronger than specified – both for the steel fasteners and the timber itself. This is an issue that designers need to be aware of and that needs to be raised with suppliers.

6 Acknowledgements

The authors would like to acknowledge the Natural Hazard Research Platform and EQC of New Zealand for providing research grants for this project. XLam NZ Ltd is acknowledged for contributing to the experimental materials. XLam NZ Ltd, Nelson Pine Industries Ltd and Pacific Steel are thanked for making their material test data available.

7 References

- Australian/New Zealand Standard, AS/NZS 4357.0:2005. (2005): Structural Laminated Veneer Lumber. Standards Australia, GPO Box 476, Sydney, NSW 2001 and Standards New Zealand, Private Bag 2439, Wellington 6140
- Australian/New Zealand Standard, AS/NZS 4671:2001. (2001): Steel reinforcing materials. Standards Australia, GPO Box 476, Sydney, NSW 2001 and Standards New Zealand, Private Bag 2439, Wellington 6140
- Brühl, F., Schänzlin, J., & Kuhlmann, U. (2014): Ductility in Timber Structures: Investigations on Over-Strength Factors. In *Materials and Joints in Timber Structures* (pp. 181-190). Springer, Dordrecht.
- Dickof, C., Stiemer, S. F., Bezabeh, M. A., & Tesfamariam, S. (2014). CLT–Steel Hybrid System: Ductility and Overstrength Values Based on Static Pushover Analysis. *Journal of Performance of Constructed Facilities*, 28(6)
- EN 338:2016 (2016). Structural timber. Strength classes. European Committee for Standardization, Brussels.
- Eurocode 3 (2008): Design of steel structures - Part 1-1: General and rules for buildings. CEN. (EN 1993-1-1).
- Eurocode 5 (2004/2014): Design of timber structures - Part 1-1: General and rules for buildings. CEN. (EN 1995-1-1).
- Franke, S., & Quenneville, P. (2011): Bolted and dowelled connections in radiata pine and laminated veneer lumber using the European yield model. *Australian Journal of Structural Engineering*.

- Gavric, I., Fragiaco, M., & Ceccotti, A. (2015): Cyclic behavior of typical screwed connections for cross-laminated (CLT) structures. *European Journal of Wood and Wood Products*, 73(2), 179–191
- Guttmann, I. (1970): Statistical tolerance regions: classical and Bayesian.
- Jorissen, A., & Fragiaco, M. (2011): General notes on ductility in timber structures. *Engineering Structures*, 33(11), 2987–2997.
- Karmazínová, M. & Melcher, J. (2012): Influence of steel yield strength value on structural reliability. In *Proceedings of the 7th WSEAS International Conference on Continuum Mechanics “CM'12* (pp. 441-446).
- Leicester, R.H. (1986): Confidence in estimates of characteristic values. *Proceedings of 19th CIB W18 Meeting*, Firenze, Italy
- Ottenhaus, L.-M., Li, M., Smith, T., & Quenneville, P. (2016): Ductility and Overstrength of Dowelled LVL and CLT Connections Under Cyclic Loading. In *Proceedings of the WCTE 2016 World Conference on Timber Engineering*, Vienna / Austria, August 22-25, 2016
- Ottenhaus, L.-M., Li, M., Smith, T., & Quenneville, P. (2017): Overstrength of dowelled CLT connections under monotonic and cyclic loading. *Bulletin of Earthquake Engineering*.
- Ottenhaus, L.-M., Li, M., Smith, T. (2018): Overstrength of large-scale dowelled connections in CLT. *Proceedings of the 2018 NZSEE Conference*, New Zealand Society of Earthquake Engineering, Auckland, April 13-15, 2018.
- Ranta-Maunus, A. (2007): Strength of Finnish grown timber. VTT Technical Research Centre of Finland.
- Sandhaas, C., & van de Kuilen, J. W. G. (2017): Strength and stiffness of timber joints with very high strength steel dowels. *Engineering Structures*, 131, 394–404.
- Smith, I., & Foliente, G. (2002): Load and Resistance Factor Design of Timber Joints: International Practice and Future Direction. *Journal of Structural Engineering*, 128(1), 48–59.
- Uibel, T., & Blaß, H. J. (2014): Joints with Dowel Type Fasteners in CLT Structures Test material. *Focus Solid Timber Solutions - European Conference on Cross Laminated Timber (CLT)*, 119–134.
- Vogt, T., Hummel, J., Schick, M., & Seim, W. (2014): Experimentelle Untersuchungen für innovative erdbebensichere Konstruktionen im Holzbau. *Bautechnik*, 91(1), 1–14.

Discussion

The paper was presented by L-M Ottenhaus

U Kuhlmann commented additional thoughts are needed about realistic resistance of the dowel as all steel connections are typically directed towards the tensile strength of the steel. H Blass said that there are lots of results available confirming that bending strength of steel is 90 to 100% of its tensile strength. U Kuhlmann further commented that the steel community has a valuable data bank containing the strength properties of steel for their code. One should get more information from the steel community for this work. L-M Ottenhaus agreed and responded that in plastic design one designs to the yield point and not the ultimate strength.

A Frangi referred to slide 13 and asked how to achieve ductile failure when minimum distances are needed. L-M Ottenhaus agreed and said that a lot of time brittle failures were experienced and this depends also on connection layup. There is a need to consider fastener distances to ensure ductile failure mode.

H Blass disagreed with the statement that EYM is pretty accurate. He said that rope effect in dowels can appear and is ignored in EYM. This can compromise the approach as the EYM equations were made for static design and not for overstrength issues in seismic design.

C Sigrist and L-M Ottenhaus discussed comparisons between full scale experimental results and the model.

PINCHING-FREE TIMBER CONNECTION

Pierre Quenneville¹

Nicholas Chan¹

Pouyan Zarnani²

¹Department of Civil and Environmental Engineering, The University of Auckland, Auckland, New Zealand

²Department of Built Environment Engineering, Auckland University of Technology, Auckland, New Zealand

Keywords: Connections, seismic, timber, low-damage design, pinching, ductile

1 Introduction

The philosophy when designing timber connections is to use many small diameter fasteners in order to ensure that a minimum amount of ductility is present and that the joint will absorb the seismic loads on the structure. However, even if brittle failure of the timber is prevented at the joint, the yielding failure of the timber/fastener combination will include an increased amount of pinching at every subsequent cycle, as shown in Figure 1.

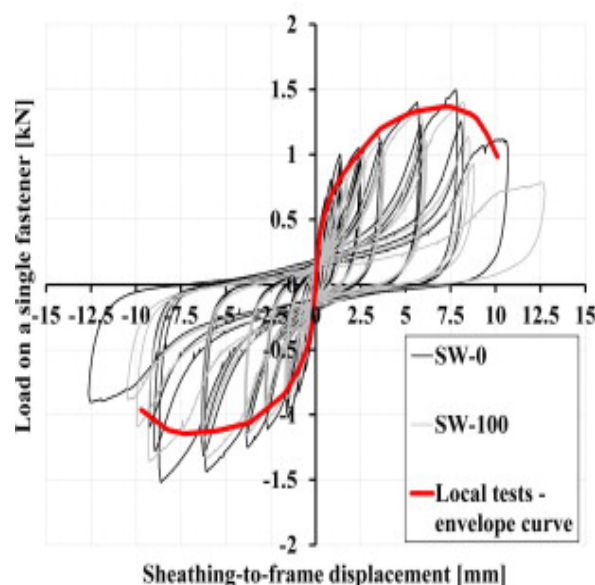


Figure 1. Load-deformation response of timber connection showing pinching behaviour [1].

Designers have accepted this pinching behaviour as a characteristic of timber connections resisting cyclic loads. A new connector has been developed to prevent this pinching behaviour in connections.

2 Current Design Approach

Building structures are occasionally subjected to extraordinary loads, such as during earthquakes. Structures are presently designed to cope with these loads without catastrophic failure. However, damage to the structure or parts of the structure is inevitable, and to an extent desirable or intended. In particular, predictable fracturing or plastic yielding of building components or materials can be intended to absorb energy of an event, reducing peak loads or displacements and thus lessening the risk of more significant failures. One example of this type of predictable damage occurs in joints between wooden members and other parts of structure. Where wooden members are connected to a flange or flanges by fastener such as bolt or bolts, extreme forces can lead to crushing of wood against the fastener. The connection resistance associated with these different yielding failures has been well studied since its introduction by Johansen [2]. This crushing/yielding can be a significant energy absorber. However, in an event, such as an earthquake, which induces cyclic forces or displacement, the wood member may be forced to move alternately relative to the fastener. Movement induced crushing in the first cycle opens up a cavity and allows a degree of “play” between the fastener and the wooden member. This play has a detrimental effect on the energy absorbency of the joint in subsequent movement cycles. In timber buildings subjected to earthquake loadings, prior art structural joint solutions for resisting and damping seismic forces are mainly based on the yielding of the fasteners (bolts or dowels) in combination with crushing of the timber fibres by the fasteners. This achieves an amount of ductility and energy dissipation. However, earthquake loads are cyclic, with repeated loading and unloading. The fibre crushing is irreversible, so the crushed timber area does not provide an immediate response in subsequent cycles of the event. This “slack” or “play” leads to a delay in the connection response, termed “pinching”. The pinching means that the amount of energy available to resist earthquake excitation in subsequent cycles is limited. This is illustrated in Figure 2 for a tension-only connection.

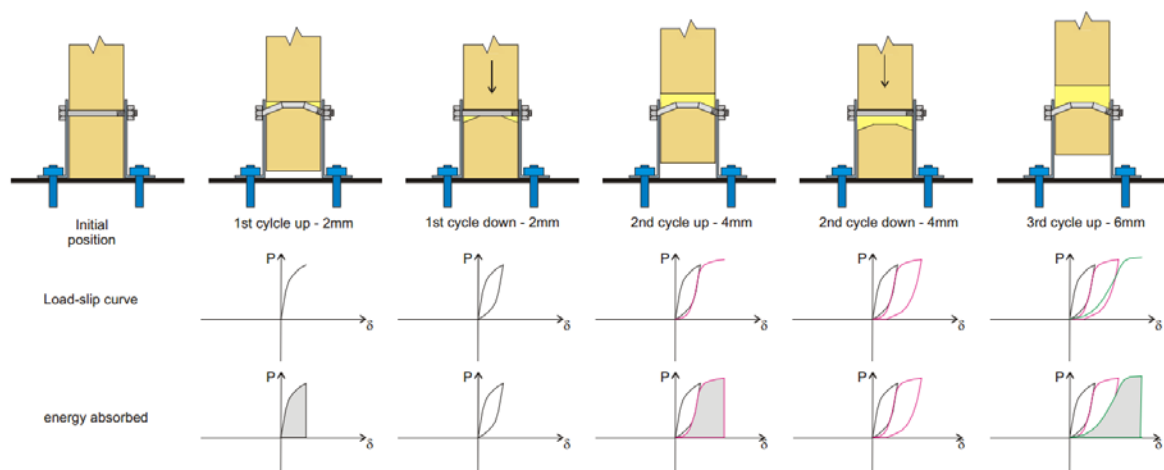


Figure 2. Conventional timber connection behaviour under cyclic loading showing pinching phenomenon.

3 Proposed Pinching-Free Connector

3.1 The Concept

To overcome the pinching behaviour from limiting the amount of energy being absorbed at every load cycle, a novel connector was developed at the University of Auckland, New Zealand [3]. The concept is based on the principle that the “play” or “slack” that occurs at every load cycle, is absorbed / eliminated. Essentially, the timber fastener can yield or remain in the elastic range but the bulk of the seismic energy is absorbed through crushing of the timber fibres. The displacement resulting from this fibre crushing is absorbed at every loading cycle. This offers the advantage that the joint fasteners, even in their bent state, are available to mobilise the full energy-absorbing capacity of the embedment of the timber. This is shown in Figure 3 for one of the PFC concept.

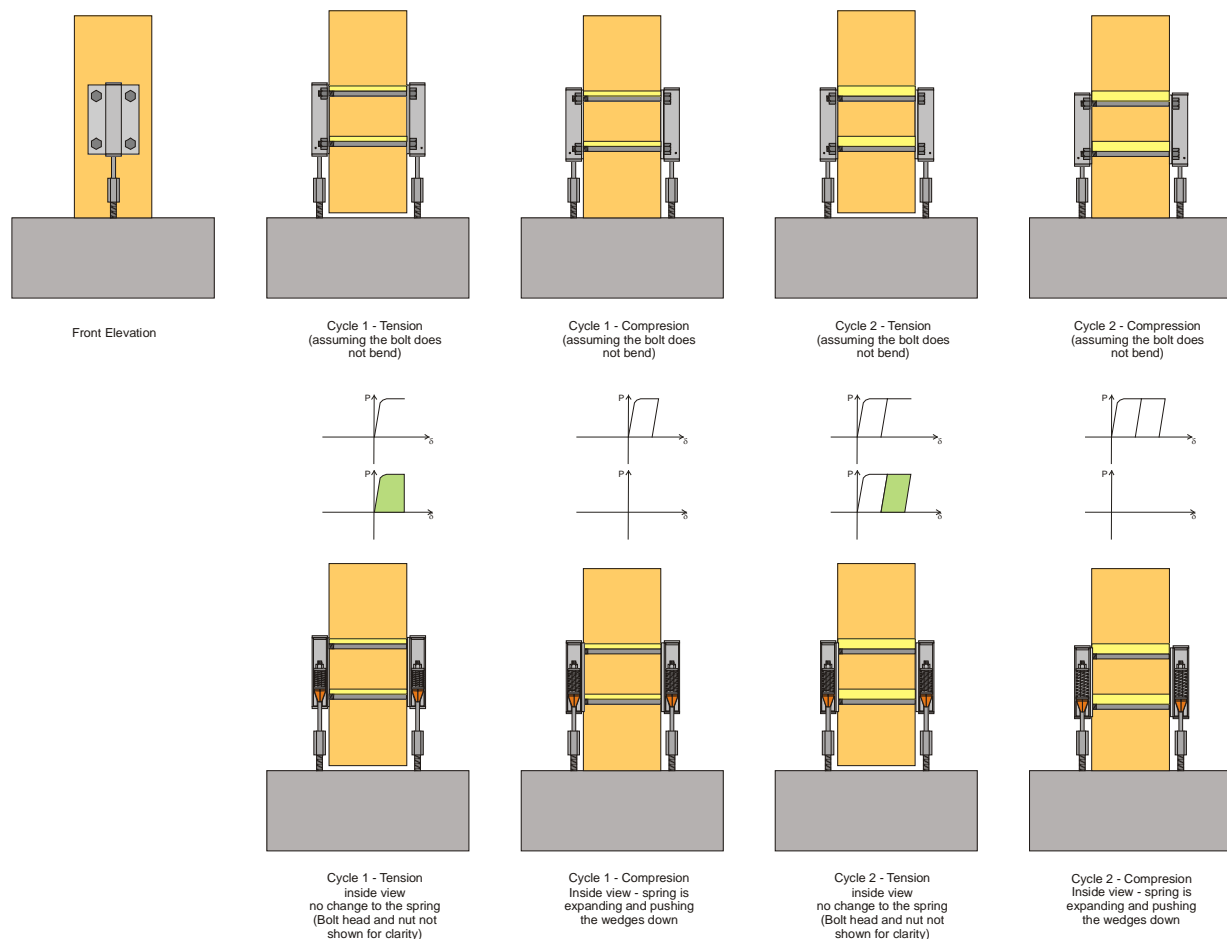


Figure 3. Proposed “Pinching-Free Connector” (PFC) with resulting load-deformation curves.

With the advantage of removing the play or slack in the connection, the governing resistance failure mode becomes Mode 1 of the European Yield Model. Although the design of the joint could be made with slender or stocky fasteners, the ultimate amount of energy absorbed at every cycle would be controlled by the Mode 1 resistance.

In the case of a PFC joint with small diameter fasteners, the fasteners would deform and yield according to the EYM and exhibit a Mode 2 or Mode 3 deformation behaviour. However, as this deformation is not an issue anymore, the fasteners will continue to resist any additional loading resulting from the imposition of additional deformation at subsequent cycles.

3.2 The Device

An illustration of the concept is shown in Figure 4. In this figure, the device is applied as a hold-down for a shear wall. It resists tensile forces at either end of the wall, which tend to lift-off the ground as the wall rocks back-and-forth under seismic excitation.

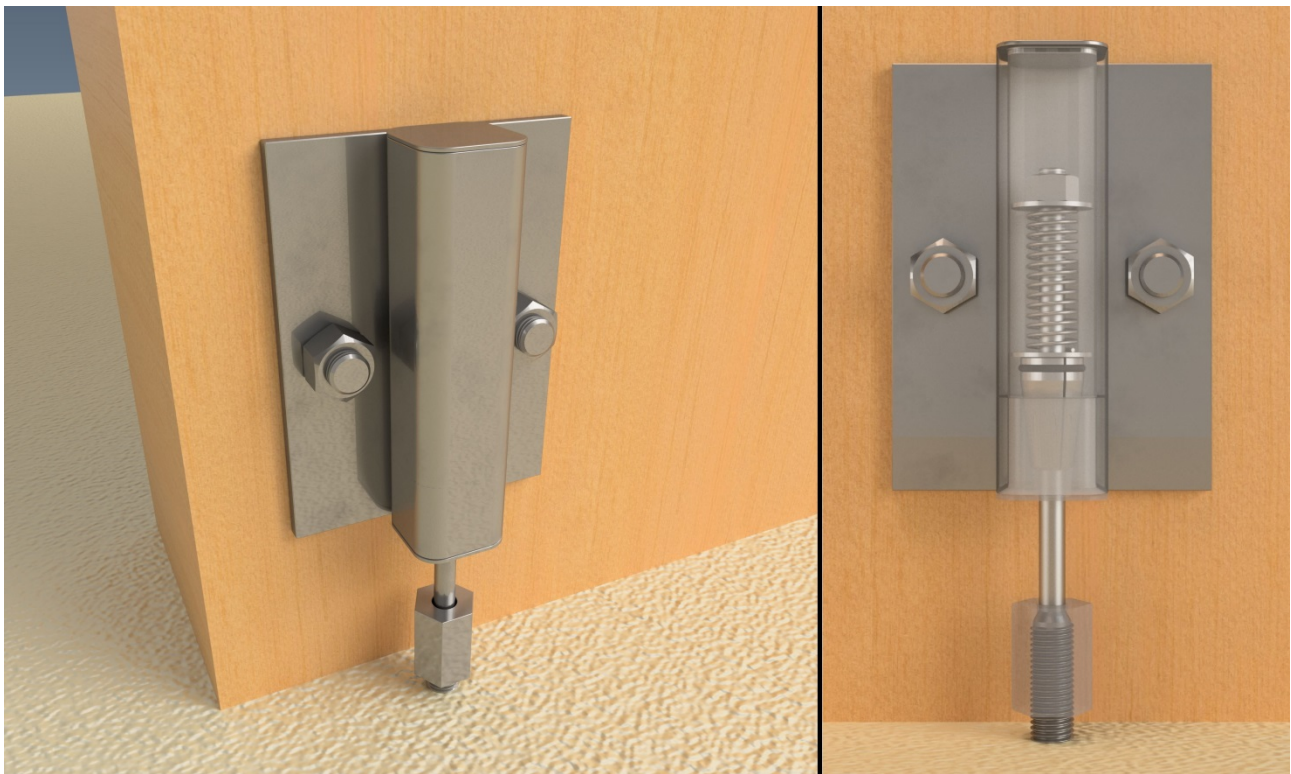


Figure 4. The proposed pinching-free connector used as a hold-down.

There are seven main parts to the PFC, as shown in Figure 5. Parts one to six are listed in order with the load path:

1. Bolts
2. Housing weldment, that consists of:
 - a. steel side-plate with bolt holes
 - b. bottom-cap with tapered hole
 - c. hollow-tube to attach (a) to (b)
 - d. top-cap to enclose (c)
3. Split-wedges

4. Rod with tapered head
5. Partially-threaded sleeve
6. Threaded anchor
7. Spring plus nut and washers

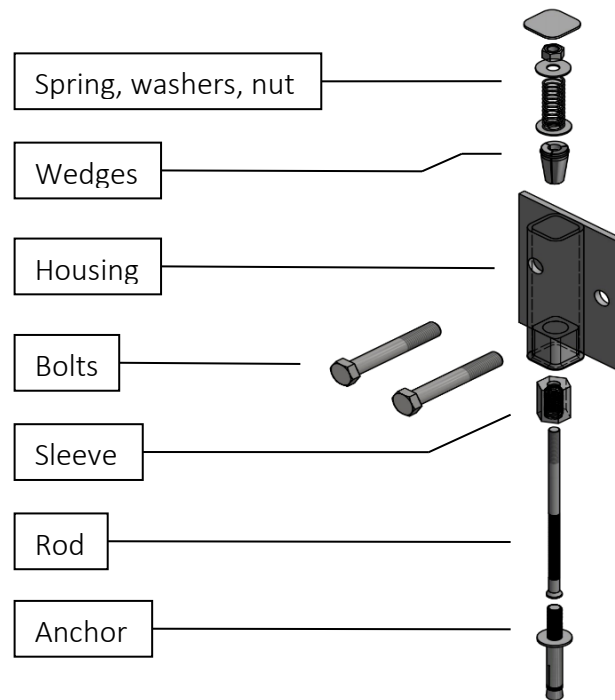


Figure 5. Components of the pinching-free connector.

3.3 How It Works

During the loading phase, the timber member is restrained from uplifting by bearing on the bolts. Bolt shear forces are transferred to the steel side-plates within the housing. The forces flow into the housing's bottom-cap, which is resisted by the split-wedges.

As there is a tapered interface between the bottom-cap and the wedges, a horizontal force component arises from the vertical load on the wedges. This squeezes the split-wedges, bringing the split pieces together so that they grip the rod, 'locking' them in place on the rod. The rod, being held-down by the sleeve, is put in tension and restrained from vertical movement because the sleeve screws into a threaded anchor. This completes the load path. When the load exceeds the yielding and/or embedment capacity, failure occurs in either Mode 1, Mode 2 or Mode 3 depending on the configuration. For a given size of timber, stiffer and stockier bolts that are well-restrained would exhibit pure embedment failure (Mode 1).

On the other hand, bolts that are relatively slender and poorly-restrained at their ends can display a combination of embedment and yielding failure (Mode 2 or Mode 3). In either case, timber fibres crush underneath the bolts. Bolt holes elongate towards the member-end, thereby reducing the end-distances of the bolts.

During the unloading phase, the split-wedges are disengaged in the absence of horizontal forces. This allows the wedge-pieces to split and release their grip on the rod. As the timber member falls toward the ground, it also brings down the bolts and the housing because they are both fastened to the timber. The bolts and housing appear to ‘travel’ or slide downwards relative to the stationary rod.

As this happens, the bolts remain at the bottom of their elongated holes and remain embedded in the timber. This preserves the reduced end-distances, and prevents slack from forming. The pre-stressed spring then pushes the freed wedges into the bottom-cap that has travelled downwards. This locks the housing and bolts at their new position, so that there is immediate resistance upon the next cycle of uplift.

4 Experimental Demonstration

4.1 Test Programme

An experimental demonstration was carried out to demonstrate the applicability of the connector to eliminate pinching and absorb the optimum amount of seismic energy at every cycle. The secondary goal was to verify whether alternative PFC configurations can control the backbone curve, in addition to the lack of pinching.

To this end, three tests were performed according to the configurations outlined in Table 1. Test 1 uses a conventional bracket connection with ‘many’ small and weak fasteners. Test 2 also uses small-diameter fasteners, but in smaller quantities and of higher yield strength. The pinching-free connection is also applied.

Test 3 utilises a pinching-free connection with ‘few’ large-diameter bolts. In this case, the aim was to keep the bolts elastic and un-deformed. Table 1 also lists the behaviour and failure modes expected for each test.

Table 1. Connection configurations tested.

Test #	Connection	Fasteners	Pinching Occurs	Bolts Yield	Timber Crushes
Test 1	Brackets	6-M10 – Grade 4.8	Yes	Yes	Yes
Test 2	PFC	4-M10 – Grade 8.8	No	Yes	Yes
Test 3	PFC	2-M16 – Grade 8.8	No	No	Yes

4.2 Test Setups

The tests attempt to simulate an uplifting timber column or shear wall, by loading Glulam columns attached to two connectors to form a steel-wood-steel joint (see Figure 5). All steel components – aside from the various fasteners tested in Table 1 – were designed to remain elastic.

A 300 kN MTS machine was used to lift the timber members, which are glue-laminated members made of New Zealand Radiata Pine. They are classified as Grade 8 (PL 8), having densities of 468 kg/m³ on average. The side-plates in all the

connections tested were similarly sized at 150 mm (width) by 200 mm (height) by 8 mm (thick) for ease of comparison. The centre of the plates was located 200 mm from the member-end. In Tests 1 and 2, these plates have identical hole sizes (12 mm diameter) and hole spacings (50 mm vertically, 100 mm horizontally). For Test 3, the middle two holes are simply enlarged to 18 mm diameter to accommodate 2-M16 bolts alone.

The PFC uses M12 rods (Grade 10.9) to transmit tensile loads into the M20 anchor (Grade 8.8). The anchor is a threaded rod that screws into the steel base-plate, which is 25 mm thick and fastened to the foundation. Portal gauges were used to measure the displacements of the timber relative to the connection. Four gauges were installed between the timber and the side-plates (two gauges per plate). Figure 6 shows the location of the gauges.



Figure 6. Connections for Test 1 (left), Test 2 (centre) and Test 3 (right).

4.3 Load Regime

Figure 7 shows the load regime that was planned for the tests. In all cases, the rate of loading was similarly set at 0.1 mm/s. However, their differences lie in the point at which each test terminates.

The plan was to terminate Tests 2 and 3 (pinching-free connector) earlier than Test 1 (conventional brackets). This is because the PFC absorbs all displacement in the form of crushed fibres. Specifically, the displacement occurring on every cycle contributes in crushing the fibres, so that the total amount of crushing accumulates considerably fast when using the PFC.

For instance, Figure 7 shows the plan for Test 2 to undergo 2 cycles each with amplitudes 1.0 mm, 1.5 mm, 2.0 mm and 2.5 mm. These add up to 14 mm of total

deformation, which surpasses the maximum deformation expected from Test 1 (at 10 mm).

It should be noted that the displacement followed in Figure 7 refers to the portal gauge outputs, which measure the relative displacement between the steel side-plate and the timber directly (rather than the displacement between side-plate and the MTS loading arm).

In doing so, the connection hysteresis could be plotted without interference from additional slack that could arise in other parts of the setup. One such source of slack is the hole clearance in the bolted connection that fastens the timber to the MTS loading arm.

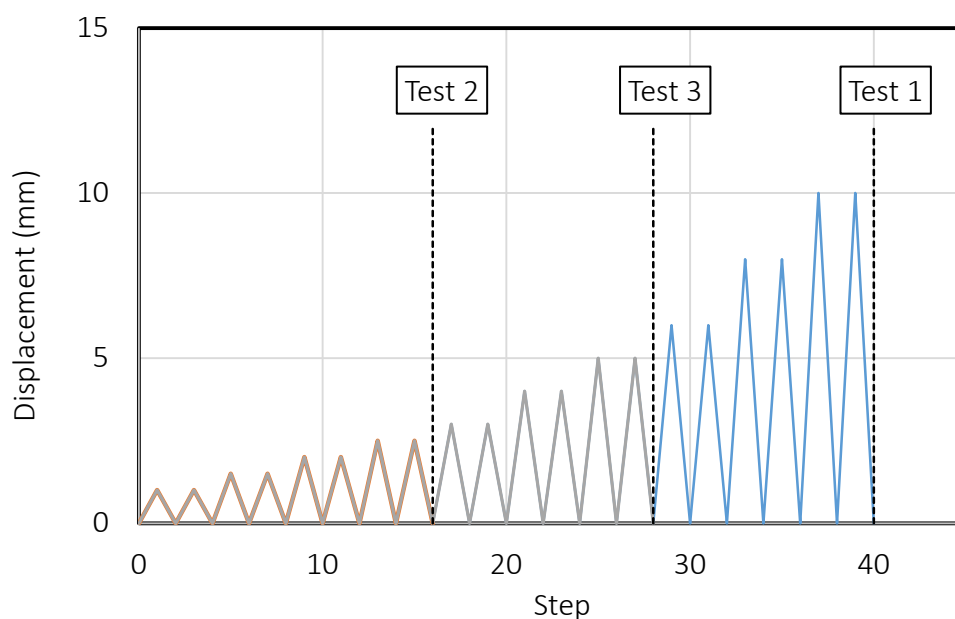


Figure 7. Load regime for Tests 1, 2 and 3.

5 Results and Analysis

5.1 Connection Behaviour

5.1.1 Test 1 – Conventional Brackets with 6-M10 [4.8] Bolts

The load-slip curve in Test 1 shows a slow and gradual gain in resistance. This is a connection with low stiffness, as a high resistance cannot be provided without significant deformation. Yet, brittle failures can occur after significant deformation, such as shear failure in the small and weak bolts, or splitting failure in the timber. However, the test was terminated before brittle failure could happen. Significant pinching was observed in every cycle. The specimen could not resist any load until it had displaced significantly on every cycle to overcome the slack, which amounts to the crushed distance previously achieved. As expected from the smallest and weakest bolts, Figure 8 shows the most severely bent bolts in Test 1. A larger proportion of

crushed timber occurred near the side-plates. Therefore, the predominant mode of failure appears to be Mode 3 of the European Yield Model.

5.1.2 Test 2 – PFC with 4-M10 [8.8] Bolts

In Test 2, the gain in strength was quicker than Test 1 because higher grade bolts were used. This reduces the bending in the bolts, and engages the full timber embedment capacity earlier. With only four bolts, the resulting capacity of the connection was similar as Test 1. Pinching was eliminated with the PFC, as compared to Test 1 with brackets. It can be seen in Figure 7 that every cycle of loading was met with an immediate resistance. The source of this resistance was initially a combination of bending and crushing (Modes 2/3). Eventually, the backbone curve plateaus into a pure embedment failure (Mode 1) despite the bolts remaining in their bent state. It should be noted that the initially stiff response on every loading cycle (approximately 20 kN to 30 kN) could have resulted from over-tightened nuts. This led to friction between the steel side-plate and the timber. The frictional resistance may have also increased in subsequent cycles due to the rope effect.

5.1.3 Test 3 – PFC with 2-M16 [8.8] Bolts

Test 3 shows a stiffer connection that almost behaves in an elastic-perfectly plastic manner. In fact, the load-slip curve bears some resemblance to that of steel as it transitions from elastic to plastic behaviour. There was no visible bending in the large-diameter bolts. Instead, Figure 8 shows great depths of crushed timber under the relatively straight bolt shanks.

This connection is governed by a pure embedment failure (Mode 1). The failure load is clearly defined by the plateau, in comparison with Test 1. In fact, the term ‘failure’ is not very appropriate because the load-carrying ability did not diminish even after 27 mm of deformation – all without any pinching.

The initial slack of 1 mm seen in the graph may have been caused by clearance for the bolt holes. Proper installation procedures would have prevented this by ensuring that the bolt shanks were in contact with the timber.

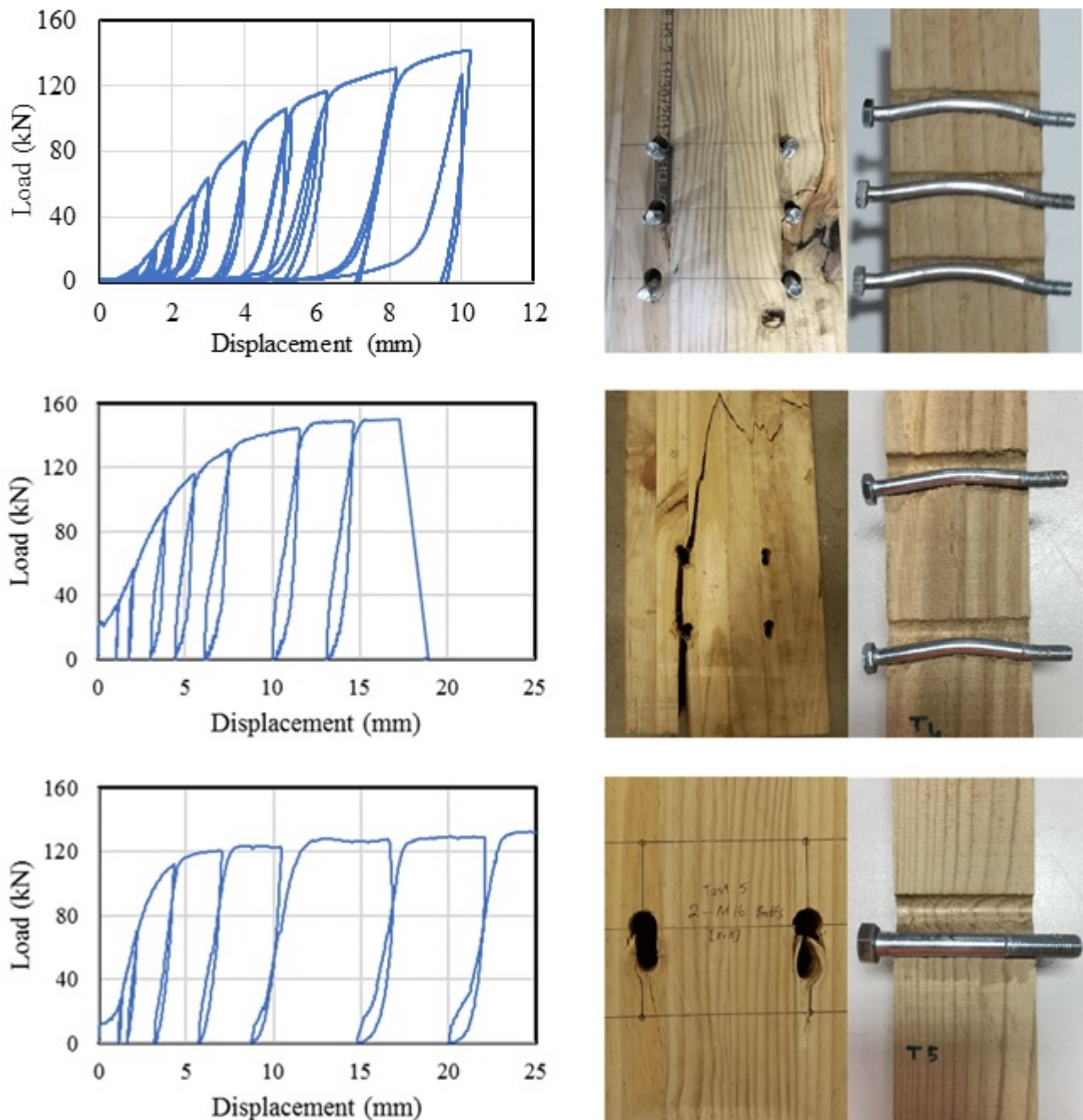


Figure 8. Load-slip graphs (left) and corresponding specimen at failure (right) for Test 1 (top), Test 2 (middle) and Test 3 (bottom). Note the different scales used by the displacement axes.

5.2 Energy Dissipation

To illustrate the potential of the PFC in dissipating energy, six complete cycles were selected from Test 1 to compare against the first six cycles of Test 3. In both cases, they consist of 2 cycles each of 2.0 mm, 3.5 mm and 6.0 mm of displacements approximately. These are highlighted in Figure 9 as the bolded curves.

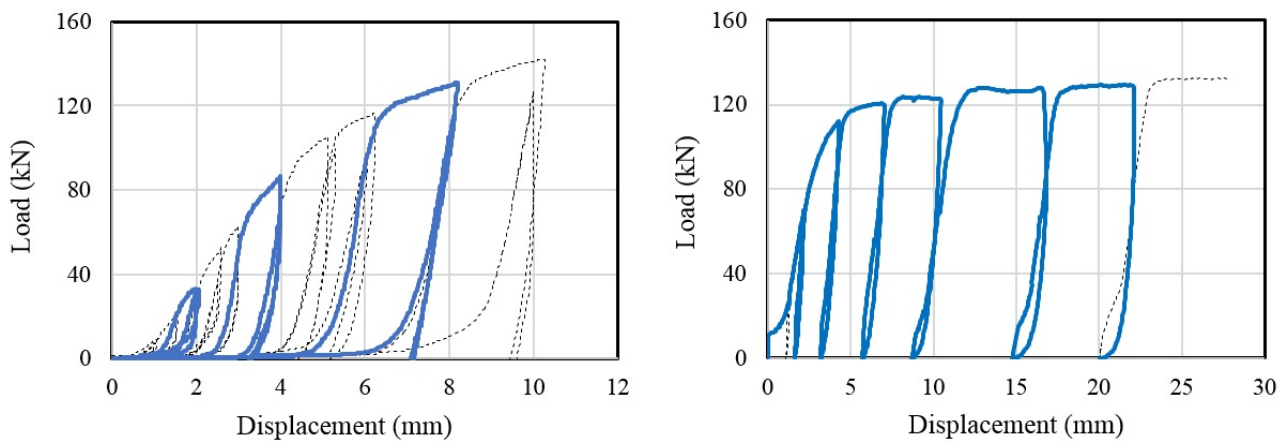


Figure 9. Six complete cycles (bolded) of similar magnitudes from Test 1 (left) and Test 3 (right).

The graph in Figure 10 compares the differences in energy dissipated over the six cycles chosen. On the y-axis, the cumulative energy dissipated was calculated via Riemann integration. These were plotted against the number of completed cycles on the x-axis.

In this graph, each loading phase was considered a half-cycle, and each unloading phase another half-cycle. The number of completed cycles at any point in time was determined based on the proportion of half-cycle completed (i.e. the ratio of displacement to the displacement interval in a half-cycle). A smooth curve can then be plotted, independent of time.

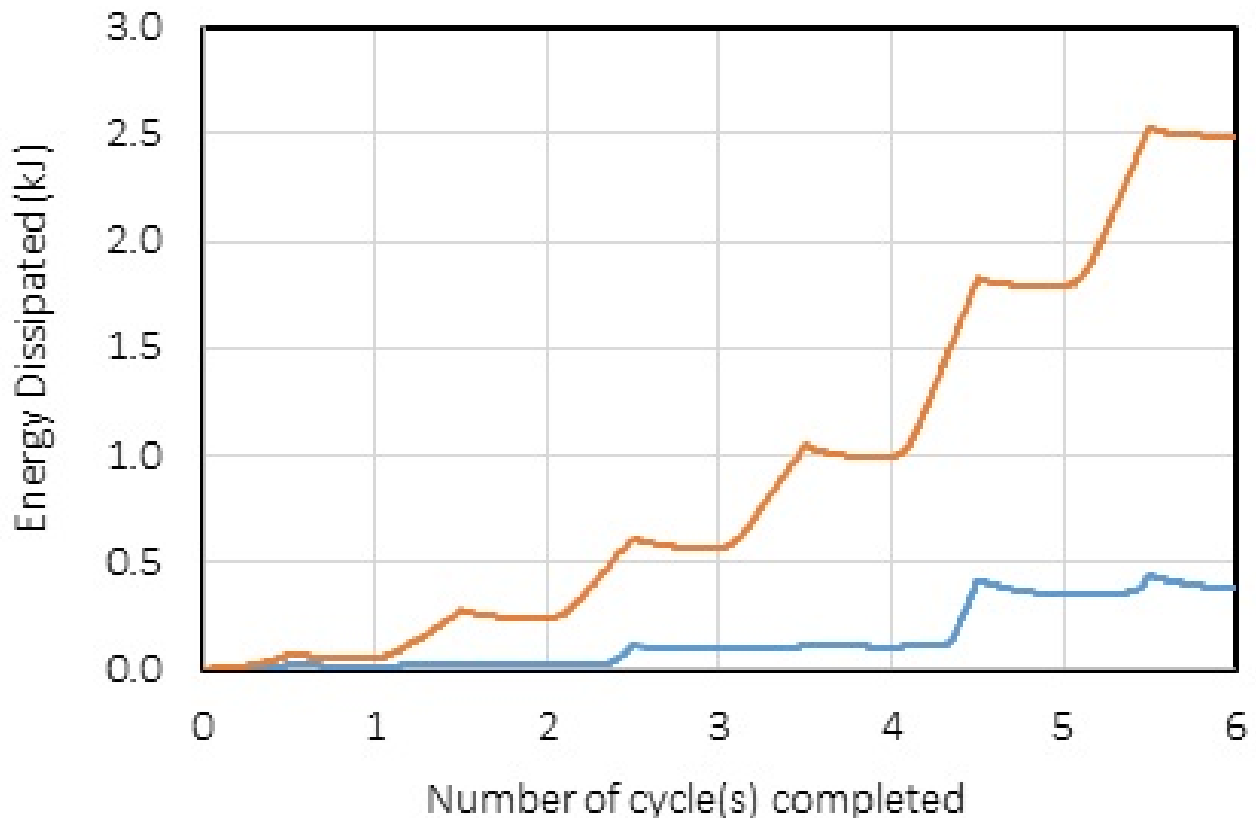


Figure 10. Comparing energy dissipated over the six chosen cycles in Tests 1 and 3.

A significant difference in the amount and manner of dissipation can be seen in Figure 10. In the absence of slack or pinching, the PFC is shown to resist forces and dissipate energy immediately upon loading. In comparison, once the bracket displaces to a new maximum there is negligible dissipation due to slack.

Physically, this means that a bracket connection can only become looser and stays loose. The PFC on the other hand stays stiff. Consequently, the bracket can only dissipate so much energy before brittle failure occurs; whereas the energy dissipated by the PFC can only keep increasing, depending on how much crushing is allowed for by the designer.

Despite having a smaller ultimate capacity in Test 3, the PFC dissipates greater quantities of energy because it mobilises its full timber embedment capacity at an early stage. In contrast, the bracket does not reach a high resistance until considerable slack has formed.

6 Implications

6.1 Design Philosophy

With this connector, the design philosophy can dramatically change from the requirement to specify many small diameter fasteners to requiring very few large and strong ones that will engage the full timber embedment capacity. This has the advantage to allow designers to predict with greater confidence the connection 95th percentile resistance and defining the over-strength requirements. One important requirement of the PFC is that there is sufficient resistance against one of the possible brittle failures (either row shear or group tear out) and this even after a large amount of embedment failure [4]. This is possible if the end distance and bolt in-row spacing are large or if there are screws perpendicular-to-grain to prevent longitudinal shear failures.

6.2 Structural Performance

A connection in the form of a PFC with few, large fasteners can provide a stiff connection with extreme ductility by allowing as much crushing as desired. With a stiffer connection, serviceability requirements can be easily satisfied and addressed in timber structures. As the PFC eliminates pinching completely, there is immediate resistance upon loading. This makes it possible to dissipate seismic energy.

Momentum imparted to the structure can be absorbed by timber members via crushed fibres under embedded bolts. Consequently, the behaviour of a timber substructure equipped with PFC more closely resembles that of a steel member. This means that ductility factors much higher will be possible for timber structures. By dissipating significant energy and damping vibrations from severe earthquakes or wind forces, peak deflections can be significantly less than that of conventional bracket connections. On smaller amplitude excitations such as aftershocks, the PFC imparts a stiff behaviour to a substructure, unlike a loose bracket connection with

slack. Ultimate and serviceability limit requirements will be more easily satisfied, thus reducing damage to the structure, non-structural components and building contents. This benefit flows onto reduced downtime and savings from costly repairs.

6.3 Construction and Maintenance

It is generally a laborious process to install conventional connections, because each joint requires numerous thin fasteners that would bend under high loads. In contrast, the PFC uses few and large bolts that remain elastic and undamaged throughout the life of the device. This entails a rapid 'plug-and-play' installation process, by simply bolting the plate onto the timber and screwing the sleeve into the anchor. All these can be done without power tools. In terms of maintenance, the device only requires attention when the designed travel or length of crushing is exhausted. So, the connection can be designed to sustain as much crushing as desired to prolong the maintenance schedule. No special training is necessary to inspect the length of travel that remains. The timber member can be remedied with a wood-filler during maintenance. The device can then be 'reset' in the same way that it was installed. There is no need to replace any steel parts, as they all remain free of damage. The implication of this is a low-damage, low-maintenance connection which reduces downtime and disruption.

6.4 Potential Applications

In theory, the PFC can be used wherever a wooden member is subjected to tensile forces. In addition to hold-down connectors, the PFC could also be applied in beam-column joints to create moment-resisting connections. This means that the entire building could be fitted with PFC at every joint to form stiff connections throughout the structure. Figure 11 shows some possible applications.

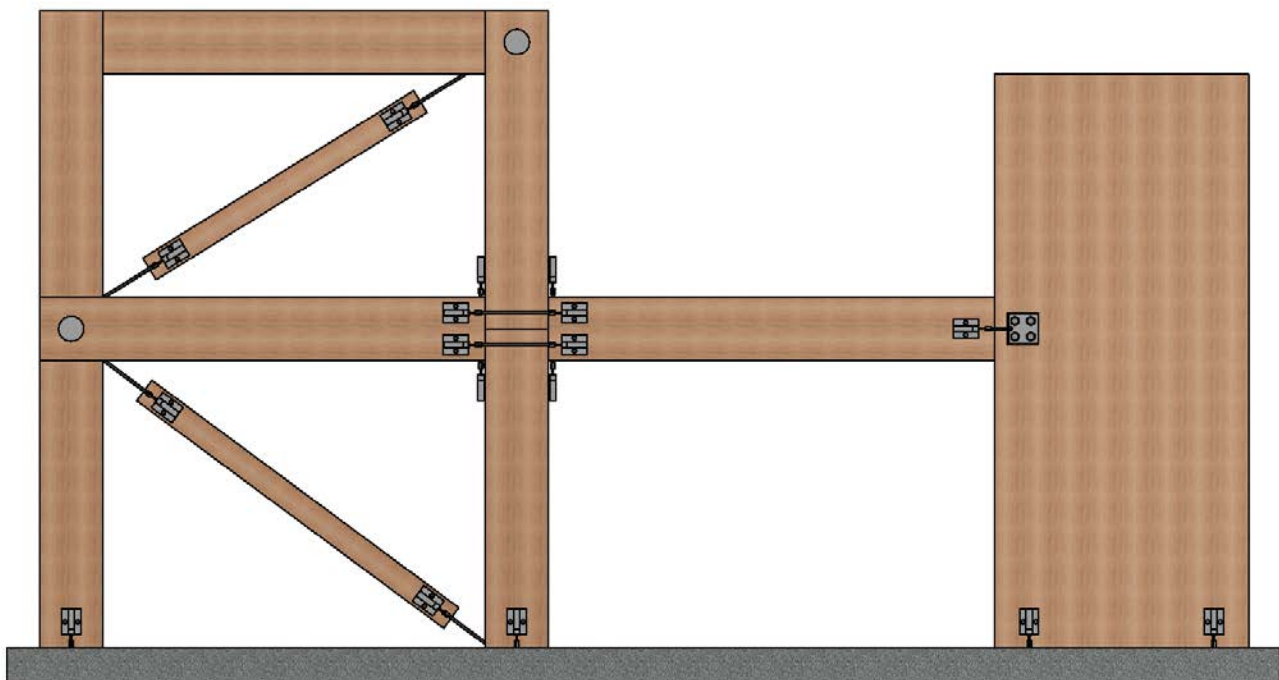


Figure 11. Potential applications of the pinching-free connector.

7 Conclusions

This paper presents a new pinching-free connector (PFC) that allows more energy-absorption during cyclic loading of structural timber components. With this connector, even small dowel-type fasteners can be used to form stiff connections without suffering from pinching.

In fact, the device turns a weakness in timber into an advantage. By crushing the fibres, small fasteners can mobilise the full embedment strength of the timber member to dissipate energy, even in their bent state. A transition occurs initially from failure Modes 2 or 3, to a predominant failure Mode 1.

Hence, the PFC has the potential to alter the design philosophy of using many small dowel-type fasteners in timber connections, to few and large ones. Test results have demonstrated the performance benefits of using fewer and larger fasteners. They can create a stiff and immensely ductile timber connection, with a clearly-defined capacity. One consequence of this is that designers can better define the over-strength requirements for timber members to avoid brittle failures.

The PFC opens up new possibilities for low-damage, pinching-free solutions. Unlike traditional bracket connections, the PFC does not need to be replaced as every single part can remain elastic and free of damage. As for the structure, the device reduces damage to building contents and non-structural elements by reducing peak deflections substantially. A low-damage solution is possible with this connector.

Rapid installation and low maintenance are additional perks that complement the device's performance. Together, these can result in substantially reduced downtime and increased resilience for timber structures in the face of natural hazards.

8 References

- [1] Germano, F., Metelli, G. and Giuriani, E., (2015). Experimental results on the role of sheathing-to-frame and base connections of a European timber framed shear wall, *Construction and Building Materials*, Vol. 80.
- [2] Johansen, K.W. (1949). Theory of timber connection, *International Association for Bridge and Structural Engineering*. 9, 249-262.
- [3] Quenneville, P. and Zarnani, P., "Pinching-free hold down for timber shear walls". Application No. 724903, Filed 4 October 2016, NZ IP Office.
- [4] Quenneville, J. H. P., and Mohammad, M. (2000). "On the failure modes and strength of steel-wood-steel bolted timber connections loaded parallel-to-grain." *Can. J. Civ. Eng.*, 27(4), 761-773.

Discussion

The paper was presented by P Quenneville

H Blass commented that this system is not for changing force directions. P Quenneville agreed.

L-M Ottenhaus commented that in a shear wall application at 2.5% drift a lot of deflection is needed to mobilize the ductility. P Quenneville agreed and commented that in some cases with high stiffness and capacity even with more ductility maybe less deflection is possible. He said that after an earthquake, reset of the fasteners can be done; however, it is not a damage connection system.

A Frangi commented that in CLT one can crush the timber without splitting; however, in glulam one would cause splitting. P Quenneville agreed and said that one would need to prevent wood brittle failure. In this case one does not want too many bolts and using bigger dowels rather than more bolts is the key.

L-M Ottenhaus commented that splitting can be reinforced by screws. P Quenneville said that in cross banded LVL splitting is not an issue.

M Frese asked about the need for maintenance work to ensure moveable gadget for the life of the structure. P Quenneville agreed and would like to verify the concept.

In-plane shear connection for CLT diaphragms

T Schmidt, Blass & Eberhart GmbH / Karlsruhe Institute of Technology, Germany

HJ Blass, Karlsruhe Institute of Technology, Germany

Keywords: cross laminated timber CLT, contact joints, in-plane shear connection, wall and floor diaphragms, bracing elements

1 Introduction

Plates or diaphragms made of cross-laminated timber (CLT) are ideal members to transfer vertical as well as horizontal loads in buildings. The excellent mechanical properties of CLT combined with a high degree of prefabrication enable CLT members to be used in residential as well as in other buildings, where steel and concrete are still the predominant building materials. Examples are industrial and commercial buildings, engineered timber structures in general and medium and high-rise inner-city buildings. However, the technical limit is far beyond 10 storeys. A recent example is the 18 storey Brock Commons Student Residence at the University of British Columbia in Vancouver, Canada. Here, a hybrid system is used with a first storey made of structural concrete and 17 storeys of mass timber construction with glulam columns and CLT floors. The vertical loads of the 53 m high building are transferred by the timber structure, while horizontal loads are transmitted by the CLT floor diaphragms to the two concrete cores. Since the building footprint is 15 m x 56 m, the floor diaphragms require a large number of joints between single panels. The accumulated length of these edge joints in the 17 floor diaphragms is about 5 km.

Earthquake or wind loads on buildings cause diaphragm action in CLT members. Because of their high shear strength and stiffness, CLT members are especially suited for these in-plane loads. However, fabrication, transport and erection limit the potential size of CLT members. Consequently, wall or floor diaphragms are often composed of several smaller CLT elements joined at the edges (Figure 1-1). Using traditional connection techniques, e.g. nails, screws or special CLT connectors (Kögl and Maderbner, 2013), the edge connection only achieves between 10 % and 30 % of the shear capacity of the CLT itself. Of course, there are high performance connection systems available Polastri et al. (2016), but they are expensive.

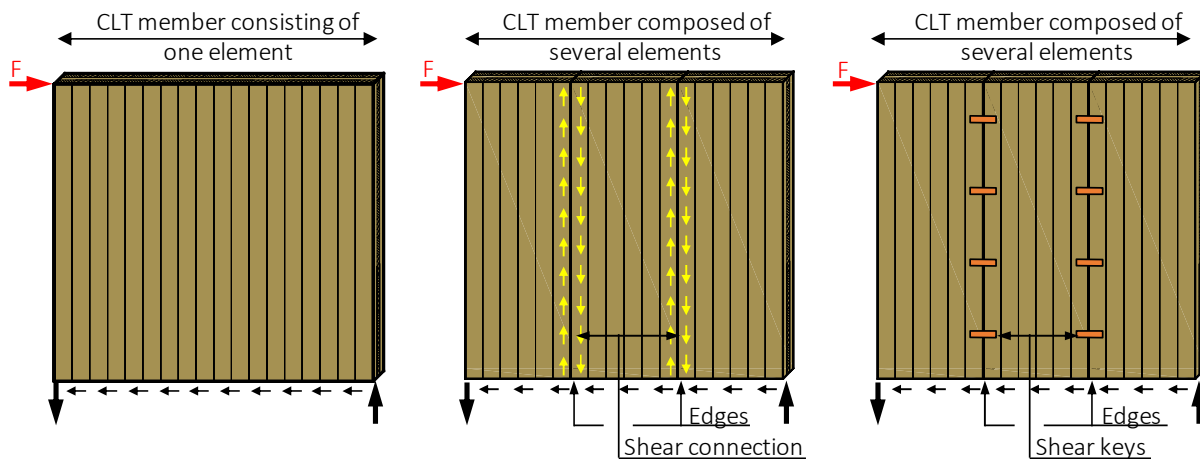


Figure 1-1 CLT shear walls.

The shear strength and stiffness of a CLT member composed of several elements are governed by the load-deformation behaviour of the edge connections. The load-carrying capacity of the CLT member and the shear connection, respectively, are hence not balanced and the high shear capacity of the CLT member cannot be exploited. To close the gap between the shear capacities of CLT and the shear connections, contact joints were developed. CNC automatic processing machines are already used to produce high capacity contact connections for linear timber members, see Enders-Comberg et al. (2015). Stecher et al. (2014) showed the use of dovetail connectors fabricated from Beech plywood to transfer shear along the edges of CLT members. In a first theoretical and experimental approach over 30 newly developed shear connections were considered Schmidt and Blass (2016).

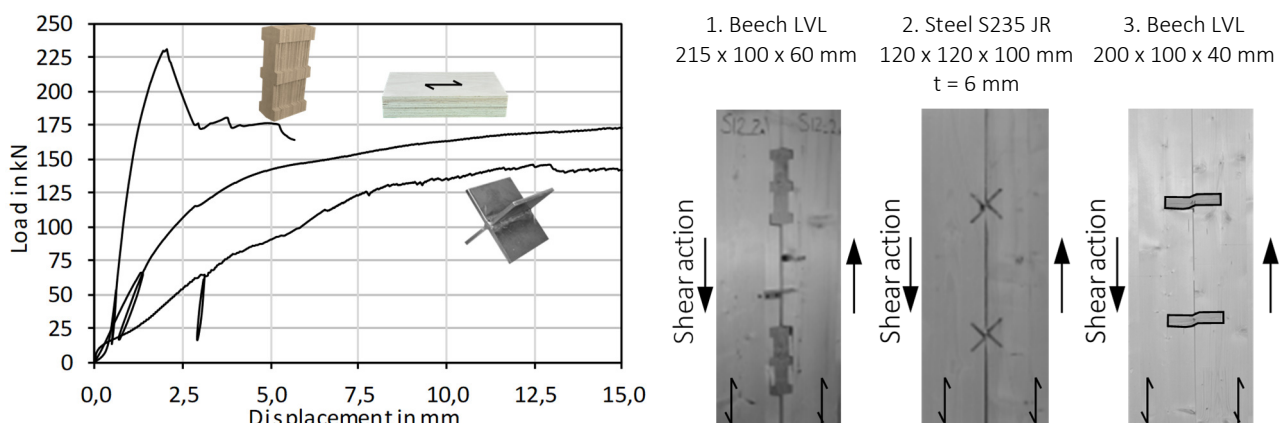
As a result of this first study two different joints with different mechanical properties were chosen for a continued and in-depth experimental and numerical study. While the first type of joint using Beech LVL shear keys is very suitable for floor diaphragms of buildings in earthquake prone regions, where high stiffness and load-carrying capacity but no energy dissipation is required, the second type including the steel plate fasteners is able to provide the necessary energy dissipation in CLT shear walls (Schmidt and Blass 2017). Both are aiming at easy fabrication using automatic processing machines and quick assembly at the construction site.

2 Contact joints for CLT wall and floor diaphragms

Figure 2-1 exemplarily shows the load-displacement curves of three different contact joints. The first connector oriented parallel to the joint line shows high initial stiffness and high load-carrying capacity. After a brittle shear failure, the connector shows a limited remaining load-carrying capacity, which mainly relies on the cross layers' shear strength. The stiffness and load-carrying capacity of the second – x-shaped – connector are significantly lower than the corresponding values of the first connector. However, the x-shaped connector advantageously is able to transfer loads parallel

as well as perpendicular to the joint line. The load-displacement behaviour of the third connector oriented perpendicular to the joint line is in between the first two connector types. Both connectors 2 and 3 reach an ultimate joint-displacement of 15 mm without a significant load decrease. In general, the load-displacement behaviour is mainly influenced by the CLT layup as well as the connectors' material, geometry, spacing and manufacturing precision.

Apart from requirements such as load-carrying capacity, stiffness or cost-effectiveness for connections in buildings, the robustness needs to be considered as well Starossek (2005). Progressive failure should be excluded as far as possible. Connections may contribute to load redistribution in structures and hence to increased robustness, if they behave in a ductile manner. Figure 2-1 shows that a shear key made of Beech LVL loaded perpendicular to the grain seems to be a suitable compromise between load-carrying capacity, stiffness and ductile behaviour resulting in robust CLT wall or floor diaphragms, Schmidt and Blass (2016). Consequently, an in-depth investigation of LVL shear keys loaded perpendicular to grain is presented in the following.



The three layer CLT had a symmetrical layup (40-20-40 mm) with a total thickness of 100 mm and a ratio of 4 between the sum of longitudinal layer thickness and cross layer thickness. The load was applied parallel to the longitudinal layers. Each specimen contains 2 connectors in the joint line.

Figure 2-1 Load-displacement curves of different contact joints.

Figure 2-2 shows the principal type of a contact joint for wall or floor diaphragms under static loads. The LVL shear keys are predominantly loaded in shear and compression perpendicular to the grain and show ductile load-deformation behaviour. Mainly the CLT members are loaded in compression parallel and perpendicular to the grain and in shear. The influence of shear key thickness t , penetration length t_e and the slenderness ratio t_e/t is studied here in order to further improve the load-carrying-capacity and stiffness of the connection and to create a basis for an analytical model and a design proposal.

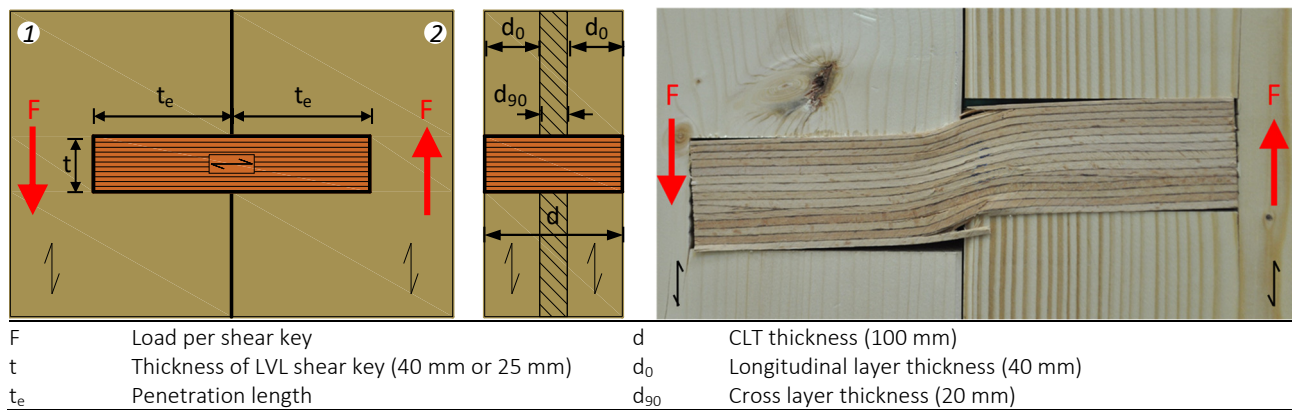
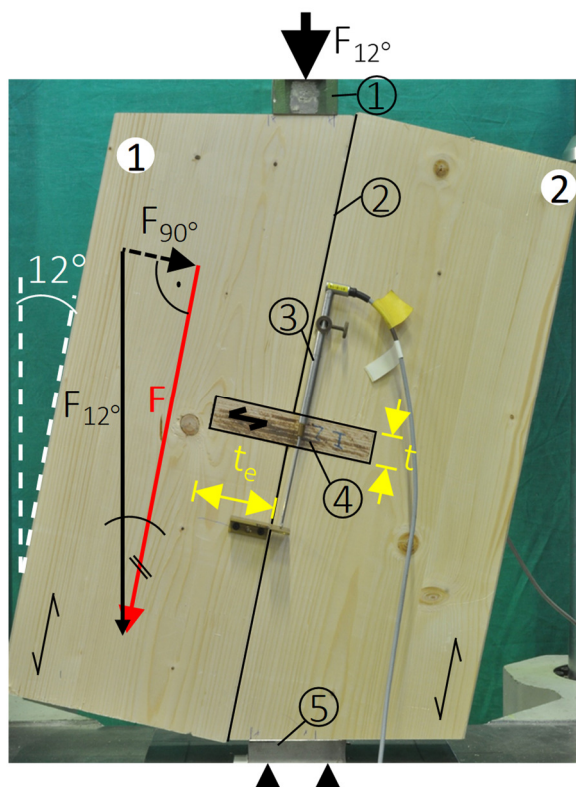


Figure 2-2 Shear key made of Beech LVL.

3 Materials and methods

The specimens including the CLT edge connection are symmetrical, i.e. the penetration length t_e is identical in both CLT members. Each specimen contained one shear key arranged in the edge of the CLT parts in the centre of the joint line. The tests were performed according to EN 26891 as compression shear tests (Figure 3-1). The slip parallel to the joint line was measured on both sides of the specimen using LVDTs. The evaluation of the test results is based on the load F parallel to the joint line and the average of both LVDT readings.



- 1 Load introduction (F_{12°)
- 2 Joint line: Length = 750 mm
- 3 LVDT (front and back)
- 4 Shear key
- 5 Steel plate support

Figure 3-1 Test set-up for compression shear tests.

European softwood (Norway spruce) CLT according to European Technical Approval ETA-11/0210 was used for the specimens. The three-layer CLT had a symmetrical layup (40-20-40 mm) with a total thickness of 100 mm and a ratio of 4 between the sum of longitudinal and cross layer thicknesses. Due to aesthetic reasons, the edges between adjacent longitudinal layer boards were bonded. However, for the edge bonding a non-structural adhesive is used and hence the edge glue lines must not be used in the determination of the in-plane shear strength of the CLT. The cross layers are not edge bonded. The effective characteristic in-plane shear strength of the CLT according to ETA 11/0210 is hence only $f_{v,k} = 1.6$ MPa for the full cross-section. The average gross density of the CLT specimens is 455 kg/m^3 with a Coefficient of Variation (COV) of 4.2 %. The average moisture content of the longitudinal layers is 10.7 % (COV 10.0 %). The shear keys were produced from Beech LVL with an average density of 800 kg/m^3 (COV 2.0 %) and a moisture content of about 7.5 %. 12 test series with 5 specimens each were performed using 25 mm or 40 mm thick shear keys with slenderness ratios between 1 and 3.5 (Table 3-1). The bending strength of some Beech LVL shear keys was determined at random for both thicknesses. For the 25 mm thick shear keys, a mean bending strength of 129 MPa with a COV of 10 % was determined; the corresponding values for the 40 mm thick shear keys is 117 MPa for the bending strength and a COV of 12 %.

Table 3-1. Test program.

t = 40 mm			t = 25 mm		
Series	λ	t_e in mm	Series	λ	t_e in mm
40-1	1	40	25-1	1	25
40-2	1.5	60	25-2	1.5	37.5
40-3	2	80	25-3	2	50
40-4	2.5	100	25-4	2.5	62.5
40-5	3	120	25-5	3	75
40-6	3.5	140	25-6	3.5	87.5

4 Results and discussion

Ductile load-deformation behaviour was observed for all test series independent of the slenderness ratio t_e/t . Figure 4-1 shows connections with different slenderness ratios after reaching the ultimate deformation of 15 mm. For lower slenderness ratios the shear keys rotated during the test while for slenderness ratios exceeding $\lambda = 2.0$ the shear keys were clamped in the CLT members. All specimens showed compression perpendicular to grain deformation in the shear keys, compression parallel to grain deformation in the CLT members and local splitting in the longitudinal layers of the CLT members at the end of the shear keys (Figure 4-1). The load carrying capacity F_{max} was defined as the maximum load before a relative displacement parallel to the joint line of 15 mm was achieved. For slenderness ratios < 2.0 the load-carrying capacity depends on the embedded length (Figure 4-2). Figure 4-3 shows the

load-displacement diagrams for the 40 mm thick shear keys. A relative displacement of 15 mm was reached for all specimens with shear key thickness 40 mm without significant load decrease. The corresponding displacement for 25 mm thick shear keys was about 12 mm. For slenderness ratios above 2 the ultimate load remains at the same level. Table 4-1 summarizes the test results. The COV of the ultimate load is between 2.1 % and 8.5 % for shear key thickness 40 mm and between 4.9 % and 13.2 % for shear key thickness 25 mm. The COV of the slip modulus is between 4.0 % and 9.5 % for shear key thickness 40 mm and between 9.6 % and 43.8 % for shear key thickness 25 mm.

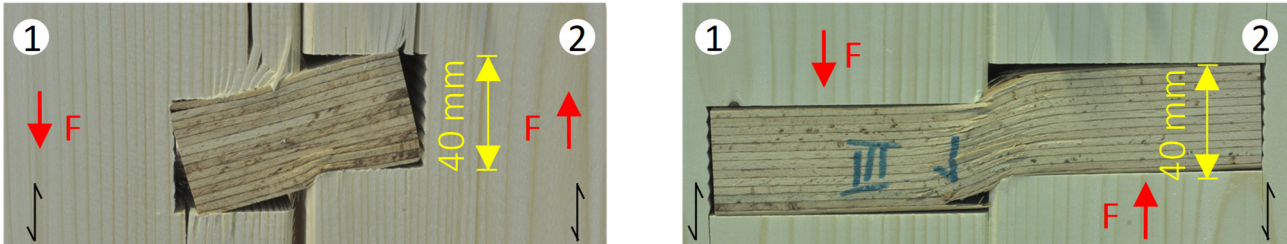


Figure 4-1 Connection with slenderness ratio $\lambda = 1$ (left) and $\lambda = 2.5$ (right) after the test.

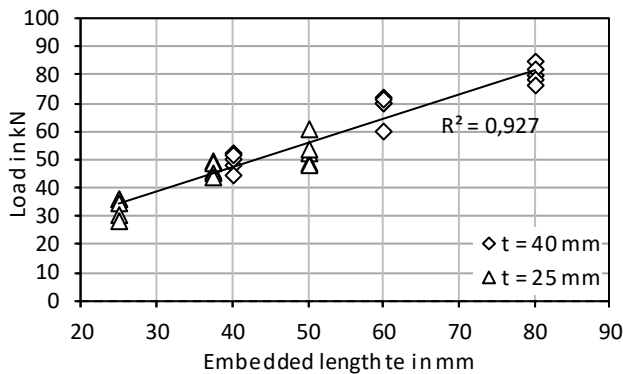


Figure 4-2 Correlation between the embedded length and the load-carrying capacity ($\lambda \leq 2.0$).

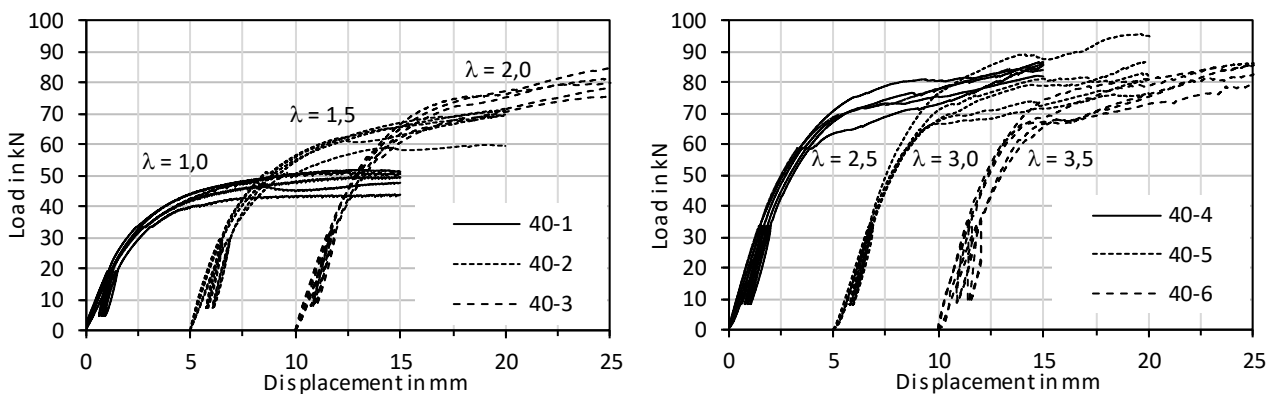


Figure 4-3 Load-displacement curves of connections with 40 mm thick shear keys. In order to improve readability, load-slip curves are partly moved to right on the abscissa.

Table 4-1. Test results.

t = 40 mm				t = 25 mm			
Series	λ	$F_{\max, \text{mean}}$ in mm	$k_{s, \text{mean}}$ in kN/mm	Series	λ	$F_{\max, \text{mean}}$ in mm	$k_{s, \text{mean}}$ in kN/mm
40-1	1	48.9	15.2	25-1	1	32.9	16.9
40-2	1.5	68.3	18.0	25-2	1.5	46.3	22.9
40-3	2	80.1	19.4	25-3	2	52.5	18.5
40-4	2.5	84.9	20.5	25-4	2.5	55.4	18.8
40-5	3	84.6	21.3	25-5	3	58.7	23.2
40-6	3.5	84.0	20.9	25-6	3.5	57.7	21.0

For larger connector slenderness ratios $\lambda \geq 2.0$ the load-deformation behaviour is significantly influenced by the compression perpendicular to grain failure of the shear key close to the joint line. The influence of other parameters decreases since the slender shear key is clamped into the indentation in the CLT member. This prevents rotation of the shear key and limits plastic compression deformation to a small area close to the joint line while connectors with a low slenderness ratio also cause plastic compression deformation at the connector ends both in the CLT parallel to the grain as well as in the connector perpendicular to the grain. Figure 4-4 left shows the distribution of compression stresses perpendicular to the grain in a 40 mm thick shear key at a joint displacement of 15 mm. The uneven stress distribution over the width of the connector caused by the different stiffness of the CLT longitudinal and cross layers is obvious. Plastic compression deformations only occur close to the joint line, at the shear key ends the stresses remain in the elastic range.

Mahler (2016)

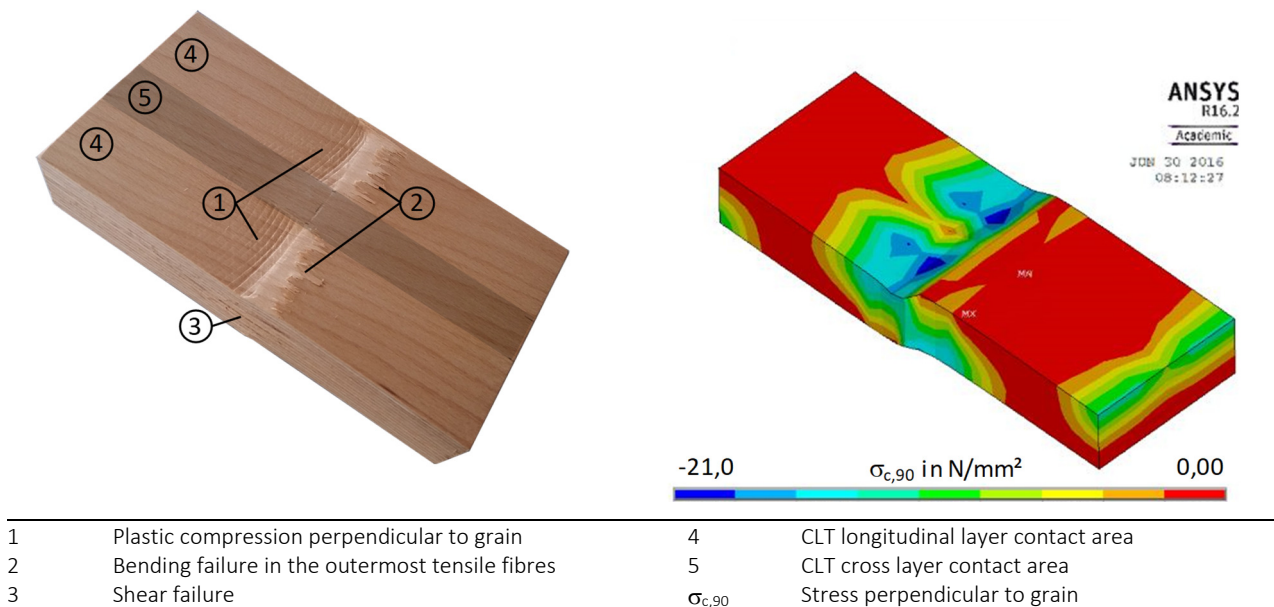


Figure 4-4 Shear key after the test (left) and distribution of compression stresses perpendicular to grain from FE results (right).

The uneven distribution of plastic compression deformation over the shear key width can also be observed in Figure 4-4 right. Apart from compression failure perpendicular to grain in the CLT longitudinal layer contact areas, the shear key also shows bending and shear failure when loaded up to 15 mm joint displacement. If the joint deformation is limited to 12 mm, the failure mode of slender shear keys predominantly is compression perpendicular to grain close to the joint line. The compression stresses further away from the joint line remain in the elastic range. A simplified design method hence should take into account this failure mode. In the load-displacement curves a significant strengthening effect couldn't be observed and consequently a significant rope effect doesn't occur. A numerical study with varying friction coefficient values not shown here confirms this observation.

5 Design method

Even though the real failure mode is a complex interaction of several failure modes including bending, shear and compression perpendicular to grain the governing failure mode is compression perpendicular to grain of the Beech LVL. In order to derive a simple and robust design method only compression perpendicular to grain of the Beech LVL is considered. This method is derived from a design method for reinforced concrete beams with a user-defined compression zone. In Germany, the same approach was used for timber columns directly clamped in concrete foundations Heimeshoff and Eglinger (1981). Figure 5-1 left shows the assumed stress distribution perpendicular to the Beech LVL shear key. After formulating moment and force equilibrium, transformations and simplifications lead to the design equation (1).

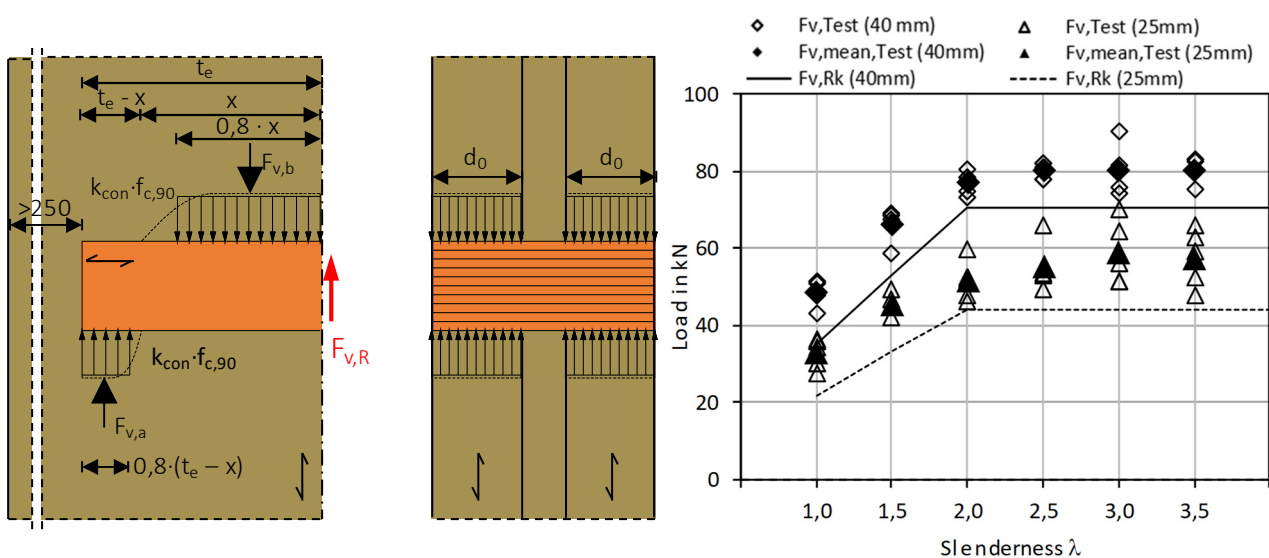


Figure 5-1 Mechanical model and assumed stresses for slenderness ≤ 2.0 (left) and test results at a displacement level of 12 mm in comparison with the determined characteristic load-carrying capacity $F_{v,Rk}$ based on the design model (right).

$$F_{v,Rk} = \begin{cases} \sum_i d_{0,i} \cdot 0,8 \cdot f_{c,90,k} \cdot k_{con} \cdot \frac{t_e}{2} & \rightarrow \text{for } 1,0 \leq \lambda \leq 2,0 \\ \sum_i d_{0,i} \cdot 0,8 \cdot f_{c,90,k} \cdot k_{con} \cdot t & \rightarrow \text{for } \lambda > 2,0 \end{cases} \quad (1)$$

Where:	25 mm ≤ t ≤ 40 mm; t _{e,1} = t _{e,2} Centre to centre spacing between two consecutive shear keys and loaded end parallel to the joint line ≥ 11·t
t	Shear key thickness
t _e	Shear key penetration depth
f _{c,90,k}	Compression strength of the LVL shear key perpendicular to grain, determined according to EN 408
k _{con}	Modification factor (k _{con} = 2.75)
Σd _{0,i}	Sum of longitudinal layer thicknesses
λ	t _e / t

Additional compression tests perpendicular to the grain of Beech LVL (Schmidt, 2018) were carried out to determine strength values depending on the deformation resp. compressive strain. In this special case, these strength values are more realistic than EN 408 based values, because the compression deformation in the additional tests complies with the deformation of the shear keys in the connection. This is in contrast to common tests, e.g. according to EN 408, where the compression strength perpendicular to grain is determined at a significantly lower deformation.

The modification factor k_{con} is calibrated based on characteristic values and considers:

- Higher strength values perpendicular to grain of the Beech LVL shear key than f_{c,90,k}-values, due to higher compressive deformation of the shear key,
- Different compression stress distributions perpendicular to the grain of the shear key between the real situation in a connection and in the additional compression tests,
- Contribution of protruding fibres of the shear key in the contact area of the CLT longitudinal layer and the shear key,
- Logarithmic normal distribution of the load-carrying capacity according to EN 14358 is assumed.

Figure 5-1 right shows the result of the calculated characteristic load-carrying capacity according to equation (1) in comparison with the test results at 12 mm displacement in the joint line. 12 mm was chosen to limit the potential inter-storey drift of the walls composed of several CLT elements. Since the contribution of the CLT cross layer to the load-carrying capacity is about 3 %, the design proposal only considers the contribution of the CLT longitudinal layers. It seems that the simple mechanical model is a sufficiently correct approach for all considered slenderness ratios to calculate the load-carrying capacity of Beech LVL shear keys loaded perpendicular to grain.

For CLT layup used in the tests a single Beech LVL shear key with 40 mm thickness and a slenderness ratio ≥ 2.0 reaches a characteristic load carrying capacity of F_{v,Rk} = 70.4 kN (f_{c,90,k} = 10 MPa). Since an in plane shear connection in the edges of CLT members consists of several consecutive shear keys in a joint line, it is obvious that

consideration of a single connector is not sufficient. A longitudinal shear failure of the CLT needs to be considered as well since this failure mode caused a significant load decrease in some load-displacement curves of the shear key connections.

6 Spacing rules and effective number of connectors

In order to determine minimum spacing in longitudinal direction two test series with 6 tests using the same CLT material as described before were carried out (shear key thickness $t = 40$ mm, slenderness $\lambda = 2.5$). The tests were performed according to EN 26891 as compression shear tests. As described before, the specimens including the CLT edge connections are symmetrical. Each specimen contained two shear keys arranged in the edges of the joint line. Two additional recesses at the beginning and the end of the joint line without a shear key make sure that the CLT shear stresses were similar to the situation in a continuous joint line. The difference between the two test series is the spacing between the shear keys.

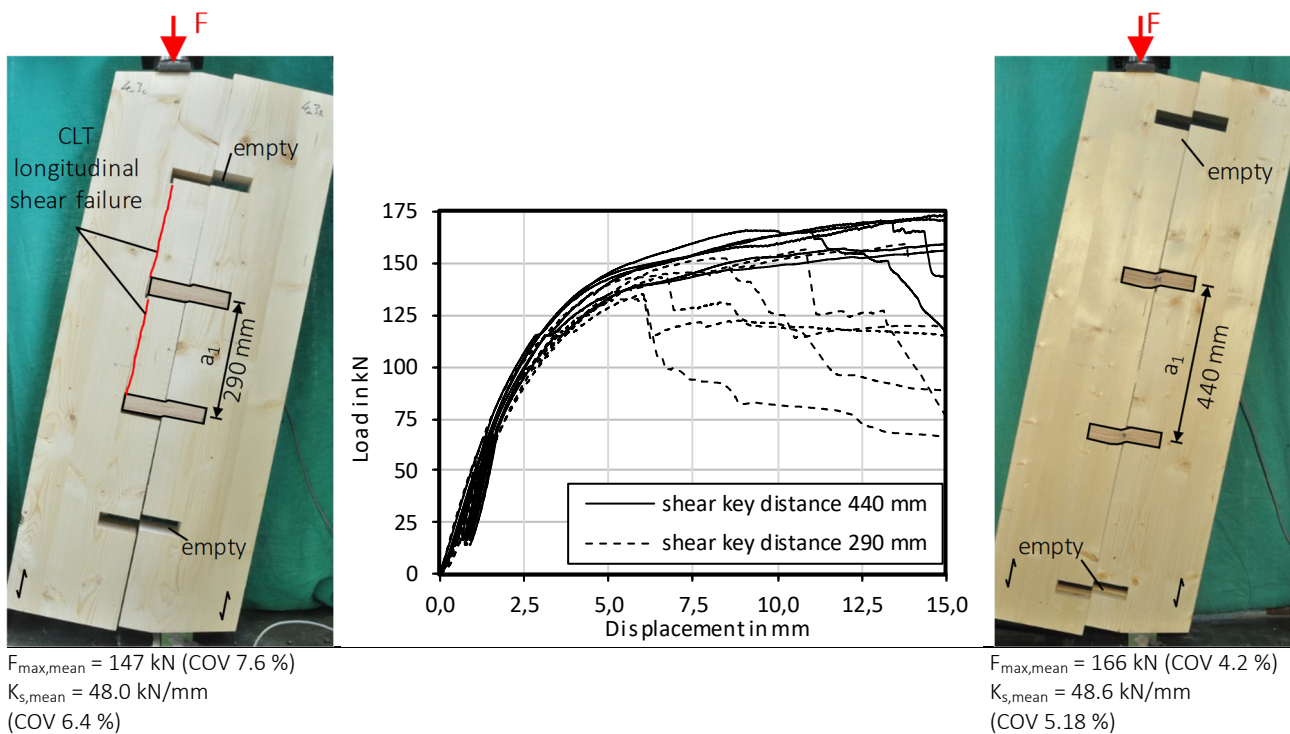


Figure 6-1 Compression shear test with different spacing with two shear keys in a joint line.

A small shear key spacing ($7.25 \cdot t$) finally leads to longitudinal CLT shear failure (Figure 6-1 left). After brittle shear failure, the connection showed a reduced load-carrying capacity. This failure mode can largely be avoided with increased spacing of $11 \cdot t$. Then mostly a displacement of 15 mm was reached without significant load decrease, while the most prominent failure mechanism is perpendicular to grain compressive

failure of the shear key (Figure 6-1 right). Furthermore, a larger shear key spacing has a significant influence on the load-carrying capacity: +12.9 % (Figure 6-1 middle). Connection stiffness was hardly influenced by shear key spacing.

The remaining load-carrying capacity after brittle shear failure of the CLT with small spacing may be explained by the following mechanism: due to the higher shear stiffness of the longitudinal layers before the first shear failure, the load is nearly completely transferred from the shear key into the end grain surfaces of the CLT longitudinal layers. After a sudden shear failure within the longitudinal layer, two possible load paths remain: part of the load is transferred from the longitudinal layers via rolling shear into the cross layer, another part into the contact area of the cross layers perpendicular to the grain. The shear capacity of the cross layer hence explains the remaining shear capacity after first brittle failure.

As expected, the average load-carrying capacity of two consecutive shear keys does not reach the same level as two times the load-carrying capacity of a single shear key (test series 40_4: $2 \cdot F_{\max} = 2 \cdot 85.2 \text{ kN} = 170 \text{ kN}$ compared to 166 kN, see Figure 6-1 right). In this configuration with 11-t, the effective number is $n_{\text{ef}} = 1.94$.

In order to verify the influence of the number of shear keys in a joint line on the load-carrying capacity a numerical study will consider consecutive shear keys with different load-displacement curves and different production inaccuracies. Preliminary results confirm this experimental finding for higher displacement levels. However, at lower displacement levels n_{ef} is significantly influenced by production tolerances. Consequently, the effective number of shear keys has to be considered in serviceability limit state, too. Otherwise, the diaphragm stiffness is significantly overestimated.

7 Conclusion

Shear keys made of Beech LVL and loaded perpendicular to the connector plane show ductile load-displacement behaviour. A possible brittle shear failure of CLT between two consecutive shear keys is avoided by minimum spacing of 11 times the shear key thickness. If additionally a minimum slenderness ratio of 2.0 is observed, the connections achieve high load-carrying capacity with low variation. The higher the slenderness ratio, the lower are fastener rotations and the subsequent forcing apart of two connected CLT members. Secondary connections are necessary to transmit forces perpendicular to the joint line.

The joints for floor diaphragms were also modelled numerically and a good agreement between test and simulation results was found. An analytical model was derived to determine the load-carrying capacity. Since the load between CLT and shear key is transferred via the longitudinal layers of CLT, the load-carrying-capacity primarily depends on the contact area between CLT longitudinal layers and Beech LVL connector. Consequently, the proposed design model only considers the accumulated

longitudinal layer thicknesses and the compression strength perpendicular to grain of the Beech LVL shear key.

Further refining of the connection geometry as e.g. a tapered shape will lead to a quick assembly. Here, further numerical and experimental studies will follow.

Although the fastener is wood-based, the joints show ductile load-slip behaviour. Beech LVL or Beech plywood seem to be very suitable materials for these wood-based connectors.

8 References

- Enders-Comberg M, Frese M, Blass HJ (2015): Beech LVL for trusses and reinforced glulam. Bautechnik 92, Heft 1, Pages 9 – 17. DOI: 10.1002 / bate.201400076. Article in German.
- Heimeshoff B, Eglinger W (1981): Einspannung von Holzstützen durch Verguss im Betonfundament (in German). Untersuchungsstufe I. Lehrstuhl für Holzbau und Baukonstruktionen, Technische Universität München. IRB Verlag. Stuttgart.
- Kögl J, Maderebner R (2013): System connectors for cross-laminated timber panels. 19. Internationales Holzbau-Forum, Garmisch-Partenkirchen.
- Mahler P (2016): Experimentelle und numerische Untersuchung zur Tragfähigkeit von Kontaktverbindungen in Brettsperrholz (in German). Master's Thesis, July 2016, Karlsruhe Institute of Technology, Timber Engineering and Building Construction, Karlsruhe.
- Polastri A, Giongo I, Pacchioli S, Piazza M (2016): Structural analysis of CLT multi-storey buildings assembled with the innovative X-RAD connections system: Case-study of a tall building. Proceedings of the 2016 World Conference on Timber Engineering (WCTE), 22-25 August, World Conference on Timber Engineering, Vienna, Austria.
- Schmidt T, Blass HJ (2016): Contact joints in engineered wood products. Proceedings of the 2016 World Conference on Timber Engineering (WCTE), 22-25 August, World Conference on Timber Engineering, Vienna, Austria.
- Schmidt T, Blass HJ (2017): Dissipative joints in CLT shear walls. Proceedings of the International Network on Timber Engineering Research 2017 (INTER), 28-31 August, Kyoto, Japan.
- Schmidt T (2018): Kontaktverbindungen für aussteifende Scheiben aus Brettsperrholz (in German). PhD thesis, KIT Scientific Publishing.
- Starossek U (2005): Progressiver Kollaps von Bauwerken. Beton- und Stahlbetonbau (in German). Sonderdruck, Heft 4, Pages 3-15.
- Stecher G, Kögl J, Beikircher W (2014): Mechanical behavior of dove-tail connections for Cross Laminated Timber wall elements, Proceedings of the 2014 World Conference on Timber Engineering (WCTE), 10-14 August, World Conference on Timber Engineering, Quebec City, Canada.

Discussion

The paper was presented by T Schmidt

R Harris stated that they studied oak dowel joints and FRP joints where compatibility between shear connector and wood and FRP connection behaviour are the key issues. Wedges were created to lock in the joint as resistance to initial horizontal movement is weak. He asked how to hold the joint together.

T Schmidt responded that it is not a problem in the test setup as compression is activated. In real structure, one needs a chord member to hold the system together.

F Lam commented that in Canada the Seismic design community suggests that diaphragms need to behave linear-elastically so that ductile energy dissipation happens in the prime lateral resistant elements. Here very large forces would need to be transmitted linear-elastically in the diaphragm splines. This is particularly true for concrete wood hybrid system. H Blass asked how would the nail spline work in the UBC Brock Commons building. F Lam said that it would not as this thinking was initiated after the building was built. In addition there exists a concrete layer which could help provide the shear transfer in the plan of the diaphragm.

P Quenneville said that this system can also be used in shear walls.

A Frangi asked about the possible initial slip from humidity effects and asked if there was initial slip in test which may be different from field application. T Schmidt and H Blass said that the ETA has conical shape of connector to provide good contact.

A Frangi and T Schmidt discussed about the depth of the shear key elements versus the depth of the panels as an issues that can be optimized.

C Sigrist asked how to get the tolerance in the building site. H Blass responded that the first shear key will align the member as CNC production can meet the 0.5 mm precision.

E Serrano and H Blass discussed the width of the CLT laminae may create a gap at the end of the shear key. H Blass said that tension test perpendicular to grain is created within the full board in cases without gaps. In cases with gaps (i.e. without a full board) different stress distribution would result but should not affect the load slip behaviour.

BJ Yeh asked about loading horizontally which could cause the diaphragm to open up. H Blass said that the diaphragm needs chord which will keep the diaphragm from opening up.

F Lam received confirmation that full scale diaphragm tests were performed.

Seismic response of connections with glued-in steel rods

Jelena Ogrizovic, ETH Zurich

Robert Jockwer, ETH Zurich

Andrea Frangi, ETH Zurich

Keywords: Glued-in rods, cyclic loading, seismic design

1 Introduction

Connections in timber with glued-in rods (GIR) have gained popularity in recent years, thanks to the high strength and stiffness that can be achieved. The field of application of these connections is diverse, ranging from the hinged connections, to beam joints and moment resisting connections (Gehri, 2010). Moment resisting connections with glued-in rods can be implemented in the connections of columns and walls to the foundation, in the beam-column connections or to provide continuity in long timber elements. Employment of moment-resisting connection in timber structures results in reduced element sizes and improved robustness, due to the load redistribution.

Extensive research has been conducted in the last 30 years (Tlustochowicz et al., 2011) and efforts are made to include design provisions for connections with glued-in rods in the European design code and in international standards. One of the essential issues related to GIR that have to be dealt in a design code are specifications regarding seismic response.

2 Connections with glued-in rods under cyclic loading

The performance of connections with glued-in rods under cyclic loading has been studied by several researchers. The experiments of Gattesco et al. (2017) showed that it is possible to achieve a ductile moment-resisting connection using mild steel

and designing with sufficient glued-in length, however the achieved ductility under cyclic loading is smaller than under monotonic loading. The experiments of Ogrizovic et al. (2017) investigated the performance of moment-resisting connections with glued-in steel rods under cyclic loading, using softwood and hardwood glued laminated timber (glulam), as well as hardwood laminated veneer lumber. Performance of connections with hardwood proved to be superior, compared to softwood. Figure 1a) illustrates the loss of capacity due to premature local failures in columns made of spruce glulam, thus hindering development of highly ductile response on the connection level that can be observed for hardwood in Figure 1b). The ductility observed in the experiments with softwood might be sufficient only in regions with low seismicity, better understanding of the connection behaviour could widen the field of application of the connections with glued-in rods. It is important to adequately estimate the strength, stiffness and ductility of the connection in order to perform seismic design of the structure. While the strength and ductility determine the capacity of the structure, the stiffness is important for calculating the seismic demand.

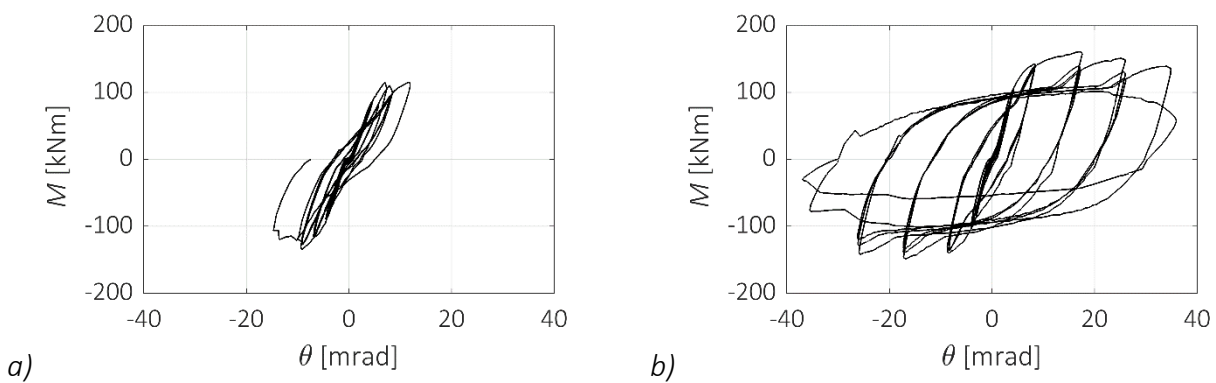


Figure 1. Examples of the moment-rotation response of two connections with the same layout and steel quality, and different timber quality (Ogrizovic et al., 2017). a) Spruce glulam. b) Ash glulam.

In the study of Ogrizovic et al. (2017) it was not possible to detect the actual cause of the early failure of the spruce columns, hence it was deemed necessary to gain more knowledge about the single-rod connection response, when subjected to cyclic axial loading. One of the possible explanations for the behaviour observed is that a combined failure mode, i.e. yielding of the steel rod followed by the pull-out failure instead of the tensile failure in steel, took place. Parida et al. (2013) performed a series of pull-out tests, demonstrating that such failure mode can occur when the pull-out capacity is larger than the yield strength but smaller than the ultimate tensile strength of the rods. Preliminary monotonic pull-out tests were performed in the study of Ogrizovic et al. (2017), on the single-rod specimens with the same geometry as those built into the full scale column. Yielding of the steel and tensile failure took place, as intended for the chosen configuration. Local failures in moment-resisting connections could only be explained as the influence of cyclic loading.

The seismic performance of the single-rod connections has not been studied before. However, fatigue of connections with glued-in rods has been investigated. One of the studies was performed in the scope of the GIROD project (Bainbridge et al., 2002). The experimental results indicate a reduction of the pull-out capacity, even for a low number of cycles, especially for the case of reversed loading. A design approach using fatigue modification factor to reduce the design fatigue strength with respect to the characteristic strength for static load was proposed. The results of studies of Tannert et al. (2016) confirmed similar fatigue behaviour for connections with fibre reinforced polymer rods.

The goal of the study presented is to investigate if a similar reduction of capacity can be observed in cyclic tests with increasing amplitude, representing the seismic loading. The features investigated are the influence of cyclic loading nature on the pull-out capacity of the connection, typical connection response under cyclic loading with presence of yielding and the influence of glued-in length on ductility.

3 Experimental investigation on single-rod connections

An experimental campaign on connections with single glued-in rods was conducted at ETH Zurich. The connections were subjected to axial loading in tension and compression. The main goal of the campaign was to investigate the behaviour of the connections subjected to cyclic loading and the failure modes that can occur. Furthermore, attention was given to evaluating the connection stiffness in both monotonic and cyclic loading.

3.1 Materials and methods

30 single-rod specimens were investigated in the experiments in a “pull-pull” configuration. Two types of experiments were performed, i.e. pull-out tests with monotonic application of tensile force and cyclic tests with half-cycles in tension and compression. The specimens were produced with the rod diameter of 16 mm. The parameters varied in the experiments were the glued-in length l_a , the unbonded length l_u and the quality of steel (see also Table 1). Failure in timber was expected in all experiments using high-strength steel, while ductile failure was predicted for experiments using mild steel.

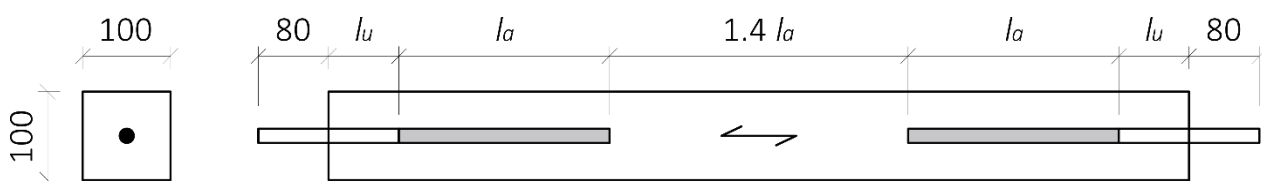


Figure 2. Schematic representation of the test specimen.

All specimens were produced with spruce glulam of grade GL24h, according to EN 14080:2013. They were produced with a cross-section of $100 \times 100 \text{ mm}^2$, as shown in Figure 2. The length of the specimen was adjusted to the glued-in length, according to the Draft standard for the testing of GIR (CEN/TC 193, 2018), while the size of the cross section corresponded to the specimens tested by Ogrizovic et al. (2017), as no splitting failure occurred during the campaign for connection with the same diameter of the rod. The steel rods were glued into the pre-bored holes using epoxy based adhesive Mastifix (Renoantic, 2018). During production, a nut was mounted on each rod to ensure the close contact between the timber specimen and the connection plate. At the control of the specimens before the experiments, drying cracks and inclination of glued-in rods up to 2 % were observed on several specimens. Although this was not ideal for the experiments, such conditions can easily be expected in real applications.

The experiments were performed in a universal testing machine with a capacity of 1600 kN. The test setup presented in Figure 3 was designed to transfer both tension and compression. Tension was transferred via steel rod, while both the rod and surrounding timber were loaded in compression half-cycles. This was accomplished by inserting the steel rods in the threaded holes in the connection plates on both ends of the specimen. The connection plates were then clamped to the ground plates of the testing machine.

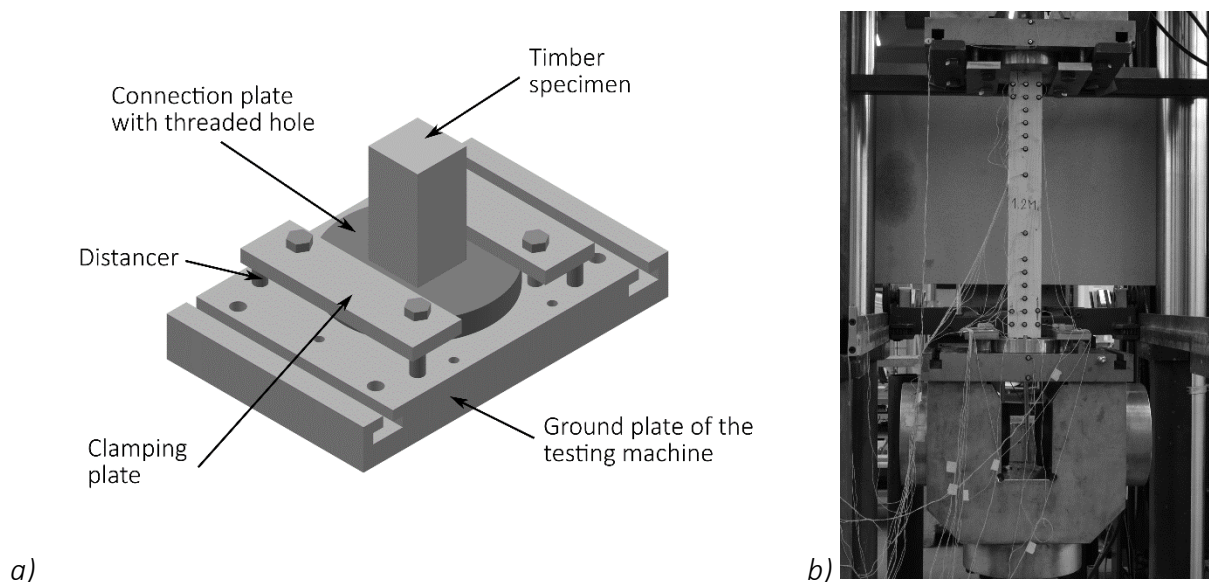


Figure 3. Test setup. a) Connection detail. b) Practical application.

Variations of parameters resulted in 9 different configurations tested, according to Table 1. Configurations 1-3 were tested under monotonic and cyclic loading, to investigate the influence of the loading nature on the pull-out capacity. Configurations 4-6 were tested only under monotonic loading, to investigate if there is significant influ-

ence of the unbonded length on the pull-out capacity. Configurations 1-6 were designed with high-strength steel to induce the bond-line failure. Configurations 7-9 were tested only under cyclic loading, to investigate the behaviour including yielding and large deformations and the influence of glued-in length on the ductility of the connection. These specimens were designed following the principle of good GIR design, namely designing the connection for ductile failure in the steel rods.

Table 1. Overview of the specimens and experiments.

Configuration No.	Steel grade	l_a [mm]	l_u [mm]	Type of experiment	Number of tests	Density [kg/m ³]
1	10.9	240	-	Monotonic	3	389/451/406
				Cyclic	3	457/382/470
2	10.9	320	-	Monotonic	3	420/398/418
				Cyclic	3	406/462/381
3	10.9	400	-	Monotonic	3	546/470/515
				Cyclic	3	475/379/391
4	10.9	240	80	Monotonic	1	406
5	10.9	320	80	Monotonic	1	375
6	10.9	400	80	Monotonic	1	406
7	4.8	240	80	Cyclic	3	416/372/412
8	4.8	320	80	Cyclic	3	395/388/374
9	4.8	400	80	Cyclic	3	403/369/381

The monotonic tensile tests were performed with displacement control. The constant displacement rate of 0.01 mm/s was chosen as to achieve the failure of the connection within 300 ± 120 s (CEN/TC 193, 2018). The specimens were firstly loaded up to 40 % of the expected pull-out capacity, unloaded to approximately 5 % of ultimate load, and reloaded until failure, defined as sudden loss of capacity.

The monotonic pull-out tests were performed in the beginning of the testing campaign, as a benchmark. The same configurations were subjected to cyclic load, to investigate the influence of cyclic loading on the pull-out capacity and the failure mode. A symmetrical loading procedure was chosen, as this is typical for the performance assessment of structural components (Krawinkler, 2009). According to experience of Bainbridge et al. (2002), reversed loading is also the most severe scenario when the fatigue behaviour of connections with glued-in rods is investigated. Symmetrical loading is to be expected in a base connection, while tensile deformation would prevail in a beam-column connection with glued-in rods. The cyclic loading procedure was adopted according to Casagrande & Piazza (2018). Constant displacement rates of 0.01 mm/s and 0.1 mm/s were used for the loading in the elastic and inelastic range, respectively, as illustrated in Figure 4. The estimated yield displacement necessary for

the specification of the loading procedure was calculated for the specimens with M16 4.8, which are the only specimens that indeed experience yielding. By using the same procedure for the cyclic experiments the resulting pull-out failure allowed a comparison of the two sets of experiments. In the experiments with mild steel, the influence of glued-in length on the ductility of the connection and the influence of large deformations due to yielding on the connection capacity were investigated.

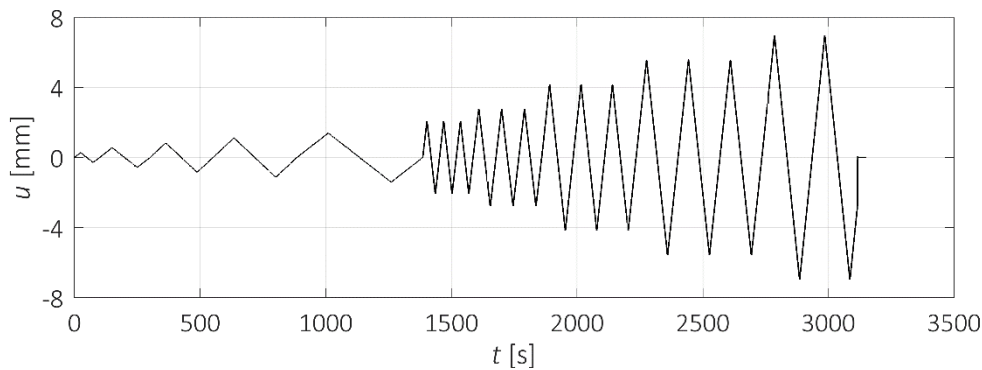


Figure 4. Loading protocol for cyclic tests.

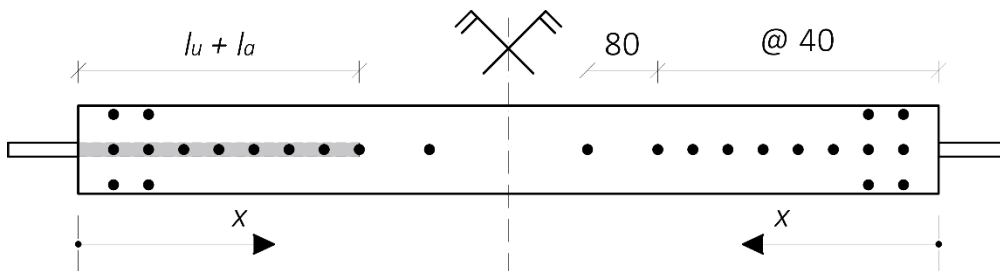


Figure 5. Layout of the sensors for the optical 3D measurement system. Distances in [mm].

Deformation of the specimens was measured with an optical 3D measurement system (NDI). The light emitting diodes were distributed along the length of the specimen, with multiple sensors positioned at both ends of the specimen, since the largest deformations were expected in these locations (Figure 5). The exact 3D coordinates of these diodes were recorded at a measurement frequency of 5 Hz by a camera unit and allowed for the determination of absolute and relative displacements in all recorded points. The applied load was measured by a load-cell together with the deformation of the testing machine and were recorded in parallel by the system NDI.

3.2 Experimental results

The experimentally measured capacity of the connections was compared with the analytical approaches in Figure 6. The presented values of pull-out force and bond shear strength contain correction to take into account the influence of density. Linear correlation between the strength and density, and reference density of 420 kg/m^3 were

adopted (CEN/TC 193, 2018). In Figure 6a), the corrected measured force is compared with the expected range of pull-out capacity $F_{est.,k}$ calculated using the proposals of prEN1995-2:2003 and Riberholt (1988). The calculations are made for brittle glue and timber density of 420 kg/m^3 . The measured pull-out capacity exceeds the predictions of characteristic pull-out strength. In Figure 6b), the results are expressed in terms of bond shear strength and compared to prediction according to Aicher & Stapf (2017). The measured bond shear strength exceeds the prediction of mean bond shear strength for the longer glued-in lengths, while the mean bond shear strength for very short glued-in lengths is overestimated by this prediction. The results of experiments performed on the specimens that contain unbonded length are in the upper range of the measured values. The experiments do not indicate significant decrease of pull-out capacity in cyclic tests, in comparison to monotonic tests.

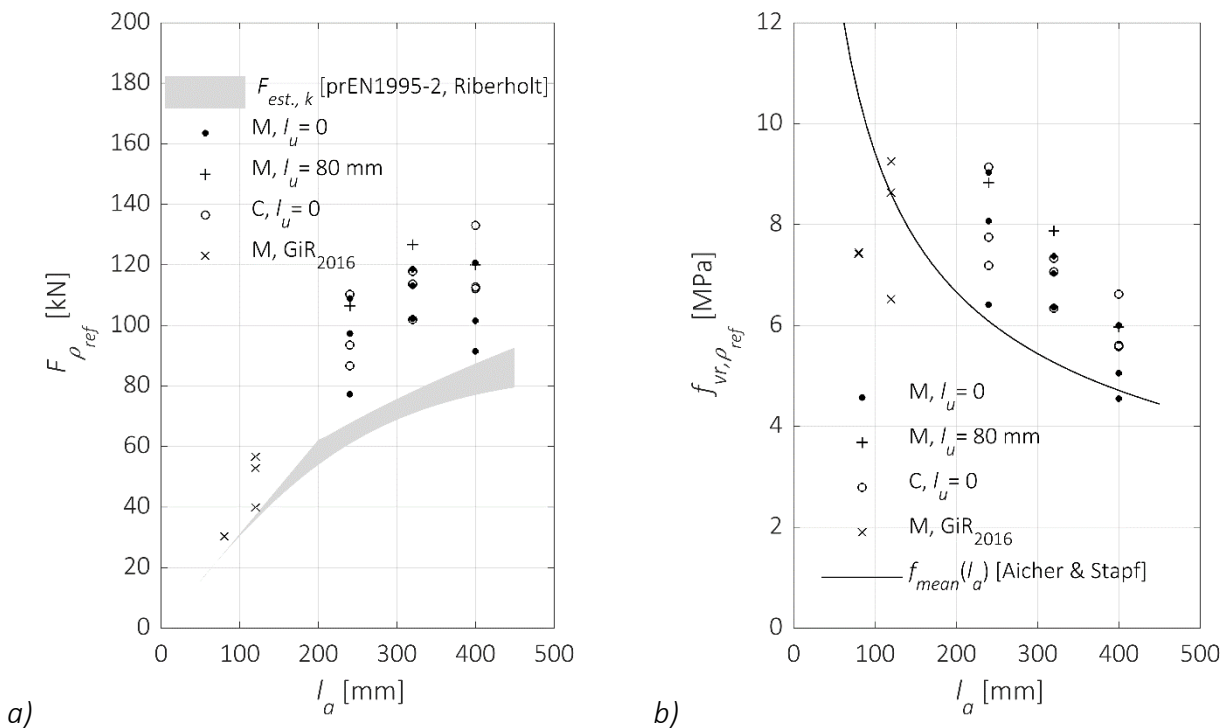


Figure 6. Results of the monotonic (M) and cyclic (C) tests with the given unbonded length l_u ; results of the monotonic tests performed within experimental campaign in 2016. a) Pull-out force and estimations of characteristic strength. b) Bond shear strength and predictions of mean strength.

The typical failure modes observed in the monotonic tests were the pull-out and the splitting failure. Brittle failure took place because the specimens were produced with high-strength steel. The pull-out failure is characterized by the shear failure in the timber or on the interface between the timber and the adhesive, as illustrated in Figure 7a). Figure 7b) depicts the splitting failure, characterized by the development of large cracks in timber and loss of bond between the adhesive and the rod. The loss of

bond is considered to be an important factor in the splitting failure, as it leads to expansion of the connection, thus introducing radial tension stresses that lead to crack formation. Splitting failure in a monotonic test is presented in Figure 8a).

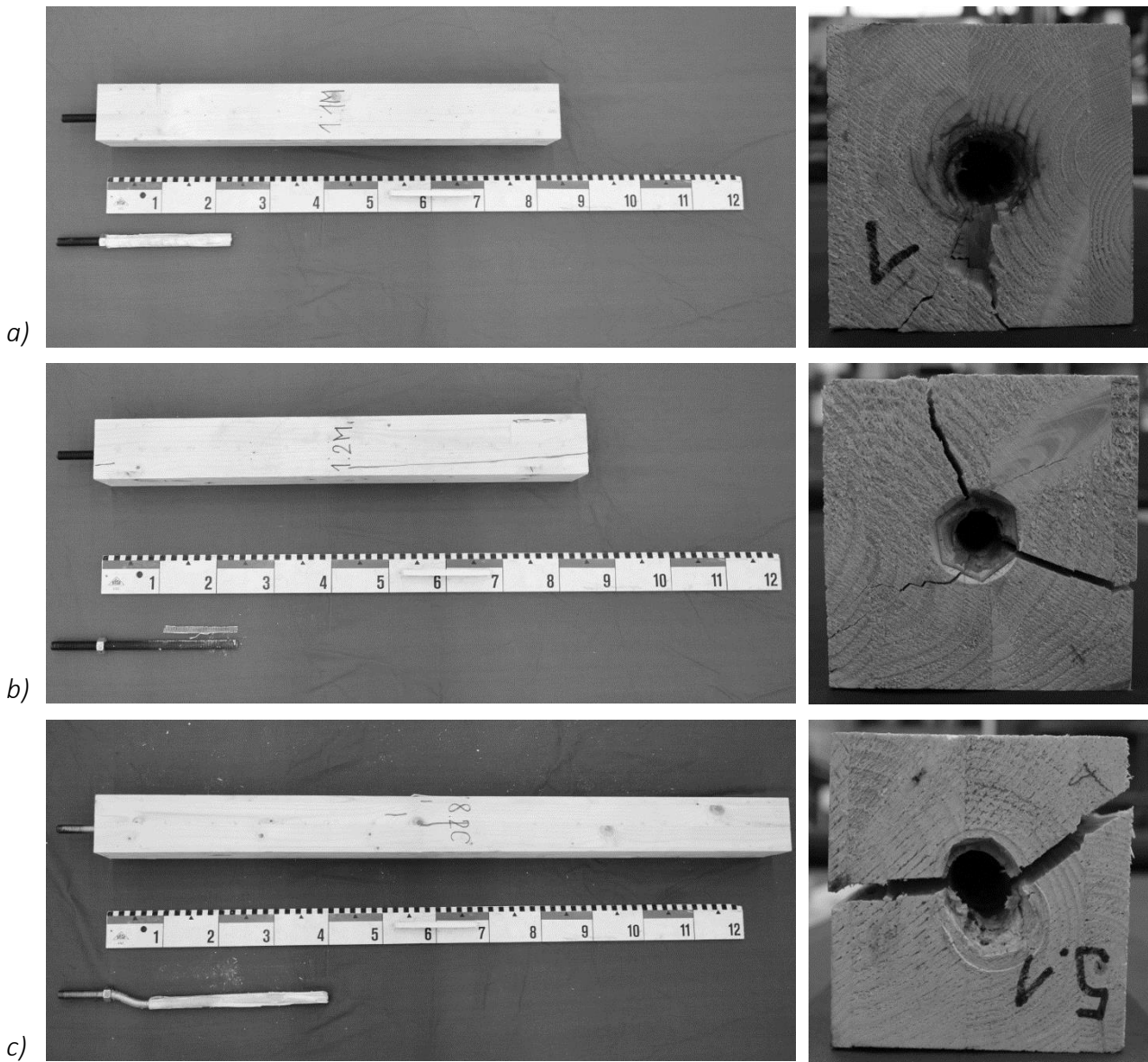


Figure 7. Failure modes. a) Pull-out failure with loss of bond between timber and adhesive. b) Splitting failure with loss of bond between steel rod and adhesive. c) Yielding of the steel rod, followed by buckling of steel rod, failure in compression parallel to grain and splitting.

The minimum rod to edge distances according to Tlustochowicz et al. (2011) were respected, hence only the pull-out failure was initially expected. Possible reason for the splitting failure could be related to excessively large forces introduced to the specimens. The specimens were produced with relatively large glued-in length, with respect to the diameter of the rod. Choosing high-strength steel, the failure of the rod was prevented and a brittle failure took place instead. Interestingly, the splitting failure cannot be related to initial imperfections, e.g. pre-existing cracks or inclination of

the rod, as both pull-out and splitting failure occurred for specimens with and without noticeable inaccuracies in the production. Furthermore, the splitting failure did not always occur at force levels lower than for pull-out failure.

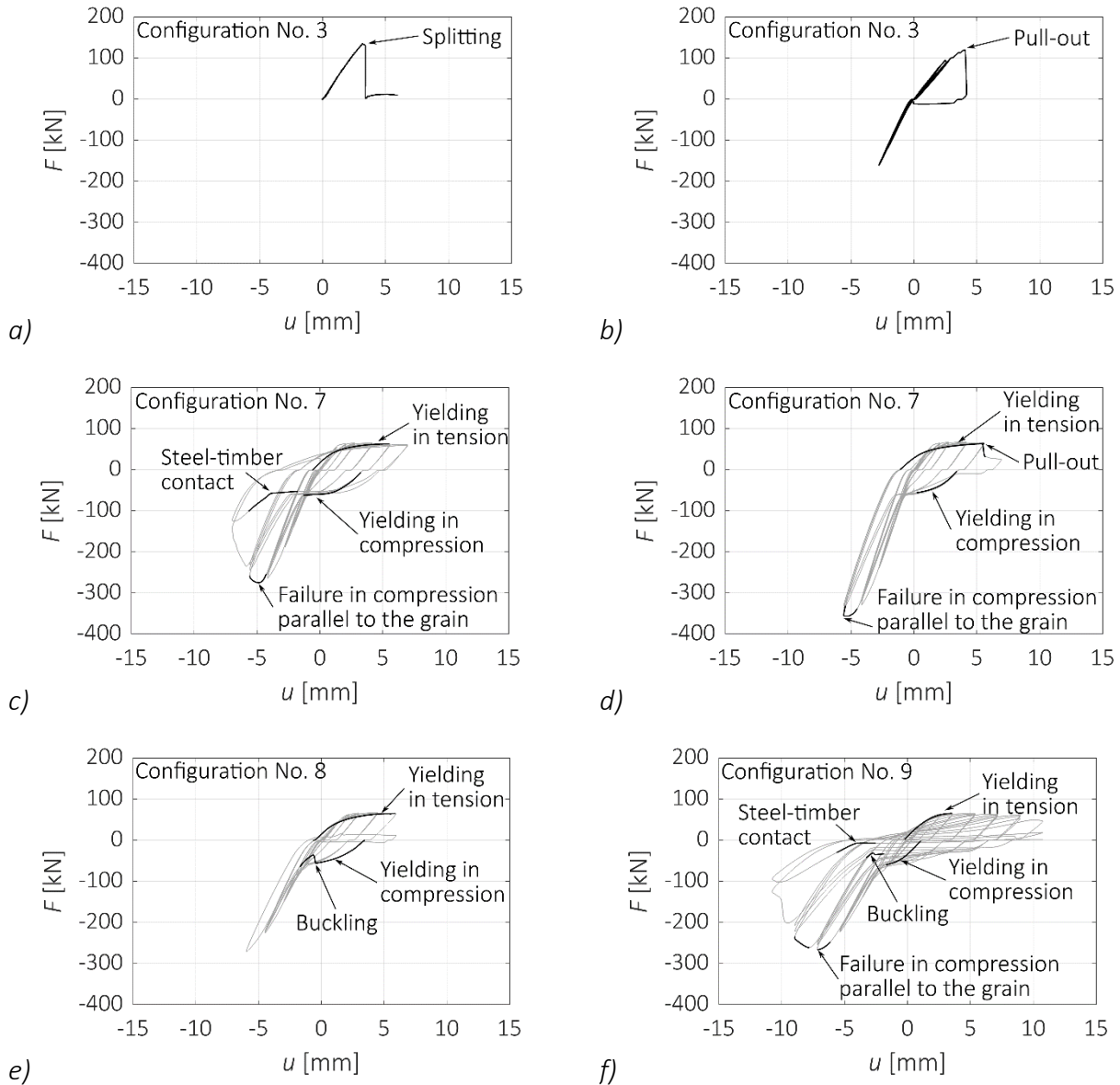


Figure 8. Failure modes representative of the testing campaign. a) Splitting in a monotonic test. b) Pull-out in a cyclic test without yielding. c) Failure in compression parallel to the grain in a cyclic test with yielding. d) Pull-out failure in a cyclic test with yielding. e) Buckling failure in a cyclic test with yielding. f) Combined failure in a cyclic test with yielding.

Typical failure modes in cyclic tests performed on the specimens with high-strength steel were the same as in the monotonic tests, i.e. the pull-out and the splitting failure. Figure 8b) depicts a pull-out failure in a cyclic test. Typical failure modes in the cyclic tests on the specimens with mild steel were yielding of steel, failure in compression parallel to the grain and buckling of steel rods, as shown in Figure 7c). Yielding in tension and compression was observed in each experiment with mild steel. The

steel rod is the only element of the connection that can accommodate tension forces, while compressive forces are accommodated by the rod and the timber section. Compression is transferred to timber via contact with the connection plate. Due to the initial imperfections, this contact is usually not present at the beginning of the experiment and it is established after the compressive force is introduced. After yielding it is easy to detect when the contact is established, which can be seen in Figure 8c) as an increase of stiffness. The response is largely influenced by the timber properties and geometry of the specimen, as the failure in compression parallel to the grain takes place. The experiments have shown that pull-out failure can also take place after yielding of the rod, on the load level lower than expected based on the results of pull-out tests in Figure 6a). This failure mode, presented in Figure 8d), was observed on a single specimen in the configuration with the shortest glued-in length. Buckling was observed for longer glued-in lengths. The conditions leading to buckling only occurred after yielding, with an increase of unbonded length and the gap between the timber specimen and the connection plate, due to plastic deformation of the steel rod. The typical failure mode with buckling is presented in Figure 8e). Figure 8f) shows that a combined failure with buckling and compression parallel to the grain can also occur. Large decrease of stiffness throughout the experiment could be observed.

The position of the sensors and the distribution of deformation along the specimen is depicted in Figure 9. The load level of 40 kN is chosen because all of the specimens respond in an elastic manner. It is possible to see that the deformation is concentrated at the end of each specimen, independent on the unbonded length. Similar distribution is observed for tension and compression.

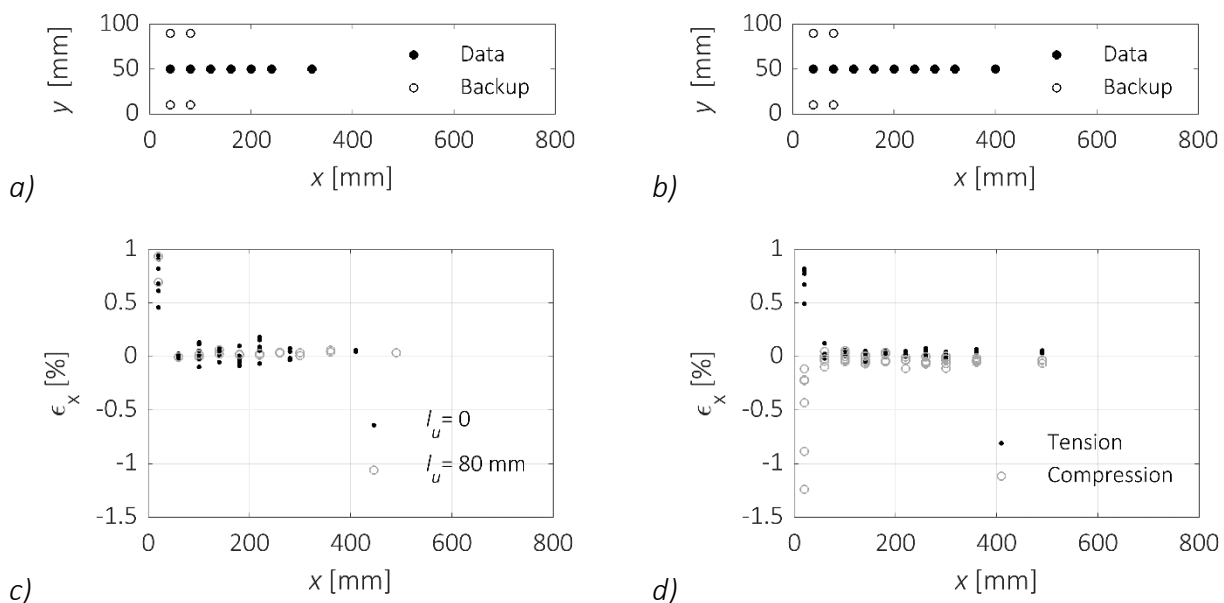


Figure 9. Typical distribution of deformation along the specimen. Results are given for $l_a = 240$ mm. a) Sensor layout, without unbonded length. b) Sensor layout, with unbonded length. c) Influence of the unbonded length. d) Tension and compression.

The stiffness of the connection was determined according to EN 26891:1991. The results are expressed in terms of the initial slip modulus k_i , namely the secant stiffness at 40 % of the ultimate load accounting for the initial slip, and slip modulus k_s , representing the slope of the linear part of the load-displacement curve between 10 % and 40 % of the ultimate load. The slip is defined as displacement measured at the end of the specimen, but it is not clear from the standard between which two points this displacement should be measured. Therefore, distribution of slip modulus along the length of the specimen is given in Figure 10, where slip is measured between the connection plate and sensor at position x . The loading type does not affect the results significantly and both the slip modulus and its variation reduce with the increase of distance x .

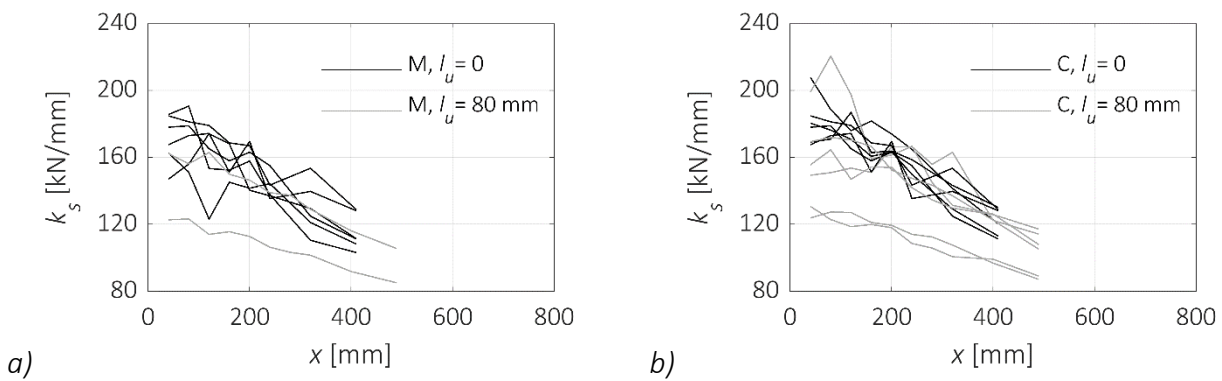


Figure 10. Distribution of slip modulus (k_s) along the specimen. Results are given for $l_a = 240$ mm. a) Monotonic tests. b) Cyclic tests.

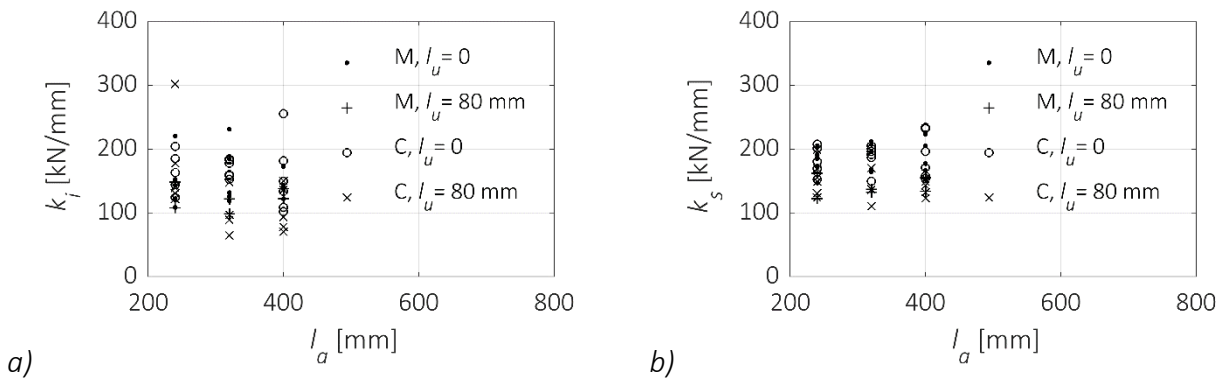


Figure 11. Influence of glued-in length on the stiffness. a) Initial slip modulus (k_i). b) Slip modulus (k_s).

Figure 11 presents the influence of glued-in length on the connection stiffness, obtained with data from the sensors with the smallest x coordinate. A decreasing trend can be observed for the initial slip modulus k_i , while the slip modulus k_s does not show variations with respect to the glued-in length. The mean values of slip modulus of $k_{s,mean} = 196$ kN/mm and $k_{s,mean} = 128$ kN/mm were measured for the specimens without and with the unbonded length, respectively. No influence of glued-in length

on the stiffness of the connection was observed. Possible dependence on the rod diameter has not been investigated, but the comparison with results of Verdet et al. (2016) indicates nonlinear dependence.

Use of mild steel allowed development of large plastic deformations in cyclic tests. Ductile behaviour was achieved for all glued in lengths by using the low strength steel. Ductility was calculated as the ratio between the ultimate displacement and the yield displacement in a cyclic test (Casagrande & Piazza, 2018). The ultimate displacement was defined as displacement at failure or 80 % of the maximum load. The yield displacement was calculated based on the equivalent energy elastic-plastic curve, which replaces the measured force-displacement curve with bilinear curve. Only the part of the curve in tension was used, because the compressive behaviour is largely influenced by the slenderness of the specimens tested.

The results are presented in Figure 12. The ductility seems to be independent on the glued-in length, but limited by the failure mode, i.e. the ductility of 5 can be reached only if the brittle failure modes are avoided. In design, the typical value of ductility should be limited to 2.5-3, unless it can be proven that no buckling or pull-out failure will occur.

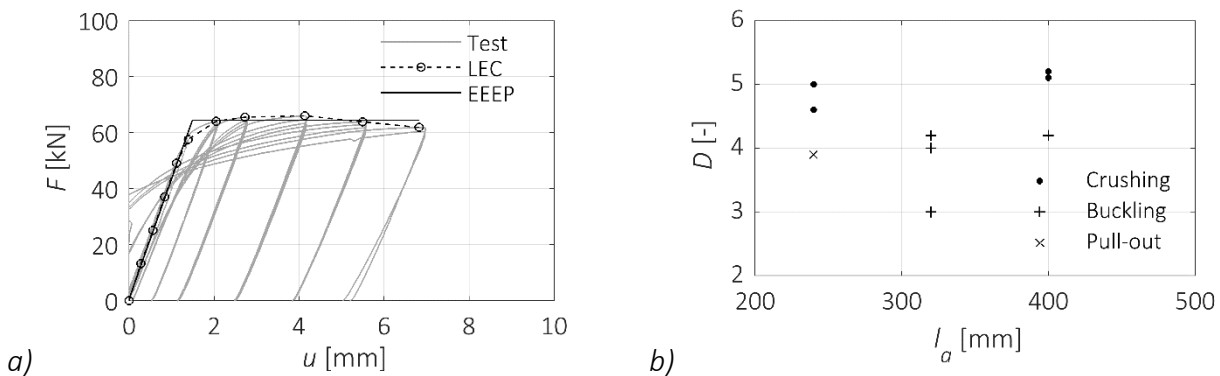


Figure 12. Ductility. a) Definition of ductility based on the load-deformation curve (F - u), load envelope curve (LEC) and equivalent energy elastic-plastic curve (EEEP), as described by Casagrande & Piazza (2018). b) Experimentally measured ductility (D) for different glued-in lengths (l_a).

4 Application of the study for the design of connections

The connections with glued-in rods present an efficient way to connect timber elements to other structural elements, including the foundations. Using mild steel with low yield strength and moderate rod diameter allows to design the connection for ductile failure of the rods. It is essential to have a good knowledge about the yield strength of the steel rods and the pull-out capacity of the connection, in order to design the connection adequately. Having in mind that ductility is especially beneficial in

seismic events, it is of utmost importance to be able to guarantee that ductility will also be provided in case of cyclic loading. Hence, the practicing engineer would benefit from design rules for connections with glued-in steel rods in regions with high seismicity.

The following recommendations with regard to the seismic design of connections with glued-in rods can be given:

- If low tensile strength of steel is ensured and design is performed with sufficient glued-in length, to avoid brittle failure, ductility in the range of 2.5-3 can be accounted for.
- The stiffness of the connection can be reliably defined between the steel plate and the end of the timber element. A value of $k_s = 200 \text{ kN/mm}$ is proposed for the connections without the unbonded length and with diameter $d = 16 \text{ mm}$ based on the experiments.
- The capacity of connection in tension and compression can be calculated separately, considering that there was no significant interaction between the corresponding failure modes in the cyclic experiments.
- A good bond between the steel rod and the adhesive should be guaranteed, e.g. by degreasing the steel rod prior to the application of adhesive, in order to reduce the radial tension stresses in the connection.
- Straightness of the rod in the borehole should be guaranteed by using spacers at the top and bottom of the glued-in length.

5 Acknowledgements

The authors would like to thank Dominik Bissig and Cyril Laube for their contribution in performing the experiments and preliminary data analysis.

6 References

- Aicher, S, Stapf, G (2017): Eingeklebte Stahlstäbe – state-of-the-art – Einflussparameter, Versuchsergebnisse, Zulassungen, Klebstoffnormung, Bemessungs- und Ausführungsregeln. In: Proceedings of the 23. Internationales Holzbau-Forum (IHF 2017), 7. and 8. December 2017, Garmisch.
- Bainbridge, R, Mettem, C, Harvey, K, Ansell, M (2002): Bonded-in rod connections for timber structures – development of design methods and test observations. International Journal of Adhesion & Adhesives 22: 47-59.
- Casagrande, D, Piazza, M (2018): A proposal for the revision of the European Standard EN 12512 – Timber structures – Test methods – Cycling testing of timber connections and assemblages for seismic design. Personal communication.

- EN 14080 (2013): Timber structures – Glued laminated timber and glued solid timber – Requirements. European Committee for Standardization CEN, Brussels, Belgium.
- EN 26891 (1991): Timber structures – Joints made with mechanical fasteners – General principles for the determination of strength and deformation characteristics (ISO 6891:1983). European Committee for Standardization CEN, Brussels, Belgium.
- prEN 1995-2 (2003): Design of timber structures, Part 2: Bridges. Final Project Team draft. Stage 34, European Committee for Standardisation, Brussels, Belgium.
- CEN/TC 193 (2018): CEN/TC 193/SC 1/WG 6 N 80: Glued-in rods in glued structural timber products - testing, requirements and bond shear strength classification. European Committee for Standardization CEN, Brussels, Belgium.
- Gattesco, N, Gubana, A, Buttazzi, M, Melotto, M (2017): Experimental investigation on the behaviour of glued-in rod joints in timber beams subjected to monotonic and cyclic loading. *Engineering Structures*, 147: 372-384.
- Gehri, E (2010): High performing jointing technique using glued-in rods. In: WCTE 2010, World Conference on Timber Engineering. Riva del Garda, Italy.
- Krawinkler, H (2009): Loading histories for cyclic tests in support of performance assessment of structural components. In: 3AESE, The 3rd International Conference on Advances in Experimental Structural Engineering, San Francisco, California.
- Renoantic (2018): http://www.renoantic.ch/sites/default/files/fiche-produit/FT_MAS-TIFIX_FR_DIF.pdf (Last checked on 13.07.2018)
- Riberholt, H (1988): Glued bolts in glulam – Proposals for CIB code. In: Proceedings of the CIB-W18 Meeting 21, Parksville, BC, Canada, Paper No. CIB-W18A/21-7-2.
- Ogrizovic, J, Wanninger, F, Frangi, A (2017): Experimental and analytical analysis of moment-resisting connections with glued-in rods. *Engineering Structures*, 145: 322-332.
- Parida, G, Johnsson, H, Fragiaco, M (2013): Provisions for ductile behavior of timber-to-steel connections with multiple glued-in rods. *Journal of Structural Engineering*, 139(9): 1468-1477.
- Tannert, T, Zhu, H, Myslicki, S, Walther, F, Vallée, T (2016): Tensile and fatigue investigations of timber joints with glued-in FRP rods. *The Journal of Adhesion*.
- Tlustochowicz, G, Serrano, E, Steiger, R (2011): State-of-the-art review on timber connections with glued-in steel rods. *Materials and Structures*, 44: 997-1020.
- Verdet, M, Salenikovich, A, Cointe, A, Coureau, J, Galimard, P, Munoz Toro, W, Blanchet, P, Delisee, C (2016): Mechanical performance of polyurethane and epoxy adhesives in connections with glued-in rods at elevated temperatures. *BioResources*, 11(4):8200-8214.

Discussion

The paper was presented by J Ogrizovic

H Blass asked why unbonded length was used. J Ogrizovic responded that the intent is for the steel to yield at the unbonded zone. H Blass said that even if you have unbonded length you have brittle failures.

P Quenneville said that transverse reinforcement was not used. Since the dowels may not be perfectly in line with loading direction, transverse reinforcement would help to prevent brittle failures. J Ogrizovic said that the connections were made with CNC machine so alignment should not be a problem. R Jockwer commented that this is not a problem; even buckling happens at high loads.

S Winter received confirmation about splitting occurring with unbonded length. He commented that their experience is that splitting can be avoided with unbonded area. He asked about the elongation of the glued in rod. J Ogrizovic responded that sensors were mounted at the steel plate. The stiffness values compare reasonably well with published information.

E Toumpanaki received clarification on the deformation measurement system.

S Aicher commented that results indicate spruce has little ductility while ash has much better ductility. So the spruce specimens may be able to handle a few more cycles. He wondered where does the ductility come from. It could come from the steel yielding but the failure mode is brittle. He said one should decouple the two modes and over-design for the brittle behaviour so that ductile behaviour is achieved. A Frangi said that these connections, especially Ash, have good ductility in spite of final failure mode being brittle.

H Blass said that the results are only valid for the edge distances used in the test; otherwise, results are unsafe. J Ogrizovic said that a minimum edge distance of 2 to 2.5 d can be used for these connections.

Cyclic Performance of a Full-scale Timber Column Equipped with Resilient Slip Friction Joints

Armin Valadbeigi, Department of Civil and Environmental Engineering, University of Auckland, New Zealand

Pouyan Zarnani, Department of Built Environment Engineering, Auckland University of Technology, New Zealand

Pierre Quenneville, Department of Civil and Environmental Engineering, University of Auckland, New Zealand

Keywords: Cyclic Test, Bi-directional Test, Finite Element Analysis, Resilient Slip Friction, Self-centring

1 Introduction

The behaviour of column elements subjected to cyclic loading is recognised as a significant research topic for building structures in earthquake-prone regions. During an earthquake, columns experience bidirectional lateral loading due to the two horizontal components of the earthquakes. The observations and the experimental studies have depicted that damage in structures is more liable when they are exposed to two directional loading or ground motions rather than uniaxial loadings. This stems from the fact that the existence of damage in one direction diminishes the load carrying resistance of the other direction and when combined, it could reduce the overall seismic resistance of the structure. Therefore, it is noteworthy to investigate structural behaviour under biaxial loading. Most of the experimental studies have focused on the cyclic behaviour of columns under uniaxial loading. This is chiefly attributed to the difficulty in performing bi-directional testing. As there is a lack of biaxial hysteresis modelling, experimental research is of great interest.

The quasi-static test method has been adopted for this research since it can provide sufficient information on tested structures regarding strength, stiffness, and ductility, as well as energy dissipation and damage propagation (Leon & Deierlein, 1996).

Current design methods are based on the statement that large hysteresis curves are necessary to mitigate the earthquake force. Since a significant portion of the input energy will be dissipated by hysteresis loops, significant residual displacements could

be remaining in a building after an earthquake (MacRae & Kawashima, 1997). Investigations after earthquakes proved that even if the conventional connections evaded fractures under the earthquakes, they still suffered considerable residual deformations. These substantial deformations led to the demolition of the structures since the structures were beyond repair. All the discussed disadvantages of traditional lateral load resisting systems have led to this suggestion that an optimal earthquake-resistant system would bring the structure to its initial position.

To enhance the performance of structures in energy dissipation capacity and to reduce the residual deformation of structures, a new connection was proposed by Ricles et al. (2001). Kim & Christopoulos (2009) improved the connection by replacing the angle with frictional energy dissipating devices (FEDs) and repeated the tests. The test results showed that the FEDs could dissipate the energy and the connection has a good self-centring capacity.

Specifically, in New Zealand, one of the earliest self-centring systems has been adopted for the design of the “stepping” rail bridge over the south Rangitikei River in New Zealand in 1981 (Cormack, 1988) (Restrepo, 2002) (Skinner et al., 1993).

In regards to concrete structures, Priestley & Tao (1993) proposed the use of partially unbounded tendons to pre-stress the precast concrete moment resisting frames as a method of adding a self-centring feature for the building. In this respect, MacRae & Priestley (1994), and Stanton et al. (1993) shortly afterwards conducted an experimental test on precast beam-column subassemblies.

Although many studies have been conducted to provide a self-centred friction damper (Khoo et al., 2012), still there is a need for an innovative and a simple method to address this lack of feature in traditional friction connection. In this research, an experimental study of a full-scale timber column equipped with RSFJs (Zarnani & Quenneville, 2015) is carried out. The column is tested under the bi-directional loads to evaluate the hysteresis response and the performance of the assembly. Self-centring and energy dissipation are two fundamental structural characteristics of RSFJs when subjected to cyclic loads. The timber column is designed to accommodate the target deflection without any damage; the input energy in the system can be dissipated through the hysteretic response of the connection, without a reduction in strength.

In this study, a finite element analysis (FEA) is conducted to evaluate the stress distribution in the connection, and to corroborate the experimental results. Moreover, the FE model assists in these two objectives as well, firstly, in designing the RSFJ for a 1000 kN capacity. Secondly, in evaluating the critical local effects in the RSFJ, which cannot be precisely measured during the experiments such as contact forces between the plates, and the bending moment through the connection because of load eccentricities. For this purpose, a full 3D ABAQUS FE (2014) model is analysed and the behaviour the RSFJ is investigated. The model includes contact and sliding between different plates, prestressing of the bolts, and geometric nonlinearity. The results from the FE

Analysis (FEA) are verified by comparing the obtained force-displacement curve with the connection experimental result.

After investigating the behaviour of the RFSJ in the connection test, tests on the LVL timber column having two RSFJs subjected to uniaxial (in-plane and out-of-plane) were conducted. The main purpose of these tests is to investigate and compare the deformation ability and self-centring feature of the column under uniaxial loadings.

2 Resilient slip friction joint

The RSF components are presented in Figure 1. The two one-sided grooved cap plates and two two-sided grooved middle plates are bolted together in which the bolts are positioned in the middle of the slotted holes of the middle plates. The disc springs are also placed on the cap plates to provide room for the upward and downward movement of the cap plate when the horizontal force exceeds the friction force between the plates. The amount of friction force depends on the pre-stressing force of the bolts, the angle of the grooves, and the coefficient of friction between the plates. The spherical plain bearing is also added to have a fully pin behaviour in the out-of-plane direction. The specification of the employed bearing is given in the following sections (SKF, 2011).

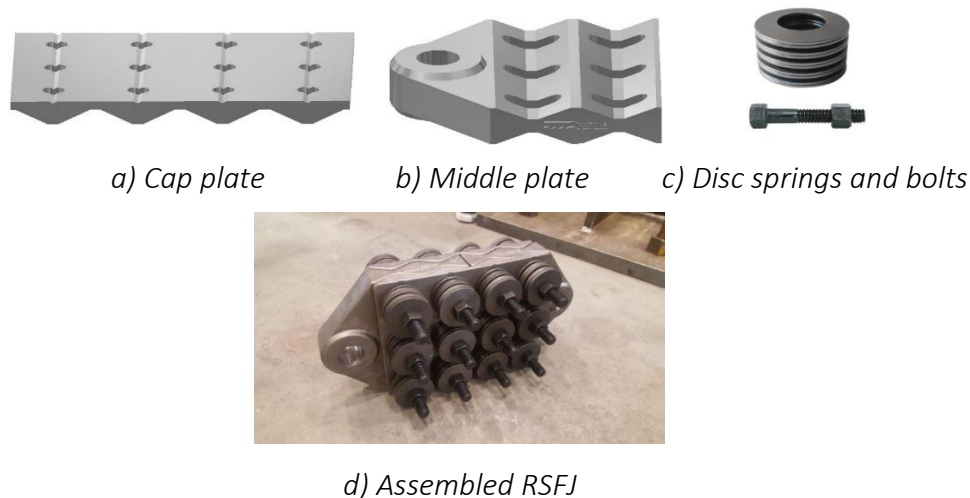


Figure 1: Schematic model of RSF joint.

Figure 2 shows the ideal behaviour of an RSF joint and identifies the important parameters of the hysteresis curve.

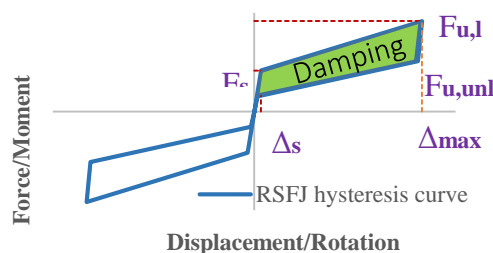


Figure 2. Ideal hysteresis curve of the RSFJ.

The connection is designed for the force of 1000 kN and the deflection of 20 mm. The RSFJ has 1000 kN capacity and the sliding force of around 400 kN. To reach this amount of sliding, a prestressing force of 55 kN has been applied to the 12 M20 bolts. In terms of the prestressing method, a hydraulic jack with a load cell was calibrated to ensure the accuracy of the prestressing force. The connection was designed to open up under the tension force and to resist the load under the compression. As there is no gap provided between the middle plates, the end face of the middle plates almost touches each other.

3 Experimental investigation of the connection

3.1 Material and specifications of the RSFJ

The cap and middle plates are made from Hardened and Tempered IC 4130 material with the yield strength of 655 MPa, the tensile strength of 795 MPa, 14% elongation and 30% reduction in area. The connection is designed for 1000 kN force and the minimum deflection of 20 mm, to go beyond 2% drift due to the building characteristics for which the connection is designed. Table 1 demonstrates the configuration of the RSFJ.

Table 1. Characteristics of the RSFJ.

Groove angles (degrees)	μ_s	μ_k	n_b	F_{slip} (kN)	$F_{ult,loading}$ (kN)	$F_{residual}$ (kN)	$F_{ult,unloading}$ (kN)
25	0.18	0.15	12	390	1032	161	408

3.2 Specification of the disc spring

Several disc springs were tested under the compression to assess their deflection and stiffness. The stiffness value was also required for both the finite element modelling of the RSFJ and specifying the amount of prestressing force. The characteristics of the disc springs have been shown in Table 2 after averaging the result of 10 tests.

Table 2. Disc springs specifications.

Flatting load (kN)	Deflection (mm)
130	1.7

The entire disc springs need to be pre-loaded first since the hysteresis curve of the first loading cycle is different from the next cycles. The test results of two disc springs are presented in Figure 3.

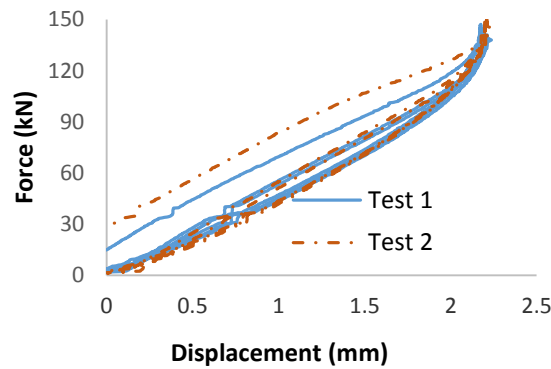


Figure 3. Disc spring load-displacement behaviour.

3.3 Experimental setup

The experimental test setup is illustrated in Figure 4. In addition to the RSFJ, the other equipment involved in the experiment includes an MTS actuator, a data logger system and a computer. The setup was assembled on the strong floor of the Auckland University's Test Hall. The end of the actuator was fixed to the strong floor with four pre-stressed anchors, and the other side of the actuator was connected to the attachment. The attachment itself was also linked to the end plate of the RSFJ. As shown in Figure 4, the portal gauge was installed between the two middle plates of the RSFJ to measure the expansion of the joint. An LVDT and a laser were placed to monitor the vertical movement of the cap plates and to ensure that the connection is behaving symmetrically. Another LVDT was also installed on the end bracket to measure any possible sliding that could influence the test result. Time histories of both displacement and force were recorded by the data logger set up on a 10 per second sampling rate. Figure 4b shows a close-up of the instrumentation and the RSFJ.



a) equipment arrangement



b) close-up view and instrumentation

Figure 4. Experimental setup for testing the RSFJ.

4 Connection test results

The load-displacement response of the specimen is shown in Figure 5. Initial stiffness (K_0) of the connection is 900 kN/mm, which could be considered a fully restrained welded connection. The connection showed a very consistent and repeatable hysteresis curve while it presented a fully self-centring hysteresis curve in all the cycles with

displacement returning to zero in every loop. Therefore, there is not any yielding in the specimen. The repeatable hysteresis behaviour stands for a fact that no major wearing or deep scratches occurred during the test. Meanwhile, the existing discrepancies between the FE and the experimental results regarding the unloading stiffness can stem from a couple of reasons including the small scratches on the surface of the plates, which were observed after disassembling the connection, and the uneven surface of the plates in the experiment. The second stiffness (k_1) of the connection is about 30 kN/mm, which is 1/30th of the initial stiffness. The ultimate unloading force is 405 kN which is in a good agreement with the analytical data. Additionally, the result confirmed that the residual force is 120 kN. In the compression stage of the test, as predicted, no buckling or yielding was observed under the compression force of 970 kN.

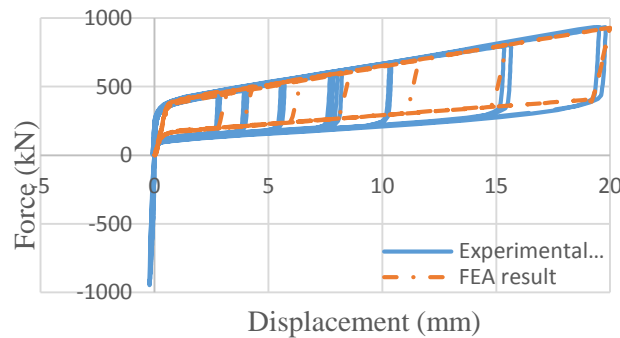


Figure 5. Load-displacement curve.

5 Finite Element Analysis

5.1 Modelling procedure

The RSFJ was modelled and analysed in ABAQUS 6.14 software (2014). The connection was optimised through a vast number of analyses. The modelling was shaped in three stages. The first stage was pre-processing, which involved modelling the geometry, property definition, and meshing. The next stage was defining the boundary condition, specifying the loading regime and then analysis. The last stage was the processing of the results including plotting different parameters.

In general, in the FE modelling the following simplifications were used:

- The bolt shank was modelled by a cylinder with a diameter of 20 mm.
- Symmetry conditions about the vertical and horizontal planes were used to reduce the computational time.

The FE model was employed to obtain the Force-Displacement curve, the initial stiffness, and the damping ratio, which was carried out by the following two-stage loading scheme:

1. The pre-loading force of the bolts was applied in the first step to pre stress the connection. Therefore, all the six bolts were loaded to 55 kN in 10 steps simultaneously.
2. Applying the displacement by following the AISC loading regime.

The non-linear geometric analysis was performed to obtain the force-displacement curve of the joint. The settings in ABAQUS included the allowable elastic slip factor (SLTO) value of 0.01; automatic stepping; and Newton–Raphson equation solver; along with contact algorithm static kinetic exponential decay function.

5.2 FEA results

The FE hysteresis curve is in a good agreement with the experimental test result. In regards to the experimental test of the RSFJ, the sliding occurs at the force of 400 kN. In the FE simulation, the static solver has been used to simulate the test procedure. Comparison of the predicted sliding force and the second stiffness of the hysteresis curve with the experimental observation are shown in Figure 5. It is found that the model could precisely simulate the flag-shaped hysteresis curve of the connection. Consequently, the model can be adopted to predict the maximum stress in the connection. The FEM confirmed the self-centring feature of the system, as the residual drift equals zero.

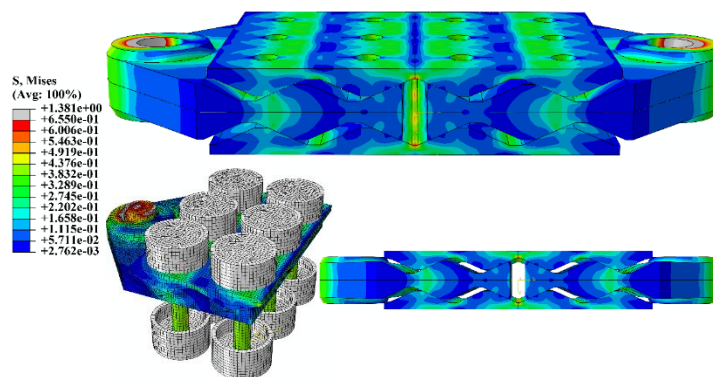
The stress distribution for the middle and the cap plates are shown in Figure 6. The maximum stress is below the yield capacity of the plates except for small areas around the pinhole where we have singularities in the model. Typical situations where stress singularities occur include the application of a point load, sharp corners, and the edge of those parts in contact as well as point restraints. Since the stress singularities are a common situation in FEA, stress values a couple of mesh elements away from these areas are considered for the evaluation of the model.



a) 3D view of the pin bracket



b) front view of the pin bracket



c) 3D view of the RSFJ FE results

Figure 6. Experimental and FE views of the RSFJ showing the RSFJ opening.

6 LVL column test equipped with the RSFJs

A spherical plain bearing was also added for the column test to provide a fully pin behaviour in the out-of-plane direction. The specification of the employed bearing is given in the following sections. Therefore, the middle plate hole is modified to accommodate the spherical bearing while the cap plate remained unchanged. The modified RSF components are presented in Figure 7.

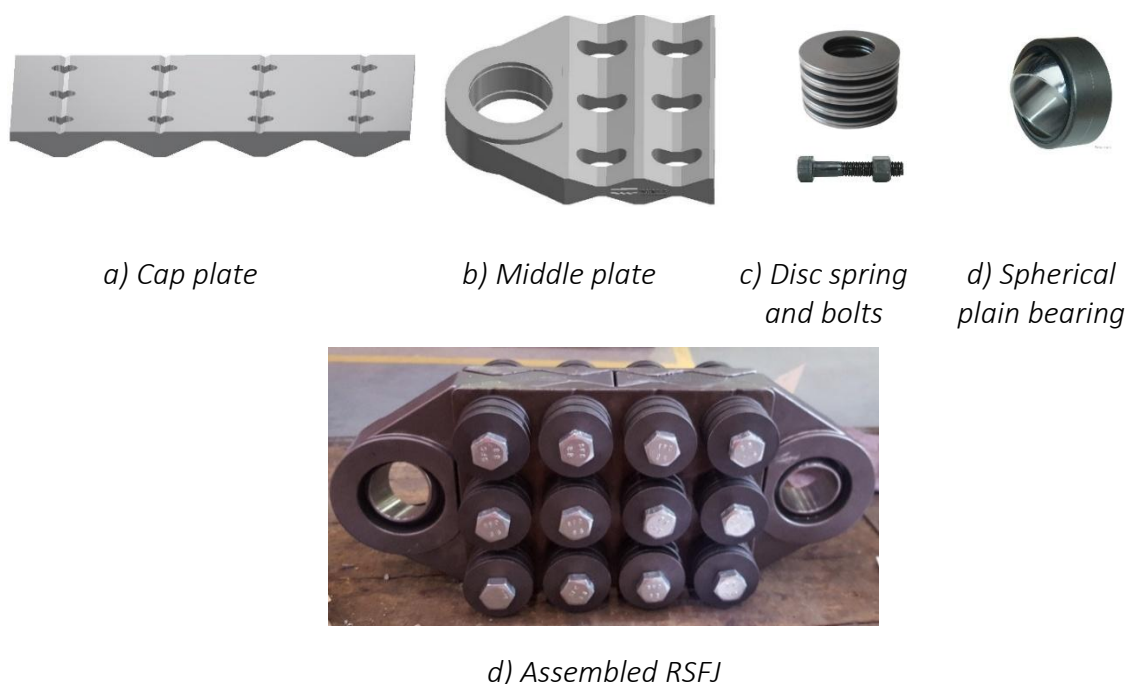


Figure 7. The new version of the RSFJ components for the column test.

6.1 LVL column details and properties

The LVL used for the column is LVL 11 (NelsonPine, 2012), manufactured in accordance with AS/NZS 4357 (1995). For limit states design to the New Zealand Code NZS 3603 (1993), LVL 11 characteristic strengths are given in Table 3.

Table 3. Characteristics of the LVL column.

Modulus of Elasticity Parallel to Grain (MPa)	Bending Strength (MPa)	Tension Strength Parallel to Grain (MPa)	Compression Strength Parallel to Grain (MPa)	Compression Strength Perpendicular to Grain (MPa)
11000	38	26	38	10

The tested column has 1700 kN.m bending strength representing a timber column of the new Nelson Airport Terminal as part of the recent research project at the University of Auckland. The tested assembly could also represent the behaviour of a beam-column connection when the test is performed in the in-plane direction. The tested column details are presented in Figure 8.

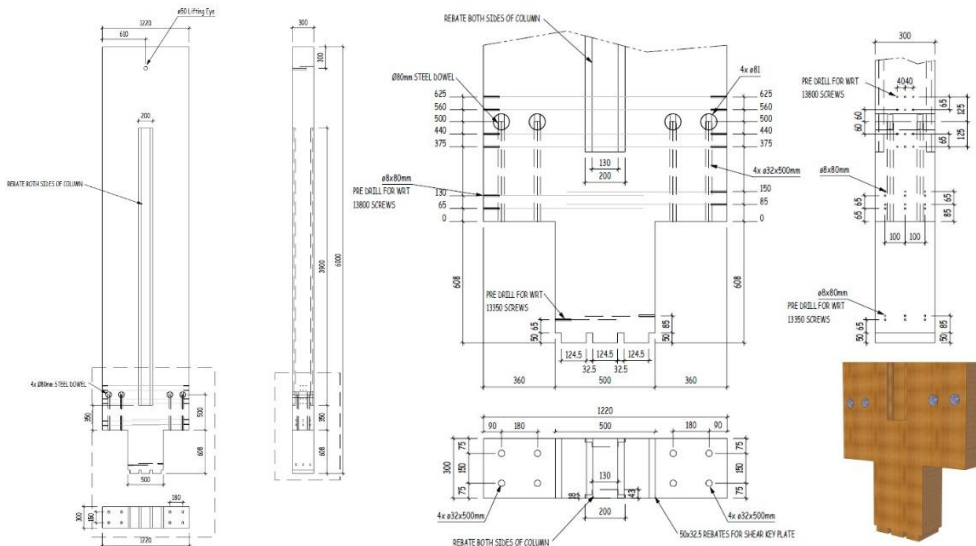


Figure 8. Detailing of the column, the shear key location and the RSFJ connection to the column.

6.2 Characteristics of the spherical bearing

As for the spherical bearing, a “GE 60 TXE-2LS” model from SKF manufacturer (2011) was used as it has enough capacity; and is also a maintenance-free bearing. This feature complies with the design goal of having a maintenance free connection after earthquakes. The specification for the spherical plain bearing is shown in Table 4. This type of bearing allows the column to move in the out-of-plane direction with minimum resistance

Table 4. Specification of the spherical bearing (SKF 2011).

Basic dynamic load rating (C) (kN)	Basic static load rating (C ₀) (kN)	Specific dynamic load factor (K) (N/mm ²)	Specific static load factor (K ₀) (N/mm ²)
695	1160	300	500

6.3 Test setup

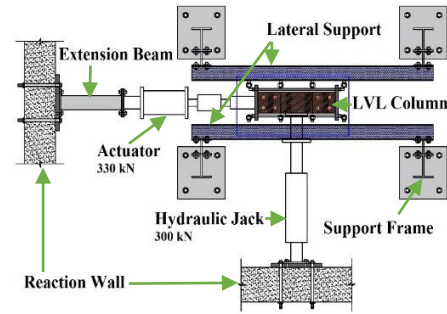
The objective of the experiments is to verify the structural characteristics as well as the cyclic performance of the proposed system. Specific attention was paid to the change in stiffness and equivalent damping ratio.

Based on the existing laboratory conditions, the test setup shown in Figure 9 was developed. In addition to the specimen, the other equipment involved in the experiment includes a hydraulic actuator with the capacity of ± 330 kN and 250 mm stroke (used for the in-plane loading) and a hydraulic jack with the same capacity and 150 mm stroke (used for applying the out-of-plane displacement). A data logger system is also hooked up to a computer to monitor the recordings. As shown in Figure 9, portal gauges were installed between the two middle plates to measure the opening of the joint. LVDTs and a laser were placed to monitor the vertical movement of the end and

the horizontal displacement of the column respectively. Time histories of both displacement and force were recorded by the data acquisition system (DAQ) set up on a 10 per second sampling rate. To prevent the column from deflecting out-of-plane, lateral supports were provided for the in-plane test. However, these supports were later removed when the out-of-plane and the bi-directional tests were conducted. The test setup was robust, and no damage observed after the tests were completed.



a) test assembly



b) equipment arrangement



c) close-up view of the RSFJs and the instrumentations

Figure 9. Experimental setup for testing the column.

6.4 Loading protocol

The specimen was loaded cyclically with the actuator. The cyclic loading protocols are in terms of inter-storey drift angle (θ). The protocol starts with four cycles at $\theta=0.005$ rad followed by four cycles at $\theta=0.01$ rad, and four cycles at $\theta=0.02$ rad in backward and forward directions. The loading protocol goes to a maximum drift of 2% for the in-plane test.

7 Column test results

7.1 In-plane test

Stiffness reduction started to appear when the RSFJ opened. The following hysteresis curves illustrate the cyclic performance of the column, and the RSFJ itself (recording the middle plates' relative displacements). It should be noted that an elastic deflection of 0.8 mm has been measured between the RSFJ top pin bracket and the column (due to the threaded rods elastic elongation). In addition, a minor 0.3 mm uplift between the bottom bracket and the base has been observed. For clarity purpose, in the result

discussion, the RSFJ refers to the casted plates, the connection relates to the entire assembly (including the pin brackets), and the column refers to the entire assembly. All column loading and displacement recordings are reported at the height of 2.6 m.

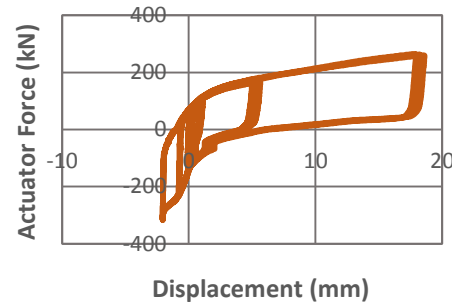
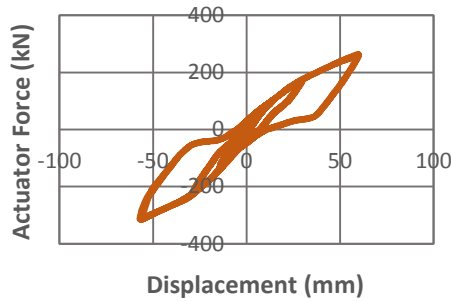


Figure 10. In-plane hysteresis curve of the column. Figure 11. In-plane hysteresis curve of the RSFJ.

Referring to the in-plane results (Figures 10 and 11), the intersection of the hysteresis curve with the displacement axis could imply some residual drift, which in fact is misleading and brings one to conclude that the column is not self-centring. To demonstrate that such behaviour is related to the test set-up and not the tested structure; separate half cycle tests were conducted under the actuator in tension, the results are shown in Figures 12 and 13, and in compression forces (Figures 14 and 15).

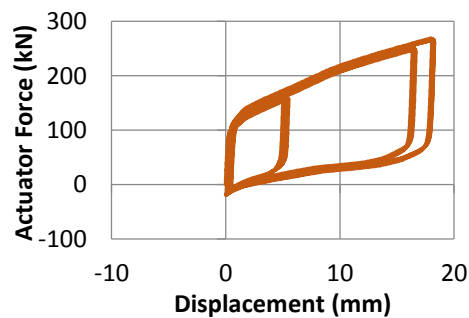
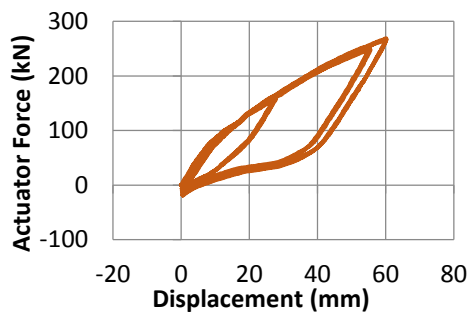


Figure 12. In-plane hysteresis curve of the column. Figure 13. In-plane hysteresis curve of the RSFJ.

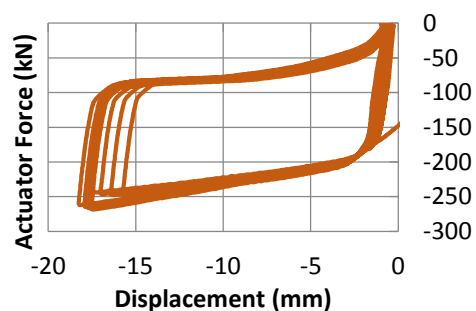
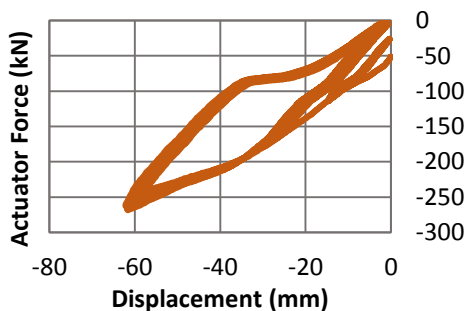
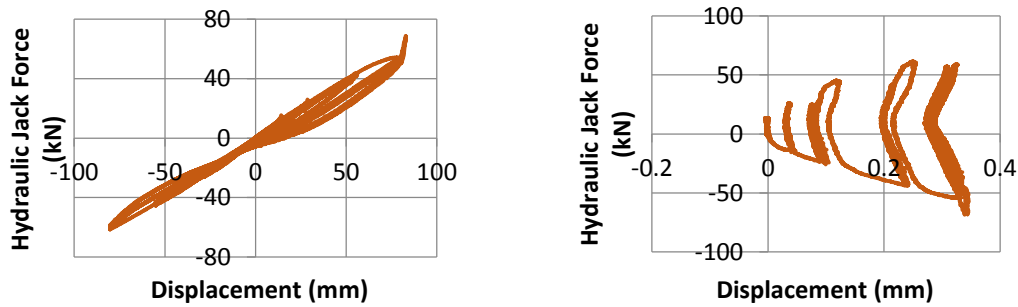


Figure 14. In-plane hysteresis curve of the column. Figure 15. In-plane hysteresis curve of the RSFJ.

As shown in Figures 12-15, the column is fully self-centring, whereas, in the full cycle, there is a small residual drift. This can be explained by some minor misalignment of the actuator under compression due to the rotation of the actuator to some extent (potentially causing some column torsion) requiring extra force to overcome the effect of this misalignment during re-centring. This torsion effect would not occur in reality.

7.2 Out-of-plane test

The load-displacement curves for the out-of-plane test are shown in Figure 16. It should be pointed out that although the application of the spherical bearing eliminates any bending moment in the connection, the column still has some resistance in the out-of-plane direction. The reason is the existence of 150 mm eccentricity (half of the column width) between the centre of rotation (edge of the column bottom plate) and the connection axis.



a) Out-of-plane hysteresis curve of the column b) Out-of-plane hysteresis curve of the RSFJ

Figure 16. Out-of-plane test load versus displacement.

The RSFJ in action and the displaced shape of the column and the joint are presented in Figure 17.

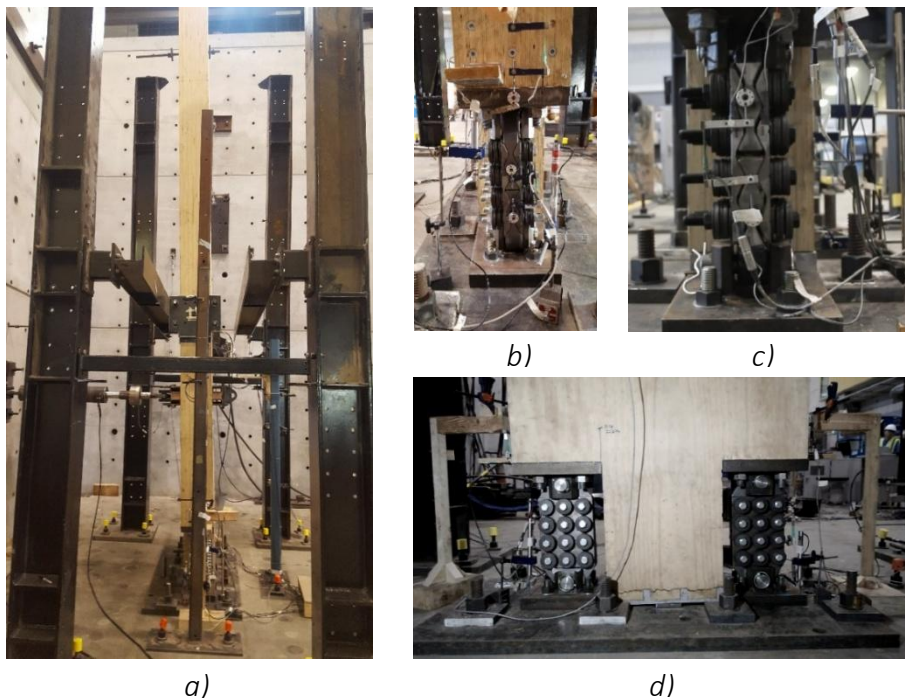


Figure 17. Structure performance during the test a) column under out-of-plane displacement b) close-up view of the joint under out-of-plane displacement c) gap opening of the RSFJ during the in-plane loading d) close-view of the rotation of the column.

8 Conclusion

Experimental investigation and the FEA of the Resilient Slip Friction Joint (RSFJ) with 1000 kN capacity corroborated the feasibility of the self-centring feature and demonstrated a repeatable flag-shaped hysteresis curve. Thus, the FEM accurately predicted the hysteresis curve of the RSFJ.

The connection presented stable and repeatable hysteresis curves validating that the steel plates did not experience substantial surface damage affecting the hysteresis loops. Furthermore, practically there is no strength degradation during the loading cycles for different drifts.

The experimental results of the uniaxial cyclic loads on the LVL column demonstrated the hysteresis response of the assembly and the joint in a real size column. This research has shown that the proposed connection is a viable resilient structural system.

The experimental study proved that the designed connection was able to open up to 20 mm and to tolerate 1000 kN force in both tension and compression without any damage. Additionally, the assembly performed well under different cycles and showed a stable behaviour.

The tested column showed a reasonable level of energy dissipation considering the innate characteristics of the flag shape hysteresis curves. The column illustrated a fully self-centring behaviour, and a considerable level of ductility without any structural damage up to 2.5% drift. The spherical bearing performed smoothly and was able to release the out-of-plane moment without being damaged. The connection presented stable and repeatable hysteresis curves validating that the steel plates did not experience substantial surface damage affecting the hysteresis loops. Furthermore, practically there is no strength degradation during the loading cycles for different drifts.

9 References

- Leon RT, Deierlein GG. (1996): Considerations for the use of quasi-static testing. *Earthquake Spectra*, Vol 12(1): 87–109.
- MacRae, G.A. & Kawashima, K. (1997): Post-Eearthquake residual displacements of bi-linear oscillators. *Journal of Earthquake Engineering and Structural Dynamics*, Vol 26: 701-716.
- Ricles, J.M., Sause, R., Garlock, M. & Zhao, C. (2001): Posttensioned seismic-resistant connections for steel frames. *Journal of Structural Engineering*, Vol 127(2): 113–121.
- Kim, H.J. & Christopoulos, C. (2009): Numerical models and ductile ultimate deformation response of post-tensioned self-centering moment connections. *Earthquake Engineering and Structural Dynamics*, Vol 38(1): 1–21.

- Cormack, L.G. (1988): The design and construction of the major bridges on the Mangaweka rail deviation. Transaction of the Institute of Professional Engineers of New Zealand, Vol 15: 16-23.
- Restrepo, J.I. (2002): New generation of earthquake resisting systems. Proceeding in FIB congress, Federation International du Béton, Osaka, Japan.
- Skinner, R.I., Robinson, W.H. & McVerry, G.H. (1993): An introduction to seismic isolation. Journal of International Development, New York.
- Priestley, M.J.N. & Tao, J.R.T. (1993): Seismic response of precast prestressed concrete frames with partially debonded tendons. Journal of Precast Concrete Institute, Vol 38(1): 58-69.
- MacRae, G.A. & Priestley, M.J.N. (1994): Precast post-tensioned ungrouted concrete beam-column subassemblage tests. Report No. SSRP-94/10, Department of Applied Mechanics and Engineering Sciences, University of California, San Diego.
- Stanton, J., Stone, W. & Cheok, G.S. (1993): A hybrid reinforced precast frame for seismic regions. Journal of Precast Concrete Institute, Vol 42(2): 20-32.
- Khoo, H., Clifton, C., Butterworth, J. & MacRae, G. (2012): Development of the self-centering sliding hinge joint with friction ring springs. Journal of Constructional Steel Research, Vol 78: 201-211.
- Zarnani, P., Quenneville, P. (2015): A resilient slip-friction joint, Patent No. WO2016185432A1, NZ IP Office.
- ABAQUS (2014): Analysis user's manual version 6.14. ABAQUS Inc.
- NelsonPine (2012): Specific Engineering Design Guide.
- AS/NZS 4357.0 (2005): Structural laminated veneer lumber, Australian/New Zealand Standard.
- NZS3603 (193): Timber Structures Standard, Standards New Zealand.
- SKF (2011): Spherical plain bearings and rod ends.

Discussion

The paper was presented by P Quenneville

A Frangi asked when the column is out of plane is there no vertical force and do you have concerns about P-Delta effect? P Quenneville responded that the max deflection is 2.5% and the engineers want to demonstrate that the out of plane movement did not cause damage. This was achieved. A Frangi asked what is the function for placing the device at the top section of the column. P Quenneville said that the engineers wanted to have the top section remain more or less as a rigid body hence the introduction of a mid-column device.

H Blass asked how did you determine the embedment strength of the 100 mm diameter dowel as equations are only valid for dowel diameter up to 30 mm. P Quenneville said it was based on judgement and the design of the engineer.

T Tannert received clarification that the apparent crack line of the LVL was the lamination of the veneer joint and not failure.

S Franke asked why different number of washers were used in one device. P Quenneville said that the connection needed more rigidity in the out of the plane direction and needed more washers to counter the prying forces; there are also dummy washers in the connection.

A Smith asked whether a bow tie profile can be used. P Quenneville answered yes and discussed the advantages of current approach.

Load-deformation behaviour and stiffness of lateral connections with multiple dowel type fasteners

Robert Jockwer

ETH Zürich, Institute of Structural Engineering, Zurich, Switzerland

André Jorissen

Technical University of Eindhoven, Eindhoven, The Netherlands

KEYWORDS: Connection, European Yield Model, Stiffness, Load-deformation behaviour, Nails, Dowels, Slip

1 Introduction

Connections with laterally loaded steel dowels are widely used in timber structures. The load-carrying capacity of these connections can be estimated using the design equations in Eurocode 5 (CEN, 2004) based on the so called European Yield model. For a reliable design of structures not only the load-carrying capacity but also the load-deformation behaviour (e.g. stiffness and ductility) of the connections are of importance.

1.1 Terminology

The non-linear load-deformation behaviour of connection is complex to describe. An example of a load-deformation curve is shown in Fig. 1. At low load levels a rather soft behaviour is observed with large initial deformations. These initial deformations are more pronounced for connections exhibiting large tolerances. With increasing deformation the load increases and shows an approximately linear load-deformation behaviour at midrange load levels. At higher load levels a non-linear load-deformation behaviour can be observed if sufficient ductility is available. The maximum load and the ultimate load can be distinguished, the latter being defined as the load at a certain ultimate displacement or a certain drop of load. Various denotations and terms are used to describe this behaviour. An example is the term for the description of slope of the load-deformation curve: in Eurocode 5 this term is called slip modulus whereas Granholm (2002) the term modulus of deformation is used. In other literature the term slip is used for the description of the deformation of structures at load levels of little or no load (Dubas et al., 1981). Within this study the following terms are used as presented in Fig. 1:

- Stiffness: slope of the load-deformation curve in N/mm. The stiffness is the force per unit deformation of a connection for a single fastener.
- Slip: deformation of a connection at zero or low load-levels in mm.

In (Dubas et al., 1981) it is highlighted that the initial slip is commonly smaller for connection tested in laboratory due to the higher precision compared to connections produced in practice.

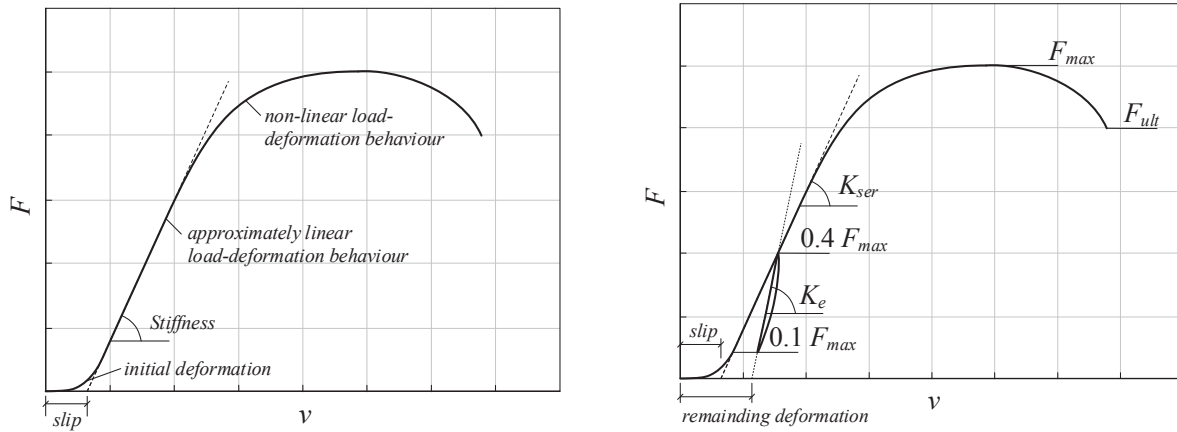


Figure 1: Characteristics of the load-deformation diagram of the connection.

1.2 Stiffness of connections

When analysing the load-deformation curve the tangential and the secant stiffness can be determined. The tangential stiffness can be calculated at a single point whereas the secant stiffness is determined between two points or load-levels. As an example the stiffness at serviceability load level could be determined as a tangential stiffness whereas the stiffness describing the ultimate load could be represented as a secant stiffness. A simplified diagram showing the load-deformation behaviour of a connection is given in Fig. 1. The stiffness is not constant along the non-linear load-deformation dependency of the connection. Depending on the respective load-level(s) different values can be observed. In general a decrease of stiffness can be observed with increasing deformation. Granholm (2002) determined the tangential and secant stiffness determined along the entire load-deformation curve of a nailed connection as given in Fig. 2. The curves were calculated based on results from 70 tests on nails $d = 5.6\text{mm}$ and length 150mm . Granholm highlights the problem how to account for the friction between the timber elements. In the case of a collapse of a bridge formwork evaluated by Granholm (2002) the stiffness at collapse due to instability of the system was only approximately 20-25% of the initial values. Gehri states in (Dubas et al., 1981) that if only the ultimate load level would be considered in the standard, the corresponding stiffness at fastener failure would be too conservative for the serviceability limit states due to the strong dependency of the relevant stiffness value on the respective load level.

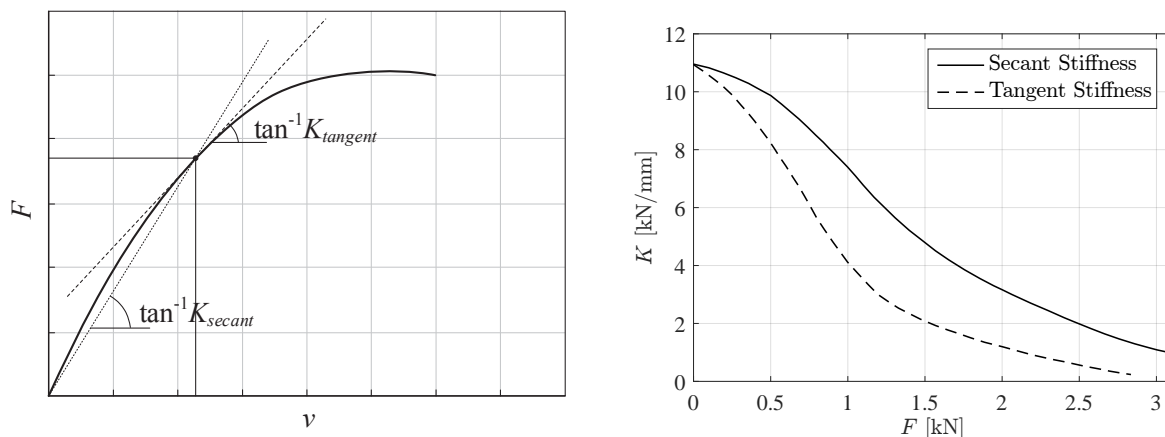


Figure 2: The secant and tangent stiffness per nail studied by Granholm (2002).

According to EC5 the stiffness K_{ser} is related to the parameter k_s that is determined as a secant stiffness between 10% and 40% of ultimate load according to EN 26891 (CEN, 1991).

Due to the almost linear-elastic load-deformation behaviour in that load range, k_s could be interpreted also as a tangential stiffness. A similar relationship between the stiffness relevant for the ultimate limit state K_u and a stiffness value determined in tests cannot be found in EC5 or related standards.

1.3 Importance of stiffness of connections

The stiffness and the load-deformation behaviour of connections is of special importance for highly undetermined structures and for combined elements with non-rigid connections such as trusses, built-up columns, timber frames, floor systems, roof diaphragms, box beams, wall panels etc. In large and complex timber structures different deformation behaviour of elements may lead to load-redistribution between connections and elements. Hence, especially when considering second order effects, the non-linear load-deformation behaviour should be accounted for in design. Examples of failure of structures due to the non-considered deformation of connections are e.g. the failure of the formwork of the Sandö bridge in the 1930s Granholm (2002). The importance of the different characteristics of the load-deformation curve of a connection can be discussed for the example of the simple beam with a combined cross-section (Fig. 3) taken from Dubas et al. (1981):

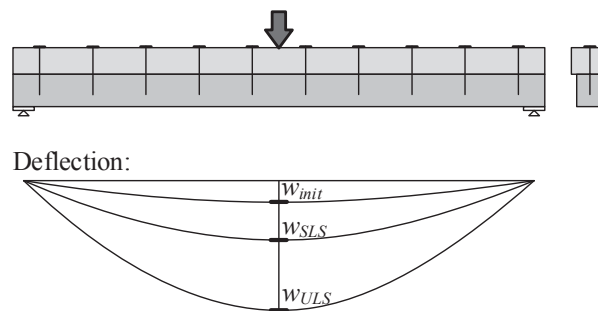


Figure 3: Simplified model and deflection of a beam with combined cross-section.

- The initial deformation under self-weight and at low load-levels is influenced by the slip of the connections.
- The deformation at serviceability limit state (SLS) can be determined by K_{ser} in the almost linear-elastic range at the respective load level between approximately 10% and 40% of ultimate load.
- The dynamic behaviour (vibration) is influenced by the elastic stiffness K_e .
- The deformation relevant for the ultimate limit state (ULS) can be calculated using the secant stiffness K_u of the connection. Ultimate failure of the entire beam will occur by failure of the individual timber members: the combined cross section without fasteners is the limit case that even after failure of the individual fasteners is carrying the load.

For other cases, such as structures and systems exhibiting stability problems, the tangential stiffness of the fasteners might be used for the determination of the critical load.

2 Background

2.1 Regulations for stiffness of connections in different European standards

The following definitions of stiffness K_{ser} at serviceability load level can be found in different design codes from Europe, in dependency of the timber density ρ and the fastener diameter d :

Table 1: Values of K_{ser} for fasteners in N/mm in timber-to-timber and wood-based panel-to-timber connections

Fastener type	EN 1995-1-1:2004	DIN 1052:2008	SIA 265:2012
Dowels			
Bolts with or without clearance	$\frac{\rho_m^{1.5} d}{23}$	$\frac{\rho_m^{1.5} d}{20}$	$3 \cdot \rho_k^{0.5} d^{1.7}$
Nails (with pre-drilling)			
Nails (without pre-drilling)	$\frac{\rho_m^{1.5} d^{0.8}}{30}$	$\frac{\rho_m^{1.5} d^{0.8}}{25}$	$60 \cdot d^{1.7}$

The stiffness of steel-to-timber connections is twice the values given in Table 1. According to SIA 265 the stiffness for connections loaded perpendicular to the grain is only half the value specified in Table 1.

The stiffness K_u at ultimate load level is given in all three standards by $K_u = 2/3 K_{ser}$. For the application in second order analysis K_u has to be charged by the partial safety factors according to DIN 1052:2008 (and the German National Annex for EC5) and SIA 265:2012.

2.1.1 Background of the DIN 1052 and EC5 equations

The theoretical derivation of the equation is given by Ehlbeck and Larsen (1993) for the example of nailed connections. The stiffness for serviceability limit state design (at approximately 40% of the ultimate resistance R) is derived as the ratio of the respective load and the instantaneous deformation. This corresponds to the definition illustrated in Fig. 4. The ultimate load-carrying capacity of a nail is derived by inserting all material dependent properties (embedment strength f_h and yield moment M_y according to EC5) into the equation for the nail capacity in single shear with two plastic hinges in the fastener. The "instantaneous" deformation v_{inst} at approximately 40% of the load-carrying capacity of the nailed connection with predrilling is given with an empirical equation in (Ehlbeck and Larsen, 1993):

$$v_{inst} = 40 \frac{d^{0.8}}{\rho_k} \quad (1)$$

For nailed connections without predrilled holes, a factor of 60 instead of 40 is used in Eq. 1. The background of this equation not explained in more detail in (Ehlbeck and Larsen, 1993). Some background on the data for the definition of the deformation v_{inst} can be found in (Ehlbeck and Werner, 1988b) and (Ehlbeck and Werner, 1988a). For a nail diameter ranging from 2 to 8 mm the following simplified equation of stiffness can be derived:

$$K_{ser,inst} = \frac{0.4R}{v_{inst}} = \frac{0.55}{100} \sqrt{100 - d} \rho_k^{1.5} d \approx \frac{\rho_k^{1.5} d}{20} \quad (2)$$

The instantaneous deformation as proposed by Eq. 1 shows the following characteristics:

- Connections with fasteners of greater diameter experience larger deformations on the respective load level of 40% ultimate load.
- The deformation of connections in timber of greater density is inversely-proportional to the density.
- This leads to a over-proportional increase of stiffness with increasing timber density.

2.1.2 Background of the SIA 265 equations

In SIA the standard values for K_{ser} listed in Tab. 1 and the relation $K_u = 2/3 K_{ser}$ is suggested if not more detailed information is available. For the experimental determination of K_{ser} , K_u and the deformation at failure v_u (for the calculation of ductility) the following information in Fig. 4 is given.

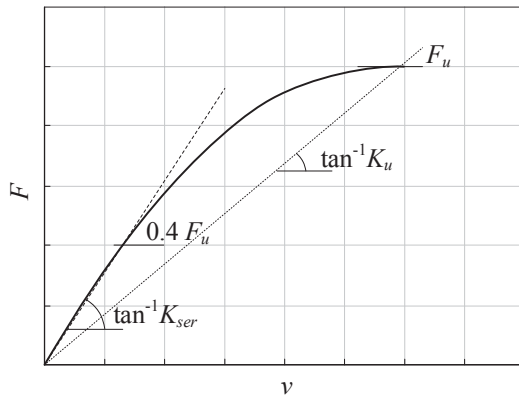


Figure 4: Definition of the stiffness of a connection for serviceability limit state and ultimate limit state as well as the reduced stiffness in the connection to take into account slip.

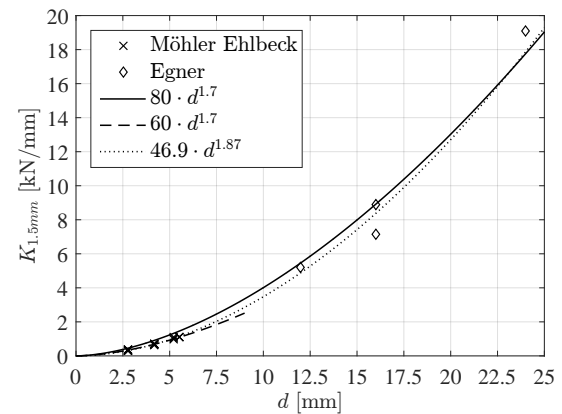


Figure 5: Size dependency of the test results on nails from Möhler and Ehlbeck (1973) (dashed line) and on dowels by Egner (1955) (solid line) for a deformation $v = 1.5\text{mm}$ with fitted curve according to Eq. 3.

The stiffness values according to SIA 265 2012 listed in Tab. 1 are based on the load at a deformation of the connections of 1.5 mm, which was defined as the deformation at permissible load-level in SIA 164 1981. Dubas et al. (1981) states that the deformation of $v = 1.5\text{ mm}$ corresponds to 1.5-2 times the serviceability load level. The constant limit of 1.5 mm results in the direct dependency of the stiffness value on the definition of (permissible) load, which is defined at this deformation in SIA 164: $F_{perm} = 60 \cdot d^{1.7}$ for predrilled nails. In SIA 164 the stiffness $K_{ser} = 40 \cdot d^{1.7}$ is given for nails without predrilling in all loading directions and the value $K_{ser} = 60 \cdot d^{1.7}$ for nails with predrilling, dowels, bolts, and screws, all of the loaded parallel to the grain.

The density dependent equations of K_{ser} in SIA 265 given in Table 1 is a fit to the value in the former version of the code using the density of $\rho_k = 400\text{ kg/m}^3$: $K_{ser} = 3 \cdot 400^{0.5} d^{1.7} = 60 \cdot d^{1.7}$. Dubas et al. (1981) has benchmarked the stiffness values against tests by Möhler and Ehlbeck (1973) and by Egner (1955) with regard to the impact of fastener diameter d as shown in Fig. 5 and suggested the following values for short term loading:

- Nails without predrilling $K_{ser} = 50 \cdot d^{1.7}$
- Nails with predrilling $K_{ser} = 60 \cdot d^{1.7}$
- Dowels and bolts $K_{ser} = 60 \cdot d^{1.7}$

The fit of all data by Möhler and Ehlbeck (1973) and by Egner (1955) yields the following

equation:

$$K_{1.5mm} = 46.9 \cdot d^{1.87} \quad (3)$$

According to Dubas et al. (1981) relatively low stiffness values were chosen in standard SIA 164 due to the higher creep in the connection compared to the other timber members (equal creep factors are used both for connections and timber members).

2.2 Other standards and codes

2.2.1 CIB Structural Timber Design Code from 1980 (CIB-W18, 1980)

In the fifth draft of the CIB Structural Timber Design Code 1980 the following regulation for the deformation v of a nailed connection is given for a load F not exceeding one third of the characteristic load-carrying capacity F_k of the connection $0 \leq F \leq F_k/3$

$$v = 0.5 \cdot d \cdot \left(\frac{F}{F_k} \right)^{1.5} \quad (4)$$

For the load $F = F_k/3$ this yields a deformation $v = 0.1d$. The stiffness derived from this formulation for nailed connections according to CIB-W18 (1980) is:

$$K = \frac{F}{v} = \frac{1/3 \cdot 200 \sqrt{\rho/1000} d^{1.7}}{0.1d} = 21.1 \sqrt{\rho} d^{0.7} \quad (5)$$

This formulation was developed by Ehlbeck and Larsen (1981) based on the studies by Mack (1966) who developed a non-linear empirical formula for the description of load-deformation curve in the range up to 2.5 mm deformation.

2.2.2 Australian Standard AS 1720

In the Australian standard AS 1720 (2010) the non-linearity of the load-deformation behaviour is highlighted. The secant stiffness $K_{sec} = F/v$ is defined with v the deformation of the joint (including duration effects) when the actual load (F) is applied. "Good estimates" of the value v are suggested for monotonic loads, for the incremental slip and changes in joint stiffness should be accounted for. In the former version of AS 1720 from 1997 the deformation v at a load F causing a deformation of maximum 0.5 mm was defined as (in the present version of AS 1720 (2010) Eq. 6 and 7 are slightly reformulated):

$$v \approx 0.5 \left(\frac{F}{0.107 d^{1.75} h_{32}} \right)^2 \quad (6)$$

The load causing a deformation of 2.5 mm is given as follows:

$$F_{2.5mm} = 0.165 d^{1.75} h_{32} \quad (7)$$

Load duration and creep factors are accounted for in addition in Eqs. 6 and 7. Some of the studies these factors are based on can be found in Leicester and Lhuede (1992).

For Australian softwood the stiffness factor $h_{32} \approx 750$, for hardwood higher values up to $h_{32} \approx 1600$ can be achieved. For these softwood species this corresponds to a load of $F_{0.5mm} \approx 80 d^{1.75} \text{ N}$ at $v = 0.5 \text{ mm}$ and $F_{2.5mm} \approx 124 d^{1.75} \text{ N}$ at $v = 2.5 \text{ mm}$. The resulting stiffness at $v = 2.5 \text{ mm}$ $K_{sec} = \frac{F}{v} = 49.6 d^{1.75} [\text{N/mm}]$ is similar to the specification of stiffness in SIA 265. As well the approximately linear dependency of stiffness on density is in line with SIA 265.

For connections with bolts, split-rings and shear-plates loaded parallel to the grain the following formulation is used as a "good approximation" for serviceability load effects:

$$v = \left(\frac{1}{h_{33}} \right) \left(\frac{F}{F_k} \right) \quad (8)$$

Creep and the initial slip in the connection has to be accounted for in Eq. 8 in addition. For bolted connections loaded perpendicular to the grain the deformation in Eq. 8 is divided by a factor 1.5-2.5 depending on the number of members in the connection. The stiffness factor h_{33} in Eq. 8 is $h_{33} = 0.75$ for bolted joints without metal side plates and $h_{33} = 1.15$ with metal side plates. This corresponds to $v = 1.33$ mm and $v = 0.86$ mm at characteristic load level for wood-wood and wood-steel connections, respectively.

2.2.3 Canada

According to CSA O.86 (2009) the lateral deformation of a nailed or spiked wood-to-wood joint may be estimated for a load $F \leq F_k/3$ as follows:

$$v = 0.5d \left(\frac{F}{F_k} \right)^{1.7} \quad (9)$$

In addition a factor accounting for creep is included in CSA (2009) for Eq. 9. For nails up to $d = 5$ mm Eq. 9 yields to similar deformations at $F = F_k/3$ compared to AS 1720.

2.2.4 Former german standard DIN 1052-2:1988

In the 1988 version of DIN 1052 the stiffness K in N/mm is given in dependency of the permissible load F_{perm} in N. In addition values for the deformation v at permissible load level are given. The values K and v per shear plane are:

- Dowels and bolts without clearance:
 $K = 1.2F_{perm}$, $v = 0.8$ mm
- Nails in single shear in timber-to-timber and steel-to-timber connections:
with predrilling $K = 10F_{perm}/d$, $v = 0.1d$; without predrilling $K = 5F_{perm}/d$, $v = 0.2d$
- Nails in multiple shear in timber-to-timber connections with and without predrilling:
 $K = 10F_{perm}/d$, $v = 0.1d$
- Nails in multiple shear in steel-to-timber connections with predrilling:
 $K = 20F_{perm}/d$, $v = 0.05d$

The permissible load F_{perm} in N of a nail in conventional softwood timber in DIN (1988) is:

$$F_{perm} = \frac{500d^2}{10 + d} \quad (10)$$

The permissible load of nails inserted in holes predrilled with $0.9d$ may be increased by 25%. A comparison of the stiffness values for nails with and without predrilling according to DIN 1052:2008 as given in Tab. 1 and the values according to DIN 1052-2:1988 as listed above is given in Fig. 6. The stiffness values according to DIN 1052:1988 are considerably higher compared to the values according to DIN 1052:2008 in Tab. 1.

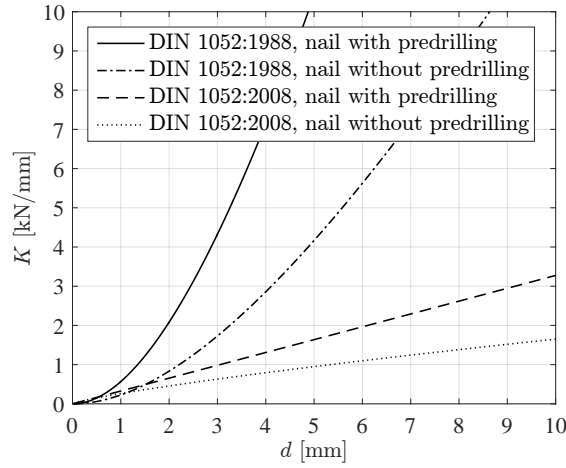


Figure 6: Comparison of stiffness values K_{ser} in Tab. 1 and Chapter 2.2.4 for $\rho_k = 350 \text{ kg/m}^3$.

2.3 Research on stiffness of connections

2.3.1 Ehlbeck (1979)

Ehlbeck (1979) states that the stiffness values tabulated in design codes are only rough estimates of the real behaviour of timber joints due to the large variability of the material properties. This should be accounted for especially when analysing complex structures or when performing sophisticated models. Ehlbeck (1979) suggest to limit the ultimate load to a deformation of the connection (summation of the deformations in both member of a connection (excluding slip)) not exceeding 7.5 mm. The problem of linking this practical definition to the safety concepts is highlighted.

Following the specifications shown in Fig. 7 by (Ehlbeck, 1979) the relation between the stiffness $k_{0.5}$ and $k_{1.0}$ of the load at deformations at 0.5 mm and 1.0 mm, respectively, can be derived as follows:

$$k_{1.0} \approx 2 \cdot k_{2.5} \approx \frac{2}{3} k_{0.5} \quad (11)$$

This relation of stiffness $k_{1.0} = 2/3 k_{0.5}$ corresponds to the relation of stiffness at ultimate and serviceability limit state in EC5: $K_u = 2/3 K_{ser}$.

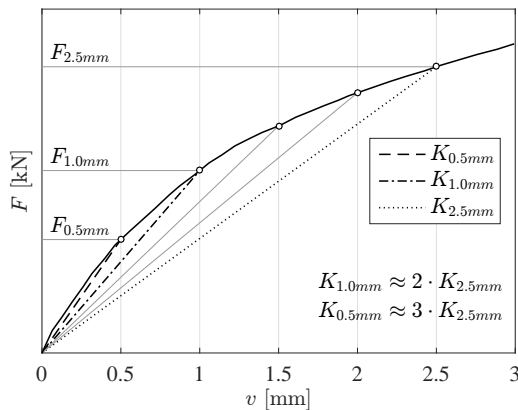


Figure 7: Schematic load-slip curve and secant slip moduli for different slip values from (Ehlbeck, 1979).

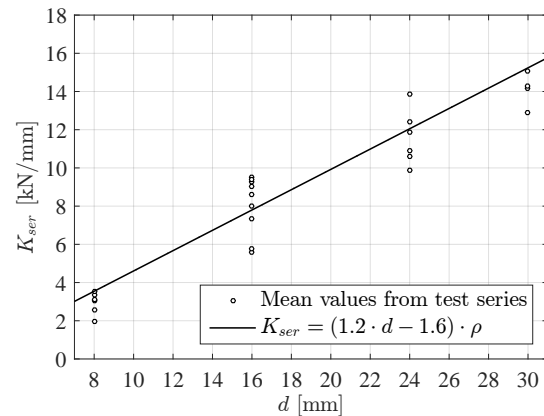


Figure 8: Stiffness k_{ser} per shear plane and dowel of a three-member joint over dowel diameter d .

2.3.2 Smith et al. (1988)

In the past considerable efforts have been made on describing the load-deformation behaviour of connections with dowel type fasteners and various models, such as beam on elastic foundation, considering elastic or plastic behaviour have been developed. Examples of literature are Kuenzi (1960), Norén (1968), Foschi (1974) or Smith (1982). Some of these models have been more curve fitting than a predictive analytical description of the load-deformation curve. By Whale and Smith (1986) it is stated that two-dimensional beam-on-elastic foundation models can give an adequate estimate of initial connection stiffness ($\pm 20\%$) and of load-carrying capacity.

Smith et al. (1988) proposed the following simplified expressions for the stiffness of a nailed connection at low load levels:

$$K = \frac{F}{v} = 5.15 \rho^{0.75} d^{0.95} \quad (12)$$

2.3.3 Ehlbeck and Werner (1988b)

In the tests reported in Ehlbeck and Werner (1988b) it was observed that the deformation at the allowable load according to DIN 1052 increases with increasing diameter d . The following equation for stiffness was derived on the basis of tests on softwood and different hardwoods:

$$k_{ser} = (1.2d - 1.6) \rho_k \quad (13)$$

The stiffness for hardwood is approximately 25% higher. In addition a simplification of Eq. 13 with $k_{ser} = d \cdot \rho_k$ is suggested.

2.4 Jorissen (1998)

Jorissen (1998) observed in his tests considerably lower stiffness values than those suggested in EC5. This is explained by the individual hole clearances, i.e. the fastener deformation at 40% of the failure load is often smaller than the hole clearance and some bolts do not contribute to the load and to the connection stiffness. The following equation for connections with multiple bolts is proposed by Jorissen (1998):

$$k_{ser} = k_{bolt} \frac{\rho_k^{1.5} d}{20} = 0.3 \frac{\rho_k^{1.5} d}{20} \quad (14)$$

3 Evaluation of the test results from TU Delft

3.1 General, geometry and configurations

A large number of tests on dowelled connections was performed at TU Delft by Jorissen (1998). One of the goals of the study by Jorissen was to determine the effect of number of fasteners in a row n and of spacing a_1 on the load-carrying capacity of connections.

The connections tested were timber-timber connections with dowels loaded in double shear. A summary of the geometry and configurations of the connections is summarized in Tab. 5 on page 17 at the very end of this paper. The following parameters were varied (see also Fig. 9): member thickness of the side (t_s) and middle (t_m) members, dowel diameter d , number of fasteners in a row n , number of rows of fasteners m , spacing of the fasteners a_1 , end-distance a_3 . The steel quality of the dowels was between 4.6 and 6.8 and the yield strength

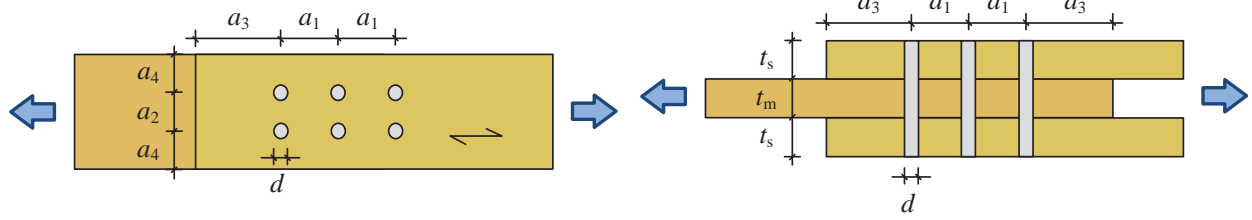


Figure 9: Denotation of geometry at a dowelled wood-wood connection.

calculated from the bending moment was approximately $f_y \approx 514 - 680 \text{ N/mm}^2$, respectively. The density ρ of the timber members was recorded. Most of the test series include 10-30 specimen, but some test series only 5-6.

The specimens were tested mainly in compression but also in tension as described in EN 1380 (2009). To reduce friction, two Teflon sheets were placed in both interfaces and steel strips were added to avoid a gap between the middle and side members.

3.2 Evaluation of the load-deformation behaviour

The following parameters were recorded in the tests: time, load, machine deformation, deformation of LVDT on both sides of the connection. For the further evaluation of stiffness and load-deformation behaviour in this study the mean deformation measured by the LVDT was used. A reloading cycle was performed according to EN 26891 (1991). The stiffness K_s and K_e were calculated according to EN 26891 (1991).

For the evaluation of the impact of individual parameters on the stiffness of connections the test series were sampled into groups of equal configurations. The following non-linear regression model was used for the evaluation of the impact of parameter X (e.g. diameter or row of fasteners) on the stiffness K :

$$K = aX^b \quad (15)$$

The stiffness values given in the following are the values per shear plane of the connection (e.g. for multiple fasteners). The different numbers of specimens tested in the different series were accounted for in the regression analysis by calculating the mean of a large number (1000) of analyses with a random selection of equal numbers of data points.

3.2.1 Diameter d

The test series according to Tab. 5 selected for the evaluation of the impact of dowel diameter on stiffness are: 11, 14, and 36. All three test series have a similar configuration: the relative thickness of the side members is $t_s/d = 3.04 - 3.38$, number of fasteners in a row $n = 5$, number of rows of fasteners $m = 1$, spacing $a_1/d = 7$ and end-distance $a_3/d = 7$. The following regressions can be fitted to the test results:

$$K_s = 0.029d^{2.24} \quad (16)$$

$$K_e = 0.9d^{1.46} \quad (17)$$

The impact of dowel diameter on stiffness K_s is considerably higher compared to the specifications in EC5, SIA 265 or other codes. Nevertheless, an over-proportional impact of dowel diameter on stiffness can be expected, if the elastic and plastic deformation is the main load-carrying mechanism in the connection.

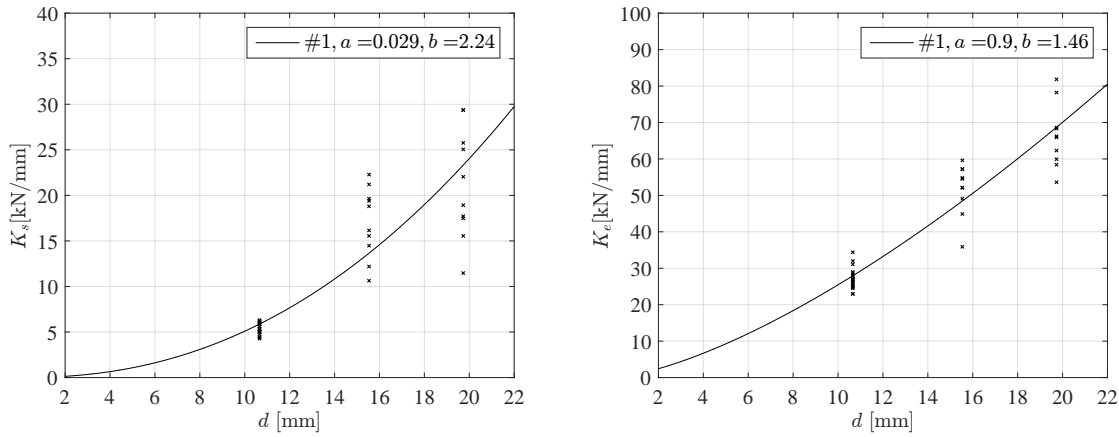


Figure 10: Impact of diameter d on stiffness K_s and elastic stiffness K_e

3.2.2 Number of fasteners in a row n

Jorissen (1998) studied in his test series the impact of the number of fasteners and of spacing on the load-carrying capacity of connections. Hence, a relatively large number of different configurations with varying number of fasteners in a row were tested. Tab. 2 shows the 10 groups of test series (according to Tab. 5) that were selected for evaluation of stiffness.

Table 2: Test series selected for evaluation of the number of fasteners in a row n .

Group #	1	2	3	4	5	6	7	8	9	10
Series	1	1	1	15	15	15	15	45	45	46
	3	2	4	17	16	18	19	47	48	51
	7	6	8	22	21	24	25	52	54	55
	13	12		29	28	31	32	56	58	
Regression parameters for K_{ser}										
a	0.64	0.65	0.75	0.58	0.58	0.55	0.52	1.27	1.25	0.79
b	1.26	1.31	1.28	1.65	1.50	1.52	1.66	1.07	1.04	1.30
Regression parameters for K_e										
a	15.4	14.9	16.0	8.91	8.61	8.01	8.38	7.17	7.49	2.24
b	0.72	0.62	0.83	0.89	0.81	0.95	0.96	1.06	1.05	1.58

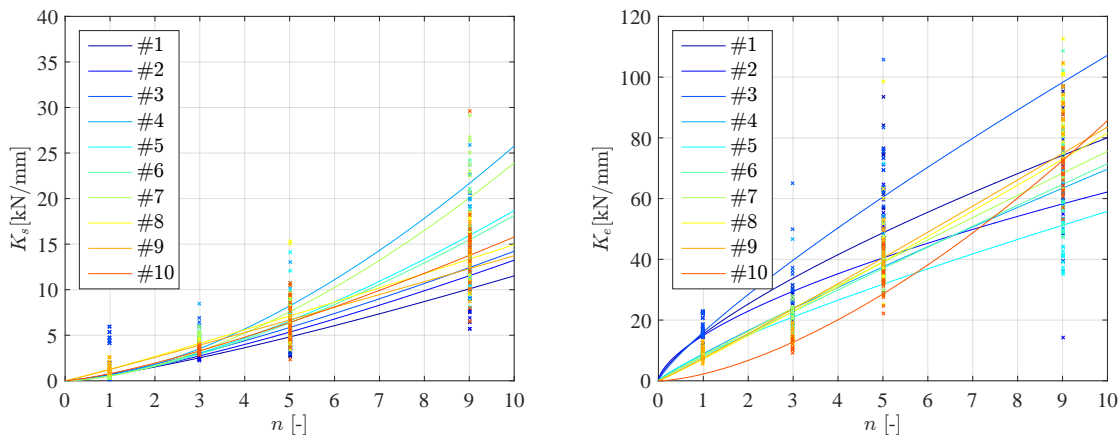


Figure 11: Impact of number of fasteners in a row n on stiffness K_s and elastic stiffness K_e

The results of the regression are given in Tab. 2 and in Fig. 11. The regression parameter b of the test series with a small relative side member thickness are larger (for K_{ser}) or smaller (for K_e) than 1. The under-proportional impact of n on K_e for connections with small side member thickness may be explained by the unequal distributes of forces within the connection due to

clearance or due to plastic embedment behaviour. The two groups 8 & 9 with larger relative side member thickness show an almost proportional impact of number of fasteners n both on K_{ser} and K_e as . Group no. 10 does not follow this trend, however, it should be noted that this is the only series without data for $n = 1$ fasteners.

3.2.3 Number of rows of fasteners m

The test series with a variation in number of rows of fasteners exhibits different spacing $a_1/d = 3$ & 7 and relatively thin side member thickness $t_s/d = 1.0 - 4.1$. All groups summarized in Tab. 3 consist of only 2 series with $m = 1$ and $m = 2$ rows of fasteners. The parameter b (exponent of the number of rows of fasteners m) is below 1 in all test series. This may be caused by an unequal load distribution between the fasteners. If due to low stiffness (provoked due to an uneven distribution of forces between fasteners), single fastener exhibit higher deformation, the risk of brittle timber failure modes (e.g. splitting or shearing) due to excessive embedment deformation at the fastener can considerably reduce the load-carrying capacity of the entire connection. In mean the impact of number of rows of fasteners could be accounted for by $m^{0.8}$ if no equal load-distribution between all fasteners can be guaranteed.

Table 3: Test series selected for evaluation of the number of rows of fastener m .

Group #	1	2	3	4	5	6	7	8
Series	5	7	20	24	34	35	40	41
	9	10	26	27	37	38	43	44
Regression parameters for K_{ser}								
a	2.64	3.65	5.75	5.12	6.28	5.36	8.19	5.93
b	1.01	0.72	0.73	0.78	0.78	0.84	0.58	0.97
Regression parameters for K_e								
a	26.0	61.5	34.7	35	23.6	27.1	31.5	34.2
b	0.85	0.31	0.45	0.71	0.80	0.85	0.45	0.79

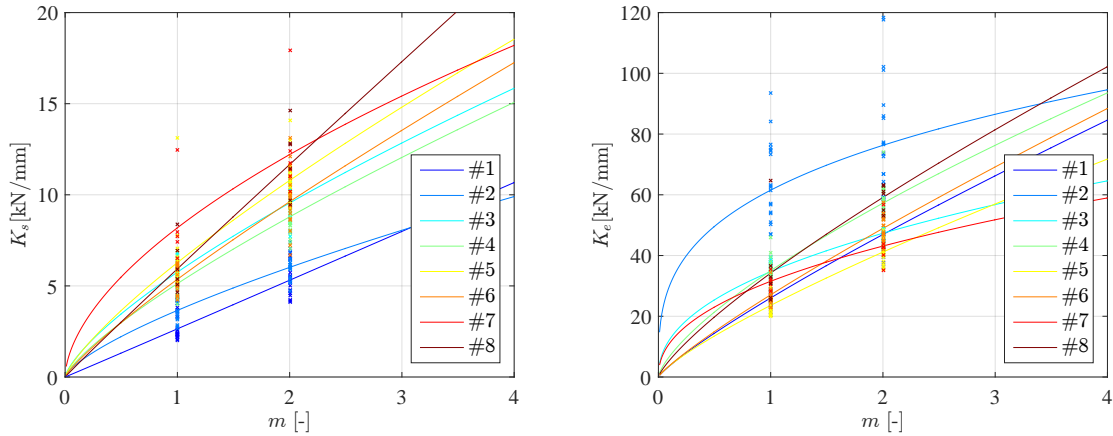


Figure 12: Impact of number of rows of fastener m on K_s and K_e

3.2.4 Selected parameters and relative thickness of the side members t_s/d

Since the side member thickness is expected to have an impact on the stiffness not only alone but also in combination with other parameters, several parameters were selected for combined evaluation: diameter d , number of fasteners in a row n , number of rows of fasteners m . The following regressions can be fitted to all test series:

$$K_s = 0.0035 \cdot n^{1.26} \cdot m^{0.61} \cdot d^{2.17} \cdot \left(\frac{t_s}{d}\right)^{0.25} \quad (18)$$

$$K_e = 0.251 \cdot n^{0.89} \cdot m^{0.53} \cdot d^{1.52} \cdot \left(\frac{t_s}{d}\right)^{-0.16} \quad (19)$$

In the test series analysed in this study, only softwood timber with a rather small range of density was used and, hence, the impact of density on the stiffness of a connection is only minor. A more detailed study of the impact of density requires a broader range of densities including the results of different hardwood species.

3.2.5 Variability of stiffness

The variability of the stiffness values is evaluated by using only n , m and d as follows:

$$K_s = 0.007 \cdot n^{1.3} \cdot m^{0.6} \cdot d^{2.0} \quad (20)$$

$$K_e = 0.16 \cdot n^{0.9} \cdot m^{0.6} \cdot d^{1.6} \quad (21)$$

The percentile values and the coefficient of variation of the stiffness K_s and elastic stiffness K_e are summarized in Tab. 4. By accounting in addition for the relative side member thickness, the variability of K_s could be reduced down to 40%.

Table 4: Percentile values and coefficient of variation of stiffness values for a connection with $n = 1$, $m = 1$ and $d = 11$ mm.

Stiffness	5% – tile	50% – tile	95% – tile	CoV
K_s	0.34	0.69	1.38	44.3%
K_e	4.95	8.11	13.3	30.6%

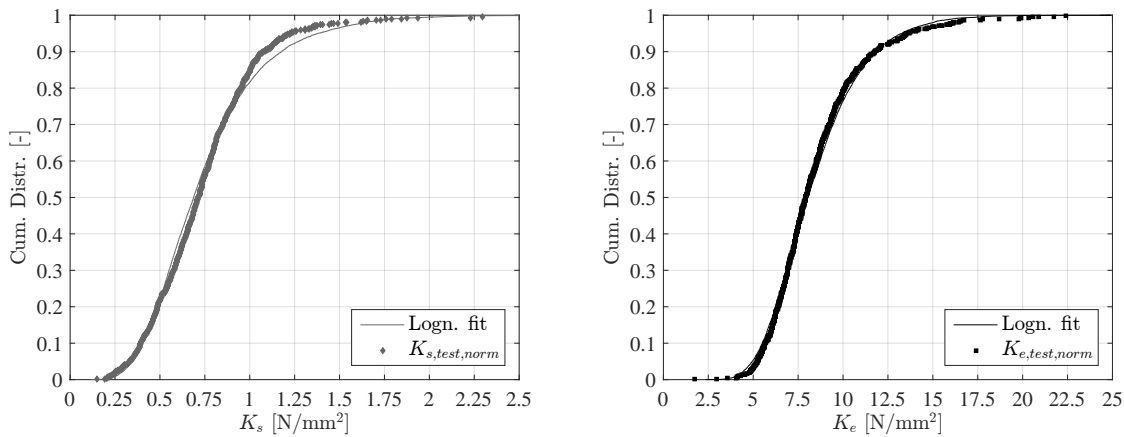


Figure 13: Cumulative distribution of stiffness K_s and K_e for $n = 1$, $m = 1$ and $d = 11$ mm

3.2.6 Determination of K_u

In the standards no method for the experimental determination of K_u are given. In EC5 K_u is defined as the "instantaneous stiffness for ultimate limit states". When considering the structural performance on mean levels, K_u could be based on the secant stiffness between 0% load and F_{max} or F_u . Due to the strong non-linearity of the load-deformation behaviour of connections with different failure modes according to EYM there are considerable differences between K_s determined in the linear part of the load-deformation curve and K_u . In Fig. 14 (left) different examples of load-deformation curves of connections are given. Depending

on the relative thickness of the side members the different failure modes according to the EYM are reached. A decrease in spacing a_1/d leads not only to decrease of maximum load but also to a reduction of the amount of ductility reached in the tests. Only if sufficient spacing and end-distances are satisfied considerable plastic deformations can be achieved (Fig. 15 (left)). The evolution of secant stiffness K_{sec} in relation to K_{ser} is shown in Fig. 14 (right). Within the linear range of the load-deformation curve up to approximately 50%-70% of F_{max} the ratio K_{sec}/K_s is approximately 1. If sufficient ductility is available, the ratio drops down to values of up to $K_{sec}/K_s \approx 0.2$, when reaching the plastic part of the curve with increasing load (see also Fig. 15 (right)). The threshold of $K_u = 2/3K_{ser}$ according to EC5 is reached at loads F exceeding 80%-100% of F_{max} . The test series with reduced spacing a_1/d show ratios $K_{sec}/K_s \approx 1$ up to failure.

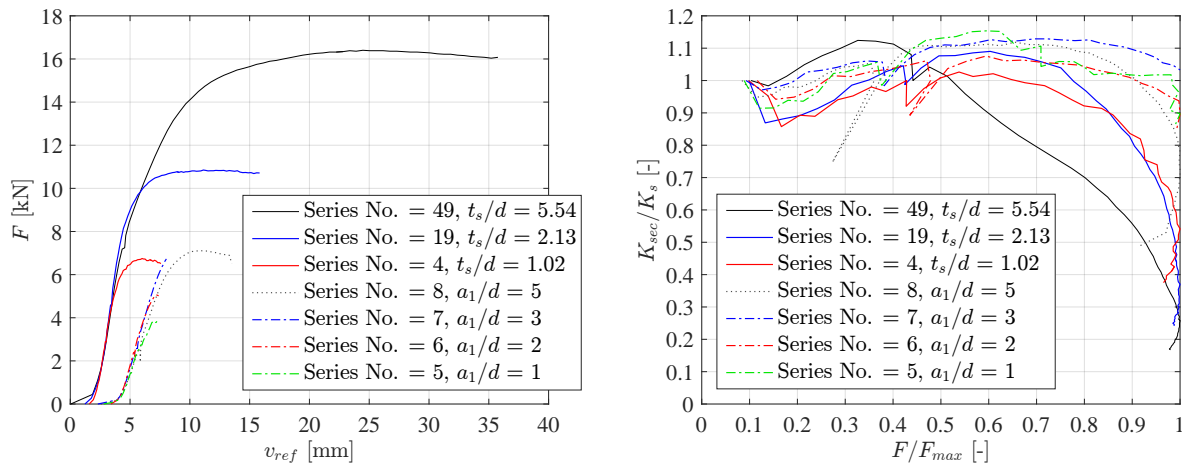


Figure 14: Examples of different load-deformation curves in dependency of the relative thickness of the side members t_s/d and the spacing a_1 (left) and the ratio of secant stiffness K_{sec} and K_s along the load-deformation curve in dependency of the load level F/F_{max} (right).

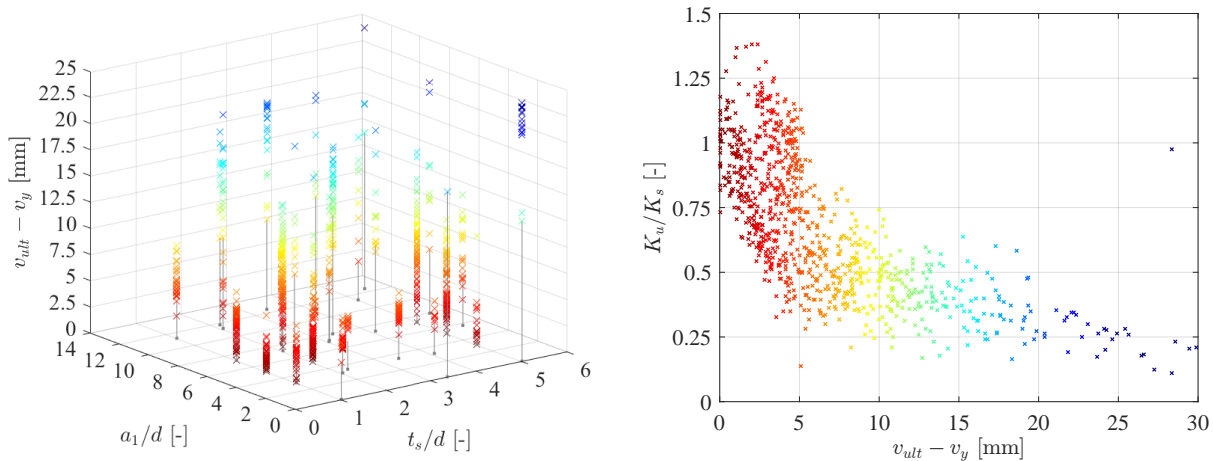


Figure 15: Impact of the relative thickness of the spacing a_1 and the side members t_s/d on the ductile deformation $v_{ult} - v_y$ (left) and the ratio of stiffness at maximum load K_u and K_s in dependency of the ductile deformation $v_{ult} - v_y$ (right).

4 Conclusions

4.1 Summary

The following conclusions with regard to code relevance can be drawn:

- The background of the equations for stiffness in EC5 is vague
- The equations for stiffness in EC5 are based partly on simplified assumptions
- Different standards and studies suggest different equations for stiffness
- The relation between stiffness for serviceability and ultimate limit states is not in line with the safety format in EC5
- The evaluation of test data from TU Delft on connections with dowels shows considerable differences compared to the stiffness values suggested in EC5
- There is a non-linear impact of number of fasteners in a row and number of rows of fasteners for small relative member thickness
- The density of the timber members shows only a minor impact on stiffness for the observed sample of tests on softwood specimens

The following recommendations with regard to design can be made:

- The fastener diameter shows a larger impact on the stiffness of a connection compared to the value currently given in EC5.
- A linear impact of the number of fasteners in a row can be assumed if sufficient member thickness, spacing and distances is satisfied.
- For connection without or with low ductility (embedment failure modes and brittle failure modes) the 5 and 95 percentile fractiles of K_{ser} , respectively, should be used.
- For connection with high ductility either K_u can be used or the ductility is considered directly (linear elastic-ideal plastic behaviour with ultimate deformation).
- The failure mode with plastic hinges in the fastener should serve as the reference when specifying stiffness values.

4.2 Outlook

Further research is needed for the following topics:

- Impact of density of timber members for a broader range of soft- and hardwoods
- Stiffness of different types of timber-to-timber, wood-based-material-to-timber and steel-to-timber connections
- Stiffness of different types of fasteners

Acknowledgement

The work presented in this paper was developed during a Short Term Scientific Mission at Technical University of Eindhoven financially supported by COST Action FP 1402 (European Cooperation in Science and Technology) (www.costfp1402.tum.de).

References

CEN (1991): EN 26891: Timber structures - Joints made with mechanical fasteners - General principles for the determination of strength and deformation characteristics (ISO 6891:1983). European Committee for Standardization CEN, Bruxelles, Belgium

- CEN (2004): EN 1995-1-1: Eurocode 5: Design of timber structures - Part 1-1: General - Common rules and rules for buildings. European Committee for Standardization CEN, Bruxelles, Belgium
- CEN (2009): EN 1380: Timber structures - Test methods - Load bearing nails, screws, dowels and bolts. European Committee for Standardization CEN, Bruxelles, Belgium
- CIB-W18 (1980): CIB-Structural timber design code
- CSA (2009): O86-09, Engineering design of wood, vol O86-09. Canadian Standards Association, Mississauga, Ontario, Canada
- DIN (1988): DIN 1052-2: Holzbauwerke; Mechanische Verbindungen. DIN Deutsches Institut für Normung e.V., Berlin, Germany
- Dubas P., Gehri E., Steurer T. (1981): Einführung in die Norm SIA 164 (1981) - Holzbau. Publication No. 81-1, Institut für Baustatik und Stahlbau, ETH Zürich, Zurich, Switzerland
- Egner K. (1955): Versuche mit Bolzenverbindungen (Schraubenbolzen). Fortschritte und Forschungen im Bauwesen, Series D, No. 20
- Ehlbeck J. (1979): Load-carrying capacity and deformation characteristics of nailed joints. In: Proc. of the CIB-W18 Meeting 12, Bordeaux, France, Paper No. CIB-W18/12-7-1
- Ehlbeck J., Larsen H. (1981): Load-slip-relationship of nailed connections. In: Proc. of the CIB-W18 Meeting 14, Warsaw, Poland, Paper No. CIB-W18/14-7-3
- Ehlbeck J., Larsen H.J. (1993): Eurocode 5 - design of timber structures: Joints. In: Barnes M., Brauner A., Galligan W., Leichti R., Soltis L. (eds) Proc. of the International Workshop On Wood Connectors, Editors, Forest Products Society
- Ehlbeck J., Werner H. (1988a): Design of joints with laterally loaded dowels. proposal for improving the design rules in the cib-code and draft eurocode 5. In: Proc. of the CIB-W18 Meeting 21, Parksville, Canada, Paper No. CIB-W18A/21-7-4
- Ehlbeck J., Werner H. (1988b): Untersuchungen über die Tragfähigkeit von Stabdübelverbindungen. Holz als Roh- und Werkstoff 46(8):281-288
- Foschi R.O. (1974): Load-slip characteristics of nails. Wood Science 7(1):69-74
- Granholm H. (2002): Der Einsturz des Bogengerüstes der Sandöbrücke. Verlag der Akademie der Wissenschaften und der Literatur, Mainz, Germany
- Jorissen A. (1998): Double shear timber connections with dowel type fasteners. PhD thesis, Technische Universiteit Delft, Delft, The Netherlands
- Kuenzi E.W. (1960): Theoretical design of a nailed or bolted joint under lateral load. United States Department of Agriculture, Forest Service, Forest Products Laboratory, Madison, Wisconsin
- Leicester R., Lhuède E. (1992): Mechano-sorptive effects on toothed-plate connectors. In: Proc. of the IUFRO S5.02 Timber Engineering Meeting, Bordeaux, France, pp 213-222
- Mack J.J. (1966): The strength and stiffness of nailed joints under short-duration loading. Div. of Forest products technological paper no. 40, CSIRO, Melbourne, Australia
- Möhler K., Ehlbeck J. (1973): Untersuchungen über das Tragverhalten von Sondernägeln bei Beanspruchung auf Abscheren und Ausziehen. Berichte aus der Bauforschung No. 91
- Norén B. (1968): Nailed joints - their strength and rigidity under short-term and long-term loading. Tech. Rep. 22, National Swedish Institute for Building Research
- SIA (1981): Standard SIA 164 - Timber Structures. SIA Swiss Society of Engineers and Architects, Zurich, Switzerland
- SIA (2012): Standard SIA 265 - Timber Structures. SIA Swiss Society of Engineers and Architects, Zurich, Switzerland
- Smith I. (1982): Interpretation and adjustment of results from short-term lateral load tests on white-wood joint specimens with nails or bolts. TRADA, Bucks, UK
- Smith I., Whale L., Anderson C., Hilson B., Rodd P. (1988): Design properties of laterally loaded nailed or bolted wood joints. Canadian Journal of Civil Engineering 15:633-643
- Standards Australia International (2010): AS 1720.1-2010, Australian Standard - Timber Structures - Part 1: Design methods. Standards Australia International Ltd., Sydney, Australia
- Whale L., Smith I. (1986): Mechanical joint in structural timberwork - information for probabilistic design. Trada - Timber Research and Development Association, Buckinghamshire, UK

Table 5: Test series with variation of parameters.

Series	Type	t_s/d	t_m/d	n	m	a_1/d	a_3/d	d	#
1	1	1.021	2.043	1	1	0	7	11.75	30
2	1	1.021	2.043	3	1	5	7	11.75	10
3	1	1.021	2.043	3	1	7	7	11.75	10
4	1	1.021	2.043	3	1	11	7	11.75	10
5	1	1.021	2.043	5	1	3	7	11.75	21
6	1	1.021	2.043	5	1	5	7	11.75	18
7	1	1.021	2.043	5	1	7	7	11.75	20
8	1	1.021	2.043	5	1	11	7	11.75	20
9	1	1.021	2.043	5	2	3	7	11.75	19
10	1	1.021	2.043	5	2	7	7	11.75	20
11	1	3.087	4.116	5	1	7	7	15.55	10
12	1	1.021	2.043	9	1	5	7	11.75	20
13	1	1.021	2.043	9	1	7	7	11.75	20
14	2	3.038	4.051	5	1	7	7	19.75	10
15	3	2.254	4.507	1	1	0	7	10.65	25
16	3	2.133	4.267	3	1	5	5	11.25	10
17	3	2.133	4.267	3	1	5	7	11.25	10
18	3	2.400	4.267	3	1	7	7	11.25	10
19	3	2.133	4.267	3	1	11	7	11.25	10
20	3	2.043	4.085	5	1	3	7	11.75	20
21	3	2.043	4.085	5	1	5	5	11.75	19
22	3	2.043	4.085	5	1	5	7	11.75	20
23	3	2.043	4.085	5	1	7	5	11.75	20
24	3	2.043	4.085	5	1	7	7	11.75	20
25	3	2.043	4.085	5	1	11	7	11.75	20
26	3	2.180	4.359	5	2	3	7	11.035	20
27	3	2.254	4.507	5	2	7	7	10.65	20
28	3	2.043	4.085	9	1	5	5	11.75	19
29	3	2.064	4.127	9	1	5	7	11.64	20
30	3	2.137	4.275	9	1	7	5	11.255	20
31	3	2.085	4.169	9	1	7	7	11.53	20
32	3	2.043	4.085	9	1	11	7	11.75	10
33	4	3.380	4.507	1	1	0	7	10.65	10
34	4	3.380	4.507	5	1	3	7	10.65	21
35	4	3.380	4.507	5	1	7	7	10.65	20
36	4	3.380	4.507	5	1	12	7	10.65	20
37	4	3.380	4.507	5	2	3	7	10.65	22
38	4	3.380	4.507	5	2	7	7	10.65	20
39	6	4.507	4.507	1	1	0	7	10.65	10
40	6	4.085	4.085	5	1	3	7	11.75	5
41	6	4.085	4.085	5	1	7	7	11.75	6
42	6	4.085	4.085	5	1	11	7	11.75	7
43	6	4.085	4.085	5	2	3	7	11.75	6
44	6	4.085	4.085	5	2	7	7	11.75	6
45	8	5.021	6.128	1	1	0	7	11.75	20
46	8	5.540	6.761	3	1	5	5	10.65	10
47	8	5.540	6.761	3	1	5	7	10.65	10
48	8	5.540	6.761	3	1	7	7	10.65	10
49	8	5.540	6.761	3	1	12	7	10.65	10
50	8	5.021	6.128	5	1	3	7	11.75	19
51	8	5.021	6.128	5	1	5	5	11.75	20
52	8	5.021	6.128	5	1	5	7	11.75	20
53	8	5.021	6.128	5	1	7	5	11.75	20
54	8	5.021	6.128	5	1	7	7	11.75	20
55	8	5.021	6.128	9	1	5	5	11.75	20
56	8	5.021	6.128	9	1	5	7	11.75	20
57	8	5.021	6.128	9	1	7	5	11.75	20
58	8	5.021	6.128	9	1	7	7	11.75	20
59	8	5.021	6.128	9	1	11	7	11.75	10

Discussion

The paper was presented by R Jockwer

Z Li said that this area of study is important for structural analysis. He asked if this can be applied to beam to column connections. R Jockwer said that most studies has parallel to grain information. It may be possible to do more research. There are works in Växjö Sweden on the topic.

L-M Ottenhaus commented about the 95th percentile and the 5th percentile curve and CLT. H Blass confirmed there may be a factor of up to 10.

C Sigrist commented that large connections may have higher stiffness. In some large connections very small deformation was observed without ductile behaviour. R Jockwer agreed and there are many more possibilities that need to be studied.

Design Parameters of Notched Connections for TCC Structures as Part of Eurocode 5

Prof. Dr.-Ing. Ulrike Kuhlmann, Head of Institute

Simon Mönch, M.Sc., Scientific Researcher

Institute of Structural Design, University of Stuttgart, Germany

Keywords: Timber-Concrete Composite, Notched Connections, Design Parameters

1 Introduction

Timber-concrete composite (TCC) structures are an economical solution for multi-storey buildings and bridges. Due to high values of stiffness and load-bearing capacity notched connections (see Figure 1.1) are one of the most efficient connections between timber and concrete of mixed structures. In addition, the fabrication of notches does not need any special skills beyond the typical knowledge of carpentering timber connections.

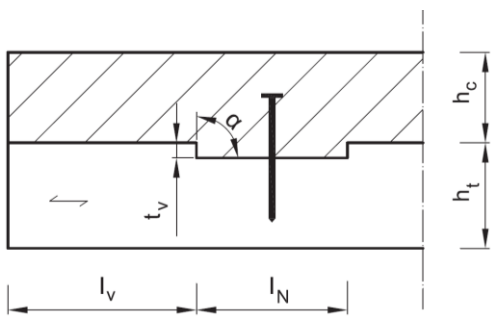


Figure 1.1. Notched connection with geometrical parameters: t_v = notch depth, l_N = notch length, l_v = timber length in front of the notch, h_t = timber thickness, h_c = concrete thickness, α = notch inclination of the edge (Kudla 2017).

All over the world, different universities and research institutions investigated notched connections. Thereby, various kinds of test setups, material properties and different

geometries of test specimens as well as different methods of evaluation and measurement devices were used.

Usually push-out tests (e.g. Figure 2.1) are conducted to investigate the load-bearing capacity, the stiffness and failure modes of notches. Thereby, the gained values can be used for the design of TCC floor or bridge systems.

In 2015 Kudla (2017) conducted 20 push-out tests within 5 test series. Therein, the geometry of the notch was varied and tests without screws and tests with different configurations of screws were conducted. To investigate the impact of further geometrical variations, in 2017 additional 12 push-out tests within 4 test series were conducted at the University of Stuttgart (Mönch & Kuhlmann (2018)). Herein, the length in front of the loaded edge of the notch as well as the orientation of the lamellae were varied. In consideration of the mentioned tests and based on extensive comparative literature studies by Kudla (2015), proposals for the design of notched connections were derived. These suggestions comprise values of the stiffness of notched connections in TCC elements as well as recommendations about corresponding assumptions concerning material properties and geometry.

A new part on TCC structures will be added as CEN Technical Specification to the future Eurocode 5. Therein, also information on joints between timber and concrete will be included and the most important characteristics and properties of a notched shear connection given. Therefore, the results presented in this paper can be helpful and lead to an improvement of the economical use of TCC structures in practice.

2 Overview of conducted push-out test program

All specimens realised in the 2 test programs in Stuttgart were made of glued-laminated timber out of spruce GL 24h according to EN 14080 (2013).

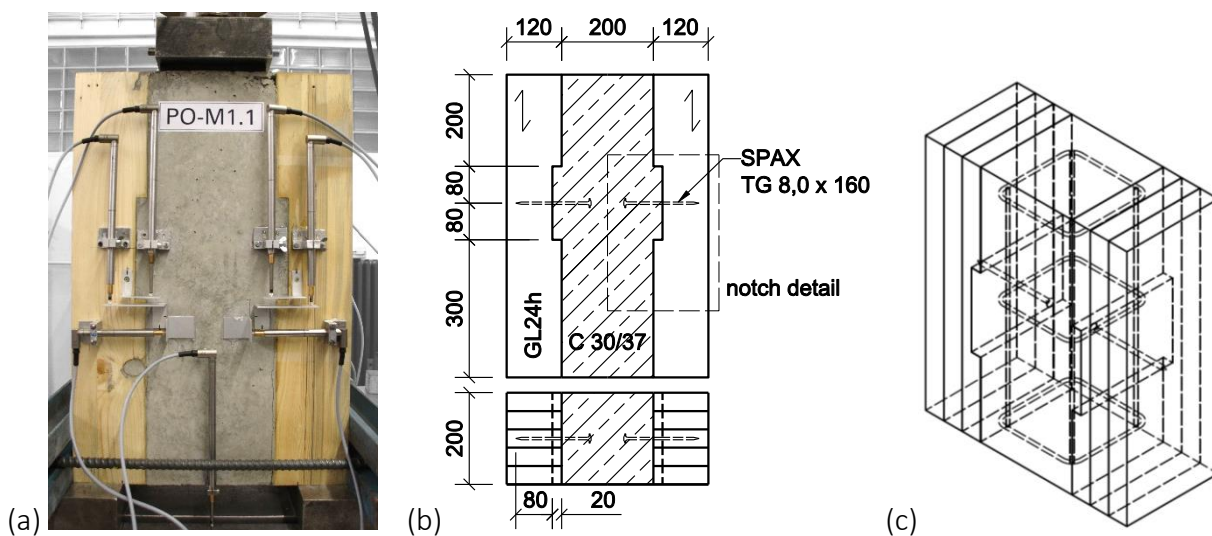


Figure 2.1. (a) Test specimen PO-M1.1 installed in test machine, (b) Front view and top view of test Series PO-1 or PO-M4 with dimensions in mm, (c) Isometric drawing of test series PO-M3 with orientation of the glulam-lamellae and reinforcement.

Each glulam-lamella had a width of 40 mm and the concrete quality was C 30/37 according to EN 1992-1-1 (2004). In all timber elements of the push-out test specimens the depth of the notch, which was milled in the timber, was $t_v = 20$ mm (see Figure 2.1). The width of one specimen was 200 mm and the same width was chosen for timber and concrete elements. In most of the test specimens in the middle of the notch one self-drilling washer head screw SPAX 8.0 x 160 according to National Technical Approval Z.9.1-449 (DIBt 2012) was applied (see Figure 2.1 (b) and Table 2.1). The secondary reinforcement (diameter of 6 mm) inside the concrete elements, which was used for all test specimens, is shown in Figure 2.1 (c).

In total, 32 symmetrical push-out tests within 9 test series were conducted, see Table 2.1 that shows the varied parameters of each test series. All test series PO-1 to PO-5, which were conducted in 2015, had a timber length in front of the loaded edge of the notch of $l_v = 300$ mm, which corresponds to 15 times the notch depth. Within these five test series also all glulam-lamellae were located in upright direction (standing lamellae). However, within test series PO-M1 to PO-M4 conducted in 2017, the timber length in front of the loaded edge of the notch as well as the orientation of the glulam-lamellae were varied. To ensure comparability, test series PO-M4 of the series in 2017 was produced with the same geometry as test series PO-1 conducted in 2015.

Table 2.1. Overview and configuration of all conducted push-out test series in 2015 and 2017

Series number	Number of specimens	Length of notch [mm]	Screw in the notch	l_v [mm]	$l_v \triangleq$	Glulam-lamellae
PO-1	7	160	X	300	$15 \cdot t_v$	upright
PO-2	3	120	X	300	$15 \cdot t_v$	upright
PO-3	3	200	X	300	$15 \cdot t_v$	upright
PO-4	4	160	-	300	$15 \cdot t_v$	upright
PO-5	3	200	X*	300	$15 \cdot t_v$	upright
PO-M1	3	160	X	300	$15 \cdot t_v$	lying
PO-M2	3	160	X	160	$8 \cdot t_v$	upright
PO-M3	3	160	X	160	$8 \cdot t_v$	lying
PO-M4	3	160	X	300	$15 \cdot t_v$	upright

* Additional screws in front of the loaded edge of the notch

The length of the notch was varied among the test series PO-1 to PO-5, see marked detail in Figure 2.1. (b). For test series PO-1, which represents the standard case, the length of the notch was chosen to 160 mm and there was always one washer head screw in the middle of the notch. For test series PO-2 and PO-3 the length of the notch was chosen to 120 mm and 200 mm, respectively. The original intention of this variation was to initiate different failure modes of concrete and timber.

Whereas usually a screw was placed inside the notch, see Figure 2.2, for test series PO-4 no screws were used in the notch to investigate the influence of the screws. In order to prevent a timber shear failure in front of the loaded edge of the notch as well as to

increase the stiffness and load-bearing capacity of the notch, for test series PO-5 four additional screws were applied in front of the loaded edge of the notch.

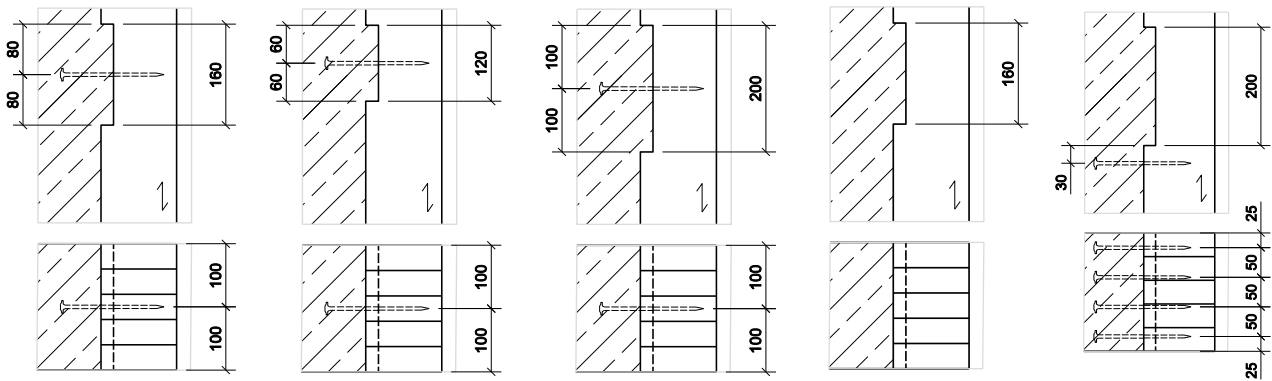


Figure 2.2. Overview of the five conducted push-out test series in 2015, from left to right: Test series No. PO-1, PO-2, PO-3, PO-4 and PO-5, dimensions in mm (Kudla 2017).

Figure 2.3 shows the varied geometrical parameters as well as the orientation of the glulam-lamellae of test series PO-M1 to PO-M4. Also, in these test series self-drilling washer head screws were applied in the middle of the notch. Differently to the other test series, the specimens of test series PO-M1 and PO-M3 were produced with lying glulam-lamellae. For test series PO-M2 and PO-M3 the timber length in front of the loaded edge was reduced to 8 times the notch depth. The intention was to investigate the effects of the timber geometry on the load-bearing behaviour and failure modes. In Figure 2.3 the possible shearing zone, in which a shear failure of the timber might occur, is marked dotted.

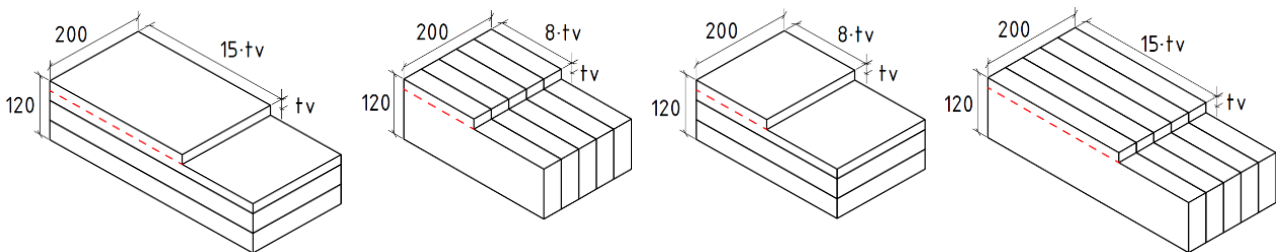


Figure 2.3. Overview of the four conducted push-out test series in 2017, from left to right: Test series No. PO-M1, PO-M2, PO-M3 and PO-M4, possible shearing zone marked dotted, dimensions in mm (Mönch & Kuhlmann (2018)).

All push-out tests were conducted under static loading applying the vertical machine load on the centre of the concrete surface. All push-out tests specimens were supported on steel bearing plates with a width 80 mm underneath the timber elements. Thus, a possible shear failure of the timber in front of the loaded edge of the notch was not excluded (see test setup in Figure 2.1 (a)).

3 Results of the conducted push-out tests

3.1 Comparison of failure modes and failure progress

In principal, the occurred failure modes of the 9 conducted push-out test series, with at least 3 tests each, may be classified into two fundamentally different types. All test

series with a timber length in front of the loaded edge of the notch of $l_v = 15 \cdot t_v = 300$ mm (PO-1 to PO-5, PO-M1 and PO-M4) showed a ductile failure mode as compression failure of the wooden fibres (see Figure 3.1 (a)). In comparison, all other test series with a timber length in front of the loaded edge of the notch of $l_v = 8 \cdot t_v = 160$ mm (PO-M2 and PO-M3) showed a brittle failure mode as shear failure of the timber in front of the loaded edge of the notch (see Figure 3.1 (b)). While all tests with ductile timber failure modes were stopped after 20 mm displacement was reached, the brittle shear failure occurred after only a displacement of around 1.5 mm at the notch.

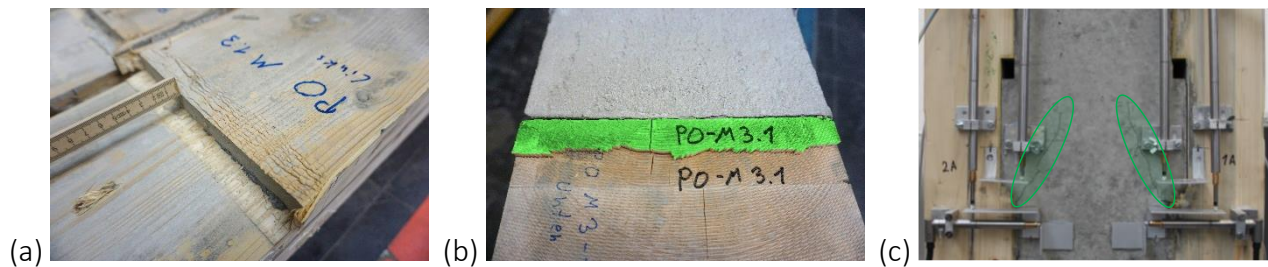


Figure 3.1. Failure modes and failure progress: (a) Timber compression failure in front of the loaded edge of the notch, (b) Timber shear failure in front of the loaded edge of the notch, (c) Concrete failure as cracks starting from the loaded edge of the notch.

As a secondary failure, shortly before reaching the maximum load, all 9 test series showed inclined cracks in the concrete elements which always started from the loaded edge of the notch at the concrete (see Figure 3.1 (c)). Table 3.1 summarises all occurred failure modes of the 9 test series.

Table 3.1. Overview on the failure modes of push-out test series conducted in 2015 and 2017

Series number	Failure mode	Failure progress
PO-1 to PO-5, PO-M1 + PO-M4	Timber: Compression Compression failure of wooden fibres in front of the loaded edge of the notch	Ductile compression of timber up to a displacement of around 20 mm, inclined concrete cracks shortly before reaching the maximum load
PO-M2	Timber: Shear Shear failure in front of the loaded edge of the notch (lamellae partially)	Brittle shear failure of timber after a displacement of around 1.5 mm, inclined concrete cracks shortly before reaching the maximum load
PO-M3	Timber: Shear Shear failure in front of the loaded edge of the notch (along entire width of the notch)	Brittle shear failure of timber after a displacement of around 1.0 mm, inclined concrete cracks shortly before reaching the maximum load

Comparing the failure modes of PO-M1 (lying lamellae) and PO-M4 (upright lamellae) or PO-M2 (upright lamellae) and PO-M3 (lying lamellae), it is obvious that the orientation of the glulam-lamellae has no relevant influence on the failure mode and that the failure mode seems only depending on the length of the timber part in front of the loaded edge of the notch.

3.2 Stiffness and load-bearing capacity

Up to a displacement of 1 mm, all specimens of all test series showed a very similar initial load-bearing behaviour, see Figure 3.2 on the mean values of the load-displacement curves for test series PO-1 to PO-5. All values were obtained from vertical measurement devices, which were placed in the area of the notch. In Figure 3.3 the corresponding load-displacement curves for test series PO-M1 to PO-M4 are shown. For better comparison, Figure 3.2 and Figure 3.3 are scaled to the corresponding maximum load F_{max} for each group of test series of 662 kN/m for Figure 3.2 and 549 kN/m for Figure 3.3. In general, all 9 test series showed a linear-elastic behaviour until 70 % to 80 % of the maximum load of the corresponding test series was reached. As a consequence, a difference between the stiffness value of the serviceability limit state or the ultimate limit state K_{ser} and K_u cannot be stated. Subsequently, a steady decrease of stiffness appeared, until a non-linear/plastic behaviour occurred. This non-linear behaviour started from an already small displacement below 1 mm.

For the test series with longer timber length in front of the loaded edge of the notch ($l_v = 15 \cdot t_v = 300$ mm) the failure mode was characterized by timber failure due to compression parallel to grain (see Figure 3.1 (a)). Thereby, the transition from linear-elastic to plastic behaviour can be characterized by a timber compression failure. As a consequence, deformation and shear cracks also occurred in the concrete. The variation of the length of the notch (between 120 and 200 mm within test series PO-1 to PO-3) did not show an effect on the resulting failure mode and the resulting stiffness. Within test series PO-4 no screws were placed in the middle of the notch. Nevertheless, the mean values of test series PO-1 (with a screw in the middle of the notch) and test series PO-4 (without screws) are similar (see Figure 3.2). Therefore, an effect of screws in the notch on the stiffness or load-bearing capacity could not be determined.

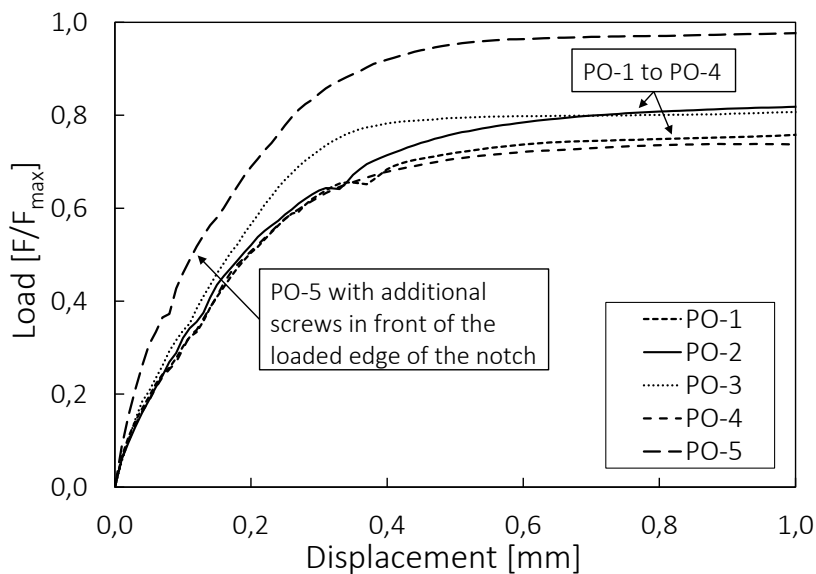


Figure 3.2. Mean values of load-displacement curves of push-out test series PO-1 to PO-5 conducted by Kudla (2017) at the University of Stuttgart in 2015.

Test series PO-5, with additional screws in front of the loaded edge of the notch, did not show a different failure mode as the other test series, but a higher load level was reached. As within the test series with longer timber length in front of the loaded edge of the notch ($l_v = 15 \cdot t_v = 300$ mm) and also in PO-5, a shear failure of timber never occurred, an effect of additional screws preventing a shear failure mode cannot be concluded. However, test series PO-5 showed that additional screws in front of the loaded edge of the notch lead to an increase of stiffness (+ 80 %) and a higher load-bearing capacity (+ 20 %) compared to test series without screws in front of the loaded edge of the notch.

Table 3.2 shows the resulting slip moduli K_{ser} , which were determined between 10 % and 40 % of the maximal load, according to EN 26891 (1991), as mean values of each test series. Additionally, the mean values of the maximum force F_{max} of each test series (referred to 1 m width) as well as corresponding coefficients of variation are shown.

Table 3.2. Resulting mean values of the slip modulus K_{ser} and maximum load F_{max} of the notch per 1 m width for all conducted push-out test series in 2015 and 2017

Series number	$l_v \triangleq$	Glulam-lamellae	K_{ser} (mean) [kN/mm/m]	Coefficient of variation [-]	F_{max} (mean) [kN/m]	Coefficient of variation [-]
PO-1	$15 \cdot t_v$	upright	1372	0.216	541	0.031
PO-2	$15 \cdot t_v$	upright	1571	0.151	602	0.053
PO-3	$15 \cdot t_v$	upright	1971	0.200	582	0.115
PO-4	$15 \cdot t_v$	upright	1629	0.265	509	0.041
PO-5*	$15 \cdot t_v$	upright	2816	0.177	662	0.057
PO-M1	$15 \cdot t_v$	lying	1327	0.060	549	0.080
PO-M2	$8 \cdot t_v$	upright	942	0.009	473	0.014
PO-M3	$8 \cdot t_v$	lying	813	0.380	462	0.034
PO-M4	$15 \cdot t_v$	upright	1133	0.168	516	0.026

* Additional screws in front of the loaded edge of the notch

Also, within the test series conducted in 2017 for all specimens with longer timber length in front of the notch ($l_v = 15 \cdot t_v = 300$ mm) all slip moduli led to values clearly above 1000 kN/mm/m. However, both test series (PO-M2 and PO-M3) with shorter timber length in front of the notch ($l_v = 8 \cdot t_v = 160$ mm) led to K_{ser} values below 1000 kN/mm/m and thus to reduced K_{ser} values by about 40 % compared with the values of the test series with longer timber length in front of the loaded edge of the notch. Table 3.3 shows mean values of groups of the test specimens for the four main variants.

Table 3.3. Resulting mean values of the slip modulus K_{ser} and maximum load F_{max} of the notch per 1 m width, summarised for the four relevant groups of push-out test series in 2015 and 2017

Series number	$l_v \triangleq$	K_{ser} (mean) [kN/mm/m]	Coefficient of variation [-]	F_{max} (mean) [kN/m]	Coefficient of variation [-]
PO-1 to PO-4	$15 \cdot t_v$	1571	0.240	551	0.082
PO-5*	$15 \cdot t_v$	2816	0.177	662	0.057
PO-M1 + PO-M4	$15 \cdot t_v$	1230	0.137	532	0.064
PO-M2 + PO-M3	$8 \cdot t_v$	878	0.220	472	0.027

* Additional screws in front of the loaded edge of the notch

Figure 3.3 shows the mean values of the load-displacement curves for test series PO-M1 to PO-M4. The test series with longer timber length in front of the loaded edge of the notch (PO-M1 and PO-M4) showed a quite similar load-bearing behaviour as the above-mentioned test series PO-1 to PO-5 (see Figure 3.2). On the other hand, test series PO-M2 and PO-M3 with shorter timber length in front of the loaded edge of notch ($l_v = 8 \cdot t_v = 160$ mm) showed a quite different load-bearing behaviour. After an initial linear-elastic behaviour a steady decrease of stiffness occurred. This non-linear behaviour only lasted shortly, until from an already small displacement of 1 mm to 1.5 mm, a brittle shear failure of timber in front of the loaded edge of the notch occurred for these test specimens (see Figure 3.3).

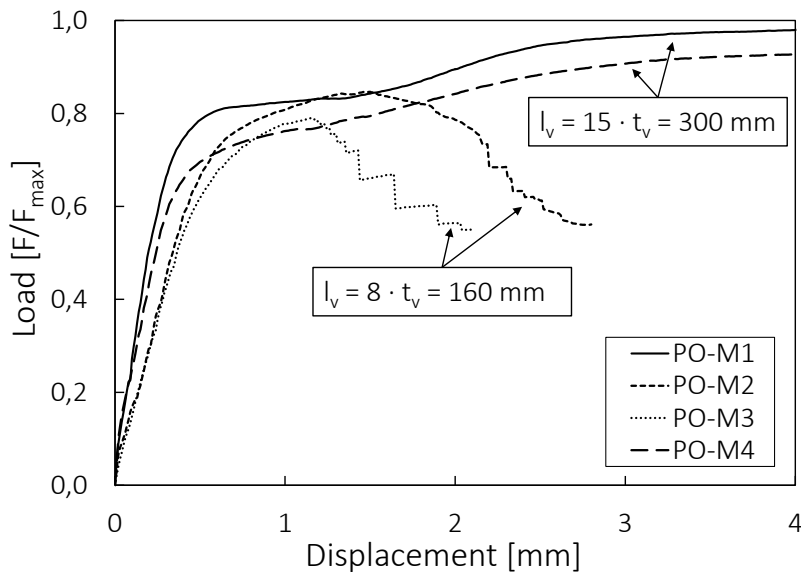


Figure 3.3. Mean values of load-displacement curves of push-out test series PO-M1 to PO-M4 conducted at the University of Stuttgart in 2017.

Due to an early brittle shear failure of the specimens of test series with shorter timber length in front of the loaded edge of the notch ($l_v = 8 \cdot t_v = 160$ mm), aside of the already mentioned lower values of stiffness, also the maximum load F_{max} reached 13 % lower values compared with the values of specimens with longer timber length in front of the loaded edge of the notch (see Table 3.3).

Additionally, the orientation of the glulam-lamellae within test series PO-M1 to PO-M4 was varied (see Figure 2.3). Comparing the resulting stiffnesses of PO-M1 and PO-M3

(both with lying lamellae) with PO-M2 and PO-M4 (both with upright lamellae) it is obvious that the lamellae orientation has no effect on the resulting slip modulus and the failure mode. Table 3.3 shows that the spreading of the resulting values of the slip modulus K_{ser} with a maximum coefficient of variation of 22 % (for test series PO-M2 and PO-M3) is significantly larger than the maximum coefficient of variation of the maximum loads of 8.2 % (for test series PO-1 to PO-4). This illustrates that the maximum load of a notched connection can be quantified in a more consistent way than the strongly spreading values of the slip moduli.

4 Further comparisons with data from literature

Within COST Action FP1402 a detailed comparison of literature about notched connections for TCC structures was conducted by Kudla (2015). Table 4.1 shows an extract of the results of further investigated push-out tests on timber-concrete composite elements with notched connections. Therein, results of test series with specimens and notches, which were comparable regarding geometry and material properties also to the own conducted tests, are considered.

Aside of the material quality and the notch size, Table 4.1 also lists the failure modes observed in the different tests series according to the given literature. It became apparent that the material quality, a variation of material properties and geometry of the specimens, the position of measurement devices and the test set-up as well as the corresponding loading protocol may have affected the resulting values of the slip modulus.

Table 4.1. Results of push-out tests with notches with a depth of $t_v = 20$ mm evaluated in a literature study by Kudla (2015)

Literature	$l_v \triangleq$	Concrete quality	Timber quality	K_{ser} (mean) [kN/mm/m]	Failure mode
Grosse (2005)	$12.5 \cdot t_v$	C 35/45	Stacked board S10 (C24)	1602	Stress in concrete / (Compression parallel to grain)
Schönborn (2006)	$18.0 \cdot t_v$	C 25/30	GL 24h	1368	Compression parallel to grain / (Shear in concrete)
Michelfelder (2006)	$12.5 \cdot t_v$	C 20/25	Stacked board S7 (C16)	706	Shear of timber in front of the notch
Simon (2008)	$12.5 \cdot t_v$	C 25/30	GL 28h	737	Compression parallel to grain / Shear of timber in front of the notch
Kuhlmann & Aldi (2010)	$10.0 \cdot t_v^*$	C 30/37	GL 32h	1757	Shear of timber in front of the notch

* $t_v = 40$ mm

In general, results of the selected test series from Schönborn (2006) and Grosse (2005) show quite similar values of slip moduli when compared to the own test series with a

timber length in front of the loaded edge of the notch of $l_v = 15 \cdot t_v$, see Table 3.3 and Table 4.1.

In contrast, the resulting slip modulus in Michelfelder (2006) and Simon (2008) is lower compared to all other tests series. Measurements in the second series at the University of Stuttgart (Mönch & Kuhlmann (2018)) showed higher values of K_{ser} for displacements measured at the notch in comparison with displacement measurements when the devices were located at the bottom of the timber element. In Michelfelder (2006) K_{ser} was determined by displacements measured at the bottom of the timber element, which might be an explanation for the relatively low values.

In Kuhlmann & Aldi (2010) a depth of the notch of $t_v = 40$ mm was investigated, and high values of slip modulus were achieved in spite of the shear failure mode, see Table 4.1 In addition, further literature studies of Kudla (2015) showed that push-out tests with notches with a depth of $t_v \geq 30$ mm led to higher values of the slip moduli compared to tests with $t_v = 20$ mm.

In addition, a parameter study was conducted on a framed model of a TCC floor system, which was validated by beam tests, in order to investigate the effects of varied slip moduli of notches as connections for TCC floors on resulting deflections and internal forces (Mönch et al. (2016)). Results are given in Figure 4.1.

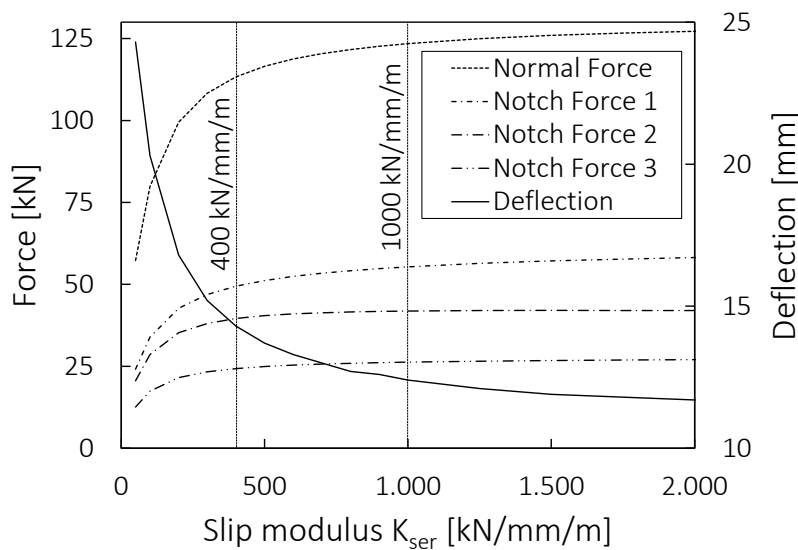


Figure 4.1. Parameter study on a 6 m TCC floor with 6 notches and a 400 mm wide section of a GL 24h timber element and a C30/37 concrete element, each of 120 mm height. Normal force and notch forces as well as deflection in midspan given for varied slip moduli K_{ser} .

As shown in Figure 4.1, slip moduli of notches with K_{ser} values below 400 kN/mm/m lead to continuously increasing internal forces and deflections of TCC floors. However, above a value of $K_{ser} = 1,000$ kN/mm/m only negligible small effects regarding the change of internal forces and deflections can be observed. As a consequence, certain “inaccuracy” of the assumption for the slip modulus in this range may be accepted.

The recent tests conducted at the University of Stuttgart as well as most of other push-out tests found in literature were carried out with a depth of the notch of $t_v = 20$ mm.

For this, under corresponding boundary conditions such as material properties and geometry (see Chapter 5.2), a value of the slip modulus $K_{ser} = 1000 \text{ kN/mm/m}$ may be assumed as a lower bound. This is supported by sufficient data. In addition, a second value of $K_{ser} = 1500 \text{ kN/mm/m}$ is recommended for notches with a depth of $t_v \geq 30 \text{ mm}$. Also for this conclusion some literature exists (see evaluation in Kudla (2015)).

While other TCC-connectors like screws are usually covered by national technical approvals, the most important characteristics and properties of notched connections are not covered and should be included in the future Technical Specification on TCC structure for the new Version of Eurocode 5. Therefore, suggestions for design parameters of notched connections and corresponding boundary conditions for material properties and geometry are given in Chapter 5.2.

5 Conclusions and Suggestions for Design Parameters of Notched Connections

5.1 Conclusions

In this paper, several experimental push-out test results, obtained from in total 32 symmetrical push-out tests within 9 test series, which were conducted at the University of Stuttgart recently, were presented. Various parameters were varied and results also from literature studies were put together to derive recommendations and provide important parameters for the design of notched connections.

The mainly observed decisive failure modes may be classified into abrupt brittle timber shearing failure and gradually increasing ductile compression failure from the timber in front of the loaded edge of the notch.

For a common notch depth of $t_v = 20 \text{ mm}$ several test series with a timber length in front of the loaded edge of the notch of $l_v = 15 \cdot t_v = 300 \text{ mm}$ always showed a ductile failure mode with a resulting slip modulus K_{ser} clearly above 1000 kN/mm/m . For the test series with shorter length of timber in front of the loaded edge of the notch ($l_v = 8 \cdot t_v = 160 \text{ mm}$), aside of a reduced maximum load capacity, also always a brittle failure mode (shear failure of timber) occurred and the slip modulus resulted in lower values. As a ductile failure mode is preferable to an abrupt brittle failure mode, a timber length in front of the loaded edge of the notch of $l_v = 15 \cdot t_v$ is recommended. This is also the case for a notch depth of $t_v \geq 30 \text{ mm}$ with a recommended stiffness value of $K_{ser} = 1500 \text{ kN/mm/m}$.

It was shown that single screws in the area of the notch do not increase or even influence the stiffness of notched connections. However, in most cases a screw was placed in the notch of the push-out specimens to prevent a separation of the composite elements, which is also recommended as a construction rule mainly. In addition, tests with several closely placed screws in the timber in front of the loaded edge of the notch

showed the possibility to even increase the already high values of stiffness and load-bearing capacity. However, it is not yet possible to quantify this effect for a design rule.

The other parameters such as the length of the notch l_N , the orientation of the glulam-lamellae, the inclination of the edge of the notch or the material qualities of timber and concrete did either not show a decisive effect or could not be varied sufficiently within the tests series so that only minimum conditions are concluded as recommendations to limit the application range for the suggestions on the design of notched connections.

5.2 Suggestions for Design Parameters of Notched Connections

The following suggestions for design parameters of notched connections are based on one hand on extensive experimental tests at the University of Stuttgart (see e.g. Kudla (2017), Mönch & Kuhlmann (2018)) and on the other hand on results of comprehensive literature studies by Kudla (2015).

Depending on commonly used values of the depth of the notch t_v it was decided to officially agree on stiffness values of the notch K_{ser} . For notches of 20 mm and 30 mm and more depth, it is proposed to determine the value K_{ser} to 1000 and 1500 kN/mm per metre width, respectively. Due to the almost constant stiffness in the load-bearing behaviour of the notches up to point when the maximum load nearly is reached, it is recommended to use the same stiffness values of the notch ($K_u = K_{ser}$) for ultimate limit state as well as for serviceability limit state.

The slip moduli K_{ser} determined above should be applied under the following conditions, which are stated mainly due to the limited amount of test specimens:

- Glued-laminated-timber (minimum GL 24h) according to EN 14080 (2013) or Stacked board elements (minimum C 24) according to EN 338 (2016)
- Concrete (minimum C 20/25) according to EN 1992-1-1 (2004)
- Concrete maximum grain size 16 mm
- Glulam-lamellae orientation “upright” or “lying”
- Washer head screws in the notch ($D \geq 6$ mm) (construction rule preventing uplift)
- Depth of the notch t_v at least 20 mm
- Length of the notch l_N at least 150 mm and at most 200 mm
- Timber length in front of the loaded edge of the notch l_v at least $15 \cdot t_v$
- Inclination of the edge of the notch α between 90° and 100°

The results will contribute to the preparation work (Technical Specification of Project Team CEN/TC 250-SC5.T2, Dias et al. (2017)) for the new TCC rules in the forthcoming new version of Eurocode 5 and will increase the economical use of notched connections in practice.

6 Acknowledgements

The research was financially supported by the Federal Ministry of Economics and Technology via the funding organisation AiF. This support is gratefully acknowledged. The additional test specimens for the experimental investigations in 2017 were financially supported by PIRMIN JUNG Deutschland GmbH. This support is gratefully acknowledged. Moreover, we thank SPAX International GmbH & Co. KG for providing screws for the specimens.

7 References

- Kudla, K. (2017): Kerven als Verbindungsmittel für Holz-Beton-Verbundstraßenbrücken (in German). Institute of Structural Design, University of Stuttgart, Mitteilung No. 2017-02, PhD thesis
- Kudla, K. (2015): Notched Connections for TCC Structures as Part of the Standard. Short Term Scientific Mission, COST Action FP 1402, University of Stuttgart
- Mönch, S. & Kuhlmann, U. (2018): Investigations on the effect of geometry in timber-concrete composite push-out tests with notched connections. In: Seoul National University (Ed.): WCTE 2018, World Conference on Timber Engineering, Seoul (Republic of Korea), 20.08.-23.08.2018
- EN 14080 (2013): Timber structures – Glued laminated timber and glued solid timber – Requirements. European Committee for Standardization (CEN), Brussels
- EN 1995-1-1 (2004): Eurocode 5: Design of timber structures – Part 1-1: General – Common rules and rules for buildings. European Committee for Standardization (CEN), Brussels, with corrections and amendments + AC:2006 and A1:2008
- EN 1992-1-1 (2004): Eurocode 2: Design of concrete structures – Part 1-1: General rules and rules for buildings. European Committee for Standardization (CEN), Brussels with corrections and amendments + AC:2010
- EN 338 (2016): Structural timber – Strength classes; European Committee for Standardization (CEN), Brussels
- EN 26891 (1991): Timber Structures – Joints made with mechanical fasteners – General principles for the determination of strength and deformation characteristics. European Committee for Standardization (CEN), Brussels
- Michelfelder, B. (2006): Trag- und Verformungsverhalten von Kerven bei Brettstapel-Beton-Verbunddecken (in German). Institute of Structural Design, University of Stuttgart, Mitteilung No. 2006-01, PhD thesis
- DIBt (2012): SPAX Schrauben als Holzverbindungsmitel. SPAX International GmbH & Co. KG. Allgemeine bauaufsichtliche Zulassung Z-9.1-449 (National Technical Approval): Deutsches Institut für Bautechnik
- Mönch, S.; Kudla, K.; Kuhlmann, U. (2016): Holz-Beton-Verbundkonstruktionen mit Kerven – Tragfähigkeit und Steifigkeit (in German). In: Forum Holzbau (Hrsg.):

- Bauen mit Holz im urbanen Raum. 9. Europäischer Kongress EBH. Köln, 19.-20.10.2016, http://www.forum-holzbau.ch/pdf/15_EBH_2016_Moench.pdf
- Simon, A. (2008): Analyse zum Trag- und Verformungsverhalten von Straßenbrücken in Holz-Beton-Verbundbauweise (in German). Institute of Structural Engineering, Bauhaus-Universität Weimar, PhD thesis
- Schönborn, F. (2006): Holz-Beton-Fertigteilelemente (in German). Leopold-Franzens-Universität Innsbruck, PhD thesis
- Grosse, M. (2005): Zur numerischen Simulation des physikalisch nichtlinearen Kurzzeittragverhaltens von Nadelholz am Beispiel von Holz-Beton-Verbundkonstruktionen (in German). Institute of Structural Engineering, Bauhaus-Universität Weimar, PhD thesis
- Dias, A.; Fragiocomo, M.; Harris, R.; Kuklík, P.; Rajcic, V.; Schänzlin, J. (2017): Technical Specification 3rd Draft – Structural design of timber-concrete composite structures – common rules and rules for buildings. Eurocode 5: Design of Timber Structures, Project Team CEN/TC 250-SC5.T2, September 2017
- Kuhlmann, U. & Aldi, P. (2010): Ermüdungsfestigkeit von Holz-Beton-Verbundträgern im Straßenbrückenbau (in German). (AiF/iVTH 15052) University of Stuttgart, Institute of Structural Design, No. 2010-60X, research report

Discussion

The paper was presented by U Kuhlmann

S Winter received confirmation that screws in front of notch mean at the loaded edge and screws in the notch did not play a role.

A Frangi agrees with the results. He said screws in the notch did not play a role because the crack was developed above the screw and anchoring it in the compression zone would work.

Bond performance of glued-in CFRP and GFRP rods in timber

Dr. Eleni Toumpanaki, Research Associate, Centre for Natural Material Innovation, University of Cambridge, 1-5 Scroope Terrace, CB2 1PX, email: et343@cam.ac.uk (corresponding author)

Dr. Michael H. Ramage, Senior Lecturer in Architectural Engineering, Director Centre for Natural Material Innovation, Department of Architecture, University of Cambridge, Cambridge, UK

Keywords: Glued-in rods, Bond strength, Engineered timber, Fibre Reinforced Polymer (FRP)

1 Introduction

A rapid growth in multi-storey and tall timber buildings¹ has been observed in the last decade (e.g. the Treet building in Bergen, Norway (14 storeys, 49 m, in 2015) and the Mjøstårnet building in Oslo, Norway (18 storeys, 80 m, in 2018)) heating the competition to build taller with wood with future building proposals (e.g. the River Beech tower (Sanner et al. 2017)) showing tremendous ambition. This growth is the outcome of recent advances in engineered timber, such as glued laminated timber (glulam) and laminated veneer lumber (LVL), the turn towards sustainable building materials in light of the Paris Agreement (2016) for CO₂ emissions cuts, and construction and design advantages. One of the limitations that hinders the use of engineered timber at greater scale is the establishment of robust and rigid timber connections that can transfer high tensile axial loads and limit lateral story drifts. Glued-in rod connections are a suitable candidate for these applications due to their high axial stiffness and load transition, superior fire performance and ease of installation. The use of

¹Definition of a tall timber building based on Foster et al. (2016)

composite materials such as carbon fibre reinforced polymer (CFRP) and glass fibre reinforced polymer (GFRP) rods can result in improved durability for these connections under high moisture contents (e.g. Service Class 3 (EC5 2004)- Relative Humidity of the surrounding air exceeding 85% for several weeks per year), lower weight and better chemical compatibility between the resin and the FRP rods. Schematic details for timber diagrid structural systems with glued-in rods connected perpendicular and at an angle to the grain are shown in Figure 1.

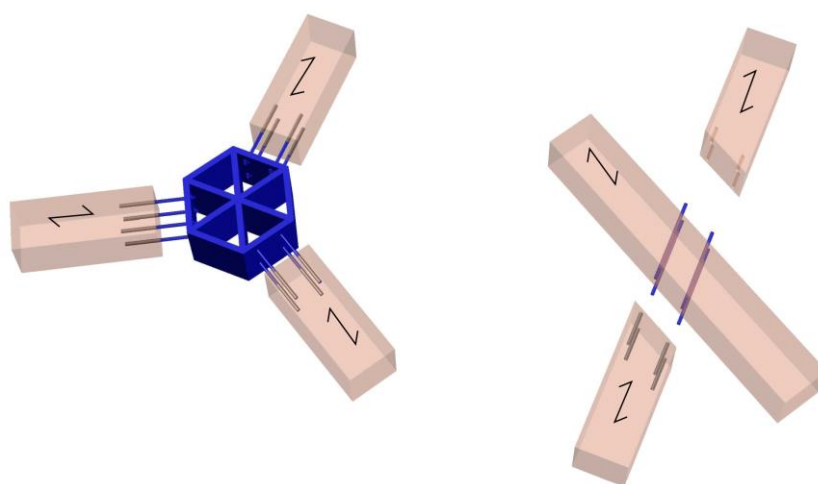


Figure 1: Schematic connection details for diagrid structural systems with glued-in rods.

Existing literature (e.g. Mettem et al. 1999 and Aicher et al. 1999) and applications (Strahm 2000) have emphasised the use of steel rods and limited research has been carried out on the use of FRP (fibre reinforced polymer) rods focusing either on GFRP (Madhoushi & Ansell 2004) or CFRP materials (De Lorenzis et al. 2005). Despite the considerable studies in glued-in steel rods (e.g. GIROD programme), there seems to be no consensus in the establishment of design methods for Eurocode 5. Various authors and national design guidelines relate the bond strength of glued-in steel rods to different parameters (e.g. timber density or glue strength), and experimental results can often be contradictory. Steiger et al. (2006) showed that the bond strength of steel rods glued parallel into the grain direction is directly influenced by the timber density, reporting bond failures by shearing off of a wooden layer at the anchorage. However, this trend was less pronounced in the experimental results by Aicher et al. (1999) with similar bond failure. Other variables such as glue line thickness, anchorage length, rod diameter, bond test methods and the lack of detailed experimental reporting (e.g. type of bond failure and mechanical properties of the glue material) inhibit firm conclusions. An increase

in the glue-line thickness is usually associated with an increase in the axial load resistance (e.g. in glued-in steel rods with a ductile epoxy adhesive in Feligioni et al. 2003 and with epoxy and polyurethane adhesives in Bengtsson & Johansson 2000), but this is highly dependent on the type of applied adhesive. The use of phenol-resorcinol has resulted in decreased bond performance with increasing glue-line thickness attributed to higher shrinkage effects and the application of polyurethane can yield bubbles at the wood/resin interface due to its reaction with the inherent timber moisture. Epoxy adhesives exhibit higher bond strength regardless of glue-line thickness. Yet, standardisation in bond performances of resins can be hindered due to constant advances in resin formulations that are usually proprietary to the manufacturers (Lees et al. 2017). Moreover, different bond test methods can result in different bond strength results and understanding of the different acting stress mechanisms is needed to enable the establishment of testing procedures. Broughton & Hutchinson (2001) showed that a pull-pull test method in timber can yield higher pull-out loads than a pull-compression test irrespective of the glue-line thickness for steel rods bonded in LVL, but these findings contradict existing literature in bond performance of steel and FRP rods in concrete structures with similar test techniques.

The aim of this study is to compare the bond performance of CFRP and GFRP rods in timber blocks under tensile static and cyclic loading and identify the relationship between bond strength and stiffness and cost for different materials. GFRP rods are usually preferred in structural applications due to their lower cost ($\sim 1/3$ of the CFRP cost). However, CFRP rods exhibit greater fatigue and creep resistance and can result in higher bond strength and stiffness due to their greater elastic modulus (Baena et al. 2009). Therefore, they can be more suitable when high strength timber connections are necessary such that their high initial cost can be justified.

2 Experimental Programme

2.1 Materials

Pultruded FRP rods (Sireg, Italy) with the same core rod diameter ($D=10$ mm), resin matrix (vinylester), fibre content ($>65\%$), and surface deformation (helically wrapped and sand coated) but different fibre type (glass versus carbon) are used in this study. The outer diameter of the rods accounting for the external sand coating layer is $D_o=10.7$ mm and $D_o=11.1$ mm for the CFRP and GFRP rods respectively according to ACI 440.3R-12 (ACI 2012) guidelines.

The rods were glued in timber specimens using a two component thixotropic adhesive of epoxy resin and special filler (Sikadur 30). The nominal mechanical properties, as provided by the manufacturers, are summarised in Table 1. The timber specimens derived from a block laminated spruce C24, made in Stora Enso Ybbs (Austria) factory using their CLT process without the cross-laminated elements.

Table 1. Material properties for FRP rods and epoxy glue.

	CFRP (Carbopree)	GFRP (Glasspree)	Epoxy glue (Sikadur 30)
Longitudinal tensile elastic modulus - E_L (MPa)	130000	46000	11200**
Average tensile strength, f_{ru} (MPa)	2450	1000	26*
Elongation at break, ε_{ru} (%)	1.8	1.8	N/A
Average shear strength, f_{vu} (MPa)	N/A	N/A	16*

*Curing conditions: after 7 days at 15°C, **Curing conditions: after 7 days at 23°C

2.2 Specimen Preparation

A 250 mm CFRP/GFRP rod was placed concentrically in a 70 x 70 x 55 mm timber block, parallel to the grain, and was glued with an epoxy layer of varying thickness ($t=1.5, 3$ and 5 mm). The bonded length was 50 mm corresponding to $5D$ where D is the core diameter of the rod. To ensure the proper alignment of the FRP rod along the bonded length, acrylic caps were prepared and applied at the loaded end (end closer to the crosshead of the Instron machine where the load is directly applied) and free end (see Figure 2a). The caps were sprayed with a demoulding agent and covered with silicone rubber (Dow Corning) to enable their easy removal after curing of the epoxy glue. The epoxy was cast vertically in the holes and the specimens were left in that position for at least 1 day before the anchorage preparation. Sleeve anchors were used, to ensure a firm grip on the FRP rods considering their inferior mechanical performance in lateral compression. The anchors consisted of black mild steel tubes with an outer diameter $D_o=31.75$ mm, thickness, $t=3.2$ mm and length $L=80-90$ mm and were filled with epoxy (Sikadur 30 or Sikadur 33). The anchors were aligned horizontally based on the rig shown in Figure 2b. Two types of anchors (Type I and Type II) were used and Type I was preferred to accelerate the alignment procedure. The specimens with a glue-line thickness $t=1.5$ and 3.0 mm were stored in the lab at $T=21.5 \pm 3.2^\circ\text{C}$ (standard deviation-STDV) and $RH=51.1 \pm 7.8\%$ (STDV) and the specimens with a glue-line thickness $t=5.0$ mm were stored

at $T = 22.0 \pm 2.3^\circ\text{C}$ (STDV) and $RH = 53 \pm 5.2\%$ (STDV). The specimens are identified here as a-b-c, where 'a' denotes the fibre type (C: Carbon and G:Glass), 'b' denotes the glue-line thickness and 'c' denotes the type of loading (s:static and c:cyclic).

To understand the bond stress transfer mechanism during pulling-out of the rod, one specimen each from the groups C-3.0-s, G-3.0-s, C-5.0-s and G-5.0-s was prepared with 4 strain gauges attached on the surface of the rod and equally distributed over the bonded length. The strain gauge cables were guided through drilled holes of 8 mm diameter from one of the 4 sides of the timber block. To enable the attachment of the strain gauges, the sand coating layer of the FRP rods was removed with a blade along the bonded length for roughly a 5 mm wide surface area.

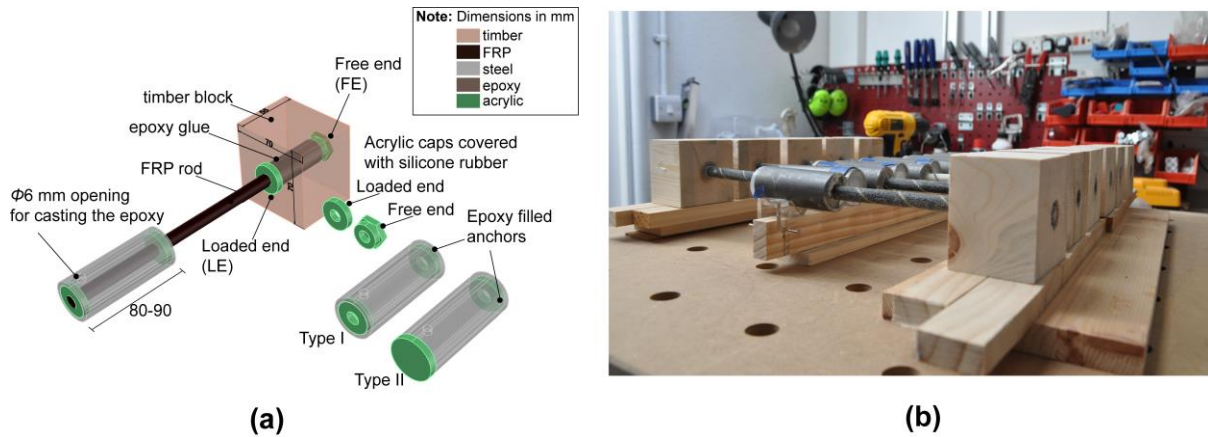


Figure 2. (a) Pull-out test specimen and (b) Alignment rig for the anchorage preparation.

2.3 Test Method

To measure the bond strength of the FRP rods glued in timber blocks, the pull-compression test method (or defined elsewhere as pull-out test) was selected due to its simplicity and ease of application for mechanical screening. The FRP rods were pulled out from the timber block that reacted against a fixed steel plate (see Figures 3a and 3b).

All specimens were tested after at least 10 days of curing of the epoxy glue. The tests were carried out in an Instron machine with a 150 kN load cell capacity in displacement control. Five specimens from each of the 12 groups (60 samples in total) were tested in a static and cyclic loading regime at a displacement rate of 0.5 mm/min. The cycling regime consisted of 3 load-unload repetitions at three target loads of $0.20-0.25F_{us}$, $0.4-0.5F_{us}$ and $0.60-0.75F_{us}$, where F_{us} is the average

pull-out failure load of each group tested statically, followed by loading up to failure. Slip values were recorded with 2 LVDTs (Linear Variable Differential Transformers) at the loaded end and 1 LVDT at the free end. Any displacement of the steel reaction plate was recorded with an LVDT during testing. Strain gauges were attached selectively at the loaded end of 4 GFRP and CFRP rods to measure experimentally their longitudinal elastic Young's modulus during the pull-compression test method. The slip values at the loaded end were corrected for the rod extension and the plate displacement and therefore the differences in the elastic modulus between the CFRP and GFRP rods were not considered. The rod extension was calculated based on the experimental elastic Young's moduli values, that were 19% and 36% higher than the nominal values of the CFRP and GFRP rods respectively, and the free unbonded length of the rod between the two anchorage points (the anchor and the loaded end). The corrected slip values were considered to be more representative of a glued in rod connection between two timber structural elements, where the unbonded length is negligible.

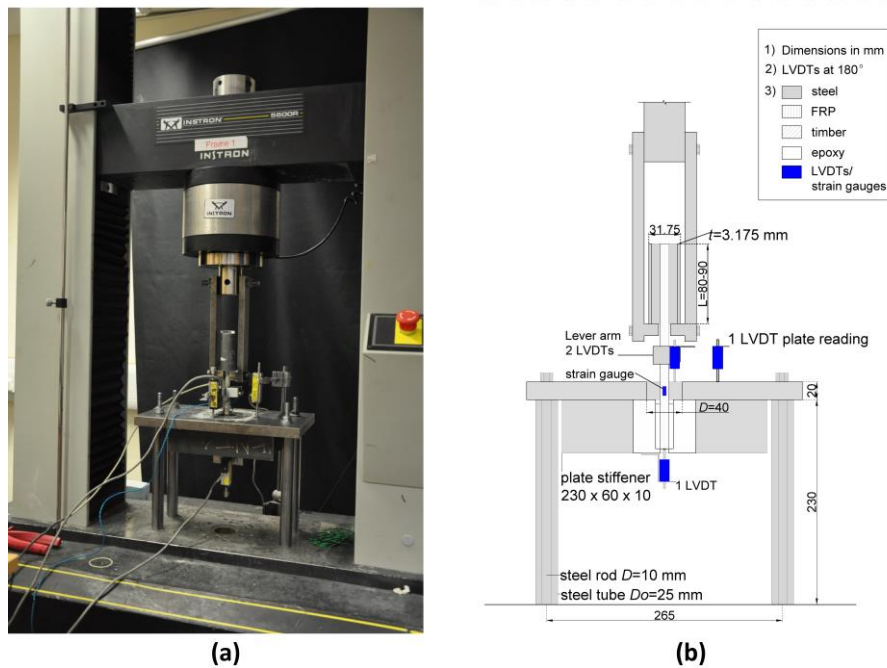


Figure 3. Pull-out test set up, (a) Photo of actual test set up and (b) Drawing.

3 Results and Discussion

3.1 Bond strength

Figure 4a shows the average pull-out load values, F_u , for each glue-line thickness ($t=1.5, 3.0$ and 5.0) and each rod material (CFRP and GFRP) after static and cyclic loading. Figure 4b shows the average bond strength values as derived

from the failure pull-out loads normalised by the surface area of the drilled hole diameter in timber, assuming a uniform bond stress distribution over the bonded length. The hole surface area was adopted as a reference area since most bond failure mechanisms occurred in the wood/resin interface. The error bars indicate one standard deviation. The red dots represent the specimens with the 4 strain gauges over the bonded length that were tested statically. These specimens were excluded from the group's average values, because it was assumed that the occupied volume of the cables from the strain gauges would result in discounted bond performance. All specimens had a timber moisture content of 9.3 ± 0.7 % (STDV) as measured with a moisture meter (EXTECH M0220) after testing.

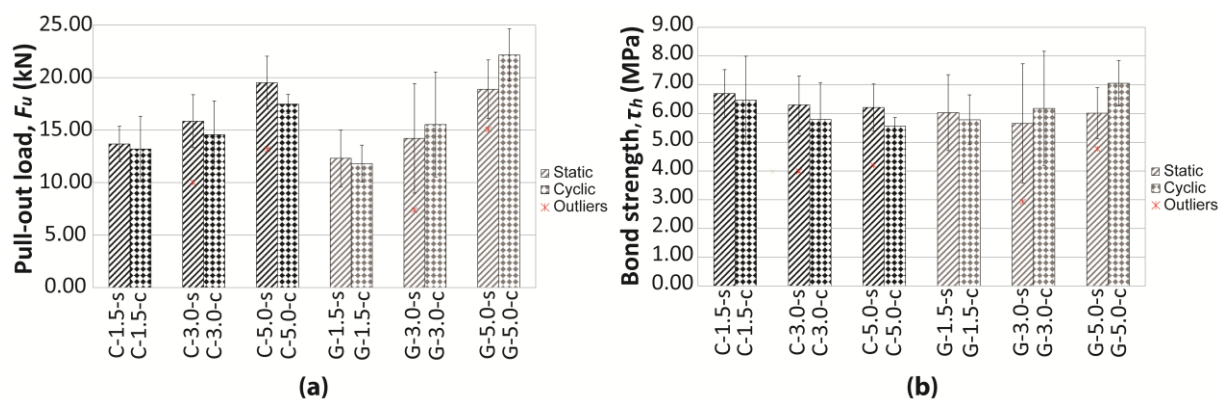


Figure 4. (a) Failure pull-out load and (b) Bond strength values after static and cyclic loading for glued-in CFRP and GFRP rod connections in timber.

All rods (CFRP and GFRP) showed an increasing trend in the average pull-out load with an increase in the glue-line thickness. Rises up to 43 and 53% were recorded under static loading with a 3.5 mm increase in the glue-line thickness for CFRP and GFRP rods respectively. Different trends were observed in terms of normalised load and bond strength values, as shown in Figure 4b. CFRP rods showed a 7% decrease in the bond strength by comparing the C-1.5-s with the C-5.0-s group and GFRP rods showed a negligible difference for the same glue-line thickness variations. In conclusion, failure loads, bond strength values and reference surface areas should be highlighted in each study in glued-in rod connections to avoid misinterpretations.

CFRP rods exhibited consistently higher average pull-out loads than the GFRP rods under static loading irrespective of the glue-line thickness. The difference between the two materials was more dominant at smaller glue-line thickness ($t=1.5, 3.0$ mm) where CFRP rods showed 11% higher axial load resistance. The cyclic loading seems to deteriorate the average axial load resistance of CFRP

rods and a maximum 10% decrease is recorded for a glue-line thickness $t=5.0$ mm (C-5.0-c versus C-5.0-s). It should be noted that one of the five specimens in group C-1.5-c failed at the first loading of the 3rd cycle ($0.66F_{us}$) at 8.09 kN. Under cyclic loading GFRP rods seemed to perform better and yielded the maximum average axial load resistance among the groups, $F_u=22.16$ kN, for a glue-line thickness $t=5.0$ mm. However, considering the observed standard deviations in the bond strength of the glued-in CFRP and GFRP rods in timber and the material variability, it can be inferred that cyclic loading does not affect the bond strength. The experimental findings agree with the existing literature. Indicatively, the G-1.5-s group yielded an average pull-out load of $F_u=12.32$ kN and Mettem et al. (1999) has reported an average pull-out load of $F_u=12.2$ kN for GFRP rods with a diameter $D=8.0$ mm glued into LVL with a 2 mm epoxy glue-line thickness and a 60 mm bonded length. The experimental results suggest that the increase in the pull-out load and the hole surface area are linearly related for both types of rods but an approximately six times increase in the glue volume can lead to a rise in axial load resistance of up to 88% (G-5.0-c versus G-1.5-c). Therefore, the relevant benefits in the axial load resistance from an increase in the glue volume and consequently cost should be estimated using engineering judgement.

3.2 Bond stress-slip plots

The bond stress-slip plots for the CFRP rods under cyclic loading are depicted in Figure 5 for the different glue-line thicknesses studied. The slip values refer to the loaded end. It can be observed that there is no decrease in the gradient and thus the stiffness of the glued-in rod connections upon cyclic loading. An increase in the residual slip values after unloading is detected and it is more pronounced with increasing loading and glue-line thickness. This is attributed to cyclic creep that is representative of viscoelastic materials such as timber and epoxy resins. The failure of the CFRP rods glued in timber parallel to the grain was brittle with a sudden drop in bond strength up to 94% of the peak values (see Figure 5d). GFRP rods exhibited similar performance.

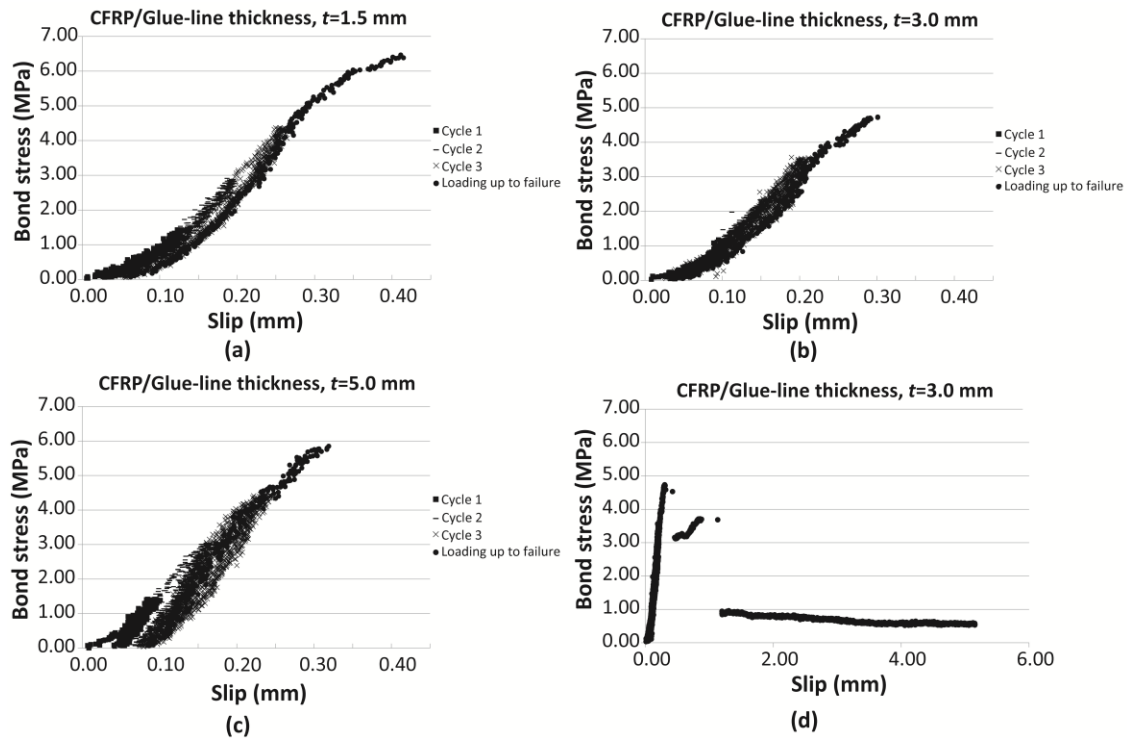


Figure 5. Bond stress-slip plots at cyclic loading for a CFRP rod with (a) glue-line thickness, $t=1.5$ mm, (b) glue-line thickness, $t=3.0$ mm, (c) glue-line thickness, $t=5.0$ mm and (d) after post-failure for glue-line thickness, $t=3.0$ mm.

3.3 Secant stiffness

Figures 6a and 6b depict the secant stiffness derived from the pull-out load versus slip plots at the Ultimate Limit State (ULS) and Serviceability Limit State (SLS). The Serviceability limit state was defined between 10 and 40% of the ultimate failure load, F_u , where structures are mostly expected to be loaded during their design life and to align with the slip modulus definition, K_{ser} , for steel dowel connections. At cyclic loading the secant stiffness was calculated as the ratio of the failure load to the loaded end slip value corrected for any residual slip at zero load. The secant stiffness at both ULS and SLS exhibited high values for a glue-line thickness of $t=5.0$ mm under both static and cyclic loading. Most specimens had a higher secant stiffness after cyclic loading with maximum values of $K_{SLS}=99.7$ kN/mm, $K_{SLS}=189.1$ kN/mm and $K_{ULS}=91.8$ kN/mm and $K_{ULS}=106.8$ kN/mm for the groups C-5.0-c and G-5.0-c respectively. This was attributed to the stiffer response observed with increasing loading combined with the corrected slip values for the residual deformations. The difference in the stiffness between glue-line thicknesses $t=1.5$ and 3.0 were limited to around $\pm 18\%$ at both static and cyclic loading except that the G-3.0-s group showed 43% lower stiffness at ULS and the C-3.0-s showed 35% lower stiffness at SLS. The slip modulus of a single dowel connection with a 10 mm steel dowel for the same timber grade is 3.7 kN/mm per shear plane according to Eurocode 5 and

can vary up to 14.8 kN/mm accounting for two shear planes and a steel-to-timber connection. However, a higher stiffness up to 38.4 kN/mm has been experimentally reported by Reynolds et al. (2016) for a single dowel connection with a 12 mm steel dowel in C16 Sitka spruce.

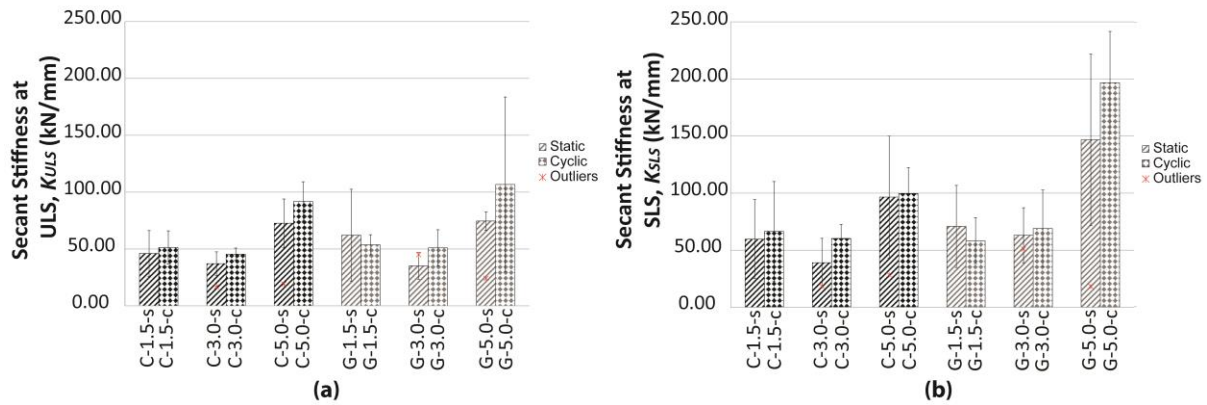


Figure 6. Secant stiffness for glued-in CFRP and GFRP rods in timber at (a) Ultimate limit state (ULS) and (b) Serviceability Limit State (SLS).

3.4 Bond failure mechanisms

The majority of the specimens failed at the wood/resin interface (W/R) (see Figure 7d) followed in some cases by a wood plug failure (WP). Mixed-mode bond failure was also observed, such as wood/resin (W/R) combined with resin/FRP (R/F) interface failure and wood/plug with resin/FRP interface failure. The definition of the bond failure mechanisms adopted in this study is depicted in Figure 7c. In the resin/FRP failure mode the failed interface was mostly between the external sand coating layer and the core rod indicating a good adhesion between the glue and the FRP. In Figures 7a and 7b the failure mechanisms with respect to the glue-line thickness and the experimental pull-out load are classified for the clear and mixed-mode bond failures. The highest axial load resistance is observed for resin/FRP interface failure modes at a glue-line thickness of $t=5.0$ mm. Considerable variations in the pull-out load lie among the W/R failure modes and firm conclusions cannot be derived. Splitting failures seem not to be linked with lower failure loads, but this can depend on the adopted test method (pull-compression).

In 15 specimens out of the 60 tested in total, the wood plug failure extended up to the hole of the reaction plate. This was mostly observed in the groups C-1.5-s and C-1.5-d. This type of failure might not have been observed in a pull-pull test procedure indicating that the bond test method can affect the bond failure and

possibly the recorded experimental bond strength values. In the wood plug failure the failed surface propagated along the growth rings at the latewood/earlywood interface or within the earlywood, as schematically shown in Figure 7c(i). During pulling out, shear stresses develop at the interface between earlywood and latewood due to the inherent differences in density and thus stiffness between the adjacent growth rings. In some specimens the wood plug failure was limited to one lamina of the timber block and the crack pattern did not expand to the adjacent one. Therefore, the wood plug failure mechanism and the relevant bond strength values are more related with the timber density (as suggested by Steiger et al. (2006)), compared with the wood/resin and resin/FRP failure mechanism. Variations in the bond strength due to material variations are also expected. By observing the wood plug failure pattern, the peak failure load seems to be related to the wood shear strength in both the longitudinal/radial and longitudinal/tangential plane. Noises of imminent failure followed with occasional visually detected radial cracks were observed during the cyclic loading at $0.75F_{us}$. Splitting was associated with 18 bond failure mechanisms (see Figures 7a and 7b) and it was mostly observed in specimens with a thicker glue-line ($t=3.0$ and $t=5.0$ mm). Splitting cracks propagated along the growth rings, were restricted in some cases within the lamina and they usually developed in the vicinity of a knot as observed in the face/edge grain of the specimen. More splitting failures were observed in GFRP rods at a glue-line thickness of $t=1.5$ mm and $t=3.0$ mm and for CFRP rods this was dominant at a glue-line thickness of $t=5.0$ mm. A higher number of splitting bond failure modes have also been recorded for Near Surface Mounted GFRP ribbed rods used in normal strength concrete when a smaller groove size and thus epoxy layer thickness was applied (De Lorenzis et al. (2002)). Similar CFRP ribbed rods but with less pronounced ribs exhibited failure at the epoxy-concrete interface. A greater splitting tendency has also been observed by Achillides & Pilakoutas (2002) in GFRP bars used as a reinforcement in concrete beams and when an adequate concrete cover was not provided. This was attributed to the lower Elastic modulus of the GFRP bars that affects their deformability both in the longitudinal and transverse direction (Poisson's ratio effect). Nevertheless, the Poisson's ratio effect should result in tensile stresses in the radial direction, where the splitting crack and radial cracks develop, based on a thick walled analysis as previously used by Tepfers (1979). De Lorenzis et al. (2005) showed that the splitting bond strength depends on the depth of the provided cover when FRP rods are glued in timber parallel to the grain by adopting a thick walled analysis. However, this analytical approach is valid for isotropic materials and might not be suitable for anisotropic materials like timber. Madhoushi & Ansell (2017) showed that the increase in glue-line

thickness for GFRP rods alleviates the axial stress concentration along the glue lines by carrying out a FE analysis. In conclusion, further investigation is needed to comprehend the effect of the glue-line thickness and the interaction of the glue and FRP (due to their inherent different material properties) in the axial stress distribution at the end grain and in the bond shear stress distribution along the bonded length.

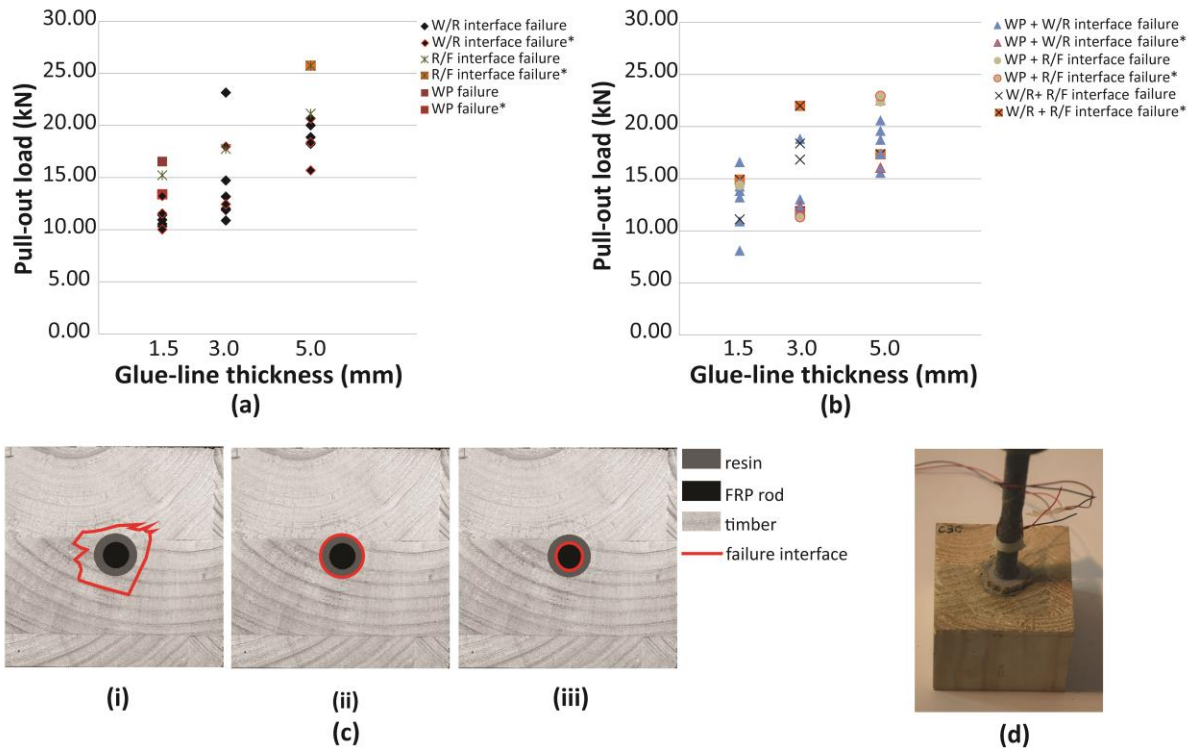


Figure 7. Pull-out load versus glue-line thickness for (a) clear bond failure mechanisms and (b) mixed-mode bond failure mechanisms, (c) Definition of bond failure mechanisms-schematic, (i) wood plug failure, (ii) wood/resin interface failure and (iii) resin/FRP failure and (d) actual photo of a typical wood/resin interface failure. Note: WP: wood plug failure, W/R: wood/resin interface failure, R/F: resin/FRP interface failure and * denotes splitting failure.

3.5 Axial strain distribution

Figures 8a and 8b depict the axial strain distribution along the bonded length for a specimen tested statically with a CFRP and GFRP rod respectively and a glue-line thickness of 5.0 mm.

In the plots the loaded and free end correspond to $x=5.0$ mm and $x=47.0$ mm respectively, where x is the centre to centre distance of the strain gauges along the bonded length. A linear strain distribution is observed for both FRP rods up to 25% of their failure load indicative of a uniform bond stress distribution. At higher loads similar strain readings are recorded at the vicinity of the loaded

end suggesting that a local debonding failure takes place. At the failure load the maximum strain values are derived at a distance, $x=19$ mm, followed by a linear strain distribution. A deviation from a linear strain distribution is observed in the CFRP rod at $x=33.0$ mm. Inspection of the specimen by splitting it open after testing showed a local void at this location for roughly $\frac{1}{4}$ of the rod surface area impeding a full wood/resin contact. The specimen with the GFRP rod had a full wood/resin contact along the bonded length. The uniform bond stress assumption seems not to be valid for bonded lengths greater than or equal to 5 times the rod diameter at a glue-line thickness of 5.0 mm due to the local debonding observed. The method adopted with the 4 strain gauges along the bonded length seemed inefficient for the 3.0 mm glue-line thickness. The strain readings were inconsistent between FRP rods and inspection of the specimens showed unbonded areas up to half the surface of the rod. This was the result of the occupied space from the cables of the strain gauges in combination with the thixotropic nature of the epoxy.

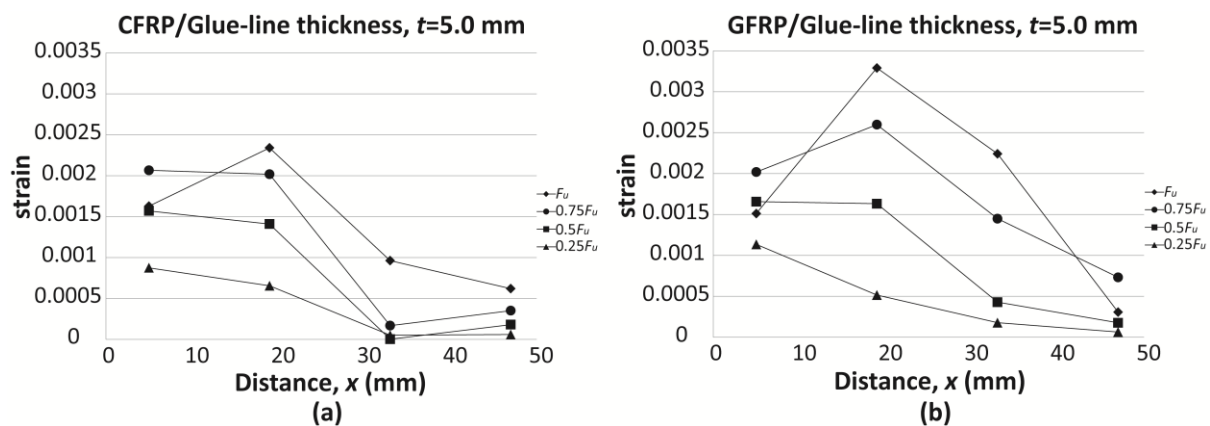


Figure 8: Axial strain distribution for (a) a CFRP rod and (b) for a GFRP rods glued –in timber with a glue-line thickness of $t=5.0$ mm.

4 Conclusions

CFRP rods exhibit a higher bond performance under static loading up to 11% compared with GFRP rods but GFRP rods yield higher bond stiffness at SLS, K_{SLS} under the same loading regime (up to 90%). Given the considerable difference in cost between the two materials, GFRP rods seem to be the optimum solution for glued-in FRP rod connections in timber. However, the long-term performance of glued-in GFRP and CFRP rods in timber (e.g. under fatigue and sustained loading) should be also investigated in the future to derive firm conclusions. The increase in the glue-line thickness increases significantly the

average axial load resistance but this is reflected in a much higher use of glue epoxy and consequently cost.

5 Acknowledgements

The presented work is supported by a Leverhulme Trust Programme Grant. The timber material was provided by Stora Enso.

6 References

- Achillides, Z. and Pilakoutas, K. (2002): Analytical approach to the bond behaviour of FRP bars in concrete. Proc., Int. Symp. on Bond in Concrete from Research to Standards, G.L. Balázs, P.J.M. Bartos, J. Cairns and A. Borosnyói eds., Budapest University of Technology and Economics, Hungary, 700-707.
- ACI 440.3R-12 (2012): Guide Test Methods for Fiber-Reinforced Polymers (FRPs) for Reinforcing or Strengthening Concrete Structures. American Concrete Institute, Farmington Hills, MI, USA.
- Aicher, S., Gustafsson, P.J. and Wolf, M. (1999): Load displacement and bond strength of glued-in rods in timber influenced by adhesive, wood density, rod slenderness and diameter. In Proceedings of 1st RILEM Symposium on Timber Engineering, 369-378.
- Baena, M., Torres, L., Turon, A., and Barris, C. (2009): Experimental study of bond behaviour between concrete and FRP bars using pull out test. Composites: Part B, 40(8), 784-797.
- Bengtsson, C. and Johansson, C.J. (2000): Test methods for glued-in rods for timber structures. Paper 33-7-8. In: Proceedings of the 33th conference of CIB-W18, Delft, Netherlands.
- Bengtsson, C. and Johansson, C.J. (2002): GIROD-glued-in rods for timber structures: Final report. SMT4-CT97-2199.
- Broughton, J.G. and Hutchinson, A.R. (2001): Pull-out behaviour of steel rods bonded into timber. Materials and Structures, 34, 100-109.
- BS EN 1995 Eurocode 5 (2004): Design of timber structures - Part 1-1: General - Common rules and rules for buildings.
- De Lorenzis, L., Rizzo, A. and La Tegola, A. (2002): A modified pull-out test for bond of near-surface mounted FRP rods in concrete. Composites Part B: Engineering, 33(8), 589-603.

- De Lorenzis L., Scialpi, V. and La Tegola, A. (2005): Analytical and experimental study on bonded-in CFRP bars in glulam timber. *Composites Part B*, 36(4), 279-289.
- Feligioni, L., Lavischi, P., Duchanois, G., De Ciechi, M. and Spinelli, P. (2003): Influence of glue rheology and joint thickness on the strength of bonded-in rods, *Holz als Roh- und Werkstoff*, 61(4), 281-287.
- Foster, R.M., Reynolds, T.P.S. and Ramage, M.H. (2016): Proposal for Defining a Tall Timber Building, *Journal of Structural Engineering*, 142(12).
- Lees, J.M., Toumpanaki, E., Barbezat, M. and Terrasi, G.P. (2017): Mechanical and Durability Screening Test Methods for Cylindrical CFRP Prestressing Tendons, *Journal of Composites for Construction*, 21(2).
- Madhoushi, M. and Ansell M.P. (2004): Experimental study of static and fatigue strengths of pultruded GFRP rods bonded in LVL and glulam. *International Journal of Adhesion and Adhesives*, 24(4), 319-325.
- Madhoushi, M. and Ansell, M.P. (2017). Effect of glue line thickness on pull-out behaviour of glued in GFRP rods in LVL: Finite element analysis. *Polymer Testing*, 62(2017), 196-202.
- Mettem, C.J., Harvey, K. and Broughton, J.G. (1999): Evaluation of material combinations for bonded in rods to achieve improved timber connections. In CIB-W18, Meeting 32, Graz, Austria, 1-14.
- Reynolds, T., Sharma, B., Harries, K. and Ramage, M. (2016): Dowelled structural connections in laminated bamboo and timber. *Composites Part B*, 90(2016), 232-240.
- Sanner, J., Snapp, T., Fernandez, A., Weihing, D., Foster, R. and Ramage, M. (2017): River Beech Tower: A Tall Timber Experiment. *CTBUH Journal*, Issue II, 40-44.
- Steiger, R., Gehri, E. and Widmann, R. (2006): Pull-out strength of axially loaded steel rods bonded in glulam parallel to the grain. *Materials and Structures*, 40, 69-78.
- Strahm, T. (2000): The GSA-system of anchorage: efficient and easy to design. *Proceedings of the 32 SAHFortbildungskurs "Verbindungstechnik im Holzbau, Weinfelden, Switzerland*, 165–169 (only available in German)
- Tepfers, R. (1979): Cracking of concrete cover along anchored deformed reinforcing bars. *Magazine of Concrete Research*, 31(106), 3-12.

Discussion

The paper was presented by E Toumpanaki

A Frangi commented that this could be a good solution. He commented that push out and pull out results are not compared. E Toumpanaki said results of different test methods can be compared with this data. H Blass said that if you want to use it as a tensile member you should test it as a tensile member.

A Smith asked why GFRP has higher bond stiffness. E Toumpanaki responded that it may be related to how the loads are transferred.

E Serrano received confirmation that one should expect better performance with compression pull through test because compression stresses are developed. He further commented that this may be different in larger specimens. F Lam commented the supporting plate in the compression pull through test may restrain the specimen from developing splitting failure mode; hence over estimation of capacity will result from this test set up besides the presence of compression stresses.

P Dietsch commented about the statement that FRP is more durable compared to steel. In service class 3 wood would be the problem. P Dietsch and E Toumpanaki discussed the potential difference in results if service class 3 condition rather than service class 1 was considered in the test.

S Aicher commented that there are significant outliers with low strength properties. One should focus on these. The difference in strength results are very low between the groups given the variability expected in wood. S Aicher and E Toumpanaki discussed the difference in stiffness is one the other hand very high. This may be attributed to the bond characteristics between the adhesive and the rod which is also related to the outliers.

Multiple shear plane timber connections with slotted-in steel plates and dowel-type fasteners: a study of the brittle failure mode in the parallel-to-grain direction

Yurrita, Miguel. Wood Chair. Department of Structural Analysis and Design. University of Navarra (Spain). myurrital@alumni.unav.es

Cabrero, J.M. Wood Chair. Department of Structural Analysis and Design. University of Navarra (Spain). jcabrero@unav.edu

Quenneville, Pierre. Department of Civil and Environmental Engineering. Faculty of Engineering. University of Auckland (New Zealand). p.quenneville@auckland.ac.nz

Keywords: Timber Connection, Multiple shear planes, Slotted-in steel plates, Brittle failure, Ductile failure, Parallel-to-grain, Dowel-type fastener

1 Introduction

The multiple shear connections with slotted-in steel plates and dowel-type fasteners are being increasingly used in both civil engineering and architecture since its origins in the 1940's (Gehri, 2000). Large structures, in height or in span, require structural elements with a high load capacity, and this connection fulfils such requirements. Several recent examples of this joint can be found, as the typical solution given by Crocetti (2016) for a timber truss node. Malo et al. (2016) studied a recent timber structure with this kind of connection: the "Treet" building in Bergen, Norway, a 14-storey building with vertical timber trusses.

A typical configuration of a four shear plane connections with two slotted-in steel plates and a total of 9 dowels distributed in 3 rows and 3 columns is depicted in Fig. 1 with its main geometric parameters.

Despite its common use, no standard deals explicitly with the multiple shear plane connections with slotted-in steel plates. Some authors have already studied the ductile failure mode of this kind of connections: Pedersen (2002), Sawata et al. (2006) and Rossi *et al.* (2016). However, no research about the brittle failure mode has

been performed. This work presents the results of the first study of the brittle failure mode on multiple shear connections with slotted-in steel plates and dowel-type fasteners. The obtained results are also compared with the most representative analysis methods.

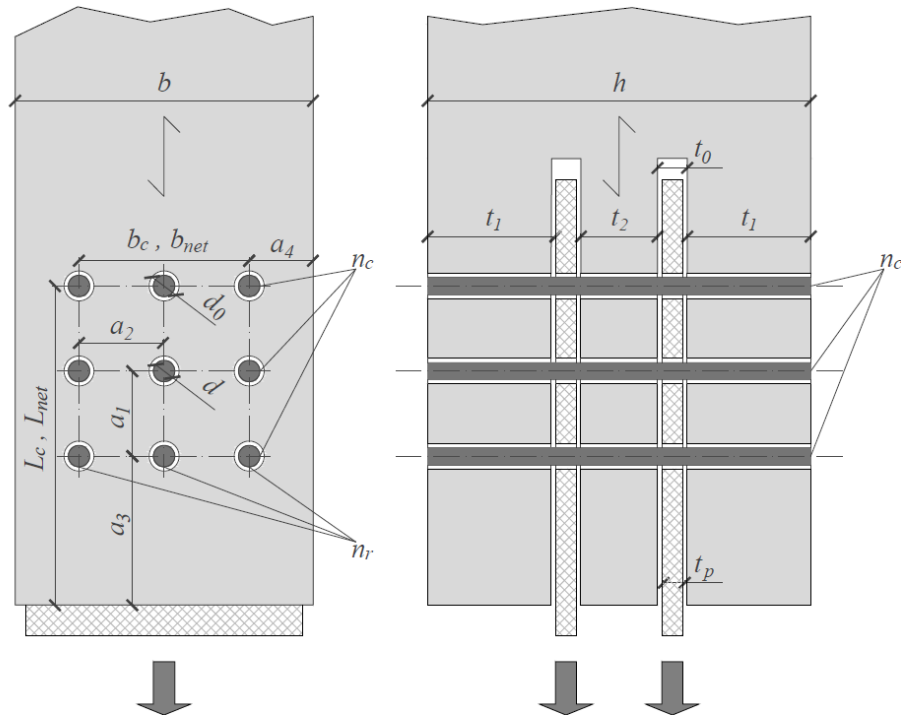


Fig. 1: Denotation of the geometrical parameters of a generic connection similar to the tested one, with four shear planes and two slotted-in steel plates.

2 Calculation models

2.1 Ductile failure mode

The European Yield Model is the most widespread calculation method for ductile behaviour of timber connections, namely embedment (Fig. 2a). The usually provided formulae consider only connections with one or two shear planes (with only wood members or combined with steel plates). The Eurocode 5 (2004) suggests that this method can be applied in connections with more shear planes, but no further information is given. Also the model from Hanhijärvi and Kevarinmäki (2007, 2008), considers that a multiple shear connection can be decomposed as the sum of several double shear joints.

First researches about multiple shear connections have focused on this failure mode. Pedersen (2002) proposed a calculation method based on the European Yield Model for connections with four shear planes, and validated it with a set of tests. Similar procedure was followed by Sawata et al. (2006). However, the latter considers connections with any number of shear planes and, instead of achieving a load capacity per each single shear plane, it obtains the effective thickness of the fasten-

er along the whole connection. The most recent study, conducted by Rossi *et al.* (2016), consisted on an experimental campaign of tests where only ductile failure is studied.

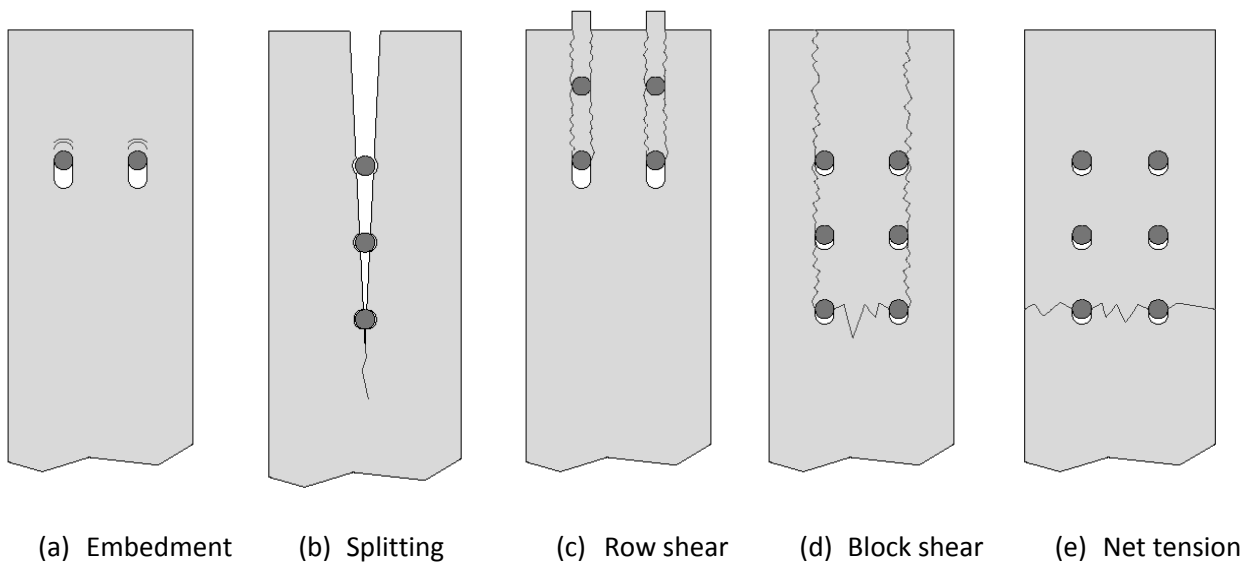


Fig. 2: Failure modes in a connection. Image from Cabrero and Yurrita (2018).

2.2 Brittle failure mode

Brittle failure mode can lead to worse consequences than a ductile failure due to a sudden collapse of the structure. However, early standards and researches focused only on the ductile behaviour. First approach to brittle failure dates from 1985, when Smith and Steck (1985) noticed the necessity of new proposals to obtain the "*ultimate capacities of joints with brittle failures*". Since then, many proposals dealing with one or more of the possible brittle failure modes, which are splitting (Fig. 2b, a crack along the fasteners originated by stresses perpendicular to the load), row shear (Fig. 2c, two shears planes generated along the perimeter of each row of fasteners), block shear (Fig. 2d, failure at the perimeter of the joint with two shear planes and one head tensile plane) and net tension (Fig. 2e, failure of the cross section area due to tension load), have appeared. Cabrero and Yurrita (2018) gathered and studied most of these proposals.

Three models have been considered on this work, as they are the only proposals that consider all the possible brittle failure modes: Eurocode 5 (2004), the model from Quenneville and Zarnani (2017) –which is the proposed for the New Zealand standard draft, and can be considered as an evolution of the method from the CSA 086 (2014), and the proposal of Hanhijärvi and Kevarinmäki (2007, 2008). However, none of them considered the case of multiple shear connections with slotted-in steel plates. A brief description of the three methods is given below.

2.2.1 Eurocode 5 (2004)

The standard Eurocode 5 (2004) considers both splitting and row shear simultaneously with the ductile failure mode by combining the European Yield Model with an effective number of fasteners per column n_{ef} , obtained from the studies of Jorissen (1998) and defined for the case of dowels as:

$$n_{ef} = \min[n_c; n_c^{0.9}(a_1/13d)^{0.25}] \quad (1)$$

where n_c is the number of columns, a_1 is the distance between columns and d is the dowel diameter.

Block shear failure was included in recent versions in Annex A. The block shear capacity $F_{B,block}$ of each timber member is defined as the maximum of the capacities of the tensile head plane and the lateral and bottom shear planes:

$$F_{B,block} = \max[1.5A_{net,t}f_{t,0,k}; 0.7A_{net,v}f_{v,k}] \quad (2)$$

where $f_{t,0,k}$ and $f_{v,k}$ are the characteristic tensile strength parallel-to-grain and the characteristic shear strength, respectively, and $A_{net,t}$ and $A_{net,v}$ are the tensile and shear net areas.

Finally, net tension is not considered as a failure mode of connections, but in section 6.1.2 of the Eurocode 5 (2004) it is established that the design strength along the grain must be higher than the design tensile stress.

2.2.2 Quenneville and Zarnani (2017)

It is the only method that considers each failure mode separately (except splitting, as it is an unexpected failure in connections of more than one row of fasteners). The brittle capacity of each timber member is the minimum of the following ones:

- Net tension:

$$F_{B,net} = A_{net,t}f_{t,0,k} \quad (3)$$

- Row shear:

$$F_{B,row} = R_v n_r \quad (4)$$

where n_r is the number of rows and R_v is the capacity of the two shear planes along a single row, defined as:

$$R_v = 0.75 f_{v,k} K_{LS} n_c 2a_{cr} t \quad (5)$$

where K_{LS} is a loading surface factor equal to 0.65 for side members and 1 for middle members and a_{cr} diminishes the length of the joint L_c and is equal to the minimum of the distances a_1 and a_3 .

- Block shear capacity is obtained as the sum of the row shear capacity of a single row plus the capacity of the head tensile plane:

$$F_{B,block} = R_v + 1.25A_{net,t}f_{t,0,k} \quad (6)$$

2.2.3 Hanhijärvi and Kevarinmäki (2007, 2008)

The model from Hanhijärvi and Kevarinmäki (2007, 2008) is the most complex one. As shown in Fig. 3, they divide the connection in outer (square pattern) and inner (line pattern) parts. For each part, the different possible failure modes that may happen in their limits (represented by dashed lines for outer parts and with continuous lines for inner parts) are accounted for. Not only all the possible brittle failure modes are considered, but also the possible interaction between them with an equation that diminishes the calculated capacities of the combined brittle failure modes.

The capacity of the timber member will be the sum of the capacities of the outer and inner parts of the joint:

- Inner parts. Embedment $F_{h,int}$ and the interaction between shear and tension $F_{t+v,int}$ are considered:

$$F_{total,int} = \min(F_{h,int}; F_{t+v,int}) \quad (7)$$

- Outer parts. Embedment $F_{h,out}$, the interaction between shear and tension $F_{t+v,out}$, and also splitting at the end of the connection $F_{spl,end}$ and the interaction between shear stress and splitting originated at the hole of the last fastener $F_{v+spl,hole}$ are considered:

$$F_{total,out} = \min(F_{h,out}; F_{t+v,out}; F_{spl,end}; F_{v+spl,hole}) \quad (8)$$

For the sake of brevity, all the equations for each case are not provided on this document. However, it is interesting to point out that they consider also an effective number of fasteners, an effective thickness of the fastener and also they introduce some parameters that depend on the used timber product (LVL, glulam, etc.).

2.3 Brittle failure in multiple shear connections with slotted-in steel plates

Nowadays, there is no method that provides a calculation method for the brittle failure of connections with multiple shear planes. Hanhijärvi and Kevarinmäki (2007, 2008) proposed that every connection can be decomposed as the sum of the capacities of simple connections (wood-steel-wood for the outer members and steel-wood-steel for the inner members of the connection), but this assumption may not be accurate enough. This proposal implies that all the timber members reach their limit load capacity at same time. As the thickness of the timber members, and also the corresponding effective thickness due to the dowel deformation can be different, the timber elements may not reach their failure capacity simultaneously.

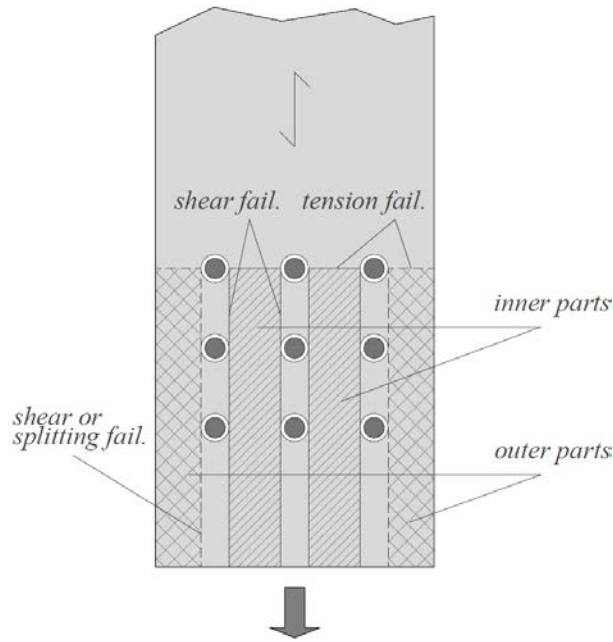


Fig. 3: Division of a connection into outer and inner parts made by Hanhijärvi and Kevarinmäki (2007, 2008), and its possible failure modes.

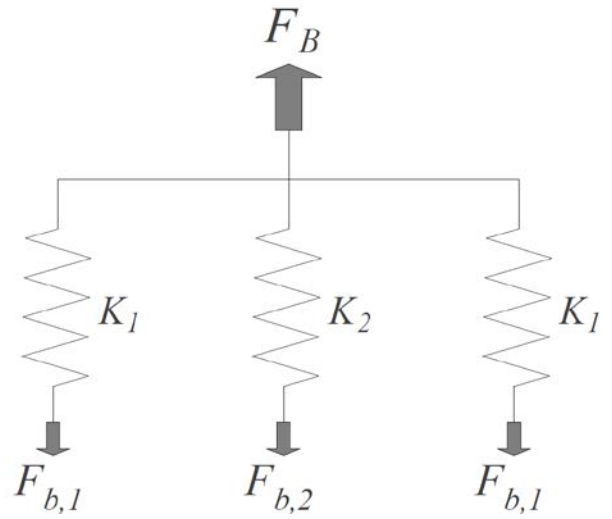


Fig. 4: Analogy of the studied connection with a spring model.

A stiffness based approach method is therefore proposed. The connection is modelled by means of a spring system (Fig. 4) where each timber element is a spring, and all of them are related. Each spring has its own stiffness K_i , and a load capacity $F_{b,i}$, directly related to the deformation Δ ($F_{b,i} = K_i \Delta$). The deformation of all the timber elements is supposed to be the same, and hence the load achieved in each of the timber members is directly related to its relative stiffness. As in a common connection the only different parameter among the members is the thickness, then the load capacity F_B of a connection with four shear planes and two slotted-in steel plates of the joint can be expressed as:

$$F_B = \min[F_{B,1}(2+t_2/t_1); F_{B,2}(1+2t_1/t_2)] \quad (8)$$

The first expression considers the failure of the outer members, and the second one the failure of the inner timber element. Both of them consider that the load capacity of the connection is achieved when one of its members reaches its own capacity. At that moment, the other element will have reached a proportional load related to the thickness ratio, which will be lower than its isolated load capacity. This stiffness based approach could be applied for a connection with any number of shear planes.

3 Materials and methods

3.1 Materials

A total of 112 tests (28 configurations with four specimens for each one) have been performed in order to study their brittle failure mode. All of them have the basic

geometry depicted in Fig. 1: three timber members with two slotted-in steel plates and a total of 9 dowels displayed in 3 columns and 3 rows. Fig. 5 shows one of the specimens ready to be tested.

All the steel plates have a thickness of 8 mm, and a steel grade G250+. The dowels are 12 mm diameter and the steel grade is 8.9. Due to budget issues, the fasteners were ordered as bolts (as can be seen in Fig. 5b) but they were used as dowels. Two common timber products from New Zealand were used: LVL-E11 and GL-8. Table 1 summarizes all the timber properties at both characteristic and mean level. Mean level is considered more adequate in order to compare the prediction ability of the calculation models with the test results.

Table 1: Characteristic and mean properties of the timber products used in tests. Characteristic properties of LVL-E11 were taken from Quenneville et al. (2011), and the ones of GL-8 from Zarnani (2013). Mean density and MOE have been obtained by experimental tests. The other mean values are obtained from a MatLab script made by Jockwer et al. (2018).

Timber Grade	Level	Density ρ [kg/m ³]	MOE E_0 [MPa]	Shear Mod. G [MPa]	Ten. parallel $f_{t,0}$ [MPa]	Ten. Perp. $f_{t,90}$ [MPa]	Shear F_v [MPa]
LVL-E11	Charac.	570.0	11,000	550.0	25.0	1.45	4.6
	Mean	583.5	11,840	686.3	34.1	2.90	5.9
GL-8	Charac.	450.0	8,000	530.0	10.0	1.19	3.7
	Mean	476.3	10,790	661.3	13.7	2.40	4.8



(a) Detail of a LVDT.



(b) Specimen ready to be tested.

Fig. 5. Images of one assembled specimen ready to be tested.

3.2 Design of the specimens

The preliminary calculations have been performed considering the method from Pedersen (2002) for the ductile case and the method from Quenneville and Zarnani

(2017) combined with the stiffness approach proposal for the brittle one. All the specimens have been designed to collapse under brittle failure. A minimum ratio of 1.5 between the two failure modes has been assumed in order to guarantee that.

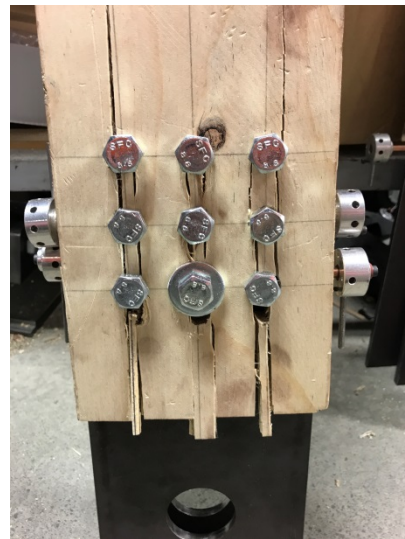
The differences between the 28 tests configurations are basically three:

- Timber product. As explained, LVL-E11 or GL-8
- Thickness of the timber elements. Three combinations: inner and outer members with same thickness ($t_1 = t_2 = 22$ mm); outer members double from the inner ($t_1 = 44$ mm, $t_2 = 22$ mm); and inner member double from the outer ones ($t_1 = 22$ mm, $t_2 = 44$ mm).
- Geometric pattern of the dowels. Several combinations of the distances between fasteners and from fastener to timber edges have been considered.

All the geometric details of the tests are provided in Table 2.



(a) Block shear



(b) Row shear



(c) Net tension



(d) "L" failure (Block+Net)

Fig. 6. Most common brittle failure modes of the tested specimens.

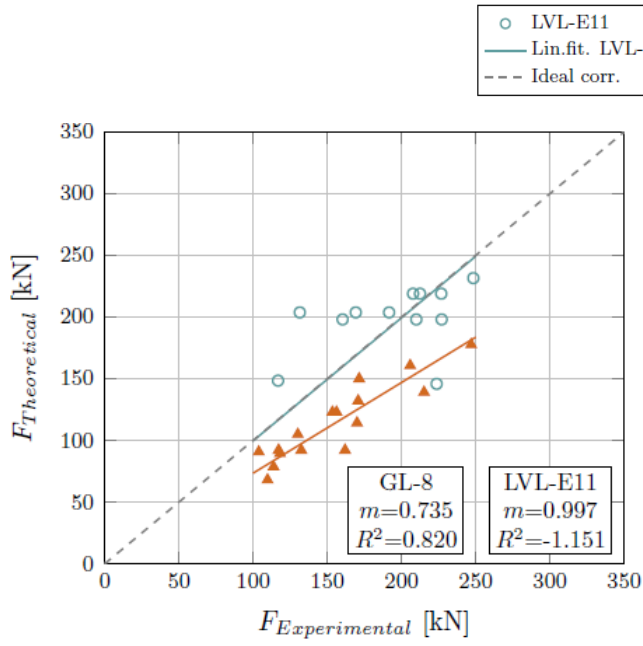
3.3 Test results

As expected, all the samples collapsed under brittle failure, although not always in the expected way. Block shear (Fig. 6a) and row shear (Fig. 6b) were the expected modes (most of the GL-8 specimens failed in block shear and the LVL-E11 samples collapsed under row shear). However, some net tension failure (Fig. 6c) and a mixed mode between block shear and net tension (Fig. 6d), named here as “L” failure do to its shape.

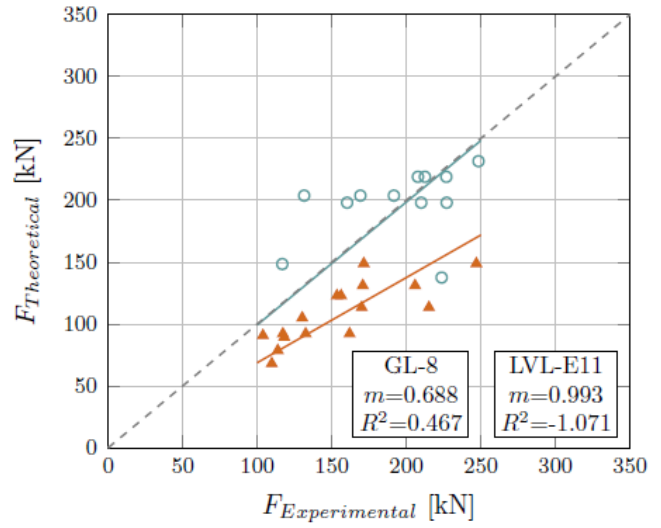
Table 2 summarises the results of the performed tests, providing the average failure value of the tests, the COV and the most common failure modes.

Table 2: Basic geometry and test results (average tested vinal load F_T , COV and most common failure modes of the four specimens per each configuration) of the 28 test configurations.

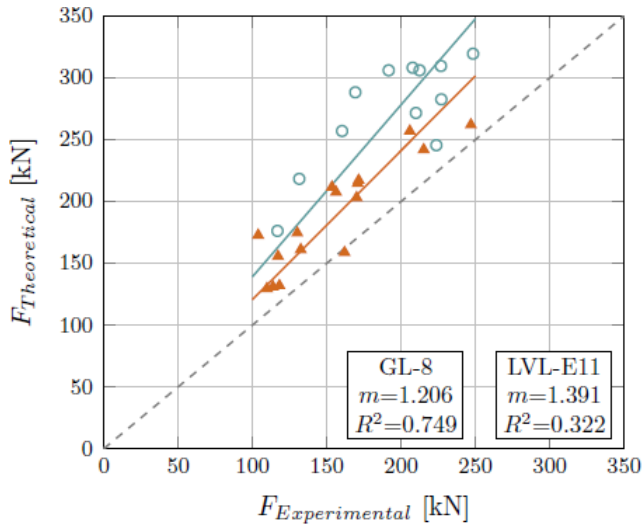
Specimen	Geometry [mm]											Test Results		
	t_1	t_2	d	d_0	a_1	a_2	a_3	a_4	b	b_c	L_c	F_T [kN]	COV	F. Mode
LVL a3.3	22	22	12	14	36	36	84	36	144	72	156	116.83	4.3%	Row
LVL b3.3	22	44	12	14	36	36	84	36	144	72	156	160.33	7.0%	Row
LVL b3.4	22	44	12	14	36	48	84	36	168	96	156	169.2	10.4%	Row
LVL b4.3	22	44	12	14	48	36	84	36	144	72	180	209.99	3.1%	Row/Block
LVL b4.4	22	44	12	14	48	48	84	36	168	96	180	212.49	8.1%	Block
LVL b5.3	22	44	12	14	60	36	84	36	144	72	204	227.09	8.7%	Row
LVL b5.4	22	44	12	14	60	48	84	36	168	96	204	248.43	10.1%	Row
LVL b4.a4	22	44	12	14	48	48	84	48	192	96	180	207.81	7.0%	Row
LVL b5.a4	22	44	12	14	48	48	84	62	220	96	180	226.84	7.1%	Row
LVL b3.a3	22	44	12	14	36	48	36	36	168	96	108	131.5	12.2%	Row
LVL b9.a3	22	44	12	14	36	48	108	36	168	96	180	191.68	1.2%	Row
LVL c3.3	44	22	12	14	36	36	84	36	144	72	156	223.72	5.2%	Row
GL a3.3	22	22	12	14	36	36	84	54	180	72	156	109.76	6.2%	Block/L
GL a3.4	22	22	12	14	36	48	84	54	204	96	156	117.22	19.8%	Block/Row
GL a4.3	22	22	12	14	48	36	84	54	180	72	180	113.81	18.9%	Block
GL a4.4	22	22	12	14	48	48	84	54	204	96	180	161.98	3.7%	Block/Net/L
GL a5.3	22	22	12	14	60	36	84	54	180	72	204	118.16	8.0%	Block/L
GL a5.4	22	22	12	14	60	48	84	54	204	96	204	132.51	10.3%	Block/Net
GL b3.3	22	44	12	14	36	36	84	54	180	72	156	103.86	21.3%	Block/L
GL b3.4	22	44	12	14	36	48	84	54	204	96	156	156.26	6.7%	Block/Row
GL b4.3	22	44	12	14	48	36	84	54	180	72	180	130.19	27.4%	L/Net
GL b4.4	22	44	12	14	48	48	84	54	204	96	180	153.5	7.8%	Block/Net
GL c3.3	44	22	12	14	36	36	84	54	180	72	156	170.07	2.1%	Block/L
GL c3.4	44	22	12	14	36	48	84	54	204	96	156	215.22	6.2%	Block/Row
GL c4.3	44	22	12	14	48	36	84	54	180	72	180	170.82	10.5%	Net/L
GL c4.4	44	22	12	14	48	48	84	54	204	96	180	205.88	16.3%	Net/L
GL c5.3	44	22	12	14	60	36	84	54	180	72	204	171.49	19.0%	L/Net
GL c5.4	44	22	12	14	60	48	84	54	204	96	204	246.98	14.0%	Net/L



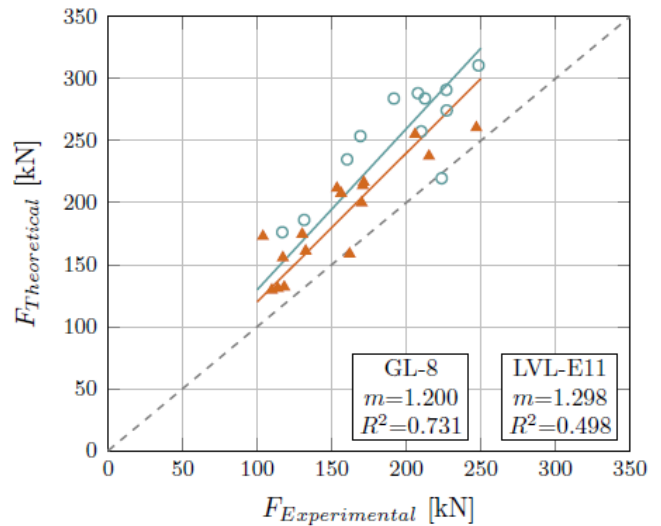
(a) Eurocode 5 (2004).



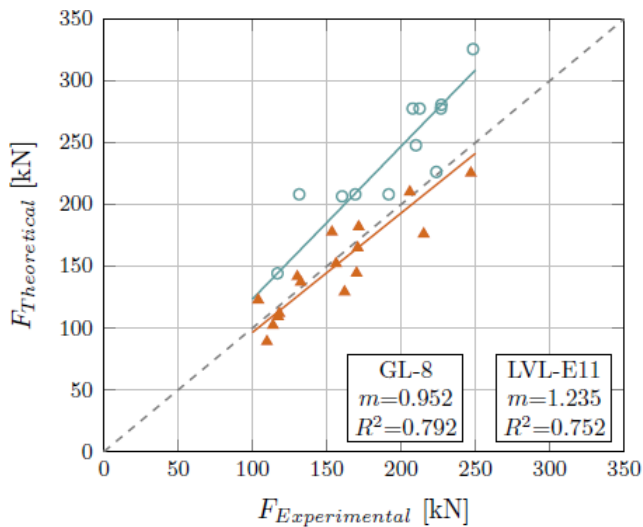
(b) Eurocode 5 (2004) + Stiffness.



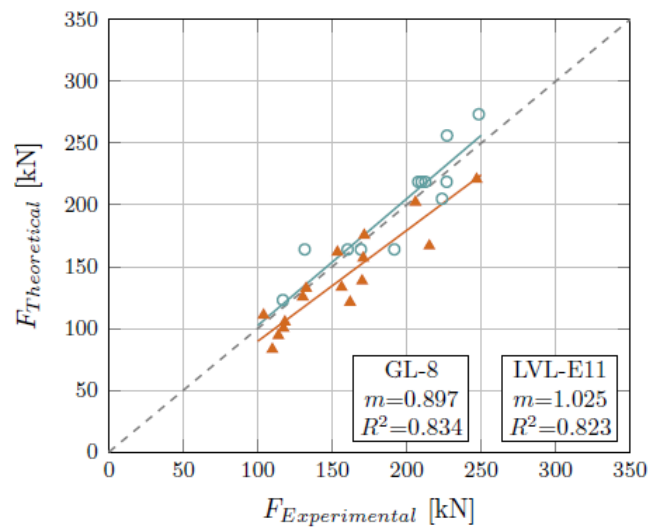
(c) Hanhijärvi and Kevarinmäki (2007, 2008).



(d) Hanhijärvi and Kevarinmäki (2007, 2008) + Stiffness.



(e) Quenneville and Zarnani (2017).



(f) Quenneville and Zarnani (2017) + Stiffness.

Fig. 7. Comparison between the test results and the predicted values of the considered methods.

4 Comparison with existing models

The obtained test results have been compared with the already three explained models that consider all the possible brittle failure modes: Eurocode 5 (2004), Quenneville and Zarnani (2017) and Hanhijärvi and Kevarinmäki (2007, 2008). Each model has been studied considering two cases: the first one by applying only the method, and the second one by combining with the proposed stiffness method.

The prediction ability of all of them is given in Fig. 7. In these graphics, the results related to each timber product, which barely match with the different failure modes (LVL-E11 with row shear and GL-8 with block shear) have been plotted separately. A linear fitting passing through the origin of coordinates of both timber products is provided with its corresponding slope and the coefficient of correlation R^2 .

The Eurocode 5 (2004) (Fig. 7a) clearly underestimates the values of the GL-8 tests. Even if the slope for LVL-E11 is almost perfect, the low resulting value (negative, indeed) of the R^2 demonstrates its poor predicting quality. When combined with the stiffness approach (Fig. 7b), the situation almost remains equal: only the values for the case of block shear differ as the row shear is included in the EYM method, which cannot be combined with this model.

The model from Hanhijärvi and Kevarinmäki (2007, 2008) (Fig. 7c) overestimates both cases. The overestimation remains when combined with the stiffness method (Fig. 7d), even if the prediction ability improves slightly. A consideration should be pointed out with this method. It considers also splitting and due to this, the tension perpendicular-to-grain strength $f_{t,90}$ has an influence on the results. This value remains constant as 0.4 in the European codes, but the values provided for the studied timber products are much higher. As the model was proposed based on the European Codes, this value may considerably distort the accuracy of the method.

The model from Quenneville and Zarnani (2017) (Fig. 7e), overestimate the results for LVL-E11, but obtains a good fitting for GL-8. When combined with the stiffness model (Fig. 7f), the average fitting of the two models improves, and can be considered as the most accurate model.

To confirm that, Table 3 summarizes the ability of all the methods, considering this time both timber products together. The ratio between the predicted value F_p and the test results F_T is studied (providing the average value, the standard deviation and the COV). Also the ability to predict the failure mode is given.

It is confirmed that the Eurocode 5 (2004) underestimates the load capacity and the model from Hanhijärvi and Kevarinmäki (2007, 2008) overestimates it. However, for this model, also the values considering $f_{t,90,k} = 0.4$ are given in brackets, which are considerably much better. The model from Quenneville and Zarnani (2017) appears still as the most accurate, especially when combined with the stiffness model, as it obtains the best values for the three given parameters (average, standard deviation and COV).

Table 3: Accuracy of the studied models (considering also the combination with the stiffness approach). Average value of the ratio between the predicted loads F_p and the test results F_T , the Standard Deviation, COV, CCC (Concordance correlation Coefficient) and the ability of the predicted failure modes are given.

Model	F_p/F_T Ratio				Fail. Mode
	Average	St. Dev.	COV	CCC	
Eurocode 5	0.880	0.228	26.0%	0.653	73.4%
Eurocode 5 + Stiffness	0.864	0.243	28.1%	0.565	73.4%
New Zealand	1.089	0.192	17.6%	0.762	88.1%
New Zealand +Stiffness	0.957	0.121	12.6%	0.902	87.6%
Hanhijärvi*	1.326 (1.083)	0.195 (0.205)	14.7% (18.9%)	0.531 (0.748)	76.0% (75.1%)
Hanhijärvi* + Stiffness	1.279 (1.054)	0.163 (0.185)	12.7% (17.5%)	0.603 (0.788)	76.0% (75.1%)

* Values in brackets are obtained considering the tensile stress perpendicular-to-grain $f_{t,90,k}=0.4$.

When considering the ability of the failure mode prediction, Eurocode 5 (2004) and Hanhijärvi and Kevarinmäki (2007, 2008) obtain similar values around 75%, while the model from Quenneville and Zarnani (2017) provides an accuracy of 88%.

5 Conclusions

Brittle failure mode in multiple shear connections with slotted-in steel plates and dowel-type fasteners has been studied for the first time by conducting a set of tests. A stiffness model which adjusts the load distribution among the timber elements is proposed to be combined with the existing models for cases of one or two shear planes. The comparison between the models and the test results demonstrates that the model from Quenneville and Zarnani (2017), combined with the stiffness approach is the most accurate. However, some inconsistencies between this model and the tests have been noticed. Further researches considering those inconsistencies may lead to a new model that may be applied for connections with any number of shear planes.

Acknowledgements

The research has been performed thanks to the COST Action FP1402 and the Department of Civil and Environmental Engineering from the faculty of Engineering of the University of Auckland, New Zealand.

The first author is supported by a PhD fellowship from the Programa de Becas FPU del Ministerio de Educación y Ciencia (Spain) under the grant agreement FPU15/03413. The authors would like to acknowledge the contribution of the COST Action FP1402. His 6-month stay in the University of Auckland has been supported by a fellowship from Fundación Caja Navarra.

6 References

- Cabrero, J. M. and Yurrita, M. (2018). Performance assessment of existing models to predict brittle failure modes of steel-to-timber connections loaded parallel-to-grain with dowel-type fasteners, *Engineering Structures*. Elsevier, (November 2017), pp. 1–16. doi: 10.1016/j.engstruct.2018.03.037.
- Crocetti, R. (2016). Large-Span Timber Structures, in *Proceedings of the World Congress on Civil, Structural and Environmental Engineering (CSEE'16)*. Prague, Czech Republic, pp. 1–23. doi: 10.11159/icsenm16.124.
- CSA 086 (2014). *CSA-O86-14 Engineering design in wood*, CSA Group.
- Eurocode 5 (2004). EN 1995-1-1:2004 - Eurocode 5: Design of timber structures - Part 1-1: General - Common rules and rules for buildings, *Eurocode 5*, 1(2004).
- Gehri, E. (2000). Multiple Shear Steel to Timber Joints, in *Behaviour of Timber Connections - Borg Madsen*. Timber Engineering Ltd., pp. 367–403.
- Hanhijärvi, A. and Kevarinmäki, A. (2007). Design method against timber failure mechanisms of dowelled steel-to-timber connections, in *CIB-W18 Timber Structures*. Bled, Slovenia, p. Paper 40-7-3.
- Hanhijärvi, A. and Kevarinmäki, A. (2008). *Timber Failure Mechanisms in High-Capacity Dowelled Connections of Timber to Steel*.
- Jockwer, R., Fink, G. and Köhler, J. (2018). Assessment of the failure behaviour and reliability of timber connections with multiple dowel-type fasteners, *Engineering Structures*, 172, pp. 76–84. doi: <https://doi.org/10.1016/j.engstruct.2018.05.081>.
- Jorissen, A. J. M. (1998). *Double shear timber connections with dowel type fasteners, Heron-English Edition*-. TU Delft.
- Malo, K. A., Abrahamsen, R. B. and Bjertnæs, M. A. (2016). Some structural design issues of the 14-storey timber framed building 'Treet' in Norway, *European Journal of Wood and Wood Products*. Springer Berlin Heidelberg, 74(3), pp. 407–424. doi: 10.1007/s00107-016-1022-5.
- Pedersen, M. U. (2002). *Dowel Type Timber Connections*. Danmarks Tekniske Universitet.
- Quenneville, P., Franke, S. and Swager, T. (2011). *New Zealand timber portal frames design guide*. Auckland, New Zealand: EXPAN.
- Quenneville, P. and Zarnani, P. (2017). Proposal for the Connection Chapter of the New Zealand Design of Timber Structures standard, *Unpublished*.
- Rossi, S. et al. (2016). Load-bearing capacity of ductile multiple shear steel-to-timber connections, in *World Conference on Timber Engineering*. Vienna, Austria.
- Sawata, K., Sasaki, T. and Kanetaka, S. (2006). Estimation of shear strength of dowel-type timber connections with multiple slotted-in steel plates by European yield theory, *Journal of Wood Science*, 52(6), pp. 496–502. doi: 10.1007/s10086-006-

0800-9.

Smith, I. and Steck, G. (1985). Influence of number of rows of fasteners or connectors upon the ultimate capacity of axially loaded timber joints, in *CIB-W18 Timber Structures*. Beit Oren, Israel, p. Paper 18-7-3.

Zarnani, P. (2013). *Load-Carrying Capacity and Failure Mode Analysis of Timber Rivet Connections*. University of Auckland.

Discussion

The paper was presented by M Yurrita

F Lam asked and received clarification about the reason why R^2 value greater than 1 and being negative was fitting the regression through the origin. F Lam commented that the brittle strength in the model is stressed volume dependent hence model should capture this aspect to be more generally applicable. H Blass agreed and said that the tensile strength failure mode is an example where failure always occurs in the same location hence stressed volume effect should indicate the tensile strength value in the model can be increased.

R Jockwer commented about the conversion of characteristic strength properties to mean values needing assumption of COV. This assumption needs to be checked as the assumed COV may be low. M Yurrita will look into this.

S Winter commented that if you are doing tests and comparing to model predictions, you should use real strength values from tests rather than conversion of properties from other references.

Group-effect of self-tapping screws in cross-laminated timber shear connections

Afrin Hossain, PhD Candidate, University of British Columbia Vancouver

Marjan Popovski, Principal Scientist, Advanced Building Systems, FPInnovations

Thomas Tannert, Associate Professor, Wood Engineering, University of Northern British Columbia, Prince George, corresponding author: thomas.tannert@unbc.ca

Keywords: Connection design; Experimental investigations; Group effect; CLT; STS

1 Introduction

1.1 Background

CLT panel-to-panel connections need to be designed for in-plane shear forces. Being rigid in nature, CLT panels need to be assembled with ductile connections in wall assemblies that are part of the Seismic Force Resisting System to dissipate energy under seismic loading. CLT wall assemblies demonstrated adequate energy dissipation under cyclic loading when connected with ductile dowel-type fasteners. In these panel-to-panel shear connections, different joint types are commonly used in practical applications such as internal spline, single or double surface spline, half-lap, or butt joints (Gavric et al. 2014), often with a large number of fasteners installed in one row.

Self-tapping screws (STS) belong to the group of dowel-type fasteners and are considered state-of-the-art in connector technology for timber structures (Dietsch and Brandner 2015). Installing STS at an angle (most often 45°) to the interface also increases the stiffness of the shear connection. Recent research (e.g. Loss et al. 2018) on STS has focused on the influence of screw and connection parameters along with models that count for the combined shear and withdrawal action of inclined screws. The withdrawal resistance of the STS can be predicted by equations provided by product approvals or the generic design equations for screws in Eurocode 5 (2004). However, the North American timber design standards NDS (2015) and CSA-O86 (2014) do not yet provide any design guidance for STS; therefore, engineers rely on the manufacturers' technical reports or apply (the conservative) lag screw provisions.

1.2 Group-effect

The phenomenon that the load-carrying capacity of timber connections with multiple mechanical fasteners is smaller than the sum of the single fastener's capacities is called 'group-effect'. This reduction can be described using the concept of an effective number of fasteners (n_{eff}) as shown in equation (1):

$$F_N = F_S \cdot n_{\text{eff}}$$

Eq. (1)

where F_N is the load-carrying capacity of a multiple fastener connection and F_S is the load carrying capacity of a single fastener.

Until the 1970s, this group-effect was not explicitly considered in timber design. Then, equations to consider the group-effect in bolted connections based on theoretical considerations were proposed. In the NDS, the group action factor, C_g was introduced in 1973. Since 1997, the NDS uses the Lantos model (Lantos 1969), in a tabulated form for bolts, lag screws, split rings, and shear plates in a row. In 1984, CSA-O86 included the modification factor J_G for lag-screw, bolt, split rings and shear plate connection for. In 2009, CSA O86 introduced a mechanics based-model for the capacity of bolted connections that accounts for brittle failure modes and the group-effect modification factor for bolts was taken out. The provisions for lag screws, remained unchanged. However, no design guidance for STS. Therefore, engineers often rely on the lag screw provisions. The current Eurocode 5 (2004) accounts for group-effect for screwed connections loaded parallel to the grain for dowel-type fasteners using the relationship $n_{\text{eff}} = n^{0.9}$. The group effect expressions implemented into Eurocode 5, NDS and CSA O86 differ significantly; e.g., the value of n_{eff} according to EC5 is twice that of CSA O86 for a larger number of screws in one row. These discrepancies indicate the need and importance for further fundamental research on multiple screw timber connections.

With respect to the group-effect in STS, Brandner (2016) investigated the withdrawal capacity of STS groups placed in the narrow face of CLT and conservatively proposed the relationship $n_{\text{eff}} = 0.9 \cdot n$, even though the test results indicated $n_{\text{eff}} > 1$. Krenn and Schickhofer (2009) performed tension tests on glulam joints connected with steel plates as outer members using inclined STS in both single and multiple rows up to a maximum of 8 screws per joint and proposed $n_{\text{eff}} = 0.9 \cdot n$ for the capacity reduction. For serviceability limit states, $n_{\text{eff}} = n^{0.8}$ was suggested to account for the group effect. Krenn and Schickhofer further showed that the influence of number of fasteners on the joint capacity is variable and inconsistent when comparing ductile and withdrawal failure modes. The influence of number of screws on stiffness in steel-to-timber joints with inclined screws was also studied, however no equation was proposed. Different technical approvals for STS use in timber and wood-concrete slab applications were considered; however, expressions for the group-effect are only given for screws loaded axially $n_{\text{eff}} = \max(n^{0.9}, 0.9 \cdot n)$, e.g. according to ETA-11/0190 (2013).

1.3 Objective

In this study, different joint types (surface splines with STS in shear, and half-lap and butt joints with STS in either shear or withdrawal) were evaluated in a total of 175 quasi-static monotonic and reversed cyclic tests, with the number of STS in one row varied between 2 and 32. The objective of the research presented herein was to develop group-effect reduction factors for shear connections that utilize STS in CLT.

2 Experimental investigation

2.1 Materials

CLT panels used for the testing met the requirements of ANSI/APA PRG-320 (2013); they were manufactured from SPF (Spruce-Pine-Fir) with a mean oven dry relative density of 0.42 and glued using Polyurethane adhesive. During the time of CLT-STC connection testing the average moisture content of the CLT panels was 10% (+/-2%), measured using a handheld electric resistance meter.

Four different types of STS with diameter $d=8\text{mm}$ with Canadian product approval CCMC 13677-R (2013) were used in the testing program: 1) 80 mm long partially threaded (PT) ASSY Ecofast CSK screws placed at $\alpha=90^\circ$ and $\beta=90^\circ$ for shear action; 2) 90mm long PT ASSY Ecofast CSK screws placed at $\alpha=90^\circ$ and $\beta=90^\circ$ for shear action; 3) 140mm long fully threaded (FT) ASSY VG CSK screws placed at either $\alpha=90^\circ$ and $\beta=45^\circ$ for shear action or $\alpha=45^\circ$ and $\beta=45^\circ$ for withdrawal action, and 4) 180mm long FT ASSY VG CYL screws placed at either $\alpha=45^\circ$ and $\beta=33^\circ$ for withdrawal action. Herein, the angle α is between the screw shaft to the joint line between the CLT panels, and β is the transverse angle of insertion. The STS were spaced using parameters meeting or exceeding the requirements according to the Canadian product approval.

2.2 Joint types

The experiments reported herein focused exclusively on the in-plane shear properties of CLT joints obtained by installing STS along the edges of CLT panels. All CLT assemblies tested were connected with STS designed for three different joint types (surface spline, lap, butt) with two different screw actions (shear and withdrawal). Five different joint configurations (types A to F) were tested.

Type A: Surface spline joints with 8x80mm STS acting in shear ($\alpha=90^\circ$) using 19mm thick D-Fir plywood surface splines with a width of either 80mm or 160mm (80mm for small-size specimens), meaning that either 40mm or 80mm wide slots were cut into the joining edges of the panels (Figure 1a). Type B: Lap joints with 8x90mm STS acting in shear ($\alpha=90^\circ$). The panel laps were 80mm wide and 50mm deep (half the panel thickness), see Figure 1b. Type C: Lap joints where the laps were cut identical to those of joint type B, but 8x140mm STS were inserted at an angle $\alpha=45^\circ$ so they were loaded predominantly in withdrawal, as shown in Figure 1c. Type D: Butt joints where no machining was required to the panels. For these joints, 8x140mm FT STS were installed at angles $\alpha=90^\circ$ and $\beta=45^\circ$ to act in shear, see Figure 1d. Type E: Butt joints where 8x180mm FT STS were installed at an angle of $\alpha=45^\circ$ to the edge of the CLT panels and at an angle of $\beta=33^\circ$ to the face of the CLT panels to act predominantly in withdrawal, as shown in Figure 1e.

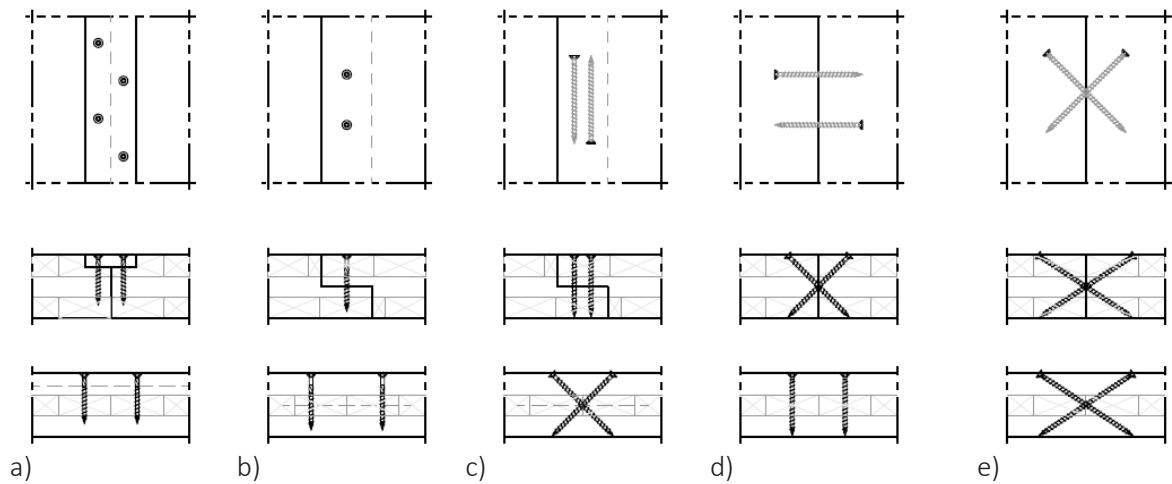


Figure 1: Joint specimen layout: spline joint with STS in shear (a), lap joint with STS in shear (b) and in withdrawal (c), butt joint with STS in shear (d) and in withdrawal (e)

2.3 Specimen description and preparation

Each of the five joint types were tested as a part of CLT assemblies which consisted of 3-ply, 99mm thick panels. The first part of testing included connections with two screws (considered one connector unit) to obtain the reference value, e.g. F_S for strength, and connections with multiple screws to obtain the values, F_N . This part was performed on CLT assemblies with three individual panels connected at two shear planes, each CLT panel being 150mm wide and 200mm long. Six replicates for each series were tested under quasi-static monotonic and cyclic loading.

For the multiple screw connections, three different specimen sizes were fabricated and subsequently tested: small, medium, and large. Small-sized specimens with two individual panels connected with one shear plane sized 145mm by 700mm and 300mm by 800mm for quasi-static monotonic and reversed cyclic tests, respectively (Figure 3a). For this specimen size, depending on screw action, four, six or eight STS were installed and three replicates of each series were tested under monotonic and cyclic loading. Medium-size and large-size specimens consisted of three individual CLT panels connected with two shear planes, each panel sized 400mm by 1200mm and 800mm by 2400mm, respectively. 16 (mid-size) and 32 (large-size) STS were installed in each shear plane with one replicate of each series been tested under quasi-static monotonic and three (mid-size) and two (large-size) under reversed cyclic loading.

The parameters of the test series are summarized in Table 1. The designation $XY-n-z$ indicates the series name, where X refers to the joint type: Spline (S), Lap (L) or Butt (B); Y refers to the STS action: Shear (S) or Withdrawal (W); n indicates the number of STS used per shear plane, and z indicates the loading type: quasi-static monotonic (m) and reversed cyclic (c).

2.4 Test methods and analyses

The small-size specimens with one shear plane were tested at an inclination of 13.5° for both monotonic (Figure 2a) and cyclic tests (Figure 2b), so that the load and reaction were aligned to the centre line of the specimen according. All results presented herein are the load components parallel to the shear planes. The actuator load and the relative vertical displacements between the individual panels were recorded using two calibrated LVDTs attached at mid-height of the assembly.

For test specimens with two shear planes under quasi-static monotonic loading (Figure 2c) the outer two CLT panels were kept in place by two HSS sections. The reversed cyclic test assembly was similar to the monotonic one, with the outer two panels kept in place by bracing the top hollow sections horizontally using threaded steel rods and HSS sections (Figure 2d). To apply the uplift forces, 25mm steel rods were attached at the centre of the CLT panel. The actuator load and the relative vertical displacements between the two panels of the assembly were recorded using two LVDTs (small-sized specimens) or four LVDTs (medium- and large-sized specimens) at a sampling rate of 10Hz. The reported displacements for all the tests are the average values between the front and back side of each shear plane.

The static load was applied according to a modified EN-26891 (1991) loading protocol at a displacement controlled rate of 2.5 mm/min for joints with STS loaded in withdrawal, and 5 mm/min for joints with STS loaded in shear. The cyclic load was applied using a CUREE loading protocol according to ASTM E2126-11 (2014) at a displacement controlled rate of 2.5mm/sec.

The yield load F_Y , maximum load F_{max} , displacement corresponding to yield load d_Y , displacement corresponding to maximum load d_{Fmax} , stiffness k , and ductility μ , were calculated for each test. EN-26891 was followed to obtain k corresponding to the range between 10% and 40% of F_{max} . Equivalent energy elastic-plastic curves were developed for both positive and negative envelopes according to ASTM E2126-11 to calculate F_Y and its corresponding d_Y . The ratio between the ultimate displacement and d_Y is usually used to calculate ductility and then the value is compared with the scale as proposed by Smith et al. (2006): brittle ($\mu \leq 2$), low ductility ($2 \leq \mu \leq 4$), moderate ductility ($4 \leq \mu \leq 6$) and high ductility ($\mu > 6$). In order to compare between test series with different load-deformation behavior (the tests of ductile joints were stopped at large deformations), the ratio between d_{Fmax} and d_Y was taken to calculate μ .

The yield load F_Y , maximum load F_{max} , displacement corresponding to yield load d_Y , displacement corresponding to maximum load d_{Fmax} , stiffness k , and ductility μ , were calculated for each test. EN-26891 was followed to obtain k corresponding to the range between 10% and 40% of F_{max} . Equivalent energy elastic-plastic curves were developed according to ASTM E2126-11 to calculate F_Y and its corresponding d_Y . The ratio between the ultimate displacement d_{Fmax} and d_Y is usually used to calculate ductility and then the value is compared with the scale proposed by Smith et al. (2006).



Figure 2: Test set-ups: one shear planes a) quasi-static monotonic, and b) cyclic; two shear planes: c) quasi-static monotonic, and d) cyclic

2.5 Results

The average values for load-carrying capacity and stiffness per screw as a function of the number of screws as well as the ductility values of the CLT assemblies and their respective Coefficient of Variations (CoV) are summarized in Table 1 and illustrated in the graphs of Figure 3. In these graphs, load values are reported per individual screw and the displacements are the averages of the two measurements from the back and the front of the specimen at each shear plane.

From the quasi-static monotonic tests, no group effect was observed for the joints where the screws acted in shear; however, for the joints where the screws acted in withdrawal, a reduction in capacity was observed which can be best described by the expression $n_{\text{eff}} = 0.9 \cdot n$. The reduction in capacity observed from the reversed cyclic tests showed a more pronounced group-effect which, independently from the type of screw action (shear and withdrawal) can be expressed as $n_{\text{eff}} = n^{0.9}$.

When evaluating the joint stiffness under quasi-static monotonic loading, no clear trend as a function of screws acting either in shear or in withdrawal was observed. Conservatively, the group effect could be described by the expression $n_{\text{eff}} = n^{0.8}$. However, a more severe reduction in stiffness (up to 70%) was observed for spline joints with the screws acting in shear. Even less consistent results were obtained from the reversed cyclic tests. While the group effect for the Lap joints can be expressed as $n_{\text{eff}} = n^{0.8}$, the butt joints with screws acting in withdrawal and the spline joints exhibited a much larger reduction and conversely the butt joints with screws acting in shear exhibited almost no reduction in stiffness as a function of the number of screws.

Joint ductility ranged between brittle (lap joints with STS acting in withdrawal), moderately ductile (butt joints with STS acting in shear or withdrawal) and ductile (lap and spline joints with STS acting in shear). The group-effect on ductility for all the joints can be reasonably expressed with the equation $n_{\text{eff}} = n^{0.9}$ for the quasi-static as well as for the reversed cyclic loading case.

Table 1: Group Test series overview and test results

Joint & Screw Type & Angle	Size (mm) & # of shear planes	Series	Repli- cates	F_{ult}		k		μ	
				Mean	COV	Mean	COV	Mean	COV
Spline_Shear, PT 8x80mm ($\alpha=0^\circ$, $\beta=90^\circ$)	150x200 (2)	SS-2-m	6	6.4	6	1.6	39	9.8	27
		SS-2-c	6	5.8	9	1.9	16	6.2	17
		SS-4-m	5	6.4	8	1.7	52	9.1	40
		SS-4-c	6	6.0	4	2.0	24	8.5	60
	145x700 (1)	SS-8-m	6	6.9	5	0.5	11	7.5	8
		SS-16-m	6	6.5	6	0.5	22	8.0	20
	300x800 (1)	SS-16-c	3	4.4	4	0.6	41	5.3	20
Lap_Shear, PT 8x90 ($\alpha=0^\circ$, $\beta=90^\circ$)	150x200 (2)	LS-2-m	6	6.2	15	0.9	21	6.3	28
		LS-2-c	6	6.9	10	1.1	45	5.8	27
	145x700 (1)	LS-4-m	6	6.4	6	0.9	38	5.3	26
		LS-8-m	6	6.7	6	1.0	14	6.6	33
	300x800 (1)	LS-8-c	3	5.1	1	0.8	17	5.6	15
		LS-16-m	1	7.3	-	0.8	-	5.1	-
	400x1200 (2)	LS-16-c	3	6.3	2	0.8	15	5.0	17
		LS-32-m	1	6.9	-	0.9	-	6.1	-
	800x2400 (2)	LS-32-c	2	5.8	-	0.8	-	5.1	-
Butt_Shear, FT 8x140mm ($\alpha=0^\circ$, $\beta=45^\circ$)	150x200 (2)	BS-2-m	6	6.1	13	0.7	58	6.0	39
		BS-2-c	6	7.1	6	0.7	22	3.8	30
	145x700 (1)	BS-8-m	6	6.8	2	0.5	10	5.0	19
		BS-8-c	3	6.4	4	0.6	15	5.1	21
	400x1200 (2)	BS-16-m	1	6.7	-	0.4	-	5.5	-
		BS-16-c	3	6.1	7	0.6	3	5.5	15
	800x2400 (2)	BS-32-m	1	6.0	-	0.6	-	5.0	-
		BS-32-c	2	5.2	-	1.0	-	7.0	-
Lap_Withdr, FT 8x140mm ($\alpha=90^\circ$, $\beta=45^\circ$)	150x200 (2)	LW-2-m	6	7.5	14	4.5	38	2.1	12
		LW-2-c	6	7.3	7	4.7	22	1.9	25
	145x700 (1)	LW-6-m	6	7.6	10	4.2	30	1.5	19
		LW-12-m	6	7.2	11	4.1	36	2.9	49
	300x800 (1)	LW-12-c	3	5.9	7	2.7	28	2.3	27
		LW-16-m	1	7.2	-	3.1	-	1.4	-
	400x1200 (2)	LW-16-c	3	6.6	4	3.6	29	1.8	49
		LW-32-m	1	6.5	-	2.8	-	1.9	-
Butt_Withdr, FT 8x180mm ($\alpha=45^\circ$, $\beta=33^\circ$)	150x200 (2)	LW-32-c	2	5.2	-	3.9	-	1.3	-
		BW-2-m	6	7.7	6	5.9	42	3.3	77
	145x700 (1)	BW-2-c	6	7.5	7	7.5	17	2.4	83
		BW-4-m	6	7.6	12	4.5	53	2.8	21
	300x800 (1)	BW-8-m	6	7.8	11	5.3	32	5.4	24
		BW-8-c	3	6.9	15	2.6	21	2.0	31
	400x1200 (2)	BW-16-m	1	6.9	-	3.6	-	6.4	-
		BW-16-c	3	6.7	7	2.9	27	5.3	12
	800x2400 (2)	BW-20-m	6	6.8	5	5.1	14	7.7	25
		BW-20-c	4	6.7	4	3.0	3	4.1	14

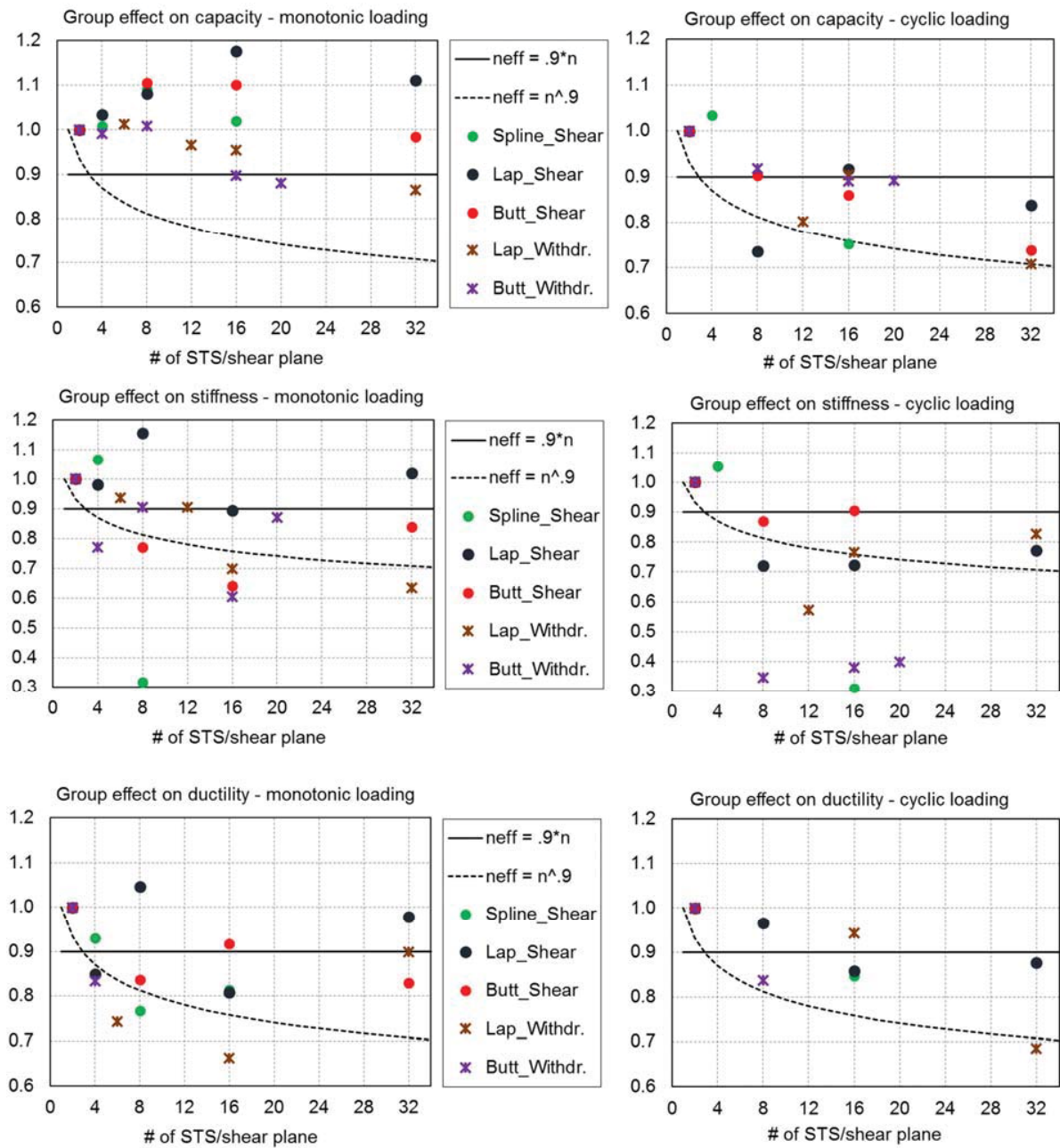


Figure 3: Group-effect on: capacity monotonic (a) and cyclic (b) loading; stiffness monotonic (c) and cyclic (d) loading; ductility monotonic (e) and cyclic (f) loading

2.6 Discussion

The tests results confirmed the established findings that CLT shear connections with STS exhibit high stiffness and low ductility when the screws are primarily loaded in withdrawal. Ductile joints with low stiffness however, were achieved when the screws were loaded primarily in shear. A relatively low CoV for capacities (7% on average) was obtained, with a clear trend towards reduced variability with a larger number of screws explained by the averaging effect of having multiple fasteners in one connection.

A comparison between the experimentally obtained group effect $n_{\text{eff}} = 0.9 \cdot n$ and the existing design guidance for lag-screws in CSA-O86 clearly demonstrates that the CSA-O86 provisions are far too conservative for connections with STS screws in CLT. Moreover, the standard only provides group effect factors for a maximum of 12 screws in one row, while the proposed reduction relationship is experimentally validated for up to 32 STS in one row.

Another finding is that the capacity of CLT shear connections under reversed cyclic loading was on average 9% lower than the capacity under monotonic loading, independently for joint type, with small differences depending on the number of screws. Furthermore, the group effect for capacity was more pronounced under reversed cyclic loading. Since most manufactures only provide information on the monotonic performance of their screws, these findings should be considered for seismic design.

Although the research presented herein did not have the objective to develop new models to estimate connection stiffness, the results point towards the existence of a significant group effect for stiffness of STS connections in CLT. The obtained values showed a relatively high scatter with an average CoV of 27% for all test series. Therefore the proposed expression $n_{\text{eff}} = n^{0.8}$ to describe the group effect on stiffness should be further evaluated and confirmed by both experimental and analytical investigations.

Comparing the shear connection stiffness as a function of loading protocol, a clear dependency on the screw action was observed: on average 19% larger values were obtained under reversed cyclic loading for the joints where the STS were loaded in shear, while a 9% reduction was observed for those joint types where the STS acted in withdrawal. Although the relatively high variation within and between test series does give reason to caution, it seems safe to state that there is no group effect for stiffness for STS joints under cyclic loading loaded in shear, but stiffness reduction was observed for the STS joints loaded in withdrawal.

The effect of the number of STS on joint ductility can be expressed by the equation $n_{\text{eff}} = n^{0.9}$ for both monotonic and reversed cyclic loading. The ductility decreased under cyclic loading, herein on average by 15%. This reduction was found to be a function of the screw action: the reduction in case of ductile joints was only 10% on average, while the ductility of the brittle joints was reduced by an average of 25%. The observed variability within test series, however, was relatively high (29%); therefore, similar to the conclusions for the stiffness, these test results will require further validation.

3 Conclusions

The objective of the research presented in this paper was to develop group-effect reduction factors for strength, stiffness, and ductility of shear connections with STS in CLT under monotonic and cyclic loading, where STS were loaded in shear or withdrawal. To achieve the objective, a total of 175 monotonic and cyclic tests were conducted with a wide range between 2 and 32 STS in one row. Based on these tests, the following conclusions can be drawn:

- 1) The expression $n_{\text{eff}} = 0.9 \cdot n$ is sufficient to describe the reduction in capacity for all joints under quasi-static monotonic loading with STS acting in shear or withdrawal. This approach is significantly less conservative than the existing Canadian design guidance for lag-screws.
- 2) The capacity (strength) obtained under reversed cyclic loading was on average 9% lower than that obtained from monotonic loading. The expression $n_{\text{eff}} = n^{0.9}$ can be used to account for the group effect of STS joints under cyclic loading.
- 3) The effect of number of screws on the joint stiffness can conservatively be described by the expression $n_{\text{eff}} = n^{0.8}$. High variation within test series and large differences between test series require further investigation.
- 4) Stiffness under reversed cyclic loading was on average 9% lower than under monotonic loading for joints with STS acting in withdrawal, while it was not reduced for STS in shear.
- 5) The group-effect on ductility for all the joints can be expressed with the equation $n_{\text{eff}} = n^{0.9}$ for both, monotonic and reversed cyclic loading cases.

The findings discussed in this paper will be presented to the Technical Committee of CSA O86 for potential inclusion into the next edition of the Canadian Standard for Engineering Design in Wood.

References

- ANSI/APA PRG-320 (2012): Standard for performance-rated cross-laminated timber American National Standards Institute (ANSI) and Engineered Wood Association (APA).
- ASTM E2126–11 (2014): Standard test methods for cyclic (reversed) load test for shear resistance of vertical elements of the lateral force resisting systems for buildings.
- Brandner R. (2016): Group Action of Axially-Loaded Screws in the Narrow Face of Cross Laminated Timber. In: *Proceedings of the World Conference on Timber Engineering*. Vienna, Austria.
- CCMC 13677-R. (2013): Evaluation report 13677-R SWG ASSY® VG Plus and SWG ASSY® 3.0 Self-Tapping Wood Screws. Canadian Construction Materials Centre.
- CSA O86 (2014): Engineering design in wood. Canadian Standard Association (CSA) Mississauga, Canada
- Dietsch P, Brandner R. (2015): Self-tapping screws and threaded rods as reinforcement for structural timber elements – A state-of-the-art report. *Construction and Building Materials* 97: 78–89.
- Eurocode 5 (2004): Design of timber structures - Part 1-1: General and rules for buildings. CEN. (EN 1995-1-1).
- EN-26891 (1991): Timber structures, joints made with mechanical fasteners, general principles for the determination of strength and deformation characteristics. Brussels, Belgium, 1991.
- ETA-11/0190 (2013): Würth self-tapping screws for use in timber constructions. European Technical Approval Berlin, Deutsches Institut für Bautechnik.
- Gavric I, Fragiaco M, Popovski M, et al. (2014): Behaviour of cross-laminated timber panels under cyclic loads. *Materials and Joints in Timber Structures* 9: 689–702.
- Lantos G. (1969): Load distribution in a row of fasteners subjected to lateral load. *Wood Science*; 1(3): 129–130.
- Loss C, Hossain A, Tannert T (2018): Simple cross-laminated timber shear connections with spatially arranged screws. *Engineering Structures* 2018
- NDS (2015): National Design Specification for Wood Construction. American Wood Council
- Krenn H, Schickhofer G. (2009): Joints with Inclined Screws and Steel Plates as Outer Members. In: *Proceedings of the 42nd CIB Working Commission W18 - Timber Structures*, Dübendorf, Switzerland.
- Smith I, Asiz A, Snow M, Chui I. (2006): Possible Canadian/ISO approach to deriving design values from test data. In: *Proceedings of 39th CIB Working Commission W18–Timber Structures*, Karlsruhe, Germany

Discussion

The paper was presented by T Tannert

F Lam asked about the R^2 or standard error of the regression fits. T Tannert said it was not done but they would be low. He said the intent is to provide guidance to code committee that group effect is not as severe as indicated in these connections while providing recommendation for a new conservative group effect. F Lam further received confirmation that only 8 mm screws were used. He commented that given the low R^2 values and limited screw diameters and screw type considered, it will be difficult to convince code committee to accept the results.

L-M Ottenhaus commented about the low cycle fatigue type failures with the ISO protocol. She said it is not sure that one can rely on the joint to dissipate energy with brittle failure mode. She said also high overstrength factor can result if you are too conservative with group effect. T Tannert agreed with the over strength factor issue. He said part of the problem is that the prototype may not be based on earthquake response. He wants to develop loading protocol for this types of screws. F Lam said that the CUREE protocol was developed by H Krawinkler with consideration of the earthquake response of light wood frame systems.

Performance of the Different Models for Brittle Failure in the Parallel-to-Grain Direction for Connections with Dowel-Type Fasteners

J.M. Cabrero, Wood Chair. Department of Building Construction, Services and Structures. University of Navarra, Spain. jcabrero@unav.edu

M. Yurrita, Wood Chair. Department of Building Construction, Services and Structures. University of Navarra, Spain

Keywords: Brittle failure, Parallel-to-grain, Splitting, Row shear, Block shear, Dowel-type fastener

1 Introduction

Usually, standards and analysis of joints deal only with ductile failure. That is the case of the well-known European Yield Model (EYM), which relies on the assumption of plastic behaviour of the steel fastener and plastic embedment of timber.

However, it has been noticed that brittle failure may govern the capacity of the connection. For that reason, the evaluation of brittle failure of connections loaded parallel-to-grain was one of the main objectives for the Working Group 3 “Connections” within the COST Action FP1402. This paper provides information on the state-of-the-art report and on the analyses done on steel-timber connections with large-diameter fasteners (namely dowels). The different existing models are compiled and benchmarked against an extensive database of connections from the literature. A similar study will be performed in the future for small-diameter fasteners.

Description of brittle failure modes dates back to the early work by Fahlbusch (1949). They sometimes are referred through the “group effect” concept, which states that, due to interaction among the fasteners, the capacity of the connection is lower than the sum of the individual contributions. As a consequence, an effective number of

fasteners, lower than the actual one, is required (Foschi and Longworth, 1975; Nozynski, 1980; Yasumura et al; 1987; Gehri, 1996; Jorissen, 1998). This kind of proposal made its way into the prenormative version of the Eurocode 5, *ENV 1995-1-1:1993* (1993), and it was finally adopted in the Eurocode 5 (2004), based on the work by Jorissen (1998).

Smith and Steck (1985) noticed the need for new models to account for this kind of failure modes and in the 1990s, Racher (1994) and Kevarinmäki (1995) proposed an approach for the analysis of block shear failure, which set the basis for the current Annex A of Eurocode 5 (2004)

Brittle failure modes were included in the Canadian Code *CSA Standard. O86*, based on works by Mohammad and Quenneville (1999), and they are also to be included in the future New Zealand standard draft following a proposal by Quenneville and Zarnani (2017).

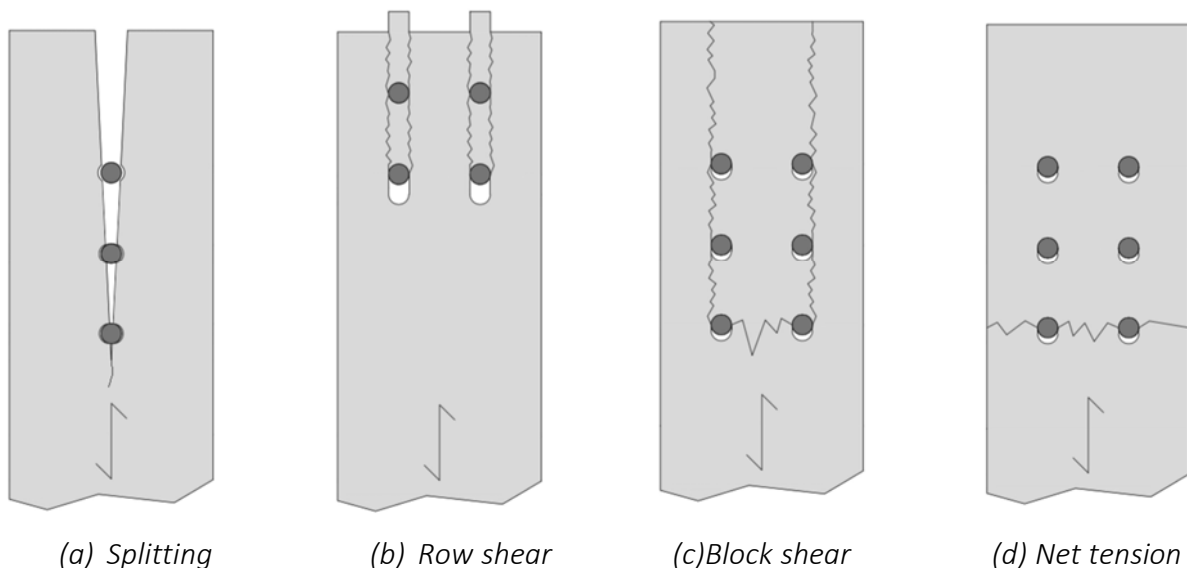


Figure 1. Brittle failure modes of large-diameter fasteners: splitting, row shear, block shear and tensile net failure (Cabrero and Yurrita, 2018).

2 Brittle failure modes for large-diameter fasteners

Figure 1 depicts the different possible brittle failure modes with large-diameter fasteners, which protrude the whole timber member. Splitting (Fig 1.a) is supposed to be produced by means of tension perpendicular to the grain, due to the fact of the dowel wedging in the timber. It is produced as a single crack, usually originating near the last hole. On the contrary, in row shear (Fig. 1b) two different cracks propagate in each fastener column parallel to the grain. They are assumed to be produced mainly by shear stress. Block shear (Fig. 1c) is characterised by the plug failure of the whole connection area, by means of two lateral failure planes (failing mainly by shear) and

one head plane (failing under tension). The final type of brittle failure would be the failing of only the head plane by tension (Fig. 1d), giving rise to a net-tensile failure.

Figure 2 shows the different nomenclature used within this paper. For the sake of simplicity, the different equations and models will be rewritten accordingly in this paper.

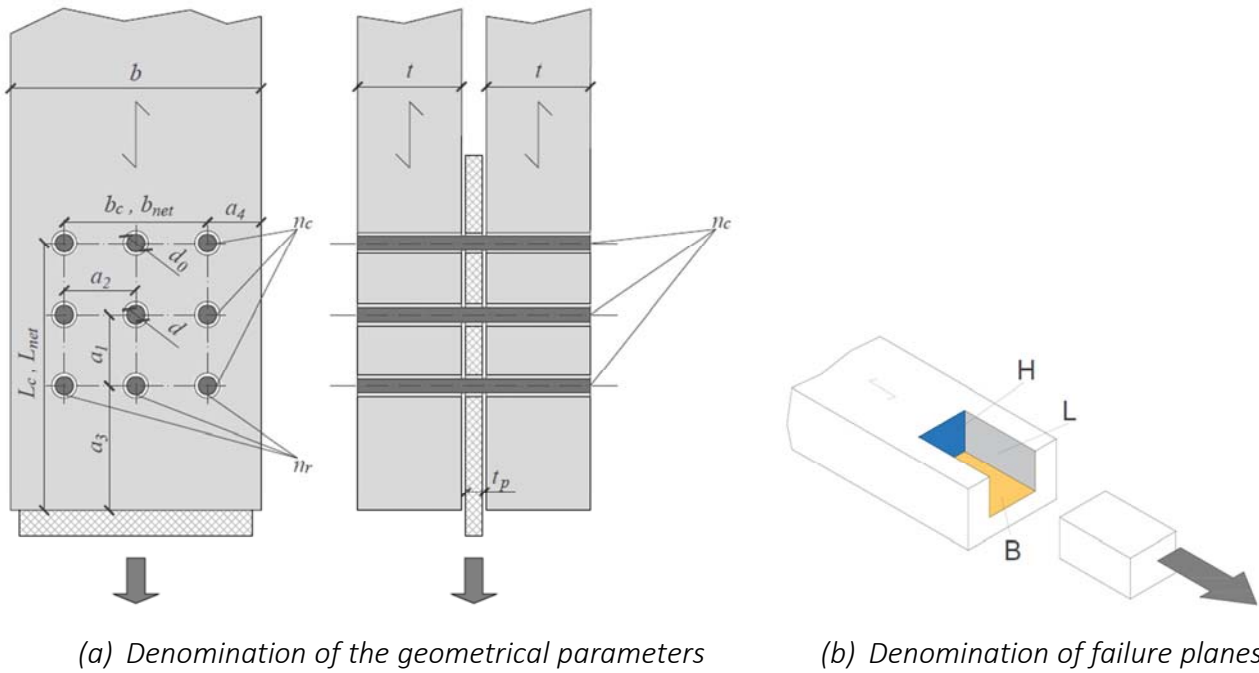


Figure 2. Denominations used in this paper

Table 1. Models for splitting failure.

Reference	Splitting capacity	Remarks
Literature		
Jorissen (1998)	$2t \sqrt{\frac{G_f E_0 \sin \alpha (b - d \sin \alpha)}{t}}$	α , angle of friction ($\alpha=30^\circ$)
Hanhijärvi and Kevarinmäki (2008)	$\frac{k_{conc}}{\beta_p} \frac{1}{s_{t90}} a_3 t f_{t,90}$	$s_{t,90}$ is a geometrical parameter different for splitting initiating at hole or end-member $k_{conc} = 0.7$
Jockwer et al. (2018)	$2 \beta_p t a_3 f_{t,90}$	
Standards		
Eurocode 5 (2004)	$n_c^{0.9} \sqrt{\frac{a_1}{13d}}$	Reduction factor of ductile capacity, connection shear plane capacity instead of member

G_f , fracture energy; $f_{t,90}$, perpendicular to grain tension strength; E_0 , parallel modulus of elasticity

2.1 Splitting failure

The different analyzed models for splitting are given in

Table 1. Splitting is assumed to be produced by means of tension perpendicular to the grain. Most of the models are based to a certain extent on the works of Jorissen (1997, 1998), who based his work on a beam on an elastic foundation and a Volkersen model. This work was the basis for the model of the effective number of fasteners in the Eurocode 5.

Most of the models consist on geometrical formulae, which account for the tension perpendicular-to-grain as a factor of the parallel load, called the wedge factor β_p . This parameter usually takes two different values, based on the friction angle: $\beta_p=1/10$ (angle of 30°), used in Hanhijärvi and Kevarinmäki (2008), or $\beta_p=1/7$ (angle of 18°), used in Jockwer, Fink and Köhler (2018). Based on experimental evidence, Jensen, Girhammar and Quenneville (2015) have proposed a higher value of $\beta_p = 0.25$.

2.2 Row shear and block shear failures

Row shear and block shear are based on the formation of two similar kinds of failure planes: lateral **L** failing under shear, and head **H** under tension. For that reason, their models can be summarised and compared in terms of how they account for the capacity of each of the different failure planes and, lastly, on how they add those capacities to obtain the capacity of the timber member. Therefore, Table 2 compiles the capacity of each single shear plane and Table 3 that of the tension plane. In Section 2.2.4, the combination proposal of each method to obtain the capacity of the timber member is given.

2.2.1 Shear capacity of the lateral failure plane

As shown in Table 2, the capacity of the lateral shear plane **L** is defined by its area (which dimensions are sometimes modified by means of an effective thickness t_{ef} - see Table 4- or a different way to account for its length), the shear strength f_v , and a parameter lower than one which accounts for the uneven load distribution.

Only the proposal from the Annex A (developed originally for small-diameter fasteners) considers the possibility of a lower bottom shear plane **B**, for the cases of a side member, a connection with a single shear plane, or when not failing by embedment.

The proposal from Jensen and Quenneville (2009, 2010, 2011) is the only one which is based on a fracture energy formulation. It is quite complicated, although all the inherent complexity is disguised in this work under the parameter ϕ . The other two formulae shown in Jensen and Quenneville (2009, 2010, 2011) are plastic limits. They verify the previously made proposal by Quenneville and Mohammad (2000) and Mohammad and Quenneville (2001), who proposed that, instead of taking into account the whole length, it should be reduced according to the minimum parallel spacing, either a_1 or a_3 , which would trigger the failure.

2.2.2 Tensile capacity of the head plane

Similar formulae have been proposed for the capacity of the head tensile plane. The different proposals consider the area of the plane (defined by the width of the connection -usually net width b_{net} - and its thickness t), and the parallel-to-grain tension strength, $f_{t,0}$. A parameter higher than one usually appears, to reflect the uneven stress distribution among the rows.

2.2.3 Effective thickness

Some of the models, instead of accounting for the whole thickness of the timber member, use an effective thickness, t_{ef} . This is a simple way to consider the stress distribution along the member thickness due to the deformation of the fastener. Some proposals obtain such effective thickness as the distance between plastic hinges in the EYM fastener yielding (Eurocode 5, 2004). Other proposals provide a simple approach by means of a simplified parameter depending on the member location (side or middle) in the joint.

2.2.4 Capacity of the whole timber member

Most of the models obtain the capacity of the whole timber member for each failure mode as the sum of the capacities of the involved failure planes. Hence, for block shear, the capacities of one head **H** (tensile, Table 3) and two lateral **L** (shear, Table 2) planes are added; while for row shear failure it corresponds to the capacity of two times the number of columns of lateral (shear) planes. After obtaining the capacity for each failure mode, the total capacity of the timber member would be the minimum of both.

Table 2. Proposals for the capacity of one lateral plane, F_V .

Reference	Shear plane capacity (per plane) F_V	Remarks
Literature		
Hanhijärvi and Kevarinmäki (2008)	$K_{v,cnctr} \frac{n_c^{0.9}}{n_c} L_c t_{ef} f_v$	$0.7 \leq k_{v,cnctr} \leq 1$
Quenneville and Mohammad (2000), Mohammad and Quenneville (2001)	$J_r n_c t a_{L,min} f_v$	$a_{L,min} = \min\{a_1, a_3\}$ $0.6 < J_r < 1$
Jensen and Quenneville (2009, 2010, 2011)	$n_c a_1 t f_v$ $n_c a_3 t f_v$ $\phi a_3 t f_v$	Minimum of the three.
Standards		
Eurocode 5 (2004)	$n_c^{0.9} \sqrt{a_1 / 13d}$ (row shear) $0.7 t_{ef} L_{net} f_v$ $0.7 L_{net} (b_{net} + t_{ef}) f_v$	Reduces ductile capacity, connection shear plane capacity <i>Embedment, inner steel/timber</i> <i>All remaining</i>
Quenneville and Zarnani (2017)	$0.75 n_c a_{L,min} t_{ef} f_v$	

Table 3. Proposals for the capacity of the head plane, F_H .

Reference	Tensile plane capacity (per plane) F_H	Remarks
Literature		
Hanhijärvi and Kevarinmäki (2008)	Inner plane: $K_{t,cnctr} n_{ef}/n_c b_{net} t f_{t,0}$	$1.7 \leq k_{t,cnctr} \leq 2$
Quenneville and Mohammad (2000)	$t b'_{net} f_{t,0}$	$b'_{net} = (n_r - 1)(a_2 - (d + 2))$
Standards		
Eurocode 5 (2004)	$1.5 b_{net} t f_{t,0}$	
Quenneville and Zarnani (2017)	$1.25 b_{net} t f_{t,0}$	

Table 4. Effective thickness.

Reference	Effective thickness, t_{ef}	
Literature		
Hanhijärvi and Kevarinmäki (2008)	<i>Side members</i> $\min \left(t, \frac{d}{1.47 \sqrt{\frac{1.5 f_{h,0}}{f_y}}} \right)$	<i>Middle members</i> $\min \left(t, \frac{d}{0.615 \sqrt{\frac{1.5 f_{h,0}}{f_y}}} \right)$
Standards		
Eurocode 5 (2004)	<i>Thin plates</i> $0.4 t$ (no hinges) $1.4 \sqrt{\frac{M_y}{f_{h,0,d}}}$ (one hinge)	<i>Thick plates</i> $2 \sqrt{\frac{M_y}{f_{h,0,d}}}$ (two hinges) $t \left[\sqrt{2 + \frac{M_y}{f_{h,0,d} t^2}} - 1 \right]$ (one hinge)
	Quenneville and Zarnani (2017) <i>Side members</i> $K_{LS} t = 0.65 t$	<i>Middle members</i> $K_{LS} t = 1.00 t$

$f_{h,0}$, embedment strength; f_y , yield strength of the fastener; M_y , yield moment of the fastener

One important difference is the model in the Annex A of the Eurocode 5, which assumes as the capacity of the member the maximum capacity of the two failure planes, either **H** or **L** (or **L+B** depending on the yield mode), considering as the capacity of the member that of the last plane to fail.

In the case of Hanhijärvi and Kevarinmäki (2008), they also obtain the timber member capacity as the sum of the failure of the inner and outer parts. Those capacities are previously reduced to consider the interaction with the other type of stresses (tension and shear; and shear and splitting in the outer part), by means of the following formula:

$$F_{i+j} = F_i \left(1 - k_{int} F_i / F_j \right), \text{ where } F_i \leq F_j \quad (1)$$

Finally, the capacities of the inner and outer parts are added. The result might be obtained by quite different and not always compatible failure modes in both parts (as an example, it could give the ductile capacity as the minimum inside, and shear –with interaction of tension- in the outer... which in the end defines just a lateral plane of failure, which could end up either in row shear or block shear). Therefore, for this analysis, their equations were combined to obtain compatible failure modes for the inner and outer part (tensile inside + shear outside would equal block shear; shear inside and out would be row shear).

Table 5. Capacity of the timber member for the different failure modes.

Reference	Row shear	Block shear	
Literature			
Hanhijärvi and Kevarinmäki (2008)	$2 n_r F_V$	$F_H + 2 F_V$	Actual proposal: $\min(\text{inner}) + \min(\text{outer})$
Quenneville and Mohammad (2000)	$2 n_r F_V$	$F_H + 2 F_V$	
Jensen and Quenneville (2009), (2010), (2011)	$2 n_r F_V$	--	
Standards			
Eurocode 5 (2004)	$n_{ef} n_r n_s F_{EYM}$	$\max(F_H, F_V)$	
Quenneville & Zarnani (2017)	$2 n_r F_V$	$F_H + 2 F_V$	

F_{EYM} , EYM capacity (per shear plane); n_s , number of shear planes of the connection.

Table 6. Summary of the tests database.

N. of config.	Joint scheme			Joint configuration			Fastener	
	Wood-Steel	Steel-Wood-Steel	Wood-Steel-Wood	Single fastener	Single row	Group	Bolt	Dowel
141	9	63	53	26	27	88	92	49
--	7.2%	50.4%	42.4%	18.4%	19.2%	62.4%	62.4%	34.8%
No. of tests	Timber product			Failure mode				
	LVL	Glulam	Lumber	Ductile	Splitting	Row	Block	Tension
1030	33	86	22	12	37	57	58	3
--	23.4%	61.0%	15.6%	8.5%	26.2%	40.4%	41.1%	2.1%

3 Procedure for the performance comparison

3.1 Database for benchmarking

For the comparison of the different models, a database of experimental tests (Jensen and Quenneville, 2011; Mohammad and Quenneville, 2001; Quenneville and Mohammad, 2000; Sjödin and Johansson, 2006; Iraola, 2016; Hanhijärvi and Kevarinmäki, 2008) has been compiled. Table 6 shows the main features of the database. The compiled tests fail mostly under brittle modes, since they come from studies which analyzed such behavior. It was also intended to have a significant number of tests with groups of fasteners, although some tests feature a single dowel or a single row.

3.2 Used metrics

The usual metric to obtain the performance of a model is the Coefficient of determination, R^2 , defined as

$$R^2 = 1 - \frac{\sum_{i=1}^n (y_i - f_i)^2}{\sum_{i=1}^n (y_i - \bar{y})^2} \quad (2)$$

where y_i is the prediction, f_i the experimental result of a particular test, and \bar{y} the mean value of the predictions. It provides a measure similar to a normalized error of the predictions. In this paper, it is used not as a measure of goodness of fitting, but applied to all the single tests, in its canonical form. For that reason, negative values may be obtained, which are just a proof of a bad correlation. In order to measure the error, the Mean Relative Error (MRE) is used.

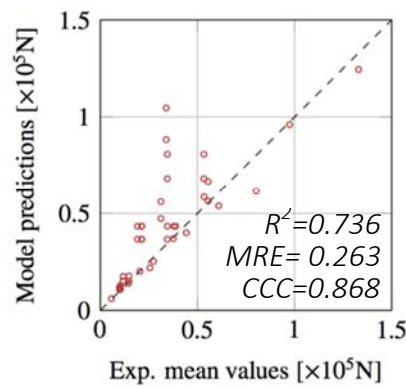
An additional criterion, which was found to be reliable, and a good summary of a certain number of desirable metrics (precision, accuracy, determination, correlation) is the Concordance Correlation Criterion (Chirico and Gramatica, 2011). A recommended threshold value is 0.85.

$$CCC = \frac{\sum_{i=1}^n (f_i - \bar{f})}{\sum_{i=1}^n (f_i - \bar{f})^2 + \sum_{i=1}^n (y_i - \bar{y})^2 + n(\bar{f} - \bar{y})^2} \quad (3)$$

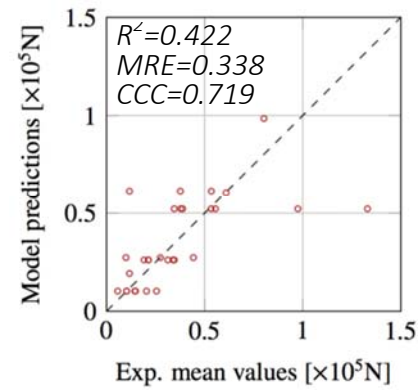
where \bar{f} is the mean of the experimental results.

4 Results

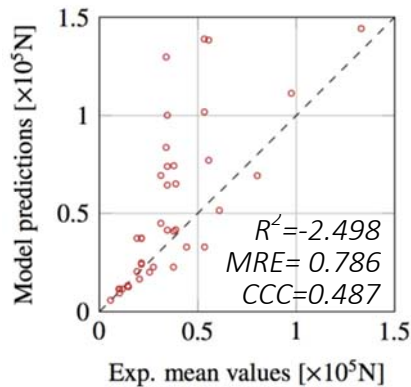
For the described analysis, the different tests were grouped by their reported failure mode, and then compared against the corresponding predictions of each model (the tests which failed under row shear were evaluated only with models predicting row shear, and so on). For that reason, the previously mentioned modification on the proposed model by Hanhijärvi and Kevarinmäki (2008) was done.



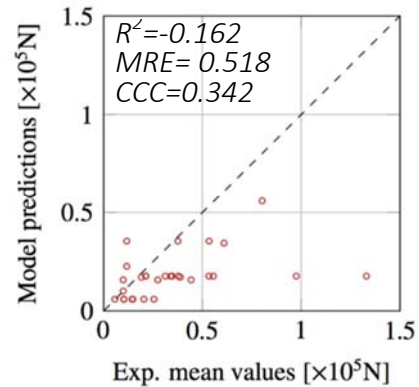
(a) Eurocode 5 (2004)



(b) Jockwer, Fink and Köhler (2018)



(c) Hanhijärvi and Kevarinmäki (2008)



(d) Jorissen (1998)

Figure 3. Splitting. Performance of the proposals, ordered according to CCC.

4.1 Levels of comparison

Since the tests feature a low number of replicas, the performance is evaluated at the mean level. The characteristic material properties used in the standards have been converted to such mean level by means of a script provided by Jockwer et al. (2018), based on the probabilistic model for timber of the Joint Committee on Structural Safety (2006)

4.2 Splitting

Figure 3 shows the obtained results for splitting. The effective number of fasteners from the Eurocode 5 stands as the best model, closely followed by the geometrical proposal by Jockwer et al. (2018). However, a significant scatter is seen for all the models.

4.3 Row shear

In the case of row shear, the model from Hanhijärvi and Kevarinmäki (2008) stands as the best one, with the best CCC, correlation factor and coefficient of determination R^2 . However, the proposal from Quenneville and Zarnani (2017) in the future New Zealand draft obtains a lower performance, although above the threshold of the CCC metric. The effective number of the Eurocode 5 (2004) provides a good performance up to a certain capacity, maybe related to the fact that it is a reduction of the EYM capacity.

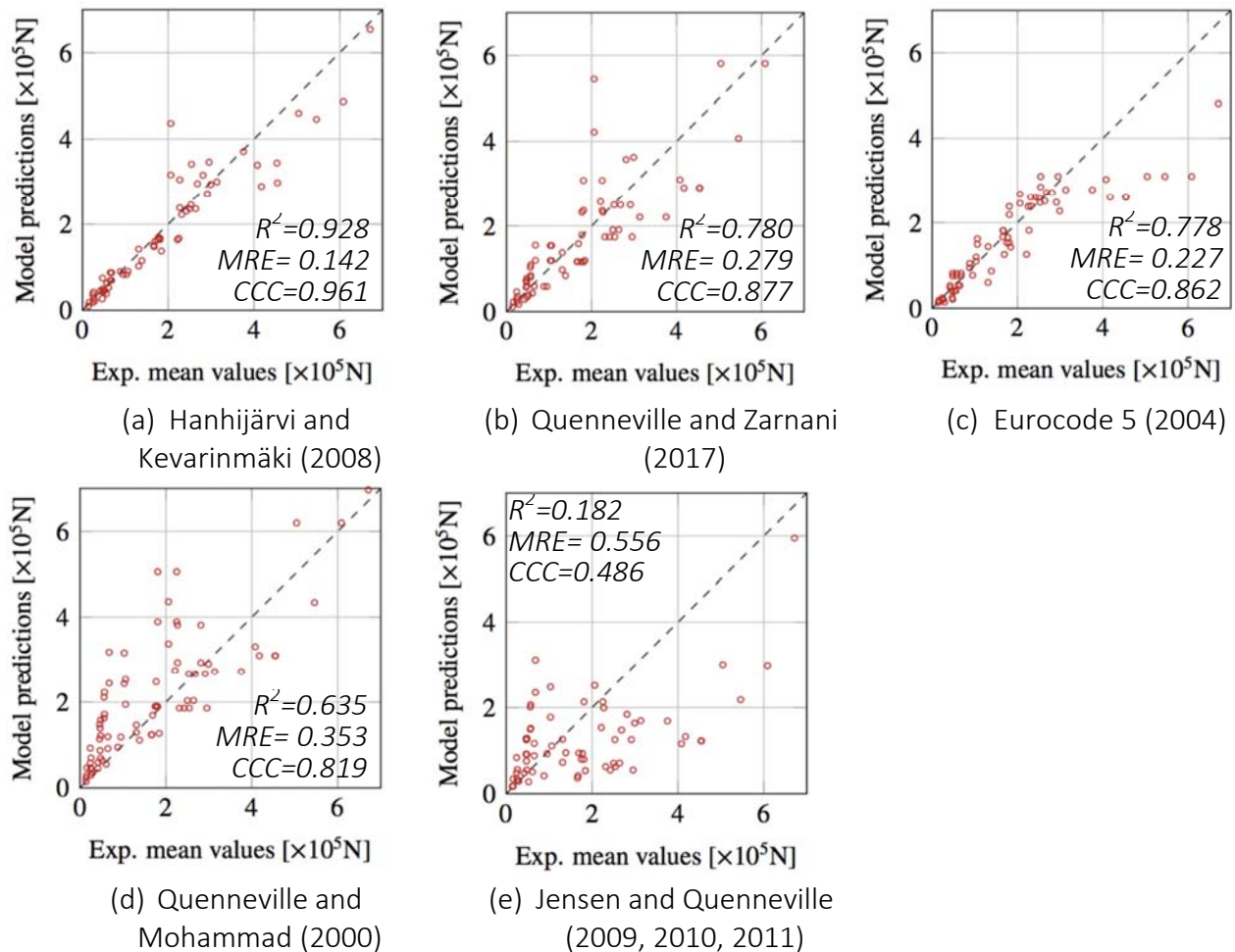


Figure 4. Row shear. Performance of the proposals, ordered according to CCC.

4.4 Block shear

In the case of block shear, none of the models obtains a CCC above the required threshold. The model from Hanhijärvi and Kevarinmäki (2008) obtains the best performance, but it might be observed that its coefficient of determination is quite low. This fact just reflects the huge variety of configurations in this set of tests, and the difficulty to obtain a formula which correctly addresses all the involved phenomena.

4.5 Discrimination ability

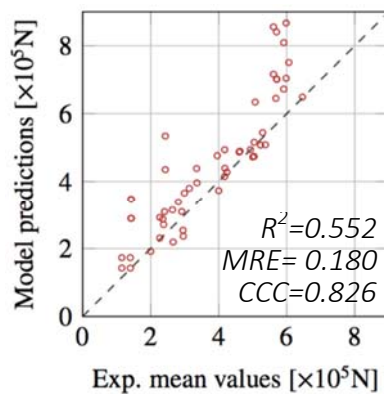
Three of the analyzed models (Hanhijärvi and Kevarinmäki, 2008; Quenneville and Zarnani, 2017; Eurocode5, 2004) provide a full set of equations which allow to discriminate among the different failure modes and, moreover, to discriminate between ductile and brittle failure. Therefore, such ability to correctly predict a brittle or a ductile failure is assessed.

The model from Hanhijärvi and Kevarinmäki (2008) provides the highest percentage of right guesses, with over 80% of true brittle and ductile failures. The proposal from Quenneville and Zarnani (2017) for the New Zealand standard is the second best, with over 70% of right predictions. The Eurocode falls way behind, but it must be stated that in its current shape, assuming that the n_{ef} provides a reduction to account

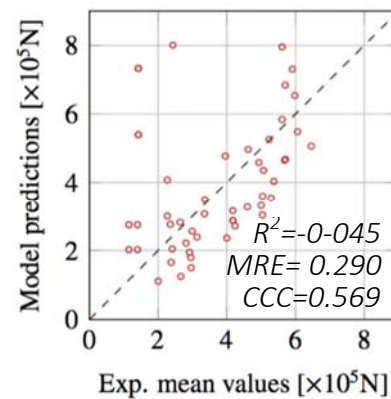
for brittle failure, it predicts ductile failure only for those specimens with only one dowel.

5 Conclusions

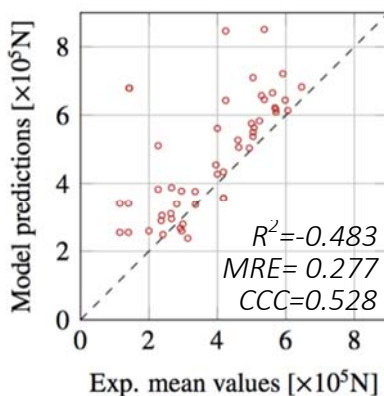
The future versions of structural standards require an improved definition of the brittle failure modes of connections. This paper provides a comparison of the different models for connections with large-diameter fasteners. Different models for each of the brittle failure modes (splitting, row shear and block shear) have been briefly described and compared. Their performance has been benchmarked against a set of tests compiled from the literature. The Eurocode 5 features an implicit model for splitting and row shear (the effective number of fasteners), and an explicit model for block shear. It is the best model for splitting, but it is surpassed by other proposals in the other analyzed failure modes.



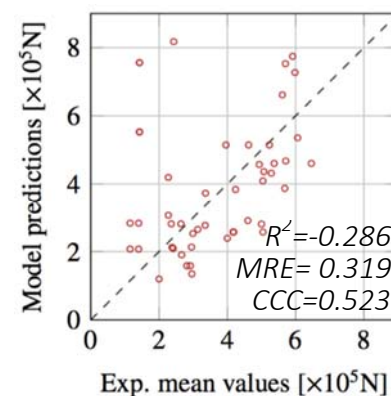
(a) Hanhijärvi and Kevarinmäki (2008)



(b) Quenneville and Zarnani (2017)



(c) Quenneville and Mohammad (2000)



(d) Eurocode 5 (2004)

Figure 5. Block shear. Performance of the proposals, ordered according to CCC.

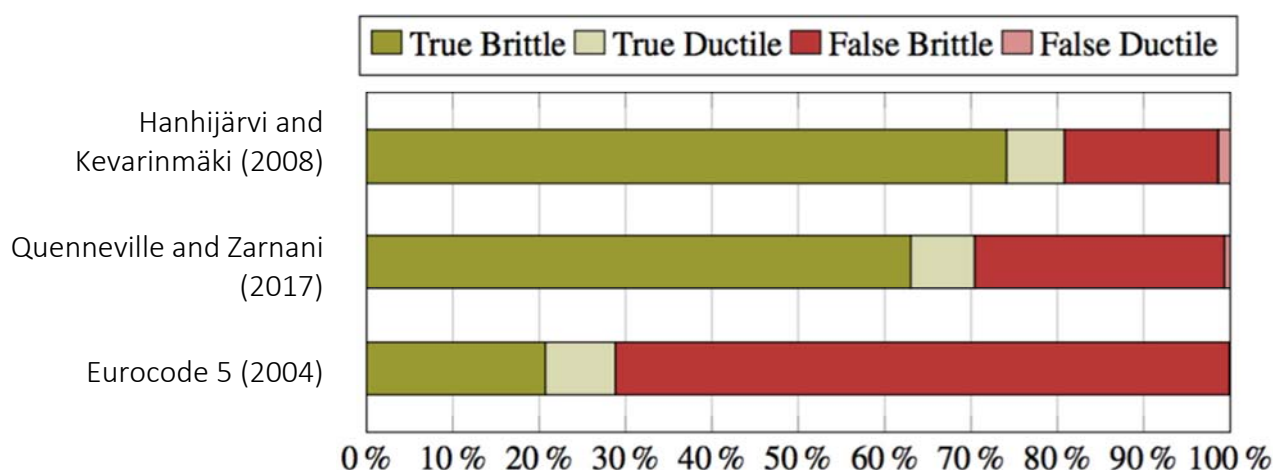


Figure 6. Discrimination ability

It is desirable that a design model is simple to use, meaningful and clear for the practitioner (so he understands the different parameters involved), and that it provides a clear description of the failure mode. The model from Hanhijärvi and Kevarinmäki (2008), which obtains the best global results, unless modified as done for the comparison in this paper, does not provide a clear view of the failure mode, due to possible incompatibilities between inner and outer parts, and due to the fact that the interaction hides the resulting failure. However, it obtains the best predictive performance in this study. The proposal from Quenneville and Zarnani (2017) for the New Zealand draft provides a clear feedback to the user of the resulting failure. It gets usually a second place in all the failure modes.

6 Acknowledgements

This work is mainly based on work done within the framework of the COST Action FP1402, funded by COST (European Cooperation in Science & Technology). The first author is in deeply gratitude to the members of the Working Group 3 within the Action, who provided feedback and “fruitful” discussions on the subject. Preliminary reports have also been presented for discussion in the Working Group 5 “Connections” in the Eurocode 5 Committee (CEN TC250/SC5/WG5).

The second author is granted by the Spanish Ministerio de Educación y Ciencia, with the grant number FPU15/03413. He was supported as well in preliminary stages by the Asociación de Amigos of the University of Navarra.

7 References

Cabrero, J. M. and Yurrita, M. (2018). Performance assessment of existing models to predict brittle failure modes of steel-to-timber connections loaded parallel-to-grain with dowel-type fasteners, *Engineering Structures*. Elsevier, In press.

- Chirico, N. and Gramatica, P. (2011). Real external predictivity of QSAR models: How to evaluate It? Comparison of different validation criteria and proposal of using the concordance correlation coefficient, *Journal of Chemical Information and Modeling*, 51(9), pp. 2320–2335.
- ENV 1995-1-1:1993. *Eurocode 5, Design of Timber Structures, Part 1-1: General Rules and Rules for Buildings* (1993). Comité Européen de Normalisation.
- Eurocode 5 (2004). EN 1995-1-1:2004 - Eurocode 5: Design of timber structures - Part 1-1: General - Common rules and rules for buildings, *Eurocode 5*, 1(2004).
- Fahlbusch, H. (1949). *Ein Beitrag zur Frage der Tragfaehigkeit von Bolzen in Holz bei statischer Belastung*. Technische Hochschule Braunschweig.
- Foschi, R. O. and Longworth, J. (1975). Analysis and design of griplam nailed connections, *Journal of the Structural Division*, 101(12), pp. 2537–2555.
- Gehri, E. (1996). Paper 29–7–6. Design of joints and frame corners using dowel-type fasteners, in *CIB-W18 Timber structures*. Bordeaux, France.
- Hanhijärvi, A. and Kevarinmäki, A. (2008). *VTT PUBLICATIONS 677: Timber Failure Mechanisms in High-Capacity Dowelled Connections of Timber to Steel*. Espoo: VTT.
- Hanhijärvi, A., Kevarinmäki, A. and Yli-Koski, R. (2006). Block shear failure at dowelled steel-to-timber connections, in *CIB-W18 Timber Structures*. Florence, Italy, pp. 175–189.
- Iraola, B. (2016). Simulación del Comportamiento Mecánico de la Madera en Uniones Estructurales y su Aplicación mediante Modelos Tridimensionales de Elementos Finitos, 1.
- Jensen, J. L., Girhammar, U. A. and Quenneville, P. (2015). Brittle failure in timber connections loaded parallel to the grain, *Proceedings of the Institution of Civil Engineers: Structures and Buildings*, 168(10).
- Jensen, J. L. and Quenneville, P. (2009). Fracture mechanics analysis of row shear failure in dowelled timber connections., *Wood Science and Technology*, 44(4), pp. 639–653.
- Jensen, J. L. and Quenneville, P. (2010). Fracture mechanics analysis of row shear failure in dowelled timber connections: asymmetric case, *Materials and Structures*, 44(4), pp. 351–360.
- Jensen, J. L. and Quenneville, P. (2011). Experimental investigations on row shear and splitting in bolted connections, *Construction and Building Materials*, 25(5), pp. 2420–2425.
- Jockwer, R., Fink, G. and Köhler, J. (2018). Assessment of the failure behaviour and reliability of timber connections with multiple dowel-type fasteners, *Engineering Structures*, 172, pp. 76–84.
- Joint Committee on Structural Safety (ed.) (2006). Properties of Timber, in *JCSS Probabilistic Model Code*.

- Jorissen, A. J. M. (1997). CIB-W18/30-7-5. Multiple fastener timber connections with dowel type fasteners, in *International Council for Research and Innovation in Building and Construction. Working Commission W18 - Timber Structures*. Vancouver, Canada, pp. 150–166.
- Jorissen, A. J. M. (1998). *Double shear timber connections with dowel type fasteners*. TU Delft.
- Kevarinmäki, A. (1995). Lecture E6. Trusses made from laminated veneer lumber, in *STEP/Eurofortech, Timber Engineering Volume 2*. The Netherlands: Centrum Hout, Almere.
- Mohammad, M. and Quenneville, J. H. (2001). Bolted wood steel and wood steel wood connections: verification of a new design approach, *Canadian Journal of Civil Engineering*, 28(2), pp. 254–263.
- Mohammad, M. and Quenneville, P. (1999). *Behaviour of wood-steel-wood bolted glulam connections*. 32. Graz, Austria.
- Nozynski, W. (1980). *Investigation of the effect of number of nails in a joint on its load carrying ability*. 13. Otaniemi, Finland.
- Quenneville, J. H. P. and Mohammad, M. (2000). On the failure modes and strength of steel-wood-steel bolted timber connections loaded parallel-to-grain, *Canadian Journal of Civil Engineering*, 27(4), pp. 761–773.
- Quenneville, P. and Zarnani, P. (2017). *Proposal for the Connection Chapter of the New Zealand Design of Timber Structures*.
- Racher, P. (1994). Lecture C1. Mechanical timber joints - General, in *STEP/Eurofortech, Timber Engineering. Volume 1*. Almere, The Netherlands: Centrum Hout.
- Sjödin, J. and Johansson, C.-J. (2006). Influence of initial moisture induced stresses in multiple steel-to-timber dowel joints, *Holz als Roh- und Werkstoff*, 65(1), pp. 71–77.
- Smith, I. and Steck (1985). *Influence of number of rows of fasteners or connectors upon the ultimate capacity of axially loaded timber joints*. 18. Beit Oren, Israel.
- Yasumura, M., Murota, T. and Naka, H. (1987). Paper 20–7– 3. Ultimate properties of bolted joints in glued laminated timber, in *CIB-W18 Timber structures*. Dublin, Ireland.

Discussion

The paper was presented by J M Cabrero

LM Ottenhaus received clarification that LVL, glulam and lumber were considered also the characteristic value of the material from standards were used to convert into mean values for evaluation of performance in the study.

A Frangi and JM Cabrero discussed the assessment of Eurocode for differentiation of brittle and ductile failure mode and effective number of fasteners. A Frangi said that Eurocode works quite well for the failure mode that it intends for. However it does not work well to distinguish between the brittle and ductile failures. They also discussed about the intent of the code to discourage the practitioners to design for brittle failure.

T Tannert commented that existing model seem to be less reliable about high capacity joints. Do they over or underestimate these cases. JM Cabrero agreed and said that they tend to overpredict the capacity in most cases.

L-M Ottenhaus commented that in seismic design it is important not to predict ductile failure if it is actually brittle. JM Cabrero agreed.

I Abeysekera asked what happens if you use all the values rather than just the mean value. JM Cabrero said that the model cannot do this now.

P Quenneville said that the moment the engineers know that there is a possibility of brittle failure mode, they will need to control it.

R Jockwer commented that it would be useful to give information with minimum spacing and distances to avoid brittle mode. JM Cabrero agreed but it is not yet available. P Quenneville disagreed as there is no one solution because there are too many variables.

P Dietsch, A Frangi and JM Cabrero discussed the role of reinforcements, practicality issues and the need for good and reliable model.

Beam-on-foundation modelling as an alternative design method for timber joints with dowel-type fasteners – Part 1: Strength and stiffness per shear plane of single-fastener joints.

Romain Lemaître, ENSTIB/LERMAB, University of Lorraine, Épinal, France

Jean-François Bocquet, ENSTIB/LERMAB, University of Lorraine, Épinal, France

Michael Schweigler, Department of Building Technology, Linnaeus University, Växjö, Sweden

Thomas K. Bader, Department of Building Technology, Linnaeus University, Växjö, Sweden

Keywords: timber joints, numerical modelling, beam-on-foundation, embedment

1 Introduction

Optimised manufacturing processes made possible the production of larger dimensions timber products, which allow for the design of outstanding structures. In the last version of the EN 1995-1-1 (Eurocode 5 (2004)), which was developed during the 1990s, it seemed important to its drafters to propose design formulas to estimate stiffness of joints in accordance with the needs of that time. Aware of the technical jump that had to be managed, the proposed rules remained simple. However, simple design equations became insufficient to cope with present-day challenges, which are, e.g., related to the design of high-rise wooden buildings. In Eurocode 5, the resistant capacity of dowel-type timber joints is no longer determined by empirical formulas but it is based on the limit analysis proposed by Johansen (1949). This methodology however shows limits for complex joints even though many improvements have been made since its introduction (Blaß & Laskewitz (2000)). In parallel with these analytical approaches, developments in computational mechanics made it possible to develop simple numerical methods (Foschi (1974), Hirai (1983)), which take even into account

nonlinear phenomena. These approaches have remained unused in practical design due to their complex implementation and their high running time, at the time of their invention, while today's computational resources would allow for fast and efficient numerical methods-based design. Numerical modelling of connections can help engineers to fill the gaps of the Eurocode 5 and to cope with variability in connection design. For this purpose, dowel-type fasteners are numerically modelled as elastoplastic beams on a nonlinear foundation in engineered wood-based products (Sawata & Yasumura (2002), Hochreiner et al. (2013)). This method is called Beam-On-Foundation (BOF) modelling and shows huge potential for engineering design. The purpose of this paper is to show how this method can substitute and complement limit analysis and empirical stiffness formulas of timber joints with dowel-type fasteners. Corresponding perspectives are exemplified after a comparison of BOF modelling with the limit state approach in EN 1995-1-1.

2 Description of the Beam-on-foundation method

The complexity in the local deformation and stress state in wood close to the dowel suggests using a phenomenological approach to describe the embedment behaviour instead of using 3-dimensional continuum models. Thus, beam-on-foundation approaches have been developed (see Figure 2.1), where nonlinear springs are used to model the contact between wood and steel dowel, by making use of mathematical functions for the nonlinear relative displacement-embedment load behaviour (see Foschi (1970), Hirai (1983) and Schweigler et al. (2018)). In most of these equations, the parameters can be related to physical properties derived from uniaxial embedment tests. The simplest approach would be to assume linear tangents with a continuous intermediate nonlinear transition. An initial nonlinear region with increasing stiffness is typically observed in test data. This is linked on the one hand to the quality and the precision of production and assembling, and on the other hand to the stochastic nature of the properties. Mathematical functions enable an integration of this initial behaviour, which would lead to a more realistic load distribution in multiple fastener joints. The dowel itself is modelled by 1-dimensional beam elements, which makes it possible to reduce the number of elements compared to a 3-dimensional model. An elastoplastic material behaviour is assigned to these beam elements. Prescription of displacements of the connected structural elements yield corresponding reaction forces, which gives access to the global load-displacement behaviour of the connection.

The sensitivity of the discretization of the embedment behaviour, i.e., the number of springs elements and their distance along the dowel on the global load-displacement curve of the connection, were investigated in Hirai (1983). In this paper, it has given rules to define the number of springs elements according to the slenderness of the connection t/d .

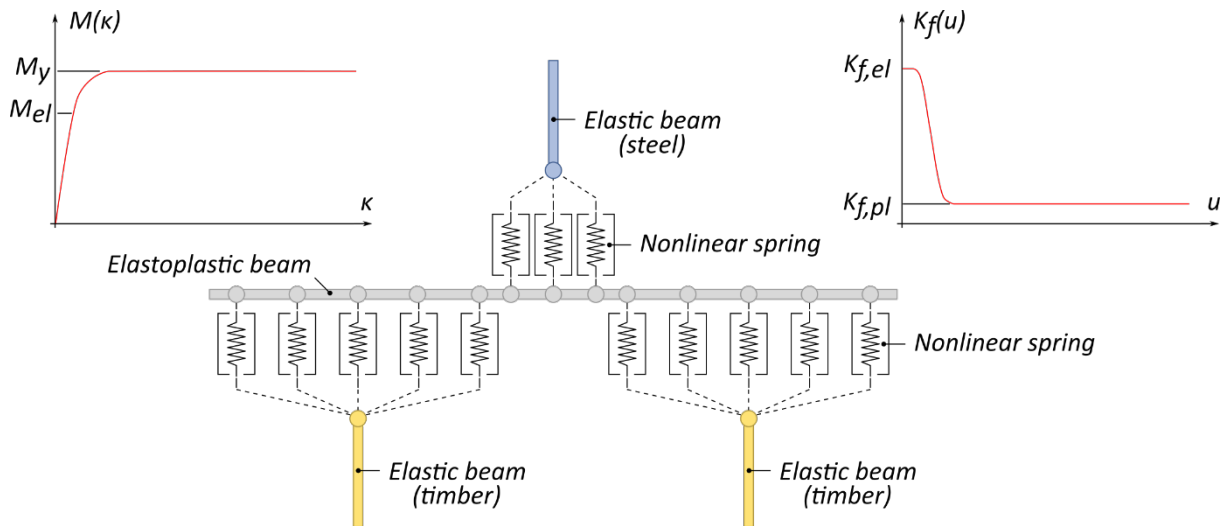


Figure 2.1. Description of the Beam-On-Foundation modelling for the design of timber joints with dowel-type fasteners (example of a meshing steel-to-timber connection with two shear planes)

3 Comparison with European Yield Model

In this part, the load-bearing capacities and the stiffness of different types of connection assemblies computed with the analytical formulas of the European yield model (EYM) are compared with the numerical results of the BOF modelling.

In order to investigate the validity of the BOF modelling and to demonstrate that it can be used as an alternative to the EYM, results of these two methods will be compared for different connections with variation in connection parameters. In particular, load-bearing capacity, i.e., the connection load at a displacement equal to 5 mm and the quasi-elastic stiffness of the connection were computed. Connection parameters were chosen to encompass all failure modes (see Figures 8-2 and 8-3 in EN 1995-1-1) and included the following variations:

- dowel diameter d in {8 mm; 16 mm; 24 mm};
- slenderness of the connection t/d in {1; 1.5; 2; 2.5; 3; 3.5; 4; 4.5; 5; 6; 7; 8; 9; 10}, where t is the thickness of the timber members;
- density of timber ρ in {420 kg/m³};
- yield strength of the dowel f_y in {240 MPa}.

The comparison is limited to timber-to-timber and steel-to-timber joints with double-shear planes (equations (8.7), (8.11), (8.12) and (8.13) in EN 1995-1-1), see Figure 3.1. Design equations specified in Figure 3.1 are based on the EYM, but contrary to EN 1995-1-1 equations, partial safety factors related to the uncertainties on the materials and the rope effect are neglected in order to be able to compare the mechanical models. Uncertainty considerations can be later added to the BOF model.

The BOF model was established with an elasto-plastic beam element representing the steel dowel. Young's modulus of steel equal to 210 GPa and a yield strength equal

to 240 MPa (f_y) was used. The yield moment M_y included in equations of Figure 3.1 was equal to the theoretical expression for a circular cross-section. The nonlinear behaviour of dowel elements was defined from a moment-curvature relationship which allowed to calculate a new bending stiffness of the dowel for each step of calculation (equal to 0.02 mm).

The foundation used to model the contact between wood and steel dowel was described by a pure elasto-plastic behaviour where the elastic limit f_h was equal to the empirical expression (8-16) of EN 1995-1-1. It was supposed that the elastic behaviour remained elastic up to a millimetre of embedment. Therefore, the elastic and plastic foundation moduli (named $K_{f,el}$ and $K_{f,pl}$) were equal to f_h and zero, respectively.

The distance between embedment spring elements was equal to $0.4d$. The nonlinear spring gave only loads parallel to the displacement direction, while the dowel was free to move along its axial direction (no friction was considered).

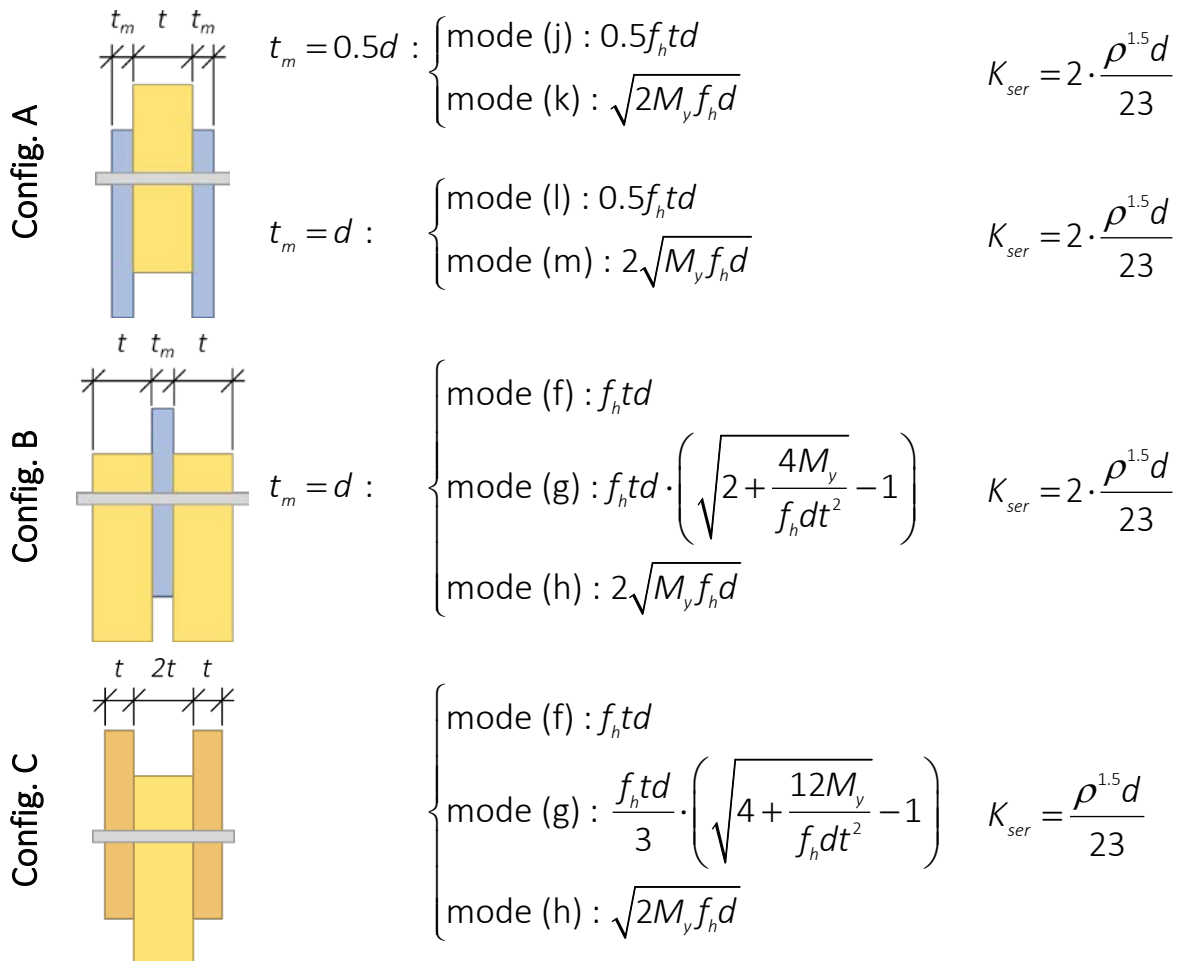


Figure 3.1. Double-shear steel-to-timber and timber-to-timber connections and design equations according to EN 1995-1-1 without partial safety factors for comparison with BOF modelling.

Load-bearing capacity according to the limit state approach ($F_{v,EC5}$) were compared to the reaction force in the BOF model for a relative displacement equal to 5 mm ($F_{v,BOF}$).

The foundation modulus K_{ser} according to EN 1995-1-1 (see Figure 3.1) was compared to the numerical simulations using two evaluations methods. In the first approach, stiffness was defined between 10% and 40% of the load-bearing capacity $F_{v,BOF}$ (empty forms of the Figure 3.2 and Figure 3.3). In the second approach, the stiffness is defined between 0% and 10% of the load-bearing capacity $F_{v,BOF}$ to guarantee all material behaviours were linear (full forms of the Figure 3.3).

It was observed that the foundation used to model the contact between steel and dowel influences numerical results. Being difficult to quantify the elastic foundation modulus for that type of contact, different numerical simulations have been realized (exemplary shown in Figure 3.2 for configuration B with a dowel diameter equal to 16 mm). Based on these simulations, an elastic behaviour with a foundation modulus equal to fifty times $K_{f,el}$ was retained in the rest of this study.

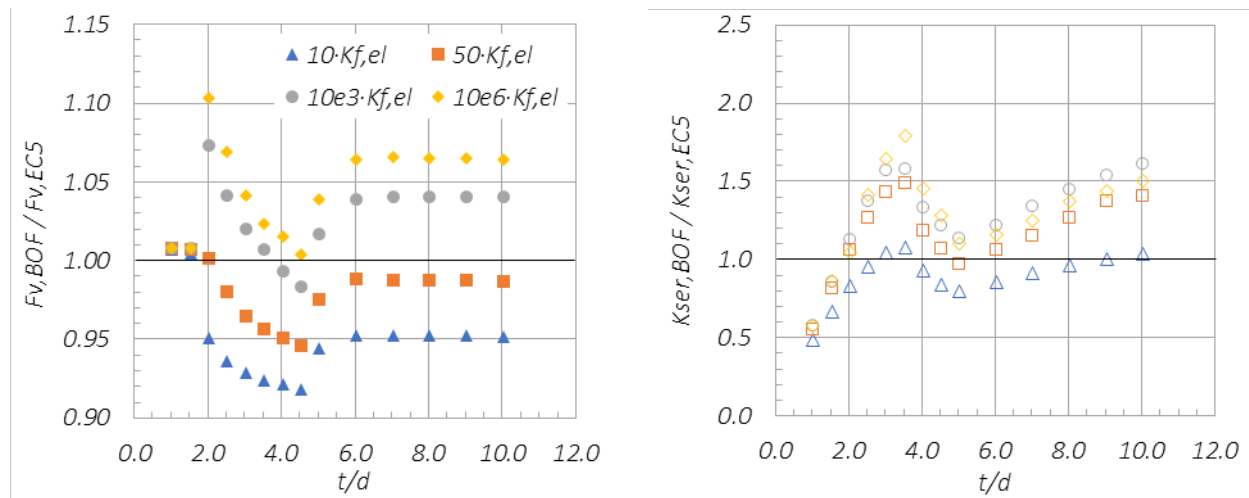
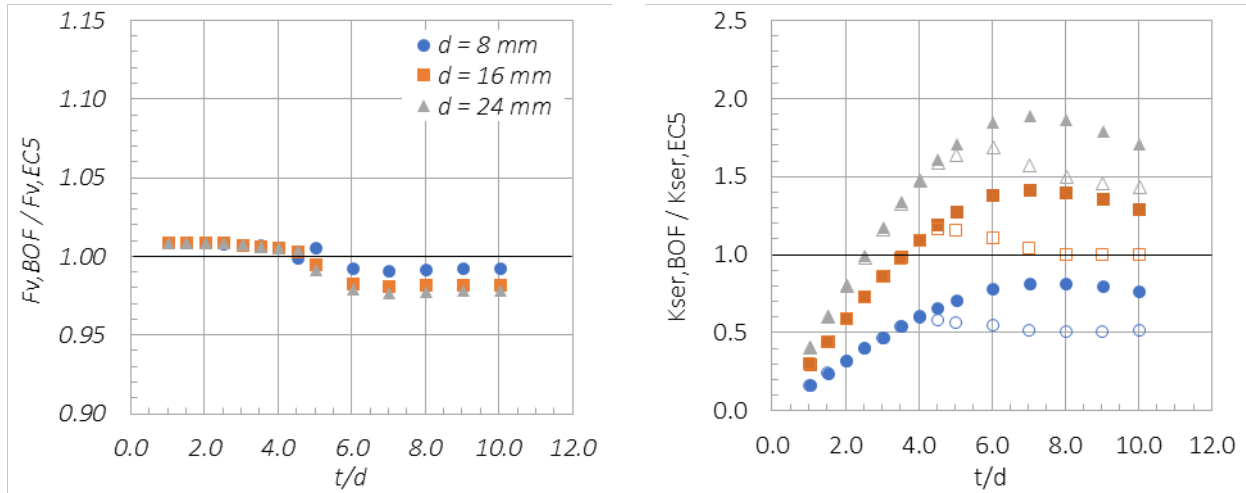


Figure 3.2. Influence of the elastic foundation modulus of the contact between dowel and steel on the ratio of numerical result to the analytical result (configuration B and $d = 16$ mm).

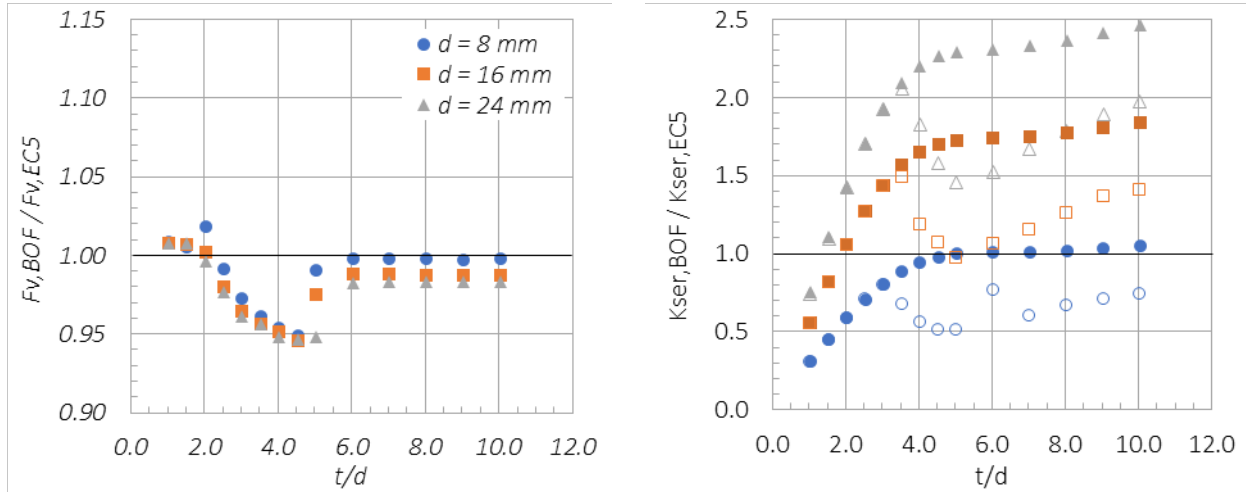
The results are grouped in the different graphs in Figure 3.3, where each point represents the ratio of numerical result to the analytical result. The numerical results show an evolution of the stiffness as a function of the slenderness, t/d , which is not predicted by the empirical formula of Eurocode 5 for K_{ser} . It is observed that the evolution of the stiffness is more marked in the first definition of the stiffness (empty forms) for configurations B and C. It could be explained by the early emergence of the first plastic hinge on the dowel (in the inner part of the connection) decreasing its bending stiffness therefore the stiffness of the connection.

For the load-bearing capacity at 5 mm slip, the numerical results are in good agreement with the load calculated by the EYM. It becomes however obvious that differences evolve in accordance with the failure modes. Indeed, for the mode with one plastic hinge in the steel dowel, whatever the configuration and the dowel diameter, the differences between the numerical and the analytical results are lower than 10%. For the failure modes without plastic hinge or more than one, whatever the configuration and the dowel diameter, the differences are lower than 3%.

Configuration A



Configuration B



Configuration C

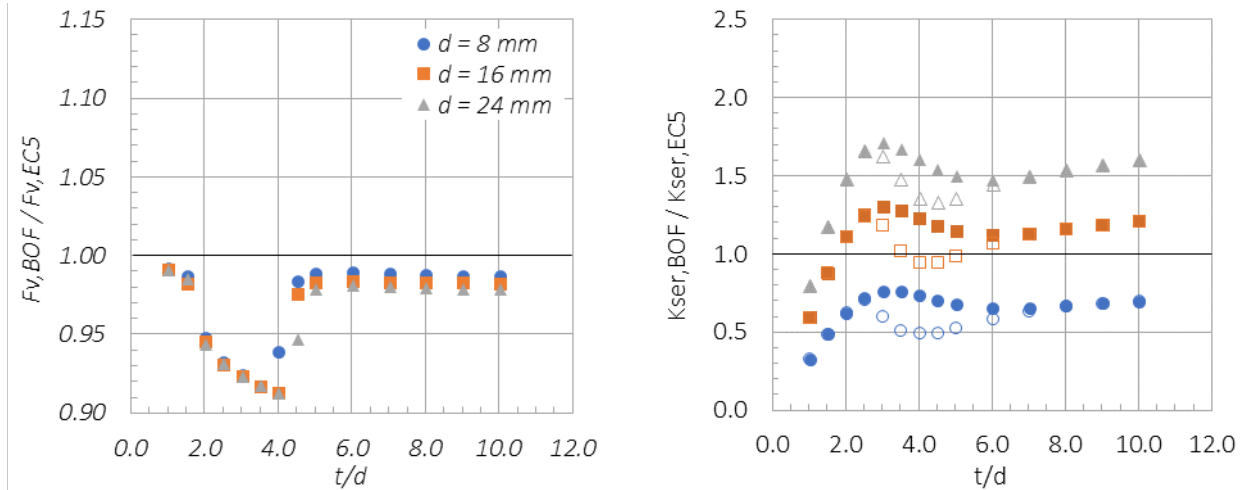


Figure 3.3. Comparison of the load-bearing capacity and the empirical equation for K_{ser} in EN 1995-1-1 with BOF modelling results for each configuration.

4 Perspectives of the method

Emergence of new engineering wood-based products (EWPs) led to the situations that design equations for connection in Eurocode 5 do not cover all EWPs. Moreover, only a limited number of connection layouts are covered by Eurocode 5 equations. The BOF modelling can thus complement and extend Eurocode 5 equations and is intended to be a universal tool for estimating the mechanical behaviour of connections (load-bearing capacity, load distribution and stiffness). In the following, perspectives of this numerical tool for configurations which are not covered or only partially covered by Eurocode 5, will be shown. These configurations do not pretend to be exhaustive but are limited to the most common practically relevant cases.

4.1 Multiple-shear plane connections: comparison analytical equations and BOF

To calculate multiple-shear planes connections, Eurocode 5 proposes to decompose the connection into series of three elements and to calculate for each decomposition the load-bearing capacity of each shear planes (§ 8.1.3 of EN 1995-1-1). However, checking the compatibility of failure modes (see Figure 4.1) remains a tedious work for some configuration of connections. It is proposed here to check the consistency of the BOF modelling for a steel-to-timber connection with four shear planes. The connection is composed of two outer timber members with a thickness of t_1 equal to 95 mm and an inner timber member with thickness t_2 equal to 90 mm. The thickness of the steel plates is taken equal to the dowel diameter, d , equal to 16 mm. Finally, the material properties (embedding strength f_h and yield strength f_y) are identical to those specified in Section 3. For this design example, analytical formulas of the Johansen theory are given below and are associated with the failure modes shown in Figure 4.1.

$$\text{mode (l + f) : } 0.5f_h t_2 d + f_h t_1 d \quad (\text{Eq. 4-1})$$

$$\text{mode (l + g) : } 0.5f_h t_2 d + f_h t_1 d \left(\sqrt{2 + \frac{4M_y}{f_h d t_1^2}} - 1 \right) \quad (\text{Eq. 4-2})$$

$$\text{mode (l + h) : } 0.5f_h t_2 d + 2\sqrt{M_y f_h d} \quad (\text{Eq. 4-3})$$

$$\text{mode (m + f) : } 2\sqrt{M_y f_h d} + f_h t_1 d \quad (\text{Eq. 4-4})$$

$$\text{mode (m + g) : } 2\sqrt{M_y f_h d} + f_h t_1 d \left(\sqrt{2 + \frac{4M_y}{f_h d t_1^2}} - 1 \right) \quad (\text{Eq. 4-5})$$

$$\text{mode (m + h) : } 2\sqrt{M_y f_h d} + 2\sqrt{M_y f_h d} \quad (\text{Eq. 4-6})$$

Results of the numerical simulation are shown in Figure 4.2 in terms of the global load-relative displacement curve (displacement at the steel plate). In this graph, both

load-slip curves of the outer parts and of the inner part are given. A substantially different behaviour in the timber members of the connection becomes obvious from the BOF model, which is not predicted by Eurocode 5 design equations. Load-bearing capacity for a dowel connection at a slip of 5 mm, as predicted by the numerical simulation, is 7% higher than EN 1995-1-1 predictions based on the EYM (predicted failure mode $(m + h)$).

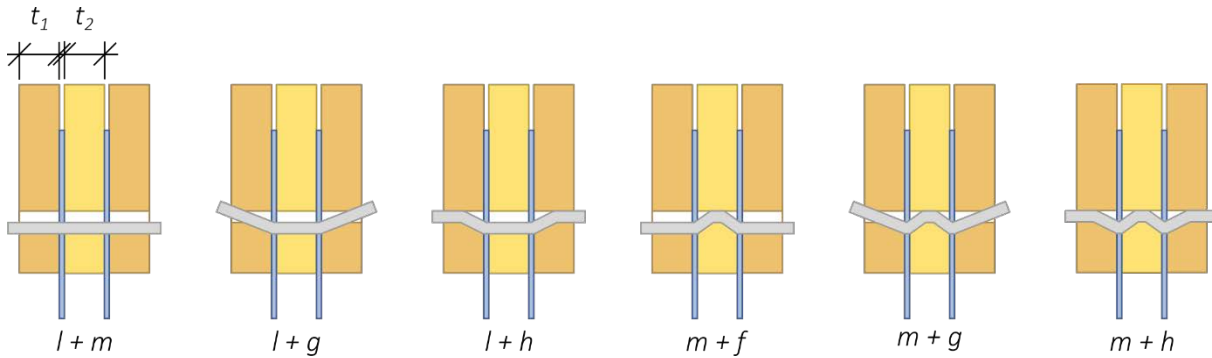


Figure 4.1. Failure modes of multiple-shear planes for steel-to-timber connection.

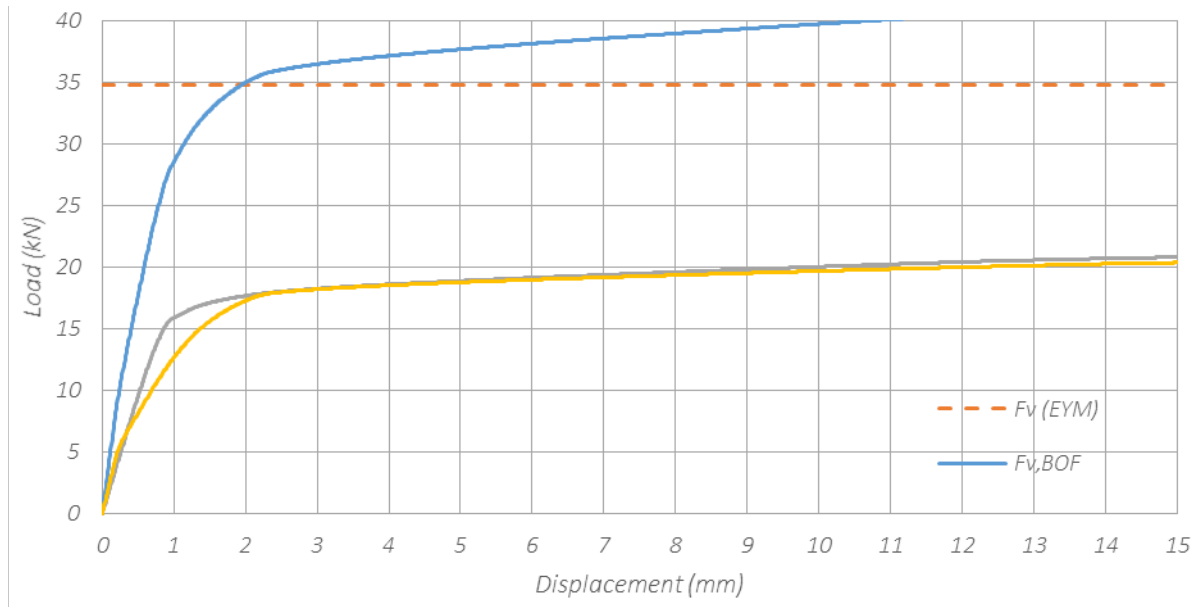


Figure 4.2. BOF modelling results of one multiple-shear plane connection compared with EYM.

4.2 Multiple-material connections: Reinforcement with plywood

The addition of plywood as reinforcement significantly increases the resistance capacity of connections (see Bouchair et al. (2007)). Analytical formulas based on the EYM, considering the contribution of plywood were derived in Werner (1993). It is proposed here to compare the BOF modelling with these formulas.

$$\text{mode (g)} : (f_{h,1}t_1 + f_{h,r}t_r)d \quad (\text{Eq. 4-7})$$

$$\text{mode (h)} : (0.5f_h t_2 + f_{h,r}t_r)d \quad (\text{Eq. 4-8})$$

$$\text{mode (j)} : \frac{\beta f_{h,1} d}{2 + \beta} \left[\sqrt{(t_1 + 4t_r)^2 + \frac{2 + \beta}{\beta} \left(t_1^2 - 4\eta t_r^2 + \frac{4M_y}{df_{h,1}} \right)} - (t_1 + 4t_r) \right] + f_{h,r} t_r d \quad (\text{Eq. 4-9})$$

$$\text{mode (k)} : \frac{2\beta f_{h,1} d}{1 + \beta} \left[\sqrt{t_r^2 - \frac{1 + \beta}{2\beta} \left(\eta t_r^2 - \frac{2M_y}{df_{h,1}} \right)} - t_r \right] + f_{h,r} t_r d \quad (\text{Eq. 4-10})$$

Where:

- $f_{h,r} = 0.11(1 - 0.01d)\rho$, $\beta = f_{h,2}/f_{h,1}$ (equal to 1) and $\eta = f_{h,r}/f_{h,1}$ (equal to 1.34)

The connection is composed of two outer timber members with a thickness of t_1 equal to 32 mm and an inner timber member with a thickness of t_2 equal to 64 mm, on which plywood panels with a thickness of t_2 equal to 10 mm (see Figure 4.3) were added at the inner shear planes. As the previous example, the material properties are identical to those mentioned in Section 3 and dowel diameter was equal to 16 mm. The results of the numerical simulation are shown in the graph of the Figure 4.4. They show good agreement with Werner's equations (predicted failure mode (j)).

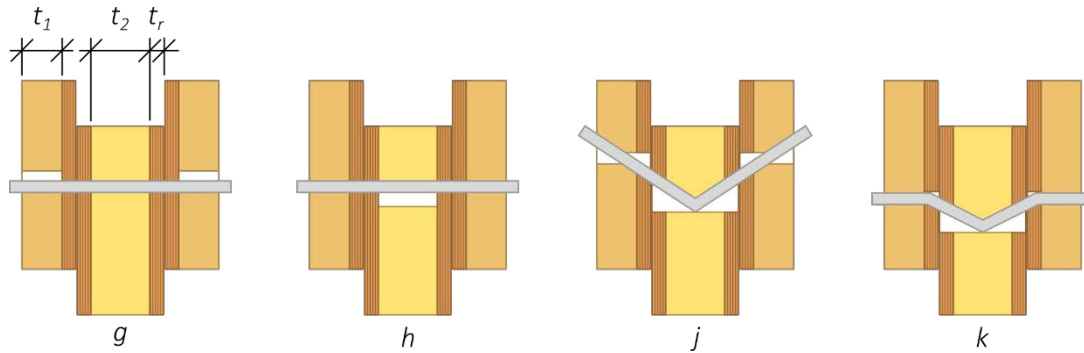


Figure 4.3. Failure modes of timber-to-timer connection reinforced with glued-on wood-based panels.

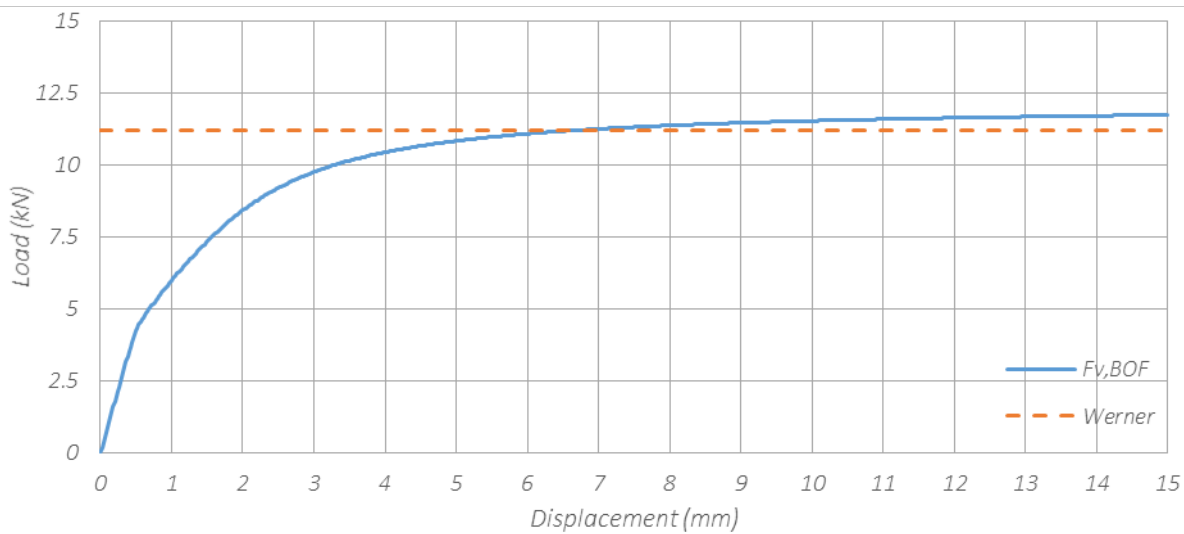


Figure 4.4. BOF modelling result of one timber connection reinforced with glued-on wood-based panels and comparison with Werner (1993) equations.

4.3 Multiple-material connections: Cross laminated timber (CLT)

The last example of the BOF modelling is related to a CLT connection with one shear plane (three layers 19-22-19 for the CLT and the thickness of the steel plate was equal to the dowel diameter 16 mm). Uibel & Blaß (2006) have proposed different analytical formulas for this type of connection. The results of the numerical simulation are shown in Figure 4.6 (predicted failure mode (d.2)). They also show good agreement between the numerical results and the analytical equations.

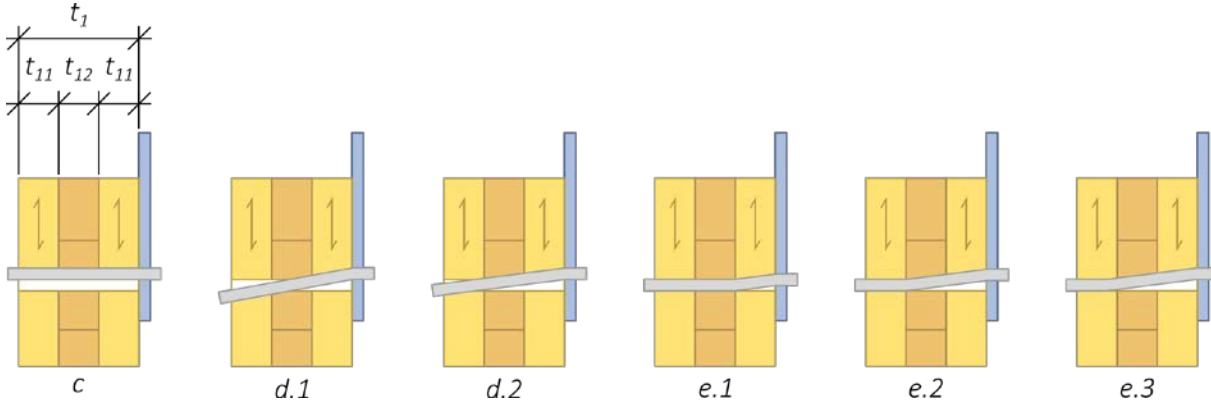


Figure 4.5. Failure modes of one-shear plane for steel-to-CLT connection.

$$\text{mode (c)} : f_h t d \quad (\text{Eq. 4-11})$$

$$\text{mode (d.1)} : f_{h,1} t d \cdot \left[\sqrt{2} \cdot \sqrt{\beta \left(\beta (2 + \psi^2 - 2\psi + 1) + 2\psi (1 - \psi) + \frac{2M_y}{f_{h,1} d t^2} \right)} - \beta \right] \quad (\text{Eq. 4-12})$$

$$\text{mode (d.2)} : f_{h,1} t d \cdot \left[\sqrt{2} \cdot \sqrt{\psi (2\beta - 2) + 2 - \beta + \frac{2M_y}{f_{h,1} d t^2} + 2\psi + \beta (1 - 2\psi) - 2} \right] \quad (\text{Eq. 4-13})$$

$$\text{mode (e.1)} : 2 \sqrt{M_y f_{h,1}} d \quad (\text{Eq. 4-14})$$

$$\text{mode (e.2)} : f_{h,1} t d \psi \cdot \left[1 - \beta + \sqrt{\beta \left(\beta - 1 + \frac{4M_y}{f_{h,1} d t^2 \psi^2} \right)} \right] \quad (\text{Eq. 4-15})$$

$$\text{mode (e.3)} : f_{h,1} t d \cdot \left[\beta (1 - 2\psi) + \sqrt{2\psi - 1 + 2\psi (\beta - 1) - \beta + 1 + \frac{4M_y}{f_{h,1} d t^2}} \right] \quad (\text{Eq. 4-16})$$

Where:

- $f_h = 0.112 d^{-0.5} \rho^{1.05}$, $f_{h,1} = 0.082 (1 - 0.01d) \rho$, $f_{h,12} = f_{h,1} / (1.35 + 0.015d)$;
- $\beta = f_{h,12} / f_{h,1}$ (equal to 0.629), $\psi = t_{11} / t_1$ (equal to 0.317).

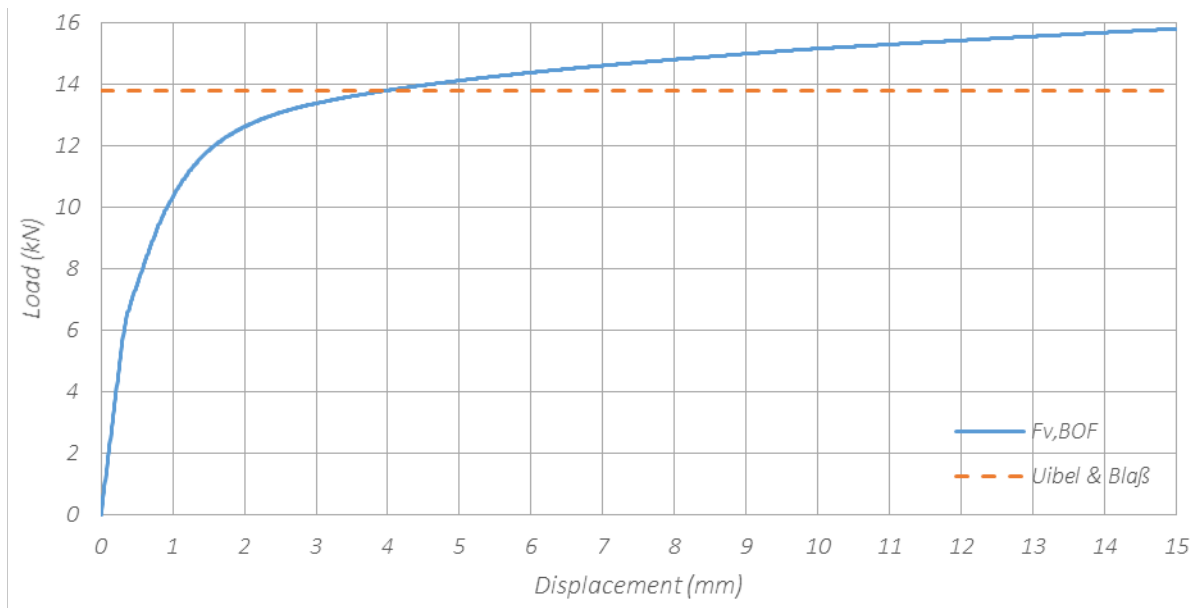


Figure 4.6. BOF modelling result of one CLT connection (three layers 19-22-19) compare with Uibel & Blaß (2006) equations.

5 Proposed modifications for the EN 383 (2007)

The stress field of the timber around the dowel during an embedding test induces tensile stresses perpendicular to the grain of the wood. These stresses can cause splitting of the timber just after or even before the timber has entered its plastic domain (for tests with low load-to-grain angles, 0° to 30°). This phenomenon is more pronounced for timber with a high density and especially for hardwoods. However, at the scale of a connection, because of the mass of the material around the dowel or possible reinforcement (screws, plywood for example), the risk for splitting might be considerably reduced and ductile connection behaviour is achieved. In order to be able to predict the behaviour of these connections, there is a need to obtain experimental curves of embedment up to high dowel displacement (about 15 mm). For this purpose, embedment test specimens should be reinforced in order to avoid splitting. The reinforcement can be achieved by glued-on plywood at the end area of the specimen or by screws. The reinforcement must not alter the mechanics of the embedment and it must be placed sufficiently far from the drilling hole: $1.5d$ (for reinforcement by plywood, see Sandhaas (2012)) and $3d$ (for reinforcement by screw). The type of reinforcement to be favoured is a reinforcement by screw because it allows a simple and fast implementation. Screws should be placed perpendicular to the wood grain to ensure maximum transverse tensile strength.

By reinforcing embedment test specimens up to load-to-grain angles of equal to 30° , it becomes possible to idealize the experimental curves of embedment tests of wood or wood-based material by a nonlinear function with linear hardening (see Figure 5.1) for all diameters, densities and load-to-grain angles. From this idealized shape, six

physical parameters related to the embedding of timber can be defined. The proposed parameters are as follows:

- $f_{h,5mm}$: embedding strength defined at a displacement equal to 5 mm;
- $f_{h,1mm}$: embedding strength defined at a displacement equal to 1 mm;
- $K_{f,el,1}$: elastic foundation modulus defined between 10% and 40% of $f_{h,5mm}$ during the first loading;
- $K_{f,el,2}$: elastic foundation modulus defined between 10% and 40% of $f_{h,5mm}$ during the first unloading;
- $K_{f,pl}$: plastic foundation modulus defined between 3 mm and 15 mm displacement;
- gap : gap between the dowel and the wood defined as the intersection of the x-axis and the line with the slope of $K_{f,el,1}$.

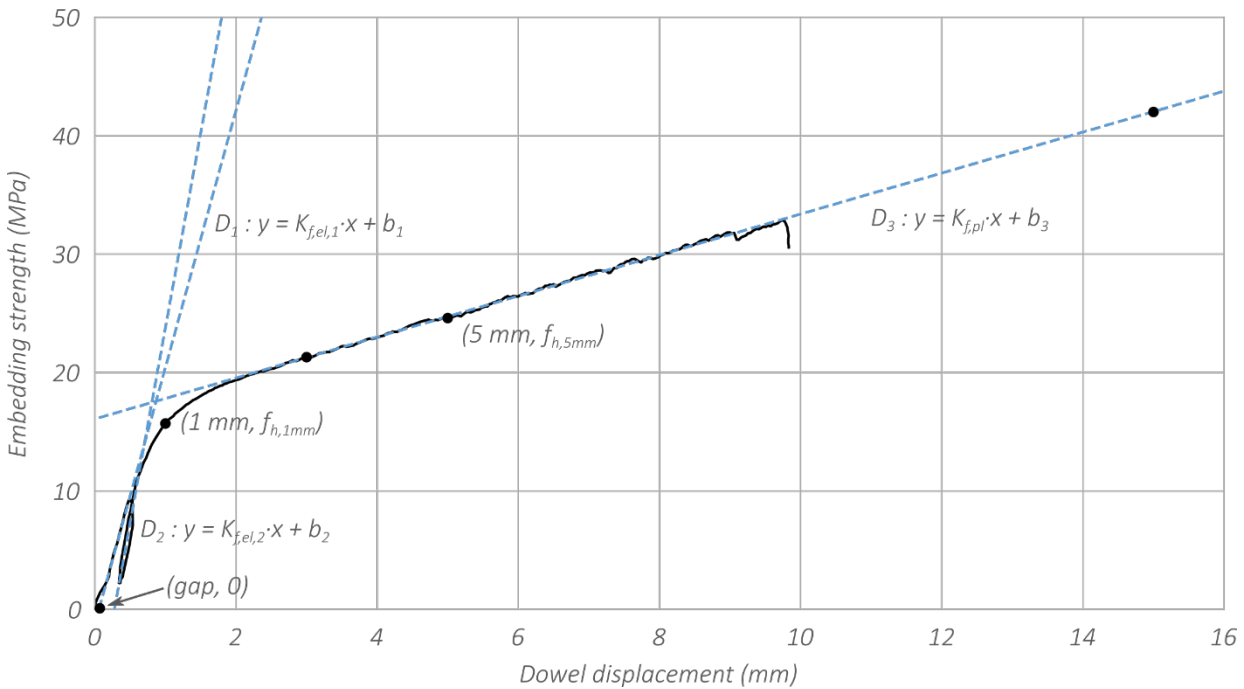


Figure 5.1. Idealized shape of an experimental curve of an embedment test with the characteristic parameters necessary to quantify the nonlinear foundation.

These six parameters have the advantage of being easily measurable (regardless of the type of material tested: softwood, hardwood, CLT, LVL, plywood, etc.) and can be used in mathematical functions describing the nonlinear foundation, no matter which one is chosen by the users of the BOF modelling (see Schweigler et al. (2018)).

Bléron & Duchanois (2006) and Schweigler et al. (2016) have shown that for embedding tests out of orthotropic axes, the relative displacement between the dowel and the wood is not collinear with the direction of the load. Both authors have used a set-up to leave free and measure the lateral displacement of the test specimen. This embedding mechanic is found in connections loaded by bending moments and that is why the embedding tests out of the orthotropic axes made to quantify the nonlinear foundation of the BOF modelling will have to take into account the previous remark.

Finally, the last proposal concerns the dimension of the test specimens for embedding tests with solid wood or glulam. The dimensions of the test specimens with load-to-grain angle tests are calculated by linear interpolation from the dimensions given in EN 383 (2007) for 0° and 90° (see Hübner et al. (2008)).

6 Discussion and conclusions

In this paper, principles of modelling dowel-type fastener connections with beam-on-foundation (BOF) models using the finite element method, was described. A comparative study of the load-bearing capacity and the stiffness of single-dowel connections with two shear planes predicted by the EYM with the prediction of the BOF method was made. This comparison included effects of parameters included in the Yield Analysis Theory of EN 1995-1-1. The study was continued by the design of connections with more than two shear planes, as well as by connections with reinforcements and multiple-material layups in order to highlight possibilities of the BOF method compared to the Yield Analysis Theory, as regards practical engineering problems.

BOF model calculations and their comparison to the design equations highlights the validity of the method and the advantage of a kinematically compatible model that allows prediction of the slip behaviour of connections in addition to the ultimate strength. Effects that are not explicitly covered in the empirical design equations, namely the influence of the slenderness on the elastic slip modulus, were demonstrated. The low identified gaps come from different approaches of kinematic, an isolated hinge for the Johansen theory and a continuous approach along the dowel for the BOF method.

Finally, recommendations for modifications of the timber engineering design standards were proposed. Since the BOF method requires additional input compared to the Yield Analysis Theory, namely kinematically compatible load-displacement data, proposed modifications mainly concern the embedment test standard EN 383 (2007). In the future a study will also have to be done to quantify the foundation of the contact between dowel and steel.

BOF calculations presented herein were limited to single dowel connections loaded parallel to the grain. The 2-dimensional model can however be applied to calculate connection behaviour for arbitrary load-to-grain angles and has been extended to a 3-dimensional foundation model. Their integration in multiple fastener connections was demonstrated in a previous work and can be used to predict load distribution.

This paper could be the first of a series of four papers, which will, in addition to this one, encompass: methodology for modelling multiple fastener joints with the BOF method and reliability, second order theory effect for considering the rope effect in dowel-type fasteners using the BOF method, basic parameters for different wood species and their exploitation in the BOF method.

7 References

- Blaß, H.J., Laskewitz, B. (2000): Load-carrying capacity of joints with dowel-type fasteners and interlayers, CIB-W18/33-7-6, Delft, Netherlands.
- Bleron, L., Duchanois, G. (2006): Angle to the grain embedding strength concerning dowel type fasteners. *Forest products journal*, 56(3), 44.
- Bouchaïr, A., Racher P., and Bocquet J. F. (2007): Analysis of Dowelled Timber to Timber Moment-Resisting Joints. *Materials and Structures* 40 (10): 1127–41.
- EN 383 (2007): Timber structures. Test methods. Determination of embedment strength and foundation values for dowel type fasteners.
- Eurocode 5 (2004): Design of timber structures - Part 1-1: General and rules for buildings. CEN. (EN 1995-1-1).
- Foschi, R.O. (1974): Load-Slip Characteristics of Nails. *Wood Science*, 17, 69-77.
- Hirai, T. (1983): Non-linear load-slip relationship of bolted wood-joints with steel side members –II – Application of the generalised theory of beam on elastic foundation. *Makusu Gakkaishi*, Vol. 29, No. 12, pp 839-844
- Hochreiner, G., Bader, T.K., de Borst, K., Eberhardsteiner, J. (2013): Stiftförmige Verbindungsmittel im EC5 und baustatische Modellbildung mittels kommerzieller Statiksoftware, *Bauingenieur* 88:275-289.
- Hübner, U., Bogensperger, T., Schickhofer, G. (2008): Embedding strength of European hardwoods, CIB-W18/41-7-5, Andrews, Canada.
- Johansen, K.W. (1949): Theory of Timber Connections, International Association for Bridge and Structural Engineering (ABSE) Pub. 9, 249-262.
- Sandhaas, C. (2012): Mechanical Behaviour of Timber Joints with Slotted-in Steel Plates. PhD thesis, Technische Universiteit Delft.
- Sawata, K., Yasumura, M. (2002): Determination of embedding strength of wood for dowel-type fasteners, *Journal of Wood Science* 48(2), 138-146.
- Schweigler, M., Bader, T.K., Hochreiner, G., Unger, G., Eberhardsteiner, J. (2016): Load-to-grain angle dependence of the embedment behavior of dowel-type fasteners in laminated veneer lumber. *Construction and Building Materials*, 126:1020-1033.
- Schweigler, M., Bader, T.K., Hochreiner, G., Lemaître, R. (2018): Parameterization equations for the nonlinear connection slip applied to the anisotropic behaviour of wood. *Composites Part B: Engineering*, 142:142-158.
- Uibel, T., Blaß, H. J. (2006): Load carrying capacity of joints with dowel type fasteners in solid wood panels. CIB-W18/39-7-5, Florence, Italy.
- Werner, H. (1993): Untersuchungen von Holz-Verbindungen mit stiftförmigen Verbindungsmitteln unter Berücksichtigung streuender Einflußgrößen. PhD thesis, Universität Karlsruhe.

Discussion

The paper was presented by R Lemaître

A Frangi stated that one needs to compare to test results rather than just comparisons with other models. R Lemaître showed some additional test results showing relatively good agreement between model and test results. A Frangi commented that one is designing for connection rather than a single connector. One will need simple equation for design. He asked about rope effect. R Lemaître showed additional information on the subject to be presented in a WCTE paper in Seoul.

R Jockwer stated that there are additional parameters such as gaps. Also there is more information that can be obtained from test results rather than a single point of capacity. R Lemaître said that the gap issue can be handled by the model.

S Winter asked about the basis for the foundation spring properties. R Lemaître said this comes from the load slip curve of the dowel embedment strength tests of different material.

H Blass commented that the model can potentially be used to give information for dowels in multiple shear plane connection.

P Dietsch elaborated on the background of the COST action for this type of work and outlook for the next step.

Formulaic Design Methods for TCC floors

Andrew Smith, Arup Advanced Technology + Research

Prof. Dr.-Ing. habil. Jörg Schänzlin, Institute for timber design, Hochschule Biberach

Prof. Dr. Maurizio Piazza, DICAM- University of Trento

Andrew Lawrence, Arup Advanced Technology and Research

Oliver Bell, Arup Advanced Technology and Research

Keywords: Timber, Concrete, Composites, TCCs, Partial Interaction

1 Introduction

There is currently significant interest in timber-concrete composites (TCCs). They perform well for strength and dynamics, enabling lightweight long-span floors. They are particularly well suited to situations where a timber solution is desired but the spans are too long for fully-timber systems. TCCs consist of one or more timber elements and one or more concrete elements, mechanically connected together. This paper focuses on TCC floors with a concrete upper part (member 1) and a timber lower part (member 2). These are joined with mechanical connectors such as notches, dowels, or glued-in plates.

Although TCCs are relatively simple to construct, they are complex to analyse: concrete and timber both creep but at different rates; concrete also shrinks and cracks; timber swells or shrinks with changes in moisture content; both materials experience thermal expansion / contraction but to different extents; the connectors are at discrete locations and often have non-linear loading characteristics; tests on connectors have only lasted up to 10 years and so no information exists on their longer term behaviour.

Little practical design guidance is currently available, and so a new Technical Specification (TS) is currently being prepared by CEN. While this will give rules for calculating connection strengths and important considerations for both design and construction, it will not give much guidance on member analysis, in-line with other sections of Eurocode. This paper is intended to act as a supplementary reference.

A TCC floor system is generally idealised as two beams connected with a number of springs along their length. One way to analyse this system is to consider it as a vierendeel truss. This is sometimes referred to as the “truss analogy” method. Non-linear spring

models can be used, and the beams can be analysed as complex as is deemed necessary. Some guidance has been published in research, for example *Grosse et al.* (2003).

The main issue with the “truss analogy” method is that can only be solved using finite element software. It is more practical and efficient to have a fast formulaic method which can be programmed into software or carried out by hand. Standard beam theory does not apply to TCC systems, and so an equivalent is required. This can be achieved by smearing the connectors along the interface.

2 Smeared connector approximation

If the connectors are identical, closer than or equal to 5% of the distance between the points of contraflexure, equally spaced all the way along the span, and always remain roughly elastic, then research has shown that the TCC system can be simplified to two beams separated by a smeared linear shear spring of stiffness k (refer *Michelfelder* (2006), *Grosse et al.* (2003), *Niederer* (2008)). This will have units of kN/mm/m (i.e. stiffness per unit length of beam). If all the connectors have linear stiffness K and spacing s , k is calculated as $k = K/s$. This smeared stiffness relates the interface shear force ν to the beam slip u ($\nu = ku$).

It is common for connectors to be concentrated towards the ends of the beam, where the interface shear is higher. Research has suggested that if the outer quarters of the beam have a smeared stiffness $k_{out} = K_{out}/s_{out}$ and the central half of the beam has a smeared stiffness $k_{in} = K_{in}/s_{in}$, or if the smeared stiffness varies linearly from k_{out} at the end to k_{in} at the centre then an approximate equivalent constant shear stiffness can be calculated as $k = 1/(0,75/k_{out} + 0,25/k_{in})$ (based on Clause 8.3.3 of *DIN 1052 Part 1 Engl.* (1988)). This is applicable if $k_{in} \geq 0,25k_{out}$ (Clause 8.3.3 of *DIN 1052 Part 1 Engl.* (1988), Clause B.1.2(1) of *Eurocode 5* (2014)).

3 Formulaic design equations

To design a TCC floor for a given loading, an engineer needs to be able to calculate the stresses in the concrete and timber, the maximum shear stress at the interface, and the deflection. To derive equations for these a set of differential equations are formulated which are then solved for common loading scenarios. Both members are assumed to be elastic, ignoring any cracking of the concrete. This is discussed further in Section 4. Concrete reinforcement is conservatively ignored.

3.1 Derivation of differential equations

The TCC can be broken down into infinitesimal elements as shown in Figure 1. Applying compatibility, equilibrium, and noting that $dN/dx = \nu$ yields the governing differential equation (1), where M_G is the global moment in the TCC section. This can be non-dimensionalised by substituting in $\phi = x/L$ which yields Eq.(2), where $\Omega = kL^2$, α and μ

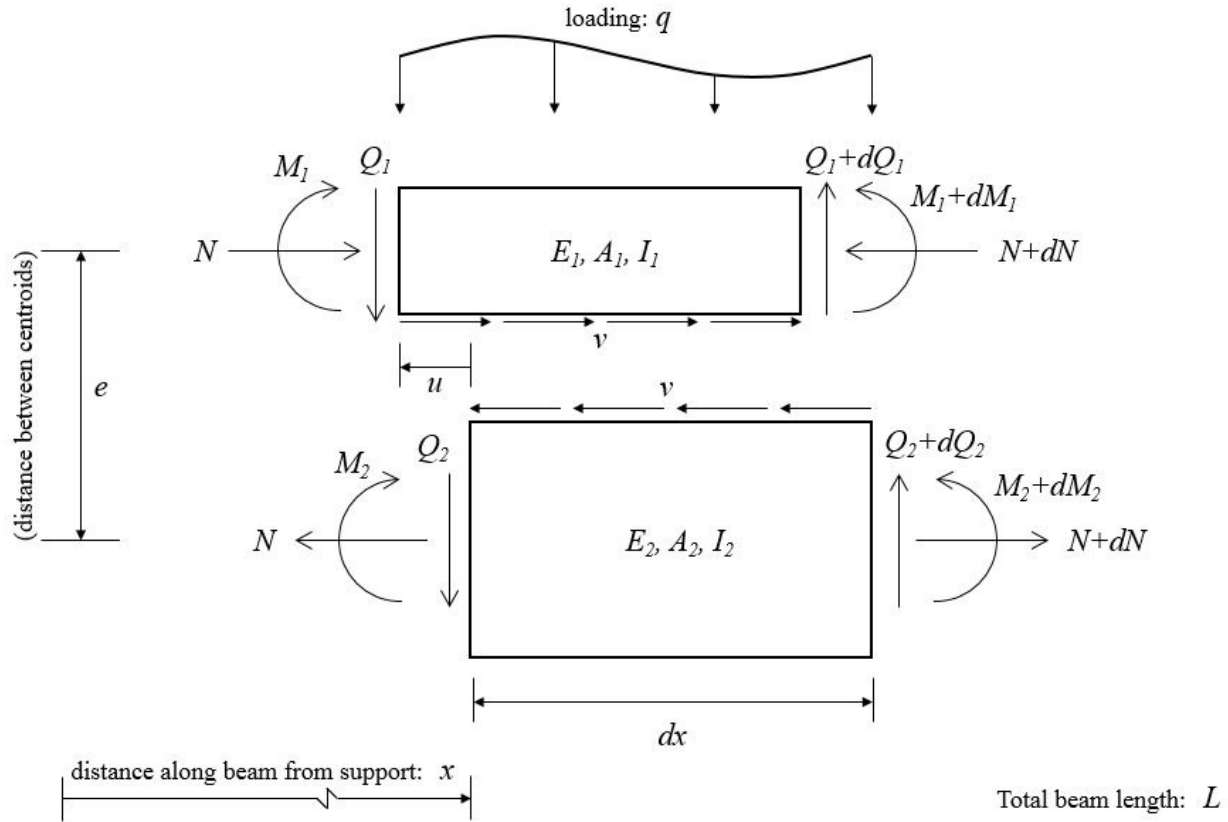


Figure 1. Equilibrium forces applied to an infinitesimal beam element of the TCC system.

are as given in Eqs. (3) and (4), and L is the beam's length. For a given member i , A_i is its cross-sectional area, E_i is its Young's Modulus, and I_i is its second moment of area. The vertical distance between the members' centroids is denoted e .

$$\frac{d^2N}{dx^2} - k \left(\frac{1}{E_1 A_1} + \frac{1}{E_2 A_2} + \frac{e^2}{E_1 I_1 + E_2 I_2} \right) N = -\frac{M_G k e}{E_1 I_1 + E_2 I_2} \quad (1)$$

$$\frac{d^2N}{d\phi^2} - \alpha^2 N = -\mu \frac{M_G}{e} \quad (2)$$

$$\alpha^2 = \left(\frac{1}{E_1 A_1} + \frac{1}{E_2 A_2} + \frac{e^2}{E_1 I_1 + E_2 I_2} \right) \Omega \quad (3)$$

$$\mu = \frac{e^2 \Omega}{E_1 I_1 + E_2 I_2} \quad (4)$$

The beam's curvature κ can be calculated from Eq.(5). This can then be used to calculate the moment in each member ($M_1 = \kappa E_1 I_1$, $M_2 = \kappa E_2 I_2$, sagging positive) which, in combination with N , allow an engineer to calculate the stresses at the top and bottom of each member. The curvature can also be integrated twice to give the beam's deflection

profile w .

$$\kappa = -\frac{d^2w}{dx^2} = \frac{M_G - Ne}{E_1I_1 + E_2I_2} \quad (5)$$

3.2 Solutions to differential equations for a simply supported beam

The majority of TCCs are analysed as simply supported. This is a reasonable approximation for most systems, and indeed mirrors how they tend to be built. Continuous spans are the subject of ongoing research, but they are very difficult to analyse due to non-linear concrete behaviour in the hogging region. Even steel-concrete composites, which have a much more mature design code, are often analysed as simply supported when the slab is actually continuous. In these situations, the new TS will adopt Clause 7.4.1(4) from Eurocode 4 as guidance for minimum reinforcement at hogging locations. As long as this is followed, it is deemed that TCCs can be analysed as simply supported. The differential equations given in Section 3.1 can be solved for basic loading cases (see Section 10). These solutions are completely elastic and so can be superimposed.

3.3 Inclusion of shrinkage, swelling, and thermal effects

Another important aspect of the design of TCCs is allowing for the longitudinal effects of volume-change phenomenon, sometimes referred to as inelastic strains. This includes shrinkage of concrete, expansion / contraction of both timber and concrete due to thermal loads, and shrinkage / swelling of timber due to moisture content variation. If the difference in longitudinal strain between sections at a cross section is denoted $\Delta\epsilon$ (positive for member 1 contracting relative to member 2), then Eqs. (1) and (2) become Eqs. (6) and (7) respectively.

$$\frac{d^2N}{dx^2} - k \left(\frac{1}{E_1A_1} + \frac{1}{E_2A_2} + \frac{e^2}{E_1I_1 + E_2I_2} \right) N = -\frac{M_G ke}{E_1I_1 + E_2I_2} + k\Delta\epsilon \quad (6)$$

$$\frac{d^2N}{d\phi^2} - \alpha^2 N = -\mu \frac{M_G}{e} + \Omega \Delta\epsilon \quad (7)$$

Setting $M_G = 0$ and solving for constant $\Delta\epsilon$ gives the theoretical solution presented in Section 10.6. Once again this is a purely elastic solution, and so it can be superimposed onto the solutions from Section 3.2.

4 Accounting for concrete cracking

All the solutions so far have ignored concrete cracking in tension. If concrete is assumed to have no tensile strength then it can be shown that the depth of the concrete compression block is constant along the beam under sinusoidally distributed loading. This

is also approximately true for uniformly distributed loading. The depth of this compression block, denoted the effective height $h_{1,\text{eff}}$, can be calculated from Eq.(8). The new effective spacing between the centroids then becomes $e_{\text{eff}} = 0,5h_2 + h_1 - 0,5h_{1,\text{eff}}$.

By setting $h_{1,\text{eff}} = h_1$ in Eq.(8) and solving for h_1 , the maximum depth of concrete for it to all remain in compression can be calculated from (14). $h_{1,\text{eff}}$ and e_{eff} can be substituted into Eqs. (1) through (7) and the solutions in Section 10, replacing h_1 and e respectively. A_1 and I_1 also need to be adjusted accordingly based on the effective height.

As a first step in design, Eq.(9) can be used to calculate an initial estimate for an appropriate depth of concrete. The new TS will direct engineers towards Eurocode 4 for calculation of minimum reinforcement which requires engineers to calculate the depth of concrete in tension. Eq.(8) can be used to estimate this depth.

$$h_{1,\text{eff}} = \min \left\{ \frac{-1 + \sqrt{1 + E_1 b_1 \left(\frac{\pi^2}{kL^2} + \frac{1}{E_2 A_2} \right) (2h_1 + h_2)}}{E_1 b_1 \left(\frac{\pi^2}{kL^2} + \frac{1}{E_2 A_2} \right)}, h_1 \right\} \quad (8)$$

$$h_{1,\text{max}} = \sqrt{\frac{h_2}{E_1 b_1 \left(\frac{\pi^2}{kL^2} + \frac{1}{E_2 A_2} \right)}} \quad (9)$$

It is important to note that Eqs. (8) and (9) are only valid for uniformly and sinusoidally distributed loadings, and conservatively ignore any reinforcement. For more complex loading cases, such as with point loads or volume-change effects, the effective depth will vary along the beam. In this case, an iterative approach could be used to find an approximate constant effective depth for use in the solutions from Section 3, or more conservatively the worst case effective depth could be used. It is, however, expected that Eqs. (8) and (9) will be sufficiently accurate for early-stage design.

5 The γ method

5.1 Overview

The majority of TCCs are currently analysed using the so-called γ method provided in Appendix B of *Eurocode 5* (2014) (see *Möhler* (1956) and Lecture B11 of *STEP 1* (1995)), which is a rearrangement of the solution given in Section 10.1. This rearrangement defines a value γ_i which is a measure of the degree of interaction of member i with member 2 ($\gamma_i = 1$ for full interaction and $\gamma_i = 0$ for no interaction). These are used to calculate an effective bending stiffness $(EI)_{\text{ef}}$. The solution in Appendix B of Eurocode 5 is generalised to 3-member systems, and so i can equal 1 or 3. For standard TCC systems, member 3 does not exist and so those parts of the equations can be ignored. As stated in Clause B.1.2 in *Eurocode 5* (2014), the γ method can be used for analysing TCC systems when the loading produces a moment which is roughly sinusoidal. This

means it can be used for uniformly distributed loadings, but not for point loads.

5.2 Inaccuracies in current and past versions of Eurocode 5

It should be noted that there have been some inaccuracies in the γ method solutions provided in Appendix B of current and past versions of *Eurocode 5*, of which three versions have been released to date (July 2018): *EN1995-1-1:2004*, *EN1995-1-1:2004+A1:2008* and *EN1995-1-1:2004+A2:2014*.

In *Eurocode 5* (2004) and *Eurocode 5* (2008), the equation for the maximum shear stress in the timber provided in Clause B.9 was as per Eq.(10). This was corrected in *Eurocode 5* (2014) to Eq.(11), where $h = 0,5h_2 + a_2$ (a_2 as defined in Appendix B of *Eurocode 5* (2014)). However, h should have a maximum value of h_2 which is not mentioned.

$$\tau_{2,\max} = \frac{\gamma_3 E_3 A_3 a_3 - 0,5 E_2 b_2 h_2^2}{b_2 (EI)_{\text{ef}}} V \quad [Do not use] \quad (10)$$

$$\tau_{2,\max} = \frac{\gamma_3 E_3 A_3 a_3 - 0,5 E_2 b_2 h^2}{b_2 (EI)_{\text{ef}}} V \quad (11)$$

In all three versions of *Eurocode 5*, Equation B.6 has been written as shown in Eq.(12). This is only correct if the three sections sit directly on top of each other. For other configurations, such as when there is a zero-strength interlayer (e.g. cracked concrete) or the side-attached I-joist section shown as the second example in Figure B.1 of *Eurocode 5* (2014), this is incorrect. It should instead be modified as per Eq.(13), where e_{12} is the distance between the centroids of members 1 and 2, and e_{23} is the distance between the centroids of members 2 and 3. It is easy to see that Eq.(12) assumes $e_{12} = (h_1 + h_2)/2$ and $e_{23} = (h_2 + h_3)/2$, but this is not always the case.

$$a_2 = \frac{\gamma_1 E_1 A_1 (h_1 + h_2) - \gamma_3 E_3 A_3 (h_2 + h_3)}{2 \sum_{i=1}^{i=3} \gamma_i E_i A_i} \quad (12)$$

$$a_2 = \frac{\gamma_1 E_1 A_1 e_{12} - \gamma_3 E_3 A_3 e_{23}}{\sum_{i=1}^{i=3} \gamma_i E_i A_i} \quad (13)$$

The authors recommend that these equations are corrected in the upcoming version of *Eurocode 5*.

5.3 Extension to include volume-change effects

An extension to the gamma method has been developed by *Schänzlin* (2003) to include volume-change effects, which cause a difference in longitudinal strains between members 1 and 2 as introduced in Section 3.3 (also refer *Schänzlin and Fragiaco* (2007)). The effects of the longitudinal strains are captured by introducing a fictitious uniformly distributed load (UDL) p_{sls} , which is added to the actual UDL q_d . p_{sls} is defined in

Eq.(14), where $C_{p,sls}$ is a scaling coefficient. This coefficient is given by Eq.(15), where γ_1 is member 1's composite coefficient as introduced in Section 5.1, $k_N = \pi^2$, and all other symbols are as defined in Figure 1.

$$p_{sls} = C_{p,sls} \cdot \Delta\epsilon \quad (14)$$

$$C_{p,sls} = k_N \cdot \frac{E_1 A_1 E_2 A_2}{E_1 A_1 + E_2 A_2} \cdot \frac{e \gamma_1}{L^2} \quad (15)$$

The effective bending stiffness $(EI)_{ef}$ from Section 5.1 is modified as per Eq.(16) to give a new effective bending stiffness $(EI)_{ef,sls}$, where $C_{J,sls}$ is the coefficient defined in Eq.(17). The beam's actual mid-span deflection w_{max} can then be calculated from Eq.(18).

$$(EI)_{ef,sls} = C_{J,sls} (EI)_{ef} \quad (16)$$

$$C_{J,sls} = \frac{q_d + p_{sls}}{\frac{E_1 A_1 + E_2 A_2}{\gamma_1 E_1 A_1 + E_2 A_2} \cdot p_{sls} + q_d} \quad (17)$$

$$w_{max} = \frac{5L^4}{384 (EI)_{ef,sls}} (q_d + p_{sls}) \quad (18)$$

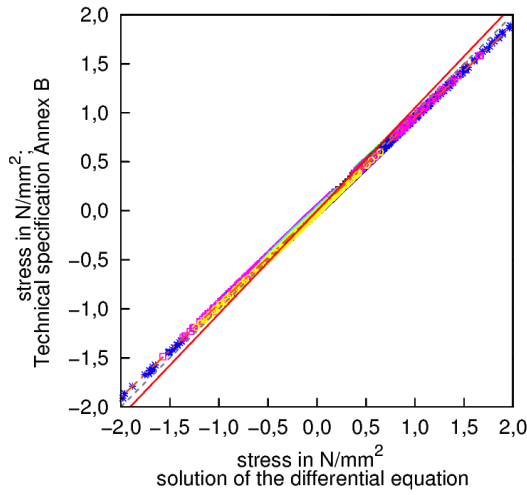
The maximum curvature κ_{max} and the maximum moments in members 1 and 2 ($M_{1,max}$ and $M_{2,max}$) can then be calculated from Eq.(19), where $M_{G,eff,sls}$ is the maximum global moment that would be caused by a total UDL of $(q_d + k_M \cdot p_{sls})$ and $k_M = 0,8$. The maximum axial force N_{max} can be calculated by applying equilibrium at a cross section, giving Eq.(20), where M_G is the global moment caused by q_d only (not including p_{sls}).

$$\kappa_{max} = - \left. \frac{d^2 w}{dx^2} \right|_{max} = \frac{M_{1,max}}{E_1 I_1} = \frac{M_{2,max}}{E_2 I_2} = \frac{M_{G,eff,sls}}{(EI)_{ef,sls}} = \frac{(q_d + k_M \cdot p_{sls}) L^2 / 8}{(EI)_{ef,sls}} \quad (19)$$

$$N_{max} = \frac{M_G - M_{1,max} - M_{2,max}}{e} = \frac{q_d L^2 / 8 - M_{1,max} - M_{2,max}}{e} \quad (20)$$

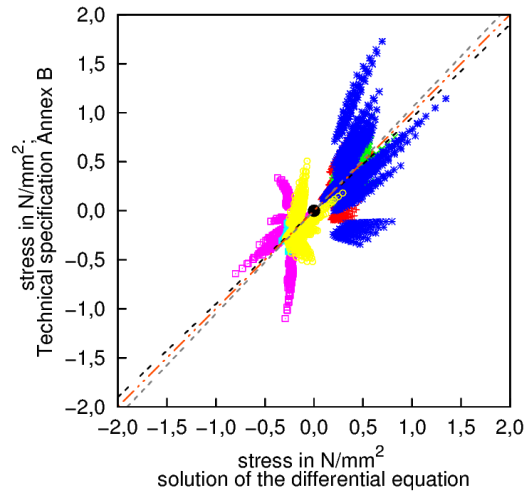
The value of $k_N = \pi^2$ comes from the assumption of sinusoidal loading made in the γ method. Using this value, the calculated p_{sls} gives reasonably accurate predictions for deflection from Eq.(18), but would lead to an over-prediction of maximum curvature κ_{max} if the whole p_{sls} were used. This in turn would lead to an unconservative under-prediction of N . Therefore, the $k_M = 0.8$ factor is introduced. Further information on this will be made available in the *Technical Specification – Background Document*.

The γ method extension was tested by *Fragiacomo and Raggiunti (2018)*. It was found that when $q_d = -p_{sls}$, $C_{J,sls} = 0$. Furthermore, when $p_{sls} = -q_d \cdot \frac{\gamma_1 E_1 A_1 + E_2 A_2}{E_1 A_1 + E_2 A_2}$, it was found that $C_{J,sls} = \infty$. Indeed, $C_{J,sls}$ can take the value of any real number. As a result, the modified effective bending stiffness $(EI)_{ef,sls}$ can vary anywhere from $-\infty \rightarrow +\infty$.



+ $\sigma_{\text{cross-section 2, lower edge}}$
 x $\sigma_{\text{cross-section 2, centroid}}$
 * $\sigma_{\text{cross-section 2, upper edge}}$
 □ $\sigma_{\text{cross-section 1, lower edge}}$
 ■ $\sigma_{\text{cross-section 1, centroid}}$

○ $\sigma_{\text{cross-section 1, upper edge}}$
 - - - 95%
 - - - 100%
 - - - 105%



+ $\sigma_{\text{cross-section 2, lower edge}}$
 x $\sigma_{\text{cross-section 2, centroid}}$
 * $\sigma_{\text{cross-section 2, upper edge}}$
 □ $\sigma_{\text{cross-section 1, lower edge}}$
 ■ $\sigma_{\text{cross-section 1, centroid}}$

○ $\sigma_{\text{cross-section 1, upper edge}}$
 - - - 95%
 - - - 100%
 - - - 105%

(a) Beams within the $C_{J,sls}$ applicability limits show good agreement between the γ method extension and the theoretical solution.

(b) Beams outside the $C_{J,sls}$ applicability limits show poor agreement between the γ method extension and the theoretical solution.

Figure 2. Comparison of stresses in TCC brams calculated using the γ method extension with stresses calculated using the theoretical solution (Dias et al., unpublished).

The main issue arises when $C_{J,sls} = 0$ (and therefore $(EI)_{ef,sls} = 0$), as w_{\max} and κ_{\max} then become infinite. In this case, to calculate w_{\max} , Eq.(17) can be substituted into Eq.(16) and then in turn into Eq.(18), as the $(q_d + p_{sls})$ terms usefully cancel and the result becomes finite. However, this is not true for κ_{\max} .

In order to tackle this issue, the applicability limits for $C_{J,sls}$ given in Eqs. (21) and (22) will be given in the TS. To demonstrate the effectiveness of these limits, a number of theoretical TCC beams were investigated. The maximum stresses were calculated for various combinations of q_d and $\Delta\epsilon$ using the γ method extension and the theoretical solutions given in Section 10. The results for beams within and outside the $C_{J,sls}$ applicability limits are shown in Figures 2a and 2b respectively. As can be seen, the limits successfully discard any beams for which the γ method extension is not applicable. In these cases, the theoretical solutions from Section 10 should be used.

$$0 < C_{J,sls} \quad (21)$$

$$0.9 \leq \frac{C_{J,sls} \cdot \left(q_d + 0,8p_{sls} \frac{E_1A_1 + E_2A_2}{\gamma_1 E_1A_1 + E_2A_2} \right)}{q_d + 0,8p_{sls}} \leq 1.1 \quad (22)$$

6 Material Properties

The solutions presented in Section 3 are completely elastic, and can therefore be superimposed. The elastic model used for timber is reasonable because it is an elastic-brittle

material, and concrete in TCCs also generally remains elastic in compression. However, concrete behaves non-linearly in tension. Section 4 presented a modification which can be applied to the solutions in Section 10 to account for this.

Timber and concrete experience long-term effects. Both creep, which is often allowed for using long-term effective E values. These can be used in the equations from Section 3 to predict long-term effects, but it is important to note that changing the material properties means that the solutions are no longer completely elastic. The solutions for stress and deflection can be superimposed, but the loadings need to be split up according to duration and the effects calculated accordingly.

In order to account for the influences of composite action and relaxation on the effective creep coefficients for timber, concrete and the connection, modification factors will be recommended in the TS based on work by *Kupfer and Kirmair (1987)*, *Kreuzinger (1994)* and *Schänzlin (2003)*.

The strength of timber is also time dependent, and so stresses need to be checked using the standard k_{mod} values given in the most up to date version of *Eurocode 5*.

7 Connection Properties

TCC connectors are generally non-linear, and so it is common practice to assume one spring stiffness for serviceability limit states (K_{ser}) and another at ultimate limit states (K_u). For dowel-type fasteners, glued-in rods, and notched connectors, the new TS will lay out rules for estimating K_{ser} and K_u , along with their characteristic strength $F_{v,Rk}$. For other connection topologies, or for more accurate values, the TS will include a testing specification to determine K_{ser} , K_u , and $F_{v,Rk}$.

Load duration also affects the connection stiffness, but there is little data on the long-term properties of connectors. The TS will therefore recommend calculating an effective k_{def}' value for the connector with Eq.(23), based on the timber's k_{def} value. This is used to modify the connection stiffnesses K_{ser} and K_u . The TS will recommend that $F_{v,Rk}$ should be modified with an effective k_{mod}' value calculated from Eq.(24), where k_{mod} is the timber's modification factor and α_{cc} is the coefficient from *Eurocode 2 (2014)* to take into account long-term effects on the compressive strength.

$$k_{def}' = 2k_{def} \quad (23)$$

$$k_{mod}' = \sqrt{\alpha_{cc}k_{mod}} \quad (24)$$

8 Critical points in time for design

During design, reinforced concrete structures will in general be checked for a short-term loading case with short-term material properties (normally governs for strength

design) and a long-term loading case with long-term properties (normally governs for serviceability design). In contrast, timber structures may need to be checked at many more points in time because timber both creeps and changes strength depending on load duration. For TCCs, the TS will recommend checking for a short-term loading case (t_0) and a long-term loading case (t_∞). Due to the different creep rates of timber and concrete and the load duration effects on timber strength, the new TS will recommend that an intermediate point in time should also be checked (t_{3-7yr}). However the TS will recommend that this intermediate point in time can be ignored if the ULS utilisations at t_0 and t_∞ are less than 0,8.

It is worth noting that the value of $h_{1,eff}$ calculated as described in Section 4 will change for different combinations of effective values of E_1 , E_2 and k . If loads of different durations are being superimposed, this can conservatively be allowed for by using the minimum $h_{1,eff}$ value calculated at t_0 , t_{3-7yr} and t_∞ for all points in time.

9 Conclusion

This paper has not intended to document all aspects of TCC design, and it is the responsibility of the engineer to adhere to all the clauses in the TS once it is released. However, it is hoped that the standard solutions presented will be useful as a reference for engineers analysing these systems. When using these it is important to always be aware of the time dependencies and non-linear effects of the materials and connections involved.

In order to design a TCC, it is suggested that an engineer first produce a rough initial design using geometry, Eq.(9), and span to depth ratios. Then, more detailed checks could be carried out either using the solutions in Section 3.2 or the γ method depending on the engineer's preference, allowing for concrete cracking as per Section 4, allowing for material properties as per Section 6, allowing for connection properties as per Section 7, and checking the structure at the points in time specified in Section 8.

10 Theoretical Solutions

This section lists solutions to differential equations (2) and (7) for simply supported beams under standard load cases. Symbols are as defined in Section 3, and reference should be made to Figure 1. Solutions are given for loading (q), global moment (M_G), axial force (N), interface shear force (ν) and deflection (w) as a function of the non-dimensionalised distance along the beam ($0 \leq \phi \leq 1$). Some solutions use the following shorthand: $\bar{\phi} = 1 - \phi$, $\bar{\beta} = 1 - \beta$

10.1 Sinusoidally distributed loading

$$q = p_0 \sin(\pi\phi) \quad \left| \quad M_G = p_0 \frac{L^2}{\pi^2} \sin(\pi\phi) \right.$$

$$N = p_0 \frac{L^2}{\pi^2} \frac{\mu}{e(\pi^2 + \alpha^2)} \sin(\pi\phi) = p_0 \frac{L^2}{\pi^2} \frac{\mu}{e\alpha^2} \left(1 - \frac{\pi^2}{\pi^2 + \alpha^2} \right) \sin(\pi\phi)$$

$$\nu = p_0 \frac{L}{\pi} \frac{\mu}{e\alpha^2} \left(1 - \frac{\pi^2}{\pi^2 + \alpha^2} \right) \cos(\pi\phi)$$

$$w = \frac{p_0}{E_1 I_1 + E_2 I_2} \frac{L^4}{\pi^4} \left(1 - \frac{\mu}{\pi^2 + \alpha^2} \right) \sin(\pi\phi)$$

10.2 Uniformly distributed loading

$$q = p \quad \left| \quad M_G = pL^2 \frac{\phi\bar{\phi}}{2} \right.$$

$$N = pL^2 \frac{\mu}{e\alpha^2} \left(\frac{1}{\alpha^2} \left[\cosh(\alpha\phi) - \tanh\left(\frac{\alpha}{2}\right) \sinh(\alpha\phi) - 1 \right] + \frac{\phi\bar{\phi}}{2} \right)$$

$$\nu = pL \frac{\mu}{e\alpha^2} \left(\frac{1}{\alpha} \left[\sinh(\alpha\phi) - \tanh\left(\frac{\alpha}{2}\right) \cosh(\alpha\phi) \right] - \phi + \frac{1}{2} \right)$$

$$w = \frac{p}{E_1 I_1 + E_2 I_2} L^4 \left(\frac{\mu}{\alpha^2} \left[\frac{1}{\alpha^4} \left(\cosh(\alpha\phi) - \tanh\left(\frac{\alpha}{2}\right) \sinh(\alpha\phi) - 1 \right) - \frac{\phi^4}{24} + \frac{\phi^3}{12} - \frac{\phi^2}{2\alpha^2} \right. \right. \\ \left. \left. - \left(\frac{1}{24} - \frac{1}{2\alpha^2} \right) \phi \right] + \frac{\phi^4}{24} - \frac{\phi^3}{12} + \frac{\phi}{24} \right)$$

10.3 Central point load

The following solutions are valid for $0 \leq \phi \leq 0,5$. The solution will be symmetric.

q : a point load P at the centre of the beam

$$M_G = \frac{PL\phi}{2}$$

$$N = \frac{PL}{2} \frac{\mu}{e\alpha^2} \left(\phi - \frac{\sinh(\alpha\phi)}{\alpha \cosh(\frac{\alpha}{2})} \right)$$

$$\nu = \frac{P}{2} \frac{\mu}{e\alpha^2} \left(1 - \frac{\cosh(\alpha\phi)}{\cosh(\frac{\alpha}{2})} \right)$$

$$w = \frac{P}{E_1 I_1 + E_2 I_2} \frac{L^3}{2} \left(\frac{\mu}{\alpha^2} \left[\frac{\phi^3}{6} + \left(\frac{1}{\alpha^2} - \frac{1}{8} \right) \phi - \frac{\sinh(\alpha\phi)}{\alpha^3 \cosh(\frac{\alpha}{2})} \right] - \frac{\phi^3}{6} + \frac{\phi}{8} \right)$$

10.4 Point load at an arbitrary location

q : a point load P at a position $x = \beta L$ along the beam.

$$M_G = \begin{cases} P\bar{\beta}\phi L & 0 \leq \phi \leq \beta \\ P\beta\bar{\phi} L & \beta < \phi \leq 1 \end{cases}$$

$$N = PL \frac{\mu}{e\alpha^2} \begin{cases} \bar{\beta}\phi - \frac{\sinh(\alpha\bar{\beta})}{\alpha \sinh(\alpha)} \sinh(\alpha\phi) & 0 \leq \phi \leq \beta \\ \beta\bar{\phi} - \frac{\sinh(\alpha\beta)}{\alpha \sinh(\alpha)} \sinh(\alpha\bar{\phi}) & \beta < \phi \leq 1 \end{cases}$$

$$\nu = P \frac{\mu}{e\alpha^2} \begin{cases} \bar{\beta} - \frac{\sinh(\alpha\bar{\beta})}{\sinh(\alpha)} \cosh(\alpha\phi) & 0 \leq \phi \leq \beta \\ -\beta + \frac{\sinh(\alpha\beta)}{\sinh(\alpha)} \cosh(\alpha\bar{\phi}) & \beta < \phi \leq 1 \end{cases}$$

$$w = \frac{PL^3}{E_1 I_1 + E_2 I_2} \begin{cases} \left[\frac{\mu}{\alpha^2} \left(\frac{\bar{\beta}\phi^3}{6} + \left[\frac{\bar{\beta}}{\alpha^2} - \frac{\beta\bar{\beta}(1+\bar{\beta})}{6} \right] \phi - \frac{\sinh(\alpha\bar{\beta})}{\alpha^3 \sinh(\alpha)} \sinh(\alpha\phi) \right) \right. \\ \left. - \frac{\bar{\beta}\phi^3}{6} + \frac{\beta\bar{\beta}(1+\bar{\beta})}{6} \phi \right] & 0 \leq \phi \leq \beta \\ \left[\frac{\mu}{\alpha^2} \left(\frac{\beta\bar{\phi}^3}{6} + \left[\frac{\beta}{\alpha^2} - \frac{\beta\bar{\beta}(1+\beta)}{6} \right] \bar{\phi} - \frac{\sinh(\alpha\beta)}{\alpha^3 \sinh(\alpha)} \sinh(\alpha\bar{\phi}) \right) \right. \\ \left. - \frac{\beta\bar{\phi}^3}{6} + \frac{\beta\bar{\beta}(1+\beta)}{6} \bar{\phi} \right] & \beta < \phi \leq 1 \end{cases}$$

10.5 Symmetric four point bending

The following solutions are valid for $0 \leq \phi \leq 0.5$. The solution will be symmetric.

q : two point loads P at positions $x = \beta L$ and $x = (1 - \beta)L$ along the beam.

$$M_G = \begin{cases} P\phi L & 0 \leq \phi \leq \beta \\ P\beta L & \beta < \phi \leq \frac{1}{2} \end{cases}$$

$$N = PL \frac{\mu}{e\alpha^2} \begin{cases} \phi - \frac{\sinh(\alpha\beta) + \sinh(\alpha\bar{\beta})}{\alpha \sinh(\alpha)} \sinh(\alpha\phi) & 0 \leq \phi \leq \beta \\ \beta - \frac{\sinh(\alpha\phi) + \sinh(\alpha\bar{\phi})}{\alpha \sinh(\alpha)} \sinh(\alpha\beta) & \beta < \phi \leq \frac{1}{2} \end{cases}$$

$$\nu = P \frac{\mu}{e\alpha^2} \begin{cases} 1 - \frac{\sinh(\alpha\beta) + \sinh(\alpha\bar{\beta})}{\sinh(\alpha)} \cosh(\alpha\phi) & 0 \leq \phi \leq \beta \\ \frac{\cosh(\alpha\bar{\phi}) - \cosh(\alpha\phi)}{\sinh(\alpha)} \sinh(\alpha\beta) & \beta < \phi \leq \frac{1}{2} \end{cases}$$

$$\text{For } 0 \leq \phi \leq \beta: w = \frac{PL^3}{E_1 I_1 + E_2 I_2} \left(\frac{\mu}{\alpha^2} \left[\frac{\phi^3}{6} + \left(\frac{1}{\alpha^2} - \frac{\beta\bar{\beta}}{2} \right) \phi - \frac{\sinh(\alpha\beta) + \sinh(\alpha\bar{\beta})}{\alpha^3 \sinh(\alpha)} \sinh(\alpha\phi) \right] - \frac{\phi^3}{6} + \frac{\beta\bar{\beta}}{2} \phi \right)$$

$$\text{For } \beta \leq \phi \leq 0,5: w = \frac{PL^3}{E_1 I_1 + E_2 I_2} \left(\frac{\mu}{\alpha^2} \left[\frac{\beta(\phi^3 + \bar{\phi}^3)}{6} + \frac{\beta}{\alpha^2} - \frac{\beta\bar{\beta}(1 + \beta)}{6} - \frac{\sinh(\alpha\phi) + \sinh(\alpha\bar{\phi})}{\alpha^3 \sinh(\alpha)} \sinh(\alpha\beta) \right] - \frac{\beta(\phi^3 + \bar{\phi}^3)}{6} + \frac{\beta\bar{\beta}(1 + \beta)}{6} \right)$$

10.6 Volume change effects

$\Delta\epsilon > 0$ for cases where the concrete contracts relative to the timber

$$q = 0 \quad \bigg| \quad M_G = 0$$

$$N = \frac{\Omega\Delta\epsilon}{\alpha^2} \left(\frac{\sinh(\alpha\phi) + \sinh(\alpha\bar{\phi})}{\sinh(\alpha)} - 1 \right)$$

$$\nu = \frac{\Omega\Delta\epsilon}{\alpha L} \left(\frac{\cosh(\alpha\phi) - \cosh(\alpha\bar{\phi})}{\sinh(\alpha)} \right)$$

$$w = \frac{\Omega L^2 e \Delta\epsilon}{\alpha^2 (E_1 I_1 + E_2 I_2)} \left(\frac{1}{\alpha^2} \left[\frac{\sinh(\alpha\phi) + \sinh(\alpha\bar{\phi})}{\sinh(\alpha)} - 1 \right] + \frac{\phi\bar{\phi}}{2} \right)$$

11 References

- Dias, A., M. Fragiaco, R. Harris, P. Kuklík, V. Rajčić, and J. Schänzlin (unpublished). *Eurocode 5: Structural design of timber-concrete composite structures – common rules and rules for buildings*. Technical Specification – Background Document.
- DIN 1052 Part 1 Engl. (1988). *Structural Use of Timber*. DIN 1052-1:1988 (English Translation). Deutsches Institut für Normung.
- Eurocode 2 (2014). *Design of concrete structures – Part 1-1: General rules and rules for buildings*. EN 1992-1-1:2004+A1:2014. Brussels, Belgium: European Committee for Standardization.
- Eurocode 5 (2004). *Design of timber structures – Part 1-1: General rules and rules for buildings*. EN 1995-1-1:2004. Brussels, Belgium: European Committee for Standardization.
- (2008). *Design of timber structures – Part 1-1: General rules and rules for buildings*. EN 1995-1-1:2004+A1:2008. Brussels, Belgium: European Committee for Standardization.
 - (2014). *Design of timber structures – Part 1-1: General rules and rules for buildings*. EN 1995-1-1:2004+A2:2014. Brussels, Belgium: European Committee for Standardization.
- Grosse, M., R. Hartnack, St. Lehmann, and K. Rautenstrauch (2003). “Modellierung von diskontinuierlich verbundenen Holz-Beton-Verbundkonstruktionen / Teil 1: Kurzzeittragverhalten”. In: *Bautechnik* 80.8, pp. 534–541.
- Kreuzinger, H. (1994). *Verbundkonstruktionen Holz / Beton*.
- Kupfer, H. and H. Kirmair (1987). “Verformungsmoduln zur Berechnung statisch unbestimmter Systeme aus zwei Komponenten mit unterschiedlichen Kriechzahlen”. In: *Bauingenieur* 62, pp. 371–377.
- Michelfelder, B. (2006). *Trag- und Verformungsverhalten von Kernen bei Brettstapel-Beton-Verbunddecken*. Dissertation, Universität Stuttgart, Institut für Konstruktion und Entwurf.
- Möhler, K. (1956). *Über das Tragverhalten von Biegeträgern und Druckstäben mit zusammengesetztem Querschnitt und nachgiebigen Verbindungsmitteln*.
- Niederer, A. (2008). “Grenzen der Anwendung des γ -Verfahrens”. In: *Bachelor-thesis, HTWG Konstanz*.
- Schänzlin, J. (2003). “Zum Langzeitverhalten von Brettstapel-Beton-Verbunddecken”. PhD thesis. Institut für Konstruktion und Entwurf, Universität Stuttgart.
- Schänzlin, J. and M. Fragiaco (Aug. 2007). *Extension of EC5 annex B formulas for the design of timber-concrete composite structures*. Bled, Slovenia: Meeting forty of the Working Commission W18-Timber Structures, CIB, International Council for Research and Innovation, no. CIB-W18/40-10-1, 2007.
- STEP 1 (1995). *Timber Engineering: Basis of design, material properties, structural components and joints*.

Discussion

The paper was presented by A Smith

A Frangi suggested that more simplification should be considered for technical specification. The suggested model is too complicated for technical specification even though it is broader in scope compared to the gamma approach. The simple gamma approach should be extended and reformulated for cracked concrete considerations. A Smith responded that issues related to the complexities in the proposed method may be important for design consideration.

H Blass commented that inclined screws rely on withdrawal capacity from concrete which need to be tested with the cracked concrete case.

R Jockwer suggested that sensitivity studies should be considered to reevaluate the impact of some of the parameters on design. A Smith responded that such sensitivities studies may have already be initiated.

R Harris commented that there were much discussions in past years on this topic. Balance between simple code provisions versus more generalized approach is a topic of discussion. He suggested the interested parties should form a group to look in this issue.

A Frangi, I Abeysekera and A Smith further discussed the need for balance between simplification in design and a more generalized approach to cover more cases.

Adaptation of Eurocode 5 standard to French hardwoods - Proposal of new hygroscopic equilibrium charts

Varnier Maximin, University of Limoges, GC2D, EA 3178, F-19300 Egletons, France

Sauvat Nicolas, University of Limoges, GC2D, EA 3178, F-19300 Egletons, France

Montero Cedric, Laboratoire de Mécanique et Génie Civil (LMGC), Univ. Montpellier, CNRS, F-34172 Montpellier, France

Dubois Frédéric, University of Limoges, GC2D, EA 3178, F-19300 Egletons, France

Gril Joseph, Clermont Auvergne University, UMR 6602, F-63170 Aubière, France

Keywords: heat and mass transfer, softwood and hardwood, hygroscopic equilibrium, Eurocode 5 application, Experimental approaches, Modelling aspects

1 Introduction

As a hygroscopic material, wood behaviour is dependent on its surrounding climatic conditions. To describe moisture content evolutions in timber structure elements it is essential to predict phenomena related to drying process, mechanical behaviour prediction, cracks, and also risk of fungal attacks. Several studies have been carried out to highlight the influence of humidity and temperature on equilibrium moisture content of wood, *Siau (1994)*, *Langmuir (1918)*, *Dent (1980)*, *Merakeb et al. (2009)*. Other studies have been focused on the influence of temperature on hygroscopic equilibrium, *Keylwerth (1964)*, *Perré & May (2001)*. But, these results were mostly obtained on softwoods, and especially for drying applications. Thus, only one equilibrium hygroscopic chart is proposed in National Annexes of Eurocode5. In this work, the specificity of species, either softwood or hardwood, is considered to adapt equilibrium charts to more realistic conditions including outdoor conditions. An analysis of sorption hysteresis is presented leading to the distinction between hardwoods and softwoods. Temperature influence is developed for every sorption property.

The main contribution of this work is the introduction of temperature variations in experimental and modelling protocols. Under these conditions, all usual characterization

approaches had to be corrected. Furthermore, since experimental tests must be conducted at variable temperatures, a numerical model had to be implemented integrating both the hygroscopic equilibrium and the diffusion process.

It's for this reason that the paper begins with a presentation of the numerical model implemented in the Castem finite element platform. Model takes into account the temperature dependence on a nonlinear mass transfer process by introducing the notion of mass buffer variation.

The second section deals with experimental approach. It presents the samples and the experimental condition to obtain diffusion kinetics in variable environment for soft-wood and hardwood species. The authors have completed their experimental results with bibliographic references and with the Tropix database, *Paradis et al. (2015)*. The coupling between experimental measurements and the numerical model allows a performant identification of parameters by separating diffusion process and hygroscopic equilibrium properties.

In the last part, it's proposed new specific and more accurate interactive charts to control the moisture content path in wood material for different applications such as the timber structures design support or the control of industrial drying conditions. This part is completed by discussions between the standard approach proposed by Euro-code 5 and the necessity to adapt usual hygroscopic equilibrium curves at realistic service conditions and other species like hardwood for instance.

2 Hygroscopic model

Under external climates, timber elements are subject to heat and mass transfer process in relation with ambient temperature (T) and relative humidity (Rh) changes. In literature, this moisture content equilibrium w is represented thru sorption isotherms which are include in the Fick's law as the buffer moisture content $\frac{\partial w}{\partial Rh}$:

$$\left(\rho_{anh} \cdot \frac{\partial w}{\partial Rh} \right) \cdot \frac{\partial Rh}{\partial t} = \vec{\nabla} \left(\delta^* \cdot p_{vs} \cdot \vec{\nabla} Rh \right) + \vec{\nabla} \left(\delta \cdot Rh \cdot \vec{\nabla} p_{vs} \right) \quad (1)$$

In which ρ_{anh} is the anhydrous density, p_{vs} the saturated vapour pressure, δ^* the apparent permeability *Kulasinski et al. (2015)*. As shown by *Stamm (1964)*, δ^* can take the following temperature dependence form:

$$\delta^* = \delta_o \cdot \exp \left(-\frac{E_a}{R \cdot T} \right) \quad (2)$$

Where δ_o designates a reference value, R is the so known perfect gas constant. E_a is the activation energy also depending to the temperature:

$$E_a = H_s - (C_{pv} \cdot T) \quad (3)$$

C_{pv} is the calorific capacity. H_s is the vapour latent heat defined by the difference between its free water value L and the latent heat dissipated during the fixation of bounded water ΔH_s such as, *Merakeb et al. (2006)*:

$$H_s = L - \Delta H_s \text{ with } \Delta H_s = A \cdot \ln\left(\frac{w}{w_s}\right) \quad (4)$$

A is a constant which can characterize the material anatomy. w_s is the saturation value of w corresponding to the moisture content equilibrium reached to 100%HR in accordance with the hygroscopic equilibrium approach.

2.1 Hygroscopic equilibrium

Usually, the hygroscopic equilibrium is approached by using sorption isotherm protocol, *Eurocode 5 (2004)*, *AFNOR (2010)*, allowing to track the equilibrium moisture content vs Relative humidity in an isothermal desiccator. Because the hygroscopic equilibrium is not appropriated for constant temperatures, our approach needs to be generalized for any temperature. Literature proposes some phenomenological models, *Dent (1980)*, *Stamn (1964)*. Temperature interaction becoming necessary, let us consider a thermodynamic approach based on Merakeb's model (2006) associated to the bounded water interaction with material. Model is based on another interpretation of the vapour latent heat, such as:

$$\Delta H_s = R \cdot T^2 \cdot \frac{\partial \ln(Rh)}{\partial T} \quad (5)$$

By taking into account expression (4), the equation (5) can be rewritten as follow:

$$\ln\left(\frac{w}{w_s}\right) = \phi_i \cdot \ln(Rh) \cdot \exp(\alpha_i \cdot Rh) \quad (6)$$

ϕ_i and α_i designate two thermodynamic parameters easily characterizable. The hysteresis phenomena is reproduced by using two sets of parameters for adsorption ($i = a$) and desorption ($i = d$). Figure 1 shows a good model fitting for Douglas fir at 23°C.

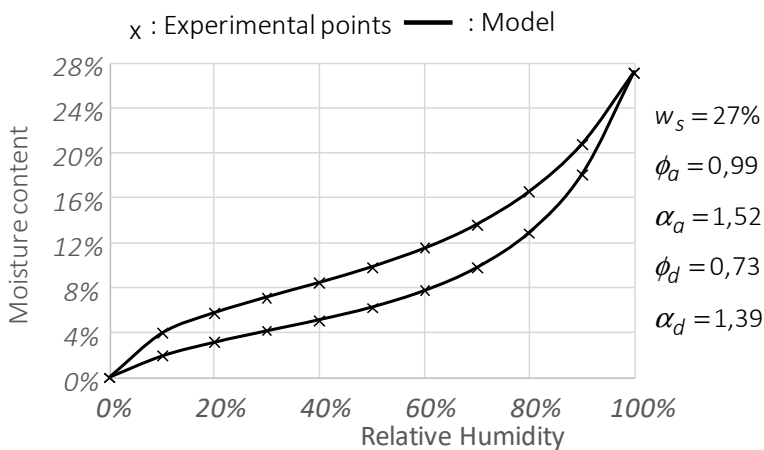


Figure 1. Hygroscopic equilibrium, experimental vs model for Douglas fir.

As proposed by *Frandsen (2007)*, the temperature mainly influences the saturation moisture content w_s . According the Le Chatelier's principle, its temperature dependence can be described by the following equation:

$$w_s(T) = \left(w_s^0 + \frac{C_{anh}}{C_{pv}} \right) \cdot \exp \left(-\frac{C_{pv}}{L} \cdot (T - 273) \right) - \frac{C_{anh}}{C_{pv}} \quad (T \text{ given in K}) \quad (7)$$

w_s^0 is the saturated moisture content at the temperature 0°C. C_{anh} is the anhydrous thermal capacity. In a usual field of use, the expression (7) can be compared to the Merakeb's model or the Eurocode 5 abacus, as shown in Figure 2. Thermodynamic parameters are bellow specified:

$$L = 2500 \text{ kJ} \cdot \text{kg}^{-1}, \quad C_{pv} = 4180 \text{ J} \cdot \text{kg}^{-1} \cdot \text{K}^{-1}, \quad C_{anh} = 1160 \text{ J} \cdot \text{kg}^{-1} \cdot \text{K}^{-1} \quad (8)$$

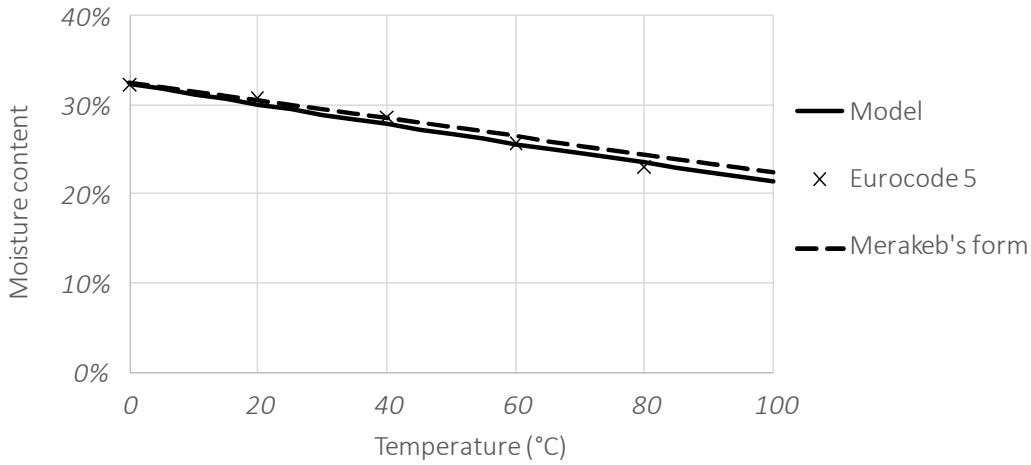


Figure 2. Saturated moisture content versus temperature.

2.2 Partial isotherm

In order to calculate the moisture content buffer, in accordance with a real climatic climate, the model needs to taking into account the partial isotherm properties ($\xi = \frac{\partial w}{\partial Rh}$). Let us consider the approach proposed by *Kulasinki et al. (2015)* which proposes two distinct formulations according to adsorption and desorption kinetics, ξ_d and ξ_a , respectively.

$$\xi_d = \frac{(w_i - w_a)^\beta \cdot \bar{\xi}_d + D \cdot (w_d - w_i)^\beta \cdot \bar{\xi}_a}{(w_d - w_a)^\beta} \quad (9)$$

$$\xi_a = \frac{A \cdot (w_i - w_a)^\beta \cdot \bar{\xi}_d + (w_d - w_i)^\beta \cdot \bar{\xi}_a}{(w_d - w_a)^\beta} \quad (10)$$

According to an incremental formulation, w_i designates the last value of moisture content. w_a and w_d designate the equivalent moisture content on the hygroscopic equilibrium curve, respectively. $\bar{\xi}_d$ and $\bar{\xi}_a$ are the moisture content buffer on the same hygroscopic equilibrium. For instance, about partial isotherm tests, the Figure 3 shows a good correspondence between model and experimental measures.

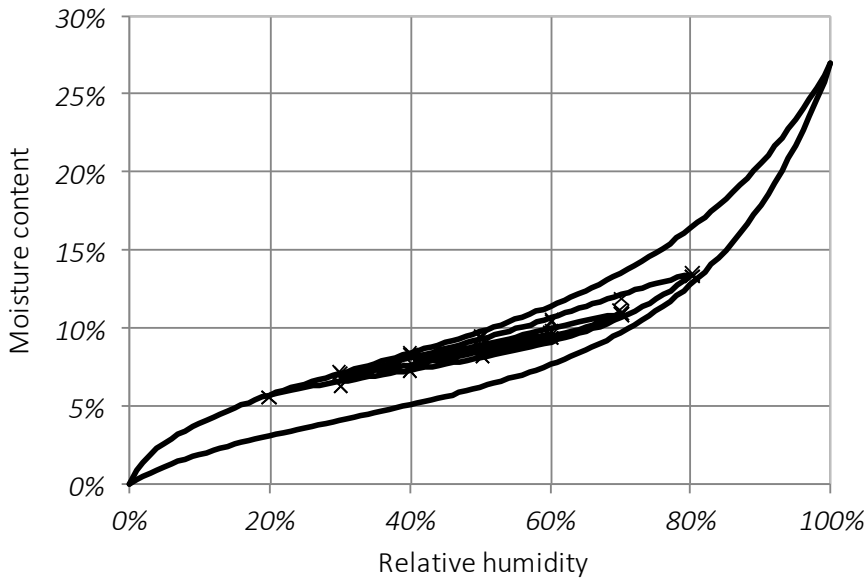


Figure 3. Partial isotherms, model vs experimentation.

3 Data base construction

3.1 Material and methods

Because hygroscopic equilibrium curves must be constructed as a function of temperature, the experimental characterization protocol must consider exposure to varying humidity and temperature. Two possibilities are offered. The first one is to gather equilibrium data available in literature. In this study, we have opted for the Tropic data base mixing softwood and hardwood families. A second way is to expose samples to a real climate. Under these conditions, we opt for a measurement of moisture content variations by weighing wood samples, Figure 4. Because the exposure conditions involve moisture exchange between wood samples and the environment, through a mass transfer process, we have implemented the previously developed model into an optimization algorithm which separates the diffusion parameters and the properties of hygroscopic equilibrium.

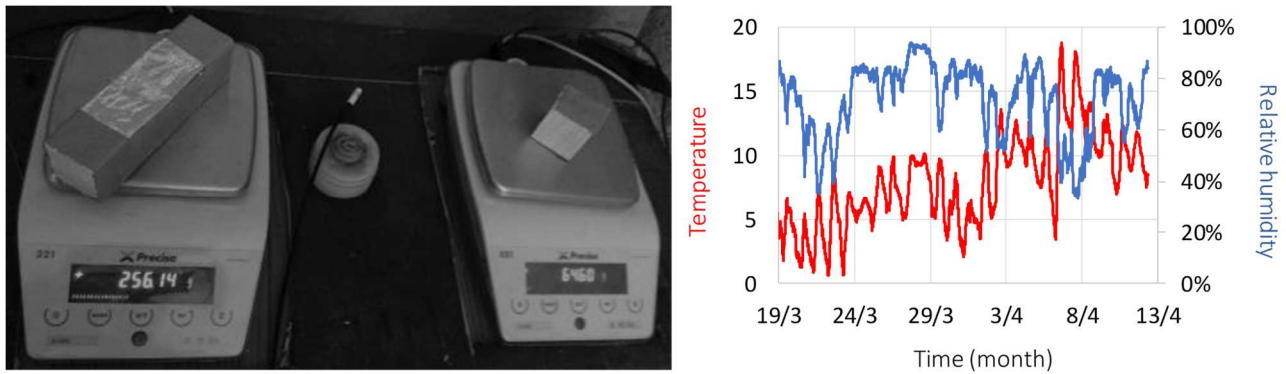


Figure 4. Sample exposition in real climate.

In this experimental protocol, some species have been tested such as Douglas fir, Oak, Beech and poplar. Thanks to the one-month optimization process for Douglas fir, the model fit good, figure 5.

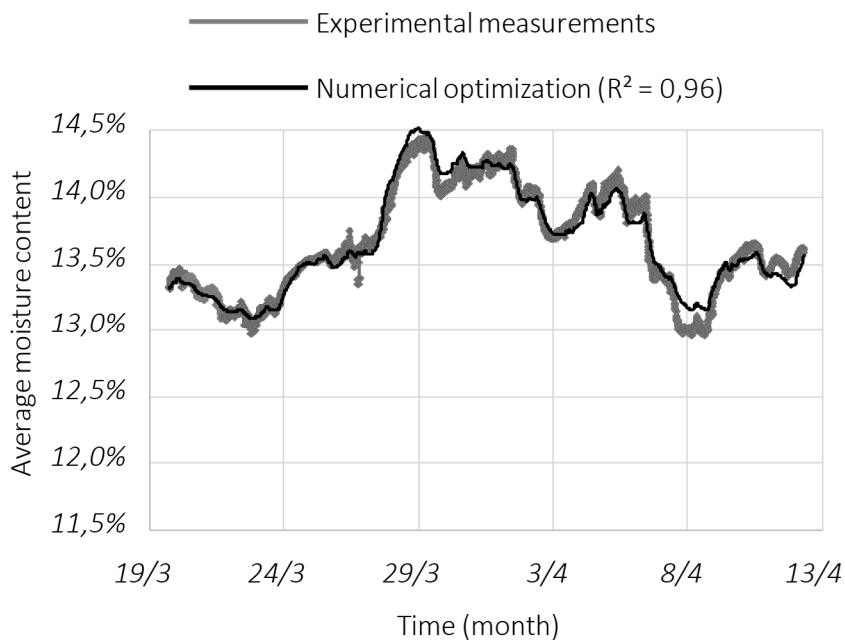


Figure 5. Results of the optimization process (Douglas fir).

3.2 Data processing

The inversion method algorithm allows tracking hygroscopic equilibrium curves for a chosen temperature, Figure 6. This graph gathers the imported data from experimental characterization and Tropix's data base, *Paradis et al. (2015)*.

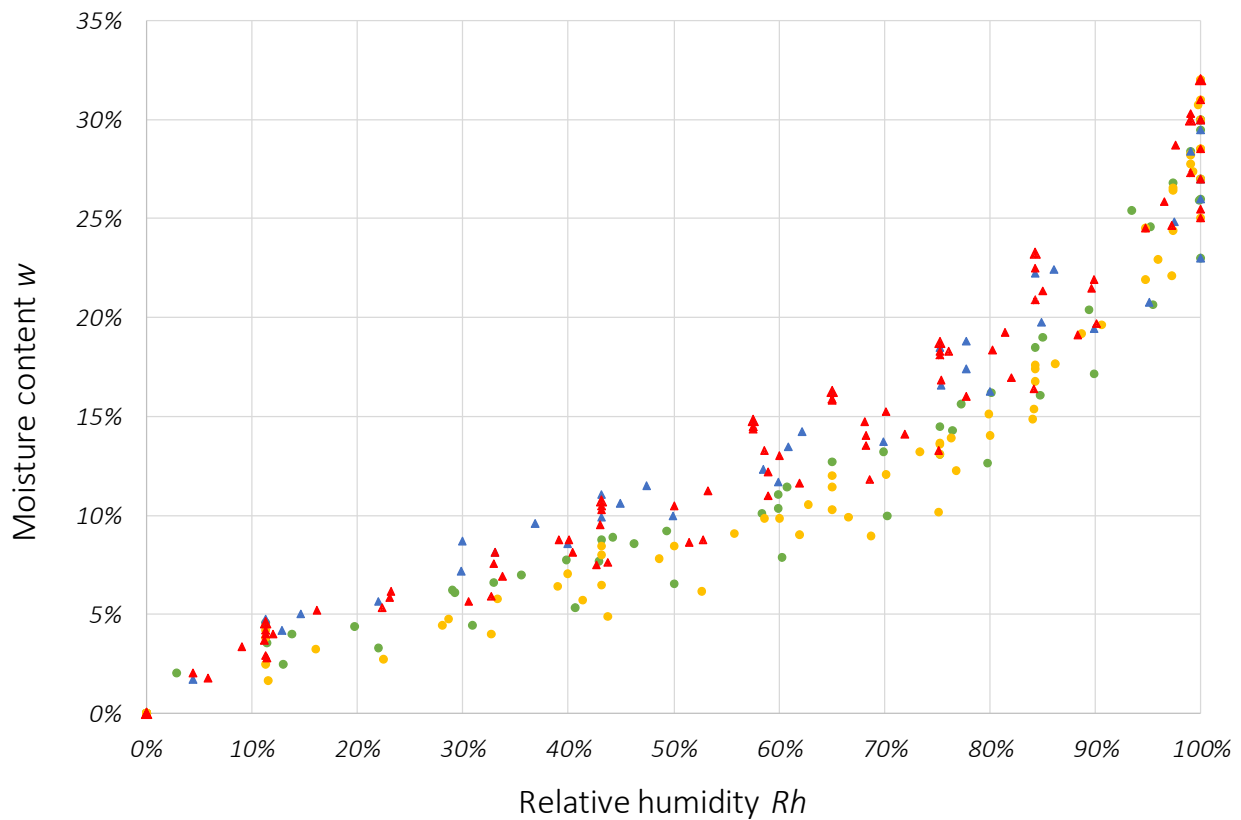


Figure 6. Curves of hygroscopic equilibrium.

By application of Le Chatelier principle, we have shown that the temperature more particularly influences saturated value of moisture content w_s , let us dimensionless hygroscopic equilibrium as shown in Figure 7 ($\frac{w}{w_s}$) to calculate the saturation ratio.

Moreover, the fitting of experimental curves with the expression (6) allows to separate two specific families, hardwood and softwood, respectively with a good correlation for adsorption and desorption phases. All properties are notified in the table 1.

Table 1. Hygroscopic equilibrium parameters for softwood and hardwood.

	Softwood	Hardwood
ϕ_a	0,82	0,85
ϕ_d	0,76	0,85
α_a	1,44	1,65
α_d	0,99	1,1

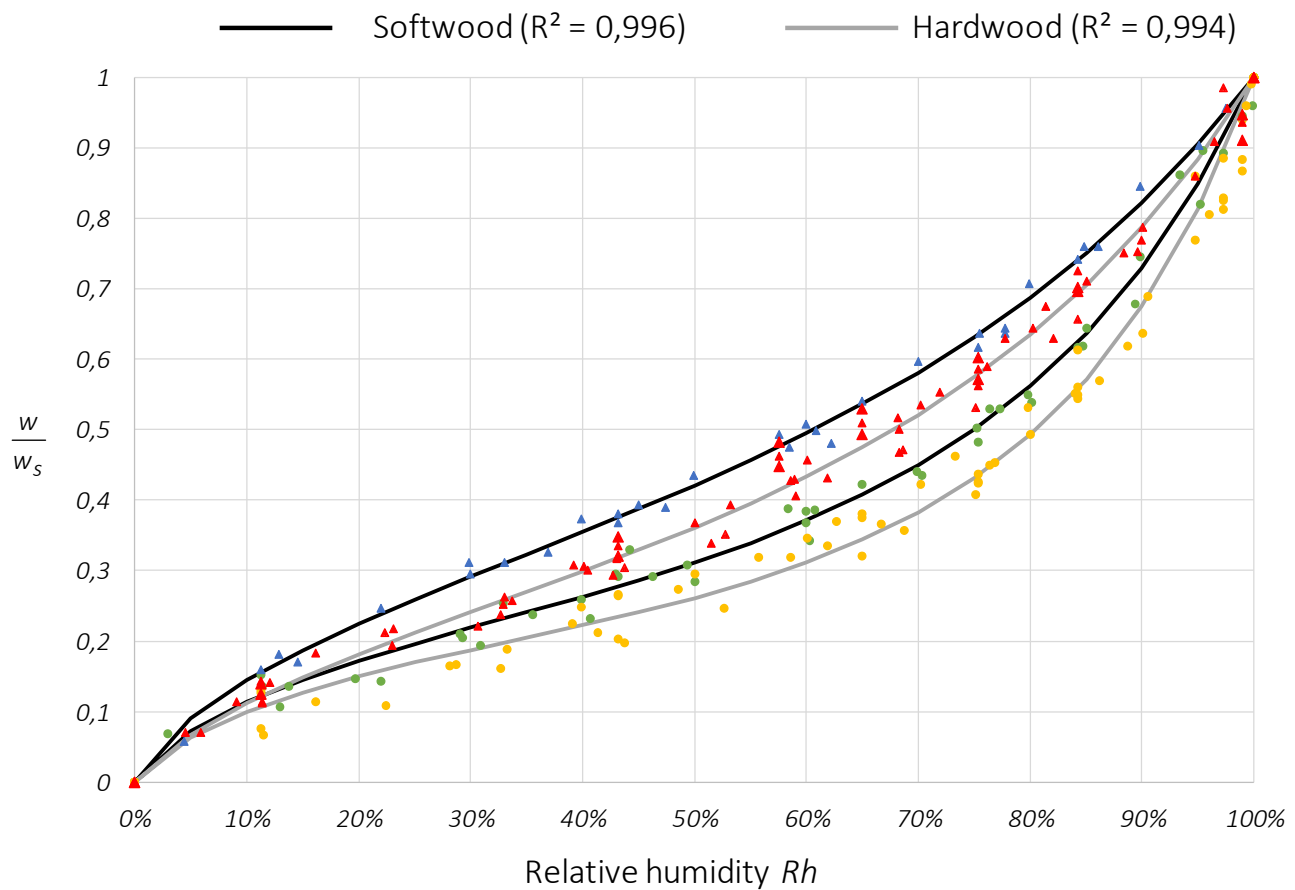


Figure 7. Sorption isotherm curves of hygroscopic equilibrium according to saturation ratio of wood and relative humidity of air.

4 Eurocode 5 positioning

4.1 Standard service classes

In accordance with Eurocode 5, timber design refers to services classes corresponding to moisture content range recalled in the table 2. These classes allow the positioning of timber element in respect to the environmental conditions. This fact induces a re-adjustment of the mechanical strength via K_{mod} and the long term deflection amplification via K_{def} . Moreover, this table is also used in order to adjust drying process parameters for the first industrial transformation.

Table 2. Service classes and moisture content range.

	Moisture content range
Service class n°1	$w \leq 12\%$
Service class n°2	$12\% < w \leq 20\%$
Service class n°3	$w > 20\%$

Today, moisture content equilibrium is estimated using a standard hygroscopic equilibrium abacus presented in Figure 8.

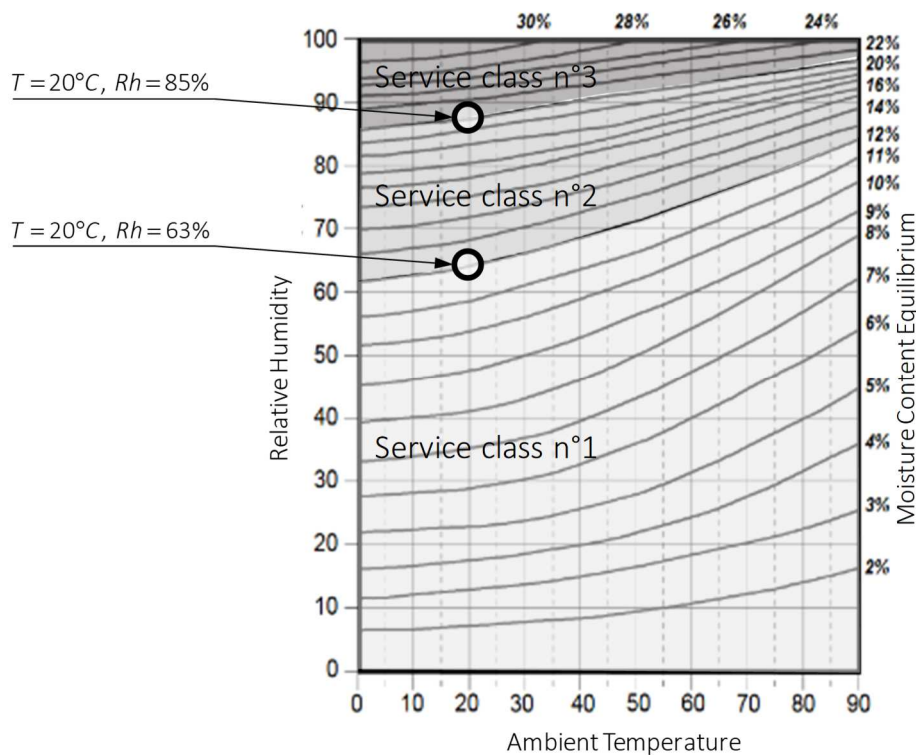


Figure 8. Standard abacus of hygroscopic equilibrium and Service classes.

Let us focus on two specific moisture equilibrium points at 20°C corresponding to the boundaries between the service classes 1 and 2 ($Rh = 63\%$, $w_{EC5} = 12\%$) and between the service classes 2 and 3 ($Rh = 85\%$, $w_{EC5} = 20\%$). Tables 3 and 4 presents differences of moisture equilibrium given by Eurocode 5 and calculated with the present approach. First of all, results highlight important differences between species. About softwoods, we can note equilibrium differences exceeding 5 points of moisture content). For instance, about the service class 2, Spruce presents excessive equilibrium moisture content which can induce biologic risks comparable to a service class 3. Hardwood family is characterized by a lower level of moisture content with a gap reaching 5 points.

Table 3. Hygroscopic equilibrium in class 1-2 conditions (20°C, 63%Rh).

Species	Adsorption phase	Desorption phase	Average equilibrium
EC5	12%	12%	12%
Softwood			
Douglas Fir	10,8%	14,2%	12,5%
Spruce	13,0%	17,3%	15,1%
Fir	11,1%	14,7%	12,9%
Scots Pine	11,9%	15,7%	13,8%
Hardwood			
Oak	9,1%	12,6%	10,8%
Beech	10,0%	13,9%	12,0%
Poplar	10,7%	14,8%	12,7%
Cherrywood	8,7%	12,1%	10,4%

Table 4. Hygroscopic equilibrium in class 2-3 conditions (20°C, 85%Rh).

Species	Adsorption phase	Desorption phase	Average equilibrium
EC5	20%	20%	20%
Softwood			
Douglas Fir	17,5%	20,6%	19,0%
Spruce	21,2%	24,9%	23,1%
Fir	18,1%	21,3%	19,7%
Scots Pine	19,3%	22,8%	21,0%
Hardwood			
Oak	15,7%	19,3%	17,5%
Beech	17,3%	21,4%	19,4%
Poplar	18,4%	22,8%	20,6%
Cherrywood	15,1%	18,7%	16,9%

Moreover, the hypothesis of initial moisture condition is essential for the prediction of the moisture content variations in service life of timber elements. In this case, the conditions of drying process need to be more controlled. It's for all these reasons that we propose an interactive abacus for the determination of hygroscopic equilibrium.

4.2 Interactive abacus for hygroscopic equilibrium

The interactive abacus integrates all Tropix data, *Paradis et al. (2015)*, *Gérard, J et al. (2011)*, and is compatible with additional experimental results. Today, the abacus is implemented in an Excel chart application driven by a visual basic subroutine.

Choose a family	Softwood
Choose a specie	Douglas fir
Do you know w_s ?	YES
$w_s =$	0,2936
Rh	85%
T	20°C

Figure 9. Input interface (screen copy).

As shown in Figure 9, the input interface allows the choice of the specie family (Softwood or Hardwood), the specie type and the environment properties. If experimental value of w_s is known, it will be preferred to its tabulated value.

The output interface has the form of three equilibrium abacus for adsorption, desorption assumptions and the average abacus, Figure 10, completed with red dots corresponding to the simulated hygroscopic equilibrium.

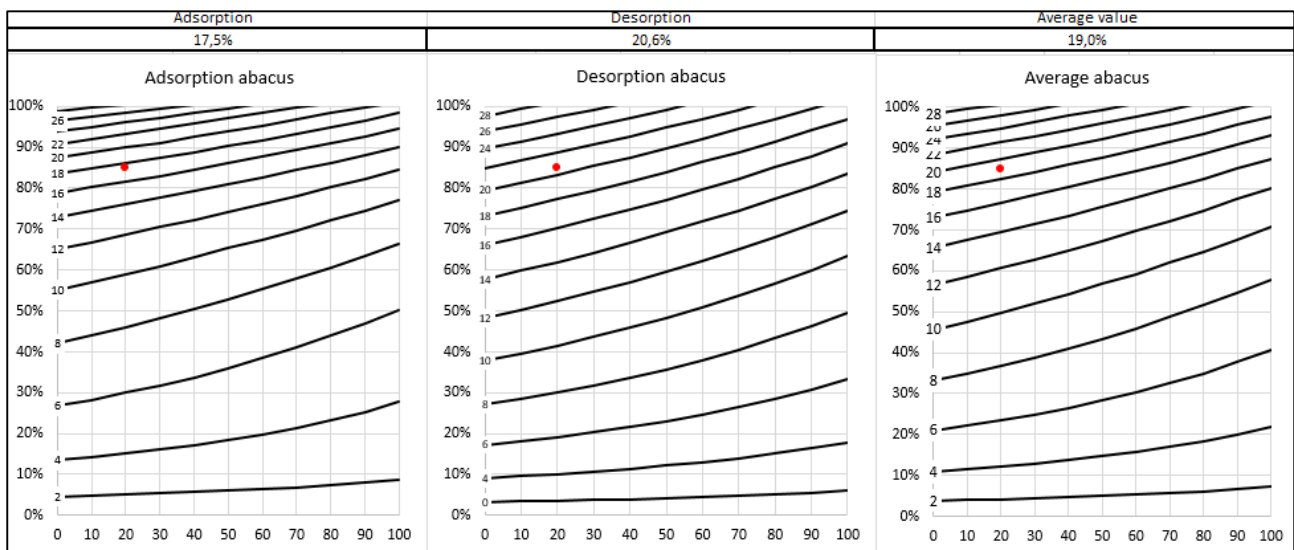


Figure 10. Output interface (screen copy).

4.3 Partial Isothermal curves

The last application allows the location of the hygroscopic equilibrium on the hysteresis for adsorption or desorption conditions. Nevertheless, the designers or drying process may need to know the future hygroscopic equilibrium in accordance with initial environment conditioning (T_{init} , Rh_{init}) and future average environment conditions (T_{final} , Rh_{final}). In this context, a second input interface allows to input initial and final environment properties, Figure 11.

Initial conditions	
$H_{rinitial}$	95%
$T_{initial}$	20°C
Do you know w_{init} ?	YES
$w_{initiale}$	24%
Final conditions	
Rh_{final}	20%
T_{final}	60°C
w_{final}	4,98%

Figure 11. Input interface (screen copy).

The output interface takes the form of a graph in which we can find the hysteresis curve given at initial temperature and moisture content way between initial and final hygroscopic equilibrium. As shown in Figure 12, a first application presents the case of a drying process at a temperature of 60°C and a relative humidity of 20%. According to an initial hygroscopic equilibrium at 24%, the model is able to calculate new equilibrium and graph show the moisture content path.

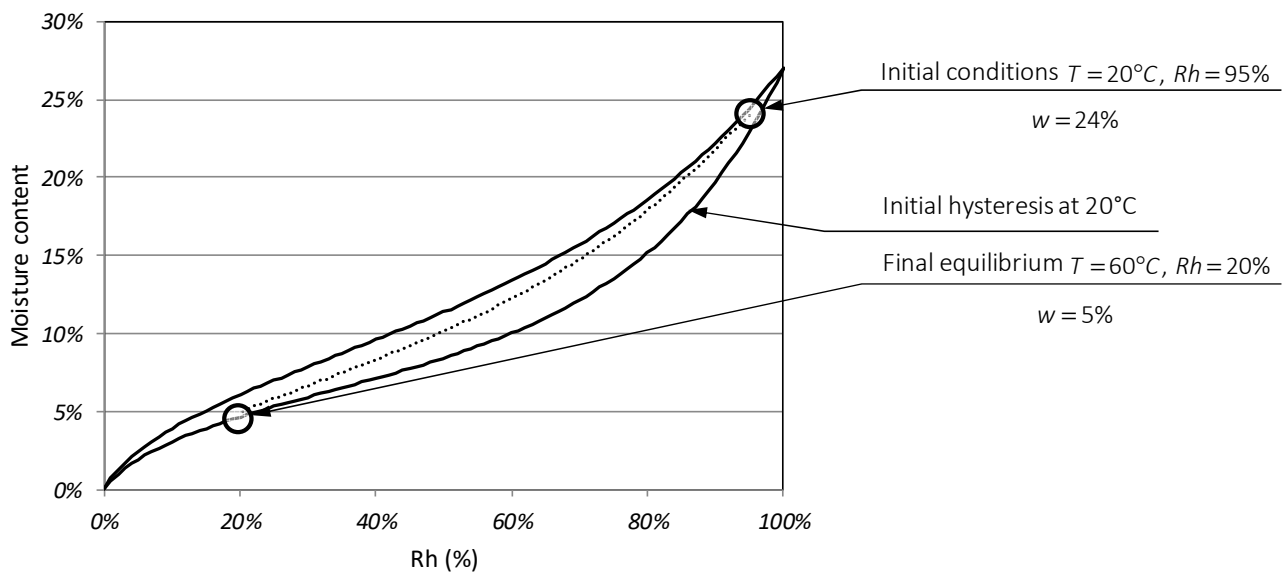


Figure 12. Moisture content evolution during drying process.

A second application deals with a timber element behavior after drying. We suppose that moisture content is controlled to 11% after dryer exit ($T = 80^{\circ}\text{C}$, $Rh = 70\%$). During the service life, we assume that timber element is placed in winter outdoor conditions ($T = 5^{\circ}\text{C}$, $Rh = 90\%$). The Figure 13 shows again the moisture content path during the wetting phase and reaching a moisture content of 21%.

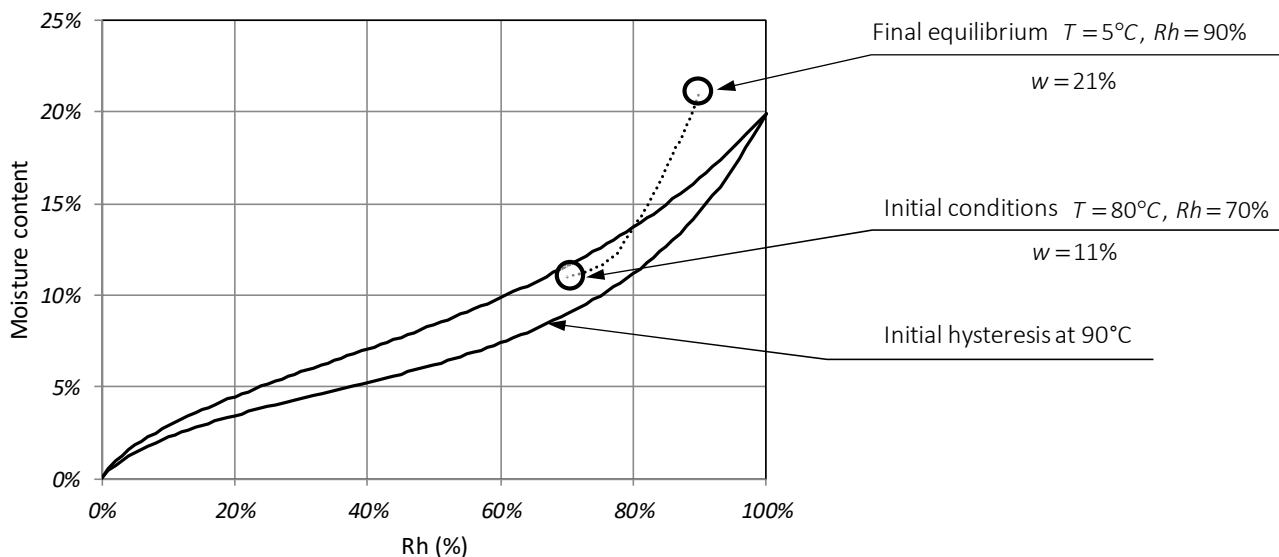


Figure 12. Moisture content evolution during wetting process.

5 Conclusion and Outlook

This work presents an experimental and numerical protocol to better apprehend hygroscopic equilibrium of wood in civil engineering constructions. This approach had allowed the construction of new interactive charts in objective of a better adaptation of Eurocode 5 for other species such as hardwoods. The paper focuses on interest of better predicting the coupling between moisture content in timber elements and the climatic environment opposite one fungal attacks in outdoor conditions or crack risks in hot and dry indoor conditions.

This paper is only one part of EFEUR5 project. The presented model also allows the characterization of orthotropic diffusion properties. In a near future, this work will be completed by the stud of long term behavior of deflected beam by adapting actual k_{def} coefficient to other species such as hardwood.

6 Acknowledgments

This work has been realised in the French National Research Agency (ANR) through EFEUR5 project. The authors would like to express appreciation to the ANR for its financial support. This work is strongly based on experimental tests. The authors sincerely thank the technical team of the civil engineering university campus, supervised by J. Dopeux, for its support.

7 References

AFNOR (2010): NF EN 1995-1-1/NA.

Dent, RW (1980): A sorption theory for gas mixtures, *Polym. Eng. Sci.*, vol. 20 : 4, pp. 286-289.

Eurocode 5 (2004): Design of timber structures - Part 1-1: General and rules for buildings. CEN. (EN 1995-1-1).

Gérard, J et al. (2011): Tropix, CIRAD, <https://tropix.cirad.fr/>

Keylwerth, R (1964): Bundesforschungsanstalt für Forst und Hozwirtschaft, Reinbek Institut für Holzphysik und mechanische Holztechnologie.

Kulasinski, K., Guyer, R., Derome, D., and Carmeliet, J. (2015): Water Diffusion in Amorphous Hydrophilic Systems: A Stop and Go Process. *Langmuir* 31, 10843–10849.

Langmuir, I (1918): The adsorption of gases on plane surfaces of glass, mica and platinum, *J. Am. Chem. Soc.*, vol. 40, pp.1361-1403.

Merakeb, S, Dubois, F, Petit, C (2009): Modelling of the sorption hysteresis for wood, *Wood Sci. Technol.*, vol. 43: 7-8, pp. 575-589.

Paradis, S., Guibal, D., Gérard, J., Beauchêne, J., Brancheriau, L., Cabantous, B., Châlon, I., Daigremont, C., Détienne, P., Fouquet, D., Langbour, P., Lotte, S., Méjean, C., Parant, M.-F., Thévenon, M.-F., Thibaut, A., Venay, M., 2015. Tropix 7.5.1 - Caractéristiques technologiques de 245 essences tropicales et tempérées (Technological Characteristics of 215 Tropical Timbers). <https://doi.org/10.18167/74726F706978>

Perré, P, May, BK (2001): A Numerical Drying Model That Accounts for the Coupling Between Transfers and Solid, Mechanics. Case of Highly Deformable Products », *Dry. Technol.*, vol. 19: 8, pp. 1629-1643.

Rijsdijk, JF (1994): Physical and Related Properties of 145 Timbers. Dordrecht: Springer Netherlands.

Siau, JF (1984): Transport Processes in Wood, vol. 2. Berlin, Heidelberg: Springer Berlin Heidelberg.

Stamm, AJ (1964): Wood and cellulose science. Ronald Press Co.

Discussion

The paper was presented by F Dubois

C Sigrist asked if the theory can be applied to fibreboard or other material. F Dubois answered that the model cannot be applied to material such as fibreboard but can be applied to heavy timber.

F Lam received confirmation that the 3D FEM model can be used to model moisture gradient and moisture movement in the timber subjected to changing relative humidity and temperature conditions.

S Franke asked since the model only deals with mean timber material properties, how can it deal with variability of material properties. F Dubois answered the model can use different material properties if they are known.

S Franke raised issues related to equilibrium and time as Service Class 2 has to deal with issues related to wind and sunshine. F Dubois said that the model and data do not take these issues into account.

H Blass asked if the model can be applied to the timber drying case. F Dubois answered that it can be extended to free water case.

S Winter commented that the model is a good start. More work is needed to cover the code related issues in Eurocode 5.

CLT under in-plane loads: Investigation on stress distribution and creep

Martin Gräfe, Philipp Dietsch and Stefan Winter
Chair for Timber Structures and Building Construction
Technical University of Munich

Keywords: cross-laminated-timber, prestressing, post-tensioning, creep, in-plane behaviour, load distribution, shear

1 Background and objective

Tall buildings need to bear high horizontal loads, particularly from wind and seismic loading. Apart from shear stresses, these loads are generating vertical forces in the bracing elements of such buildings. In steel and concrete structures, vertical tension loads are transferred by reinforcement bars, prestressing tendons, or the steel structure itself. As timber structures feature a comparatively low self-weight to counterbalance vertical tension forces and are typically made up of a relatively large number of single elements, a rather large quantity of fasteners such as screws or dowels is required to transfer the vertical tension forces.

This led to the idea of introducing vertical prestressing elements in order to counterbalance these tension forces. With this system, the horizontal joints only have to bear compression and shear stresses, which are easier to handle and enable the use of e. g. form-fitting connections without additional fasteners.

For the application of this system, it needs to be clear how a concentrated in-plane load introduced by the anchorage of a prestressing tendon into the CLT-panel distributes downwards. In addition, the creep behaviour of CLT loaded under in-plane compression loads is a prerequisite for the application of such systems. The objective of the project described in the following was to contribute answers to these two questions, based on experimental tests and parameter studies.

2 Load distribution in-plane

2.1 Definition of the load distribution angle

A single in-plane load on the narrow edge of an orthotropic plate distributes downwards in a nonlinear manner, governed by several material and geometric parameters. The bearing force on the bottom edge or any horizontal section is distributed in a bell-shaped curve, whose integral over the horizontal length represents the single load applied on the top (Fig. 1 left). For engineering applications (e. g. steel, concrete, masonry) it is widely accepted common practice, to assume a linear distribution over a certain horizontal length, which is normally defined by a fixed angle of load distribution for each material (e. g. 30° for (any type of) masonry, up to 45° for concrete or steel). (Wallner-Novak et al. 2018) recommend an angle of 25° for CLT with 33 % cross-layer proportion, and indicates a range between 15° and 45° between 0 % and 100 % cross-layer proportion.

The approach presented in this paper uses a calculated, respectively measured total width of load distribution (until the strain curve converges to zero), then cuts off 5 % of the integral, and calculates

the angle of load distribution to the point, at which 95 % of the force are covered (Fig. 1 left). The width of the strain distribution was firstly calculated by an FE-parameter study (Westermayr 2016), and subsequently verified by mechanical tests in a specialized test setup.

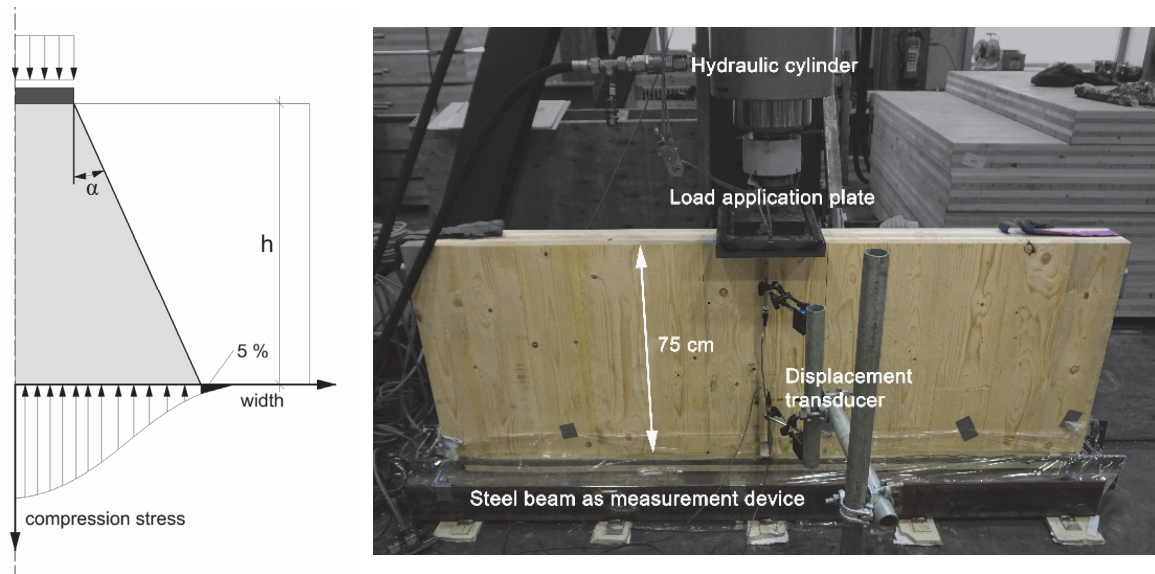


Figure 1 left: definition of the load distribution angle α , right: specimen placed in the test setup

2.2 Parameter Study

A parameter study was realized by means of a FE-model to determine the influence of the parameters on the load distribution angle: narrow face bonding, cross layer proportion, variability of material properties, range of mechanical material parameters, the position of the load application and the height/width proportion of the CLT-element. With the 3-D model, the bearing force of each configuration was calculated and plotted on a diagram over the length of the linear support at the bottom edge. This enabled the calculation of the load distribution angle for each set of parameters.

The model was a volume model representing single boards, which were defined with the material properties shown in table 1. The gaps between single boards were set with a width of 2 mm, the supports were defined as rigid nodal supports, and the FE-mesh featured a squared mesh width of 20 mm (Fig. 2 left). A typical load distribution diagram is shown in Fig. 2 right, similar diagrams were derived for all parameters mentioned above.

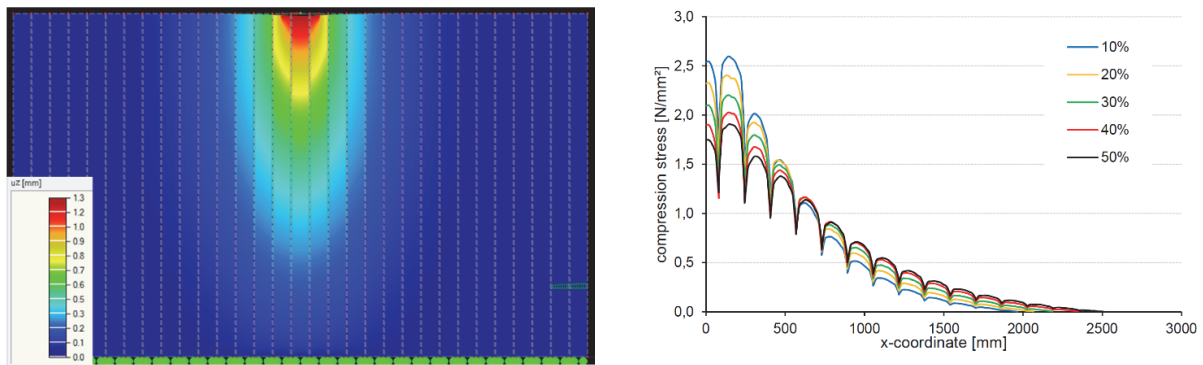


Figure 2 left: FE-model, deformation u_z , right: diagram of load distribution with different cross layer proportions (Westermayr 2016)

Table 1 Material properties for the FE-model, according to (Neuhaus 2009)

E-modulus [N/mm^2]			Shear-modulus [N/mm^2]			Poisson ratio		
L	R	T	LR	TR	TL	LR	TR	TL
10.000	800	450	600	40	650	0,027	0,6	0,033

The following conclusions from the parameter study can be drawn:

- The cross layer proportion has a significant influence on the width of the load distribution
- Narrow-face bonding leads to a smoother strain distribution, and in total to an increase of the load distribution angle of 2° to 3°
- The poisson ratio and varying material properties show a very low influence
- The wall height in a typical range from 2 m to 5 m has a very small influence
- The board width was 160 mm, broader boards lead to broader load distribution angles, the maximum is identical with the values for narrow face bonded CLT
- The bottom support was ideally rigid. This can never be achieved in practice, leading to broader distributions as calculated.
- The angle of load distribution, taking into account all models and parameters, ranged between 21° (10 % cross layer proportion) and 28° (50 % cross layer proportion)

2.3 Experimental investigation

2.3.1 General

To verify and calibrate the results from the FE-model, a series of mechanical tests was conducted. The objective was to measure the force per unit length along the bottom edge of a CLT-plate, which was loaded on the upper edge by a concentrated in-plane load.

2.3.2 Test setup

The measurement of the force per unit length at the bottom of the CLT-panel was done by placing it on a specially designed steel beam, which was equipped with 56 vertically oriented strain gauges. The steel beam was slotted into single elements, featuring 50 mm horizontal length in the middle and 100 mm on the sides of the beam (Fig. 3). The strain gauges provided the vertical compression strain in these elements, which could be converted into compression stress in the steel, correspondingly the force per unit length in the contact line between steel and CLT, and thus the stresses and distribution of stresses in the CLT-element. All strain gauges were calibrated after application to the beam by applying compression strain by calibrated test equipment and verifying the correct readings.

The steel beam was supported sidewise by two steel beams in order to prevent possible lateral deflection, and placed on the concrete floor of the laboratory in a thin layer of high-strength cement grouting to achieve the highest possible vertical stiffness. The joint between steel and CLT was smoothed accordingly with a thin ($\approx 1\text{ mm}$) layer of cement grouting, to ensure a full surface contact regardless to minor unevenness.

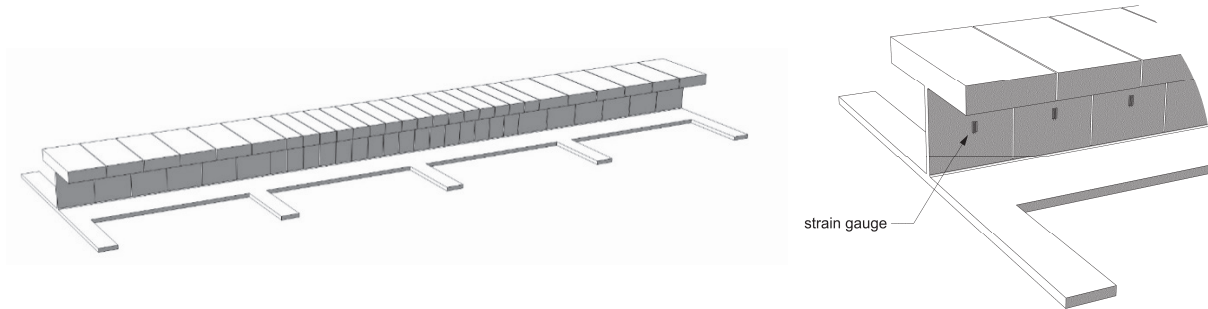


Figure 3 left: steel beam as measurement device, right: detail of single elements with strain gauge

Three different CLT-layups were used, featuring five or seven layers, total thicknesses from 150 to 200 mm, and a proportion of cross layers from 25 % to 40 %. The CLT-elements were not-narrow-face-bonded, graded as C24, and featured a height of 750 respectively 1500 mm, and width of 2000 mm. The load was applied in three steps from 5 N/mm² to 15 N/mm² on the CLT-layers with vertical orientation, by a steel plate of 300 mm length and a force controlled hydraulic cylinder (Fig. 1 right).

2.3.3 Test results

The measured strain and derived mechanical stress distribution showed a bell-shaped curve, as expected with the maximum value in the symmetry line of the load application (Fig. 4 left). This result fitted well with the derived load distribution angle from the results of the FE-model. The strain was plotted over the bottom length, and then a gaussian bell curve fitted to the measurements with the least square method. To this curve the same 95 % rule as used in the FE-study was applied, and the resulting angle calculated. This angle showed a range from 21° at 25 % cross layer proportion, to 23,2° at 40 % cross layer proportion (Fig. 4 right).

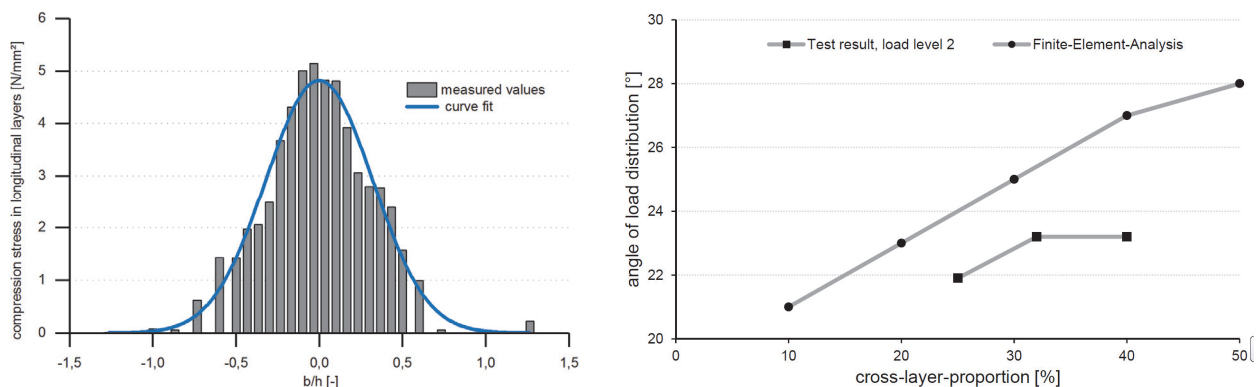


Figure 4 left: measured data and curve fit (40 % cross-layer-proportion), right: comparison between FE-model and test results

2.4 Conclusion

The angle of load distribution in CLT panels is primarily dependent on the bonding of the narrow faces, the width of the single boards, the height of the CLT-element, the proportion of cross layers, the wall height, and the stiffness of the contact surface at the bottom edge. Finite-Element studies as well as mechanical tests showed, that a single load applied on the narrow edge of a CLT panel distributes downwards in an angle of 21° to 28°. For practical engineering use, the assumption of this angle to 25° and a linear strain distribution in any horizontal section appears justified for CLT-walls

up to 5 m height, with or without narrow face bonding, and a cross layer proportion of at least 20 %. This simplified assumption takes into account, that the bottom contact surface in any application of CLT in reality is not “ideally stiff” but always featuring a certain flexibility in z-direction. This leads to a broader distribution of load, and therefore to lower compression stresses as calculated theoretically. Furthermore, the distribution is always nonlinear, with its peak level normally in the centre line under the load application. The approach suggested in this paper uses a linear load distribution, and consequently underestimates the maximum value in the centre. Such an approach is widely used and well established in engineering practice for typical structural materials (masonry, concrete, steel), some of which show typical brittle failure behaviour. The authors consider this approach to be appropriate for CLT as well, bearing in mind its ability for elastic-plastic redistribution of loads to lower stressed regions within the panel under in-plane loads. In addition, the verification against buckling of 2-dimensional CLT panels is typically on the safe side when it is realized as uniaxial verification on a “representative 1-m-strip” e. g. with the equivalent member method.

Regarding the question of standardisation it may be taken into account that practice asks for calculation methods as manageable, less error-prone and less time-consuming as possible. More detailed approaches may be more accurate in some cases, but tendency for misinterpretation or disapproval of practice is higher due to reasons of time and qualification of engineers.

3 Creep behaviour of CLT under compression stresses in plane

3.1 Influencing factors

The creep behaviour of timber is mainly dependent on the type of mechanical stresses (bending, shear, tension, compression), size, type and grade of specimens, moisture content and changes in moisture content and load level. In particular the ambient conditions and resulting changes in timber moisture content contribute a large share to the long-term behaviour, generally intensified with reduction of size of specimens. The type of processing, respectively the type of the final timber product is relevant as well, as influences like grading, cut type, thickness of lamellas and added glue may add additional uncertainty and statistic scatter to any mathematical prediction of the creep behaviour. Due to this broad range of parameters, tests results and – to an even higher extent – extrapolated final creep ratios found in literature show an extensive variety.

3.2 Literature und existing test results

Most creep tests described in literature were realized as bending tests in different setups, often with rather small specimens and in some cases from ungraded timber.

Literature on creep tests can be roughly divided into two areas of interest: The first group is represented by the creep behaviour of bending beams, which are loaded by quasi-permanent loads perpendicular to the longitudinal axis. Depending on the geometry, different proportions of tension, compression and shear stresses result in this type of specimen, and lead to corresponding creep behaviour. Consequently, deflections perpendicular to the longitudinal axis were measured over time (e. g. (Gressel 1983), (Rautenstrauch 1989), (Jöbstl et al. 2007)). The second group is represented by creep and load carrying capacity tests with slender compression members. This research intended to investigate, describe and predict the long-term-load capacity in terms of a possible stability failure due to increasing strain induced by second order effects. Usually, the specimens were loaded with

combined compression and bending strain, and different imperfections where applied. The measured parameter was normally the deflection perpendicular to the member's axis, similarly to the method known from bending tests. ((Härtel 2000), (Becker 2002), (Hartnack 2004), (Morlier 2007), (Moorkamp et al. 2001))

Unfortunately, especially in older literature, the load levels were often not specified. This makes it difficult to compare tests results, and to draw conclusions on the behaviour of real-size CLT from graded and kiln-dried boards loaded in compression. Some scientific evidence (Glos et al. 1987), (Blaß 1988) suggests, that creep test results from bending, or combined bending and compression may not fit to the creep behaviour of timber under pure compression load. For a realistic design of prestressed timber members, the creep behaviour in longitudinal direction is the only relevant parameter for the prediction of losses in prestressing force. The question of stability, or respectively long term load carrying capacity is to be answered in an additional second step, by using creep values derived from bending tests as mentioned above.

On this basis, a specific series of creep tests in different load grades and climate conditions was realized, to get more specific results for the application "CLT under longitudinal compression".

3.3 Experimental test setup

3.3.1 General layout

The test series consisted of seven creep tests, with three different load levels and three different climate conditions (Table 2). All test specimens were made of 5-layered CLT, without edge bonding, featuring a length of 8,0 m and a width of 150 mm (Fig. 5 and Fig. 6). The CLT was made of spruce, graded as CL24, and retrieved from the normal production line of Züblin Timber GmbH in Aichach, Germany. The average density was 440 kg/m^3 , the timber moisture content was $u = 10,8 \%$. No abnormal visual characteristics or damages were observed, the precision of machining, gluing and straightness was as planned and ordered.

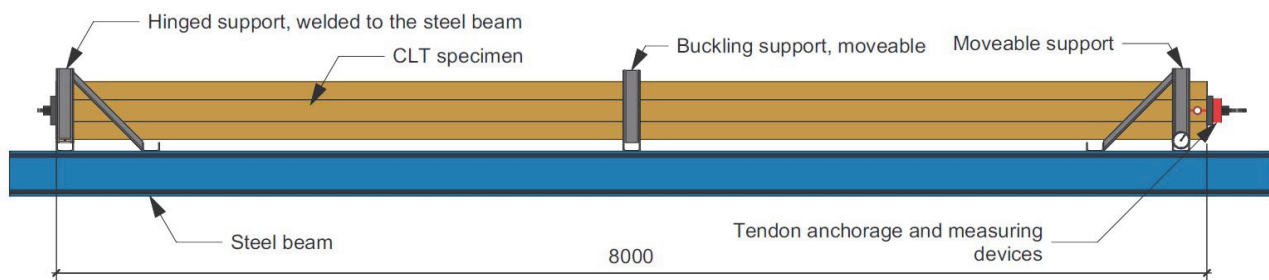


Figure 5 General layout of the test setup

The compression stress applied to the longitudinal lamellas was 5, 10 and 15 N/mm^2 . The compression force was applied by a single unbonded monostrand tendon St 1660/1860, $A_p = 150 \text{ mm}^2$, which was inserted in a centric slot of $34 \times 34 \text{ mm}^2$ (Fig. 6 left). This slot was applied during production of the panels by adding and later removing corresponding spacers. This method is described in detail in (Gräfe et al. 2018). The specimens were placed in pairs on a steel beam, which was equipped with welded-on hinged and moveable supports. One side of each specimen was fixed against the steel beam, while the other end was able to move freely in longitudinal direction. The moveability of the supports was ensured by roller bearings, and partly PTFE-sheating between timber and steel. This setup ensured that the steel beam was free of any force resulting from deformations of the timber,

and that the measured force was completely transferred by the corresponding specimen. The distances of the lateral supports were calculated as to prevent buckling in any direction, and were set to 4,0 m for the specimens type A, and 2,0 m for the specimens type B and C (Fig. 5 and 6 left).

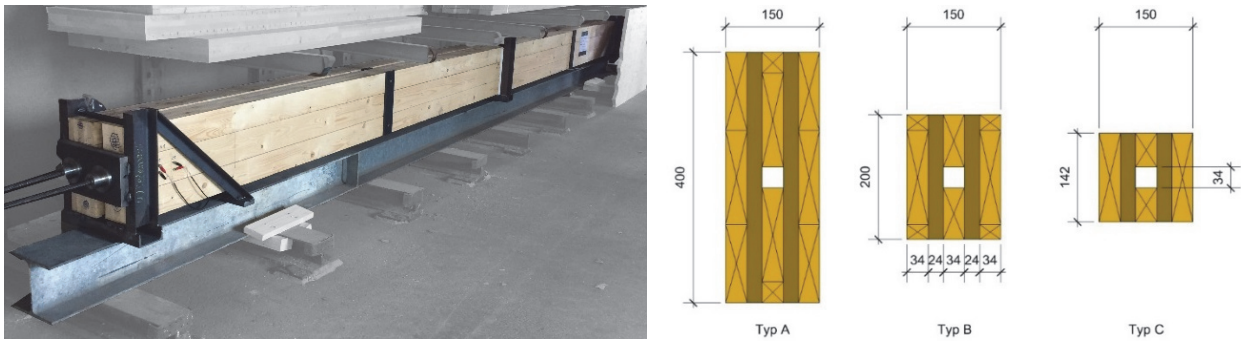


Figure 6 left: view of specimen B2 and C2 at the outdoor test location, right: cross sections of test types A, B, C

3.3.2 Prestressing process

Each tendon, resp. specimen, was prestressed to approximately 220 kN by a hand-driven hydraulic jack. After the wedges were driven into their seats and the hydraulic pressure released, the force dropped to the $P_{m,0}$ value, which was between 203 kN and 210 kN. During the prestressing process the deformations and forces were measured, allowing to subsequently calculating the individual modulus of elasticity of each specimen (Table 2).

Table 2 Specimen properties, prestressing forces, deformations and calculated modules of elasticity

Test No.	A1.1	A1.2	B1	B2	C1	C2	C3
P_{max} [kN]	220,0	221,0	222,0	221,5	222,9	220,5	222,5
$P_{m,0}$ [kN]	203,7	206,5	207,7	209,5	210,3	208,2	210,5
u_0 [mm] @ $P_{m,0}$	4,40	3,76	7,65	7,40	9,91	10,10	11,02
E [N/mm ²]	9.379	11.083	11.292	12.738	12.738	11.466	11.466
σ_c [N/mm ²]	5,0	5,0	10,0	10,0	15,0	15,0	15,0
A_{net} [mm ²]	39.644	39.644	19.244	19.244	13.328	13.328	13.328
$\sigma_c/f_{c,0,mean}$ [%]	14	14	28	28	42	42	42
Climate type (see. 3.4)	1	1	1	2	1 + 3	2	3
Duration [h]	1.400	1.400	2.000	9.800	9.800	9.800	7.300

3.3.3 Measuring systems – force, ambient conditions, deformation

In climate 2, the measurements of tendon force, ambient conditions, the material temperatures of the CLT specimen and the supporting steel beam and deformation of the specimens were realized electronically by means of load cells (500 kN Type 722, Induk GmbH), relative humidity and air temperature sensors from the modularized programmable e *Tinkerforge* System, and inductive displacement sensors. The deformation of the specimens in climate 1 and 3 (laboratory at TUM) was measured by mechanical gauges (Fig. 7). Both the inductive sensors and mechanical gauges had an accuracy of 1/100 mm, while the load cell had a guaranteed accuracy of ± 1 %.

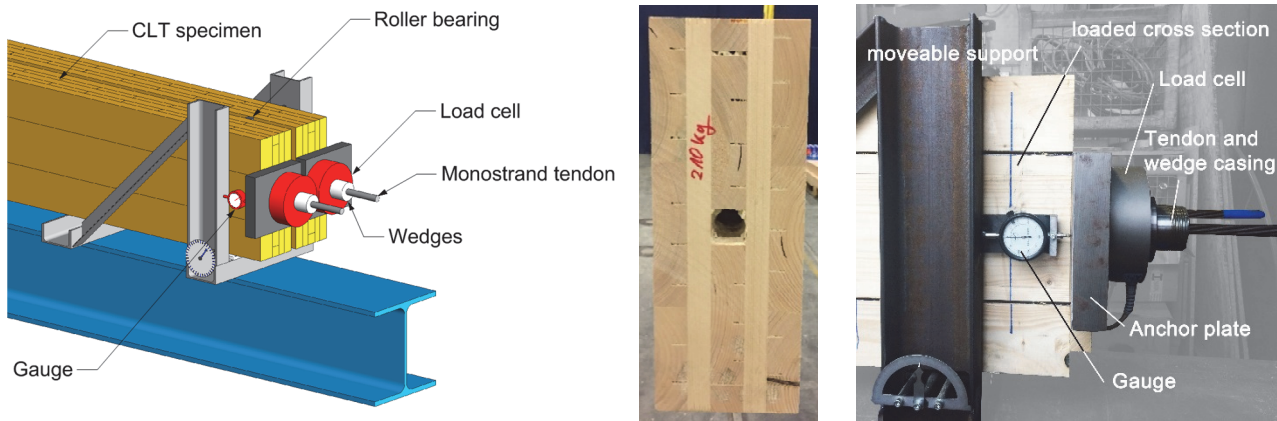


Figure 7 left: detail drawing of measuring devices, middle: cross section type A, right: side view of measuring devices

3.3.4 Measuring systems – timber moisture content

The timber moisture content for the specimens in climate 1 and 3 was measured continuously with the electric resistance method and permanently installed electrodes. The applied method and technical equipment was identical with the systems described in (Dietsch et al. 2015). (Mugrauer GmbH, Gigamodul and Softfox software). Eight pairs of electrodes were applied in depths from 15 mm, 25 mm, 40 mm and 70 mm at representative locations throughout the specimens. Representative timber moisture contents are plotted over time in fig. 9 left.

The timber moisture content of specimen B2 and C2 in the outdoor test in Aichach was measured at least every four weeks by a hand-held electric resistance-type measuring device (Type GANN Hydromette RTU 600), at eight permanently installed pairs of electrodes in 15 mm and 25 mm depth.

3.4 Ambient climate conditions

3.4.1 Types of climate

Three different climate conditions were used: a constant climate of 20° C and 60 % RH (Climate 1), the natural outdoor climate in Aichach, southern Germany (Climate 2), and a climate cycle with weekly changes between 40 % and 90 % RH (Climate 3).

3.4.2 Climate 1

The tests were performed in the timber test laboratories of TUM, in which relatively constant ambient conditions are ensured by a heating and air moisturising system. Slight variations in the climate conditions typically occur by the occasional opening of windows and entrance gates, and by the influence of the outdoor air temperature in summer as no cooling system is installed.

3.4.3 Climate 2

The location was a rain-sheltered, shady place in an all-side open storage shed in Aichach, Germany (48°26'29.2"N 11°07'11.0"E, fig. 6 left). The described test period lasted from May 2017 to June 2018, the climate was typical for the region of southern Germany. The measured relative humidity and temperature is shown together with the Savitzky-Golay-filtered data in fig. 8. The filtered relative humidity ranged from approximately 60 % RH to 90 % RH, while the according temperature range was – 3 °C to 22 °C (Fig. 8).

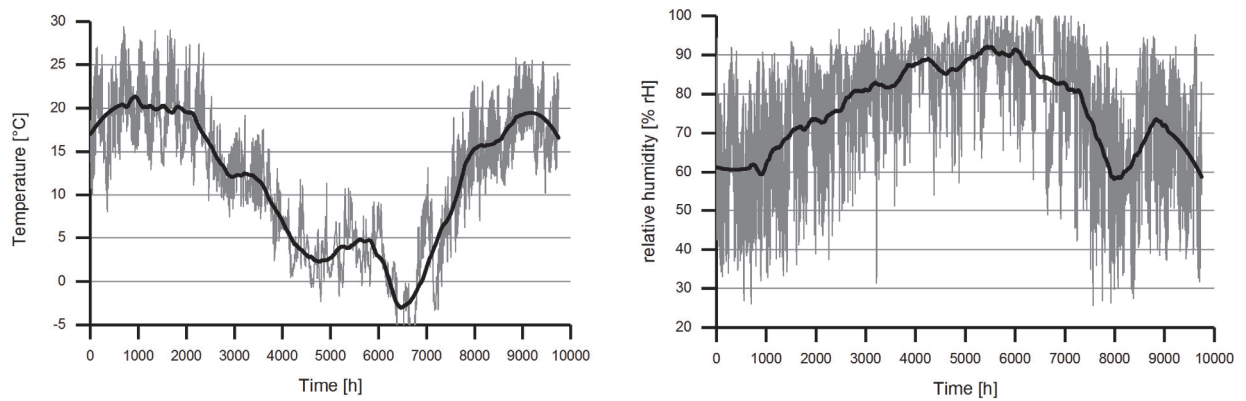


Figure 8 Air temperature (left) and relative humidity (right) in Aichach, Germany from May 2017 to May 2018 (Climate 2)

3.4.4 Climate 3

After the tests in constant climate 1 conditions were finished, the test setup in the laboratory was encased with plastic sheeting, followed by the placement of a customary ultrasonic air humidifier and a condensation dryer inside. This machinery was fitted with integrated sensors and controllers, which kept the conditions automatically at the preselected values. The volume of the casing was approximately 10 m^3 , which was constantly circulated by an electric fan with a capacity of $125 \text{ m}^3/\text{h}$ to ensure even conditions within the whole volume. As the temperature in the laboratory was conditioned to a relatively constant level, the temperature in the test casing remained constant as well at any humidity conditions inside. The climate cycles consisted of four dry (40 % RH) and four wet (90 % RH) 7-day phases, followed by a four-week wet, and a five week dry phase. The measured relative humidity over time is shown in fig. 9 left, together with the intended nominal values. Before and after the cyclic changes the conditions were constant as described for climate 1. Some scattering occurred around 2.000 h due to testing procedures of the air conditioning machinery.

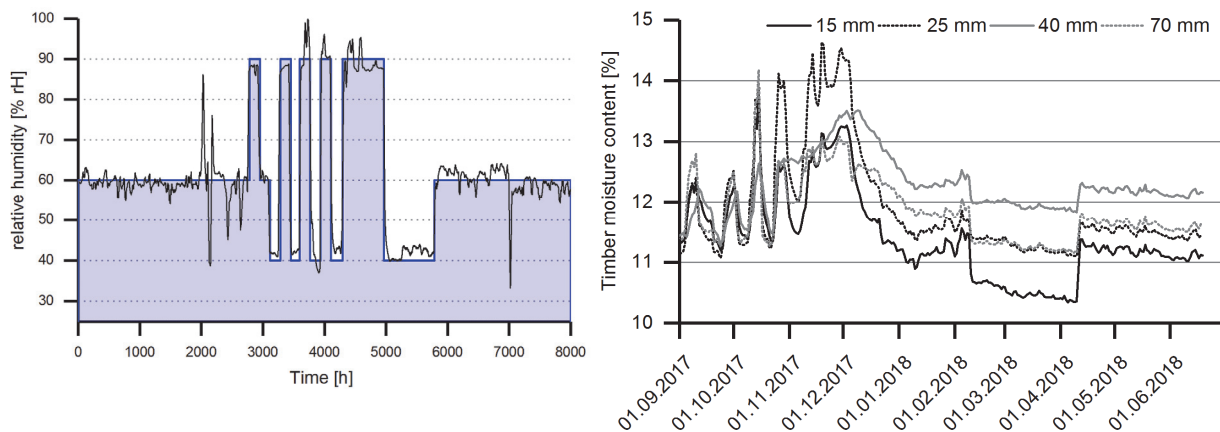


Figure 9 Relative humidity (left) and measured timber moisture content (right) in climate 3

3.5 Modelling of creep deformations

3.5.1 Calculation method for creep deformations

The reading of the gauges, respectively of the inductive deformation sensors show the superposition of influences from creep, shrinkage, swelling, variations in tendon force and temperature. To derive the desired creep deformation, the gauge reading has to be corrected by these parameters. As influences from changing timber moisture content are difficult to describe and to calculate, only time periods with identical timber moisture contents were investigated for the creep evaluation.

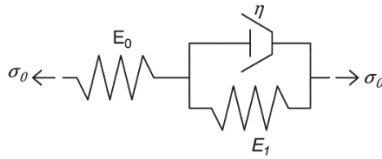
The tendon force was measured over time. In combination with the known individual modulus of elasticity, this allowed easily to account for varying deformation due to variations of compression force, respectively compression strain in the CLT elements.

Temperature changes were taken into account by using the measured material temperatures, and assuming thermal expansion coefficients of $6,0 \cdot 10^{-6}$ for timber longitudinally and of $12,0 \cdot 10^{-6}$ for steel. All deformation plots and derived creep values presented hereinafter are correspondingly corrected values according to the following formula:

$$u_{creep} = u_{measured} + u_{T,steel} + u_{T,timber} + u_{\Delta P} + u_{S+S}$$

3.5.2 Creep model and extrapolation

The test results in this research project were analysed and extrapolated by the rheological model introduced by (Pfefferle 1971), see fig. 10. This model consists of two springs, and one non-linear damper. The model was introduced originally to describe the behaviour of concrete, adapted to timber by changing the linear to a non-linear damper by (Rheinhardt 1973), and evaluated by test results from (Möhler and Maier 1970) and (Kollmann 1964). The model is equivalent to the standard solid model, but uses a damping element whose force is proportional to the square root of the time. The element deforms faster in the beginning, but converges significantly slower to its final value compared to the standard solid model.



$$\varepsilon(t) = \frac{\sigma_0}{E_0} + \frac{\sigma_0}{E_1} \cdot \left(1 - e^{-\frac{E_1}{\eta} \cdot \sqrt{t}}\right)$$

Figure 10 left: Rheological model from Pfefferle, right: formula

Advantages of this model are its good fit to the natural behaviour of wood, and the relatively simple interpretability. More complex models which integrate directly e. g. the mechano-sorptive effects (Hanhijärvi 1995), (Toratti 1992) provide theoretically a better fit to test results, with the difficulty to correctly determine the necessary parameters, which are mutually dependent in a rather complex, highly nonlinear manner. Although even simpler models such as the exponential model (used e. g. by (Wanninger 2015)) may provide a good fit to the initial time of a creep test, they seem to be less adequate to correctly approximate the behaviour over longer periods.

After extensive literature review the *Pfefferle*-model was chosen from as the best compromise between a good fit to natural material behaviour, and simplicity und comprehensibility of its parameters.

3.6 Results

3.6.1 General observations

The tendon forces decreased only slightly (less than 5 %) over time, mostly due to relaxation of the tendons. This is understandable, as the lengthening of the tendons during initial prestressing was about 100 mm, while the creep deformations of the timber reached only to 3 mm in the maximum. No buckling or visible lateral deflections were observed.

The reaction of the specimens to changes in relative humidity was very sensitive. For instance a temporary opening of windows with a resulting drop in relative humidity of up to 10 % led to a clear reaction to the length of the specimen of some 1/100 *mm* within approximately half an hour.

Shrinkage due to drying of the timber has a strong impact on total deformation, while swelling due to moisturizing in the same extent leads to lower values. All changes in timber moisture content lead to a clear increase of creep deformation.

3.6.2 Tendon force

The losses in tendon force fit well to the calculated values derived from the technical approval (Z-12.3-84) of the used monostrand tendons St 1660/1860 with *very low relaxation* (Fig. 11). Therefore the calculation approach stated in the approval was subsequently used to determine relaxation losses.

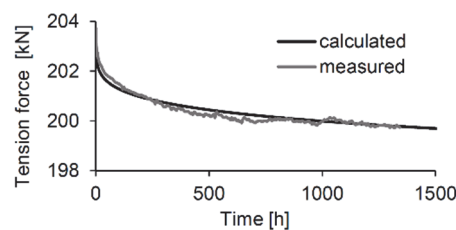


Figure 11 Measured and calculated values of tendon force, Test A1.1

3.6.3 Tests in indoor climate, specimens A1, B1, C1

The test results of the specimen A1, B1, C1 together with the related creep model curves are shown in fig. 12. Clearly visible is a better fit and clearer creep curve, as higher the load level is. Test A showed a considerable scatter and no clear measurements, as the influence of interferences like slight changes in temperature or relative humidity is relatively high. Specimen B1 and C1 show a pretty good fit to the selected creep model, and a clear decrease in the speed of creep deformations. The creep ratios were approximately 0,06 after 2000 h for specimen B1, and 0,10 for C1 respectively.

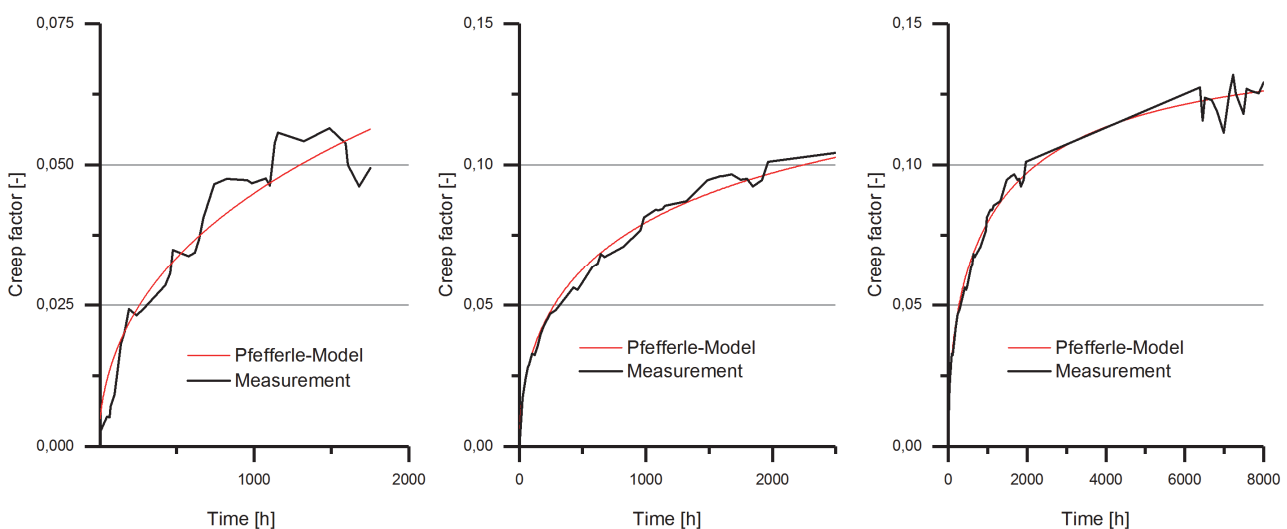


Figure 12 Creep test results and Pfefferle-models for constant climate, from left to right Tests B1, C1 to 2500 h, C1 to 8000 h

The parameters for the *Pfefferle*-models of specimen B1 and C1 were determined as follows:

$$\varphi_{B1}(t) = 0,15 \cdot (1 - e^{-0,01125 \cdot \sqrt{t}})$$

$$\varphi_{C1}(t) = 0,2 \cdot (1 - e^{-0,01652 \cdot \sqrt{t}})$$

For specimen A1 no parameters were calculated, as the measurements were not sufficiently stable and generally very low.

3.6.4 Tests in cyclic climate, specimens C1 and C3

The measured deformation of specimen C1 is plotted together with the nominal relative humidity in fig. 13 left. The strong dependency of deformations on the relative humidity – and according timber moisture content – is clearly visible. Specimen C3 followed the behaviour of C1 very closely, although it was loaded initially at the beginning of the cyclic climate change at around 2500 h.

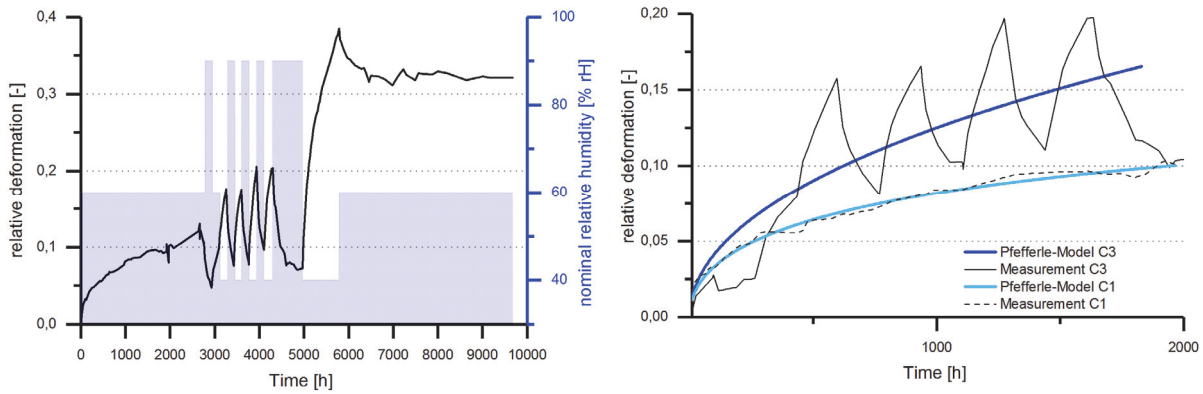


Figure 13 left: Measured deformation and nominal relative humidity of C1, right: comparison of the deformations of C1 and C3

The creep deformations in the cyclic climate are approximately twice as high as in constant climate (Fig. 13 right). Interestingly, the creep deformation does not increase further after ≈ 6000 h, which supports the assumption of the existence of a final creep ratio (Fig. 13 left). The parameters for the *Pfefferle*-model of specimen C3 were determined as follows:

$$\varphi_{C3}(t) = 0,4 \cdot (1 - e^{-0,01193 \cdot \sqrt{t}})$$

3.6.5 Tests in natural outdoor climate, specimens B2 and C2

The relative deformation of specimens B2 and C2 is shown in fig. 14 left as smoothed and temperature- and force-corrected (see section 3.5.1) measurement data. The grey line comparatively represents the *Pfefferle*-model of specimen C3 (section 3.6.4), which is considered to be representative for service class 2 conditions. Remarkable is the strong dependency of deformation to relative (air) humidity. The relative deformation grew with its maximum speed by about 0,2 in 1000 h. In the timespan up to approximately 7000 h (March 2018), the creep deformation is superimposed by the lengthening of the specimen due to swelling, resulting in *negative* relative deformations. As the relative humidity decreased substantially starting in March 2018, the timber moisture content followed accordingly (Fig. 14 right). As the test was started in March 2017, the moisture content of both specimen was on average $u = 10,8$ % and increased subsequently to its maximum of $u = 15,6$ % in December 2017. Until summer 2018 the specimen dried to a moisture content of $u = 12$ %. As swelling is partly impeded by the compression stress of the prestressing, the *lower* compression strain of specimen B2 resulted in *larger* swelling effects compared to specimen C3. Both tests B2 and C2 deformed to a lesser extent as the model C3 (grey curve) suggests.

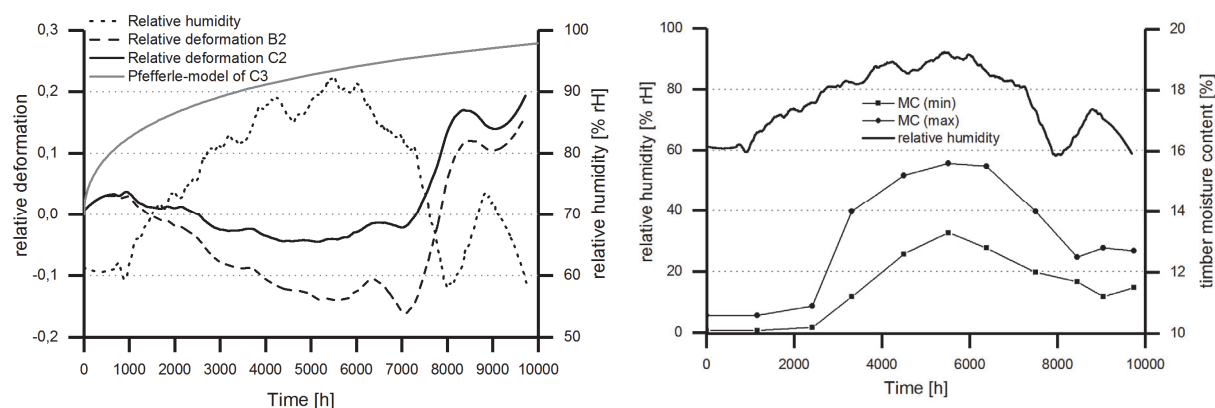


Figure 14 left: relative deformations of specimen B2 and C2, plotted together with relative humidity over time, right: dependency of relative humidity and timber moisture content

3.6.6 Extrapolated final creep ratios

Recommendations for final creep ratios derived from the creep models are shown in table 3. They represent the expected relative creep deformation after an assumed timespan of 500.000 h, which is about 57 years.

Table 3 Final creep ratios derived from the Pfefferle-model after 500.000 h, CLT from spruce loaded by compression in grain direction

Load level $\sigma_c/f_{c,0,mean}$	SC 1	SC 2
over 30 %	0,2	0,4
from 15 % to 30 %	0,15	0,3
under 15 %	0,1	0,2

3.7 Conclusion

All test results show creep deformations which are significantly lower than expected from literature data and design standards (e. g. (Gressel 1983) and (Eurocode 5)). This applies to the comparison of measured data at any specific time, as well as to final creep ratios derived from extrapolations with the applied creep model.

The difference between test results and literature can be explained by the different test setup and boundary conditions. Most tests reported in literature were conducted as bending tests either with small clear specimen, or solid wood. In the present test series, real-size CLT-specimen made from graded, kiln-dried, finger jointed sawn timber were used and stressed by compression in grain direction at specified practical load levels. *Glos et al.* (1987) report similar results from tests with specimens under compression stress. Based on this data *Blaz* (1988) recommends a final creep ratio of 0,1 for compression stress at constant climate, and twice this value (0,2) for changing climate conditions as typical in SC 2. This approach can be confirmed by the comparison between tests C1 and C3, where the changing conditions lead to a doubling of the creep deformations (Fig. 13 right). The tests in outdoor climate show a strong dependency of deformations on the variation of relative humidity over the course of the year. Anyway, the overall creep deformations in the natural climate do not exceed the deformations realized in the artificial climate with weekly cycles in climate type 3.

The test results lead to the first recommendation, that creep tests on timber should be conducted always with boundary conditions similar to the intended practical application (size and type of specimen, load level, direction of strain, climate conditions, moisture content and grading). Any setup

using test specimen and boundary conditions with properties diverging significantly from the intended application will result in measurements which are difficult to transfer into practice. Although improvements have been made in the last years in the field of computational creep modelling, related results are still associated with significant uncertainties.

Secondly, the conclusion may be drawn that current creep values stated in (Eurocode 5) significantly overestimate the creep behaviour of CLT or glulam under compression stresses in grain direction, especially for service class 1 conditions and stresses below 15 N/mm². The test results do not confirm the assumption that bending and compression creep has more or less the same level, instead compression creep seems to be significantly lower.

Following this, for the design of prestressed timber elements primarily loaded in grain direction it is proposed to answer the following two questions separately: The design regarding *bending* effects (including buckling and other stability cases) should be performed using creep factors derived from *bending tests*, the known data from standards and literature may apply. The calculation of *prestressing losses* is a question of creep due to *compression in grain direction*, and accordingly a shortening of the element. Consequently, creep factors derived from *compression* tests will result in correct calculation results. As only few references provide such test data, results from (Glos et al. 1987) and additionally this publication may be used.

4 References

- Becker, P. (2002) *Modellierung des zeit- und feuchteabhängigen Materialverhaltens zur Untersuchung des Langzeittragverhaltens von Druckstäben aus Holz*, Dissertation, Bauhaus Universität Weimar, Shaker Verlag, Aachen
- Blaß, H.-J. (1988) *Einfluss des Kriechens auf die Tragfähigkeit von Holzdruckstäben*, Holz als Roh- und Werkstoff 46 S. 405-411, DOI 10.1007/BF02608201
- Eurocode 5 (2010) *Design of timber structures - Part 1-1: General and rules for buildings*. CEN. (EN 1995-1-1).
- Glos, P., Heimeshoff, B., Kelletshofer, W. (1987), *Einfluss der Belastungsdauer auf die Zug- und Druckfestigkeit von Fichten-Brettlamellen* Holz als Roh- und Werkstoff 45, p. 243-249, DOI 10.1007/BF02616418
- Dietsch, P., Gamper, A., Merk, M., Winter, S. (2015) *Monitoring building climate and timber moisture gradient in large-span timber structures* Journal of Civil Structural Health Monitoring, Vol. 5, No. 2, DOI 10.1007/s13349-014-0083-6
- Gräfe, M., Dietsch, P., Hipper, A., Wild, M., Winter, S. (2018) *Vorspannung von Brettsperrholzkonstruktionen*, Abschlussbericht, Technical University of Munich, Chair for Timber Structures and Building Construction, München
- Gressel, P. (1983) *Rheologisches Verhalten von Holz und Holzwerkstoffen* Abschlussbericht, Versuchsanstalt für Stahl, Holz und Steine, Karlsruhe
- Hanhijärvi, A. (1995) *Modelling of creep deformation mechanisms in wood*, Dissertation, Helsinki University of Technology, Technical Research Centre of Finland, Helsinki

- Härtel, J. (2000) *Experimentelle und theoretische Untersuchungen zum Kriechverhalten hölzerner Druckstäbe unter baupraktischen Bedingungen*, Fortschritt-Berichte VDI Reihe 4, Bauingenieurwesen, Vol. 159, VDI-Verlag, Düsseldorf
- Hartnack, R. (2004) *Langzeittragverhalten von druckbeanspruchten Bauteilen aus Holz*, Dissertation, Bauhaus-Universität Weimar, Weimar
- Jöbstl, R., Schickhofer, G. (2007) *Comparative Examination of Creep of GLT- and CLT-Slabs in Bending*, Paper 40-12-3, CIB-W18, Meeting 40, Bled, Slovenia
- Kollmann, F. (1964) *Über die Beziehungen zwischen rheologischen und Sorptions-Eigenschaften (am Beispiel von Holz)*, Rheologica Acta 3, Nr. 4, p. 260–270
- Möhler, K., Maier, G. (1970) *Kriech- und Relaxations-Verhalten von luftgetrocknetem und nassem Fichtenholz bei Querdruckbeanspruchung*. European Journal of Wood and Wood Products 28, No. 1, p. 14–20, ISSN 0018-3768
- Morlier, P. (2007) (Ed.) *Creep in Timber Structures*. Taylor & Francis, New York
- Moorkamp, W.; Becker, P.; Schelling, W.; Rautenstrauch, K. (2001) *Long-term experiments with columns: Results and possible consequences on design*. Paper 34-2-1, CIB-W18, Meeting 34, Venice, Italy
- Neuhaus, H. (2009) *Ingenieurholzbau: Grundlagen - Bemessung - Nachweise – Beispiele*. 2. Ed., Vieweg + Teubner, Wiesbaden
- Pfefferle, R. (1971) *Zur Theorie des Betonkriechens*, Dissertation, Technische Hochschule Karlsruhe, Karlsruhe
- Rautenstrauch, K. (1989) *Untersuchungen zur Beurteilung des Kriechverhaltens von Holzbiegeträgern*, Dissertation, Universität Hannover, Hannover
- Reinhardt, H.-W. (1973) *Zur Beschreibung des rheologischen Verhaltens von Holz*, Holz als Roh- und Werkstoff 31 p. 352–355. – ISSN 0018-3768
- Toratti, T. (1992) *Creep of timber beams in a variable environment*, Dissertation, Helsinki University of Technology, Technical Research Centre of Finland, Espoo
- Wallner-Novak, M.; Augustin, M.; Koppelhuber, J.; Pock, K. (2018) *Brettsperrholz Bemessung: Anwendungsfälle* proHolz Austria, Wien
- Westermayr, M. (2016) *Mechanical behaviour of CLT under concentrated loads in-plane: A finite element analysis*, Master's Thesis, Technical University of Munich, Chair for Timber Structures and Building Construction, München

Discussion

The paper was presented by M Gräfe

H Blass commented that the steel tendon is used to pre-stress and creep is defined as deformation under continuous load. He questioned whether the loading can be considered continuous. M Gräfe agreed that they do not have continuous loading.

S Aicher discussed the use of steel supporting rail and asked how the buckling load was determined under such loading condition. M Gräfe responded that an average load at mid height was used.

H Blass and M Gräfe discussed the meaning of buckling of the CLT whether it is bending stiffness based or compression failure based.

S Aicher asked which width of the load distribution is considered. M Gräfe answered that it is the load corresponding to the width at mid height of the CLT panel. He also said that some FEM studies on 2D elements has been performed which show high capacity compared to individual columns.

A Frangi asked what happens when the load is not applied at the middle. M Gräfe said that the situation is not the same and will be different. He said that it will be a good future topic. A Frangi received confirmation that the beams were end sealed.

H Blass asked about the effective width for buckling design. M Gräfe explained that it is based on the load distribution angle to establish the width at mid height. H Blass said that if you have continuous load versus concentrated load and you cut out a strip, it would be too conservative. You could use a large effective width from the remaining part of the member which takes some loads.

U Kuhlmann commented that the load distribution needs to be examined carefully. There is a big different between parallel to face grain and perpendicular to face grain loading and the angle should be bounded to stiffness. M Gräfe responded that this is already considered based on the percentage of cross layers in the panel.

I Abeysekera asked how conservative is the proposed method compared to the length of effective width approach. I Abeysekera and M Gräfe discussed about the load distribution angle always between 20 to 30 degrees.

Tensile and Compression Strength of Small Cross Section Beech (*Fagus s.*) Glulam Members

Maximilian Westermayr, Wood Technology, Technical University of Munich,
Winzererstrasse 45, 80797 Munich, Germany, westermayr@hfm.tum.de

Peter Stapel, Wood Technology, Technical University of Munich

Jan-Willem van de Kuilen, Wood Technology, Technical University of Munich,
Biobased Structures and Materials, Delft University of Technology, The Netherlands

Keywords: Beech, Glulam, Truss member, Tensile strength, Compression strength, Grading

1 Introduction

The proportion of the wood species beech (*Fagus s.*) is currently increasing in central European forests. Simultaneously, a decreasing amount of forest areas covered by the economically important softwood species spruce (*Picea a.*) can be observed (German Federal Ministry of Food and Agriculture, 2015). As a result, a higher amount of beech timber is expected on the markets within the next years. Today, higher shares of beech stems grow into dimensions suitable for sawing.

Timber construction is a quantitatively interesting market for beech timber, as the hardwood species shows high mechanical potential. However, its application is currently limited to medium and high quality lamellas for glulam. For example, beech lamellas with pith are generally rejected according to the German visual grading standard for hardwoods DIN 4074-5. Lamellas for beech glulam must at least fulfil the requirements for the visual grade LS10 (Z-9.1-679), which excludes boards with pith. Based on the volume of the beech stems, the yield of lamellas suitable for glulam production reaches only ~20% (Torno et al., 2013). The use of lower lamella qualities could lead to a significantly higher profitability of beech glulam. Beside glulam subjected to bending, the application of beech glulam is conceivable in truss systems. Thereby, the truss members are stressed primarily in tension or compression.

This paper deals with the mechanical performance of beech glulam members loaded in tension and compression. Of special interest are the influences of different glulam built-ups on the load carrying capacity as well as lamination effects by applying different raw material qualities. These results can be used in the current standardization work for a hardwood glulam standard. Currently, corresponding findings for softwood are standardized in EN 14080. A further focus of this study is the prediction of glulam strength and stiffness properties by applying dynamic Modulus of Elasticity (*dyn. MoE*).

2 State of the Art

The German approval for beech glulam Z-9.1-679 refers to the visual grades given in DIN 4074-5. Lamellas must at least fulfil the requirements of visual grade LS10 for the lowest beech glulam strength class GL28h. For higher beech glulam strength classes, lamellas of the visual grades LS10 and LS13 in combination with additional threshold values for knots and *dyn. MoE* are required. However, strength grading of beech lamellas according to the visual parameters given in DIN 4074-5 does not appear to be very efficient for two main reasons.

First, the distinction into classes LS10 and LS13 does not lead to any class-wise differences in terms of mechanical properties. Westermayr et al. (2018) performed tensile testing on 214 low quality beech boards, which were visually graded according to the knot values valid for LS7, LS10 and LS13. In general, the application of a stricter knot threshold value did not result in a higher characteristic tensile strength. Furthermore, they found great mechanical potential in currently rejected lamella material.

Second, the high proportion of rejected lamellas leads to very low yield and thus often uneconomic products (Torno et al., 2013; Fischer, 2011). Dichtl (2018) examined the interaction between grading and yield. Amongst others, he found high amounts of rejected lamellas due to pith, which nevertheless showed tensile strength and stiffness suitable for structural applications.

As a consequence, in this investigation, current visual grading requirements for beech glulam lamellas are not applied except for those defects that might cause major problems in the glulam production process. Further on, finger-jointing was not implemented, which followed the intension of an easy and economic production process.

Investigations so far focused mainly on high quality beech timber and glulam subjected to bending (Ehrhart et al., 2016a, Frühwald et al., 2003; Glos et al., 2004). The results showed high mechanical potential for beech sawn timber as well as glulam. However, research focusing on low quality beech glulam stressed in tension or compression for the application in truss systems does not exist.

3 Materials and Methods

Raw material for the production of the glulam members were beech lamellas from Central Germany. As the influence of lamella quality on the mechanical performance of the glulam members was of special interest, two different collectives of beech lamellas were used for glulam production. Collective A consisted of the lowest sawn timber quality grade of sawmill *Pollmeier Massivholz* called “*Common Shop*”. The slightly steamed sawn timber includes a high amount of wood defects, like fibre deviation, pith, cracks, discoloration as well as knots and is sorted according to company specific visual characteristics. Preliminary tensile testing on a third collective consisting of 214 “*Common Shop*” beech boards showed high scatter in mechanical properties with a mean tensile strength of 33.6 N/mm² and a *COV* of 45% (Westermayr et al., 2018).

Collective B was available at TU Munich and consisted of middle and high quality beech lamellas, which were free of significant grain deviations and included just a low number of wood defects. Both collectives represented equal lamella numbers. A visual pre-grading was performed to exclude lamellas, which would cause major problems in glulam production, like big knot holes, a high variation in cross section along the lamella or decay. Thus, the initial lamella number of 248 was reduced by 8 to 240 lamellas. Half of the ~3100 mm long lamellas had the initial cross section of 100x24 mm² and 130x24 mm² respectively. Before glulam production, density, moisture content and *dyn. MoE* by eigenfrequency were determined for each lamella. Mean density of the lamellas was 723 kg/m³ with *COV* of 6 %, mean moisture content was 10.2 % with *COV* of 10 %. Two different glulam built-ups were realized, as shown in Figure 1.

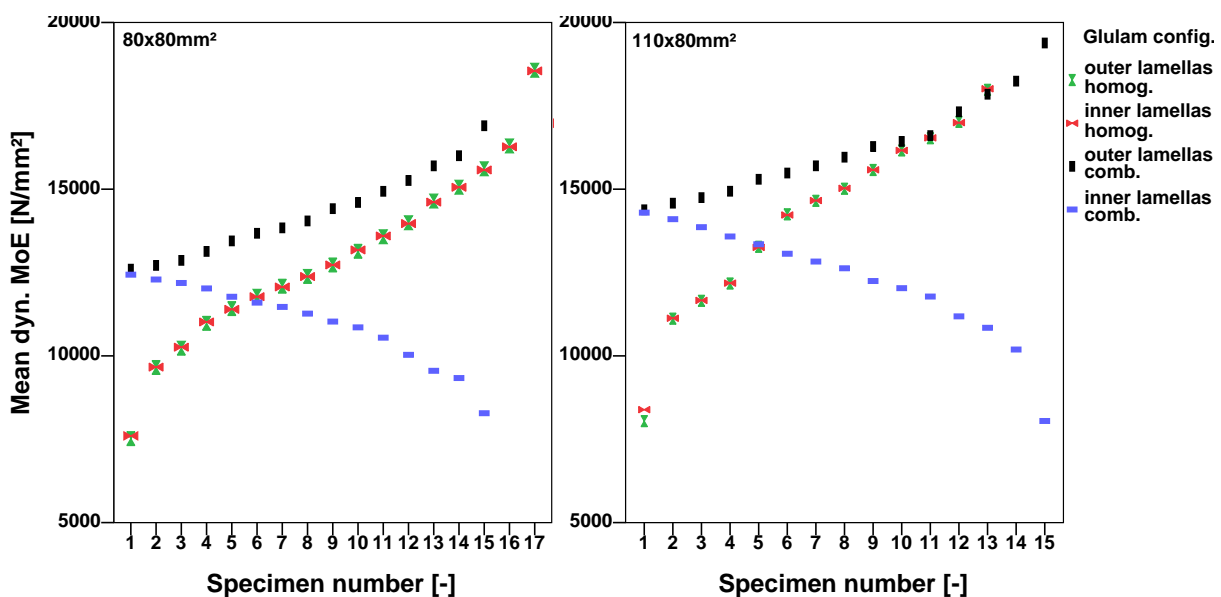


Figure 1: Mean *dyn. MoE* of the inner/outer lamellas depending on glulam configuration and cross section.

The figures show the mean *dyn. MoE* of the two inner and the two outer lamellas respectively for glulam cross sections of 80x80 mm² (Figure 1, left) and 110x80 mm²

(Figure 1, right). The inner and outer lamellas of the homogeneous glulam members, represented by the red and green symbols, show similar mean *dyn. MoE* values within a single glulam member. Values of the members/single lamellas range between $\sim 8000 \text{ N/mm}^2$ and $\sim 18000 \text{ N/mm}^2$. For combined glulam members, the mean *dyn. MoE* of the inner lamellas (blue symbols) decreases while mean *dyn. MoE* of the outer lamellas increases (black symbols). This results in an increasing *dyn. MoE* gradient between inner and outer lamellas, reaching a maximum gradient of around 10000 N/mm^2 for the $110 \times 80 \text{ mm}^2$ specimen with number 15. Instead of using random glulam layups, this approach allows the systematic examination of lamination and homogenization effects.

Glulam was produced by *Schaffitzel Holzindustrie*. The beech lamellas were planed to 20 mm thickness and glued with the MUF adhesive *Kauramin 683+688* of *BASF* according to the producers' specifications. After pressing and curing, the glulam members were planed to the final cross sections of $80 \times 80 \text{ mm}^2$ and $110 \times 80 \text{ mm}^2$, both made with 4 x 20 mm lamellas.

Tensile and compression specimens were cut out of the $\sim 3100 \text{ mm}$ long glulam members according to Figure 2.

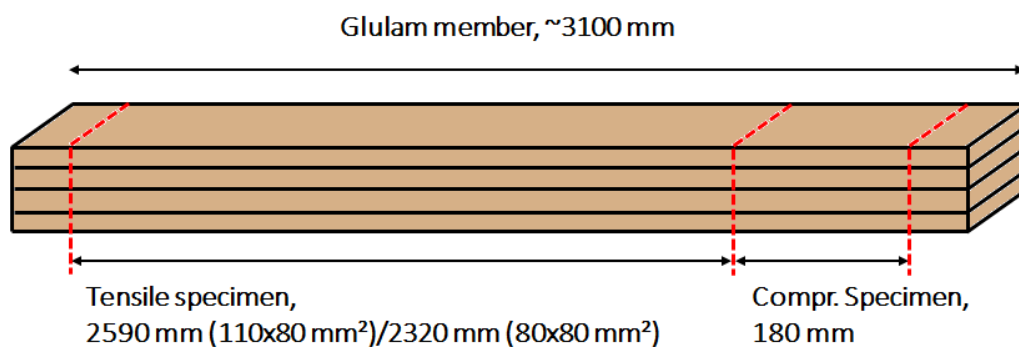


Figure 2: Sampling of the tensile and compression specimens.

Tensile specimens and tensile testing fulfilled the regulations of EN 408. Tensile specimens had total lengths of 2590 mm and 2320 mm and testing lengths of 990 mm and 720 mm depending on the cross section. Where possible, the weakest point was positioned within the testing length. Before tensile testing, the *dyn. MoE* of the tensile specimen got measured using eigenfrequency. The *dyn. MoE* measured on the tensile specimens was used in the data analysis for the corresponding compression specimens, which were cut out of the same glulam member.

Independent of the cross section, all compression specimens had a length of 180 mm and static *MoE* was measured over a length of 120 mm. The intention for the reduced testing length was the determination of a pure compression strength/stiffness value, as longer testing lengths may lead to buckling. Compression specimens were preferably free of defects. This was not always possible, especially for the bigger cross section, as only a short length of glulam remained after the tensile specimen was cut.

Before testing, specimens were stored at 20 °C and 65 %rh until constant mass was reached. Immediately after tensile testing, a piece was cut out of the tensile specimens to determine density and moisture content. Static *MoE* was adjusted to 12 % moisture content according to EN 384. *Dyn. MoE* was adjusted to 12 % moisture content according to Unterwieser & Schickhofer (2010).

4 Results and Discussion

4.1 Main results

The following table summarizes the results of the study. The results are distinguished between homogeneous and combined glulam members as well as cross sections.

Table 1. Main results of the investigation.

	Cross section	Configuration	n	Mean	COV	Min	Max
Tensile strength [N/mm ²]	80x80mm ²	Homog.	17	57.6	31%	25.4	85.0
		Comb.	15	63.2	18%	45.4	86.7
	110x80mm ²	Homog.	13	69.8	36%	31.9	100.7
		Comb.	15	72.5	12%	62.0	88.4
Tensile MoE [N/mm ²]	80x80mm ²	Homog.	17	12873	16%	9958	17564
		Comb.	15	12769	6%	11595	13832
	110x80mm ²	Homog.	13	14733	16%	10215	17287
		Comb.	15	14728	6%	13197	16297
Compression strength [N/mm ²]	80x80mm ²	Homog.	17	60.5	10%	49.7	70.8
		Comb.	15	59.8	5%	54.8	64.2
	110x80mm ²	Homog.	13	57.2	8%	48.5	62.6
		Comb.	15	58.2	5%	51.8	63.0
Compression MoE [N/mm ²]	80x80mm ²	Homog.	17	13272	15%	10936	16172
		Comb.	15	13487	10%	11381	15509
	110x80mm ²	Homog.	13	13781	12%	11908	17975
		Comb.	15	14669	12%	11784	18430

Mean tensile strength is ~60 N/mm² concerning the small cross section (80x80 mm²) and ~70 N/mm² concerning the big cross section (110x80 mm²). Furthermore, the mean tensile *MoE* of the big cross section is higher and exhibits a value of ~14730 N/mm² compared to the small cross section with ~12800 N/mm². Regarding compression, results are very homogeneous for both cross sections with strength values of ~60 N/mm² and stiffness values of ~13500 N/mm², the 110x80mm² specimens with combined lamellas excluded.

In general, the combined glulam members show two major differences compared to the homogeneous glulam members:

First, the minimum strength and stiffness values for tension and compression are higher. In terms of tensile strength, the minimum values increase from 25.4 N/mm² to 45.4 N/mm² for the small cross section and from 31.9 N/mm² to 62.0 N/mm² for the big cross section, which is an increase of ~50 %. Tensile stiffness values of the combined glulam members are around 25 % higher than the corresponding values of the homogeneous glulam members. This trend can also be observed in compression, although the increase in minimum strength is much lower.

Second, the scatter in the mechanical properties of the combined glulam members is lower than of the homogeneous glulam members. Depending on the cross section, the *COV* drops from 31 % to 18 % and from 36 % to 12 % concerning tensile strength and by ~50 % concerning tensile stiffness. The trend of lower *COVs* of combined glulam members than homogeneous glulam members is also noticeable regarding compression. An exception for both observations is the compression *MoE* of the bigger cross section, as minimum values and *COV* of combined and homogeneous glulam members appear to be similar.

The mentioned relations are confirmed when the cumulative frequencies of tensile and compression strength values are plotted, see Figure 3.

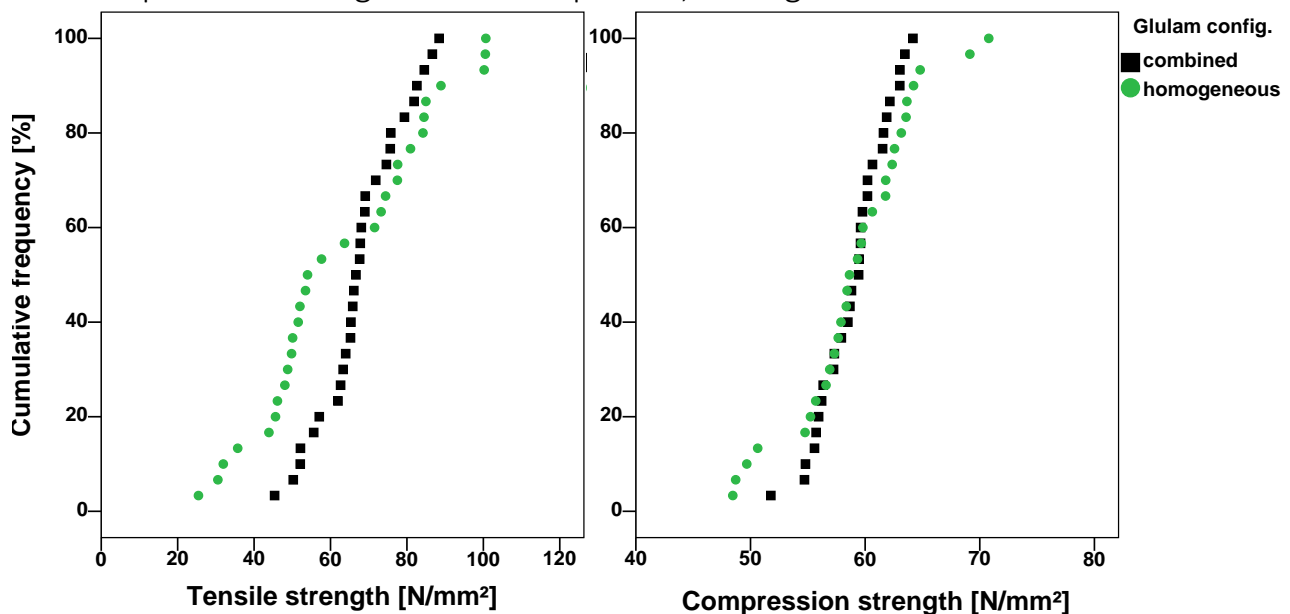


Figure 3: Cumulative frequencies of the tensile and compression strength depending on glulam configuration.

The combined glulam members show higher minimum and lower maximum strength values in tension and compression than the homogeneous glulam members. Thus, the specimens with combined lamella arrangement show a lower number of extreme values as well as a lower scatter of the strength around the mean value.

An explanation for these findings is a higher degree of homogenization by applying combined glulam members. Especially very low quality lamellas with high amounts of wood defects are compensated by the combination with higher quality lamellas. This was also observable during the testing procedure of the combined glulam members,

especially for specimens with a high gradient in the *dyn. MoE* between inner and outer lamellas. In many cases, one or even two of the low quality inner lamellas already failed, nevertheless load continued to increase just by the two outer lamellas taking up force. The effects of homogenization may also partly explain the higher mean tensile strength and stiffness values reached by the bigger cross section, as single wood defects like knots do not impact the 110 mm wide lamellas as much as the 80 mm wide lamellas. Further on, the wider lamellas included slightly higher wood qualities.

4.2 Relation between tensile and compression strength and stiffness

Looking at Table 1, it becomes obvious, that compression strength and stiffness values are very homogeneous with low scatter and do not differ a lot in terms of cross sections and lamella arrangement. In contrast, tensile strength and stiffness are heavily affected by cross section as well as glulam built-up and show in general a higher scatter. This may be a result of the different testing approaches defined in EN 408. On the one hand, the weakest point is within the testing range concerning tensile testing, which leads to high scatter of tensile strength and stiffness depending on the weak points' characteristic. On the other hand, compression testing is performed on specimens, which are preferably free of obvious wood defects and thus lead to more uniform compression strength and stiffness values.

An additional reason for the differences in tensile and compression strength and stiffness is the varying testing length. As testing lengths in this investigation were 720 mm and 990 mm for tensile testing depending on the cross section, compression testing was continuously performed on 180 mm long specimens. In consequence, the long testing lengths of the tensile specimens included a lot more wood defects than the compression specimens, which resulted in higher scatter of strength and stiffness values. All the mentioned effects are intensified as the lamellas represent the full range of timber qualities in combination with excluded visual grading before glulam production.

Hence, the relation between tensile and compression strength and stiffness need to be assessed carefully, as the following Figure 4 exemplifies.

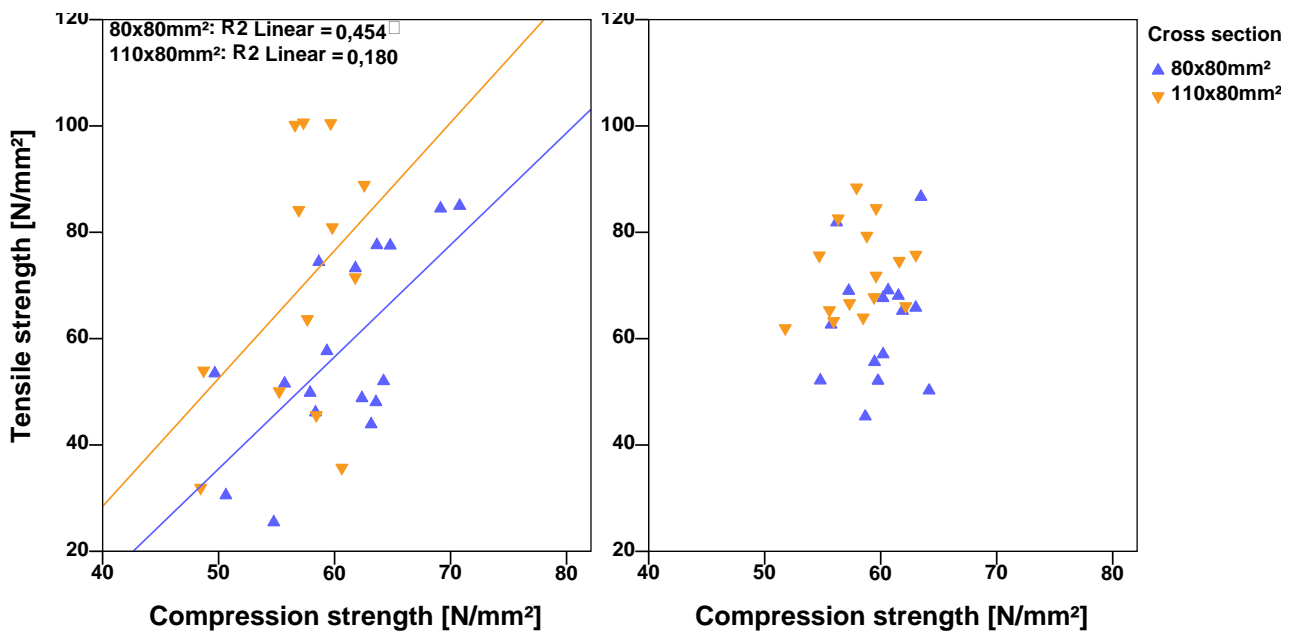


Figure 4: Relation between tensile and compression strength for homogeneous (left) and combined (right) glulam members.

The figure shows the relation of tensile and compression strength for homogeneous glulam members. The homogeneous glulam members with a cross section of 80x80 mm² exhibit a coefficient of determination of $R^2=0.45$ between tensile and compression strength, during the bigger cross section just exhibits a value of $R^2=0.18$. This may again be a result of volume effects. As the specimens with bigger cross section reach higher tensile strength values due to homogenization than the 80x80 mm² glulam members, the mainly defect free compression specimens remain on the same strength level for both cross sections. No correlation between tensile and compression strength was found for the combined glulam members as $R^2 < 0.1$. Low correlations were found regarding tensile and compression stiffness of homogeneous and combined glulam members.

4.3 Prediction of strength and stiffness properties

4.3.1 Relation of dyn. MoE single lamellas and dyn. MoE glulam member

For grading, it was of interest, if the *dyn. MoEs* of the four lamellas within one glulam member correlate with the *dyn. MoE* of the whole glulam member. Therefore, the *dyn. MoE* was measured once on the ~3100 mm long lamellas as well as on the resultant tensile specimens. The results are shown in Figure 5 separated by glulam configuration and cross sections.

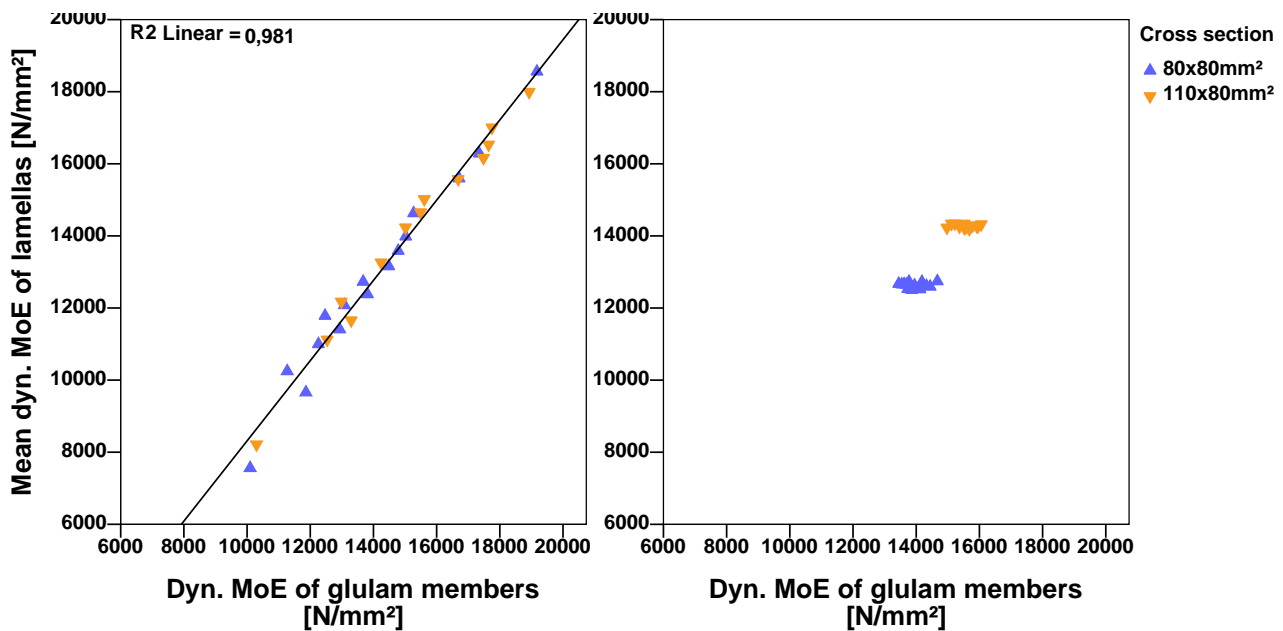


Figure 5: Relation between mean dyn. MoE of lamellas and dyn. MoE of homogeneous (left) and combined (right) glulam members.

The mean *dyn. MoE* of the four lamellas within a glulam member showed high correlation with the *dyn. MoE* of the glulam member. Concerning homogeneous glulam members, a correlation of $R^2=0.98$ was found (see Figure 5, left). Thereby, the glulam members showed slightly higher *dyn. MoE*s as the mean *dyn. MoE* of the single lamellas, especially for lower *dyn. MoE* values. The same trend can be observed concerning the combined glulam members (see Figure 5, right). The last mentioned showed a clear difference in the *dyn. MoE* values depending on the cross section as the bigger cross section included slightly higher lamella qualities.

4.3.2 Relation of *dyn. MoE* and strength/stiffness concerning homogeneous glulam

The relation between *dyn. MoE* and tensile strength is shown in figure 6.

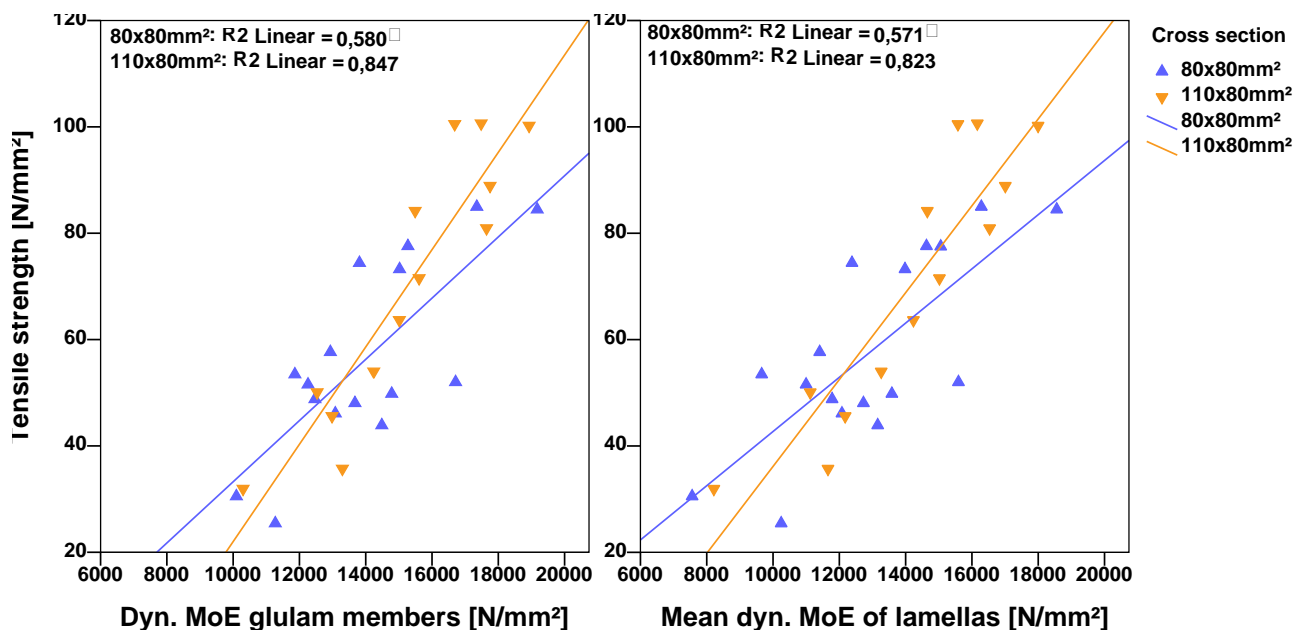


Figure 6: Relation of tensile strength and *dyn. MoE* of glulam members and lamellas.

The *dyn. MoE* of the glulam members (Figure 6, left) show good correlation with the tensile strength for both cross sections. Thereby, the bigger cross section shows higher correlation with $R^2=0.85$ than the smaller cross section with $R^2=0.58$. Applying the mean *dyn. MoE* of the single lamellas instead of the *dyn. MoE* of the glulam members leads to negligible lower correlations (Figure 6, right).

The correlation between *dyn. MoE* of the glulam members and stiffness gets even higher than strength with correlations of $R^2=0.95$ for the cross section of $110 \times 80 \text{ mm}^2$ and $R^2=0.72$ for the cross section of $80 \times 80 \text{ mm}^2$. Applying mean *dyn. MoE* of the single lamellas instead *dyn. MoE* of glulam members exhibit almost congruent correlations.

The different correlations concerning the cross sections may be a result of homogenization effects. Local wood defects of the same size have a greater effect on the smaller cross-section than on the larger one. This in turn leads to a greater variance in the mechanical properties of the smaller cross section.

Regarding the relation between *dyn. MoE* and compression strength, the exact opposite correlation can be observed concerning the cross sections, as it is given in Figure 7.

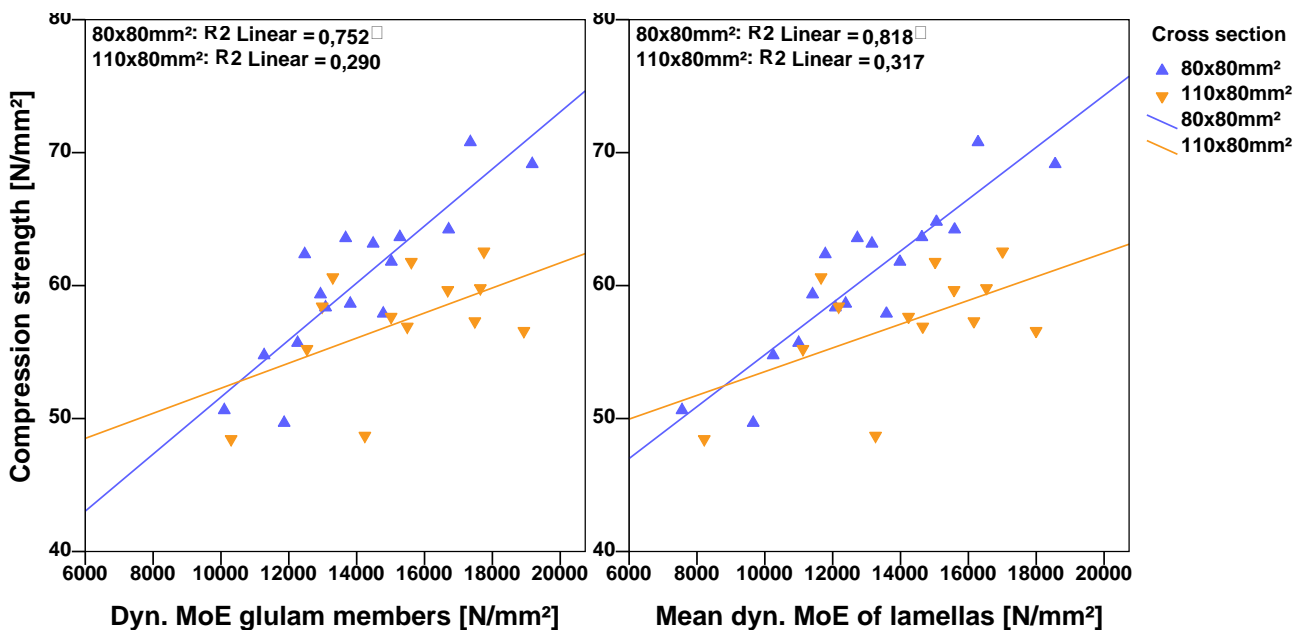


Figure 7: Relation of compression strength and *dyn. MoE* of glulam members and lamellas.

The *dyn. MoE* of the glulam members show high correlation with the smaller cross section as $R^2=0.75$ and lower correlation with the bigger cross section as $R^2=0.29$ (Figure 7, left). Applying the mean *dyn. MoE* of the lamellas instead of the *dyn. MoE* of the glulam members slightly increases the correlation to $R^2=0.82$ for the bigger and to $R^2=0.32$ for the smaller cross section (Figure 7, right).

Correlations of $R^2=0.4$ and $R^2=0.28$ are found for the cross sections $110 \times 80 \text{ mm}^2$ and $80 \times 80 \text{ mm}^2$ concerning *dyn. MoE* of the glulam members and static *MoE*. Applying mean *dyn. MoE* of the lamellas instead of *dyn. MoE* of the glulam members leads to similar correlations.

One reason for the lower correlation of *dyn. MoE* and strength regarding the bigger cross section may be a result of the specimen production. As the tensile specimens with a length of 2590 mm were cut out of the 3000 mm long glulam members, only around 300 mm remained for the choice of the compression specimen. In contrast, around 600 mm remained regarding the smaller cross section. In consequence, the probability to produce 110x80 mm² specimens free of defects was lower. This also results in lower mean as well as lower minimum and maximum compression strength values, see Table 1. In addition, defects within the specimens with bigger cross section are even more difficult to exclude by visual inspection, which consequently leads to lower strength values, too.

4.3.3 Relation of *dyn. MoE* and strength/stiffness concerning combined glulam

The increasing *dyn. MoE* of the outer lamellas with simultaneous decreasing *dyn. MoE* of the inner lamellas leads to more or less uniform mean *dyn. MoE* values on lamella and on glulam level. The resulting low scattering of the mechanical properties means that the use of vibration measurement in combined layups cannot be used to further limit the scattering of the mechanical properties. Figure 8 shows the mean *dyn. MoE* of the inner and of the outer lamellas and the corresponding strength values for the 80x80 mm² glulam members.

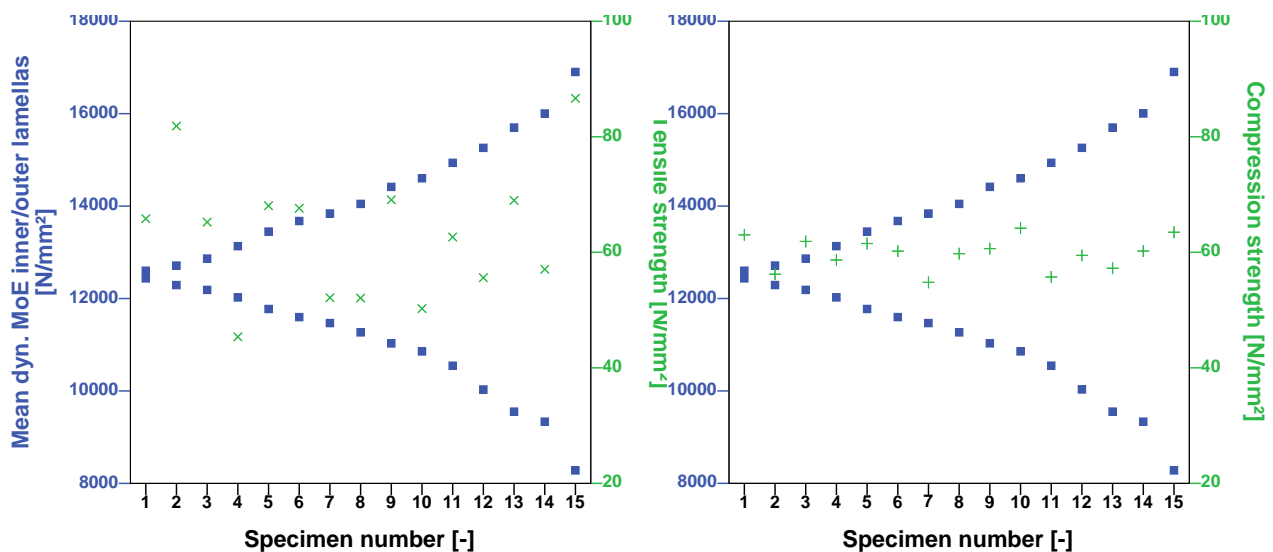


Figure 8: Relation between mean *dyn. MoE* of the inner/outer lamellas and the tensile strength (left) and compression strength (right).

The rising blue squares show the mean *dyn. MoE* of the outer lamellas and the corresponding declining blue squares the mean *dyn. MoE* of the inner lamellas. It can be seen, that tensile and compression strength show scatter independent of the gradient in the *dyn. MoE* between inner and outer lamellas. It seems, that a high proportion of low quality lamellas could be utilized in tensile and compression loaded combined glulam members. Simultaneously, lower scatter in the mechanical properties as well as higher mean tensile strength can be achieved by combined glulam members compared to homogeneous glulam members.

The relation between mean *dyn. MoE* of the inner/outer lamellas and the corresponding stiffness values is shown in Figure 9 for the 80x80 mm² glulam members.

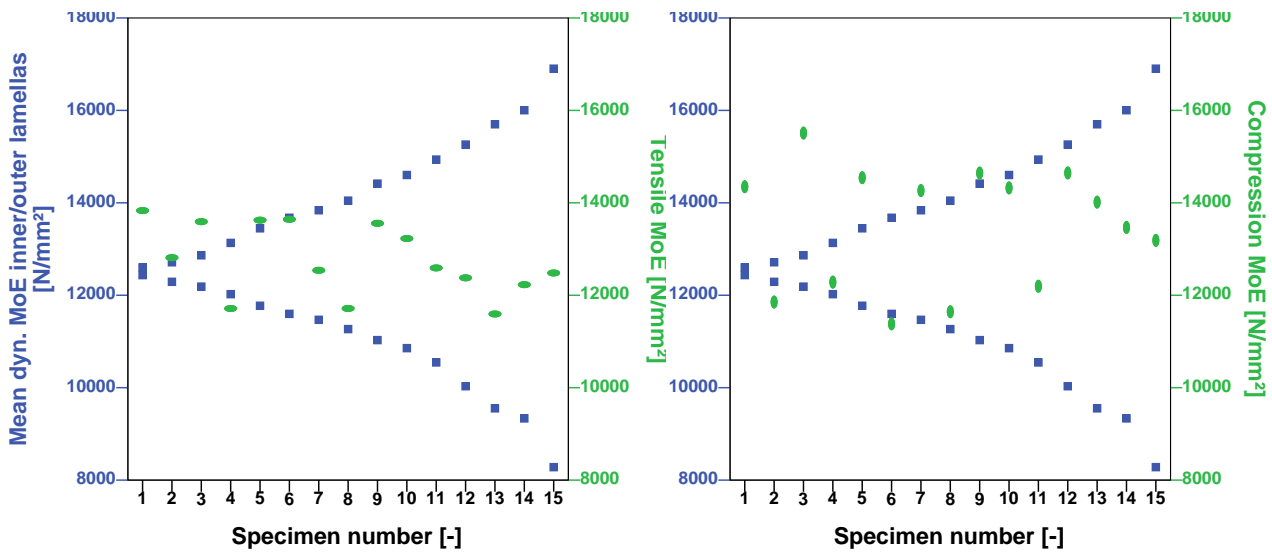


Figure 9: Relation between mean *dyn. MoE* of the inner/outer lamellas and the static tensile *MoE* (left) and static compression *MoE* (right).

The rising blue squares show again the mean *dyn. MoEs* of the outer lamellas and the declining blue squares the mean *dyn. MoEs* of the inner lamellas. Concerning tensile stiffness, the mean *dyn. MoE* of the lamellas allow a good estimation of the static *MoE*. The compression *MoE* shows higher scatter. Clearly, the *MoE* is determined on a much smaller and more homogeneous specimen than the tensile *MoE*, probably resulting in a higher scatter. There is a slight tendency that an increasing gradient in the mean *dyn. MoE* between outer and inner lamella leads to lower scatter of the static *MoE*.

The combined glulam members with a cross section of 110x80 mm² showed similar behavior.

4.3.4 Relation of density and strength/stiffness

No correlation between density of the glulam members and tensile strength is found. The same findings are observable regarding compression strength as well as tensile and compression stiffness and confirm the lacking correlation between density and tensile strength concerning beech given in literature in many occasions (e.g. Ehrhart et al., 2016b; Westermayr et al., 2018).

5 Conclusions

The tested beech glulam members show high mechanical performance in tension and compression. The comparatively low scatter in strength and stiffness is astonishing considering the partly extremely low raw material quality and the fact that only *dyn. MoE* was used as a single grading parameter. In addition, the *dyn. MoE* allows a good prediction of strength and stiffness properties on lamella or glulam level, while density shows no correlation with mechanical properties. Summarizing, the currently given

requirements for beech lamellas concerning visual grading according to Z-9.1-679 and DIN 4074-5 appear doubtful for beech lamellas. Data analysis showed lower scatter and higher mean values regarding tensile strength and stiffness values for glulam with combined built-up than for homogeneous glulam members.

The implementation of an additional knot threshold value might probably lead to even higher tensile strength values and less scatter, as minimum strength values may increase. On the other hand, this study illustrates possibilities of an economic product by applying high amounts of low quality beech sawn timber and easy grading. The findings of this study will be complemented with further investigations. Data analysis of a second compression collective is in progress, which was stored in service class 2 conditions according to EN 1995-1-1. Further on, buckling tests are going to be performed, consisting of combined and homogeneous beech glulam members with different slenderness ratios.

6 Acknowledgements

We want to thank the Bavarian Institute of Forestry (LWF).

7 References

- Dichtl T. (2018): Mechanical characteristics of low quality beech boards under tensile stress. In German. Masters Thesis Technical University of Munich.
- Erhart T., Fink G., Steiger R., Frangi A. (2016a): Experimental investigation of tensile strength and stiffness indicators regarding European beech timber. WCTE Conference, Vienna, Austria.
- Erhart T., Fink G., Steiger R., Frangi A. (2016b): Strength grading of European beech lamellas for the production of GLT & CLT. INTER Conference, Graz, Austria.
- Federal Ministry of Food and Agriculture (2015): The forests in Germany. Selected results of the third national forest inventory.
- Fischer C. (2011): Untersuchung zur Herstellung von Buchen-Brettschichtholzlamellen mittels Profilzerspanertechnologie. In German. Masters Thesis Technical University of Munich.
- Frühwald A., Ressel J.B., Bernasconi A. (2013): Hochwertiges Brettschichtholz aus Buchenholz. In German. Institut für Holzphysik und mechanische Technologie des Holzes, Bundesforschungsanstalt für Forst- und Holzwirtschaft Hamburg.
- Glos P., Denzler J. K., Linsenmann P. (2004): Strength and stiffness behavior of beech laminations for high strength glulam. Paper 37-6-3, CIB-W18 Proceedings Edinburgh, Scotland, Meeting 37.
- Torno S., Knorz M., van de Kuilen J.-W. (2013): Supply of beech lamellas for the production of glued laminated timber. ISCHP Conference, Florence, Italy.

- Unterwieser H., Schickhofer G. (2010): Influence of moisture content of wood on sound velocity and dynamic MOE of natural frequency- and ultrasound runtime measurement. European Journal of Wood Products 69: 171-181. DOI 10.1007/s00107-010-0417-y
- Westermayr M., Stapel P., van de Kuilen J.-W. (2018): Tensile strength and stiffness of low quality beech (*Fagus sylvatica*) sawn timber. Will be published in WCTE Conference proceedings, Seoul, South Korea.
- DIN 4074-5:2008: Strength grading of wood – Part 5: Sawn hard wood.
- EN 384:2016: Structural timber – Determination of characteristic values of mechanical properties and density.
- EN 408:2010+A1:2012: Timber structures – Structural timber and glued laminated timber – Determination of some physical and mechanical properties.
- EN 1995-1-1:2010: Eurocode 5: Design of timber structures – Part 1-1: General – Common rules and rules for buildings.
- EN 14080:2013: Timber structures - Glued laminated timber and glued solid timber – Requirements.
- Z-9.1-679:2014: Allgemeine bauaufsichtliche Zulassung BS-Holz aus Buche und BS-Holz Buche-Hybridträger. Deutsches Institut für Bautechnik.

Discussion

The paper was presented by M Westermayr

H Blass commented that the conclusion about the performance of combined glulam built up depends on the built up used. M Westermayr agreed and said that it may be considered in a later study.

F Lam commented that in N. America tension test of glulam is rarely done with its characteristic strength taken as a percentage of the bending strength. He asked whether there are plans to do some bending tests as a benchmark. M Westermayr answered no plans at this time.

S Franke commented that connection values are also important. M Westermayr said that they are working on screw values.

S Aicher commented that build up is important and depends on the number of laminates. Also tension strength of the laminae is important and will provide important information. M Westermayr responded that there are concerns about the dimensional stability of the laminae hence testing on members was studied. P Stapel added that there was previous test data on the strength properties of the low quality laminae and increase of sample size will not change the results.

A Frangi and M Westermayr discussed the merit of the concept of using beech as structural material and the continuing going after low quality laminae to achieve high strength. H Blass said that Beech LVL is a good example of high strength product made of low quality material.

T Ehrhart commented that EN 408 requires clear specimens for compression testing. M Westermayr said that with this quality of wood it is not always possible to find clear specimen easily. H Blass commented that as a research project one should look at the weakest part of glulam material.

T Ehrhart also discussed issues regarding material with reject grade which could be upgraded by cutting out the defects and finger joining.

M Frese commented that the size of the members in the material approval being different from the size of material considered in the testing and direct comparison should not be made.

Behaviour of Glulam and LVL Beams Loaded Perpendicular to the Grain

Lukas Windeck, Hans Joachim Blass

Karlsruhe Institute of Technology (KIT), Timber Structures and Building Construction

Keywords: Compression, Perpendicular to grain, Eurocode 5, Design, Model

1 Introduction

In most cases, wood behaves very ductile under a compression load perpendicular to the grain. Once the elastic limit is passed, only a small load increase can be measured with increasing deformation. Even if large deformations occur, a decrease of the load is rarely detected.

The design model in Eurocode 5 (EN 1995-1-1:2010-12) is based on the work of (Madsen 2001) and further on (Blaß and Görlacher 2004). The load carrying capacity perpendicular to the grain can be calculated with eq. (1).

$$\frac{F_{c,90,d}}{A_{ef}} \leq k_{c,90} \cdot f_{c,90,d} \quad (1)$$

A_{ef} is an effective contact area calculated with the existing contact length and a supporting grain length up to 30 mm per side. The factor $k_{c,90}$ depends on the support situation and is differentiated between sills and beams. For sills a value up to $k_{c,90}=1.5$ and beams a value up to $k_{c,90}=1.75$ is possible. Even though a real failure does not occur, the main focus of the model is on the ultimate limit state (ULS).

While the deformation of timber members may be easily calculated based on stiffness parameters E or G , and the deformations of mechanical connections are described by the slip moduli K_{ser} or K_u , timber design codes generally do not provide information regarding deformations in contact areas under loads perpendicular to grain. In consideration of the non-linear ductile behaviour and the reached deformations, a displacement based design model seems desirable.

Such a model is presented in the following which is derived from load deformation curves of tests. It is shown that the load can be split up in two parts: an effective compression stress perpendicular to the grain in the contact area itself and an additional part that can be described as the influence of the contributing grain length. For an overview of different models see (Leijten 2016).

2 Tests

To evaluate the model in EC5 and to create a basis for the development of a deformation based design approach, 386 tests (101 on glulam, 134 on softwood LVL beams and 151 on hardwood LVL beams) were performed. In the case of glulam, the contact length and the load situation were varied as shown in Figure . In tests with LVL the veneer orientation was additionally varied. Standard tests according to (EN 408:2012-10) were performed for all materials to generate the basic $f_{c,90}$ strength value for the sample. The tests were carried out with a loading speed of 3 mm/min up to a deformation of 15 mm over the beam height.

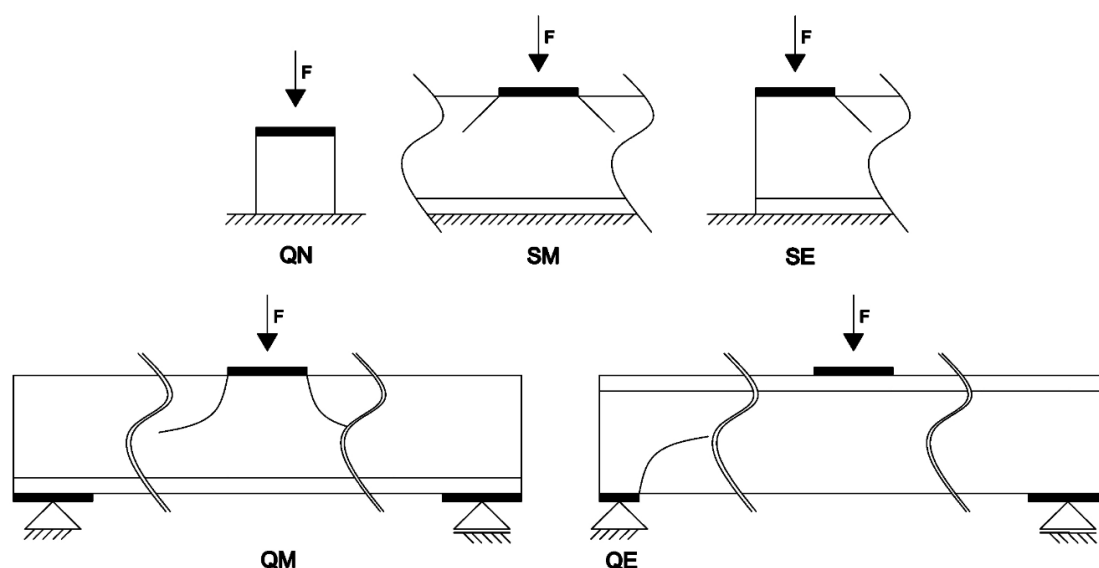


Figure 1 Tested load situations

2.1 Tests with Glulam

In the glulam tests, the contact length was varied from 50 to 200 mm with a constant beam width of 100 mm and a height of 300 mm. An overview of the tests is given in Table 1. The deformations were measured in three ranges: The upper 50 mm directly beneath the

Table 1 Performed tests on glulam

Contact length [mm]	number of tests				total
	50	100	150	200	
Tests according to EN 408 (QN)	-	-	-	20	20
Beam, two sided (QM)	6	6	6	6	24
Beam, one sided (QE)	6	6	-	-	12
Sill one sided (SE)	5	6	4	6	21
Sill, two sided (SM)	6	6	6	6	24

support were measured separately from the rest because plastic deformations only appear in this section. The lower 200 mm of the total measurement range of 250 mm were divided in two 100 mm long sections. The lowest lamella was made of beech LVL to avoid bending failure in the beam tests QM and QE. Every beam was loaded on different positions with a minimum clearance of 150 mm between contact areas to avoid influences of the neighboured contact areas. The tests which were performed according to EN 408 (series QN) provided a strength value of $f_{c,90,mean} = 3.24$ MPa and a modulus of elasticity of $E_{90,mean} = 326$ MPa. By means of (EN 14358:2013-09) a characteristic strength value of $f_{c,90,k} = 2.75$ MPa was calculated. A decrease of the load with increasing deformation values could not be measured.

Table 2 shows the measured deformations in the separate sections. The main part of the deformations occurs in the top part of the beam. The percentage in the top section is by far the biggest in all test series, and decreases with increasing contact length. In the following, the deformations over a beam height of 250 mm are considered taking into account deformations that occur in the middle and lower beam depth.

Table 2 Measured deformations in the separate sections on glulam

Series	Max. Mean Deformation [mm]	Deformation [mm]			Percentage of max. Deformation [%]		
		Top	Middle	Bottom	Top	Middle	Bottom
Q50	7,9	6,5	1,1	0,2	83,2	14,4	2,4
Q100	7,9	5,9	1,5	0,5	74,5	19,5	6,0
Q150	7,6	5,5	1,7	0,3	73,0	22,9	4,1
Q200	7,6	5,5	1,7	0,4	72,3	22,2	5,5
QE50	6,6	5,1	1,3	0,2	77,3	19,3	3,3
QE100	5,6	3,9	1,3	0,3	69,4	24,0	6,6
SM50	6,8	5,6	0,9	0,3	82,4	13,4	4,3
SM100	7,6	5,4	1,7	0,5	71,6	21,6	6,8
SM150	8,0	5,5	1,9	0,6	69,0	23,6	7,4
SM200	8,6	5,5	2,3	0,8	64,1	26,5	9,4
SE50	7,8	5,6	1,7	0,5	71,5	21,8	6,7
SE100	8,6	5,5	2,3	0,9	63,5	26,0	10,4
SE150	9,2	5,4	2,7	1,1	58,8	28,8	12,3
SE200	10,9	5,3	4,1	1,5	50,1	36,5	13,4

2.2 Tests with softwood LVL

Tests were carried out only with sills and according to EN 408. In total, 134 tests were performed with contact lengths from 50 to 400 mm. Additionally the veneer orientation was varied: The load was applied either parallel or perpendicular to the veneer orientation. The beams with a perp. veneer orientation had a height of 280 mm and a

Table 3 Performed tests on softwood LVL

	Orientation	Type	Contact length [mm]				total
			50	100	200	400	
Type C	⊥	SE	5	5	5	5	20
		SM	5	5	5	4	19
		QN	-	-	5	-	5
		SE	5	2	5	5	17
		SM	5	5	5	4	19
		QN	-	-	5	-	5
Type P	⊥	SE	2	3	4	3	12
		SM	4	2	2	-	8
		QN	-	-	3	-	3
		SE	3	4	3	-	10
		SM	3	4	3	-	10
		QN	-	-	6	-	6

width of 100 mm (89.25 mm in the case of LVL type P⊥). Those with a veneer orientation parallel to the load had a height of 220 mm and a width of 80 mm (105.5 mm in the case of LVL type P||). LVL with only parallel (type P) and with 20 % cross laminated (Type C) veneers was tested. Table 3 shows an overview of the tests. Tests according to EN 408 with specimens loaded perp. to the veneer orientation resulted in $f_{c,90,mean} = 3.6$ MPa independent of type P or Type C. With EN 14358 $f_{c,90,k} = 3.0$ MPa ($E_{c,90} = 170$ MPa) for type P ⊥ and $f_{c,90,k} = 3.2$ ($E_{c,90} = 180$ MPa) for Type C ⊥ was calculated. The stress direction parallel to the veneer orientation resulted in $f_{c,90,mean} = 8.9$ MPa ($f_{c,90,k} = 8.0$ MPa, $E_{c,90} = 460$ MPa) for LVL-P and $f_{c,90,mean} = 9.3$ MPa ($f_{c,90,k} = 8.2$ MPa, $E_{c,90} = 1800$ MPa) for LVL-C. If the beam was loaded perpendicular to the veneer orientation no decrease in the load could be detected on type P and Type C beams. In contrast, the specimens loaded parallel to the veneers show a decreasing load as a result of veneer buckling (Figure 2).

2.3 Tests performed on hardwood LVL

For hardwood LVL the same geometries and contact lengths were tested as for softwood LVL. Only



Figure 2 Failure of parallel loaded LVL due to buckling (left)



Figure 3 Failure of hardwood LVL Type P loaded perpendicular to the veneers

Table 4 Performed tests on hardwood LVL

	Orientation	Type	Contact length [mm]				total
			50	100	200	400	
Type C	⊥	SE	5	5	5	-	15
		SM	5	5	5	-	15
		QN	-	-	5	-	5
		SE	5	5	5	-	15
		SM	5	5	5	-	15
		QN	-	-	5	-	5
Type P	⊥	SE	5	5	5	3	18
		SM	5	4	5	2	16
		QN	-	-	15	-	15
		SE	4	5	3	-	12
		SM	5	5	-	-	10
		QN	-	-	10	-	10



Figure 4 Veneer buckling at hardwood LVL Type C loaded parallel to the veneers

for hardwood LVL Type C the contact length of 400 mm was not considered. An overview of the tests is shown in Table 4. For hardwood LVL type P loaded perpendicular to the veneers a decrease of the load with increasing deformation could be observed. The same applies to hardwood LVL Type C with a one sided projecting end (Test SE). Type P shows a rolling shear failure (Figure 3). One reason for this failure mode could be the use of a spherical calotte. Because of the high loads it was necessary to use a different testing machine for which only a spherical calotte could be used. If the load was oriented parallel to the veneers on type P only the tests according to EN 408 showed a decreasing load. This behaviour could not be detected during tests performed with sills.

The tests according to EN 408 on type P ⊥ resulted in $f_{c,90,mean} = 16.5$ MPa ($f_{c,90,k} = 14.8$ MPa, $E_{c,90} = 790$ MPa) and type P || in $f_{c,90,mean} = 18.2$ MPa ($f_{c,90,k} = 16.3$ MPa, $E_{c,90} = 860$ MPa). The strength value for Type C ⊥ calculates as $f_{c,90,mean} = 16.3$ MPa ($f_{c,90,k} = 14.6$ MPa, $E_{c,90} = 800$ MPa) and for Type C || as $f_{c,90,mean} = 21.2$ MPa ($f_{c,90,k} = 18.5$ MPa, $E_{c,90} = 3100$ MPa).

The failure of Type C loaded parallel to the veneer orientation is also characterised by buckling of the veneers (Figure 4).

3 Displacement based Design Approach

3.1 Introduction

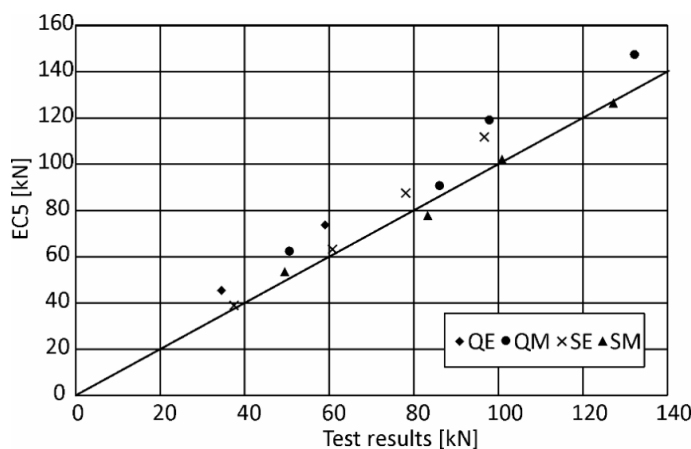


Table 5 Calculated values for $k_{c,90}$ and according to EC5

series	$k_{c,90}$	
	EC5	Tests
QM	1,75	1,52
QE	1,75	1,37
SM	1,50	1,50
SE	1,50	1,37

Figure 5 Calculated values according to EC5 in comparison to the test results at 5 mm deformation

For the comparison of the test results with the calculated values according to EC5 a total deformation of 5 mm is assumed. This corresponds to a strain of 2 % over the measured 250 mm which is a common value for the load carrying capacity perpendicular to the grain. Figure 5 shows the calculated load carrying capacities according to EC5 compared to the test results at a total deformation of 5 mm. For the calculation the $f_{c,90,mean}$ -value was used. It is apparent that the calculated values for the configuration SM (triangles) agree well with the test results. But for every other configuration the values according to EC5 are higher than the test results and deviate up to 24 %. Considering all investigated load situations, the mean ratio between EC5 and the tests is 1.11 with a standard deviation of 0.09 (COV = 8.5 %)

In EC5, the value for $k_{c,90}$ is distinguished between the support situation of sills or beams. If the coefficient $k_{c,90}$ is recalculated with the test results and eq. (1) for all assessed configurations, it is evident that $k_{c,90}$ depends on the load distribution (see Table 5, one sided or two sided) rather than on the sill or beam situation.

3.2 Derivation on the basis of glulam test results

Because of these observations it appears to be necessary to develop a new design approach for perpendicular to the grain loads. In accordance with (Madsen 2001) the load perp. to the grain is split into two parts: an effective compression stress perp. to grain in the contact area and a part that can be described as the influence of projecting grain. This is shown by comparing tests with different contact lengths see (Figure 6). A load-slip curve from one configuration with a certain contact length only provides the combined resistance of contact area and projecting ends. In order to isolate both contributions, the following hypothesis is assumed:

Both, the contribution of the contact area as well as the one from the projecting ends are independent of the contact length.

Based on this hypothesis, the load deformation curves of two test configurations with different contact lengths are subtracted from each other. Since the contribution from the projecting ends constitutes the same part in each load-deformation curve, the result from the subtraction is the pure contribution from the contact length $\ell_1 - \ell_2$ similar to a result from a test performed according to EN 408.

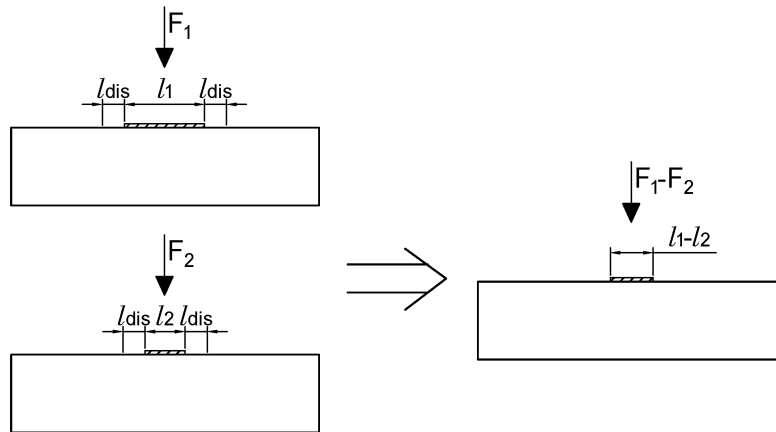


Figure 6 Procedure for the calculation of the effective compression stress perp. to the grain

The effective compression perp. to grain stresses for glulam, test series SE, are shown as an example in Figure 7.

It is obvious that the calculated stress deformation curves result in similar stress values. This means that every contact area provides the same resistance, independent of the

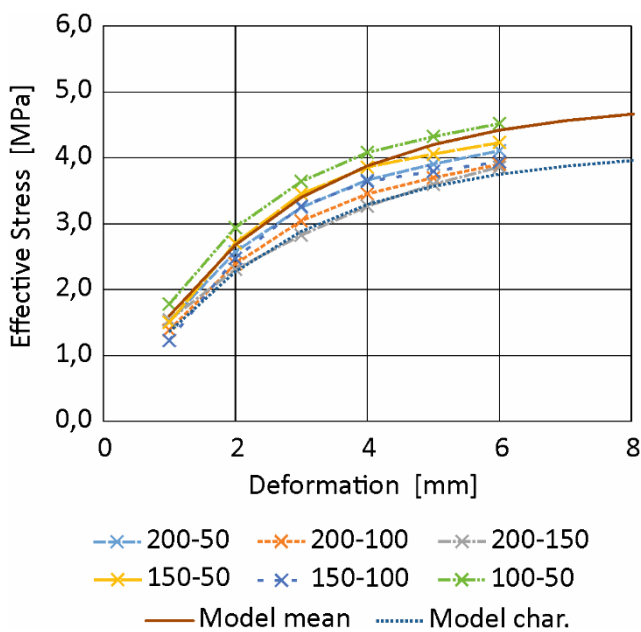


Figure 7 Calculated effective stresses for Glulam series SE

contact length. The curves can be approximated based on the compression perp. to grain strength $f_{c,90}$ determined according to EN 408. For this purpose, an effective stress depending on the deformation perp. to grain is calculated with eq. (2). The factors k_a and k_b are material specific and amount to $k_a = 1.5$ and $k_b = 0.4$ for glulam with a one sided load distribution. The calculated values are pictured in Figure 7 as well. The approximated values agree well with the calculated effective stresses. If the effective compression stresses perp. to grain are calculated with the **characteristic** strength value $f_{c,90,k}$, the values are as expected on the lower end of the array of curves (see Figure 7).

$$\sigma_{c,90,eff}(u) = k_a \cdot (1 - e^{-k_b \cdot u}) \cdot f_{c,90} = k_{c,90}(u) \cdot f_{c,90} \quad (2)$$

In the next step, the contribution of the projecting grain length ℓ_{dis} is determined. For this purpose, the contribution from the contact area is deducted from the load-displacement curves from the tests. In the subsequent calculation of the load the strength value according to EN 408 is used. Therefore, the contributing grain length is calculated with this value. Eq. (3) results in the contributing grain length for each step of deformation. These values are pictured in Figure 8. It is apparent that with increasing deformations the contributing grain length increases as well. This seems plausible since the continuous wood fibres provide higher resistance for larger deformations perp. to the grain. Because of the nonlinearly increasing values, an elastic-plastic material behaviour of the contributing grain length is assumed as well.

$$\ell_{dis}(u) = \frac{F(u) - \sigma_{c,90,eff}(u) \cdot b \cdot \ell}{f_{c,90,mean} \cdot b} \quad (3)$$

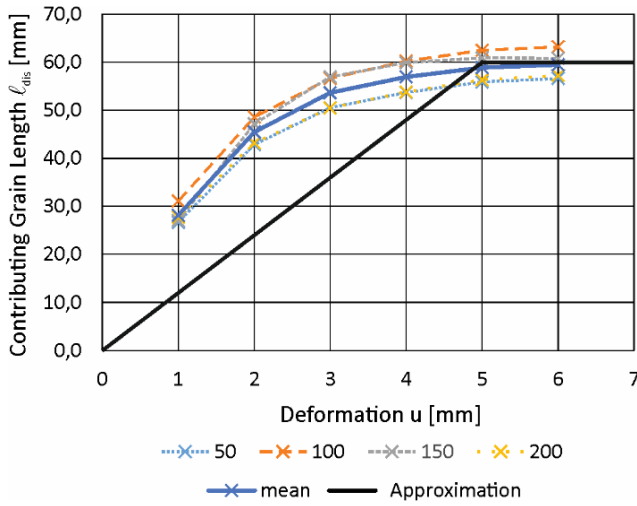


Figure 8 Contributing grain length depending on the deformation for glulam, series SE

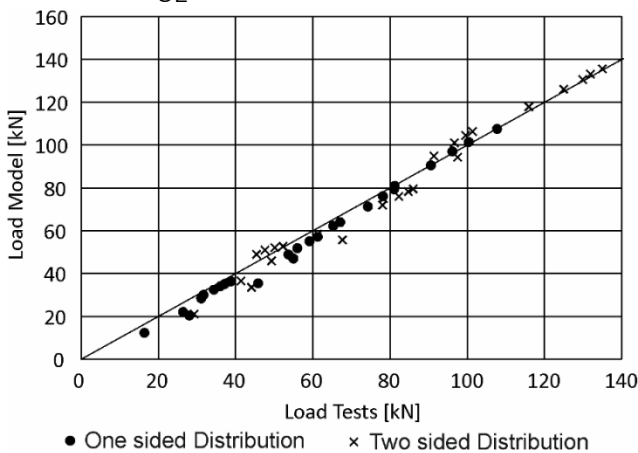


Figure 9 Comparison of model values and test results for glulam in a range of 1 to 12 mm deformation

To keep the calculation of the load simple, the contributing grain lengths is approximated as well. In a range of 5 mm to 15 mm of deformation, a constant share of 60 mm can be assumed. For smaller deformations the values may be interpolated with $u = 0$ mm and $\ell_{dis} = 0$ mm.

The same calculation process is performed for a middle loaded sill (two sided load distribution) resulting in $k_a = 1.7$, $k_b = 0.6$ and $\ell_{dis} = 40$ mm. For simplicity, the same contributing grain length of $\ell_{dis} = 40$ mm per support side is proposed, even though the calculated length for a one sided load distribution is larger than for a two sided distribution.

For the calculation of the deformation dependent load perp. to the grain both contributions are added resulting in eq. (3.3). For the determination of ℓ_{dis} a distinction between one or two sided projecting member ends is necessary.

$$F_{c,90,R}(u) = b \cdot (\ell \cdot k_{c,90}(u) + \ell_{dis}) \cdot f_{c,90} \quad (4)$$

Figure 9 shows the calculated values according to eq. (4) compared to the test results in steps of 1 mm deformation. The values are calculated with $f_{c,90,mean} = 3.24$ MPa. A good agreement is evident and the deviations of the model to the test values are lower compared to the EC5 values. The overall mean ratio is 0.99 with a standard deviation of 0.08 (COV = 7.8 %).

3.3 LVL

The same approach is used for softwood and hardwood LVL. In the following, the different test series are considered and the design approach is applied.

3.3.1 Softwood LVL Type P

At first, a load perpendicular to the veneer orientation is considered. Figure 10 shows the calculated effective stresses of an end loaded sill for a load perpendicular to the veneers. The same applies as for glulam. All the calculated stress values are between 4 MPa and 5.5 MPa for large deformations. The calculation of the factors for Eq. (2) results in $k_a = 1.6$ and $k_b = 0.2$ for a one sided load distribution and $k_a = 1.8$ and $k_b = 0.2$ for a two sided load distribution (not shown). The contributing grain length ℓ_{dis} is calculated with

the procedure given above as 46 mm for a one sided and 41 mm for a two sided load distribution in a range of 5 to 15 mm deformation. A constant value of $\ell_{dis} = 40$ mm is used in the model whereas the values are interpolated in a range of 0 to 5 mm deformation.

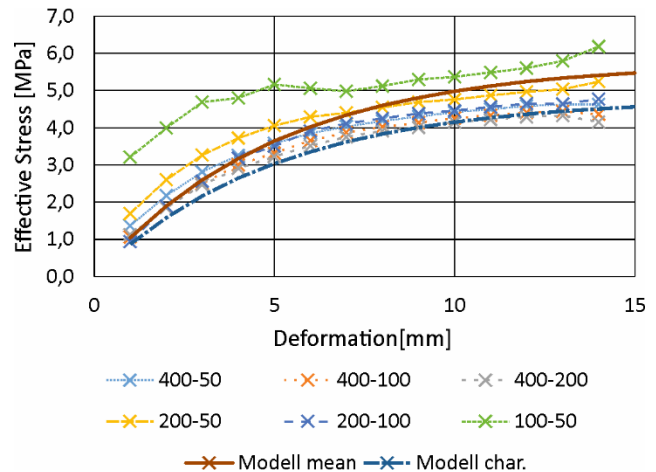


Figure 10 Calculated effective stresses for softwood LVL P \perp , series SE

3.3.2 Softwood LVL Type C

Softwood LVL Type C behaves similarly for both load configurations as softwood LVL type P. Due to the cross laminated veneers, the behaviour is stiffer, especially if the load is applied parallel to the veneers.

If the load is applied perpendicular to the veneers, no load decrease can be detected. Therefore, the deformation based design approach is suitable. Figure 11 shows the effective stresses for an end loaded sill depending on the deformation. The effective stresses in the contact area are in a range of 4 MPa to 5 MPa as well. If the factors k_a and k_b for the use with eq. (2) are set to $k_a = 1.4$ and $k_b = 0.2$, a good agreement with the calculated stresses is evident (see Figure 11).

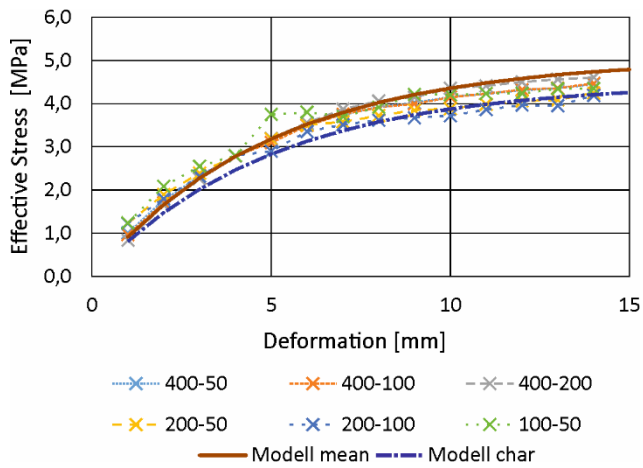


Figure 11 Calculated effective stresses for softwood LVL type C \perp , series SE

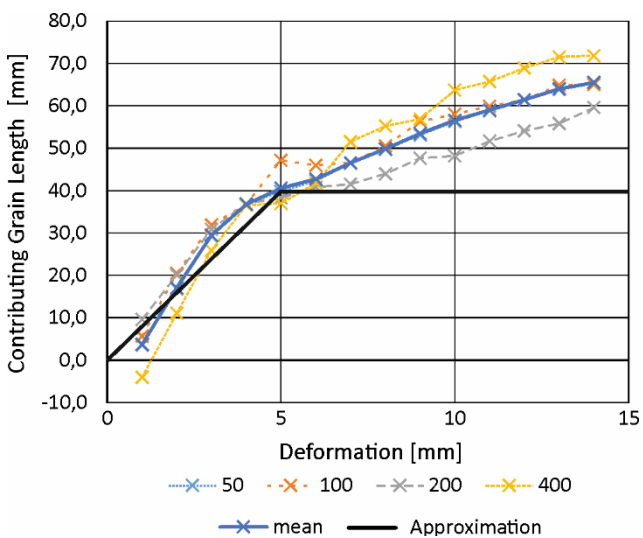


Figure 12 Contributing grain length for softwood LVL type C \perp , series SE

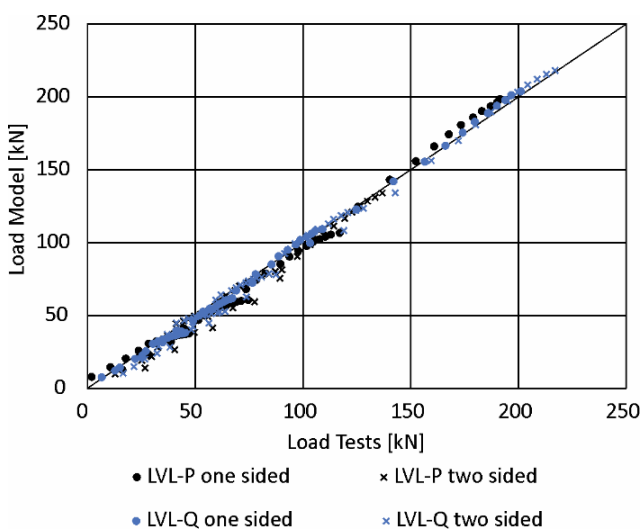


Figure 13 Comparison of the calculated load carrying capacities to the test results for softwood LVL \perp in the range of 1 to 15 mm deformation

Figure 12 shows the contributing grain length for softwood LVL Type C with a load perpendicular to the grain. At the beginning, a linear increase is visible. Plastic effects occur when the loads are above the proportional limit. The negative value for the series SE400 can be explained with slip in the experimental setup. A calculation of ℓ_{dis} results in a value of 45 mm for a one sided distribution and 40 mm for a two sided distribution. A constant value of 40 mm is assumed in the model for deformations between 5 and 15 mm.

In Figure 13 a comparison between the calculated values according to eq. (4) and the test results at a deformation from 1 mm to 15 mm is shown. All tested contact lengths are included. The mean ratio is 0.98 and the standard deviation 0.08 (COV = 8.2 %).

3.3.3 Hardwood LVL Type P

A decrease in load was not observed for hardwood LVL type P \parallel . Figure 14 shows the calculated effective stresses for hardwood LVL type P \parallel , series SE. For a deformation of 14 mm, values of 20 MPa to 25 MPa are reached whereby the behaviour at large deformations is stiffer than for glulam or softwood LVL. With $k_a = 1.6$ and $k_b = 0.15$, a good fit is reached. For larger deformations, the approximated values deviate from the calculated stresses. This is because the chosen value for the contributing grain length ℓ_{dis} in the model deviates from the calculated value for a one sided load distribution. The values for the contributing grain length are pictured in Figure 15. A constant value of 37 mm for a one sided and 28 mm for a two sided distribution can be calculated, and a value of $\ell_{dis} = 30$ mm is chosen for

the model in a range of 5 to 15 mm deformation. For a two sided distribution the same values for k_a and k_b are valid.

Figure 16 shows a comparison between the calculated and the measured loads for hardwood LVL type P ||. This leads to a mean ratio of 0.99 with a standard deviation of 0.09 (COV = 9.1 %).

3.3.4 Hardwood LVL Type C

As stated in section 2.3, hardwood LVL Type C behaves like softwood LVL Type C. Therefore, the load configuration perpendicular to the veneers is considered first. Figure 17 shows the calculated effective stresses of hardwood LVL Type C \perp , series SE. At 14 mm deformation an effective stress of 20 MPa is reached. With the factors $k_a = 1.5$ and $k_b = 0.15$ for eq.(2), the values for a one sided distribution can be approximated depending on the deformation. A consideration of the contributing grain length shows a very low scattering of the calculated values independent of the deformation and contact length (see Figure 18). Even at large deformations no completely plastic behaviour is visible. A constant value of $\ell_{dis} = 40$ mm is calculated for a one sided load distribution for larger deformations. For a two sided load distribution the values $k_a = 2.0$ and $k_b = 0.1$ can be used for an approximation of the effective stresses. A value of $\ell_{dis} = 40$ mm results for a two sided distribution for deformations between 5 and 15 mm as well. Figure 19 shows the calculated loads in comparison to the test values in a range of 3 mm to 15 mm. The mean ratio is 0.99 with a standard deviation of 0.08. Due to the higher residual stiffness at larger deformations and the assumption of a constant share of the

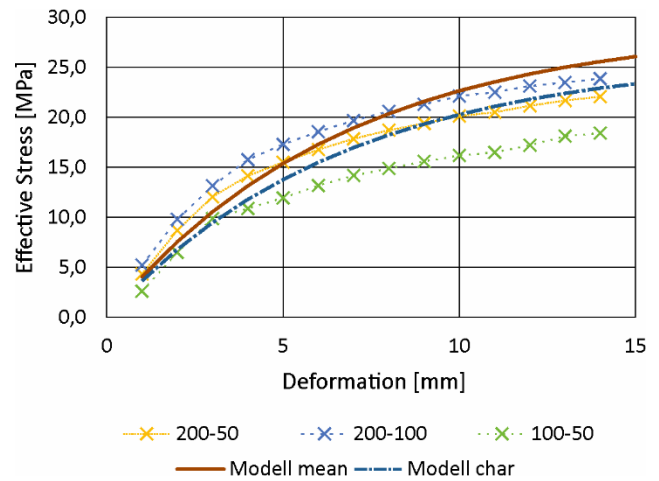


Figure 14 Calculated effective Stresses for hardwood LVL type P ||, series SE

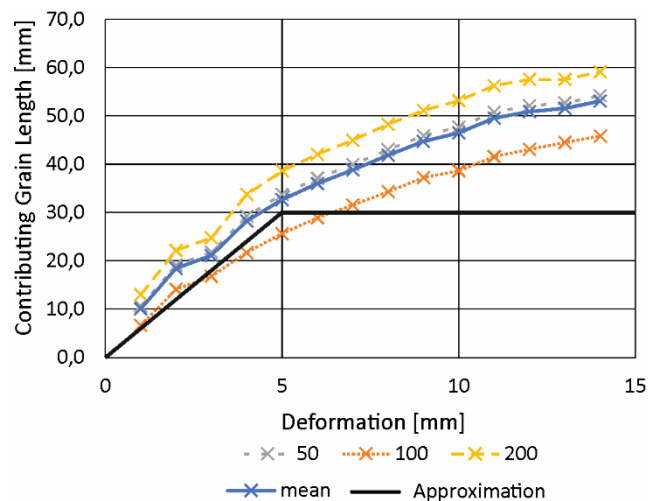


Figure 15 Contributing grain length for hardwood LVL type P ||, series SE

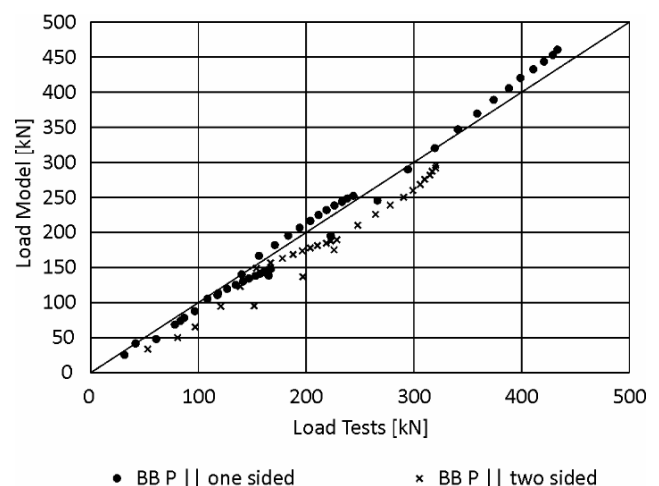


Figure 16 Comparison of the calculated load carrying capacities to the test results for hardwood LVL type P || in the range of 1 to 15 mm deformation

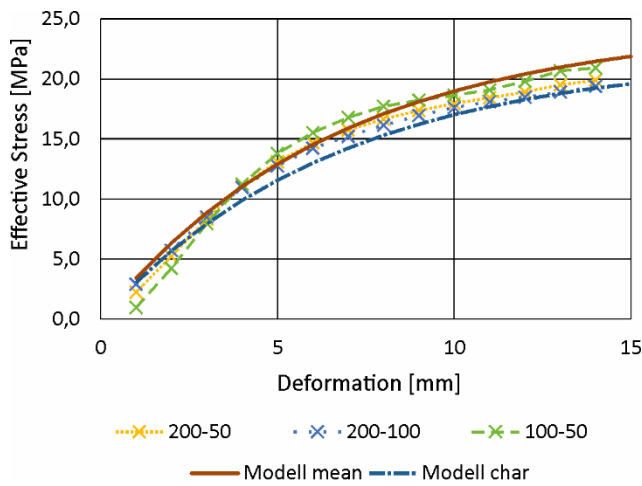


Figure 17 Calculated effective stresses for hardwood LVL Type C ⊥, series SE

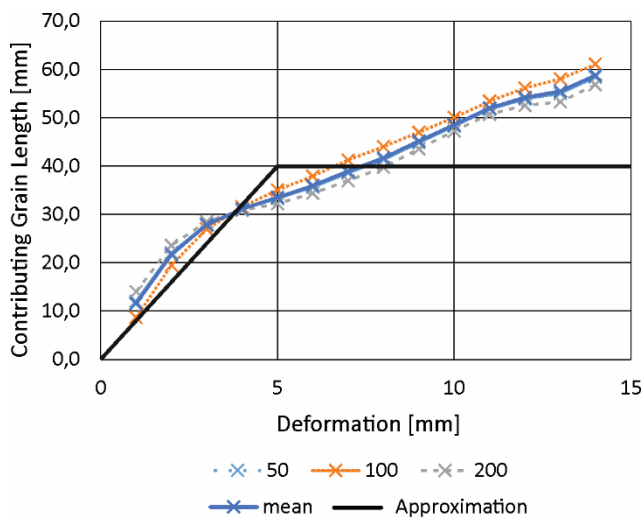


Figure 18 Contributing grain length of hardwood LVL Type C ⊥, series SE

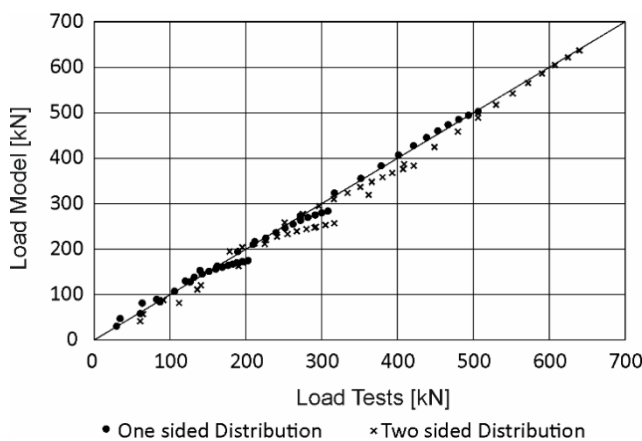


Figure 19 Comparison of the calculated load carrying capacities to the test results for hardwood LVL Type C ⊥ in the range of 1 to 15 mm deformation

contributing grain length, the deviations increase with increasing deformations, but are conservative.

3.4

Materials with a decreasing load at larger deformations

Some of the tested materials show decreasing loads at larger deformations. For these, the presented approach is not suitable. The maximum load carrying capacity, however, can be expressed in a similar way. For this purpose, a factor $k_{c,90}$ is introduced that can be calculated with the maximum effective stress and the compression strength perp. to the grain.

In the case of softwood LVL type P ||, a decreasing load due to veneer buckling (see Figure 2) with increasing deformation was observed. Therefore, the calculation of $k_{c,90}$ is only suitable up to a deformation of 6 mm because the maximum value is reached in this point. A value of $k_{c,90} = 1.0$ is appropriate for softwood LVL type P ||. A calculation of the contributing grain length ℓ_{dis} with the same method is possible up to the start of the load decrease. This results in a value of $\ell_{dis} = 25$ mm.

For softwood LVL Type C || a decreasing load with increasing deformation was observed as well. As for LVL type P ||, it is possible to calculate the contributing grain length ℓ_{dis} until the maximum load carrying capacity is reached at a deformation of 2 to 3 mm. This results in a value of $\ell_{dis} = 25$ mm and a $k_{c,90} = 1.3$ can be calculated at this point.

Due to the ductile rolling shear failure in hardwood LVL type P ⊥ at higher deformations, a decreasing load was observed.

A calculation of ℓ_{dis} results in 30 mm per side as well. Although the load can be increased up to a deformation of 14 mm, only one value of $k_{c,90} = 1.6$ is proposed for hardwood LVL type P loaded perpendicular to the veneers because the damage is not local as for glulam but can be seen throughout the whole cross section (see Figure 3).

As stated in section 2.3, a decreasing load with increasing deformation for hardwood LVL Type C || could be detected. Therefore, the approach is not suitable. Nonetheless, the contributing grain length can be calculated to 30 mm as well. The maximum load carrying capacity occurs at a total deformation of 10 mm. For this, a $k_{c,90}$ of 1.35 can be calculated.

4 Discussion

The currently valid design model for the load carrying capacity perpendicular to the grain does not allow assessing deformations. A pure ULS is assumed. Also a consideration of the load carrying capacity depending on the strain (see (van der Put 2008)) seems not suitable. A short example is supposed to illustrate this: On a beam with a height of 400 mm 4 % compression result in a deformation of 16 mm while on a 100 mm high beam the same compression results in only 4 mm of deformation. Therefore, a limitation of the beam height needs to be performed as proposed by (Leijten 2016), where a maximum height of 140 mm is stated.

In many cases the consideration of an ULS for specific wood products seems not necessary. This particularly applies to sills. Exceptions are locally supported beams, e. g. intermediate supports in continuous beams, where a local deformation reduces the effective beam height required for the bending and shear capacity. Therefore, a large deformation caused by a load perpendicular to the grain may lead to a failure not perpendicular to the grain but in bending. On the contrary, for continuously supported beams or end supports of locally supported beams, a serviceability limit state (SLS) is more suitable because no failure under compression perpendicular to the grain occurs. So in every case the engineer needs to decide if a secondary failure caused by deformation perpendicular to the grain is possible or not. In both cases it is possible to limit the load by a restriction of the allowed deformation. Due to the lower partial safety factors ($\gamma = 1.0$) in the SLS it is possible to transfer loads that are significantly higher without risking wood failure. Of course the probability of an occurrence of the assumed deformations are significantly higher than in an ULS. Similar to connections with mechanical fasteners a maximum deformation of 15 mm is used for an example on glulam: In some cases, this deformation will be reached in a SLS due to the partial safety factors of 1.0 whereas in an ULS only 1.5 to 3.0 mm deformations are to be expected under service loads. The deformation is limited due to the assumption of maximum for $k_{c,90}$ and the partial safety factors γ_F and γ_M .

The proposed design model gives a reasonable approach because a direct calculation of the load perpendicular to the grain depending on a certain deformation is possible.

The main part of the deformations is limited to a close range of the contact area. This also applies to higher beams whereas for shallow beams conservative load carrying capacities are calculated. A two sided load distribution can be assumed if the distance to the beam end is at least 200 mm because this configuration was examined in the tests and is part of the proposed values. For the contributing grain length ℓ_{dis} the same limits as in EC5 apply. Nevertheless, an independent evaluation of this model with regard to a bigger sample and the application to beams higher than 250 mm is planned.

5 Exemplary Calculation

Table 6 Exemplary calculation for glulam

EC5	
A_{ef}	$= 100 \cdot (100 + 2 \cdot 30) = 16000 \text{ mm}^2$
$k_{c,90}$	$= 1.5$
$f_{c,90,k}$	$= 2.75 \text{ MPa}$
$F_{c,90,k}$	$= A_{ef} \cdot k_{c,90} \cdot f_{c,90,k} = 66.0 \text{ kN}$
$F_{c,90,d}$	$= \frac{1.0}{1.3} \cdot 66.0 = 50.7 \text{ kN}$
Model	
u	$= 15 \text{ mm in ULS}$
$k_{c,90}$	$= 1.7 \cdot (1 - e^{-0.6 \cdot u}) = 1.70$
$F_{c,90}^{ULS}$	$= 100 \cdot (1.70 \cdot 100 + 80) \cdot 2.75 = 68.7 \text{ kN}$
$F_{c,90,d}$	$= \frac{1.0}{1.3} \cdot 68.7 = 52.9 \text{ kN}$
u	$= 15 \text{ mm in SLS}$
$F_{c,90}^{SLS}$	$= 100 \cdot (1.70 \cdot 100 + 80) \cdot 2.75 = 68.7 \text{ kN}$
u	$= 5 \text{ mm in SLS}$
$k_{c,90}$	$= 1.7 \cdot (1 - e^{-0.6 \cdot u}) = 1.62$
$F_{c,90}^{SLS}$	$= 100 \cdot (1.62 \cdot 100 + 80) \cdot 2.75 = 66.5 \text{ kN}$

An exemplary calculation on glulam and hardwood LVL type P is supposed to show the differences between EC5 and the proposed model. For both materials a sill with projecting ends on both sides, a contact length $\ell = 100$ mm and a width of 100 mm is considered. The beam height is 250 mm. For this example, k_{mod} is set to 1.0.

It is apparent that the model is able to reproduce the reached deformations in the test for the sill considered here. For this case the model according to EC5 depicts the load carrying capacity for middle loaded sills made of glulam very well (see Table 6 and Table 7). For other load configurations there will be larger differences in the deformations because EC5 overestimates the load carrying capacity perpendicular to the grain. The advantage of the proposed model is obvious as well: The partial safety factors on the load and the resistance side need to be considered in EC5. But

in the proposed model a conversion of the load into design values is not necessary because a real failure of the wood does not occur. Therefore, in many cases it is not necessary to consider an ULS. The calculated loads in SLS seem low but it should be noticed that the partial safety factors γ_F on the load side can be set to 1.0. Therefore, the applied load will be much higher than in EC5. If a deformation of 15 mm is compatible with the structure, the characteristic load can be increased by up to 90 % for glulam and by 130 % for hardwood LVL type P || compared to the EC5 under consideration of all partial safety factors. For LVL especially, different loads are calculated for a deformation of 5 mm compared to 15 mm because of the high residual stiffness at large deformations. If a deformation of 5 mm is compatible with the structure, a load of 235 kN can be applied whereas the characteristic load according to EC5 calculates to 201 kN/ $\gamma_F = 143$ kN. Even under the consideration of rather small deformations, the characteristic load can be increased by 65 % in a deformation based calculation compared to the EC5.

Table 7 Exemplary calculation for hardwood LVL type P||

EC5	
A_{ef}	$= 100 \cdot (100 + 2 \cdot 30) = 16000 \text{ mm}^2$
$k_{c,90}$	$= 1.0$
$f_{c,90,k}$	$= 16.3 \text{ MPa}$
$F_{c,90,k}$	$= 261 \text{ kN}$
$F_{c,90,d}$	$= \frac{1.0}{1.3} \cdot 261 = 201 \text{ kN}$
Model	
u	$= 15 \text{ mm in ULS}$
$k_{c,90}$	$= 1.6 \cdot (1 - e^{-0.15 \cdot u}) = 1.43$
$F_{c,90}^{ULS}$	$= 100 \cdot (1.43 \cdot 100 + 60) \cdot 16.3 = 331 \text{ kN}$
$F_{c,90,d}$	$= \frac{1.0}{1.3} \cdot 331 = 255 \text{ kN}$
<hr/>	
u	$= 15 \text{ mm in SLS}$
$F_{c,90}^{SLS}$	$= 100 \cdot (1.43 \cdot 100 + 60) \cdot 16.3 = 331 \text{ k}$
<hr/>	
u	$= 5 \text{ mm in SLS}$
$k_{c,90}$	$= 1.6 \cdot (1 - e^{-0.15 \cdot u}) = 0.84$
$F_{c,90}^{SLS}$	$= 100 \cdot (0.84 \cdot 100 + 60) \cdot 16.3 = 235 \text{ k}$
<hr/>	

6 Conclusion

On the basis of 386 tests it was shown that the factor $k_{c,90}$ should be differentiated for one or two sided load distributions. The proposed design model in eq. (5) for use in SLS and eq. (6) for use in ULS was developed based on this differentiation basically describing the load deformation curves of the performed tests. The factor $k_{c,90}$ according to (7) is introduced describing the adjustment of the strength value $f_{c,90}$ and may be less than unity for small deformations. The model enables the calculation of the load perpendicular to the grain depending on the allowed deformation and allows an estimation of the stiffness of a connection under a compression load perpendicular to the grain. The consideration of a serviceability limit state design for all materials mentioned in Table

8 is possible. Generally, an ultimate limit state design is not necessary because the materials do not show a decrease of the load with increasing deformations. An ULS should be considered only in cases, where an exceeding deformation leads to a reduction of the cross-sectional area and therefore to a higher stress in bending or shear. In contrast, the materials mentioned in Table 9 show a decreasing load with increasing deformations and the ULS should hence be verified. If the load is calculated with the proposed values in Table 9 and eq. (6), a deformation of two to four mm is to be expected under service loads.

$$F_{c,90}^{SLS}(u) = b \cdot (\ell \cdot k_{c,90}(u) + \ell_{dis}) \cdot f_{c,90,k} \cdot k_{mod} \quad (5)$$

$$F_{c,90}^{ULS}(u) = b \cdot (\ell \cdot k_{c,90}(u) + \ell_{dis}) \cdot \frac{k_{mod}}{\gamma_M} \cdot f_{c,90,k} \quad (6)$$

$$k_{c,90} = k_a \cdot (1 - e^{-k_b \cdot u}) \quad (7)$$

Table 8 Values for k_a , k_b and ℓ_{dis} for the use in a SLS with eqs. (5) and (7)

Material ¹	One sided		Two sided		ℓ_{dis} ² [mm]	$f_{c,90,k}$ [N/mm ²]
	k_a	k_b	k_a	k_b		
Softwood and glulam made of softwood	1.50	0.4	1.70	0.6	40	2.75
Softwood-(G)LVL-P \perp	1.60	0.2	1.80	0.2	40	3.0
Softwood-(G)LVL-C \perp	1.40	0.2	1.40	0.2	40	3.2
Hardwood-(G)LVL-P \parallel	1.60	0.15	1.60	0.15	30	16.3
Hardwood-(G)LVL-C \perp	1.50	0.15	2.00	0.1	40	14.6

¹ P: parallel glued veneers, C: LVL with up to 20 % cross laminated veneers; \perp : load perpendicular to veneer orientation; \parallel : load parallel to veneer orientation

² Valid for a deformation from 5 to 15 mm. For a smaller deformation the value can be interpolated between $u = 0$ mm and $\ell_{dis} = 0$ mm as well as $u = 5$ mm and ℓ_{dis}

Table 9 Values for $k_{c,90}$ and ℓ_{dis} for a one sided and two sided projecting end for the use in an ULS with eq. (6)

Material	$k_{c,90}$	ℓ_{dis} [mm]	$f_{c,90,k}$ [N/mm ²]
Softwood-(G)LVL-P \parallel	1.00	25	8.0
Softwood-(G)LVL-C \parallel	1.30	25	8.2
Hardwood-(G)LVL-P \perp	1.60	30	14.8
Hardwood-(G)LVL-C \parallel	1.35	30	18.5

The developed approach is in good accordance with the test results in a range of one to 15 mm overall deformation (overall mean is 0.99 with a COV of 8.4 %). The direct consideration of the allowed deformations distinguishes the proposed design approach from all other models (see e. g. (Leijten 2016)). The model enables the engineer a more detailed view of compression perpendicular to the grain because he is able to

decide in any particular case which deformation is acceptable for the structure, which stiffness is to be expected in the connection and further if a ULS or SLS is present. In the latter case the partial safety factors are assumed to be 1.0. However, the factor k_{mod} considering the moisture content and the load duration class should be applied in the SLS as well.

7 Literature

Blaß, H. J.; Görlacher, R. (2004): Compression Perpendicular to the Grain. In: *Proceedings of the 8th World Conference on Timber Engineering*.

EN 1995-1-1:2010-12: Eurocode 5: Design of timber structures - Part 1-1: General - Common rules and rules for buildings; German version.

Leijten, A.J.M. (2016): The bearing strength capacity perpendicular to grain of Norway spruce – Evaluation of three structural timber design models. In: *Construction and Building Materials* 105, S. 528–535. DOI: 10.1016/j.conbuildmat.2015.12.170.

Madsen, B. (2001): Behaviour of timber connections. In: *Can. J. Civ. Eng.* 28 (3), S. 546. DOI: 10.1139/l01-016.

EN 14358:2013-09: Timber structures - Calculation of characteristic 5-percentile and mean values for the purpose of initial type testing and factory production control; German version.

EN 408:2012-10: Timber Structures - Structural timber and glued laminated timber - Determination of some mechanical properties; German version.

van der Put, T.A.C.M. (2008): Derivation of the bearing strength perpendicular to the grain of locally loaded timber blocks. In: *Holz Roh Werkst* 66 (6), S. 409–417. DOI: 10.1007/s00107-008-0258-0.

Discussion

The paper was presented by L Windeck

C Sigrist and L Windeck discussed the method of checking for stiffness.

J Hakkarainen and L Windeck discussed cross lamination effects and the difference in performance between spruce and pine.

P Quenneville asked for comments on load distribution angle theory in relation paper 51-12-1. L Windeck responded that for serviceability performance the approach in this paper works and is more appropriate.

A Frangi stated that one should try to convince engineers to avoid compression perpendicular to grain. Especially if you apply this work to taller buildings, it will not work. H Blass agreed and said this work shows compression perpendicular to grain is okay for three stories and commented that this type of issue are no different from issues related to tension perpendicular to grain.

Mechanical properties of European beech glued laminated timber

Thomas Ehrhart ¹⁾²⁾, René Steiger ²⁾, Pedro Palma ²⁾, Andrea Frangi ¹⁾

¹⁾ ETH Zürich, Swiss Federal Institute of Technology, Institute of Structural Engineering (IBK), CH-8093 Zürich, Switzerland

²⁾ Empa, Swiss Federal Laboratories for Materials Science and Technology, Structural Engineering Research Laboratory, CH-8600 Dübendorf, Switzerland

Keywords: European beech timber, glued laminated timber, mechanical properties

1 Introduction

The use of European beech (*Fagus sylvatica* L.) wood for structural purposes has been very limited so far, despite its potential regarding mechanical properties (Glos et al., 2004; Frese and Blaß, 2005; Frühwald and Schickhofer, 2005) and abundant availability in Central Europe. One main reason for this is the lack of standards regulating the production process, the quality control, and specifying the mechanical properties of glued laminated timber (GLT) made from European beech wood. Aiming at closing this gap, CEN/TC124/WG3/TG1 has restarted working on a standard on the production and performance requirements for GLT made from hardwood, as EN 14080 (2013) does for GLT made from coniferous species and poplar.

This paper summarises and discusses the outcomes of extensive bending, shear, and compression parallel to grain tests on European beech GLT. The tests were conducted at the *Swiss Federal Laboratories for Materials Science and Technology (Empa)* in 2017 and 2018 in the framework of the program *Aktionsplan Holz* of the *Swiss Federal Office for the Environment (FOEN)*.

Whereas bending and compression parallel to grain tests could be carried out in a straight forward way according to EN 408 (2012), no test configuration is available in European standards for determining the shear strength of full-size GLT beams. Several issues with regard to the *correct* shear test configuration have been discussed in CIB/W18 and INTER meetings. So far, research related to the shear strength of GLT is predominantly focused on coniferous timber species.

Lam et al. (1995) investigated the shear strength of Canadian softwood structural lumber using five-point bending tests. Comparisons with results of finite element models that used values obtained of ASTM D143 (1994) shear block tests as input parameters and considered Weibull weakest link theory showed good agreement. However, longitudinal shear failure was achieved in only 40 % of the tests. Yeh and Williamson (2001) evaluated the shear strength of GLT made of Northern American softwoods based on full-size four-point bending tests with a small distance between the two central load application points. A shear failure was achieved in 70 % of the tests. Based on the investigations by Yeh and Williamson (2001), the full-size shear test method was adapted in ASTM D3737-99 (2000).

To increase the probability of achieving shear failures, the use of I-shaped cross-sections is advisable. Schickhofer (2001) conducted three-point and five-point bending tests on beams with I-shaped cross-sections to determine the longitudinal shear strength. Different strength classes, beam heights, and overhang lengths were evaluated. A shear failure rate of more than 80 % was achieved. Schickhofer (2001) recommended to abandon shear tests on small specimens (including the block shear test according to former versions of EN 408) and to establish the three-point bending test with an I-shaped cross-section as standardised shear test configuration instead. However, this proposal had not been followed so far.

Pure shear stress states hardly occur in structural timber elements and it is thus neither simple nor necessary to aim for a pure shear stress state when determining the shear strength of full-size GLT beams. Material properties should be determined for volumes and types of stresses that are representative of situations that the material will be subjected to in real structures (Gehri, 2010). Extensive investigations on the longitudinal shear strength of timber beams and the size effect were done inter alia by Foschi and Barrett (1976, 1977, 1980) and Colling (1986), who introduced the so-called *fullness parameters* that describe the stress-distribution.

Usually, shear stresses are accompanied by stresses perpendicular to grain that influence the determined shear strength. Steiger and Gehri (2011) investigated the interaction of shear stresses and stresses perpendicular to grain in full-size GLT beams using a three-point bending test configuration. A positive influence of compression stresses perpendicular to grain, and good agreement of experimental test results and data from literature (e.g. Mistler, 1979; Spengler, 1982; Eberhardsteiner, 2002) with the design approach given in the standard SIA 265 (2012) was reported.

Aicher and Ohnesorg (2011) investigated the shear strength of GLT made from European beech timber. A four-point loading configuration with a beam length of 3530 mm and an I-shaped cross-section with a height of 608 mm was used. The mean value of shear strength found was 6.1 MPa. Van de Kuilen et al. (2017) conducted shear tests on small beech wood specimens using the configuration described in EN 408 (2012) reporting a mean shear strength of 13.4 MPa.

2 Material and Methods

2.1 Material

For the production of the GLT beams and columns, 98.4 m³ of planed European beech timber boards were ordered from four sawmills located in the Swiss cantons Aargau (7.6 %), Bern (15.2 %), Jura (60.5 %), and Zurich (16.7 %). Boards containing pith, rot, and insect damage were excluded. After cutting, the boards were air-dried (partly loaded with weights) and then dried to the target moisture content of MC = 8 ± 2 % using fresh air/exhaust air drying kilns or vacuum chambers. All boards were planed to a thickness of $t_{\ell,1} = 30$ mm.

2.1.1 Strength grading

Rules for the strength grading of European beech lamellas were previously developed (Ehrhart et al., 2016), taking into account visual and physical indicators. In total 5740 timber boards were strength graded and assigned to the strength classes T26, T33, T42, and T50. 603 timber boards (10.5 %) were rejected due to pith (31.7 % of rejects, pre-grading had not been done properly), curvature (26.9 %), knots (13.8 %), unplanned or uneven surface (10.1 %), and drying checks (6.5 %). Table 1 provides an overview of the number of timber boards (n), density (ρ), dynamic MOE (E_{dyn}), and coefficients of variation (COV) per T class.

Table 1: Sample size (n), density (kg/m³), and dynamic MOE (MPa) per T class; MC = 8 ± 2 %.

T class	n	ρ_{mean}	$\rho_{0.05}$	COV[ρ]	$E_{\text{dyn,mean}}$	$E_{\text{dyn,0.05}}$	COV[E_{dyn}]
T26	1334	694	628	0.06	15060	12400	0.11
T33	1107	686	619	0.06	15480	13490	0.08
T42	1634	699	630	0.06	16980	14670	0.09
T50	1062	711	651	0.05	18130	16370	0.06

2.1.2 Production of GLT beams and columns

The GLT beams and columns were produced at the production facility of the industrial project partner *neue Holzbau AG* in Lungern, Switzerland. All boards were planed to their final thickness of $t_{\ell,2} = 25$ mm before flat face gluing using a one-component polyurethane adhesive (HS 709; 180 g/m²), combined with a primer (10 % concentration; 20 g/m²). This adhesive system had been chosen based on previous tests, in which adhesives for the gluing of hardwoods had been compared.

Homogeneous GLT of (target) strength classes GL 40h, GL 48h, and GL 55h (columns) was produced from boards of T classes T33, T42, and T50, respectively. Combined GLT of (target) strength classes GL 40c, GL 48c, and GL 55c (beams) was produced from boards of T classes T33 (2 × outer 25 % of the height) + T26 (inner 50 %), T42 + T26, and T50 + T33, respectively. For beams intended to be tested in shear, the outermost laminations were always of the T class T50 to prevent bending failures.

2.2 Methods

Bending tests ($n_m = 39$), shear tests ($n_v = 42$), and compression tests parallel to grain ($n_c = 35$) were conducted, taking into account standardised test setups described in literature and new test configurations. Table 2 gives an overview of the performed tests and the configurations used.

For I-shaped cross-sections, the web width amounted to 75 % of the flange width and the flange height was 20 % of the beam height. Different-sized elements were tested in order to investigate potential size effects related to the bending, shear, and compression properties of European beech GLT.

Digital image correlation (DIC) analyses were conducted using the 3D-system *ARAMIS* by *GOM*, to obtain detailed information on the distribution of surface strains.

Table 2: Test plan including the type of test and number of specimens per series.

Bending tests ($n_m = 39$)					
Dim. [mm]	200/80/3800	400/160/7600	600/160/11400	800/180/15200	
GL 40c	-	7	-	-	
GL 48c	7	7	7	4	
GL 55c	-	7	-	-	
Shear tests ($n_v = 42$)					
Type	3P	3P	3P	3P	4P
Cross-section	I	I	I	R (rectangular)	I
Dim. [mm]	200/120/700	400/160/1200	600/160/1700	400/160/1200	400/160/3200
GL 48c	7	3	7	5	7
GL 55c	-	7	-	-	-
Compression tests ($n_c = 35$)				Type	EN 408
Dim. [mm]	150/150/900	200/200/1200	280/280/1680	Cross-section	R (rectangular)
GL 40h	-	7	-	Dim. [mm]	200/120/614
GL 48h	7	7	7	GL 48c	6
GL 55h	-	7	-	GL 55c	-

2.2.1 Bending tests

Four-point bending tests (Figure 1) were carried out in accordance with EN 408 (2012). Three strength classes (GL 40c, GL 48c, GL 55c) and four beam heights ($h = 200, 400, 600, 800$ mm) were tested. The reference height was specified as $h = 400$ mm. Information on the number of tests per series can be found in Table 2. The local and global bending MOE, the bending strength, and the shear modulus were determined in accordance with EN 408 (2012).



Figure 1: Four-point bending test on a GLT beam (0.80 m high and 15.20 m long).

2.2.2 Compression parallel to grain tests

Compression tests parallel to grain were carried out in accordance with EN 408 (2012). Three strength classes (GL 40h, GL 48h, GL 55h) and three different quadratic cross-sections ($h_c = 150, 200, 280$ mm) were tested. The length of the columns was $l_c = 6 \times h_c$. The compression MOE parallel to grain was determined in accordance with EN 408 (2012) based on local vertical displacement over a length of $l_{E,c} = 4 \times h_c$ recorded with laser displacement sensors on two opposite sides.

2.2.3 Shear tests

As discussed in the introduction of the present paper, there is no test configuration available in European standards for the determination of shear strength of full-size GLT beams. It was thus necessary develop an approach to determine the shear strength, accounting for the influence of the test setup and stressed volume. The shear stresses τ_v were calculated using Equations (1) and (2).

$$\tau_{v,beam} = \frac{V \cdot S(z)}{I \cdot w(z)} \quad (1)$$

$$\tau_{v,408} = \frac{F_{max} \cdot \cos 14^\circ}{l \cdot w} \quad (2)$$

The reference test setup chosen within this study was a three-point bending test (3P) with a span of $2.5 \times h$ and an I-shaped cross-section (Figure 2). Most beams were of the strength class GL 48c, but beams of the strength class GL 55c with $h = 400$ mm were also tested. Each series (height and GL-class) included seven specimens. Supports and load application points on beams with heights of 400 and 600 mm were reinforced with glued-in threaded steel rods (M20, $l_{GIR} = 2/3 \times h$) in order to avoid premature failure under compression perpendicular to grain. Beams with a height of 200 mm were strengthened with fully threaded screws (diameter $d = 9$ mm, pre-drill diameter $d_{pd} = 5.5$ mm, $l_{screw} = 2/3 \times h$).

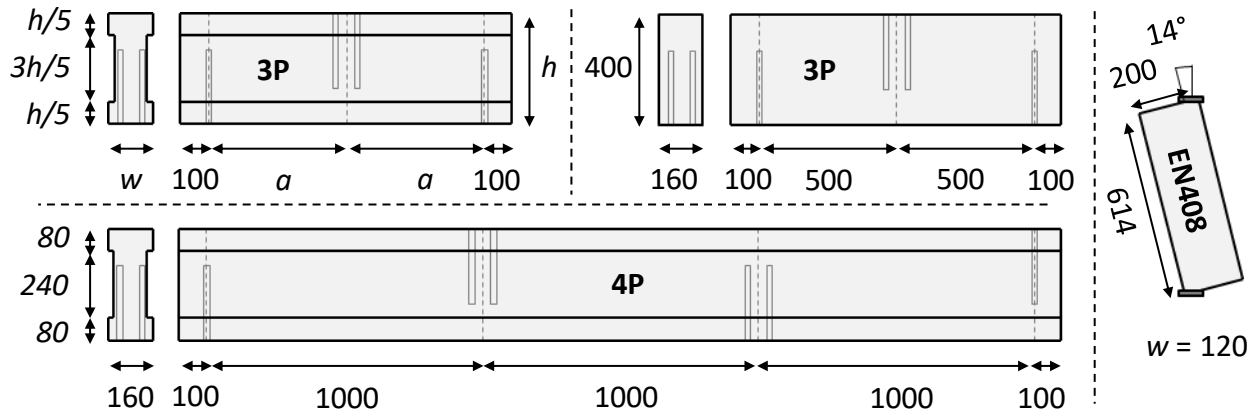


Figure 2: Different shear test setups used in this study; all measures in mm.

Five specimens ($h = 400$ mm, GL 48c) with rectangular cross-sections ($w = 160$ mm) were tested in three-point bending in order to check the necessity of testing I-shaped cross-sections to achieve shear failures.

Additionally, an *asymmetric four-point bending test setup* was developed and applied in shear testing of beams with I-shaped cross-sections (Type = 4P in Table 2 and Figure 2). This test setup is based on a configuration presented by Basler et al. (1960). It was developed to reach high shear forces accompanied by only small bending moments (Figure 3) and, hence, to reduce the probability of premature bending failure. Seven GL 48c beams with a height of $h = 400$ mm were tested.

In addition, block shear tests were carried out using an EN 408 (2012) alike test configuration (Figure 2, right). These test specimens were cut from five apparently undamaged parts of the smallest bending beams ($h = 200$ mm, $w = 120$ mm). One additional specimen was produced from a pre-cracked part. As described in EN 408 (2012), the angle between the specimen's longitudinal axis and the force was 14° .

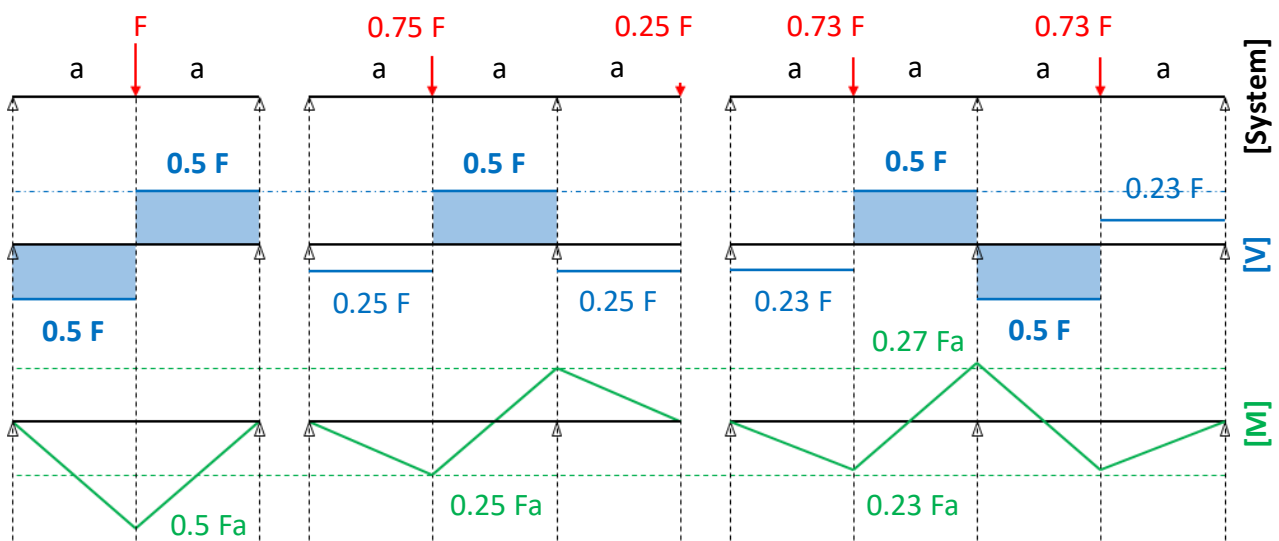


Figure 3: Comparison of test setups and distribution of shear force [V] and bending moment [M] for three different shear tests configurations: three-point- (3P, left), asymmetric four-point- (4P, middle), and five-point bending test (right). For a given shear force V and field length a , the maximum bending moment M is smallest for the asymmetric four-point bending setup.

Following the JCSS probabilistic model code (2006), a lognormal distribution was assumed for estimating all bending-, compression-, and shear strength and stiffness properties and a normal distribution for density.

Data analysis accounted for the problem of the unintended *bending* and *compression perpendicular to grain* failure modes, which frequently occur before a shear failure is observed (e.g. Lam et al., 1995; Schickhofer, 2001; Yeh and Williamson, 2001; Brandner et al., 2012). These test results were considered as censored data, i.e. the shear strength is only known to be higher than the shear stress when the bending or compression failure occurred. Censoring was considered in the data analysis following the recommendations by Steiger and Köhler (2005).

3 Results and Discussion

The main test results are summarised in Figure 4, Figure 6, and Figure 8. In the box-plots, the box boundaries are the lower (Q_{25}) and upper quartiles (Q_{75}) and the line within the box represents the median. The horizontal bars outside the box indicate the smallest and largest sample points less than 1.5 times the interquartile-distance away from the box. Extreme values are indicated with a circle. Boxes of strength classes GL 48c and GL 48h are highlighted with grey colour.

3.1 Bending

The differences in bending strength between the strength classes GL 40c ($f_{m,mean} = 63.2$ MPa / $f_{m,0.05} = 52.0$ MPa), GL 48c (63.1 MPa / 57.6 MPa), and GL 55c (66.1 MPa / 55.8 MPa) were less pronounced than expected (Figure 4, $h = 400$ mm).

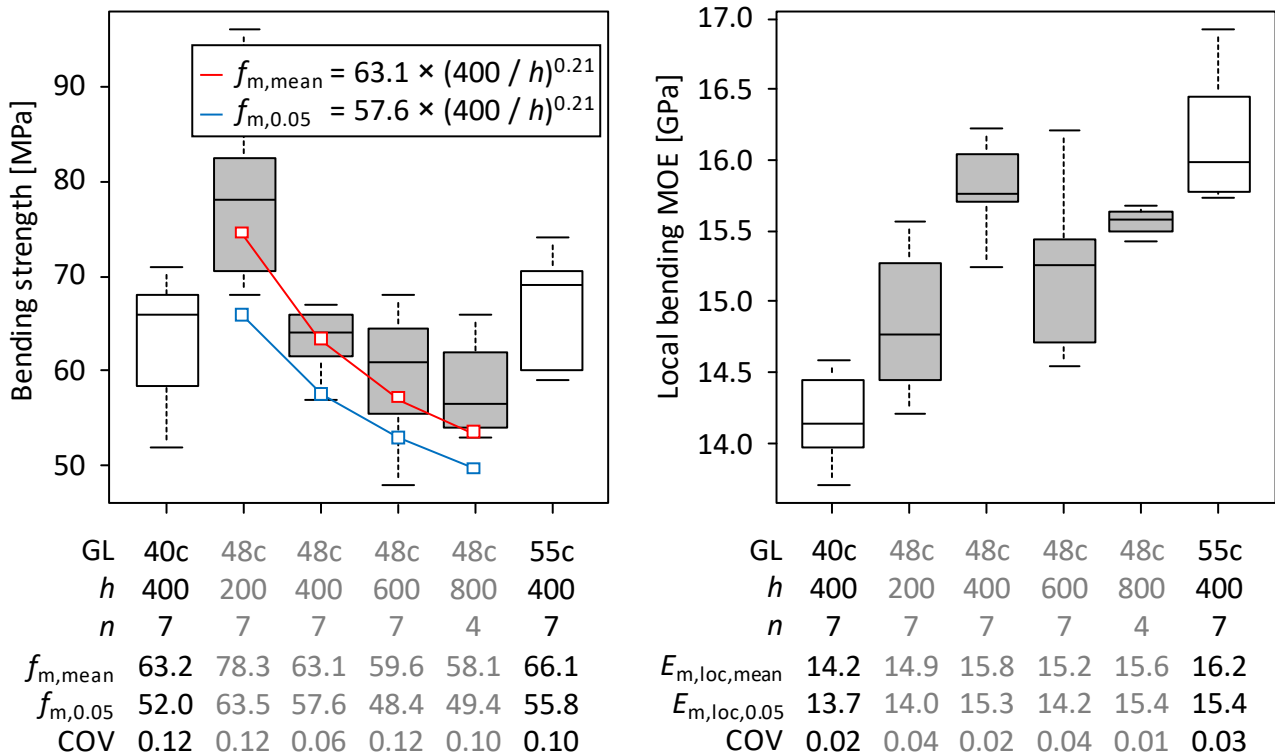


Figure 4: Bending strength f_m (MPa) and local MOE $E_{m,loc}$ (GPa) derived from the bending tests.

A pronounced size effect could be observed. For increasing heights ($h = 200$ to 800 mm), the bending strength decreases from $f_{m,mean} = 78.3$ to 58.1 MPa and from $f_{m,0.05} = 63.5$ to 49.4 MPa. The equations given in Figure 4 with a reference height of 400 mm and an exponent of 0.21 describe the influence of the beam height on the bending strength. Final equations will be proposed based on additional probabilistic and numerical investigations.

Both the non-existent correlation between GL strength classes and bending strength, and the pronounced size effect can be explained taking a closer look at the governing failure mechanisms. These were failures of finger joints (Figure 5, left), and shear failures along the medullary rays in the outermost laminations (Figure 5, right). With increasing beam height, there is an increasing number of finger joints in the critical (bending-tension) zone, which affects the bending strength.

During strength grading, only obvious fibre deviations were considered due to the lack of sufficient methods for the determination of fibre orientation in European beech wood at that time (meanwhile, a solution for this problem has been proposed by Ehrhart et al., 2018). In addition, the number of finger joints (weak points) is independent of the strength class. Consequently, both potential causes of failure occur almost equally in all strength classes and the differences in bending strength between the strength classes are rather small. For European beech GLT, this issue can only be solved by introducing a strength grading system that accounts for the fibre orientation (Aicher et al., 2001).



Figure 5: Failure of a finger joint (left), and shear failure along the medullary rays (right) in the outermost lamination were the most frequent failure mechanisms observed in the bending tests.

Nevertheless, it has to be emphasised that the target characteristic values of bending strength were achieved for all strength classes GL 40c (52.0 MPa), GL 48c (57.6 MPa), and GL 55c (55.8 MPa) for the height of $h = 400$ mm, which had been defined to be the reference height in this study.

Mean values of local bending MOE of $E_{m,loc,mean} = 14.2$ GPa (GL 40c), 15.4 GPa (GL 48c, including all heights), and 16.2 GPa (GL 55c) were determined in the tests. The marked difference between the strength classes in terms of MOE can be attributed to the strength grading process, where the dynamic MOE, a strong indicator for the static MOE, had been used as criterion.

For coniferous timber species, EN 384 (2016) provides Equation (3) to estimate the local bending MOE based on the global bending MOE (with $G_v = \infty$). Ravenhorst and van de Kuilen (2010) reported a ratio of 1.17 (for tropical hardwoods) and 1.11 (for chestnut) to describe the relationship between the local and global bending MOE. The results of the present study for European beech GLT suggest using Equation (4), which was derived by means of linear regression analysis ($r^2 = 0.88$).

$$E_{loc,EN384} = E_{m,glob} \cdot 1.30 - 2690 [MPa] \quad (3) \quad E_{loc,beech} = E_{m,glob} \cdot 1.17 - 1890 [MPa] \quad (4)$$

In total 22 shear field measurements were made in beams of the strength class GL 48c with heights of $h = 600$ mm (7×2) and 800 mm (4×2). A mean value of shear modulus $G_{v,mean} = 1082$ MPa ($G_{v,0.05} = 816$ MPa, COV = 0.16) was found.

3.2 Compression parallel to grain

The main results of the compression parallel to grain tests are summarised in Figure 6. The variation in compression strength $f_{c,0}$ was very low with minimum and maximum values of 55.8 and 67.7 MPa (COV = 0.05) including all series.

Slightly increasing mean and characteristic values of compression strength were observed for increasing strength classes (Figure 6, left). No size effect could be detected. The differences in the compression MOE parallel to grain are much more pronounced. Mean values of $E_{c,0,mean} = 15.1$, 15.7, and 17.0 GPa were found for the strength classes GL 40h, GL 48h (all heights), and GL 55h (Figure 6, right).

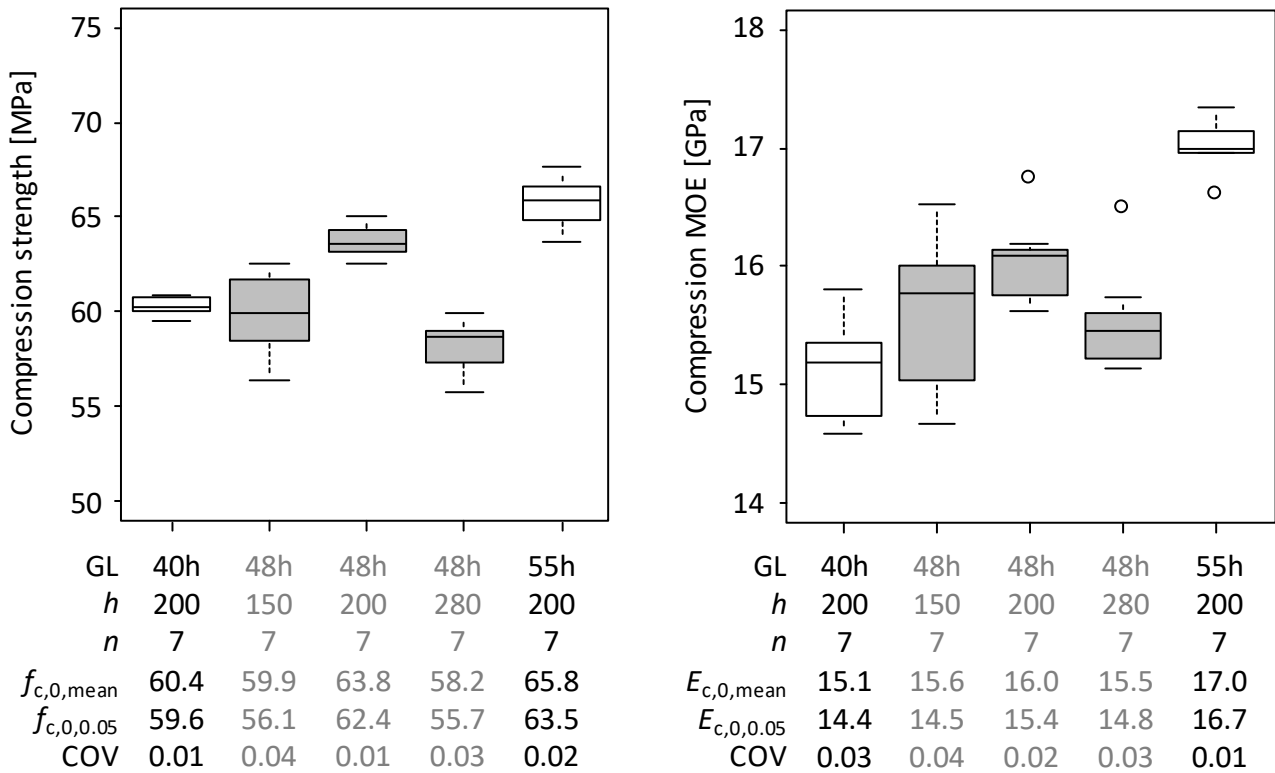


Figure 6: Compression strength parallel to grain $f_{c,0}$ (MPa) and compression MOE parallel to grain $E_{c,0}$ (GPa) derived from the compression tests.

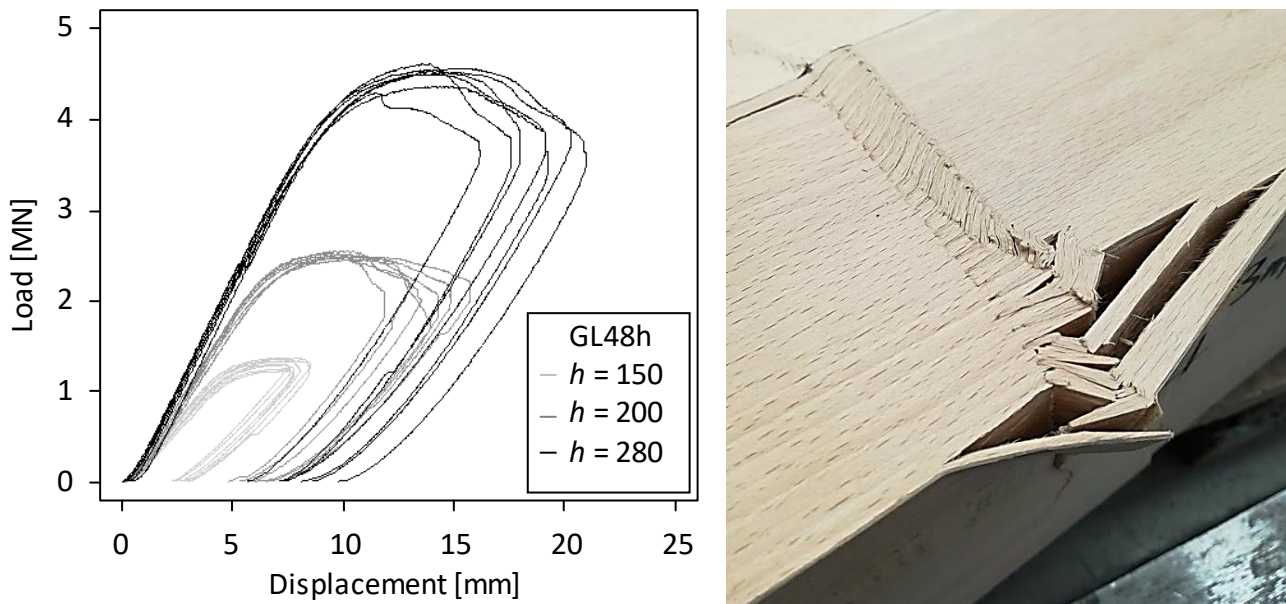


Figure 7: Load-displacement curves determined in compression tests (GL 48h) with specimen heights of $h = 150$, 200 , and 280 mm (left). Local crushing of wood fibres in a finger joint (right).

A rather ductile failure behaviour in compression parallel to grain was observed. The load-displacement curve was almost linear until reaching a level of approximately 85 % of the ultimate load (Figure 7, left). The remaining 15 % demanded about 45 % of the total displacement at the ultimate load. Local crushing of wood fibres, initiated near finger joints (Figure 7, right), knots, and zones with local fibre deviations, were observed with all specimens, resulting in the described ductile failure mechanism.

3.3 Shear

The shear tests aimed not only at determining strength values, but also at comparing the various test configurations. Figure 8 presents the main results of the shear test series with different test configurations (type), strength classes (GL), cross-section geometries, and beam heights (h). The total number of specimens per series (n_{tot}), the number of specimens failed in shear (n_{shear}), the mean ($f_{v,\text{mean}}$) and characteristic values of shear strength ($f_{v,0.05}$) with and without censoring the data (cd), and the coefficients of variation (COV) are also presented in Figure 8. The symbols used in Figure 8 indicate the observed failure mode (shear, bending, compression, or none) of each of the tested specimens. In order to analyse the strain fields with the DIC system, a beam of series 5 (three-point bending, GL 48c, rectangular cross-section $h = 400$ mm) was initially loaded to a force of 1000 kN ($\tau_v \approx 10.4$ MPa), and unloaded before failure occurred (circle in Figure 8, series 5).

In three-point bending tests on I-beams with different heights (series 1-3) and strength classes (series 4), 22 out of 24 specimens failed in shear. Both non-shear failures belong to series 1 (GL 48c, $h = 200$ mm). One specimen was tested with a span length increased by 20 % (aiming at observing changes in the strain fields), resulting in a bending failure. The repeated use of a (pre-damaged) set of screws is the reason for the failure in compression perpendicular to grain of the second beam.

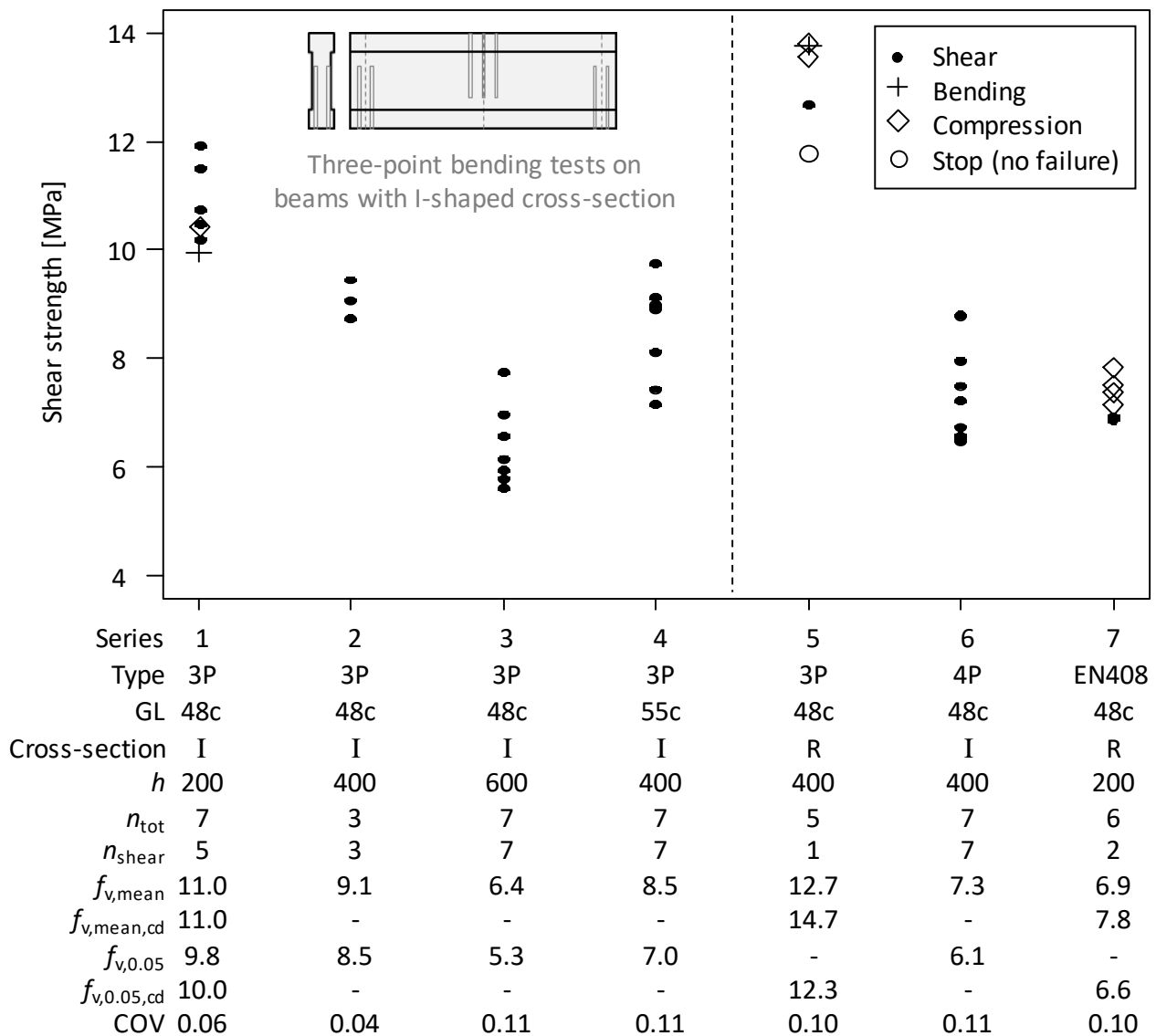


Figure 8: Comparison of shear strength f_v determined with different test methods, strength classes, cross-sections, and heights.

Using the asymmetric four-point bending test setup (series 6), a shear failure was observed in all tests. Compared to the three-point bending tests of the same height $h = 400$ mm (combined data set of series 2 and 4), considerably lower values of mean and characteristic shear strength were found, respectively - 16 % and - 17 %.

This difference is attributed to the lower compression stresses perpendicular to grain (Steiger and Gehri, 2011), also observed when analysing the DIC data (Figure 10, right), and to the larger undisturbed test volume in the 4P bending test, as the distance between the glued in rods (free shear length) is increased by a factor of two.

In agreement with Schickhofer (2001), it was not possible to determine a major influence of the overhang length (neighbouring fields). The analysis of the DIC data clearly shows that shear failure is caused by local stress concentrations and interactions, usually in areas close to knots (Figure 9, right). However, the overhang length and the glued-in rods finally determined how the test specimen behaves after the first failure has occurred.

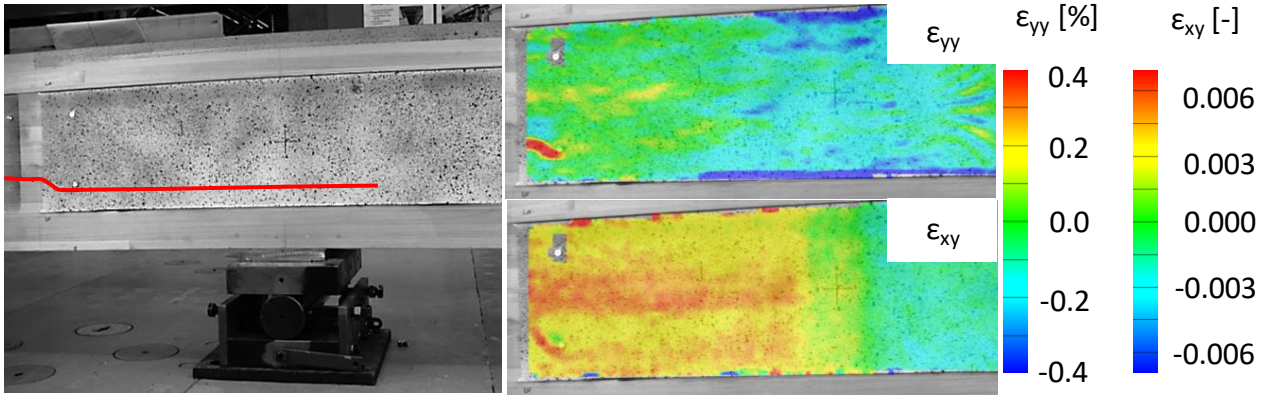


Figure 9: Shear failure path (left), and distribution of vertical strain (ϵ_{yy} , top-right) and shear distortion (ϵ_{xy} , bottom-right) immediately before failure.

Thanks to the glued-in rods and the multi-span effect, it was possible to re-increase the force to a level of 70 % of the maximum force after the first shear fracture occurred. In future, this beneficial behaviour could also be taken into account in an economic design of multi-span beams that are reinforced at supports and load application areas.

A pronounced size effect was observed. For increasing beam heights (series 1-3), the mean and characteristic values of shear strength dropped significantly (Figure 8). In agreement with Schickhofer's (2001) results, no significant difference in shear strength was found for different strength classes (series 2 vs. 4). However, the sample size of series 2 was limited to only three specimens.

Foschi and Barrett (1976, 1977, 1980) state that the shear strength f_v depends on the stressed volume (size effect coefficient k), loading conditions (β , which also depends on k), beam volume ($A \times L$), and reference shear strength $f_{v,0}$ for a reference volume V_0 (Equation 5).

In this study, a similar but simplified approach was developed to describe the size and setup effects (Equation 6). The critical volume (V_{cri}) is defined by the volume, inside which the shear stresses are higher than a threshold of $\tau_{v,cri} \geq \frac{2}{3} \times \tau_{v,max}$. For rectangular cross-sections and a shear stress distribution according to Equation (1), the critical height is $h_{cri} = 0.58 \times h$. The critical height of I-beams depends on the actual geometry, but it is very likely equal to the height of the web. The parameters ω (test setup coefficient) and θ (size effect coefficient) were calibrated to fit the experimental data (Figure 10). A reference volume $V_0 = 20 \text{ dm}^3$ was chosen, as proposed by Foschi and Barrett (1980).

$$f_v = \beta \cdot f_{v,0} \cdot \left(\frac{V_0}{A \cdot L} \right)^{1/k} \cdot \frac{Q_M}{Q_0} \quad (5)$$

$$f_v = \omega \cdot f_{v,0} \cdot \left(\frac{V_0}{V_{cri}} \right)^{\theta} \quad (6)$$

The test setup coefficient ω takes into account the differences in the stress interactions resulting from different test setups. In Figure 10 (right), the vertical strains ϵ_{yy} for the test setups 3P and 4P are compared with each other. Obviously, most of the

critical volume is subjected to compression stresses perpendicular to grain for the test setup 3P (Figure 10, top-right). Due to the positive effect of this stress interaction for the shear strength, a larger setup effect factor ω is necessary to estimate the shear strength for the test setup 3P as compared to test setup 4P.

The lines in Figure 10 (left) represent Equation (6) fitted to the 3P (red) and 4P test data (blue = reference test setup, $\omega_{4P} = 1.00$) on a mean (continuous lines) and characteristic value level (dashed lines). The reference shear strengths for a reference volume of $V_0 = 20 \text{ dm}^3$ are $f_{v,0,0.05} = 6.47 \text{ MPa}$ and $f_{v,0,\text{mean}} = 7.74 \text{ MPa}$. A size effect factor $\theta = 0.21$, and test setup coefficients $\omega_{3P} = 1.10$ and $\omega_{4P} = 1.00$ (reference) were adopted.

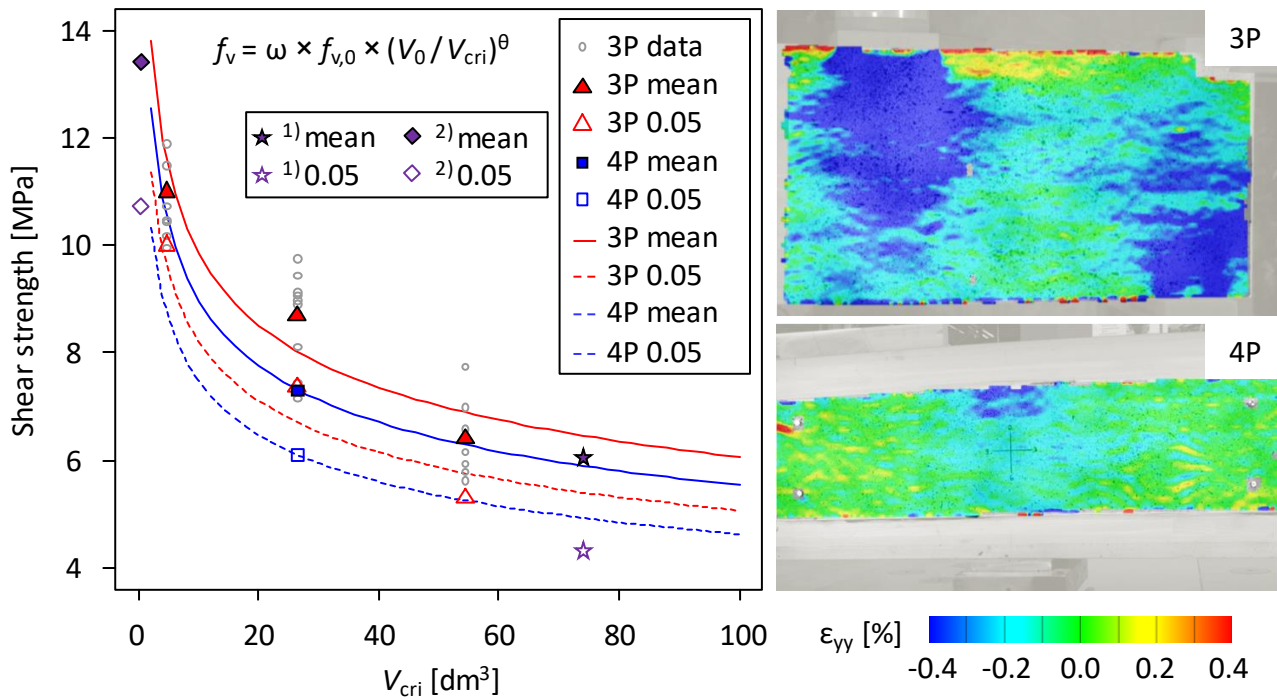


Figure 10: Size and setup effects in shear, compared to data from ¹⁾ Aicher and Ohnesorg (2011) and ²⁾ van de Kuilen et al. (2017) (left). Vertical strains recorded in tests with setups 3P and 4P (right).

For comparison, results reported by Aicher and Ohnesorg (2011) (similar stress interaction as in the 4P tests setup, $\omega \approx 1.00 \approx$ blue lines) and van de Kuilen et al. (2017) (EN 408 test setup) are also plotted in Figure 10 with star and square symbols.

Only the pre-cracked and one more specimen of the six EN408-alike block shear specimens exhibited longitudinal shear failure. The other four specimens failed in compression, with large displacements and decreasing load, with a corresponding compression stress parallel to the grain of more than 80 MPa. This setup may work for block shear tests on softwood GLT, however, the apparently larger ratio between shear strength and compression strength parallel to the grain does not allow using this type of test for determining the shear strength of European beech GLT. For block shear tests on European beech GLT, the EN408-alike block shear test setup would have to be adjusted in order to regularly achieve shear failures. Such adjustments could involve milling I-shaped cross-sections or reinforcing the load application areas.

4 Conclusions

It is possible to produce glued laminated timber of strength classes GL 40c, GL 48c, and GL 55c from European beech. Mean values of local bending MOE of $E_{m,loc,mean} = 14.2, 15.4,$ and 16.2 GPa were determined in the presented test campaign. For European beech GLT, Equation (4) is proposed to be used instead of the relationship provided in EN 384 (2016) to estimate the local bending MOE based on the global bending MOE. A mean value of shear modulus $G_{v,mean} = 1080$ MPa ($G_{v,0.05} = 816$ MPa, COV = 0.16) was found.

Regarding the bending strength, a pronounced size effect, which can be described with a power function $(h_{ref} / h)^\theta$ with an exponent of $\theta = 0.21$ was observed for bending strength.

Low variation was found for the compression strength parallel to grain. The characteristic value ($f_{c,0,0.05}$) for all strength classes was higher than 55 MPa. Mean values of compression MOE parallel to grain of $E_{c,0,mean} = 15.1, 15.7,$ and 17.0 GPa were determined for the strength classes GL 40c, GL 48c, and GL 55c, respectively.

Values for shear strength in a range between 5.6 to 12.7 MPa were found, strongly depending on the test configuration and the specimen size. Consideration of the size and setup effects is thus strongly recommended when suggesting shear strength values for the design of timber structures. Equations that allow taking into account the size (parameter $\theta = 0.21$) and setup effect (parameter ω) were developed. The resulting curves (Figure 10) describe the test results well and show a good agreement with data reported by Aicher and Ohnesorg (2011) and van de Kuilen et al. (2017).

The investigation of different test configurations showed that it is advisable to use I-shaped cross-sections in order to achieve predominantly shear failures when testing European beech GLT. Due to the optimised ratio between bending and shear stresses and its ability to reflect the actual stress state in multi-span beams, the presented asymmetric four-point bending test setup is recommended to be implemented in EN 408 (2012) for the determination of shear strength of full-size GLT beams. The EN 408-alike block shear test setup may work for block shear tests on softwood GLT, however, the apparently larger ratio between shear strength and compression strength parallel to the grain does not allow using this type of test for determining the shear strength of European beech GLT.

This paper (i) contributes to a better understanding of the mechanical properties of European beech GLT (EN 384), (ii) may contribute to the ongoing standardisation of hardwood GLT in Europe (prEN 14080-2), and (iii) suggests a test configuration for the shear testing of full-size GLT specimens (EN 408).

5 Acknowledgement

The authors acknowledge the support of the project by the Swiss Federal Office for the Environment FOEN within the framework of Aktionsplan Holz.

6 References

- Aicher, S; Höfflin, L; Behrens, W (2001): A study on tension strength of finger joints in beech wood laminations. *Otto-Graf-Journal*, 12, pp. 169-186.
- Aicher, S; Ohnesorg, D (2011): Shear strength of glued laminated timber made from European beech timber. *European Journal of Wood and Wood Products*, 69, pp. 143-154.
- ASTM D143 (1994): Standard methods of testing small clear specimens of timber.
- ASTM D3737-99 (2000): Standard practice for establishing stresses for structural glued laminated timber (glulam).
- Barrett, JD; Foschi, RO (1977): Longitudinal shear in wood beams: a design method. *Can. J. Civ. Eng.*, 4(3), pp. 363–370.
- Basler, K; Yen, BT; Mueller, JA; Thürlimann, B (1960): Web buckling tests on welded plate girders. *Welding Research Council Bulletin Series*.
- Brandner, R; Gatternig, W; Schickhofer, G (2012): Determination of shear strength of structural and glued laminated timber. Paper 45-12-2. CIB - Meeting Forty-Five. Växjö, Sweden, pp. 237-254.
- Colling, F (1986): Influence of volume and stress distribution on the shear strength and tensile strength perpendicular to grain. Paper 19-12-2. CIB - Meeting Nineteen, Volume 2. Florence, Italy, pp. 254-276.
- Eberhardsteiner, J (2002): *Mechanisches Verhalten von Fichtenholz – Experimentelle Bestimmung der biaxialen Festigkeitseigenschaften* (in German). Springer.
- Ehrhart, T; Fink, G; Steiger, R; Frangi, A (2016): Strength grading of European beech lamellas for the production of GLT and CLT. Paper 49-5-1. INTER - Meeting Forty-Nine. Graz, Austria, pp. 29-43.
- Ehrhart, T; Steiger, R; Frangi, A (2018): A non-contact method for the determination of fibre direction of European beech wood (*Fagus sylvatica* L.). *European Journal of Wood and Wood Products*, 76(3), pp. 925-935.
- EN 14080 (2013): Timber structures - Glued laminated timber and glued solid timber - Requirements. CEN.
- EN 384 (2016): Structural timber - Determination of characteristic values of mechanical properties and density. CEN.
- EN 408 (2012): Timber structures - Structural timber and glued laminated timber - Determination of some physical and mechanical properties. CEN.
- Foschi, RO; Barrett, JD (1976): Longitudinal shear strength of Douglas-Fir. *Canadian Journal of Civil Engineering*, 3(2), pp. 198–208.
- Foschi, RO; Barrett, JD (1980): Consideration of size effects and longitudinal shear strength for uncracked beams. Paper 13-6-2. CIB - Meeting Thirteen. Otaniemi, Finland, pp. 40-49.

Frese, M; Blaß, HJ (2005): Beech glulam strength classes. Paper 38-6-2. CIB - Meeting Thirty-Eight. Karlsruhe, Germany, pp. 100-110.

Frühwald, K; Schickhofer, G (2005): Strength grading of hardwoods. 14th International Symposium on Nondestructive Testing of Wood. Hanover, Germany, pp. 198–208.

Gehri, E (2010): Shear problems in timber engineering - analysis and solutions. WCTE 2010. Riva del Garda, Italy.

Glos, P; Denzler, JK; Linsenmann, P (2004): Strength and stiffness behaviour of beech laminations for high strength glulam. Paper 37-6-3. CIB - Meeting Thirty-Seven. Edinburgh, Scotland, pp. 82-94.

JCSS (2006): Probabilistic Model Code Part 3: Resistance Models.

van de Kuilen, JW; Gard, W; Ravenshorst, G; Antonelli, V; Kovryga, A (2017): Shear strength values for soft- and hardwoods. Paper 50-6-1. INTER - Meeting Fifty. Kyoto, Japan, pp. 49-65.

Lam, F; Yee, H; Barrett, JD (1995): Shear strength of Canadian softwood structural lumber. Paper 28-6-1. CIB - Meeting Twenty-Eight. Copenhagen, Denmark, pp. 118-134.

Larsen, HJ (1987): Determination of shear strength and strength perpendicular to grain. Paper 20-6-3. CIB - Meeting Twenty, pp. 155-160.

Mistler, HL (1979): Die Tragfähigkeit des am Endauflager unten rechtwinklig ausgeklinkten Brettschichtträgers (in German). Technische Hochschule Karlsruhe, Germany.

prEN 14080-2 (no date): Timber structures - Part 2: Glued laminated timber and glued laminated solid timber made with hardwood - Requirements. CEN.

Ravenshorst, G; van de Kuilen, JW (2010): Relationships between local, global and dynamic modulus of elasticity for soft- and hardwoods. Paper 42-10-1. CIB - Meeting Forty-Two. Dübendorf, Switzerland, pp. 236-247.

Schickhofer, G (2001): Determination of shear strength values for GLT using visual and machine graded spruce laminations. Paper 34-12-6. CIB - Meeting Thirty-Four. Venice, Italy, pp. 383-409.

SIA 265 (2012): Timber Structures. Schweizerischer Ingenieur- und Architektenverein.

Spengler, R (1982): Festigkeitsverhalten von Brettschichtholz unter zweiachsiger Beanspruchung – Teil 1: Ermittlung des Festigkeitsverhaltens von Brettelementen aus Fichte durch Versuche (in German). Technische Universität München. Germany.

Steiger, R; Gehri, E (2011): Interaction of shear stresses and stresses perpendicular to the grain. Paper 44-6-2. CIB - Meeting Forty-Four. Alghero, Italy, pp. 135-149.

Steiger, R; Köhler, J (2005): Analysis of censored data - examples in timber engineering research. Paper 38-17-1. CIB - Meeting Thirty-Eight. Karlsruhe, Germany, pp. 386-399.

Yeh, B; Williamson, TG (2001): Evaluation of glulam shear strength using a fullsize four-point test method. Paper 34-12-2. CIB - Meeting Thirty-Four. Venice, Italy, pp. 327-339.

Discussion

The paper was presented by T Ehrhart

S Aicher commented that finger joint strength information is missing and shear strength comparison with ASTM test method is missing. T Ehrhart agreed that finger joint strength information is important. He explained that the shear test is intended for load configuration similar to one encounters in practice with multiple spans.

BJ Yeh discussed four point bending test method in terms of the reactions and double curvature of the member under load. He asked why failure occurred in the end section where there were low shear stresses. T Ehrhart said that secondary failure occurred in the end section and initial failure occurred in the interior section.

BJ Yeh said that the reaction force can stop the propagation of shear failure. T Ehrhart responded that the initial failure was independent of the presence of glued-in-rod or screw reinforcements.

P Dietsch commented that the assumption of shear crack not being influenced by the reinforcing screws was ok. He commented that industry may not follow the 8% moisture content rule and reinforcement may create confinement and promote crack development. T Ehrhart said that the intent is to create shear failures in multiple span beam structures which is a practical issue.

F Lam commented that 7 replicates is low based on experience in Canada on glulam testing. T Ehrhart responded that this database is intended for use to verify a model with more attention paid to testing of laminae properties. F Lam said this was also the approach taken in Canada but with a large number of replicates especially for the reference depth. F Lam further commented that the three-point bending with an I-section is simpler compared to the multiple span four point tests with fewer issues related to the interpretation of the results.

S Aicher and T Ehrhart discussed issues related to beam width in shear and volume effect versus depth effect and the need for simplification of design rules for practicing engineers.

S Winter received confirmation that effect of laminae thickness was not considered. Also issues related to influence of failure mode on compression perpendicular to grain were discussed. S Winter commented that field experience indicates that even in stable environment beech glulam suffers cracks. Production at 8% MC and testing at 8% MC is idealized. Testing with moisture content variation is needed.

Cross laminated timber at in-plane beam loading – New analytical model predictions and relation to EC5

Mario Jeleč, Department of Materials and Structures, University of Osijek, Croatia

Henrik Danielsson, Division of Structural Mechanics, Lund University, Sweden

Erik Serrano, Division of Structural Mechanics, Lund University, Sweden

Vlatka Rajčić, Department of Structures, University of Zagreb, Croatia

Keywords: CLT, beam, in-plane loading, shear failure, lay-up, FE-analysis

1 Introduction

Beams made of cross laminated timber (CLT) offer several advantages over solid or glued laminated timber beams. Thanks to their orthogonal laminar structure, the transversal layers have a reinforcing effect with respect to the stress perpendicular to the beam axis. Due to the layered composition of CLT, the stress state is however complex and several failure modes and geometry parameters need to be considered in design. Several experimental tests on CLT beams have been conducted, e.g. by Bejtka (2011), Flaig (2013) and Danielsson *et al* (2017a, 2017b).

An analytical model for stress analysis and strength verification has been presented by Flaig & Blass (2013), including stress based failure criteria for relevant failure modes. This model has been used as a basis for the design equations for CLT beams in the current draft version of the new Eurocode 5 (CEN/TC 250/SC5, 2018).

The model by Flaig & Blass includes two basic assumptions related to the shear stresses acting in the crossing areas between the longitudinal and transversal laminations and relevant for shear failure mode III: 1) the stresses are, irrespective of the element lay-up, uniformly distributed in the beam width direction and 2) the torsional moments/stresses are uniformly distributed over all crossing areas in the beam height direction. Based on comparison to 3D FE-analyses as presented by Jelec *et al* (2016) and Danielsson *et al* (2017a), both these assumptions seem to be inaccurate.

The aim of the paper is to present a new model in terms of improvements of the original analytical model by Flaig & Blass (2013). Model improvements as presented by Danielsson & Serrano (2018) are reviewed and further improvements of that model are also presented. The differences between the models concern internal force and stress distributions relevant for shear failure mode III of CLT beams. Predictions of the original and the new analytical models are compared to results of 3D FE-analyses and design proposals based on the new analytical model are presented.

2 Analytical model and relation to EC 5

A brief review of the model presented by Flaig & Blass (2013) for stress analysis and strength verification of shear failure mode III for CLT beams is presented below. The equations presented are based on notation according to Fig. 1 and relate to prismatic CLT beams without edge-bonding and composed of longitudinal laminations of width b_0 and transversal laminations of width b_{90} . The laminations are assumed to have identical stiffness properties.

Index i refers to the position of the longitudinal laminations in the beam height direction and index k refers to their position in the beam width direction. Cross sectional forces and moments are considered at four separate levels: (V, N, M) refer to the total forces and moment acting on the gross cross section, (V_k, N_k, M_k) refer to the total forces and moments acting in the k :th longitudinal layer consisting of m longitudinal laminations, (V_i, N_i, M_i) refer to the total forces and moments acting in the k longitudinal layers at position i in the beam height direction and $(V_{i,k}, N_{i,k}, M_{i,k})$ refer to the forces and the moment acting in an individual longitudinal lamination i, k .

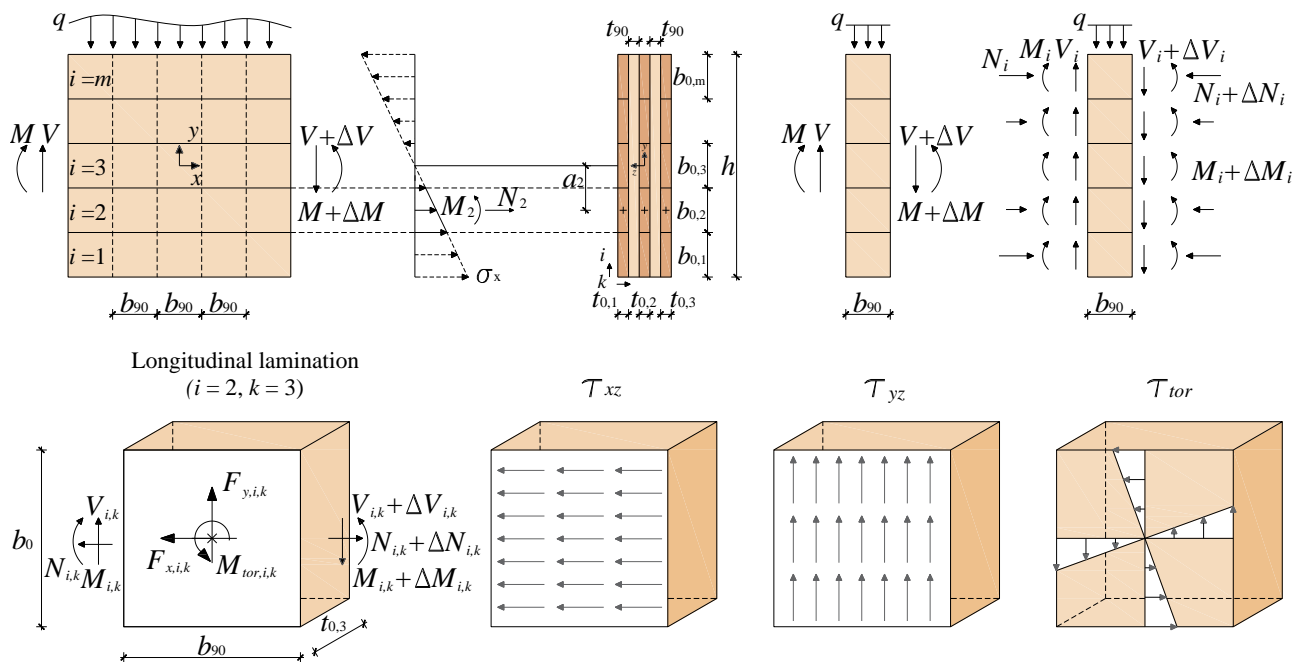


Figure 1. Illustration of beam model and definition of load and geometry parameters.

2.1 Shear mode III

According to the model presented by Flaig & Blass (2013), three shear stress components acting in the crossing area should be considered: (a) shear stress parallel to the beam axis τ_{xz} , (b) shear stress perpendicular to the beam axis τ_{yz} and (c) torsional shear stress τ_{tor} . Assumed shear stress distributions for a single crossing area are shown in Fig. 1. The *maximum* stresses for a beam composed of m longitudinal laminations in the beam height direction and having n_{CA} number of crossing areas in the beam width direction can, according to Flaig & Blass, be expressed as

$$\tau_{xz} = \frac{6V}{b_0^2} \frac{1}{n_{CA}} \left(\frac{1}{m^2} - \frac{1}{m^3} \right) \quad (1)$$

$$\tau_{yz} = \frac{q}{h} \frac{1}{n_{CA}} \quad (2)$$

$$\tau_{tor} = \frac{3V}{b_0^2} \frac{1}{n_{CA}} \left(\frac{1}{m} - \frac{1}{m^3} \right) k_b \quad \text{with } k_b = \frac{2b_{max}b_0}{b_0^2 + b_{90}^2} \quad (3)$$

where b_0 and b_{90} are the longitudinal and transversal lamination widths, respectively, and where $b_{max} = \max(b_0, b_{90})$.

For failure in the crossing areas, based on experimental tests of crossing areas loaded in either uni-axial shear, pure torsion, or a combination of both, failure criteria according to the following equations are proposed by Flaig & Blass (2013)

$$\frac{\tau_{tor}}{f_{v,tor}} + \frac{\tau_{xz}}{f_R} \leq 1.0 \quad (4)$$

$$\frac{\tau_{tor}}{f_{v,tor}} + \frac{\tau_{yz}}{f_R} \leq 1.0 \quad (5)$$

Test results indicate a mean value of the torsional strength of about $f_{v,tor} = 3.5$ MPa and a mean value of the rolling shear strength of about $f_R = 1.5$ MPa, according to Flaig & Blass (2013). The proposed failure criterion according to Eq. (5) includes shear stress perpendicular to the beam axis τ_{yz} which has local influence at supports and load introduction points. This shear stress component is not further considered here.

The shear stress parallel to the beam axis, τ_{xz} , increases with the distance from the neutral axis and Eq. (1) gives the *maximum* value which is found at the lower- and uppermost crossing areas in the beam height direction. The torsional moments and the torsional shear stress τ_{tor} are by assumption equal for all crossing areas in the beam height direction. Therefore, according to the stress interaction criterion given by Eq. (4), the upper- and lowermost crossing areas are the ones relevant for strength verification. Assuming equal torsional moments in the beam height direction corresponds from a static equilibrium point of view to assuming equal lamination shear forces in the beam height direction, i.e. $V_i = V/m$.

3 Model improvements – New analytical model

Improvements of the original model presented by Flaig & Blass (2013), concerning the distributions of internal forces and moments, are presented by Danielsson & Serrano (2018) and reviewed below.

3.1 Longitudinal lamination shear forces $V_{i,k}$

The shear force, V , is carried by the *longitudinal* laminations *only* at locations (in the beam length direction) corresponding to a section between adjacent transversal laminations without edge bonding. The shear force V is for these locations assumed to be distributed between the individual longitudinal laminations i,k according

$$V_{i,k} = \alpha_i \beta_k V \quad (6)$$

where α_i and β_k are dimensionless weighting factors defining the distribution in the beam height (α_i) and in the beam width (β_k) directions. The weighting factors α_i can be derived by considering the parabolic shear stress distribution τ_{xy} known from conventional engineering beam theory and shown in Fig. 2. Based on a dimensionless parabolic function $T(y)$, the weighting factors α_i are expressed as

$$\alpha_i = \int_{-\frac{m}{2} + (i-1)}^{\frac{m}{2} + i} T(y) dy = \frac{6i - 6i^2 + m(6i - 3) - 2}{m^3} \quad (7)$$

A distribution of the lamination shear forces in the beam width direction according to

$$\beta_k = \frac{t_{0,k}}{t_{net,0}} \quad (8)$$

with $t_{net,0} = \sum t_{0,k}$ is further assumed in the proposal by Danielsson & Serrano (2018).

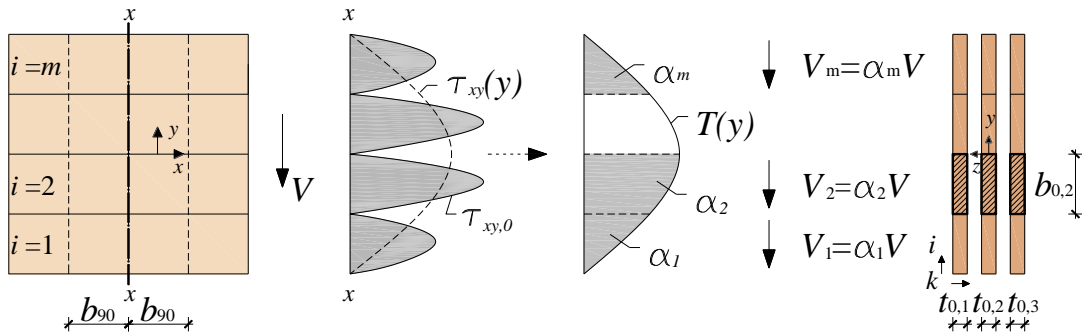


Figure 2. Illustration of shear force/stress distribution according to Danielsson & Serrano (2018).

3.2 Parallel to beam axis forces $F_{x,i,k}$ and stresses $\tau_{xz,i,k}$

The parallel to beam axis force $F_{x,i,k}$ balances the change in the lamination normal force $\Delta N_{i,k}$ over the length b_{90} , see Fig. 1. Considering constant normal stress in the beam width direction and a linear variation in the beam height direction, the parallel to beam axis forces $F_{x,i,k}$ can, by equilibrium considerations, be found as

$$F_{x,i,k} = \frac{12Vb_{90}}{m^3b_0^2} \frac{1}{n_{CA,k}} \frac{t_{0,k}}{t_{net,0}} a_i \quad \text{with} \quad a_i = b_0 \left(\frac{m+1}{2} - i \right) \quad (9)$$

where a_i is the distance in the y -direction between the centre-line of the beam and the centre-line of lamination i,k . Assuming a uniform shear stress distribution over each crossing area gives

$$\tau_{xz,i,k} = \frac{12V}{m^3 b_0^3} \frac{1}{n_{CA,k}} \frac{t_{0,k}}{t_{net,0}} a_i \quad (10)$$

The maximum parallel to beam axis shear stress with respect to the beam height direction is found at the lower- and uppermost crossing area. The stress distribution in the beam width direction is governed by the ratios of $t_{0,k}$, the longitudinal layer widths, to $n_{CA,k}$, the number of crossing areas that an individual longitudinal lamination shares with adjacent transversal laminations (= 1 or 2), i.e. $t_{0,k}/n_{CA,k}$.

3.3 Torsional moments $M_{tor,i,k}$ and stresses $\tau_{tor,i,k}$

Expressions for the torsional moments $M_{tor,i,k}$ and the torsional stresses $\tau_{tor,i,k}$ can be derived by considering equilibrium of a part of a single longitudinal lamination, see Fig. 1. For zero external load q and by using lamination shear forces $V_{i,k}$ according to Eq. (6), the torsional moments may be found as

$$M_{tor,i,k} = \frac{V b_{90}}{n_{CA,k}} \left(\alpha_i \beta_k - \frac{t_{0,k}}{t_{net,0}} \frac{1}{m^3} \right) \quad (11)$$

with α_i and β_k as defined in Section 3.1. Assuming a torsional shear stress distribution according to Fig. 1, the *maximum* torsional shear stress, found at the mid-points of the four sides of crossing area i,k , is then given by

$$\tau_{tor,i,k} = \frac{3V}{b_0^2} \frac{1}{n_{CA,k}} \left(\alpha_i \beta_k - \frac{t_{0,k}}{t_{net,0}} \frac{1}{m^3} \right) k_b \quad \text{with } k_b = \frac{2b_{max}b_0}{b_0^2 + b_{90}^2} \quad (12)$$

Eqs. (11) and (12) give maximum values of the torsional moments and the torsional shear stresses at the crossing areas located closest to the beam centre-line, in-line with the lamination shear force distribution as discussed in Section 3.1.

4 Comparison between analytical and FE-models

Numerical parameter studies were carried out on 3D FE-models in order to investigate the distribution of internal forces and stresses in the beam height and the beam width directions, respectively. The FE-analyses were performed using Ansys 2018 and they present an extension of the FE-analyses presented by Danielsson *et al* (2017). Thus, the same considerations with respect to material (see Table 1) and contact properties, as well as loading and supporting conditions, were used.

Table 1. Material stiffness parameters used for FE-analyses

E_L	E_T	E_R	G_{LT}	G_{LR}	G_{TR}	V_{LT}	V_{LR}	V_{RT}
[MPa]	[MPa]	[MPa]	[MPa]	[MPa]	[MPa]	[-]	[-]	[-]
12000	400	600	750	600	75	0.50	0.50	0.33

The analyses of force and moment distributions in the beam height and width directions were carried out separately considering 3-layer elements (3s) and 5-layer elements (5s), respectively. Due to the highly non-uniform shear stress distributions within the individual crossing areas, results are presented in the form of resulting forces and moments obtained from FE-models by integration of stresses over relevant areas. An illustration of the considered beam geometry and notation for considered forces and moments is shown in Fig. 3. Several influencing parameters were investigated with the underlined values used as reference values:

- Number of laminations in the beam height direction ($m = 2 \dots \underline{4} \dots 8$)
- Lamination width ($b = b_0 = b_{90} = 100, \underline{150}, 200$ mm)
- Width of gap between laminations ($t_{\text{gap}} = \underline{0.1}, 1, 5$ mm)
- Element lay-up for 5-layer elements ($t_{0,2}/t_{0,1} = t_{0,2}/t_{0,3} = 0.31 \dots \underline{2.0} \dots 2.62$)
- Transversal layer width ($t_{90} = 10, \underline{20}, 30$ mm)
- Contact stiffness ($K = 10, \underline{100}, 1000$ N/mm³)
- Approximate FE-mesh size (4, 5, 10 mm)

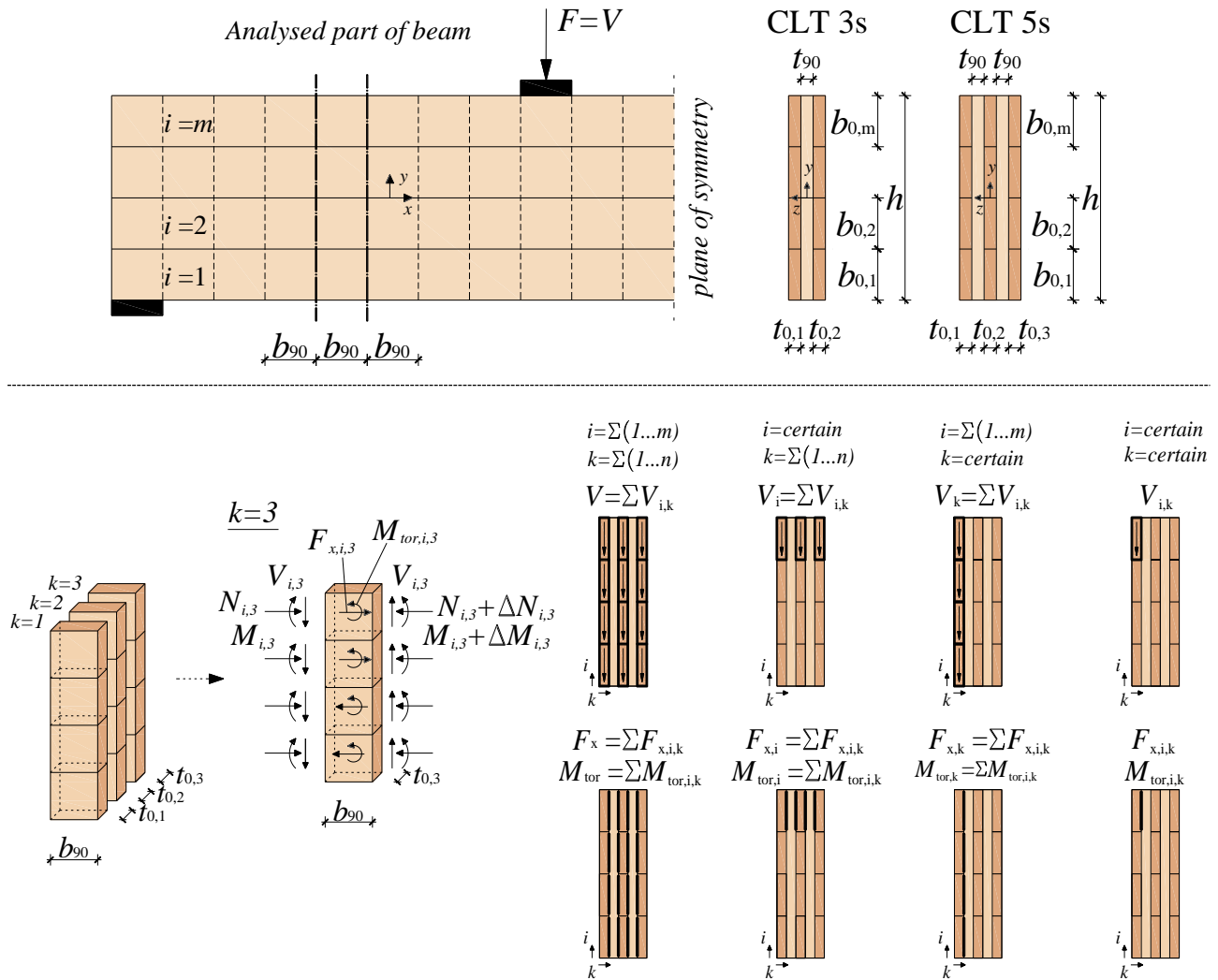


Figure 3. Illustration of geometry and considered forces of FE-analysis

The FE-results presented below are based on reference values of parameters as stated above according to: $b_0 = b_{90} = 150$ mm, $t_{\text{gap}} = 0.1$ mm, $K = 100$ N/mm³ and a FE-mesh based on cubically shaped elements with a side length of about 10 mm. FE-analyses considering other values of parameters as stated above were also carried out but were found to yield only very small influence on the results.

4.1 Results regarding force distribution in the beam height direction

A parameter study of the force distribution in the beam height direction was carried out on 3-layer elements with lay-up 40-20-40, by varying the number of longitudinal laminations m from 2 to 8. Results according to the FE-analyses, the analytical model presented by Flaig & Blass (2013) and the proposed new model are presented for the shear forces V_i in Fig. 4, for the torsional moments $M_{\text{tor},i}$ in Fig. 5 and for the parallel to beam axis forces $F_{x,i}$ in Fig. 6. Forces and moments are presented in a normalized manner as V_i/V , $M_{\text{tor},i}/M_{\text{tor}}$ and $F_{x,i}/F_x$ with definitions according to Fig. 3.

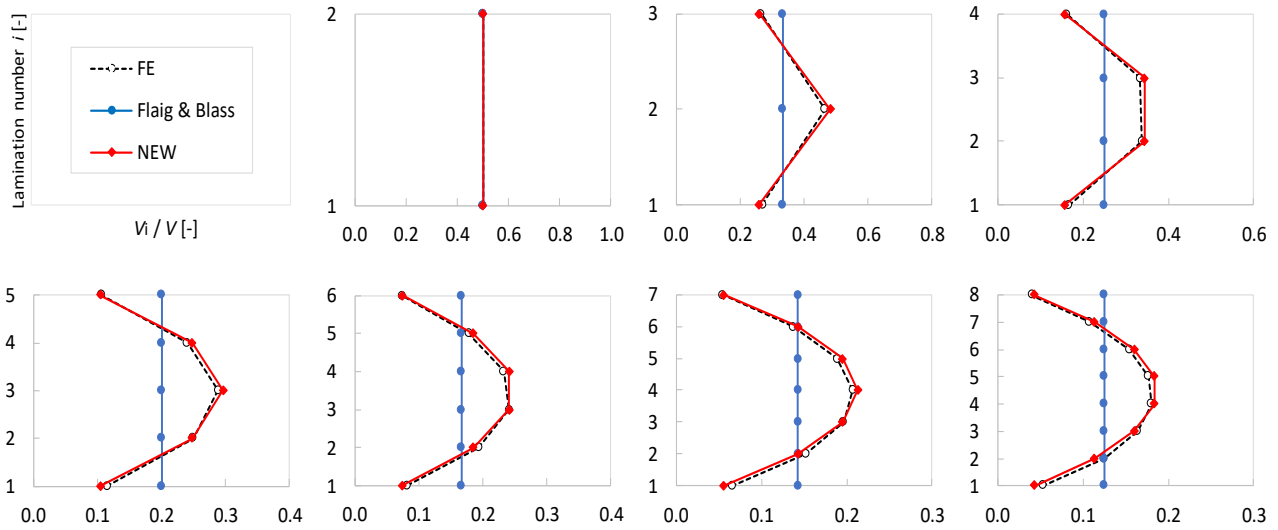


Figure 4. Distribution of shear forces in the beam height direction for CLT 3s (40-20-40).

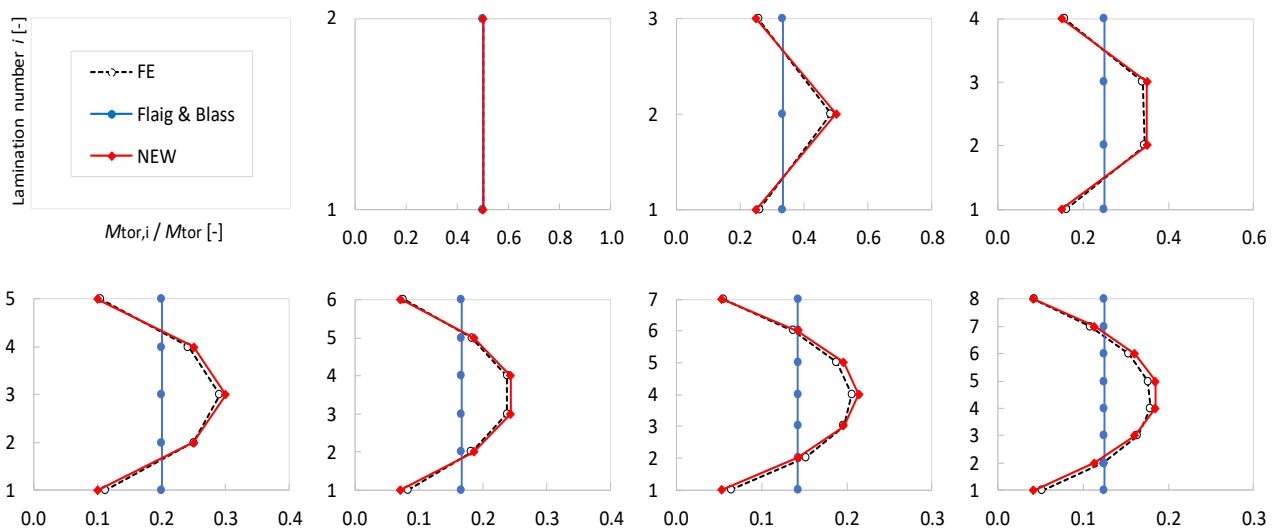


Figure 5. Distribution of torsional moments in the beam height direction for CLT 3s (40-20-40).

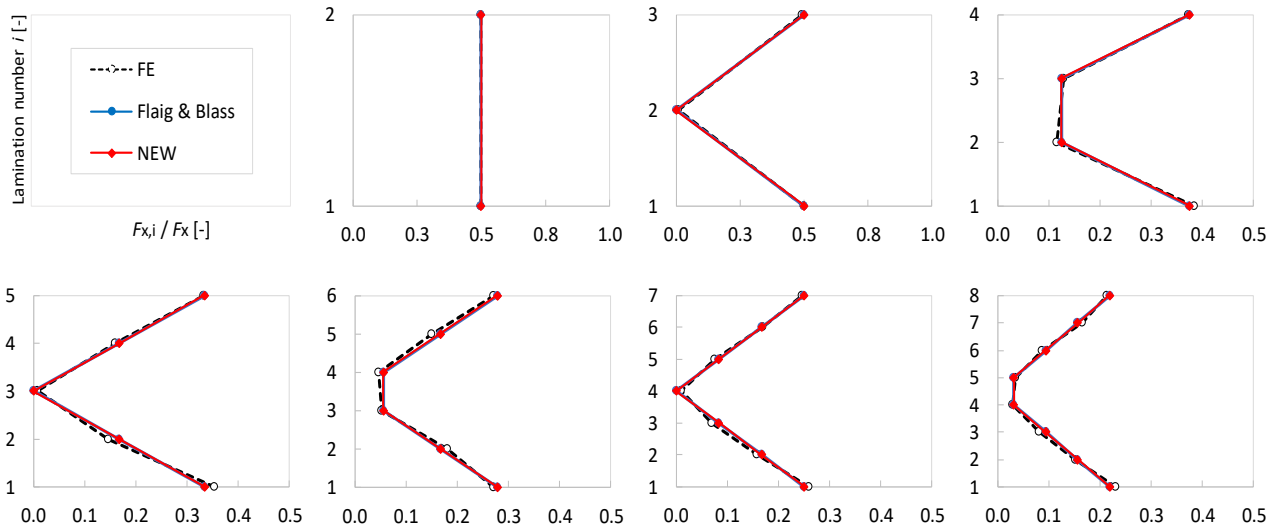


Figure 6. Distribution of parallel to beam axis forces in the beam height direction, CLT 3s (40-20-40).

The graphs presented in Figs. 4 and 5 show very good agreement between FE-results and the new analytical model. Both the FE-analyses and the new analytical model predict significantly higher values of the shear forces V_i and the torsional moments $M_{\text{tor},i}$ close to the beam centre-line than in the upper and lower parts of the beam. The analytical model presented by Flaig & Blass assumes constant torsional moments in the beam height direction, which also corresponds to constant laminations shear forces in that direction. Hence, that model underestimates the torsional moments close to the beam centre-line and overestimates the torsional moments in the upper and lower parts of the beam. The respective ratios V_i/V and $M_{\text{tor},i}/M_{\text{tor}}$ according to the new analytical model are very similar, but not identical.

The comparison of the absolute values of the parallel to beam axis forces $F_{x,i}$, as presented in Fig. 6, show very good agreement between results of the FE-analyses and both analytical models. The two analytical models predict the same forces $F_{x,i,k}$ and shear stresses $\tau_{xz,i,k}$ since the ratio $t_{0,k}/n_{\text{CA},k}$ is constant for 3-layer elements and the assumption of equal shear stress distribution in the beam width direction hence is valid.

4.2 Results regarding force distribution in the beam width direction

A parameter study of the force distribution in the beam width direction was carried out on 5-layer elements composed of $m = 4$ longitudinal laminations in the beam height direction. The influence of the element lay-up was investigated by considering ratios of interior to exterior longitudinal layer widths in the range $t_{0,2}/t_{0,1} = t_{0,2}/t_{0,3} = 0.31 \dots 2.62$ for a fixed net cross section width $t_{\text{net},0} = t_{0,1} + t_{0,2} + t_{0,3} = 120$ mm.

Results for shear forces V_k , torsional moments $M_{\text{tor},k}$ and parallel to beam axis force $F_{x,k}$ are presented in Fig. 7 using definitions according to Fig. 3. Results for shear forces V_k are presented as normalized with respect to the total shear force V (upper left) and also as normalized with respect to the total shear force V and the relative longitudinal layer width $t_{0,k}/t_{\text{net},0}$ (lower left). Results for $M_{\text{tor},k}$ and $F_{x,k}$ are presented in a similar manner: normalized with respect to the totals M_{tor} and F_x (upper centre and upper

right) and also normalized by the totals M_{tor} and F_x , the relative longitudinal layer width $t_{0,k}/t_{\text{net},0}$ and the number of crossing areas $n_{\text{CA},k}$ (lower centre and lower right). For the lower row of Fig. 7, the value 1.0 represents forces and torsional moments as predicted by the new analytical model presented in Section 3.

FE-results regarding the parallel to beam axis forces $F_{x,k}$ and their distribution in the beam width direction agree very well with predictions according to the new analytical model as presented in Section 3. The shear forces and torsional moments found from the FE-analyses show, however, partly different distributions in the beam width direction compared to the new analytical model. For the lay-up $t_{0,2}/t_{0,1} = t_{0,3}/t_{0,1} = 2.0$, the distribution of lamination shear forces V_{ik} according to Eq. (6) using $\beta_k = t_{0,k}/t_{\text{net},0}$ according to Eq. (8) agrees very well with the FE-results. For $t_{0,2}/t_{0,1} = t_{0,3}/t_{0,1} \leq 2.0$, the FE-analyses yield larger shear forces and torsional moments for the interior longitudinal layer ($k = 2$) compared to the analytical model predictions.

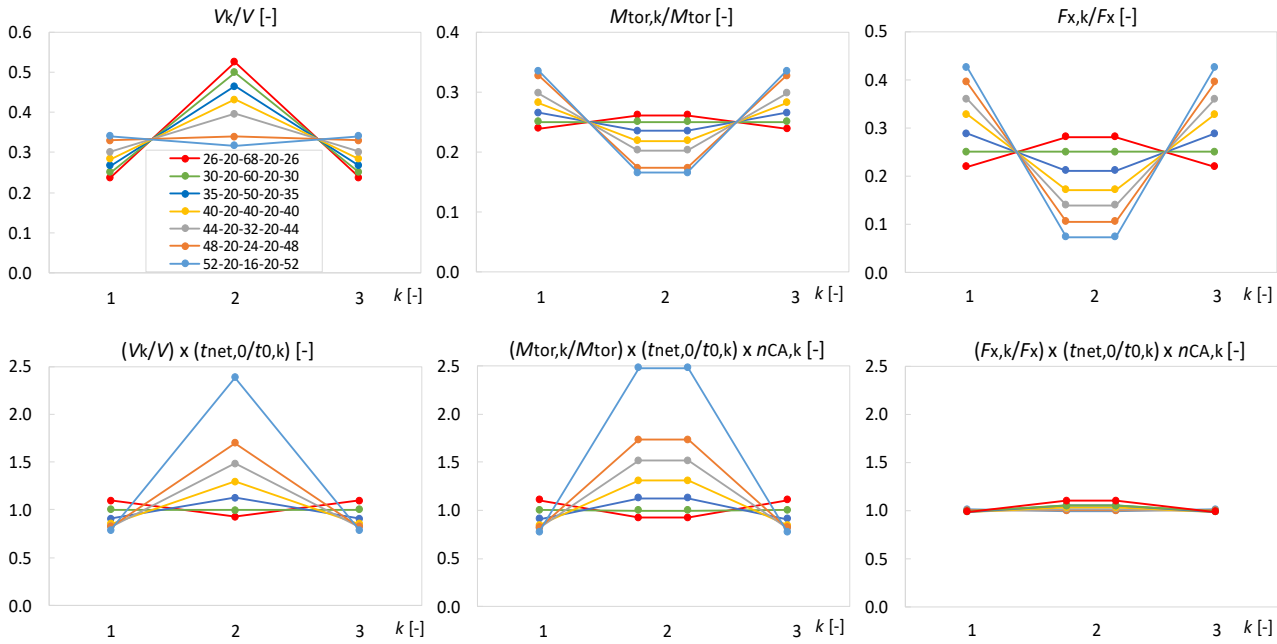


Figure 7. FE-results of influence of lay-up on distribution in beam width direction for CLT element 5s.

Alternative expressions for the weighting factors β_k were determined by manual curve-fitting to the shear force distribution found from the FE-analyses. Weighting factors according to

$$\beta_k = \begin{cases} \frac{1}{8} \left(1 + 4 \frac{t_{0,k}}{t_{\text{net},0}} \right) & \text{for } k = 1, 3 \\ \frac{1}{4} \left(1 + 2 \frac{t_{0,k}}{t_{\text{net},0}} \right) & \text{for } k = 2 \end{cases} \quad (13)$$

where found to yield good agreement for the 5-layer element lay-ups considered in the parameter study. For the special case of $t_{0,2}/t_{0,1} = t_{0,2}/t_{0,3} = 2.0$ with constant ratio $t_{0,k}/n_{\text{CA},k}$, Eq. (13) gives the same weighting factors β_k as Eq. (8). Weighting factors β_k

given in Eq. (13) are not included in the model by Danielsson & Serrano (2018) and hence represent an extension of that model.

A comparison between FE-results and the new analytical model is presented in Fig. 8 regarding lamination shear forces V_k , torsional moments $M_{\text{tor},k}$ and parallel to beam axis forces $F_{x,k}$. The marks represent FE-results and predictions according to the new analytical model as presented in Section 3 are represented by solid lines. Dashed lines represent the shear forces V_k and the torsional moments $M_{\text{tor},k}$ according to the new analytical model and use of weighting factors β_k according to Eq. (13).

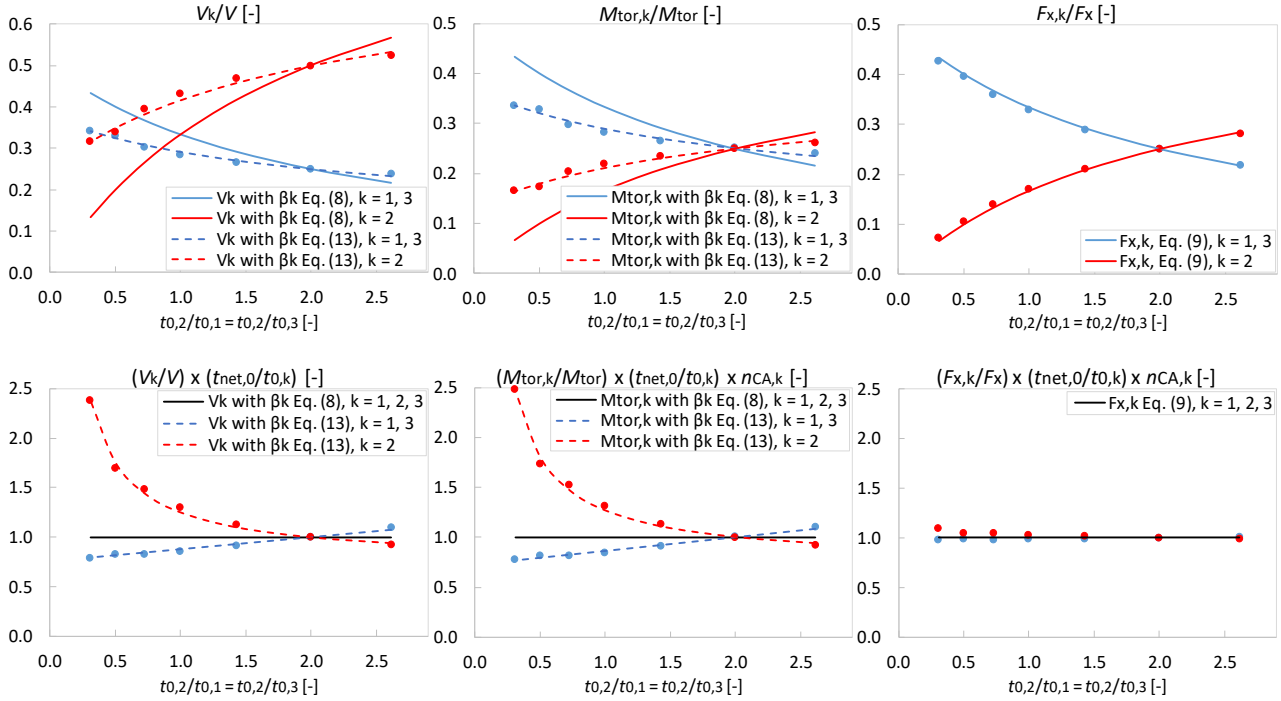


Figure 8. Comparison between FE-results (marks) and proposed new model (lines) regarding the influence of the element lay-up on the distribution of forces in the beam width direction for CLT 5s.

5 Discussion and background of design proposals

The original model according to Flaig & Blass (2013) and new model improvements have here been compared to a numerical model based on 3D FE-analyses. The non-uniform distribution of the torsional moments $M_{\text{tor},i,k}$ in the beam height direction based on weighting factors α_i as proposed by Danielsson & Serrano (2018) shows very good agreement with the FE-results. It is further evident that the element lay-up in terms of the relative longitudinal layer widths $t_{0,k}/t_{\text{net},0}$ and the ratio $t_{0,k}/n_{\text{CA},k}$ influence the stress distribution in the beam width direction.

The distributions of the lamination shear forces $V_{i,k}$ and the torsional moments $M_{\text{tor},i,k}$ in the beam width direction based on β_k according to Eq. (8) differ partly compared the FE-results. For 5-layer CLT elements typically used in practice, with lay-ups in the range of $0.5 \leq t_{0,2}/t_{0,1} = t_{0,2}/t_{0,3} \leq 1.0$, the maximum torsional moment is found for crossing areas at the exterior longitudinal layers, i.e. for $k = 1, 3$. Within this range of lay-ups

and for the exterior crossing areas, the torsional moments $M_{\text{tor},i,k}$ according to Eq. (11) with θ_k according to Eq. (8) are about 20% higher than found from the FE-analyses. Regarding practical design, calculation of the torsional moments in this manner hence yields a (safe side) overestimation compared to the FE-results. The alternative expression for θ_k according to Eq. (13) gives good agreement with the FE-results.

The maximum torsional moment and the maximum parallel to beam axis force occur at different crossing areas, see Figs. 5 and 6. Using the failure criterion in Eq. (4) with the maximum value of $\tau_{xz,i,k}$ according to Eq. (10) and the maximum value of $\tau_{\text{tor},i,k}$ according to Eq. (12) would then be mechanically incorrect (and conservative).

Since the failure criterion in Eq. (4) is based on consideration of two different shear strengths, $f_{v,\text{tor}}$ and f_R , it is not straightforward to determine which crossing area that is mostly stressed. Distributions of the maximum values of $\tau_{\text{tor}}/f_{v,\text{tor}}$, τ_{xz}/f_R and $\tau_{\text{tor}}/f_{v,\text{tor}} + \tau_{xz}/f_R$ for the individual crossing areas in the beam height direction are presented in Fig. 9, considering a fixed ratio of the strength values as $f_{v,\text{tor}}/f_R = 3.5/1.5 = 2.33$. The stress components are normalized in such a way that $\max\{\tau_{\text{tor}}/f_{v,\text{tor}} + \tau_{xz}/f_R\} = 1.0$. The critical crossing areas are here found as either the two most centrally placed ($m = \text{even}$) or the two crossing areas placed next to the centric crossing area ($m = \text{odd}$).

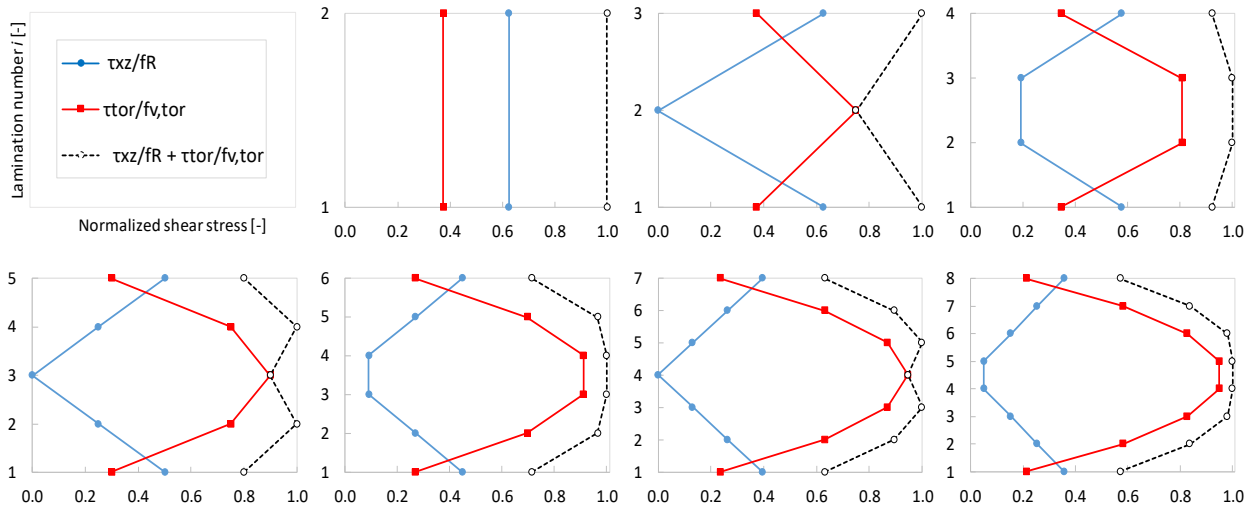


Figure 9. Distributions of $\tau_{\text{tor}}/f_{v,\text{tor}}$, τ_{xz}/f_R and $\tau_{\text{tor}}/f_{v,\text{tor}} + \tau_{xz}/f_R$ in beam height direction for $2 \leq m \leq 8$ for CLT beam 5s (40-20-40-20-40) considering θ_k according to Eq. (13) and $b_0 = b_{90} = 150$ mm

For practical design purposes, it is desirable to increase the ease-of-use by finding reasonably simple expressions for the torsional shear stress τ_{tor} and the parallel to beam axis shear stress τ_{xz} for the critical crossing area, irrespective of m being odd or even. Two designs proposals are presented in Section 6, based on the discussion and comparisons presented in Sections 5.1 and 5.2.

5.1 Background of design proposal 1

An approximation of τ_{xz} for the critical crossing area can be found from Eq. (10) by considering $a_i = b_0/2$, giving

$$\tau_{xz} = \frac{6V}{b_0^2} \frac{1}{n_{CA,k}} \frac{t_{0,k}}{t_{net,0}} \frac{1}{m^3} \quad (14)$$

which is exact for even numbers m compared to the analytical model as presented in Section 3 and shown in Fig. 9. For odd m , Eq. (14) represents an overestimation of τ_{xz} for the centrally placed crossing area and an underestimation of τ_{xz} for the critical crossing areas placed next to the centric one.

The maximum torsional shear stress according to Eq. (12) is determined by the maximum value of α_i according to Eq. (7). Considering the two cases of even and odd number of longitudinal laminations in the beam height direction separately, exact maximum values of α_i are given by

$$\max\{\alpha_i\} = \frac{3m^2 - 4}{2m^3} \quad \text{for } m = 2, 4, 6 \dots \quad (15)$$

$$\max\{\alpha_i\} = \frac{3m^2 - 1}{2m^3} \quad \text{for } m = 3, 5, 7 \dots \quad (16)$$

The maximum values of α_i for the general case given by Eq. (7) and according to Eqs. (15) and (16) are illustrated in Fig. 10. Eq. (15) yields an underestimation of the maximum value of τ_{tor} for odd m while Eq. (16) yields an overestimation of the maximum value of τ_{tor} for even m . For the critical crossing areas, Eq. (15) does however yield an overestimation of the design relevant value of τ_{tor} also for odd m since the critical crossing area is placed next to the most centric crossing area.

To arrive at reasonably simple expressions for design purposes, the torsional shear stress in the critical crossing area can be determined using Eq. (12) with $\max\{\alpha_i\}$ according to Eq. (15) while the parallel to beam axis shear in the critical crossing area can be determined using Eq. (14). This approach yields exact results compared to the analytical model as presented in Section 3 for even m . For odd m , the underestimation of τ_{xz} in the critical crossing area is compensated by an overestimation of τ_{tor} in the same crossing area and overall accurate predictions are obtained. This proposal is presented in Section 6 as design proposal 1.

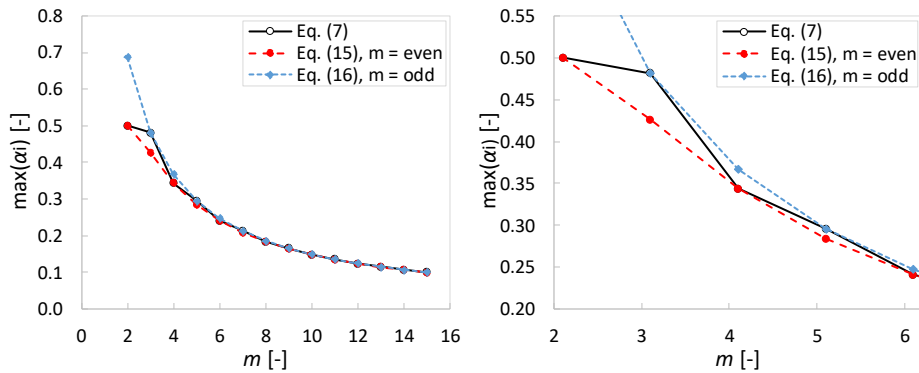


Figure 10. Comparison of $\max\{\alpha_i\}$ according to Eqs. (7), (15) and (16) for $2 \leq m \leq 15$.

5.2 Background of design proposal 2

To arrive at more simplified design equations compare to proposal 1, the factors α_i and β_k can be combined into a single factor γ . The maximum torsional shear stress according to Eq (12) may then be expressed as

$$\tau_{tor} = \frac{3V}{b_0^2} \frac{t_{0,k}}{t_{net,0}} \left(\frac{1}{m} - \frac{1}{m^3} \right) k_b \gamma \quad (17)$$

where the dimensionless factor γ is given by

$$\gamma = \frac{\left[\max\{\alpha_i\} \beta_1 \left(t_{net,0}/t_{0,k} \right) - 1/m^3 \right]}{\left(1/m - 1/m^3 \right)} \quad (18)$$

Exact values of the factors γ according to Eq. (18) are shown in Fig. 11 for CLT 5s with $2 \leq m \leq 15$ and for the two options of β_1 ; as defined in Section 3 and denoted as γ_1 and as found by curve-fitting to FE-results in Section 4 and denoted as γ_2 , respectively. Weighting factors α_i are according to Eq. (7). Based on this, simplifications as illustrated in Fig. 11 (right) can be made to avoid including the factors α_i and β_k in the design equations. A conservative simplification is $\gamma_1 = 1.5$, based on the maximum value of γ using β_1 according to Eq. (8). Another simplification, and in relation to the presented FE-results an overall more accurate one, can be made based on the mean values of the factors γ , denoted as γ_2 , within the interval $3 \leq m \leq 15$ for each of the individual lay-ups and using β_1 according to Eq. (13). The conservative simplification $\gamma_1 = 1.5$ is valid also for CLT 3s.

Concerning τ_{xz} , approximation according to Eq. (14) may be used also here. This proposal is presented in Section 6 as design proposal 2.

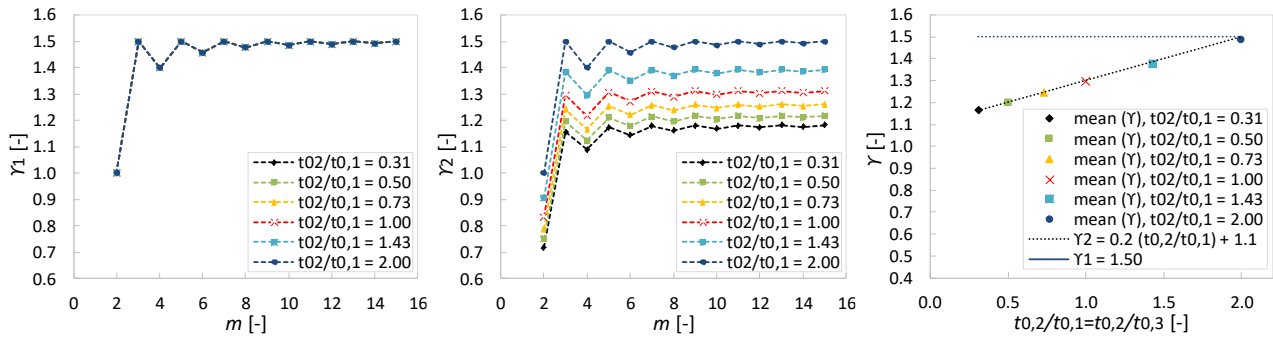


Figure 11. Factors γ_1 and γ_2 according to Eq. (18) with β_k according to Eq. (8) (left) and Eq. (13) (centre) and the mean values of γ_1 and γ_2 within the interval $3 \leq m \leq 15$ for different lay-ups of CLT 5s (right).

6 Design proposals and concluding remarks

Two alternative design proposals are presented below, based on the discussion in the previous section. Both proposals are based on:

- comparison of forces and moments between analytical and FE-analyses,

- crossing area shear stress distributions as illustrated in Fig. 1,
- shear mode III failure criterion according to Eq. (4) with a ratio between the proposed strength values as $f_{v,tor}/f_R \approx 2.3$.

Design proposal 1 is aimed at being as exact as possible in relation to the FE-results while keeping design equations fairly simple. Design proposal 2 is aimed at obtaining further simplification of the design equations while yet retaining as much as possible of the important design aspects and being exact or conservative in relation to the FE-results.

6.1 Design proposal 1

Design relevant crossing area shear stresses τ_{xz} and τ_{tor} are approximated as

$$\tau_{xz} = \frac{6V}{b_0^2} \frac{t_{0,1}}{t_{net,0}} \frac{1}{m^3} \quad (19)$$

$$\tau_{tor} = \frac{3V}{b_0^2} \left(\alpha_{i,max} \beta_1 - \frac{t_{0,1}}{t_{net,0}} \frac{1}{m^3} \right) k_b \quad \text{with } k_b = \frac{2b_{max}b_0}{b_0^2 + b_{90}^2} \quad (20)$$

where

$$\alpha_{i,max} = \frac{3m^2 - 4}{2m^3} \quad (21)$$

$$\beta_1 = \begin{cases} \frac{t_{0,1}}{t_{net,0}} & \text{for 3-layer CLT beams} \\ \frac{1}{8} \left(1 + 4 \frac{t_{0,1}}{t_{net,0}} \right) & \text{for 5-layer CLT beams} \end{cases} \quad (22)$$

6.2 Design proposal 2

Design relevant crossing area shear stresses τ_{xz} and τ_{tor} are approximated as

$$\tau_{xz} = \frac{6V}{b_0^2} \frac{t_{0,1}}{t_{net,0}} \frac{1}{m^3} \quad (23)$$

$$\tau_{tor} = \frac{3V}{b_0^2} \frac{t_{0,1}}{t_{net,0}} \left(\frac{1}{m} - \frac{1}{m^3} \right) k_b \gamma \quad \text{with } k_b = \frac{2b_{max}b_0}{b_0^2 + b_{90}^2} \quad (24)$$

where

$$\gamma = \begin{cases} 1.5 & \text{for 3-layer CLT beams} \\ 0.2 \frac{t_{0,2}}{t_{0,1}} + 1.1 & \text{for 5-layer CLT beams} \end{cases} \quad (25)$$

6.3 Comments on design proposals and concluding remarks

Both proposals are valid for 3- and 5-layer elements, with the restriction on element lay-up as $t_{0,2}/t_{0,1} = t_{0,2}/t_{0,3} \leq 2.0$ for 5-layer elements. The proposals are further limited in validity to element orientation such that the surface layers are oriented in the beam

length (x) direction. Further studies of CLT beam with inverted layer orientation and also studies of 7-layer elements should preferably be carried out.

A third proposal can be found from further simplification of design proposal 2, by using $\gamma = 1.5$ also for 5-layer CLT beams. This safe side assumption would render design equations no more complex, yet more accurate, than the equations found in the current draft version of the new Eurocode 5 (CEN/TC 250/SC5, 2018).

The proposals are based on assuming equal longitudinal lamination width b_0 for all m laminations in the beam height direction. Dimensions and placement of laminations with respect to the element edges are however in general not known in the actual design situation since the CLT beams in general are cut from larger elements, with no consideration of the location of the individual laminations. Following the recommendation in the draft version of the new Eurocode 5 (CEN/TC 250/SC5, 2018), in cases where the lamination width is not known, it should be assumed as $b_0 = b_{90} = 80$ mm.

The two proposals are solely based on comparison between analytical model predictions and FE-analyses, assuming the crossing area shear stress distributions and the failure criterion proposed by Flaig & Blass (2013) to be valid. Verification of the proposed models by comparison to experimental test results should be carried out.

7 Literature

Ansys Inc. 2018 (2017)

Bejtka I (2011): Cross (CLT) and diagonal (DLT) laminated timber as innovative material for beam elements. KIT, Karlsruhe, Germany.

CEN/TC 250/SC5 (2018): Working draft of design of cross laminated timber in a revised Eurocode 5-1-1, Version 2018-04-13, part of N892.

Danielsson H, Serrano E, Jeleč M, Rajčić V (2017a): In-plane loaded CLT beams – Tests and analysis of element lay-up. In: Proc. INTER, INTER/50-12-2, Kyoto, Japan.

Danielsson H, Jeleč M, Serrano E (2017b): Strength and stiffness of cross laminated timber at in-plane beam loading. Report TVSM-7164, Division of Structural Mechanics, Lund University, Sweden.

Danielsson H, Serrano E (2018): Cross laminated timber at in-plane beam loading – Prediction of shear stresses in crossing areas. Engineering Structures, <https://doi.org/10.1016/j.engstruct.2018.03.018>.

Flaig M (2013): Biegeträger aus Brettsper Holz bei Beanspruchung in Plattebene. PhD thesis, KIT, Karlsruhe, Germany.

Flaig M, Blass HJ (2013): Shear strength and shear stiffness of CLT-beams loaded in plane. In: Proc. CIB-W18, CIB-W18/ 46-12-3, Vancouver, Canada.

Jeleč M, Rajčić V, Danielsson H, Serrano E (2016): Structural analysis of in-plane loaded CLT beam with holes: FE-analysis and parameter studies. In: Proc. INTER, INTER/49-12-2, Graz, Austria.

Discussion

The paper was presented by M Jeleč

H Blass commented that constant shear distribution across the beam width was not considered in earlier work as only one layup was studied. M Jeleč agreed. H Danielsson discussed previous work when this was also assumed.

Seismic Resilient CLT buildings Using Resilient Slip Friction Joints (RSFJs) with Collapse Prevention Mechanism: Ductility, Design Methods and Numerical Validation

Ashkan Hashemi, University of Auckland, New Zealand

Pouyan Zarnani, Auckland University of Technology, New Zealand

Farhad Mohammadi Darani, Auckland University of Technology, New Zealand

Seyed Mohammad Mahdi Yousef-Beik, Auckland University of Technology, New Zealand

Pierre Quenneville, University of Auckland, New Zealand

Keywords: Cross Laminated Timber, CLT, seismic, resilient, self-centring, ductility, design, earthquake.

1 Introduction

Many researchers have investigated the seismic performance of CLT structures. These panels are recognised to have high lateral strength and stiffness, however, might have low ductility and low energy dissipation capacity respecting the type, location and capacity of the connectors (force and displacement capacity).

In recent years, Cross Laminated Timber (CLT) has been widely used for different types of buildings such as offices, commercial buildings, public buildings and multi-story residential complexes. Since these panels are also the main lateral load resisting members, the seismic performance of the system relies on their lateral strength and stiffness. Therefore, extensive research on the seismic behaviour of these structures are being conducted by many research groups around the world in order to evaluate the feasibility of adopting this structural system in high seismic active areas.

The most extensive experimental research about the seismic performance of CLT structures has been conducted within the SOFIE project (Ceccotti et al. 2013). That project included quasi-static tests on a single-story CLT building with different layouts, shake table tests on a three story CLT building and a series of full scale shake table tests on a seven story CLT platform structure. The results confirmed that the CLT structures with traditional connections are relatively stiff and could survive the design level earthquakes with minimum damage. Nevertheless, some of the steel connections (such as nailed hold-downs and nailed shear brackets) yielded in bending and some withdrew from the timber elements. Furthermore, high response accelerations mainly in the upper levels with a maximum of 3.8 g were recorded. Accelerations this high evidently have the potential to seriously harm the occupants, and thus it is reasonable to consider a method to reduce them.

Popovski et al. investigated the seismic response of the CLT wall panels with various arrangements and connection layouts for application in platform structures (Popovski et al. 2010; Popovski and Karacabeyli 2012). The data would seem to suggest that these walls have satisfactory lateral resistance when nails or slender screws are used together with steel brackets. Moreover, the use of hold-downs with nails at the corners of the walls was proven to improve the resistance to overturning from the lateral forces. That can be attributed to the increased moment lever arm for the wall panels.

Gavric et al. experimentally investigated the cyclic behaviour of single and coupled CLT walls with different connections (Gavric et al. 2015). The test results suggested that the layout and design of the connections govern the overall behaviour of the wall. While the in-plane deformations of the panels were almost negligible, inelastic deformations in the connection parts lead to local failures in the system.

Popovski et al. conducted a series of full scale quasi-static tests on a two story CLT structure (Popovski and Gavric 2015). No global instability was observed not even at the maximum design lateral force. Regardless of the rigid connections between the floors and walls, rocking movement of the wall panels was not totally restricted by the floor above.

Yasumura et al. studied the mechanical performance of low-rise CLT platform building with large and small panels subjected to reversed cyclic lateral loads (Yasumura et al. 2015). It was concluded that in the buildings with small panels, rotation of the panels was the major cause of the total deformation of the building. They also proposed a numerical model to predict the seismic behaviour of such structures based on the connectors in use.

Regardless of the satisfactory seismic resistance of the abovementioned CLT structures, in most cases, the connections suffered from large plastic deformations at the end of the earthquake or the end of the cyclic test (Varoglu et al. 2006). This means that many of these connectors should be repaired or replaced after a major seismic

event which can be significantly costly or even impossible because of accessibility issue.

While the seismic behaviour of the conventional CLT structures may be acceptable, however, they have three significant shortcomings. Firstly, the irrecoverable inelastic behaviour of the fasteners not only reduces the lateral stiffness of the building but also considerably decreases the energy dissipation capacity over time resulting in instability in large/long earthquakes. Secondly, these structures mostly rely on the gravity loads and their self-weight to return them to the initial position after the earthquake that is not necessarily sufficient. Previous studies showed that residual drifts greater than 0.5% in steel structures may result in the complete loss of the structure from an economic point of view (McCormick et al. 2008).

This paper introduces a new damage avoidance seismic solution for CLT structures where traditional connectors are replaced with Resilient Slip friction Joints (RSFJs). Furthermore, a simple step-by-step structural analysis and design procedure for these structures is proposed that is based on the use of Equivalent Static Method (ESM). The proposed procedure is applied to a five-story CLT structure and verified by non-linear static pushover and non-linear dynamic time-history simulations.

2 Seismic resilient CLT structures with Resilient Slip Friction Joints (RSFJs)

Passive sliding friction dampers were originally developed by Pall et al. for the steel braced frames and concrete panels (Baktash et al. 1983; Pall et al. 1980; Pall and Marsh 1982). Popov et al. later introduced the symmetric slotted bolted connection for steel moment frames which dissipates energy through friction while producing equilateral load-deformation curves in tension and compression (Popov et al. 1995). Clifton et al. proposed the asymmetric Sliding Hinge Joint (SHJ) for steel moment resisting frames which had non-rectangular yet stable hysteretic behaviour (Clifton et al. 2007). For timber structures, Filiatrault utilized the sliding friction devices for timber sheathed shear walls (Filiatrault 1990). His studies revealed a promising improvement in the hysteretic behaviour of the walls compared to traditional timber shear walls. Large amounts of dissipated energy were also observed at various lateral drifts up to a maximum of 1.5%.

Loo et al. investigated the application of flat slip friction connections as a replacement of traditional hold-downs for timber Laminated Veneer Lumber (LVL) walls (Loo et al. 2014). Their experiments showed a significantly improved seismic performance compared to traditional systems in terms of stability and hysteretic damping. Never-

theless, it was shown that a self-centring behaviour could only be achieved by applying the gravity loads to the rocking wall. This research was later expanded to the CLT coupled walls and hybrid timber-steel core walls (Hashemi et al. 2016b; a) and it was shown that in spite of reliable low damage seismic performance of the proposed systems, an additional mechanism is required to provide the self-centring behaviour.

Resilient Slip Friction Joint (RSFJ) technology was invented and introduced by Zarnani and Quenneville (Zarnani and Quenneville 2015). This joint is a friction-based energy dissipation device that can absorb the seismic energy and provide a self-centring behaviour resulting in a flag-shaped hysteresis. Figure 1 illustrates the components and hysteresis related to the RSFJ. Similar to the conventional friction dampers, RSFJ dissipates energy via sliding movement of the clamped plates. However, owing to the special grooved shape of the sliding plates, the elastic energy preserved in the compacted disc springs allows to plates to return to their original position without any additional mechanism. In other words, RSFJ provides energy dissipation and self-centring behaviour all in one compact device.

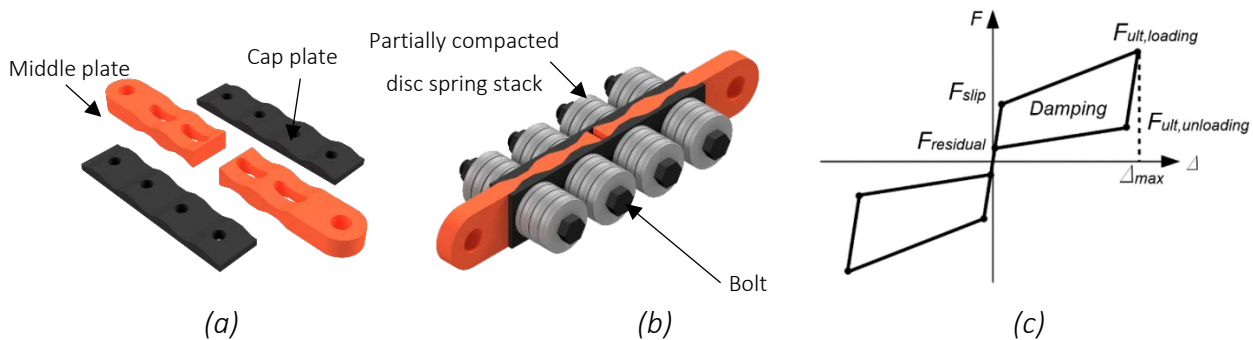


Figure 1. Resilient Slip Friction Joint (RSFJ): (a) sliding plates (b) assembly (b) hysteresis

RSFJ hysteretic parameters (F_{slip} , $F_{ult,loading}$, $F_{ult,unloading}$, $F_{residual}$ and Δ_{max}) shown in Figure 1(c) can be determined based on the design requirements. In other words, this technology offers a significant level of flexibility in design in such that the designer can almost achieve any target flag-shaped hysteresis that suits the design requirements. Hashemi et al. experimentally investigated the hysteretic behaviour of the RSFJ in the component level and large-scale level (Hashemi et al. 2017a). Figure 2(a) shows the first full-scale manufactured RSFJ that was subjected to joint component testing. It was demonstrated that the performance of the RSFJ is stable and in accordance with the theoretically predicted behaviour (see Figure 2(c)).

Similar RSFJs were later used as hold-down connections for a rocking CLT wall (Figure 2(b)). The experimentally obtained results confirmed the excellent performance of the proposed concept that yet again seem to be consistent with the proposed analytical equations (Figure 2(d)). The performance of the system was stable with a fully self-centring behaviour.

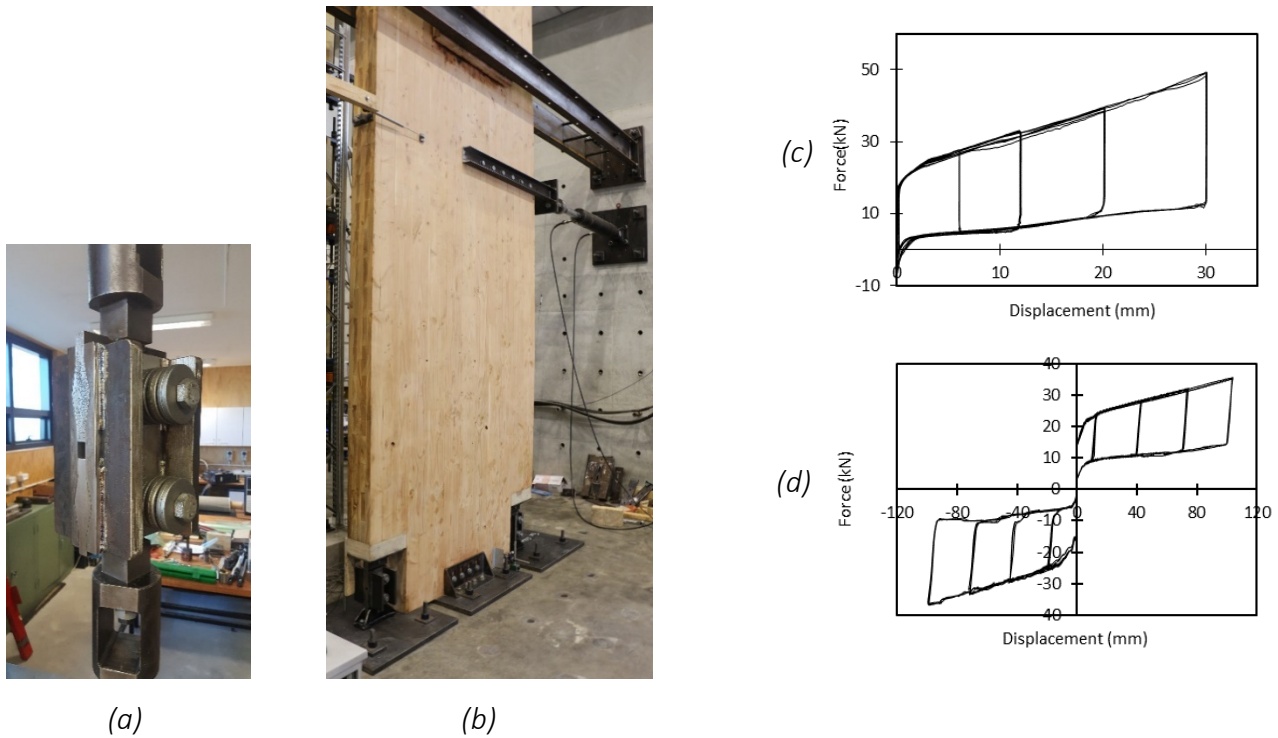


Figure 2. Experimental investigation of the CLT wall with RSFJs (a) joint component testing (b) large-scale CLT shear wall testing (c) joint component test results (d) large-scale CLT shear wall test results

It should be pointed out that when it is required by design, a collapse-prevention secondary fuse can be considered within the body of the RSFJ to act as the over-strength mechanism for the system. As can be seen in Figure 3, when the RSFJ reaches the maximum capacity (either in tension or compression) and discs are flat, the clamping bolts will yield to provide more elongation for the joint. This mechanism is usually used for Maximum Considered Event (MCE) level seismic loads. More details can be found in (Hashemi et al. 2018) including the design equations for the secondary fuse and the conducted experimental tests to verify its behaviour. It should be noticed that based on the experimental results, an over-strength factor of 1.25 to 1.4 is recommended based on the size and grade of the yielding bolts (or rods).

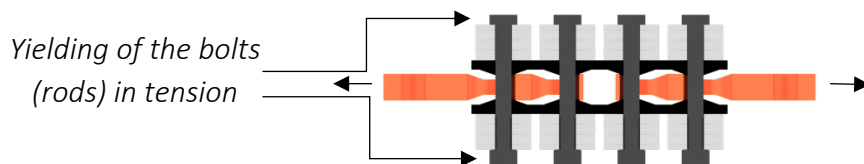


Figure 3. The optional over-strength mechanism of the RSFJ (secondary fuse)

3 The analysis and design procedure recommended for CLT structures with RSFJs

The Equivalent Static Method (ESM) is the most favourable way to calculate the seismic forces worldwide. The reason is firstly the simplicity of this method and secondly the fairly accurate (yet conservative) results. In this method, the earthquake excitations are represented as horizontal static loads applied to story levels in which the amount of loads usually depend on soil type, period of the structure, importance level and type of the lateral load resisting system. When a ductile behaviour is expected from the structure, the calculated elastic seismic loads are reduced by a factor which is related to the level of ductility. In the New Zealand standard for structural design actions, this factor is defined as the “inelastic spectrum scaling factor (k_μ)” which is related to the structural ductility factor (μ) and the period of the structure (T_1). k_μ can be calculated using the following equations:

$$k_\mu = \mu \quad \text{for } T_1 \geq 0.7 \text{ sec} \quad (1)$$

$$k_\mu = \frac{(\mu-1)T_1}{0.7} + 1 \quad \text{for } T_1 < 0.7 \text{ sec} \quad (2)$$

The calculated elastic base shear for the structure is reduced by the k_μ factor to account for the ductility introduced to the structure.

The step-by-step structural analysis and design procedure shown in Figure 4 is recommended when designing seismic resistant structures with RSFJs. This procedure which is based on the ESM in the New Zealand standard, requires non-linear static push-over simulations (in general) and non-linear dynamic time-history simulations when a more sophisticated design is targeted. It should be noted that although this procedure is based on the New Zealand standard, most of the building codes around the world use a similar approach where the calculated elastic seismic loads is reduced by the a ductility related reduction factor. Thus, this procedure is easily adoptable for other building standards.

As can be seen in Figure 4, the procedure has two sections. The right procedure is recommended when the designer wishes to perform non-linear dynamic time-history simulations. In this case, an equivalent ductility factor of $\mu = 3$ is adopted at the start and will be verified and optimised by the time-history analyses at the end. When adopting the right procedure, iterations may be required to achieve the accurate equivalent ductility factor and the optimised design. Alternatively, the left procedure in Figure 4 can be adopted if the time-history verifications are not aimed for. In this case, a more conservative equivalent ductility factor $\mu = 2$ is recommended to be adopted at the start.

START

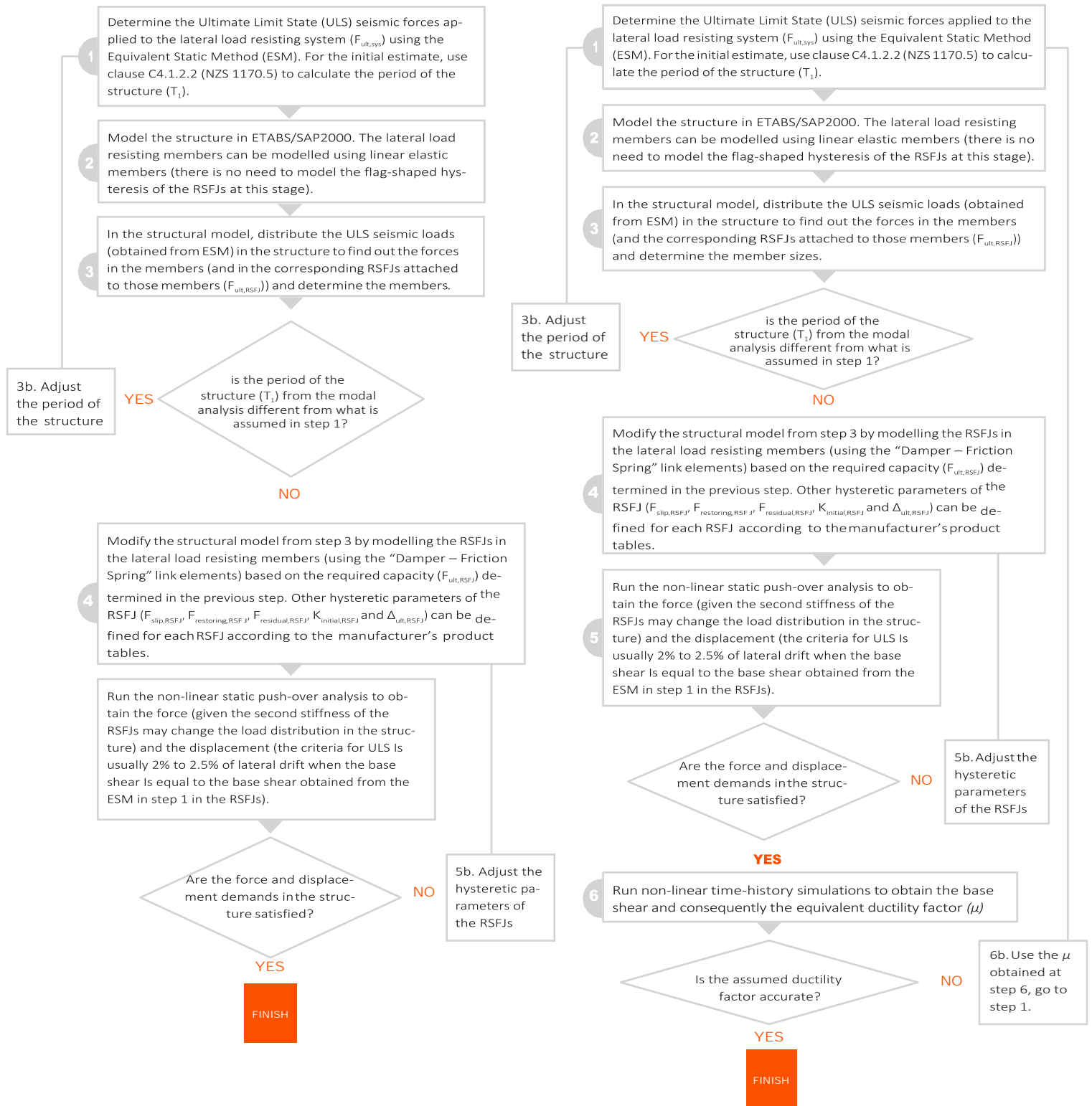
Assume an equivalent ductility of $\mu=2$ Assume an equivalent ductility of $\mu=3$ 

Figure 4. The recommended structural analysis and design procedure for the structures with RSFJs

4 The Numerical modelling of a five-story case study CLT structure with RSFJs

A design example case study is provided here following the proposed analysis and design procedure. The considered prototype building uses CLT floors, CLT load-bearing walls as the gravity loads resisting members and balloon type CLT shear walls with RSFJ hold-downs as the Lateral Load Resisting System (LLRS). The RSFJs can be connected to the CLT shear walls using a configuration similar to what was shown in section 2 for the rocking CLT wall experiment. It was assumed that the CLT floors and the CLT walls are 200 mm thick panels with five layers of MSG8 timber (Buchanan 1999). The load-bearing CLT panels were assumed to be 150 mm thick with three layers.

The building is designed for soil type C in Christchurch, New Zealand. The total height of the structure is 15 m with 5 m wide spans. Figure 5 shows the typical plan view of the structure where each wall uses two RSFJs at the base level. The design dead loads including the CLT panels, services, ceiling, cladding and self-weight of the structure were specified as 3 kPa and 1.6 kPa for the first four floors and the roof, respectively. The design live loads were assumed 2.0 kPa and 0.5 kPa for the first four floors and the roof, respectively. The abovementioned design loads correspond to seismic masses of 1.9×10^5 kg and 1.0×10^5 kg for the first four floors the roof, respectively. The target ULS design drift is considered as 1.5%.

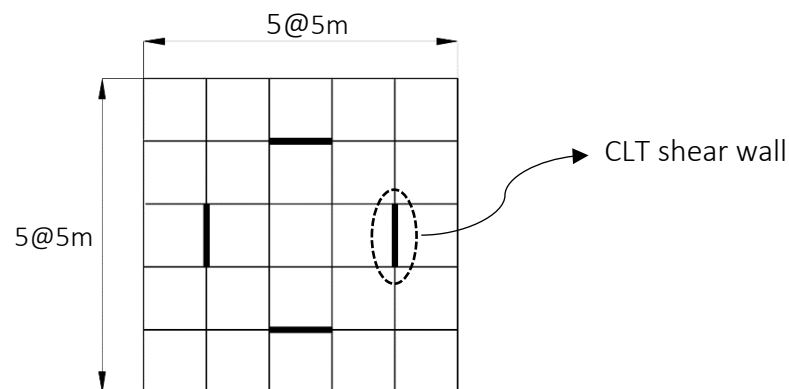


Figure 5. Typical plan view of the prototype structure

The right procedure in the provided step-by-step design flowchart (Figure 4) is used where the assumed equivalent ductility factor (μ) is verified by non-linear dynamic time-history simulations:

-Assume an equivalent ductility factor of $\mu = 3$.

1. Determine the Ultimate Limit State (ULS) seismic forces applied to the lateral load resisting system ($F_{ult,sys}$) using the Equivalent Static Method (ESM). For the initial estimate, use clause C4.1.2.2 (NZS 1170.5) to calculate the period of the structure (T_1):

The period of the structure is estimated as $T_1 = 0.48$ sec using the empirical equation in NZS 1170.5 (New Zealand Standards 2004). According to the assumed specification for the structure, the overall seismic mass of the building is 8500 kN. Following the ESM in this step, the base shear of the structure is calculated as 1150 kN. The spectral shape factor $C_h(T)$, the hazard factor Z , the return period factor R_u and the near-fault factor $N(T,D)$ are determined as 2.07, 0.22, 1.0 and 1.0, respectively. The annual probability of exceedance of 1/500 is considered for the Ultimate Limit State (ULS) design. The structural performance factor (Sp) is assumed as 0.7.

2. Model the structure in ETABS/SAP2000. The lateral load resisting members can be modelled using linear elastic members (there is no need to model the flag-shaped hysteresis of the RSFJs at this stage):

The structure is modelled in SAP2000 version 19.0 (Computers&Structures 2017). Figure 6 shows the general arrangement of the numerical model at this stage.

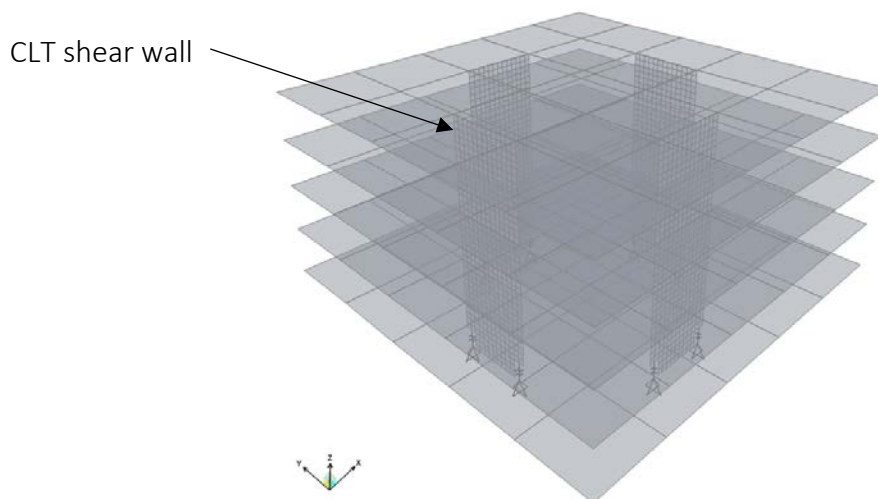


Figure 5. Typical plan view of the prototype structure

3. In the structural model, distribute the ULS seismic loads (obtained from ESM) in the structure to find out the forces in the members (and the corresponding RSFJs attached to those members ($F_{ult,RSFJ}$)):

- Is the period of the structure (T_1) from the modal analysis different from what is assumed in Step 1?

The period of the structure (T_1) at this stage is determined as 0.56 seconds from the modal analysis which is higher than what was assumed in step 1. Therefore, steps 1 to 3 should be repeated with this new value. Following the ESM with the new period, the base shear of the structure is reduced to 956 kN from 1150 kN. The force de-

mand in the RSFJs at this stage is 1160 kN. The lever arm for the RSFJ hold-down is assumed as 4.8 m given the width of the RSFJs is considered as 200 mm.

4. Modify the structural model from step 3 by modelling the RSFJs in the lateral load resisting members (using the “Damper – Friction Spring” link elements) based on the required capacity ($F_{ult,RSFJ}$) determined in the previous step. Other hysteretic parameters of the RSFJs ($F_{slip,RSFJ}$, $F_{restoring,RSFJ}$, $F_{residual,RSFJ}$, $K_{initial,RSFJ}$ and $\Delta_{ult,RSFJ}$) can be defined for each RSFJ according to the manufacturer’s product tables.

At this stage, an elastic drift (the drift of the structure at the slip force of the RSFJs ($F_{slip,sys}$) before they start to open) of 0.2% is assumed for the structure. Based on this and the target ULS drift (1.5%), the displacement demand of the RSFJ hold-downs was estimated as 62 mm. The specifications for the required RSFJs are determined with respect to the force demands (specified in the previous step) and based on the RSFJ design tables from the manufacturer (they also can be calculated using the RSFJ design equations provided in (Hashemi et al. 2017a)) and are provided in Table 1.

Table 1. Initial configuration of the RSFJ hold-downs

Initial stiffness (kN/mm)	F_{slip} (kN)	$F_{ult,loading}$ (kN)	$F_{ult,unloading}$ (kN)	$F_{residual}$ (kN)	Δ_{max} (mm)
600	580	1160	435	235	62

Following step 4, the RSFJs were re-modelled using the “Damper – Friction Spring” link element (available in SAP2000 and ETABS). For each RSFJ, the numerical parameters of the corresponded link element were calibrated using the definitions described in (Hashemi et al. 2017b).

5. Run the non-linear static push-over analysis to obtain the force and the displacement in the RSFJs.

The results of the non-linear static pushover analysis are displayed in Figure 6. The structure is pushed to 1.5% of lateral drift corresponding to 225 mm of deflection at the roof. Please note that the terminology “non-linear static pushover analysis” is used but the non-linearity is provided by the non-linear geometrical behaviour of the RSFJs. All structural components up to 1.5% drift are still behaving within their elastic limit.

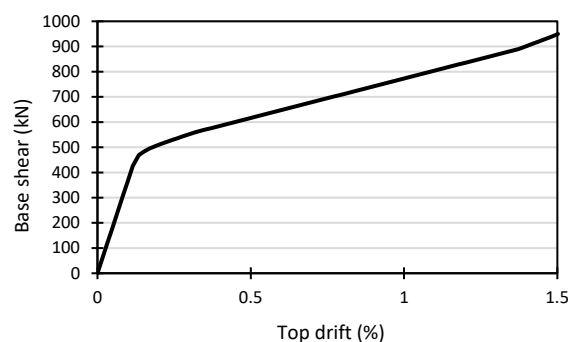


Figure 6. Results of the first non-linear static push-over analysis

- Are the force and displacement demands in the structure satisfied?

It can be seen in Figure 6 that the maximum force in the system in the given drift (1.5%) is 948 kN which is consistent with the base shear from the ESM (956 kN).

6. Run non-linear time-history simulations to obtain the base shear and consequently the equivalent ductility factor (μ)

Non-linear dynamic time-history simulations were carried out to investigate the behaviour of the structure. 10 records were chosen for the analysis which were scaled based on the New Zealand standard for ULS (with 1/500 probability of exceedance).

Figure 7 shows the maximum base shears recorded during the time-history simulations. As can be seen, the average is 840 kN. Furthermore, the results showed that the average top roof drift was 1.28% that is lower than the target drift (1.5%). Thus, the new equivalent ductility factor is calculated as $\mu = 3.4$. Given that this ductility factor is higher than the first assumption in Step 1 ($\mu = 3$), the procedure needs to be repeated from the start with the new equivalent ductility factor of $\mu = 3.4$.

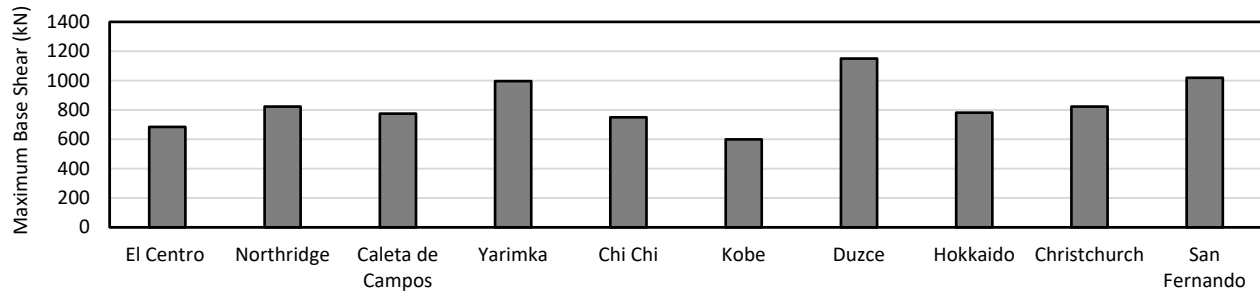


Figure 7. Results of the first non-linear dynamic time-history analysis

Following the right design procedure in Figure 4 with $\mu = 3.4$, the new base shear of the structure is determined as 830 kN. Note that the period of the structure (T_1) at this stage is increased to 0.58 seconds from the modal analysis which is not that much different from what was considered in the first iteration (0.56 seconds). The force demand in the RSFJs is reduced to 1020 kN and the specifications are revised accordingly (see Table 2).

Table 2. Revised configuration of the RSFJ hold-downs

Initial stiffness (kN/mm)	F_{slip} (kN)	$F_{ult,loading}$ (kN)	$F_{ult,unloading}$ (kN)	$F_{residual}$ (kN)	Δ_{max} (mm)
500	505	1020	370	200	62

Following step 4, the revised RSFJ hold-downs are modelled in SAP2000 using the “Damper – Friction Spring” link element. Following step 5, the results of the revised non-linear static pushover simulation are displayed in Figure 8. As can be seen, the structure performs as expected by reaching the calculated base-shear at 1.5% drift.

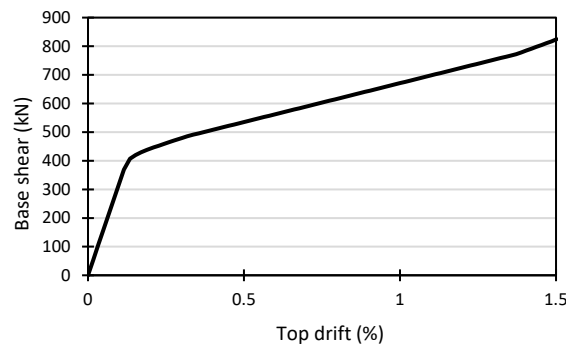


Figure 8. Results of the revised non-linear static push-over analysis

Following step 6 of the procedure, non-linear dynamic time-history simulations were re-conducted on the system. The average inter-story drift is increased to 1.47% which is consistent with the target drift (1.5%). Moreover, the average base shear of the structure is 814 kN which is reasonably close to what was specified following the ESM (830 kN). This shows that the adopted ductility factor in the second iteration ($\mu = 3.4$) is consistent with the reality given that the difference between the calculated base shears is under 2%.

This design example shows the efficiency of the proposed procedure and also demonstrates that a structural ductility factor as high as 3.4 is achievable for CLT structures when using the RSFJ technology.

5 Conclusions

The Resilient Slip Friction Joint (RSFJ) technology is a novel seismic energy dissipation system that has recently been introduced to the construction industry. This joints not only provides energy damping but also a fully self-centring behaviour meaning that the structure will actively return to its initial position at the end of the seismic event. The flag-shaped hysteresis of the RSFJ has been verified by full-scale experimental tests. Owing to the unique characteristics of the RSFJs, they can be used in different applications in timber structures such as (yet not limited to) tension-compression braced frames, tension-only braces frames, shear walls and moment-resisting frames.

This paper provides a step-by-step analysis and design procedure for the CLT structures that uses RSFJs in their lateral load resisting system. This procedure which is based on the Equivalent Static Method (ESM) involves numerical modelling of the structure in ETABS/SAP2000, performing non-linear static pushover analysis in general and non-linear dynamic time-history simulations when a more sophisticated design is targeted. The proposed design procedure was implemented for a five-story CLT structure with RSFJ hold-downs. The findings of this study showed that an equivalent ductility factor of $\mu = 3.4$ is applicable for the prototype structure. Overall,

the findings of this investigation showed that the proposed analysis and design procedure could be efficiently used when RSFJs are employed in seismic resilient CLT structures. Given the ESM is internationally accepted and widely being used, the proposed analysis and design procedure can be revised to be used along with the international building codes such as Eurocode.

6 Acknowledgements

The authors would like to thank the Ministry of Business, Innovation and Employment of New Zealand (MBIE) and the Earthquake Commission (EQC) of New Zealand for the financial support of this research.

7 References

- Baktash, P., Marsh, C., and Pall, A. (1983). "Seismic tests on a model shear wall with friction joints." *Canadian Journal of Civil Engineering*, NRC Research Press, 10(1), 52–59.
- Buchanan, A. H., and Federation, N. Z. T. I. (1999). *Timber design guide*. New Zealand Timber Industry Federation.
- Ceccotti, A., Sandhaas, C., Okabe, M., Yasumura, M., Minowa, C., and Kawai, N. (2013). "SOFIE project–3D shaking table test on a seven storey full scale cross laminated timber building." *Earthquake Engineering & Structural Dynamics*, Wiley Online Library, 42(13), 2003–2021.
- Clifton, G. C., MacRae, G. A., Mackinven, H., Pampanin, S., and Butterworth, J. (2007). "Sliding hinge joints and subassemblies for steel moment frames." *Palmerston North, New Zealand: Proc of New Zealand Society for Earthq Eng Conf*.
- Filiatrault, A. (1990). "Analytical predictions of the seismic response of friction damped timber shear walls." *Earthquake engineering & structural dynamics*, Wiley Online Library, 19(2), 259–273.
- Gavric, I., Fragiaco, M., and Ceccotti, A. (2015). "Cyclic behavior of CLT wall systems: Experimental tests and analytical prediction models." *Journal of Structural Engineering*, American Society of Civil Engineers, 141(11), 4015034.
- Hashemi, A., Loo, W. Y., Masoudnia, R., Zarnani, P., and Quenneville, P. (2016a). "Ductile Cross Laminated Timber (CLT) Platform Structures with Passive Damping." *World Conference of Timber Engineering WCTE2016, Vienna, Austria*.
- Hashemi, A., Masoudnia, R., and Quenneville, P. (2016b). "Seismic performance of hybrid self-centring steel-timber rocking core walls with slip friction connections." *Journal of Constructional Steel Research*, 126, 201–213.
- Hashemi, A., Zarnani, P., Darani, F. M., Valadbeigi, A., Clifton, G. C., and Quenneville, P. (2018). "Damage Avoidance Self-Centering Steel Moment Resisting Frames (MRFs) Using Innovative Resilient Slip Friction Joints (RSFJs)." *Key Engineering Materials*, Trans Tech Publ, 726–734.
- Hashemi, A., Zarnani, P., Masoudnia, R., and Quenneville, P. (2017a). "Experimental testing of rocking Cross Laminated Timber (CLT) walls with Resilient Slip Friction (RSF) joints."

- Journal of Structural Engineering*, 144(1), 04017180-1 to 04017180-16.
- Hashemi, A., Zarnani, P., Masoudnia, R., and Quenneville, P. (2017b). "Seismic resistant rocking coupled walls with innovative Resilient Slip Friction (RSF) joints." *Journal of Constructional Steel Research*, 129, 215–226.
- Loo, W. Y., Kun, C., Quenneville, P., and Chouw, N. (2014). "Experimental testing of a rocking timber shear wall with slip-friction connectors." *Earthquake Engineering & Structural Dynamics*, Wiley Online Library, 43(11), 1621–1639.
- McCormick, J., Aburano, H., Ikenaga, M., and Nakashima, M. (2008). "Permissible residual deformation levels for building structures considering both safety and human elements." *Proceedings of the 14th world conference on earthquake engineering*, 12–17.
- New Zealand Standards. (2004). "Structural Design Actions (NZS 1170.5)." *Wellington, New Zealand*.
- Pall, A. S., and Marsh, C. (1982). "Response of friction damped braced frames." *Journal of Structural Engineering*, 108(9), 1313–1323.
- Pall, A. S., Marsh, C., and Fazio, P. (1980). "Friction joints for seismic control of large panel structures." *PCI JOURNAL*, 25(6), 38–61.
- Popov, E. P., Grigorian, C. E., and Yang, T.-S. (1995). "Developments in seismic structural analysis and design." *Engineering structures*, Elsevier, 17(3), 187–197.
- Popovski, M., and Gavric, I. (2015). "Performance of a 2-Story CLT House Subjected to Lateral Loads." *Journal of Structural Engineering*, American Society of Civil Engineers, E4015006.
- Popovski, M., and Karacabeyli, E. (2012). "Seismic behaviour of cross-laminated timber structures." *Proceedings of the World Conference on Timber Engineering, Auckland, New Zealand*.
- Popovski, M., Schneider, J., and Schweinsteiger, M. (2010). "Lateral load resistance of cross-laminated wood panels." *Proceedings of the World Conference on Timber Engineering, Trentino, Italy*.
- Computers and Structures, (2017). "SAP2000 Ver. 19 (2017)." Berkeley, CA.
- Varoglu, E., Karacabeyli, E., Stiemer, S., and Ni, C. (2006). "Midply wood shear wall system: Concept and performance in static and cyclic testing." *Journal of Structural Engineering*, American Society of Civil Engineers, 132(9), 1417–1425.
- Yasumura, M., Kobayashi, K., Okabe, M., Miyake, T., and Matsumoto, K. (2015). "Full-Scale Tests and Numerical Analysis of Low-Rise CLT Structures under Lateral Loading." *Journal of Structural Engineering*, American Society of Civil Engineers, E4015007.
- Zarnani, P., and Quenneville, P. (2015). "A Resilient Slip Friction Joint." NZ IP Office; Patent No. WO2016185432A1.

Discussion

The paper was presented by P Quenneville

H Blass stated running non-linear timing history analysis with different earthquakes will influence the ductility factor and asked how did you decide the ductility factor of 3.4. P Quenneville received confirmation from A Hashemi that 3.4 was the average value of the ductility ratios for all of the different seismic analysis.

Z Li commented that the capacities of these connections are high and how much restoring forces can these connectors produce. P Quenneville said angles less than 15 degrees will allow restoring forces to be developed which is approximately 1/3 of the ultimate capacity. Z Li commented that in pseudo dynamic tests good results can be obtained and the real dynamic behaviour of structures may be different. P Quenneville agreed and said that snap back test was done and good results were obtained.

I Abeysekera asked about the cost. P Quenneville stated that the economics must be considered especially for high importance building.

L-M Ottenhaus asked for comments on overstrength forces in the hold down which must be resisted by the CLT. P Quenneville responded that there are reinforcement methods or other connection methods that can be employed to take the required loads. He added that the performance of these connectors is reliable therefore a lower overstrength factor of 1.25 is recommended. L-M Ottenhaus and P Quenneville further discussed how to achieve the high post tension forces in the system.

M Yasumura asked whether these systems need to be installed at every floor or just at the base of the panels. P Quenneville said that the position and placement of these connectors depend on the building shape and building height but they will not be placed at every story.

F Lam commented that the recommendation from NZ engineering community to demolish timber buildings with residual drift of ½% seems harsh especially for light wood frame structures.

An Improved Design Model for Fire Exposed Cross Laminated Timber Floors

Joachim Schmid, Michael Klippel, Reto Fahrni, Andrea Frangi,
ETH Zürich Eidgenössische Technische Hochschule Zürich, Switzerland

Norman Werther, TUM Technical University Munich, Germany

Alar Just, TUT Tallinn Technical University, Estonia

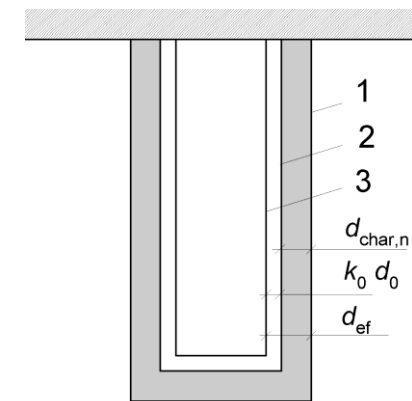
Keywords: timber, fire, cross-laminated timber, design model, bending

1 Introduction

The solid wood product cross-laminated timber (CLT) is a successful building product due to the attractive surface and the sustainability provided. However, the most important characteristic of a building product is the design efficiency (Jones et al., 2016) accounted by design models. Due to the complex behaviour of wood in fire in general and in particular of CLT, simplified fire design models are essential for designers to verify the fire resistance of timber structures. Currently, the fire part of Eurocode 5, EC5, (CEN, 2004) does not give design rules valid for CLT.

The popular effective cross-section method (ECSM) considers (i) the reduction of a timber section by charring and (ii) the reduction of strength and stiffness by an additional so-called zero-strength layer (ZSL), d_0 . The idea of the method is that an effective cross-section (CS) with strength and stiffness properties as at normal temperature provides the same resistance as the heated, fire exposed section (Schaffer et al. 1986). In the past, some CLT producers have optimized their products in a way that the ZSL of 7 mm intended for solid timber members was located solely in the transversal layers. Thus, the reduction by the ZSL has no effect on the verification. At the World Conference on Timber Engineering 2010, WCTE 2010, a first design model for fire exposed CLT was presented (Schmid et al., 2010). This method (the 2010 method) aimed to use the terminology of EC5 where the ZSL is traditionally defined (traditional ZSL), i.e. simply as the difference between the residual and the effective CS, see Eq. 1. However, the 2010 method has some limitations and drawbacks, which are discussed in Section 3 of this paper. For this study, the current CLT product

portfolio was investigated and a more flexible terminology, i.e. a new definition of the ZSL, was considered to develop design models for CLT in bending with its exposed side in tension relevant for floor elements.



Key:

- 1... original CS d_0 ZSL
- 2... residual CS $d_{char,n}$ char depth
- 3... effective CS d_{ef} effective char depth

Figure 1. Graphic definition of the ZSL (d_0) modified from Eurocode 5 (CEN 2004).

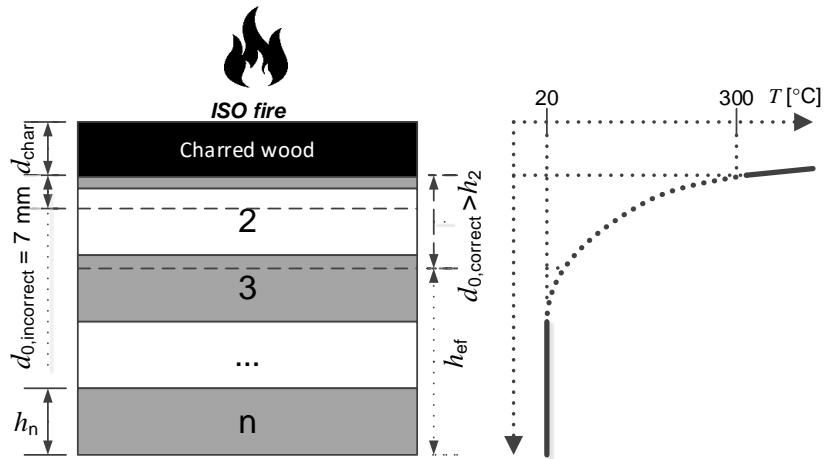


Figure 2. Overlay of a CLT layup with a typical temperature profile under ISO 834 fire.

2 The effective cross-section method for fire exposed timber members

The design model ECSM for the design of timber members exposed to fire was based on direct measurements of the strength in tension and compression and the stiffness at various temperatures using clear wood samples. The results were overlaid with temperature profiles observed in members exposed to standard fire (Schaffer et al. 1986). The relative mechanical properties were lumped together over a depth of about 40 mm. Although the proposed ZSL of 7.62 mm fits well for glued-laminated timber in bending at 30 min standard fire exposure (fire exposed on three sides), understanding the development of the ZSL suggested by Schaffer et al. (1986), it is clear that the concept is generally flawed as the stress distribution over the depth in a bending member is not constant. Further, the two-dimensional temperature distribution in members does not allow for a linear application of the “lumped strength concept” suggested by Schaffer et al. (1986). Thus, the simplified model was investigated for beams and columns by several authors and improvements were suggested by Schmid et al. (2012). It was found that many fire resistance test results cannot be used for the verification of the ECSM or that results indicate deviating ZSLs, see Schmid et al. (2014). For the revision of EC5, it is expected that an improved ECSM will be proposed for timber beams and columns based on further investigations.

3 The 2010 design model for CLT

The design model presented for CLT (Schmid et al. 2010) was determined conducting thermal simulations with SAFIR (Franssen 2007) and mechanical simulations with a self-written software code, CSTFire.

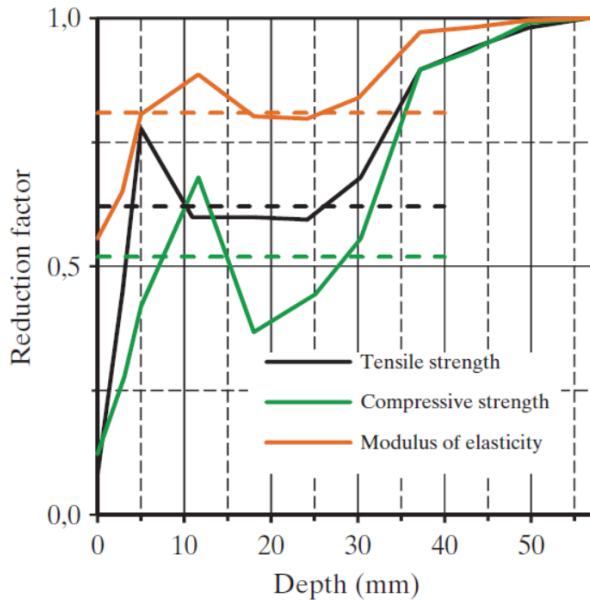


Figure 3. Relative strength and stiffness vs. distance from the char line as used in (Schaffer et al. 1986). From Schmid et al. 2015.

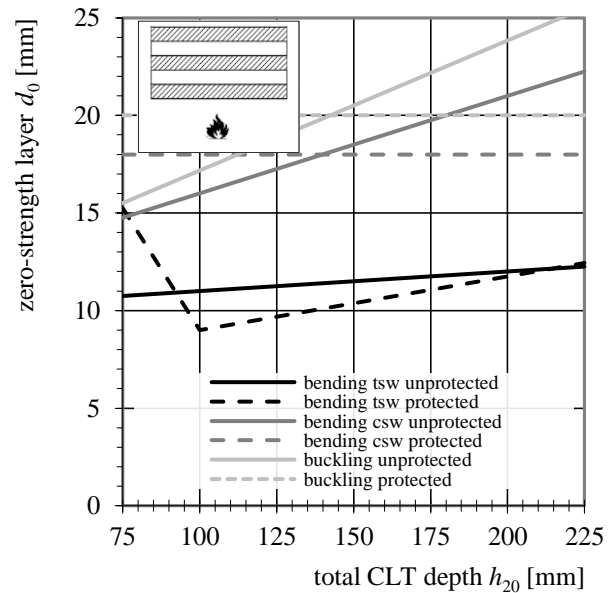


Figure 4. Zero-strength layer for five layer CLT (Schmid et al. 2010) with exposed side in tension (tsw) and compression (csu) and for buckling.

The methodology, verified by means of model scale and large scale fire tests in bending, is presented in detail in Schmid et al. (2018b). While in EC5 a general ZSL got implemented ($d_0 = 7\text{mm}$), the 2010 model for CLT gives linear functions depending on the layup, the state of stress on the fire exposed side and the depth of the product. In 2010, linear equations for three, five and seven layer CLT were given, e.g. for five layer CLT in Figure 3. The original ZSL for bending members was developed for single span beams with the exposed side in tension (tsw); the corresponding value for five layer CLT is between 11 and 12 mm, see Figure 4. In some cases, the temperature impact depth, i.e. temperatures above the normal in the temperature profile of about 40 mm beyond the char line (assumed to be at 300°C) exceeds the transversal layer as qualitatively given in Figure 2. For the extreme case when the residual section's outer lamella on the heated side is a transversal layer, the ZSL would be greater than the thickness of the transversal layers which is unable to carry loads perpendicular to the lamellae. In this case, it is obvious that the ZSL for CLT exceeds the depth of the transversal layer and is, thus, larger than 7 mm. This is due to the definition used in EC5 implicitly given in Figure 1, described using the residual depth h_{res} and the effective depth h_{ef} as follows:

$$d_0 = h_{res} - h_{ef} \quad (1)$$

Since 2010, the CLT production and the use has increased considerably and the industry pointed out the limited efficiency of the model presented in 2010, which is conservative in many cases. Thus, the authors have decided together with the industry to improve the design concept answering different needs of different end users.

4 The new design concepts

Generally, the room for improvements was defined in the CEN (European Committee for Standardization) Horizontal Group Fire, HGF, as part of the revision of the Eurocode, which should result in a new generation of codes for all materials in 2022. The HGF gave the possibilities for different design concepts on different levels of complexity. Together with the CLT industry, authors defined so-called preferred layups. Within the framework of COST FP1404 (www.costfp1404.com) an enquiry about the available product was performed involving all European CLT producers.

Table 1. Layup of preferred CLT floor elements with layup specification and total thickness of the CLT in mm.

Layup specification	Total thickness $h_{20^{\circ}C}$
20+20+20	60
40+40+40	120
20+20+20+20+20	100
40+20+20+20+40	140
40+20+40+20+40	160
40+30-40-30-40	180
40+40+40+40+40	200

Twelve CLT layups were identified representing the largest share on the European market, whereby seven layups are CLT used for floor elements. These three- and five-layer CLT define the preferred layups and are specified in Table 1. For the revision of Eurocode, it was decided for the fire parts that design models can be given on three different levels of complexity.

The intention is to fulfil needs of different groups of end users. These are (1) tabulated values, (2) simplified rules and (3) advanced models. For CLT, it is intended to give tabulated values for typical solutions, the preferred layups, and simplified rules for a more general application of CLT. Advanced models comprise Finite Element simulations. This paper provides data for (1) and (2) performing a large range of simulations using advanced models (3), which are often too complex for everyday use by engineers.

Besides the design models on different levels (1), (2) and (3), it was decided together with the European CLT industry to allow for more open definitions of the ZSL. EC5 contains an intuitive definition of the ZSL, which is the difference between the residual cross-section, see Figure 1 and Eq. (1), i.e. the original cross-section reduced by charring, and the effective cross-section. This definition is appropriate as long as a

homogeneous section is available, i.e. with homogeneous strength properties. Since CLT comprises longitudinal and transversal layers cross the load-bearing direction, compare Figure 2, this definition is challenged especially when the last uncharred, outer lamellae is a transversal layer.

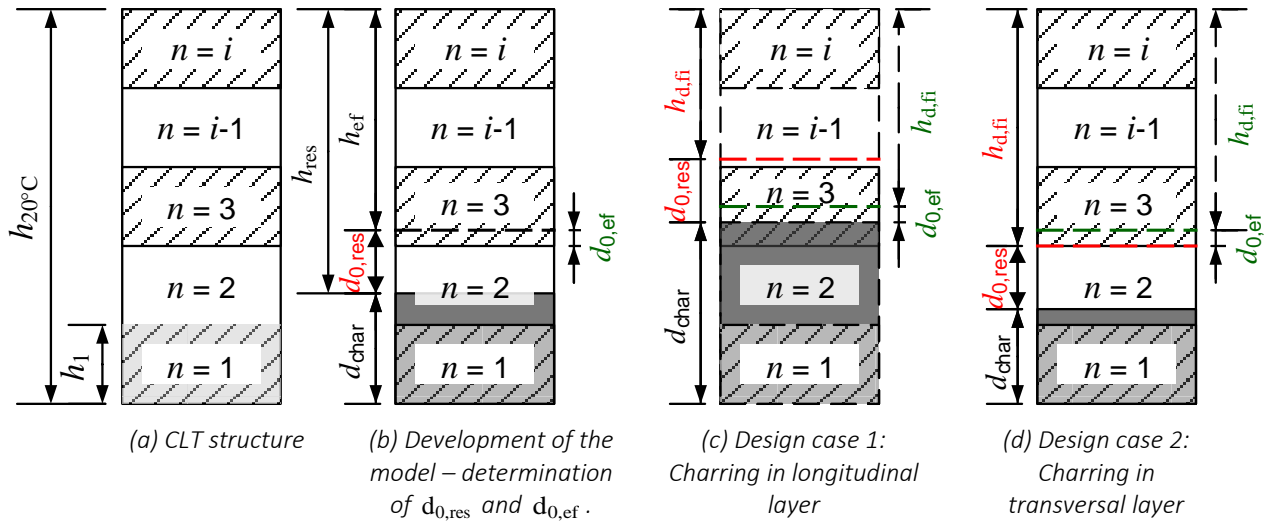


Figure 5. Determination of $d_{0,res}$ and $d_{0,ef}$ for a cross-section and two different design cases.

The improved design model makes use of a further definition, i.e. an effective ZSL, $d_{0,ef}$. This effective ZSL considers only parts of a section with its grain direction parallel to the main load-bearing direction, i.e. the longitudinal layers, parts of transversal layers are not considered. Following the introduction, the hitherto existing ZSL referring simply to the residual cross-section is indicated as $d_{0,res}$. The development and differences of both ZSL is shown in Figure 5: The development is consistent regardless the symmetrical structure with an uneven number of layers with the fire exposed layer number 1, see Figure 5 (a). Deducting the char depth in correspondence to an appropriate charring model, e.g. the stepped model or the linear charring rate of EC5, a residual cross-section h_{res} can be determined, see Figure 5 (b). The simulations deliver the corresponding cross-section with equivalent load-bearing capacity with normal temperature material properties as in the fire situation, h_{ef} . Both ZSL (indicated in red and green) are able to describe this effective depth and are intended to be applied for other design cases for this section, see (c) and (d). From (c) it becomes obvious that the determined, effective cross-sections are significantly different and more economic for the effective (green) ZSL while for (d) it is irrelevant whether to use the effective ZSL $d_{0,ef}$ or the traditional definition $d_{0,res}$.

5 Development of the improved design model

The preferred layups given in Table 1 were simulated thermally and mechanically using SAFIR and CSTFire respectively as done for the model presented in 2010, see Sec-

tion 2. For the model presented here, in addition to the preferred layups further intermediate layups were included aiming for a systematic analysis. Below, the five-step procedure for the development are presented for selected examples and followed by the results of the simulations. In a final step, design models are proposed in Section 6.

5.1 Simulation and analysis procedure

(1.) Prior to any simulation of the load-bearing capacity in bending in the fire situation, the ultimate bending capacity at normal temperature M_{20} was determined. This was done using CSTFire (Schmid et al., 2018b) utilizing a compression to tension strength ratio of $f_t / f_c = 0.9$ as observed in reference tests. Perfect plasticity was assumed in compression. Using standardized strength values does not allow for correct prediction of the ultimate load-bearing capacity (Schmid et al. 2010). The possible plasticity allows for CLT elements exposed on the side in tension (tsw) for a decreased ZSL in the beginning of the fire exposure, i.e. when the first lamellae undergoes charring.

(2.) In a second step, the residual cross-section was simulated including the corresponding temperature profile within the uncharred heated section. In addition to the unprotected case (Type 2), in total ten different cases for initially protected CLT were investigated with temperature fall-off criteria between 270°C and 800°C on the unexposed face of the fire protection, i.e. gypsum plasterboards. In general, the temperature profile drops to normal temperature, i.e. 20°C within about 40 mm for unprotected members. However, this value can be up to 80 mm for initially protected CLT. The effect of the protection was simulated for typical protection applied by the industry. Protection by single and double gypsum plasterboards were simulated. Generally for initially protected CLT, charring is delayed and reduced, thus any protection is favourable. Sufficient anchorage was assumed and fall-off of the gypsum plasterboard(s) was as observed in full-scale fire resistance tests (Just et al., 2010). Gypsum plasterboards Type F (GtF) and Gypsum plasterboards Type A (GtA), typically 15 mm and 12.5 mm thick were included in the simulations which were performed with SAFIR (Franssen, 2007). Fall-off times were taken mainly from tests with timber frame assemblies. Due to the reduced heat accumulation when attached directly to CLT, the fall-off occurs usually slightly later than in case of timber frame assemblies with insulation in the cavity, which was considered in the simulations. However, it should be noted that the database for fall-off times of gypsum protecting CLT panels is rather limited and verification is needed.

(3.) In a third step, the bending capacity of the heated section was calculated; result is the relative capacity with respect to the ultimate bending capacity of Step 1, M_{fi} / M_{20} (blue line in Figure 6).

(4.) In a fourth step, a corresponding CLT section height $h_{ef,calculation}$ with a bending capacity of a cold section corresponding to the simulated heated section was calculated (broken line in Figure 6).

Graphs as presented in Figure 6 were developed for in total 15 CLT layups (preferred layups and intermediate layer thicknesses for a systematic analysis) for initially unprotected and initially protected CLT.

(5.) In a fifth step, the ZSLs were calculated with respect to the available definitions, i.e. the effective ZSL $d_{0,ef}$ and the ZSL $d_{0,res}$ with respect to the residual cross-section (the traditional understanding of the ZSL). While the latter follows a simple relationship, described in Eq. (1), for the effective ZSL the layup was considered, i.e. the location of the longitudinal layers which are represented by the grey highlighted zones in Figure 6. Thus, depending on the progression of char, i.e. the residual cross-section, a so-called relevant cross-section (neglecting uncharred transversal layers if they are the outer layer) was defined, see Figure 7.

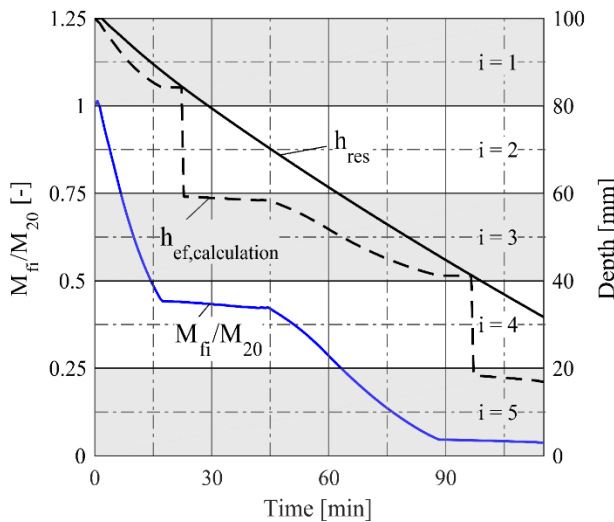


Figure 6: Residual cross-section h_{res} , simulated relative bending capacity M_{fi}/M_{20} and the corresponding section height $h_{ef,calculation}$ of a five layer CLT (5x20).

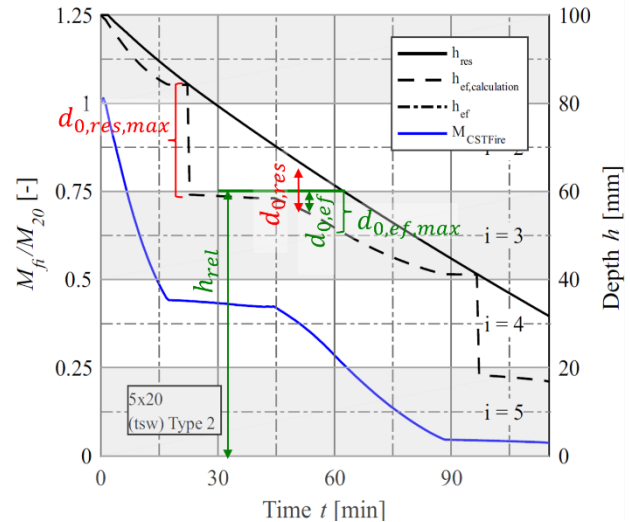


Figure 7: CLT shown in Figure 6 with the development of the effective ZSL considering a relevant depth considering layers 3 to 5 only during charring of layer 2 (transversal layer).

In Figure 7, the relevant cross-section between about $t = 30$ and $t = 62$ min is shown. Further, Figure 7 indicates both ZSL for about 50 min. Finally, Figure 7 shows maximum ZSLs over the simulated time of 120 min. In Figure 7, it is clearly visible that the traditional ZSL at about $t = 25$ min is larger than 20 mm, i.e. the thickness of the transversal layer $i = 2$.

The ZSL for this CLT (5x20), $h_{20} = 100$ mm, is smaller than in the model of 2010 where a practical range for M_{fi}/M_{20} between 40 and 20% had been used, i.e. in this case between about $t = 30$ and $t = 70$ min.

5.2 Data analysis procedure

For the analysis of results, the ZSLs were collected with respect to the definition and the design concept. The following four options were investigated based on Figure 7:

Option A: maximum ZSL over the total time, i.e. until the relative bending capacity M_{fi} / M_{20} drops under about 10%. For the example of the five layer CLT 5x20, this results in $d_{0,res,tot} = 24.8$ mm and $d_{0,ef,tot} = 9.5$ mm.

Option B: As in the model of 2010, a practical load level range for M_{fi} / M_{20} between 40 and 20% has been introduced. For the example of the five layer CLT 5x20, this is $d_{0,res,tot} = 11.1$ mm and $d_{0,ef,tot} = 9.5$ mm.

Option C: The maximum ZSL during charring of the longitudinal layers. For five layer CLT layers $i = 1$ and $i = 3$ were evaluated. For the example of the five layer CLT 5x20, this is $d_{0,ef,i=1} = d_{0,res,i=1} = 4.5$ mm $d_{0,ef,i=3} = d_{0,res,i=3} = 9.5$ mm.

Option D: especially aiming at the design concept of tabulated data, effective ZSL values at 30, 60 and 90 min were evaluated. However, to provide a measure of safety, effective ZSL within ± 5 min of these times were considered. For the example of the five layer CLT 5x20, this is $d_{0,ef,R30} = 3.3$ mm, $d_{0,ef,R60} = 9.5$ mm and $d_{0,ef,R90} = 5.4$ mm.

Here, it becomes obvious that the values are strongly dependent on the charring model used. Thus, individual charring rates implemented in technical approvals or falling-off of charring lamellae is not acceptable.

5.3 Limitations

The actual model aims for the description of the load-bearing capacity of the residual cross-section by an effective cross-section with material properties as at normal temperature. The ZSLs presented in the following are intended to describe the bending behaviour of CLT when exposed to standard fire which is generally connected with fire resistance classification R. Simulations covered fire exposures of up to 120 min with the exposed side in tension. The mechanical model is a single span beam as current jointing technique does not allow for consideration of two-span floors elements in fire.

Currently, the behaviour of timber members in non-standard fires are investigated, e.g. Lange et al. (2015). So far, authors of this study conclude that the standard fire should be used as reference to compare structural elements. Further, the validity of furnace tests is currently discussed, results show that they are a proper measure for fully developed fires (Schmid et al. 2018a and c).

5.4 Initially protected CLT

Exemplarily, in the following, the development of the ZSL for a five layer CLT 5x30 is shown. Figure 8 presents results for a protected CLT (indicated as configuration type 10 in Figure 8) using double layer of gypsum plasterboards with 15 mm thickness

each and a falling-off temperature criterion of 800°C. It is clearly visible that the bending resistance starts to decrease not earlier than at around $t = 30$ min. This is due to the delay of the heating of the CLT and the possibility of stress redistribution to the compression side where plastic deformations are possible. Further, it is clearly visible that the load-bearing capacity drops at $t = 30$ min before the section gets reduced by char at

$t = 82$ min. Finally, the ZSL can be determined to be slightly below 12 mm. Generally, it can be stated for the investigated initially protected CLT that the Option B could not be successfully applied as some of the elements do not reach those load levels within 120 minutes. Further, it was observed for all results that ZSL thicknesses tend to be slightly higher with protection than without but the maximum for the effective ZSL was not greater than 12 mm.

5.5 Effect of falling-off of charring layers

The value of the ZSL is linked to the temperature profile within a timber member. Generally, the steeper a temperature profile, the smaller the ZSL to compensate for the losses in load-bearing capacity due to heat. On the contrary, the smoother the temperature profile, i.e. the larger the temperature impact depth, the larger the corresponding ZSL. Consequently, fire protection by e.g. gypsum plasterboards entail larger ZSL while falling-off of charring layers would result in smaller ZSL. To simulate falling-off of charring layers, the thermal simulations considered a failure criteria of 300°C in the bond line, then all charred elements were manually deleted and the simulation was continued. Figure 11 shows exemplary the simulation of the ZSL of CLT.

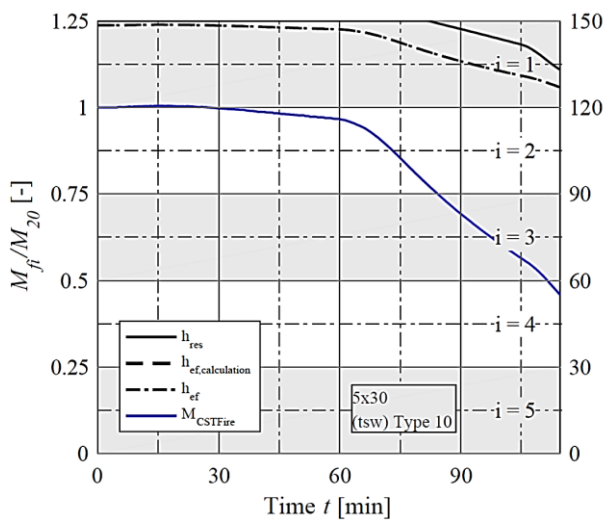


Figure 8: Residual cross-section h_{res} , simulated relative bending capacity M_{fi} / M_{20} and the corresponding section height $h_{ef, calculation}$ of a five layer CLT (5x30) initially protected by 2xGtF (Type 10).

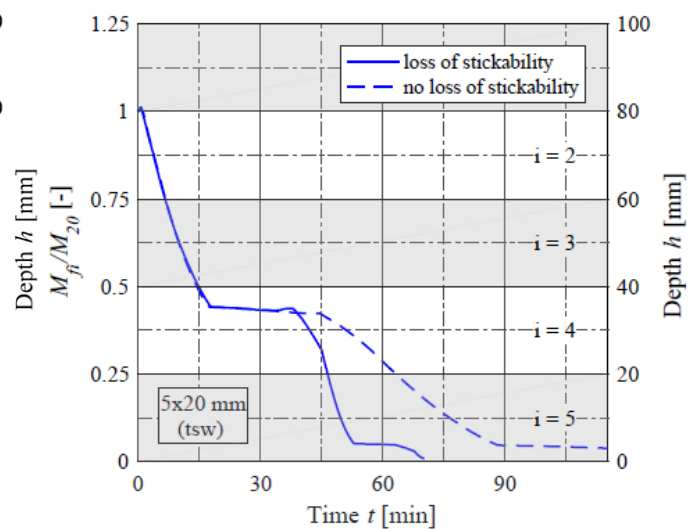


Figure 9: Relative bending moment with and without falling-off of charring layers (loss of stickability) of a five layer CLT.

5.6 Outcome

In the following, the data evaluation of some selected options and definitions of ZSLs are presented.

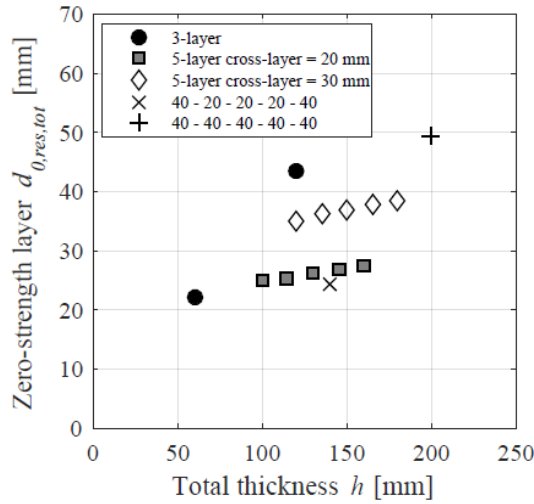


Figure 10: Option A - Traditional ZSL as function of total thickness of the CLT element.

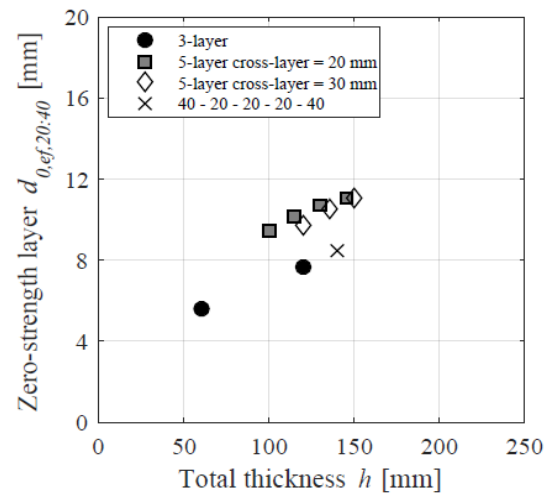


Figure 11: Option B - effective ZSL in a practical range for the relative bending capacity as function of total thickness of the CLT element.

Figure 10 shows the extreme values if a traditional definition for the ZSL, see Eq. (1), was applied. The application would result in large ZSLs and uneconomic design in many cases which was already observed presenting the 2010 model (Schmid et al., 2010). Already in the 2010 model, it was found that the introduction of the practical range between 40% and 20% M_{fi} / M_{20} would result in a higher accuracy for the traditional ZSL. The introduction of the effective ZSL exceeds the improvements implemented in 2010 and results are shown in Figure 11. The introduction of the effective ZSL would result in values between 7 and 12 mm which can be later seen as values implemented in the tabulated data, see Section 6.1.

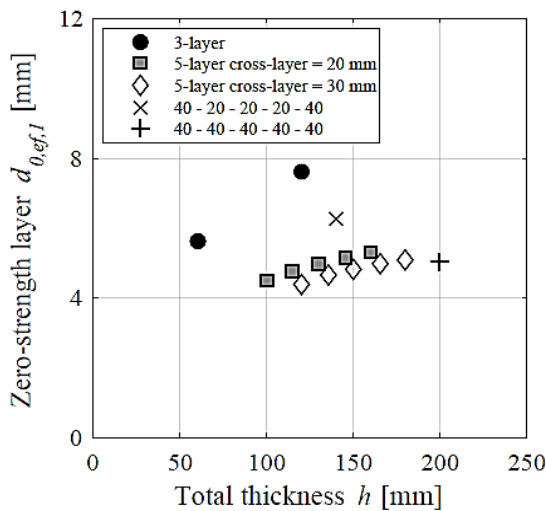


Figure 12: Option C - effective ZSL in layer $i = 1$ as function of total thickness of the CLT element.

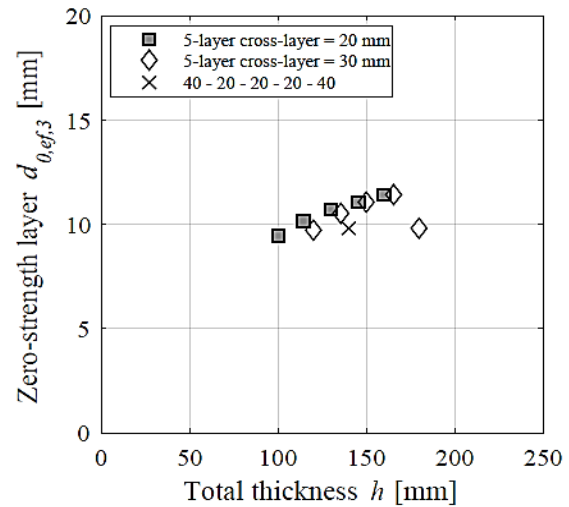


Figure 13: Option C - effective ZSL in layer $i = 3$ as function of total thickness of the CLT element.

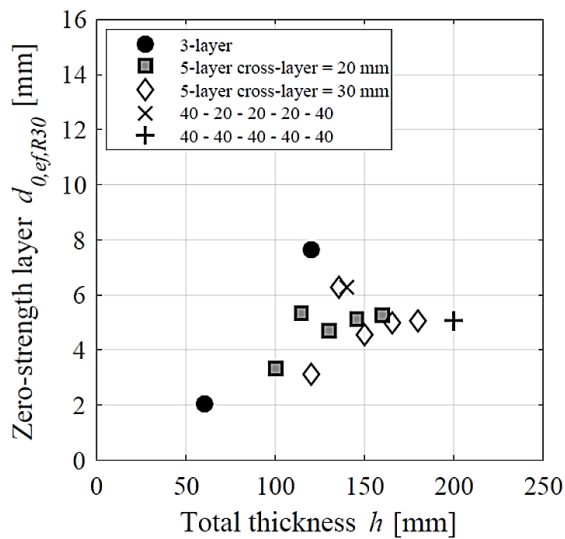


Figure 14: Option D - effective ZSL for R30 as function of total thickness of the CLT element.

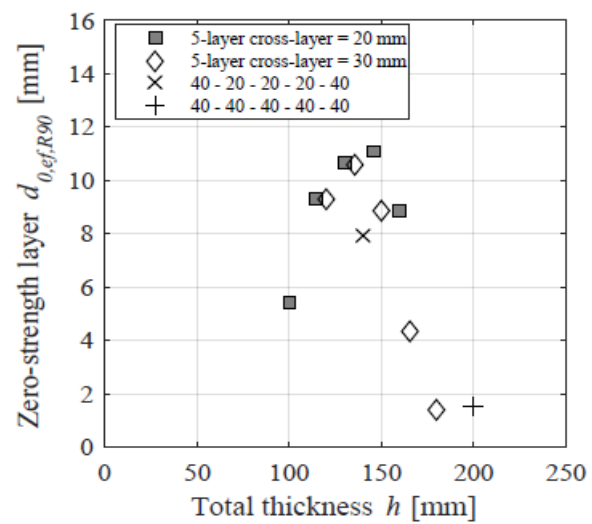


Figure 15: Option D - effective ZSL for R90 as function of total thickness of the CLT element.

An interesting finding showed the analysis of the effective ZSL for the time when charring is in the longitudinal layers $i = 1$ (see Figure 12) and $i = 3$ (see Figure 13). While the effective ZSL for layers $i = 1$ seems to be limited to about 7.5 mm, the effective ZSL for layers $i = 3$ is limited to about 12.0 mm.

Findings of Option C were later used to develop the simplified design model, presented in Section 6.2. Exemplarily, results for R30 and R90 are shown for Option D. As for R60, a large scatter of the effective ZSL can be highlighted reaching from about 2.0 mm and 7.8 mm (R30), see Figure 14, and 1.5 mm to about 12.0 mm (R90), see Figure 15.

6 Results

6.1 The tabulated data

Effective ZSLs are provided as tabulated data for CLT floor elements for 30, 60 and 90 min fire exposure. It should be noted that the values are only valid for the charring model used in simulations whereby the differences to the charring model given in EC5 are limited and acceptable. Charring models defined in ETAs based on tests can not be used together with the values given for this design concept in this Section. Maximum values were found to be 7, 10, and 12 mm, respectively. The individual effective ZSL for the preferred CLT layups are given in *Table 2*.

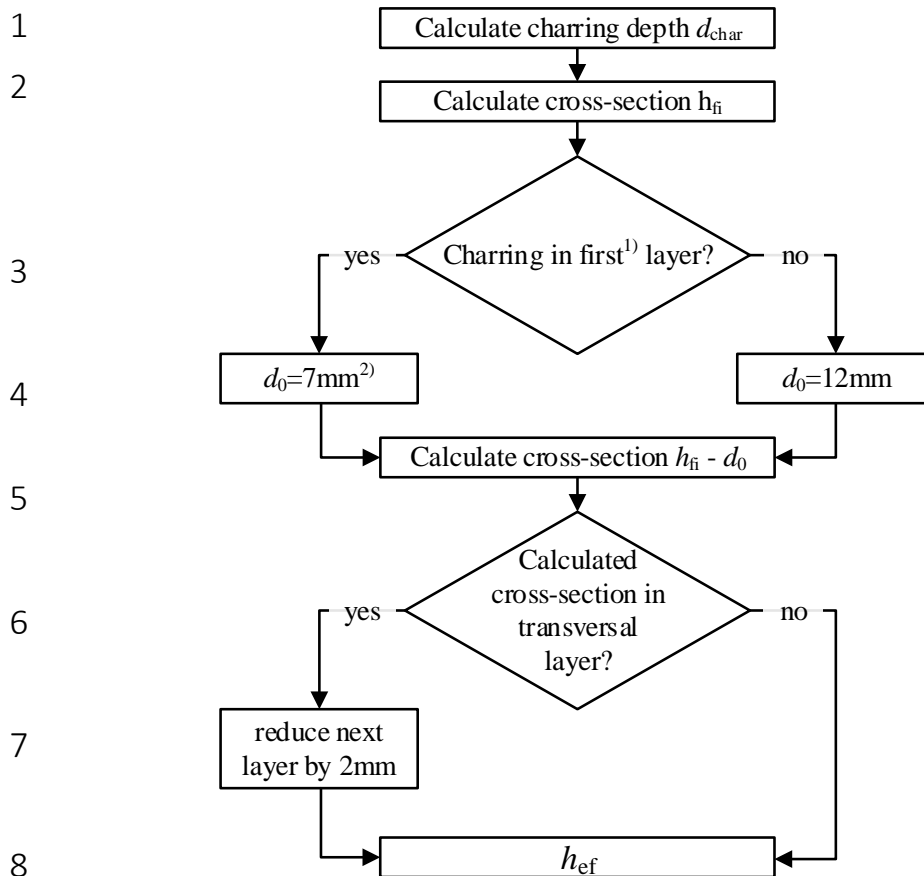
Table 2. Layup of preferred CLT floor elements with layup specification and total thickness of the effective ZSL in mm.

Layup specification	30 min	60 min	90 min
20+20+20	2.0	7.0	n.a.
40+40+40	8.0	4.0	n.a.
20+20+20+20+20	3.0	9.5	5.0
40+20+20+20+40	6.0	5.0	8.0
40+20+40+20+40	5.0	6.0	9.0
40+30-40-30-40	5.0	5.0	3.0
40+40+40+40+40	5.0	5.0	2.0

6.2 The simplified design model “twelve AND two”

The aim of the simplified rule is to increase the application range exceeding the preferred layups.

Step



1) Cover laminations with the same grain direction as the consecutive layer can be considered both as first layer.

2) 7 mm only for initially unprotected CLT; in other cases 12 mm shall be applied.

Figure 16. Determination “twelve and two” simplified design for CLT. The Eight-step procedure to determine the effective cross-section.

A large range of CLT layups was simulated and analysed systematically with respect to available products. Simulations were performed with three- and five layer CLT. The outcome is a simple design methodology which can be applied using the original definition of d_0 since the transversal layers are taken into account explicitly as shown in the flow chart in Figure 16.

To execute the resulting rule, the designer has to check whether the residual cross-section starts (i.e. the depth at the char front) in a longitudinal layer.

- d_0 of 12 mm has to be deducted from the residual cross-section unless the residual cross-section comprises parts of the first layer, then $d_0 = 7$ mm applies. However, a reduction from 12 mm to 7 mm is only possible if the CLT is initially unprotected due to the increased temperature impact depth for initially protected CLT.
- When the calculated cross-section starts in a transversal layer, the effective depth of the following longitudinal has to be reduced by 2 mm.

6.3 Accuracy of the Simplified Model

The agreement of the model “twelve and two” was compared for the simulated CLT and is shown exemplary for a three and a five layer CLT in Figure 17.

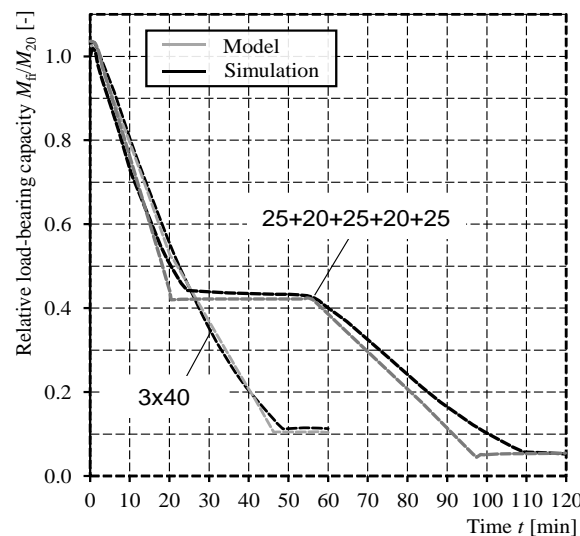


Figure 17: Comparison of the simulated relative bending moment and the result of the model “twelve and two” for two CLT layups.

Deviations are very limited; the model allows for conservative design showing a conservative solution for most of the simulated times. The economic design is granted and maximum deviations can be observed ahead of the plateau of M_{fi} / M_{20} , i.e. during the pre-heating (temperatures between 20 and 100 degrees) of the following longitudinal layer. However, neglecting the step 7 in the design process, compare Figure 16, would result in conservative design close to the end of the plateau (vertical shift of the plateau). The proposed simplified design model “twelve and two” suits also

protected CLT where the thermal penetration depth tends to be increased which resulted in higher values for d_0 proposed 2010, see Section 3.

7 Conclusions

Based on the available calculation technique, thermal and mechanical simulation, new definitions for the ZSL, new design concepts and a limited product portfolio two design concepts for CLT floors exposed to fire on the side in tension were developed in this study.

All presented methods base on the ECSM, thus, methods similar to beams and columns can be introduced for CLT in the new EC5. On one hand, tabulated data were made available, on the other hand a simplified model was presented. Both methods were already tested by the industry reference group (COST FP1404/WG2/TG1), both methods seem to be practical, whereby the simplified model “twelve and two” gave more economic results. This is in line with the intention of the levels of the design concepts.

Further work will include the buckling behaviour of CLT whereby the reduction of stiffness is expected to be crucial for wall elements. The design should make it possible to use the actual buckling model implemented in EC5 for normal temperature design. Further, in correspondence to the model presented here, preferred layups and several design concepts will be considered.

8 Acknowledgements

The authors would like to acknowledge the COST Action FP1404 and its active members from industry and research which allowed for technical discussions and a competent solution finding process as a base for the topic presented here. Further, the authors would like to express their thanks to Stora Enso, Martinsson and the Wood Wisdom network who co-funded the original work developing CSTFire for CLT. Finally, the authors would like to thank the Austrian Wood association for partly funding the work for the improvements presented here.

9 References

- EN 520:2004, Gypsum plasterboards – Definitions, requirements and test methods. European Committee for Standardization, Brussels, 2004.
- EN 1995-1-2, Eurocode 5: Structural fire design of timber. CEN, 2004.
- Franssen, J.-M.: "User's manual for SAFIR 2007. A computer program for analysis of structures"; University of Liege, Department ArGEnCo, Service Structural Engineering; 2007.
- Jones, Kell, et al. "Adoption of unconventional approaches in construction: The case of cross-laminated timber." *Construction and Building Materials* 125 (2016): 690-702.

- Just A, Schmid J, König J. Gypsum plasterboards used as fire protection-Analysis of a database. SP Report 2010:29. ISSN 0284-5172 Stockholm, Sweden, 2010.
- Lange D, Boström L, Schmid J, Albrektsson J. The reduced cross-section method applied to glulam timber exposed to non-standard fire curves. *Fire technology*. 2015 Nov 1;51(6):1311-40.
- Schaffer EL, Marx CM, Bender DA, Woeste FE. Strength validation and fire endurance of glued-laminated timber beams. US Department of Agriculture, Forest Service, Forest Products Laboratory; 1986.
- Schmid, König, Köhler. Fire-exposed cross-laminated timber-Modelling and tests, WCTE 2010. Italy, 2010.
- Schmid J, König J, Just A. The Reduced Cross-Section Method for the Design of Timber Structures Exposed to Fire—Background, Limitations and New Developments. *Structural Engineering International*. 2012 Nov 1;22(4):514-22.
- Schmid J, Klippel M, Just A, Frangi A. Review and analysis of fire resistance tests of timber members in bending, tension and compression with respect to the reduced cross-section method. *Fire safety journal*. 2014 Aug 1;68:81-99.
- Schmid J, Just A, Klippel M, Fragiaco M. The reduced cross-section method for evaluation of the fire resistance of timber members: discussion and determination of the zero-strength layer. *Fire technology*. 2015 Nov 1;51(6):1285-309.
- Schmid J, Just A, Klippel M, Fragiaco M. The reduced cross-section method for evaluation of the fire resistance of timber members: discussion and determination of the zero-strength layer. *Fire technology*. 2015 Nov 1;51(6):1285-309.
- Schmid J, Klippel M, Liew A, Just A. Analysis of fire resistance tests on timber column buckling with respect to the Reduced Cross-Section Method, INTER Meeting 2015, 48-16-01, Sibenik 2015.
- Schmid, J., Klippel, M, Frangi, A., Just, A., Tiso, M., Note: An improved design model for fire exposed Cross Laminated Timber, Proceedings of INTER Meeting August 2017 in Kyoto, Japan, 2017.
- Schmid J, Brandon D, Werther N, Klippel M. (2018a). Thermal exposure of wood in standard fire resistance tests. *Fire Safety Journal*. 2018.
- Schmid. J., Klippel, M., Frangi, A., Just, A., Tiso, M. (2018b). Simulation of the Fire Resistance of Cross-laminated Timber (CLT), *Fire Technology*, 2018.
- Schmid J, Klippel M, Fahrni F, Frangi A, Brandon D, Lange D, Sjöström J, Just A. (2018c). Thermal exposure of timber structures - the use of furnace tests to describe real fires, World Conference on Timber Engineering in Seoul, WCTE 2018, South Korea, 2018.

Discussion

The paper was presented by J Schmid

S Aicher asked how does one account for the non-edge glued CLT with variable gap sizes and whether the model only accounts for edge glued CLT. J Schmid discussed the 6 mm gap allowance for CLT which is deemed to be inappropriate. He added that in European research 2 mm gaps will not allow heat to go into the gap as the wood chars. Also most CLT producers using vacuum press has a gap limit of 2 mm which is deemed acceptable. H Blass added that the 6 mm gap size was fixed at the earlier stage of CLT production. Nowadays the gap value is much smaller.

Press Glued Connections - Research Results for Discussion and Standardization

Steffen Franke, Bern University of Applied Sciences, Biel, Switzerland

Marcus Schiere, Bern University of Applied Sciences, Biel, Switzerland

Bettina Franke, Bern University of Applied Sciences, Biel, Switzerland

Keywords: nail press gluing and screw press gluing, composite structures, head pull-through capacity, adhesive bond quality.

1 Screw and nail press gluing

Press glued connections performed with screws, nails, or staples is used in multidisciplinary applications in wood industry. The fasteners are used to hold two timber elements together while the adhesive cures in between them, or to provide curing pressure on the adhesive. Full composite action between assembled elements can be achieved. It is used in new structures to assemble hollow box elements for instance, but also to reinforce damaged structural components. The ExpoDach in Hannover, Germany, and the Sibelius Hall in Lahti, Finland, contain screw press glued load bearing elements, see Figure 1. Other examples are the the Waldau Stadium in Stuttgart, Germany, and the Leonardo da Vinci bridge in Ås, Norway.

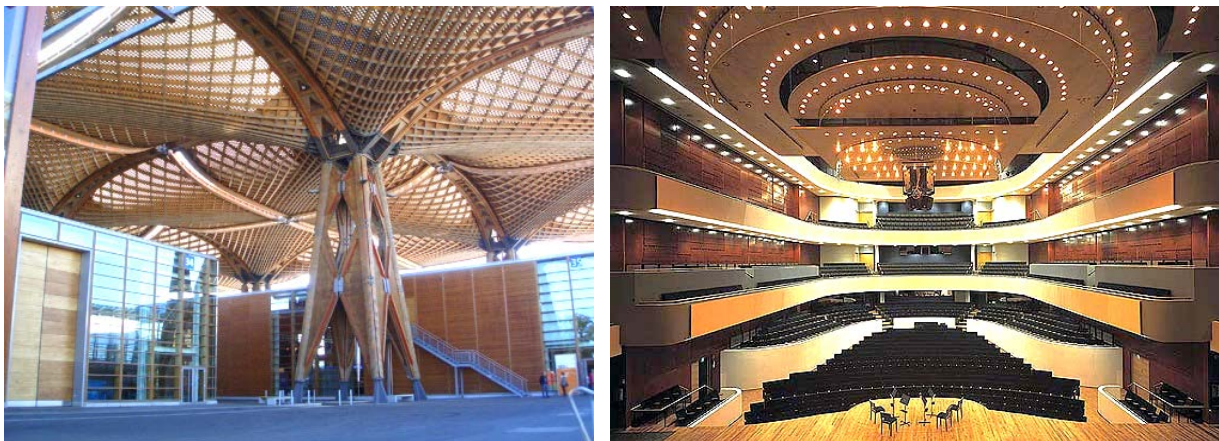


Figure 1: Outstanding example of structures manufactured using the press gluing technique: the ExpoDach in Germany (Boller 2006) (left), and the Sibelius Hall in Finland (Artec 2015) (right)

The main advantage of the press gluing methods is that they can be used on a construction site or on locations where use of presses is impractical. More common is to apply the method in workshops of small-, or in production halls of large, companies. It allows them to remain flexible and competitive and still meet a wide variety of customer requirements to size and dimensions of a product.

The opinion amongst the wood construction industry about the final quality and strength of the achieved bond varies. This is explained perhaps by the lack of a broadly supported standards and the many combinations of adhesives, materials, methods, and production conditions under which the press glued bond is established. One of the main doubts is whether the chosen fasteners can generate sufficient curing pressure for the used adhesive. Standardised methods to test or qualify the final bond are not available either. Hence, there is a need to evaluate methods and materials used.

The presented work first discusses the state of the art of the nail and screw press gluing methods by presenting earlier work and contents of current standards. Then the achievable average curing loads are measured for staples, nails and screws. After the evaluation of bond quality resulting from different production conditions, recommendations to industry and for further work are given. The presented work is a summary of work also reported in Franke et al. (2018).

2 Application and state of the art

2.1 Applications of screw press glued connections

Screw gluing and nail press gluing techniques are used to produce ribbed panels, hollow box elements, box beams, I-beams, join glued laminated timber beams, etc., see Steck (1988) and Kairi (2000). Some examples of basic structural components are shown in Figure 2 and Figure 3.

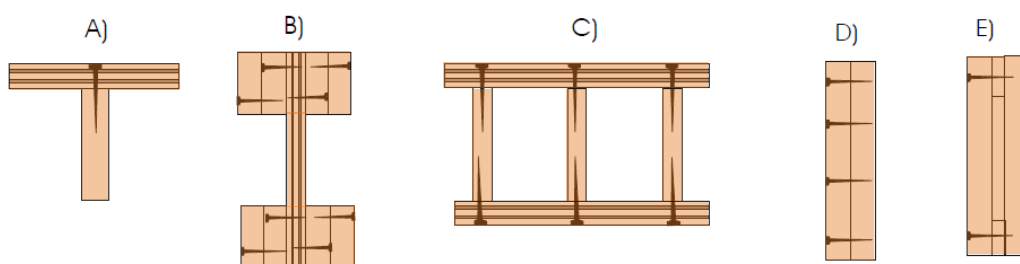


Figure 2: Structural members produced with press glued connections, T-Beam (A), I-Beam (B), Ribbed panel (C), Double Beam (D), Box-Beam (E) (Kairi, 2000)

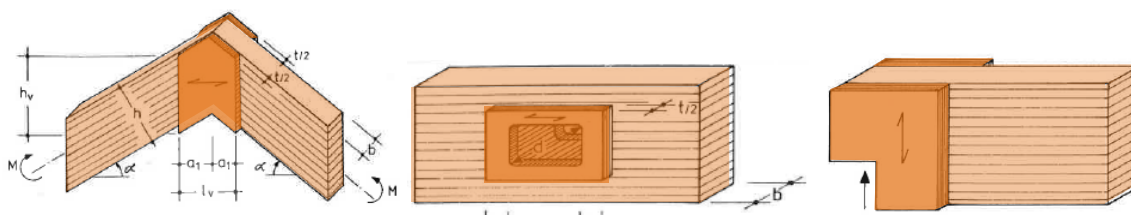


Figure 3: Connection assembled, reinforced end notch or hole (Steck, 1988)

Kairi (2000) and Hillmer (2014) list different dimensions and materials used for box elements and ribbed panels using Kerto and solid wood. Steck (1988) and Widmann (2014) provide examples of how plywood or solid wood panels are used as external reinforcement of holes and notches in beams. Damaged curved and tapered beams with tensile cracks perpendicular to the grain are repaired by applying external reinforcements. Stiffness and strength of load bearing timber elements in (historic) structures is increased by press gluing extra lamellas onto them. Bratulic & Augustin (2016) carried out experiments to join Cross Laminated Timber elements using washer head screws with head diameters of 22 mm and 35 mm. Glued laminated timber beams were joined using double threaded fasteners, see Sieber (2003). The listed examples illustrate the wide variety of applications and materials used.

2.2 Standards and recommendations

Screw press gluing is only regulated in the German National Annex of Eurocode 5, which refers to the DIN 1052-10:2012 valid previously. Up to 2004 nails were also allowed through the DIN 1052-1:1988. Now, only screws with a thread diameter larger than 4 mm are to be used. The reference surface per fastener is 15000 mm² with a maximum intermediate distance between fasteners of 150 mm. The fasteners should have a smooth shaft throughout the head side material so that it is possible to pull two assembled elements together. The maximum difference in moisture content of the joined materials should be 4 M% and both should be lower than 15 M%. Maximum allowed material thicknesses are 50 mm and 45 mm for wood based panels and solid wood, respectively. The adhesives used should have been tested according to the DIN EN 301:2006-09 type 1 test, where resistance to temperatures above 50 °C is tested. Material temperatures should be at least 18 °C and guidelines described in technical data sheets should be followed.

Engineering companies have listed additional recommendations such as the use of counter head fasteners with minimum thread diameters of 5 mm and suggest a list of adhesives. Application quantities are about 250 g/m² and the resulting glue line thicknesses should be lower than 0.3 mm. The adhesive in the assembled elements should at least be allowed to cure for three hours before further machining or transport is done. The final bond quality is to be tested by assembling additional elements for destructive tests. The bond quality could be tested by splitting the bond and evaluate the amount of substrate failure. Finally, a log should be maintained in which the used materials, production conditions, etc. should be documented per produced element (Besmer und Bruning, Pirmin Jung 2010).

Pneumatic or vacuum presses offer an alternative to the screw and nail press gluing. Hydraulic presses are used only when curing pressures above 0.6 N/mm² are needed.

2.3 Used fasteners

Figure 4 shows an overview of fasteners that are - or could - be used for press gluing applications. Common are the counter head screws, and new might be the fully

threaded screws with a varying thread angle. The slope of the thread changes at a certain point along the length of the fastener, and are ideal to tighten two materials onto each other. Some structures are assembled with scrails but continuous quality control is maintained at the production line. The advantage of the scrail is that they can be inserted with nail guns, but can also be removed once the adhesive has cured. The use of staples is economically very attractive, since these fasteners can be inserted at frequencies up to 5 Hz. The fasteners are also cheap to produce and many can be loaded into a magazine. Wave nails were also observed but the resulting bond was not used as a load bearing connection.

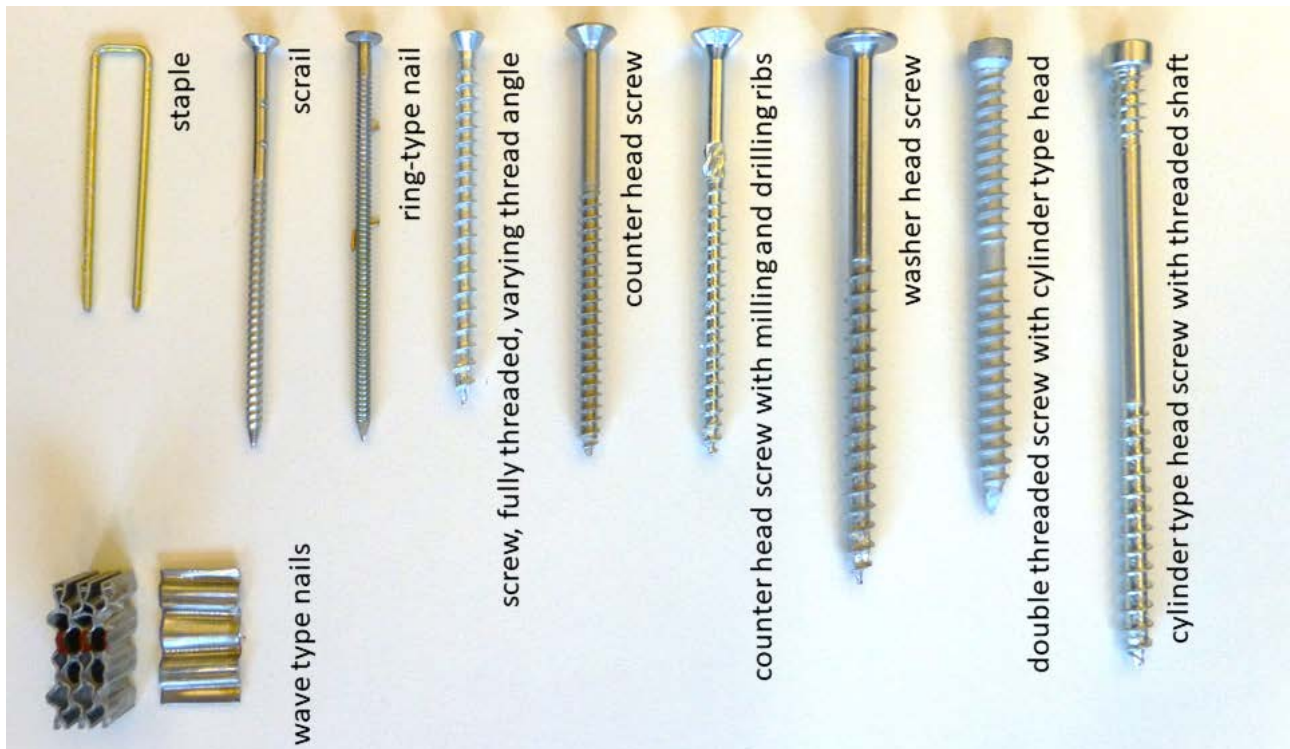


Figure 4: Overview of different pin type fasteners used already and suggested to be suitable for screw- or nail press gluing applications.

2.4 Used adhesives

Kairi et al. (1999) joined Kerto panels using one-component polyurethane (1C-PUR) adhesive Purbond HB110, applied with a quantity of 250 g/m^2 . Bond shear capacity of 6 N/mm^2 were achieved with a glue line thickness under 0.3 mm . Kurt (2003) used Gap-filling Phenol Resorcin Formaldehyde (G-PRF) to join Douglas fir Plywood to spruce beams with screws. Glue line thicknesses up to 0.508 mm still produced sufficient mean shear capacities around 6 N/mm^2 . Gerber et al. (2006) compared a synthetic rubber adhesive (RBA) to a 1C-PUR adhesive when joining plywood and engineered strand board to radiata pine beams. Average shear capacity of 4.4 N/mm^2 were achieved using the PUR adhesive. Rug et al. (2010) joined solid wood, birch plywood panels, and laminated veneer lumber to glued laminated timber beams using PRF and Epoxy adhesives using scrails. Hillmer (2014) obtained average shear capacity around 5.5 N/mm^2 and 4.5 N/mm^2 with screws and scrails, respectively.

Screws press gluing generally results in a better bond capacity. Most obtained bond shear capacities were said to be better than the material properties. Sufficient shear capacity can however be obtained with an insufficient substrate failure ratio. Gerber et al. (2006) makes an important note, claiming that the presence of the fasteners is an advantage, as they contribute to a ductile failure of the connection once the adhesive has failed.

1C-PUR adhesives are popular nowadays, but Beaud et al. (2006) warns that these might not properly cure at wood moisture contents below 8 M%. It is logically recommended to join materials at sufficient moisture contents as PUR adhesives require water during the curing process. The study also showed that even if the moisture contents of the material were sufficient during the adhesive's curing, shear load capacities could drop once moisture contents were below 8 M%. Dry conditions can be accounted for by moisturizing the wood prior to gluing, see also Kägi (2005) and Kläusler (2014). Humid conditions will accelerate the PUR-curing, requiring faster assembly of materials.

3 Measurement of compression loads

3.1 Typical load histories and evaluation of curing loads

The surface integral of the pressure distributed around the fastener, between the bonded surfaces, is equal to the tensile load present in the fastener itself, see Figure 5 (left). Miniature load cells were used to measure this tension/total compression load. The load cells were arranged in a triangular setup so that fasteners could be inserted in between these. A gap of 2 mm was maintained between the plate and rib: enough to prevent contact, but also allowed tests with short fasteners.

A typical load history of the generated compression load by the fastener is shown in Figure 5 (right). Common is the peak load that develops when the fastener is inserted, a rapid drop afterwards that changes into a converged curing load. Depending on the fastener type, sampling frequencies of 20 Hz to 100 Hz are needed to measure this peak, although it is not a representative curing load. The compression load ob-

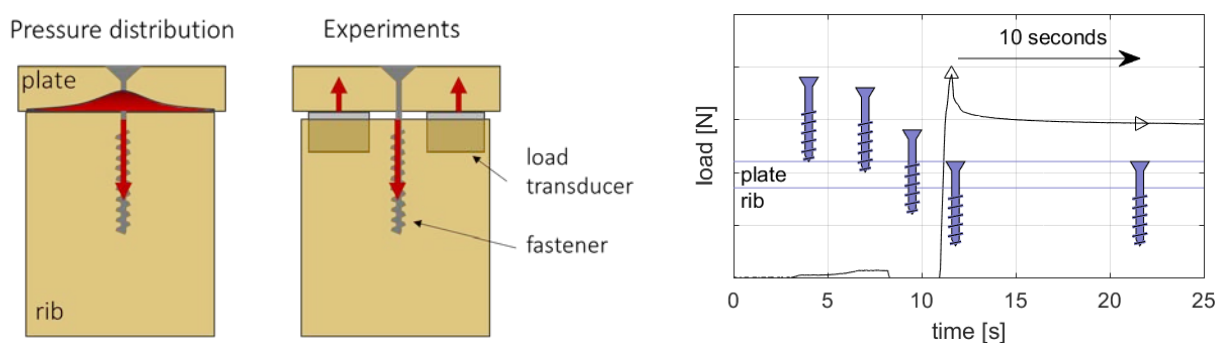


Figure 5: Visualisation of the pressure between two joined elements, and the measurement of curing load (left). The screw position during the drilling and the measured load, the maximum load, and the determination of the curing load 10 second after the peak load are visualised (right).

tained from the experiments was obtained 10 seconds after the peak occurred. To calculate the 5% quantiles of the compression loads, the lognormal distribution described in FprEN 14358:2015, Section 3 was used.

3.2 Previous research on achievable compression loads

Bratulic & Augustin (2016) suggest that the generated compression load is closely related to the head diameter of the fastener. If the used head diameter is too large, Kairi et al. (1999) warn that tip pull-out capacity can be exceeded. Hillmer (2014) and Rug et al. (2012) tested scrails and obtained loads around 200 N. Tests with 4 mm fasteners resulted in compression loads around 600 N. Kairi et al. (1999) and Bratulic & Augustin (2016) obtained loads between 2000 N and almost 9000 N with different washer head screws. These values are used later in Section 3.5. Kairi et al. (1999) also measured the compression loads of double threaded screws in Kerto and obtained a range from 0 N to 1970 N. The low values were said to be caused by a small difference in the two thread angles, through which the head and point side member could not be pulled together.

3.3 Head pull-through and tip pull-out capacities

The achieved compression loads are compared to the characteristic head pull-through capacities in Section 3.5 using the DIN EN 1995-1-1:2010. The head pull through capacity for screws was calculated using:

$$F_{head,Rk} = f_{head,k} d_h^2 (\rho_k/350)^{0.8} \quad (1)$$

Parameters affecting the head pull through capacity are the strength $f_{head,k}$, head diameter d_h , and material characteristic density ρ_k . $f_{head,k}$ is provided by manufacturers. One way to achieve greater head pull-through capacities is to use larger head diameters. Then, the head pull through capacity of the double threaded screws was calculated using the formulations for the pull-out capacity of threaded part. This is calculated using the length of the full or effective threaded length l_s , the characteristic withdrawal capacity $f_{ax,k}$ and thread diameter d .

$$F_{ax,Rk} = f_{ax,k} d l_s (\rho_k/350)^{0.8} \quad (2)$$

The fasteners are to be oriented 90° perpendicular to the fibre direction. Material densities of 350 kg/m³ were used through which the equations can be simplified somewhat. The calculated values were similar to those given in the individual product data sheets. An illustration of a screw with the indicated geometrical parameters is observed in Figure 6.

The head pull through capacity for smooth nails is calculated using the characteristic strength $f_{head,k}$ and the head diameter d_h , see also in Figure 7.

$$F_{head,Rk} = f_{head,k} d_h^2 \quad (3)$$

Material density is included in the formulation of $f_{head,k}$. Once a part of the shaft in the head side material is shanked or has rings, the capacity of this part may be added us-

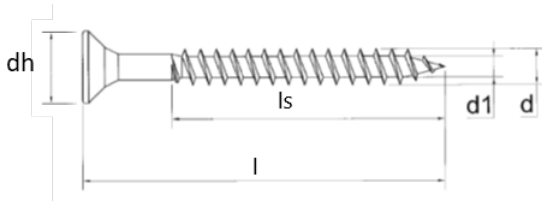


Figure 6: Partially threaded fastener with counter sunk head



Figure 7: Ring nail with almost fully shanked shaft

ing the equation for the withdrawal capacity. This uses the characteristic strength $f_{ax,k}$, the shanked length (in the head side member) l_{ef} and the shaft diameter d .

$$F_{ax,Rk} = f_{ax,k} l_{ef} d \quad (4)$$

Material densities are included in the formulation of $f_{ax,k}$.

3.4 Obtained compression loads for all fasteners

Table 1 lists the tested nails, staples and screws, some are also observed in Figure 4. The geometries of these fasteners are not uniform. The choice for these fasteners was based on whatever was provided by manufacturers, observed in practice, or recommended in literature and product folders. Tests with smaller fasteners were performed in three-layer solid wood panels of 27 mm thickness. The larger screws ($d > 6$ mm) were tested in solid wood boards of 40 mm thickness.

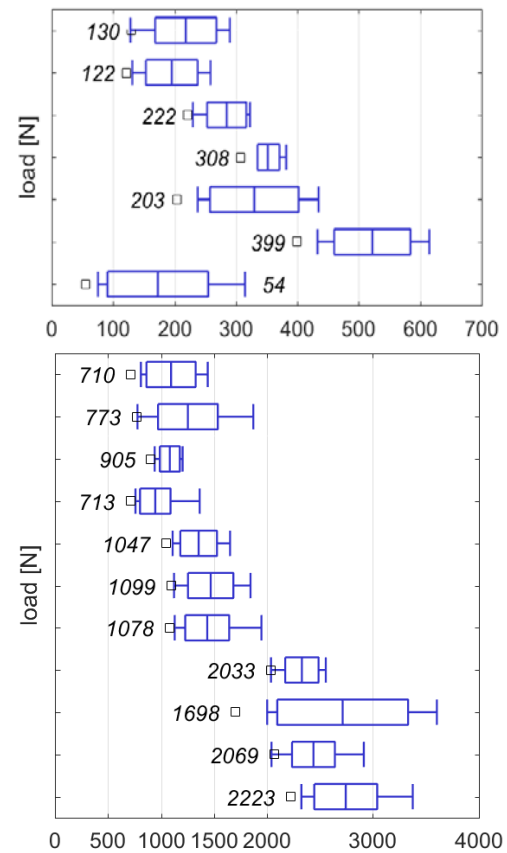
The achieved loads by the nail type fasteners were between 100 N to 600 N. The staples showed the largest spread with a Coefficient of Variation (CV) of 48 %. The reluctant attitude towards staples in press gluing applications is understood when the 5% quantile is calculated, i.e. very low values are obtained.

The counter head screws generated compression loads between 700 N and 2000 N. Some of the screws also showed a large spread with a CV up to 32 %. Varying thread screws generated higher average compression loads and had a smaller CV of 20 %. The fasteners with thread diameters of 6 mm and more proved that high adhesive curing loads can be generated. The washer head screw could be less preferred over the double threaded fasteners due to the large spread, CV of 36 %, in generated loads. Optically, washer head screws might not be preferred either in a finished product. The double threaded fasteners can generate similar loads as the washer head screws, but have a smaller spread and smaller head diameters.

Literature mentions that compression loads reduce 25 % to 30 % during the three hours after initial fastening. This is calculated with respect to the measured peak loads, see Figure 5. Now, the long-term load is compared to the load measured 10 seconds after the nailing/screwing. The tested scrails showed a remarkable average increase of 6 %, accounted to cooling of the fastener. The highest decrease was 2 %. Loads measured with the counter head screws reduced between 6 % and 12 % after three hours, the double threaded fasteners reduced between 14 % and 19 %. Since there is a correlation between the generated compression load and the reduction over three hours, it is expected that this could also be related to the moment after

Table 1: Tested fasteners, nails, staples and screws, with head diameters, thread diameters, (threaded) lengths (left) and box plots with minima, maxima, means and 5% quantile values (right).

	ID	d	d_h	l	l_s/l_{ef}
Nails/staples		mm	mm	mm	mm
Scrails	NS1.1	3.2	5.9	75	40
Scrails	NS1.2	3.2	6.9	75	40
Ring nails	NR2.1	2.8	6.8	75	
Ring nails	NR2.2	3.1	7.1	90	
Ring nails	NR2.3	3.4	7.4	100	
Ring nails	NR2.4	3.8	7.9	110	
Staples	NC3		15	75	
Screws					
CH/Würth	SC1	5.0	9.6	80	50
CH/SPAX (HR)	SC2	5.0	9.7	80	50
CH/Fischer (HR/SR)	SC3	5.0	9.7	80	50
CH/Rothoblaas (HR/SR)	SC4	5.0	10	80	40
VT/Heco	SV5.1	4.0	6.1	70	Full
VT/Heco	SV5.2	4.5	6.8	70	Full
VT/Heco	SV5.3	4.5	6.8	80	Full
VT/Heco	SV5.4	5.0	9.6	80	Full
WH/SPAX	SW6	6.0	13.6	100	60
DT/SFS WT-T	SD7	6.5	8	90	40/35
DT/Würth	SD8	6.0	8.2	120	50/15



CH (counter head), VT (varying thread), WH (Washer head), DT (double thread), HR (milling ribs under the fastener head), SR (milling ribs on the fastener shaft)

the peak load, from which the initial compression load is obtained. This point needs to be chosen smart in future measurements. More results concerning group loads, production methods, and use of other materials are found in Franke et al. (2018).

3.5 Comparison of achieved values with those available in literature

Section 3.2 already listed previously measured compression loads. Materials used throughout these studies were not uniform. Results obtained from literature and from above mentioned experiments are normalized to a material density of 350 kg/m^3 using the 5% quantile of the material density and Equation (1):

$$F_{\text{head},5\%,350} = F_{\text{head},5\%} (350/\rho_{5\%})^{0.8} \quad (5)$$

The 5% quantiles are plotted in Figure 8, where the compression load is compared to fastener head diameter. The filled markers are own experiments, and the empty markers are obtained from literature. The latter were multiplied by 0.7 to account for a 30 % reduction of the maximum measured values.

The 5% quantile of the load generated by the scrails are a little over than 100 N. The ring type nails perform better at values around 200 N to 300 N. The varying thread,

the washer head, and double threaded screws perform better than the counter head screws.

Figure 9 illustrates the relation between the measured compression loads against their characteristic head pull through capacities. Literature values were not added. The scrails, nails, counter head, and washer head fastener generate lower compression loads than can be calculated from their head pull through capacities. Those of the varying thread fastener are higher.

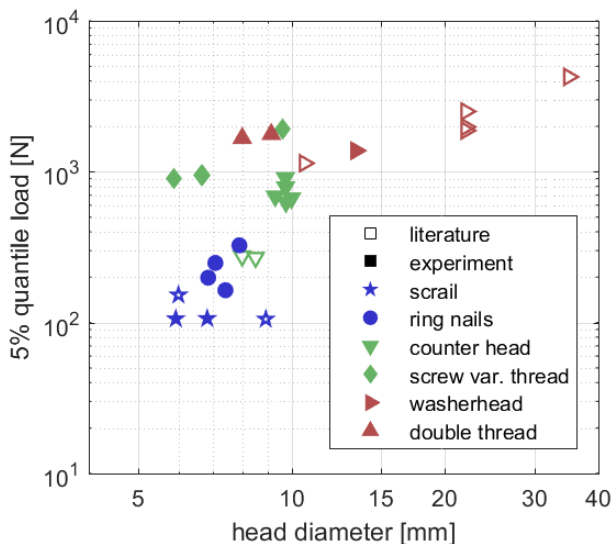


Figure 8: Comparison of obtained experimental results corrected to 350 kg/m^3 density as a function of fastener head diameter

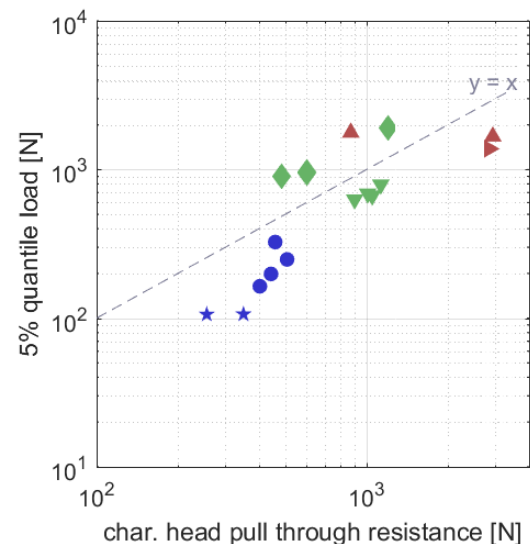


Figure 9: Experimental results corrected to 350 kg/m^3 density compared to characteristic head pull through capacities

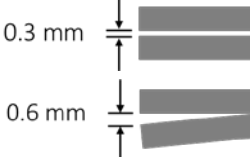
4 Methods to evaluate the resulting bond

4.1 Material and test matrix

The tests were performed using two 1C-PUR adhesives, a more liquid and viscous one, adhesive A and adhesive B respectively. Both adhesives recommended a curing pressure of at least 0.1 N/mm^2 . A quantity of 250 g/m^2 was used which was achieved within 6 % of the targeted value. Adhesive A and adhesive B recommended a maximum glue line thickness of 0.1 mm and 0.3 mm, respectively.

Three separate conditions were investigated: ideal conditions (IC), the production conditions (PC) and other conditions (OC), see also Table 2. The pressure levels on the adhesive in the ideal conditions was maintained at a constant level during the curing process. Boards 30 mm thick and 100 mm wide were used here. In the production conditions, three fastener dimensions were used to supply curing pressure between a three-layer solid wood panel and a 100 mm wide rib: A scrail, a 5 mm counter head screw, and a 6 mm counter head screw. The lowest achievable curing pressure was generated with a scrail at an intermediate fastener distance of 150 mm. The heads of the 5 mm and 6 mm screws were drilled 2 mm deeper than usual into the wood to generate higher adhesive curing pressures. In the remaining tests (OC), an

Table 2: Overview of different tests with ideal conditions, production conditions, and remaining conditions that were carried out.

Condition	Low pressure	Medium pressure	High pressure
Constant pressure	0.02 N/mm ² , IC1	0.13 N/mm ² , IC2	0.20 N/mm ² , IC3
Fasteners every 150 mm	Scrail, 0.02 N/mm ² , PC1	5 mm screw 0.11 N/mm ² , PC2	6 mm screw 0.17 N/mm ² , PC3
Worst case		Uneven application, OC1 Constant spacing 0.3 mm, OC2 Wedge spacing 0.6 mm, OC3	
Constant glue line thickness		Adhesive A, OC4 Adhesive B, OC5	

uneven application of adhesive was performed and intentionally created constant and wedge shaped spacing were created between the glued elements. In the two remaining conditions, the glue line thickness was maintained constant throughout the adhesive curing with the universal testing machine. The used timber was conditioned two weeks in a climate of 20 °C and 65 % relative humidity. The shear tests were performed two weeks after the gluing.

4.2 Resulting bond quality

The EN 14080:2013 provides a method to evaluate bond quality by suggesting minimum relations between shear capacity and substrate failure ratio. This relation is given for each individual sample, but also for the mean of all samples. Both relations should be passed. A lignin activator was used to facilitate the evaluation of substrate failure ratio since the used PUR was colorless. The results are shown through the box plots in Figure 10 and the pass/failed evaluation of the EN 14080:2013 in Table 3.

Figure 10 shows that shear capacity only does not provide a complete evaluation of the bond. Although shear capacities over 6 N/mm² are obtained, substrate failure ratio can still show a large spread and be insufficient: IC1, PC1, OC2-OC4. Curing of the adhesive while the bond thickness is maintained constant resulted in higher shear capacities, but also in a greater spread of the substrate failure rate. Tests with the intentionally created large gaps showed that glue lines in PUR adhesives are to be maintained to a minimum if a good bond is needed.

5 Discussion

5.1 Optimization of achievable curing pressure through choice of fastener

The experiments with fasteners proved that fastener head design affects the achievable compression loads. Drilling ribs under the fastener's head reduce the spread of the measured loads. The double threaded fasteners achieve similar mean loads as the washer head screws, but with a small spread. It is noted though that this depends on the difference in thread angle that the double threaded fasteners have. Varying

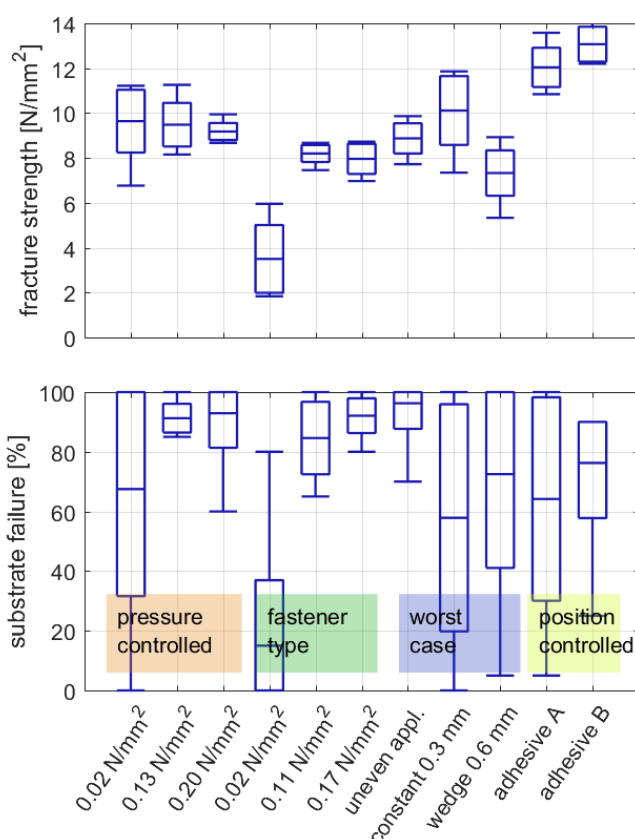


Figure 10: Shear fracture and substrate failure rate as function of different adhesive application and curing method

thread fasteners outperform counter head screws too, although care should be taken as to where the transition in thread angle occurs.

The wood industries' reluctant attitude towards use of staples in press gluing applications is understood: a low mean and large spread. The mean compression loads are similar to what was measured with scrails. A large potential for application of staples is imagined once compression loads can be better controlled, either by spread of the staple's legs or application of a choice of coating to improve the friction between wood material and staple.

5.2 Fastener distances to generate an average curing pressure of 0.1 N/mm²

Not all adhesives used in press gluing methods require a curing pressure. When they would, the obtained compression loads can be used to estimate the needed number of fasteners per distance covered or area. For instance, some 1C-PUR adhesives require minimum curing pressures of 0.1 N/mm² in their technical data sheets. This threshold is used together with the average curing load to calculate a theoretical fastener distance on different rib widths in Table 4. The maximum intermediate distances of 150 mm suggested earlier in Section 2.2 are maintained. Once fastener distances are too close, a double row of fasteners could be imagined too. The fastener dis-

Table 3: Overview of pass and fail for the different test setups to requirements set by the EN 14080:2013.

Test	Single values	Average	Total
IC1	Fail	Pass	Fail
IC2	Pass	Pass	Pass
IC3	Pass	Pass	Pass
PC1	Fail	Fail	Fail
PC2	Pass	Pass	Pass
PC3	Pass	Pass	Pass
OC1	Pass	Pass	Pass
OC2	Fail	Pass	Fail
OC3	Fail	Fail	Fail
OC4	Fail	Fail	Fail
OC5	Pass	Pass	Pass

tance s was calculated by dividing the achieved mean load F by the product of minimum curing pressure P and rib width w .

$$S = F/(P w) \quad (6)$$

Table 4: Theoretical fastener distances along a rib for a curing pressure of 0.1 N/mm²

	Mean load [N]	Fastener distance as single row for rib width of		
		60 mm	80 mm	100 mm
Scrail 3.2 mm	200	33	25	20
Ring nail 2.8 mm	250	42	31	25
Counter sunk head 5 mm	1000	150	125	100
Varying thread 4.5 mm	1400	150	150	140
Washer head 6 mm	2700	150	150	150

For example, one scrail every 33 mm on a 60 mm wide rib is close, but is also realistic. The additional advantage of using thinner ribs is also that gaps due to slight torsion of ribs, such as simulated in OC3, remain small. It should be noted that scrails and ring nails have limited tightening capacities. It is recommended to ensure sufficient spread of the adhesive before shooting the fasteners.

5.3 Choice of adhesive and final bond quality

The EN 14080:2013, Appendix D, provides a helpful way to quantify the quality of the bond. The test is relatively easy to perform. It is perhaps too conservative due to neglected additional ductility of the connection such as suggested by Gerber et al. (2006). The test allows for low material rolling shear down to 4 N/mm² under the condition that a 100 % material failure is achieved.

Epoxy and PRF adhesives are frequently used in screw and nail press gluing applications. The first adhesive requires almost no curing pressure at all but is more brittle, which could lead to stress concentrations in the bond. PRF is used when it is likely that glue line thicknesses are expected to be large.

6 Conclusions and recommendations

It is important to realize that fastener distance, fastener type, used adhesive is not the complete part of the puzzle. Parameters like achieved glue line thickness, surface quality, production conditions, etc., are elements that are all important to guarantee the final bond quality.

A measurement setup was successfully developed which allowed the measurement of compression loads generated by fasteners. The measured peak load should however not be used as reference to estimate the average curing pressure. Instead, a load measured after this peak should be used. For nails and staples, the 10 seconds seems to be a reasonable point. It could be stretched a little for screws in the future.

Press gluing with nails or staples is not popular amongst wood construction industry. The large spread in generated compression loads is a possible explanation. They do offer economical solutions, but additional quality control is recommended.

The variety of screws tested showed that some fasteners can provide high adhesive curing pressures. The head typology affects this curing load and fasteners could be optimised to achieve higher curing loads without much redesign of the fastener.

The EN 14080:2013 provides a first evaluation of the remaining bond quality. It is believed to be too conservative since the ductility of the fastener is not considered in the failure behaviour. A test setup could be redesigned to include this in future assessments of the bond quality.

7 Acknowledgements

The project was funded by the Swiss State Secretariat for Education, Research and Innovation in scope of COST Action FP1402 (SERI C15.0052). Also acknowledged are Haubold Passlode Switzerland and Brawand Zimmerei for contributing equipment, material, time, and expertise. Further thanks go to the students Desbele Teklebrhan, Lukas Ryffel, and Konstantin von Mitzlaff, who contributed to the experiments.

8 References

- Beaud P, Niemz P, Pizzi A (2006): Structure-Property Relationships in One-Component Polyurethane Adhesives for Wood: Sensitivity to Low Moisture Content, *Journal of Applied Polymer Science*, Vol. 101, pp. 4181-4192.
- Besmer und Bruning GMBH: Schraubenpressverklebung im Holzbau, www.holzmitschwung.ch
- Bratulic K and Augustin M (2016): Screw Gluing – Theoretical and experimental approach on screw pressure distribution and glue line strength, WCTE 2016 conference proceedings, Vienna, Austria.
- DIN 1052-1:1988-04; Holzbauwerke, Teil1: Berechnung und Ausführung, Deutsches Institut für Normung e. V., Beuth Verlag GmbH, Berlin, Germany.
- DIN EN 1995-1-1:2010-12: Eurocode 5: Bemessung und Konstruktion von Holzbauten Teil 1-1: Allgemeines – Allgemeine Regeln und Regeln für den Hochbau, Deutsches Institut für Normung e. V., Beuth Verlag GmbH, Berlin, Germany, 2010.
- DIN EN 1995-1-1/NA:2010-12: Nationaler Anhang – National festgelegte Parameter – Eurocode 5, Deutsches Institut für Normung e. V., Beuth Verlag GmbH, Berlin, Germany, 2010.
- DIN 1052-10:2012-05: Herstellung und Ausführung von Holzbauwerken – Teil 10: Ergänzende Bestimmungen, Deutsches Institut für Normung, Beuth Verlag GmbH, Berlin, Germany, 2012.
- FprEN 14358:2015: Holzbauwerke - Berechnung und Kontrolle charakteristischer Werte, Europäisches Komitee für Normung (in revision).

- Franke S, Schiere M, Franke B (2018): Investigation and analysis of press glued connections for timber structures, report number K.007404.77FE-V1, Bern University of Applied Sciences, Switzerland.
- Gerber C, Crews K, Sigrist C (2006); Screw- and nail-gluing techniques for wood composite structures, Proceedings of the 19th Australasian Conference on the Mechanics of Structures and Materials, pp.1023-1029.
- Hillmer V (2014); Nagelpressverklebung – Einflüsse von Maschinellem Fertigung und örtlicher Versetzung, Bachelorarbeit HAWK, Studiengang Holzingenieurwesen.
- Kägi A (2005): Untersuchung zum Einfluss der Holz-feuchte und ausgewählter technologischen Parameter auf die Verklebungsgüte von Fichtenholz mit einem 1K PUR für tragende Holzbauteile, Bern University of Applied Sciences, Thesis Nr. F/4/D/389/05/5.
- Kairi M, Kaloinen E, Koponen S, Nokelainen T, Fonselius M, Kevarinmäki A (1999): Screw gluing Kerto-LVL structures with Polyurethane, Otawood publication, HUT Laboratory of Wood Technology, HUT Laboratory of Structural Engineering, VTT, Espoo.
- Kairi M (2000): Schraubenverleimungen erlauben neue Möglichkeiten im Ingenieurholzbau, Holzbauforum Conference Proceedings, Garmisch-Partenkirchen, Germany.
- Kläusler O (2014): Improvement of One-Component Polyurethane Bonded Wooden Joints under Wet Conditions, Doctoral Thesis 22157 ETH Zürich, Switzerland.
- Kurt, R (2003): The strength of press-glued and screw-glued wood-plywood joints, Holz als Roh- und Werkstoff (61), pp. 269-272.
- Pirmin Jung Holzbauingenieure (2010): Schraubenpressklebung im Holzbau, Merkblatt Intern und Extern.
- Rug W, Linke F, Eichbaum G (2013); Vergleichende Untersuchung zum Pressdruck von Nagelschrauben in Langzeitversuchen, Hochschule Eberswalde, Bericht Nummer 2012-PB-00-010.
- Rug W, Gümmer K, Gehring S (2010): Schraubenpressklebung mit Nagelschrauben, Bautechnik 87 (Heft 1).
- SN EN 14080:2013 (2014): Holzbauwerke - Brettschichtholz und Balkensschichtholz – Anforderungen, Schweizer Ingenieur und Architektenverein, Zürich, Switzerland
- Sieber, D (2003): Brückenschlag über Fünf Jahrhunderte, SFS-intec PraxisReport 15: p. 6–7.
- Steck, G (1988): Bau-Furniersperrholz aus Buche, Informationsdienst Holz, Entwicklungsgemeinschaft Holzbau (EGH), Düsseldorf, Germany.
- Widmann R (2014): Sanierung und Verstärkung von Brettschichtholz, S-WIN Fortbildung Kurs Tagungsband.

Discussion

The paper was presented by S Franke

P Quenneville asked about the cost effectiveness for so many screws being used. S Franke responded that this depends on individual companies. Some firms feel that it could be economically effective. P Quenneville received confirmation that the screws can be removed after curing if one desires.

S Aicher commented that one should make sure about the 0.1 MPa pressure requirement as this is currently not certified for structural use in Europe. He questioned whether the screws are used just to achieve the required pressure of 0.1 MPa. He stated that one component PU is not allowed for screw gluing in structural use for a range of reasons. He also stated that in principle gluing does not require pressure; however, pressure at 0.6 MPa and 1.0 MPa are needed to bring the two gluing surfaces together. Furthermore, in CLT rolling shear dominates so shear strength of the board and glue bond may not be critical. Finally the performance of the glue bond should be measured in terms of glue line thickness which dominate glue bond strength. S Franke agreed in general and commented that washer head screws may not be desirable to some companies as they are more visible. S Aicher added that nail bonding is not under consideration in Eurocode now and bond thickness is decisive. There is a need to consider dry-wet type testing. S Winter agreed with S Aicher and commented that the system of glue performance considered should be delamination tests with the screws removed. S Franke said that they are doing tests. S Aicher commented that for serviceability requirements the 0.1 MPa level may be okay but not for strength considerations.

A new design method for timber floors – Peak Acceleration approach

Wen-Shao Chang¹, Thomas Goldsmith², Richard Harris³

¹ Sheffield School of Architecture, The University of Sheffield, Sheffield, UK

² Department of Architecture and Civil Engineering, University of Bath, UK

³ Time for Timber Ltd., UK

Abstract

This paper presents a new proposal to design timber floors that harmonises Eurocode 5 and two other alternative methods that are currently used by industry. A total of 16 timber floors with different systems (CLT, Profi Deck and joist floors) were tested. The measured response and predicted response were compared, using two existing design metrics, Response Factor and vibration dose value (VDV) and the results showed large discrepancies in the likelihood of inhabitant complaints between the two metrics. It has been concluded that the Response Factor method would pose significant design challenges to timber floors as: (1) it implies that timber floors are much more responsive than their competitors, such as concrete floors; and (2) in the design stage, most of the estimations of floor performance using the Response Factor would exceed the limits prescribed by the guidelines. At the end of the paper, a new approach is proposed which harmonise the different design guidelines and standards. In addition, the proposed method would enable engineers to design timber floor systems that are not covered by current Eurocode 5.

1. Background

Human-induced vibration of timber floors is considered as a serviceability issue that primarily relates to discomfort of occupants. In the UK, there are more than 300,000 timber floors built each year. In recent years, there has been an increase in demand for building new floor systems with larger spans. Once constructed floors that are shown to have excessive vibration are expensive to rectify.(Huang & Chang, 2018). Currently, engineers design conventional joist floors based on the approach given by Eurocode 5, which employs the frequency based criterion, also known as the 8Hz limit criterion. It limits the design of timber floors as being only applicable to residential floors with spans up to 6 metres. For floors with a fundamental frequency greater than 8Hz, further checks, including static deflection and unit impulse velocity response checks should be carried out. For floors with a fundamental frequency less than 8Hz, a special investigation is required. Several alternative design criteria for

mass timber floors have been proposed, notably by Hamm et al. (Hamm, Richter, & Winter, 2010) and Hu & Chui (Hu & Chui, 2004). Other relevant standards that deal with human exposure to vibration exist; these include BS 6472 (BSI, 2008) and ISO 10137 (ISO, 2007), which do not fully harmonise with the Eurocode.

Currently, when designing new timber floors against human induced vibration, there is no design method and associated limiting criteria for the serviceability design of mass timber floors or joist floors with spans greater than 6 metres. Thus, when considered with the disharmonisation of standards, there is a risk that the growth in the use of timber for longer spans and floors in non-domestic situations will be stifled. In this paper, we will propose a new design method that will enable engineers to design new types of timber floors, which will harmonise with relevant standards, and will produce floors that compare well with the current design practice.

2. The Response Factor versus the Vibration Dose Value

2.1 The Response Factor method

Response Factors have long been successfully used as a criterion in the design of concrete and steel framed buildings and form the basis of many design codes, including CCIP-016 (Willford & Young, 2006), SCI P354 (Smith, Hicks, & Devine, 2007) and AISC DG11 (Murray, Allen, Ungar, & Davis, 2016). The Response Factor gives the ratio between a floor's RMS response (either acceleration or velocity) under a single footfall load and a baseline response value (such as those given in BS 6472-1:2008 or BS EN ISO10137:2007 as shown in Figure 1).

$$R = \frac{a_{w,RMS}}{a_{R=1}} \quad [1]$$

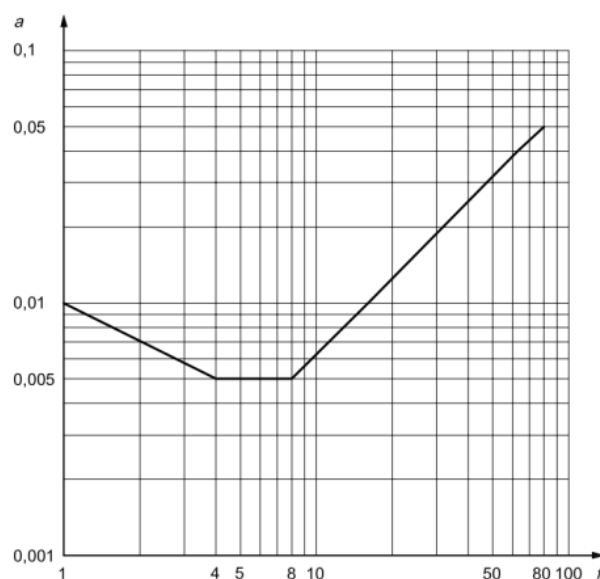


Figure 1 Base curve for perception of vibration from ISO 10137

Typical limiting values for Response Factor have been reproduced from SCI P354 (Smith et al., 2007) and are given in Table 1:

Table 1 Recommended maximum Response Factors for single person excitation

Place	Multiplying factor for exposure to continuous vibration
Office	8
Shopping mall	4
Dealing floor	4
Stairs (light use)	32
Stairs (heavy use)	24

These criteria have been formulated for steel and concrete framed buildings and have been used in some practices to design timber floors when Eurocode 5 does not cover them. However, their applicability to timber floors has not been verified. The current practice accepts a higher Response Factor for timber floors, which indicates that timber floors respond more to footfall loading than steel or concrete floors. This implies that timber floors tend to perform less well than concrete and steel floors. It should be noted that there is currently no test data to suggest an appropriate Response Factors for different types of timber floors, which poses a question on the feasibility of using this method to design timber floors.

2.2 The Vibration Dose Value Method

The Vibration Dose Value Method is currently mostly used for assessing the response of existing floors but its use for design is permitted in SCI P354 (Smith et al., 2007) and ISO 10137 (BS EN ISO10137:2007) for floors exhibiting an impulsive response that exceeds the Response Factor limit. Vibration Dose Value (VDV) can be calculated from the frequency weighted floor acceleration-time response as:

$$VDV = \left[\int_0^T a_w^4(t) dt \right]^{\frac{1}{4}} \quad [2]$$

Where T is the total time over which the floor is being excited. The total VDV is normally summed over an exposure period of a 16-hour day or 8-hour night depending on the occupancy type of the space and hence allows for comfort limits to be exceeded for short periods. Typical limiting values are given in Table 2.

Table 2 VDV ranges that might result in various probabilities of adverse comment within residential buildings (BS 6472-1:2008)

Place and time	Low probability of adverse comment ($\text{ms}^{-1.75}$)	Adverse comment possible ($\text{ms}^{-1.75}$)	Adverse comment probable ($\text{ms}^{-1.75}$)
Residential buildings 16 h day	0.2 to 0.4	0.4 to 0.8	0.8 to 1.6
Residential buildings 8 h night	0.1 to 0.2	0.2 to 0.4	0.4 to 0.8

It should be noted that BS 6472 states “for office and workshops, multiplying factors of 2 and 4 respectively should be applied to the above vibration dose value ranges for a 16h day.” The VDV method introduces a frequency weighting, i.e. the vibration data should be filtered according to the frequency weighting as shown in Figure 2 before being processed. The use of the weighting filter follows the assumption that people are more sensitive to vibration within a particular frequency range, around 8-10Hz, and therefore reduction factors are applied to the vibrations with frequencies outside this range.

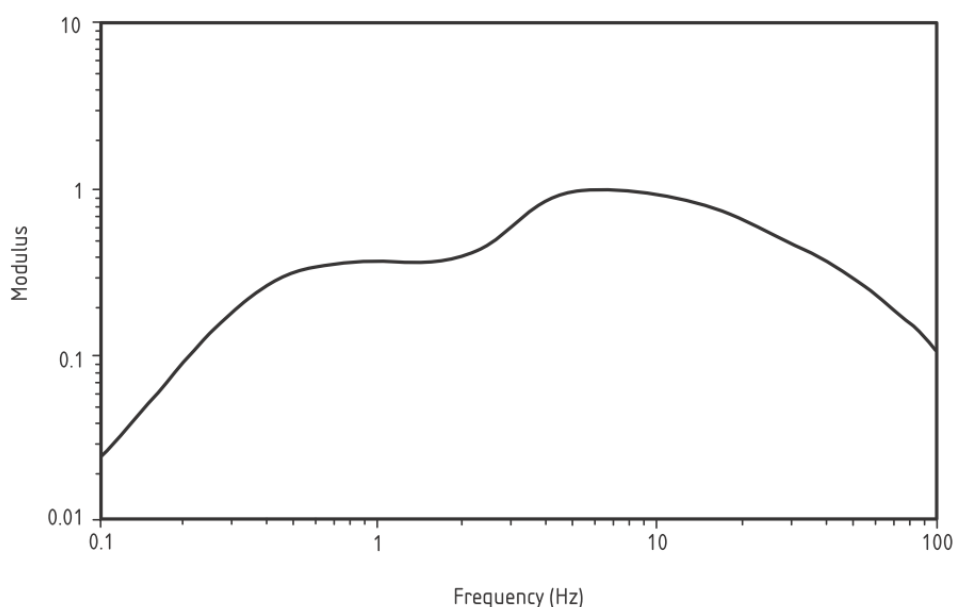


Figure 2 Frequency weighting curve for vertical vibration proposed by BS 6472

The VDV method, which was established through the European Physical Agent (Vibration) Directive (Mansfield, 2004), has been widely used to assess the acceptability of vibration and it is not only used for floor vibration. The application of VDV has been extended to assessment of vibration from different sources, such as

vehicles. (Lewis & Johnson, 2012). The method is normally used to control the vibration exposure limit of a person within a designated period of time. Where it has been used to assess the acceptability of timber floor, these floors have generally been normally constructed. There is no current method that can be used to predict VDV in the design stage and hence, to make it a useful criterion, there is a need to develop a method that be used in the design stage to predict the VDV in the finished floor.

3. Timber floor test programme

This paper reports a total of five cross laminated timber (CLT) floors, four Profi Deck timber floors and five domestic timber floors that were tested to assess the feasibility of using Response Factor (RF) and VDV methods as a prelude to development of a design method to predict the response of timber floors excited by human footfall. The details of the floors tested are tabulated in Table 3.

Table 3 Information and the outcomes of the measured timber floors

Floor	Country	Floor system	Span	Use of building
A	UK	Timber joist	4.2	Residential
B	UK	Timber joist	5.0	Residential
C	UK	Timber joist	4.1	Residential
D	UK	Timber joist	5.8	Residential
E	UK	Timber joist	4.5	Residential
F	UK	Timber joist	3.6	Residential
G	UK	Timber joist	3.6	Residential
H	UK	Timber joist	4.2	Residential
I	UK	CLT	8.9	Office
J	Germany	CLT	7.2	Residential
K	Germany	CLT	7.2	Office
L	Austria	CLT	9.0	Office
M	UK	Profi Deck	7.2	School
N	UK	Profi Deck	7.2	School
O	UK	Profi Deck	14.0	School
P	UK	Profi Deck	6.2	School

To extract dynamic properties of the timber floors, accelerometers were placed in the middle of the floors, where maximum displacement was expected to occur. Three walking events by a single tester were recorded in each room as shown in Figure 3.

The tester weighed 76kg and measured 1.85m in height. For each event, the walking pace was varied to give a complete picture of how the floor might respond under normal use. It was not felt essential to control the walking pace exactly, but an attempt was made in each room to walk at what was felt to be natural 'Slow', 'Medium, and 'Fast' paces. A walking frequency was back-calculated for each test by determining the time-period between acceleration peaks (corresponding roughly to the period between foot strikes) for each set of measured response data.



Figure 3 Tester walking on the joist timber joist floor

Once raw data had been collected frequency weighting (W_b) was applied using the filter given in BS 8041:2005. Frequency weighting is necessary as humans are more responsive to certain frequency bands of vibration. This weighting process involves the application of digital filters to the data in the frequency domain to modulate the response. The results of the frequency weighting process can be seen in Figure 4. The original response has been smoothed and attenuated, more closely reflecting what a human might perceive. The interesting range of the frequency is below 50Hz therefore the sampling rate of the data acquisition was set to be 500Hz (Chang, Huang, & Harris, 2016). There are several ways to analyse the vibration data, Fast Fourier Transfer is the most common method in the frequency domain approach

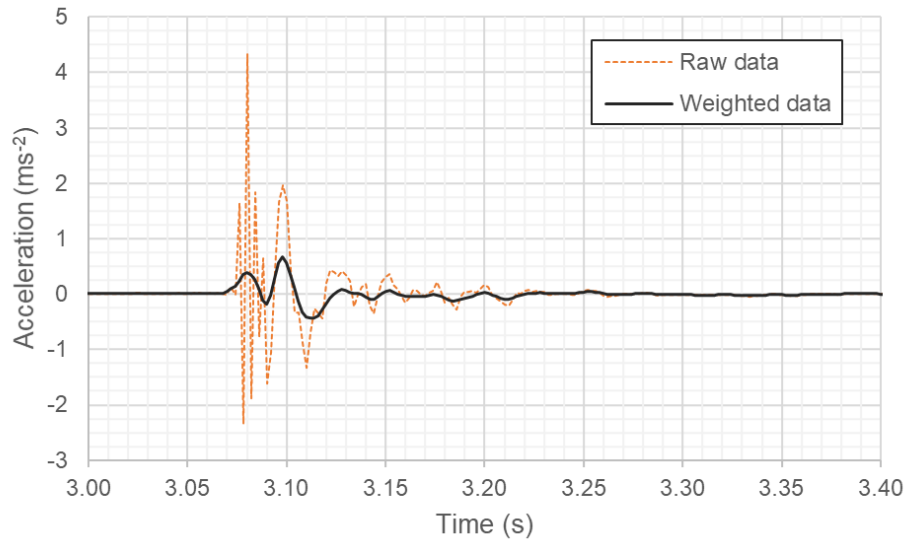


Figure 4 Acceleration-time domain response of floor to single footfall

4. Prediction of timber floor response

4.1 Acceleration of timber floors

The acceleration response of a floor can be predicted using equation [3], as given in both SCI P354 and CCIP-016.

$$a_{w,e,r}(t) = \sum_{n=1}^N 2\pi f_n \sqrt{1 - \zeta^2} \mu_{e,n} \mu_{r,n} \frac{F_l}{M_n} \sin(2\pi f_n \sqrt{1 - \zeta^2} t) \cdot e^{-\zeta 2\pi f_n t} W_b \quad [3]$$

$a_{w,e,r}$	Acceleration (ms ⁻²)
t	Time interval between each acceleration value (s)
N	Number of modes up to twice the fundamental mode
f_n	Frequency of the nth mode (Hz)
ζ	Critical damping ratio of the nth mode (%)
$\mu_{e,n}$	Mode shape amplitude at the footfall location (unity or mass normalised)
$\mu_{r,n}$	Mode shape amplitude at the receiver location (unity or mass normalised)
F_l	Footfall impulse force (Ns)
M_n	Modal mass of the nth mode (kg)
t	Time interval between each acceleration value (s)
W_b	Frequency weighting factor

The footfall impulse force is calculated differently, depending on the design guidance document being used. The Concrete Centre Guide CCIP-016 (Willford & Young, 2006) gives the footfall impulse force as a function of walking frequency, f_w (Hz) and the fundamental natural frequency of the floor as shown in Equation [4]:

$$F_I = 54 \frac{f_w^{1.43}}{f_n^{1.30}} \quad [4]$$

The footfall force was considered to be independent of floor type, making equation [4] appropriate for use with mass-timber.

4.2 Finite Element Analyses

Finite element models of each floor were constructed using the commercial software Oasys GSA. To ensure the correct model set-up, the modal results for each floor were compared to the dynamic modes extracted from the measured heel-drop data using frequency domain decomposition. GL24h characteristic strength values were assigned according to BS EN 1194 (CEN, 1998), excluding the across beam stiffness. The footfall analysis solver built into Oasys GSA was then used to generate acceleration response data at each tested walking frequency. Median damping ratios calculated from on-site test data were used for each floor. In general, the predicted acceleration response of the floors aligned reasonably well with the measured response, as shown in Figure 5.

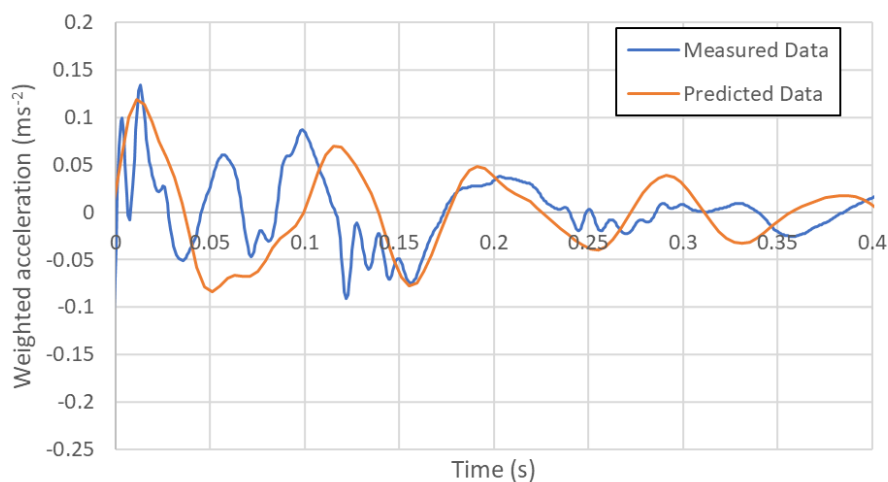


Figure 5 Weighted response to single footfall at 1.28Hz walking frequency

5. Results and discussion

5.1 Predicted response versus measured response

A total of 204 tests were carried out on the floors listed in Table 3. The predicted and measured Response Factors for the peak footfall have been plotted in Figure 6, which shows that, in the cases of Profi Deck floors, we tend to overpredict the Response Factor whereas in CLT and joist floors we tend to underpredict the Response Factors. Another noticeable phenomenon is that the Response Factors of all the floors tested are generally higher than 8, which means that if the criteria proposed by SCI P354 (Smith et al., 2007) had been adopted in the design, then most of the timber floors

would have not been built.

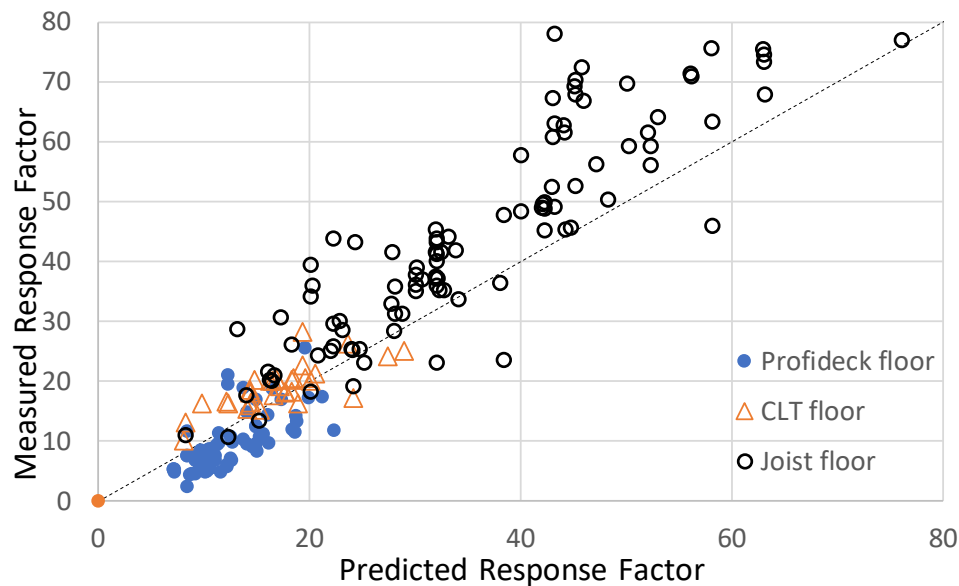


Figure 6 Measured against predicted footfall Response Factor for all the floor test events

If we increase the Response Factor limit to 12, approximately 80% of the predictions would exceed the limitation; and if we increase the Response Factor limit to 18, then approximately 55% of the predictions would exceed the limit. This implies that even if we increase the Response Factor limit, a large proportion of the timber floors would have exceeded the limitation in the design stage, and therefore design engineers would have need to be more conservative and more materials would have been needed.

5.2 Relationship between Response Factor and Vibration Dose Value

Figure 7 shows the comparison between predicted Vibration Dose Values and measured Response Factors, which shows good correlation between the two indicators. It implies that if we can predict VDV in the design stage then there is the potential to predict the measured Response Factors of the timber floors. Equation [2] shows that the VDV relates to the sum of the vibration a person has experienced over a period of time, therefore it will increase with the increase in weighted initial acceleration and decrease with the increase of the damping ratio of a floor.

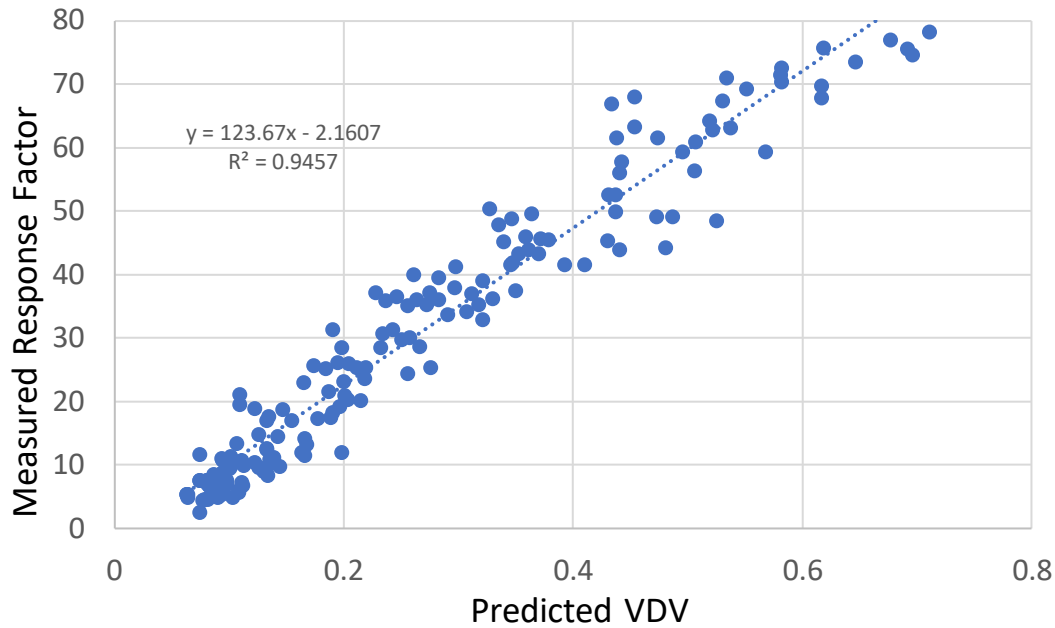


Figure 7 Predicted Vibration Dose Value versus Measured Response Factors of all the floors

To demonstrate the potential of using peak acceleration of a test event to represent the response of the timber floor, comparisons between these two indicators are plotted in Figure 8. It can be shown that peak acceleration of timber floor in a walking event can be used to predict the measured Response Factor. There is also a strong relationship between predicted VDV and the peak acceleration.

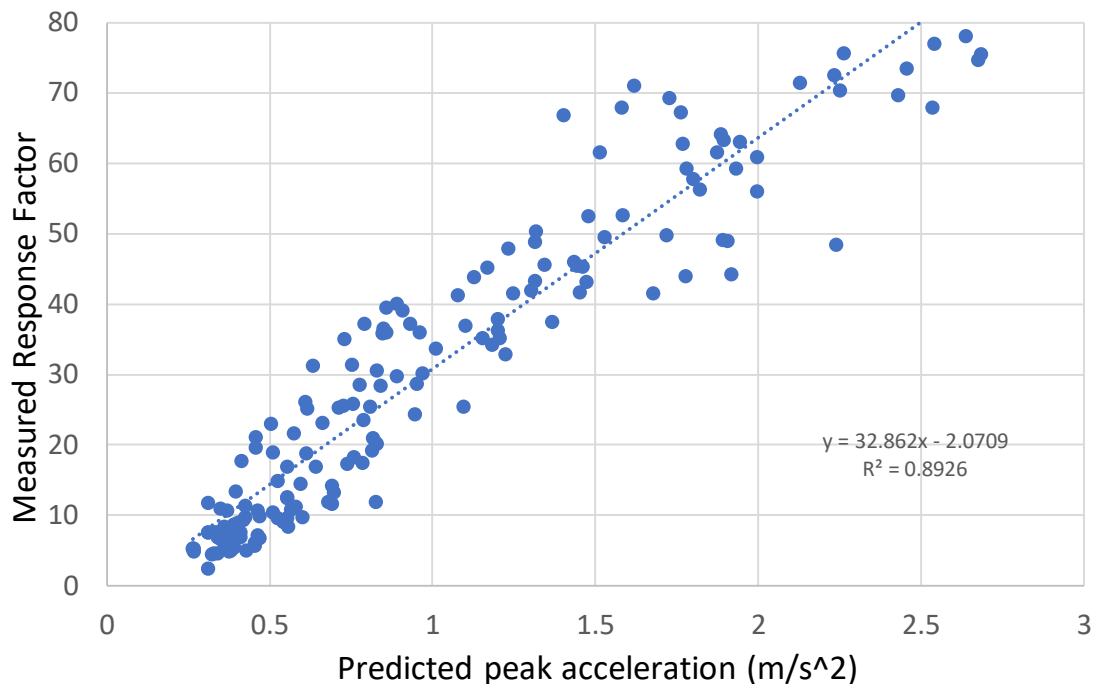


Figure 8 Predicted peak acceleration of timber floors versus Measured Response Factors

5.3 A new proposal for timber design harmonising with VDV

The weighted peak acceleration of different types of timber floors can be estimated by modifying equation [2] as:

$$a_{w,peak} = 2\pi K f_n \sqrt{1 - \zeta^2} \frac{F_l}{M_n} W_b \quad [5]$$

Where

$a_{w,peak}$	Weighted peak acceleration (ms^{-2})
K	Factor that modify the timber floor system
f_n	Frequency of the nth mode (Hz), normally take as the fundamental frequency
ζ	Critical damping ratio of the nth mode (%), normally we can assume damping ratio of timber floors to be 2-3%
F_l	Footfall impulse force (Ns), can be estimated by equation [4]
M_n	Modal mass of the nth mode (kg)
W_b	Frequency weighting factor

The factor K is to modify the system of the timber floors empirically, and has been obtained from the floor tests. The value of K can be estimated as:

$$K = \begin{cases} 2.8, & \text{for CLT floors} \\ 3.5 & \text{for profideck floors} \\ 4.6 & \text{for joist floors} \end{cases} \quad [6]$$

The frequency weighting ratio can be determined by using the natural frequency of the timber floors:

$$W_b = \begin{cases} 1 & \text{if } 8 < f_n < 16 \\ \frac{16}{f_n} & \text{if } f_n > 16 \end{cases} \quad [7]$$

For a panel simply supported on all four sides, the modal mass can be calculated by multiplying the total mass by a factor of 0.25. This factor is reduced to 0.17 for a fully fixed slab. The relationship between the weighted peak acceleration and the measured VDV can be established in Figure 9, therefore the Measured VDV of a walking event can be estimated by:

$$VDV \cong 0.27 \cdot a_{w,peak} \quad [8]$$

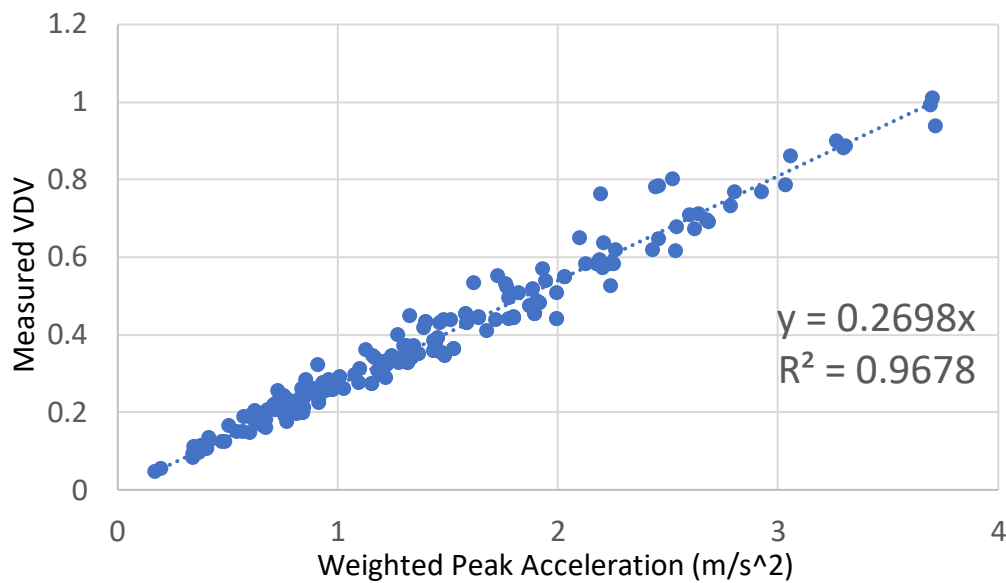


Figure 9 Relationship between peak acceleration and the measured VDV

Similar discussion of the vibration dose value predictions is hampered by the fact that criteria are applied over a longer exposure period than a single footfall. SCI P354 (Smith et al., 2007) offers a means of estimating the vibration dose value due from the predicted RMS acceleration of the peak footfall, but close inspection of Ellis (2001) shows this to be only applicable to floors exhibiting a resonant response. A relationship between total event dose value and the peak footfall dose value can instead be obtained from the measured data, as in Figure 10.

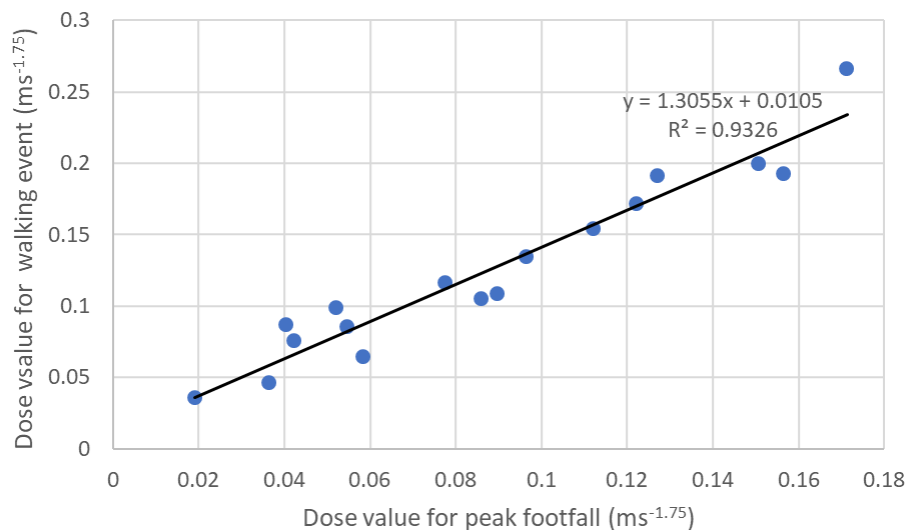


Figure 10 The relationship between peak footfall dose value and overall event dose value

Therefore the VDV for the entire exposure period can be estimated by that of a single event by using:

$$VDV_{total} = 1.31 \cdot n^{0.25} \cdot VDV_{event} \quad [9]$$

Hence the procedure of designing timber floor is demonstrated as Figure 11.

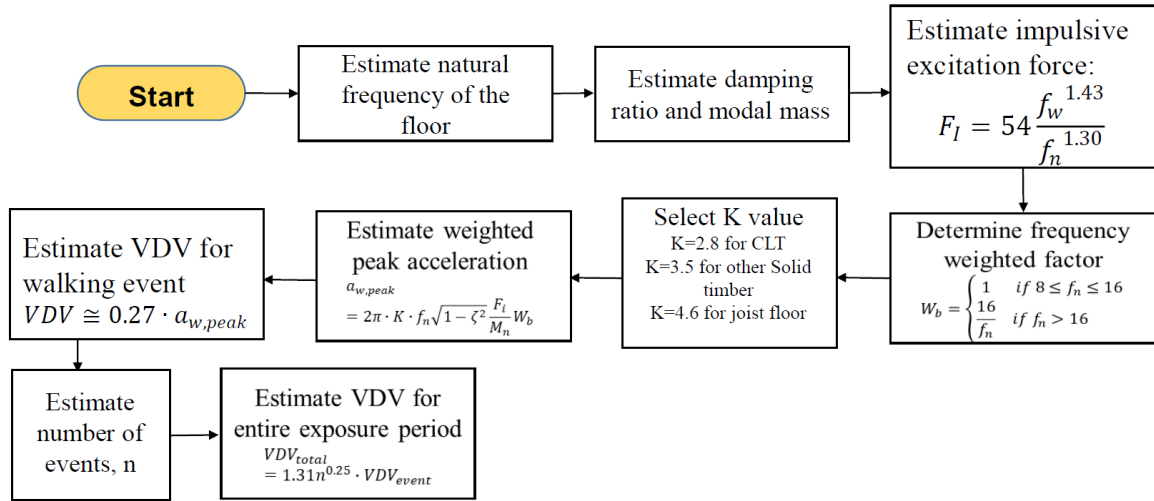


Figure 11 Proposed procedure to design timber floors

6. Conclusions

This paper presents a new proposal for the design of timber floors that covers those systems not included in the Eurocode 5, the following conclusions can be drawn:

- The Response Factor method could be used as a limiting criterion for use with mass timber (CLT and Profi Deck) floors, provided the limiting values are revised. However, in the case of the mass timber floors tests in this study, results show that a Response Factor Limits of 12 or even 18 are more appropriate figures than the current value of 8 proposed by steel industry. This implies that timber floors are very responsive to human induced vibration and could be used as an indication of lower performance when compared with concrete floors.
- Excessive Response Factors were found in the tests on the joist floors in residential buildings and most of these joist floors would not have been built if they had been designed using the Response Factor method.
- The Vibration Dose Value method is highly effective. The VDV can be predicted from the peak footfall acceleration response, allowing an estimation of VDV for an entire day. The number of allowed events can be estimated by using the criteria established by SCI P354.

Reference:

- BSI. (2008). BS 6472-1:2008 Guide to evaluation of human exposure to vibration in buildings. London: British Standard Institution.
- CEN. (1998). BS EN 1194:1999 Timber structures. Glued laminated timber. Strength classes and determination of characteristic values *Bruxelles, Belgium*.
- Chang, W.-S., Huang, H., & Harris, R. (2016). *Design of timber floor for vibration: some design and test questions*. Paper presented at the International Network on Timber Engineering Research Meeting Forty-nine, Graz, Austria.
- Ellis, B. R. (2001). Serviceability evaluation of floor vibration induced by walking loads. *The Structural Engineer*, 79(21), 30-36.
- Hamm, P., Richter, A., & Winter, S. (2010). *Floor vibrations - new results*, Riva del Garda.
- Hu, L. J., & Chui, Y. H. (2004). Development of a design method to control vibrations induced by normal walking action in wood-based floors. *Proceedings of the 8th World Conference on Timber Engineering*, 2, 217-222.
- Huang, H., & Chang, W.-S. (2018). Application of pre-stressed SMA-based tuned mass damper to a timber floor system. *Engineering Structures*, 167, 143-150.
- ISO. (2007). ISO 10137: Bases for design of structures-Serviceability of buildings and walkways against vibrations *International Standard Organisation (ISO)*. Geneva: International Standard Organisation (ISO).
- Lewis, C. A., & Johnson, P. (2012). Whole-body vibration exposure in metropolitan bus drivers. *Occupational medicine*, 62(7), 519-524.
- Mansfield, N. J. (2004). *Human response to vibration*: CRC press.
- Murray, T., Allen, D., Ungar, E., & Davis, D. (2016). *AISC Design Guide 11: Vibrations of Steel Framed Structural Systems due to Human Activity*.
- Smith, A., Hicks, S., & Devine, P. (2007). *SCI P354: Design of Floors for Vibration: A New Approach*. Retrieved from
- Willford, M. R., & Young, P. (2006). *A design guide for footfall induced vibration of structures*: Concrete Society London, UK.

Discussion

The paper was presented by R Harris

T Toratti commented that the response factor method deals with square of the acceleration and asked why the proposed acceleration based method would be different.

R Harris responded that timber floors are more responsive than concrete floors even though timber floors still have good performance. In the proposed method the whole sequence of event is taken into consideration. If you measure a sequence of event, the timber floor is less responsive compared to the response factor method.

I Abeysekera asked how one can predict the number of events that will occur within a certain period. He asked what would happen to floors built with other materials using the proposed method. R Harris answered that the proposed method is material independent and there is no special criterion for timber floors. Further details to the questions need to be addressed with W-S Chang.

Discussion took place about the applicability of VDV to floors built with other materials which could lead to equal improved predicted response and increase of their spans. I Abeysekera pointed out that the VDV is not used by the industry. A Smith discussed the value of adopting a consistent approach for all materials. R Harris agreed that it would be desirable but there is an inconsistency with wood being penalized.

Development of a floor vibration design method for Eurocode 5

I K Abeysekera, Arup Advanced Technology and Research

P Hamm, Biberach University of Applied Sciences, Germany

T Toratti, Federation of the Finnish woodworking industries, Finland

A Lawrence, Arup Advanced Technology and Research

Keywords: floor, vibration, design, vibration criteria, acceleration, velocity, frequency, serviceability

1 Introduction

The current design rules in Eurocode 5 date from the 1980s and are based on studies in Sweden for small single-family houses with simple joisted floors. Since then, timber floor structures and understanding of their behaviour has evolved. Development of multi-storey multi-family construction means that a more rigorous method of verification is now needed. In multi-family buildings where floors cross from one dwelling to another, performance requirements of floors are higher as occupants are more likely to complain about vibration which they can feel but cannot see the source of. The development of new materials such as CLT and LVL have also created the possibility of longer span floors. Increased acoustic requirements have also made timber floors more complex with added resilient layers. Therefore, design methods for floor vibration need updating, including more rigorous calculation procedures and clearer criteria.

Sensitivity to floor vibration is highly subjective. This can be seen by the many different ways in which the current rules in EC5 are applied in different European countries. Cost Action FP0702 has summarised differences in vibration design across Europe (see Zhang & al 2013). Floor vibration is also an important topic of ongoing Cost Action FP1402. A large number of research projects and Phds have been carried out during the last 30 years in many countries including Austria, Canada, Germany, Finland, Sweden, Norway and the UK. A recent JRC European Commission report describes the results of an EU project on steel floors.

This paper discusses the new design rules for the vibration performance of floors which are currently being drafted in CEN TC250/SC5 within WG3 Sub-group 4 “Vibrations”, including hand calculation methods and performance based criteria. These are being tested against existing timber floors. The hand calculation methods are applicable to timber floors on rigid (wall) supports. Work is being currently carried out to include floors on flexible (beam) supports.

2 Perception of floor vibration

Human perception of vibration is defined in ISO 10137 Annex C, which includes examples of possible vibration criteria. The curve in Figure 1 from ISO 10137 shows the limit of human perception of vertical r.m.s. acceleration. Perception is frequency dependent people being most sensitive to vibration between 4 and 8 Hz.

The inclusion of floor acceleration or related velocity criteria based on a codified vibration perception curve, has the benefit of relating the floor vibration design values to real human disturbance levels as transparently as possible.

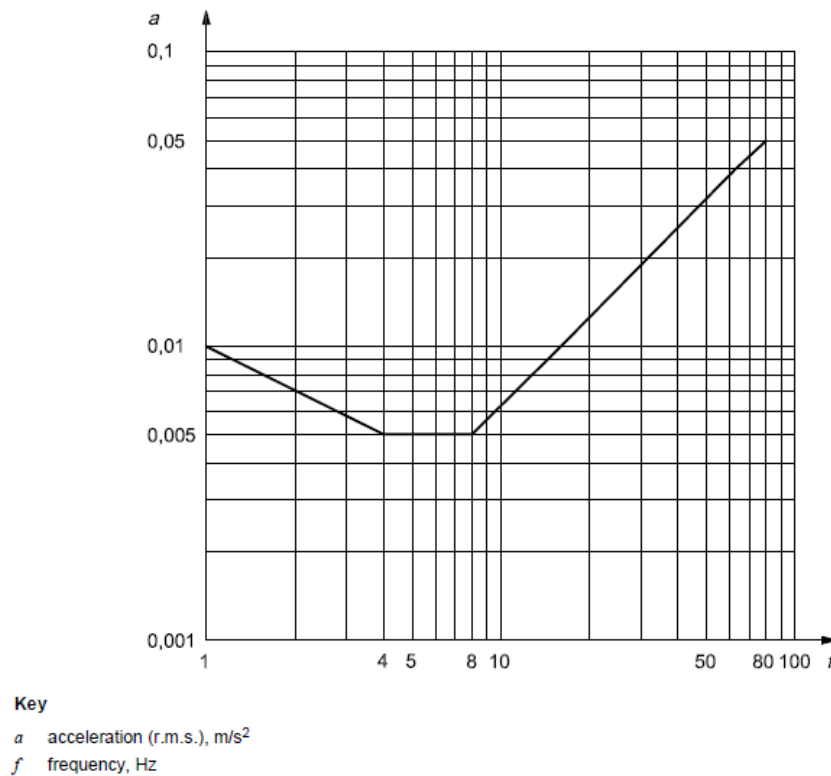


Fig. 1. Vibration base curve (vertical direction). (ref: ISO 10137:2007)

As can be seen in Figure 1, above 8 Hz the minimum perception level is not constant in terms of acceleration. However, when this part of the curve is integrated, it can be shown that it is constant in terms of velocity with a value of $v_{\text{rms},\text{base}} = 0,0001 \text{ m/s}$. Floor vibration criteria can be expressed as a multiple of this base curve referred to as a response factor. Below a floor frequency of 8 Hz an acceleration criteria can be applied and above 8 Hz a velocity criteria can be applied.

$$\begin{aligned}
 a_{\text{rms}} &< \text{Response factor} \times a_{\text{rms},\text{base}} && \text{when } f_1 < 8 \text{ Hz} \\
 v_{\text{rms}} &< \text{Response factor} \times v_{\text{rms},\text{base}} && \text{when } f_1 \geq 8 \text{ Hz}
 \end{aligned}$$

ISO 10137 suggests several ranges of response factor values for different building use categories depending whether the vibration is continuous or intermittent. Vibrations caused by footfall are intermittent. As the human perception to floor vibrations is subjective and is affected by what the person is doing, their mood and audio or visual

cues. Therefore it is difficult to set absolute criteria. There is also cultural factor based on the floor performance that people are used to in a particular country. This can be seen in the large difference between national annexes.

3 Footfall Loads for design

To predict the response of a floor it is necessary to have an agreed footfall loading model.

When the floor frequency is much higher than the walking frequency, the floor response dies out in between footfalls (known as transient response). Hence footfall loading can be idealised as a mean impulsive load (Wilford et al) by:

$$I = \frac{42f_w^{1.43}}{f_n^{1.3}} \quad (1)$$

Where f_w is the walking frequency and f_n is the modal frequency of the floor.

Where the floor frequency is low and matches the frequency of one of the harmonics of human footfall, resonant build-up is likely. In this instance loading can be idealised as a harmonic load with up to 4 significant harmonics. Hence resonant response is likely in floors with natural frequencies less than four times walking speed. Figure 2 below gives harmonic loading due to footfall in terms of dynamic load factors (DLF), where DLF is the ratio of the harmonic force amplitude to the static weight of the walker. The harmonics are based on real footfall time histories from several studies quoted in Wilford et al. It can be seen that most of the applied force is in the 1st harmonic and that the force levels in successive harmonics decrease as the harmonic number increases. It can also be seen that the force in a given harmonic increases as walking (harmonic) frequency increases. Finally it can be seen that the envelope of the 2nd to 4th harmonics is close to a straight line.

The downward trending DLF is from the Austrian National Annex and is an attempt to capture the downward steps of harmonics quoted in Hamm et al.

It should be noted that the above loading models are only applicable for floors with a mass of at least 10 times that of the walker.

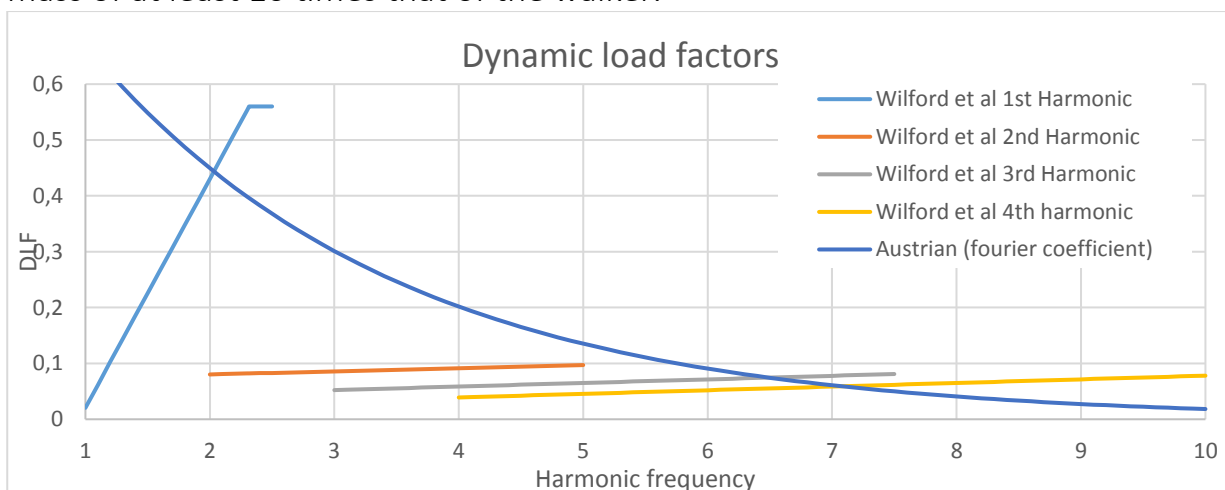


Fig. 2. Loading model when response is likely to be resonant.

4 Design procedures for transient floors

By definition transient floors are high frequency and therefore coincide with the upward slope constant V_{rms} criterion in Figure 1. For the simple case of a rectangular bay on rigid line supports (ie walls) it is possible to develop a hand calculation method. This has been done as follows based on the previous work done by Wilford et al. The procedure is as follows:

1. Calculate frequency of 1st mode of the floor using the standard formula below, where delta is the deflection of the floor assuming one way span and pinned supports, D_x/D_y is the ratio of transverse to longitudinal stiffness, l is the span of the floor and w is the width.

$$f_n = \frac{18}{\sqrt{\delta}} \times \sqrt{\frac{D_x l^4}{D_y w^4} + 1} \quad (2)$$

2. Calculate mean modal impulse of the floor using equation 1 in section 3 based on a suitable walking frequency (see section 10).
3. Calculate peak velocity response of the first mode using the standard equation below assuming a modal mass (M^*) of 25% of the floor mass including a realistic proportion of live load, which is based on the assumption that floor behaves like a pin supported plate. It is well known that the ratio of modal mass to total mass of the 1st mode of a plate is 25%.

$$V_{1,peak} = \frac{l}{M^*} \quad (3)$$

4. Multiply $V_{1,peak}$ by a factor K_{imp} to account for the contribution of higher modes. The number of higher modes that contribute to the response and therefore K_{imp} is a function of the ratio of the stiffnesses of the floor in the two directions and is therefore a function of w , l , D_x and D_y . The equation for K_{imp} below has been obtained from a parametric analysis accounting for variations of w/l from 1 to 10 and D_x/D_y from 0,05 to 1.

$$K_{imp} = \max \left\{ 0,48 \left(\frac{w}{l} \right) \left(\frac{D_y}{D_x} \right)^{0,25} \right. \\ \left. 1 \right\} \quad (4)$$

Hence the total peak response:

$$V_{Tot,peak} = K_{imp} V_{1,peak} \quad (5)$$

5. Finally to obtain a V_{RMS} value of velocity between footfalls it necessary to multiply the total peak by a reduction factor again obtained from a parametric analysis:

$$V_{rms} = \beta V_{Tot,peak} \quad (6)$$

Where β is calculated as follows:

$$\beta = (0,65 - 0,01f_n)(1,22 - 0,11\xi)\eta \quad (7)$$

Where ξ is the damping ratio.

If K_{imp} between 1 and 1,5 then

$$\eta = 1,52 - 0,55K_{Imp} \quad (8)$$

else

$$\eta = 0,69 \quad (9)$$

6. Finally divide V_{rms} by the minimum perceptible acceleration to obtain the response factor.

$$R = \frac{V_{rms}}{V_{perceptable}} \leftrightarrow R = \frac{v_{rms}[\frac{m}{s}]}{0,0001[\frac{m}{s}]} \quad (10)$$

The parametric analyses described above in which 4000 cases were investigated of varying proportions and stiffnesses, damping and walking frequencies, enable a potentially complex design procedure to be simplified into a quick hand method.

5 Design procedures for resonant floors

As in Section 4, for the simple case of a rectangular bay on rigid line supports (ie walls) it is possible to develop a hand calculation method.

When the natural frequency of the floor is lower than four times the walking frequency which is roughly in the same range as the constant acceleration part of the base curve (Figure 1), then the root mean square acceleration due to resonant response needs to be calculated. The equation to calculate the full build up rms- acceleration from 1st principles (if only one mode governs) is given as follows:

$$a_{rms} = \frac{F_{Dyn}}{\sqrt{22}\zeta \cdot M^*} \quad (11)$$

a_{rms} is the root mean square acceleration, in m/s^2

F_{Dyn} is the dynamic force amplitude calculated as DLF x walker weight

ζ modal damping ratio as listed below

M^* modal mass, in kg as:

$M^* = \frac{m \cdot l \cdot w}{4}$ assuming that the floor is rectangular and pin supported on all 4 sides

The equation suggests that increasing the floor width increases the modal mass leading to a floor response which is directly proportional to $1/M^*$. In reality this is not the case since increasing the floor width also reduces the transverse stiffness of the floor

leading to an increase in the number of significant modes that contribute to the response. For resonant response, the resonant mode will contribute the most whilst “off resonant” modes will contribute less. Work done by Wilford et al suggests the use of a resonant multiplier to account for the contribution of higher modes. They go on to suggest that for 3% damping a resonant multiplier of 0,4 times K_{imp} from section 5 is used; the multiplier should not be less than 1. Whilst this value of multiplier is conservative for damping of 3% or less it is likely to be unconservative for damping ratios higher than 3%. This is due to the fact that for higher levels of damping off resonant modes will make a larger contribution to the total response. Work is currently underway to calculate a resonant multiplier for higher levels of damping.

In reality achieving full build-up of resonant response requires several footfalls. In reality full build-up may not be possible as the walker might walk off the bay that is being excited and also since the walker may not be always walking in the centre of the floor plate (this is more likely to be the case for smaller residential floors). Hence it is common to apply a reduction factor to equation 8 to account for this. The Austrian national annex suggests a reduction factor of 0,4. Whilst Wilford et al suggests explicitly calculating this factor based on stride length and dimensions of the floor.

Finally the response factor is determined as:

$$R = \frac{a_{rms}[\frac{m}{s^2}]}{0,005[\frac{m}{s^2}]} \quad (12)$$

6 Floor damping values

Realistic floor damping values are needed for the design procedures. Eurocode 5 currently proposes a damping value of 1%. However, subsequent shows that the value should be significantly higher (Hamm & al 2010, Homb and Kolstad, Järnerö 2014, Sedlacek and Heinemeyer 2009, Toratti and Talja 2006, Weckendorf & al. 2015, Zimmer and Kolstad 2016, ISO 10137:2007). For simply supported bare timber floors in test conditions, the values may be lower. The current measured values are between 2-6 % depending on the structure, support conditions, presence of non-load bearing partitions and whether or not there were people on the floor.

For the different floors and supporting conditions, the following is proposed:

$\zeta = 0,02$ for joisted floors

$\zeta = 0,025$ for timber-concrete and mass timber floors

$\zeta = 0,03$ for joisted floors with a floating layer

$\zeta = 0,035$ for timber-concrete composite and mass timber floors with a floating layer

$\zeta = 0,04$ for all floors with a floating layer and supported on 4 sides

$\zeta = 0,06$ for all floors with a floating layer, supported on 4 sides by timber walls via flexible bearings.

7 Floor performance levels and vibration criteria

Six different floor performance levels and respective floor vibration criteria have been proposed by CEN/TC250/SC5/WG3/SG4 as shown in Table 1. It is intended that for different use categories, the floor performance level will either be specified in national annexes or by the client or structural designer.

- Six different floor performance level are offered. This is needed to account for cultural variations between countries.
- For low frequency floors there is an acceleration criterion a_{rms} .
- For high frequency floors there is a velocity criterion v_{rms} .
- For all floors there is a 1 kN point load stiffness criterion; this is empirical based on historic practice and is particularly useful for light joisted floors for which the methods in this paper are less applicable (refer to section 3).
- The easiest way to compare how current national annexes compare to the performance classes is to check on the 1 kN stiffness criteria given. However, because the point load criterion ignores the mass of the floor it is not a perfect measure and is only applicable to the traditional floor types on which it was developed.
- In the Austrian national annex there are two floor classes, Class 1 (w_{1kN} [mm] $\leq 0,25$ mm and $a_{rms} < 0,05$ m/s²) and Class 2 (w_{1kN} [mm] $\leq 0,50$ mm and $a_{rms} < 0,10$ m/s²). These approximately match floor performance levels II and III respectively.
- In Finland the national annex requires that w_{1kN} [mm] $\leq 0,50$ mm and VTT (Toratti and Talja; 2006) suggests a base acceleration of $a_{rms} < 0,075$ m/s². This would coincide approximately to floor performance level III.
- JRC report (Sedlacek et al.;2009) recommends response factors for residential and office use between 8 and 32 (Class C). This covers the whole performance level range given in table 1.

Table 1. Floor vibration criteria according to the floor performance level.

	Floor performance levels					
Criteria	level I	level II	level III	level IV	level V	level VI
Frequency f_1 [Hz] \geq	4,5					
<u>Stiffness criteria</u> w_{1kN} [mm] \leq	0,25		0,5	0,8	1,2	1,6
Response factor R	4	8	12	16	20	24
<u>Acceleration criteria</u> <u>when $f_1 < 8$ [Hz]</u> a_{rms} [m/s ²] \leq	$R \times 0,005$					
<u>Velocity criteria when</u> <u>$f_1 \geq 8$ [Hz]</u> v_{rms} [m/s] \leq	$R \times 0,0001$					

Tentative floor performance levels for residential and office uses are given in Table 2, however this is still in discussion as in many countries the lower levels would not be acceptable.

Table 2. Tentative floor performance levels for use categories A (residential) and B (office).

Use category	Quality choice	Base choice	Economy choice
A (residential)	level III	level IV	level V
B (office)	level II	level III	level IV

8 Comparison of proposed design method with existing test data

Most of the existing test data is for transient floors, as timber floors on wall supports tend to be high frequency. A comparison has been made of the method proposed in this paper with existing test data collected by Patricia Hamm, Antje Richter and Tomi Toratti. Values calculated using the method are compared against measurements of real timber floors.

Three sets of data presented below. The first (Figure 3) shows measured vs calculated velocities (transient calculation); the second (Table 2) gives measured response factors vs a subjective evaluation of floor performance for transient floors (based on data from Patricia Hamm); the third (Figure 4) is a graph of measured response factors vs subjective evaluation and frequency based on test data from Toratti et al (Toratti T., Talja A.: 2006). These graphs show that on the whole, the method gives a good prediction of the vibration performance of the floor. The cases where the method gives a response higher than measured (ie those significantly above the line in Figure D) can be explained by the fact that the walker was not always in the centre of the floor in the tests (a conservative assumption built into the method) and the fact that on some floors heavy partitions that were present were not accounted for in the calculation as full details of these are not known. Both these effects can be accounted for in the proposed method by including the mass of the partitions and also a factor that accounts for the difference in the walker and receiver location on the floor span; this would however lead to the method being more involved. Further including some amount of live load is likely to give a better match between measured and predicted response factors as this is more realistic. Table 2 suggests that response factors below 8 correspond to a good floor; above this there are likely to be an increasing number of complaints.

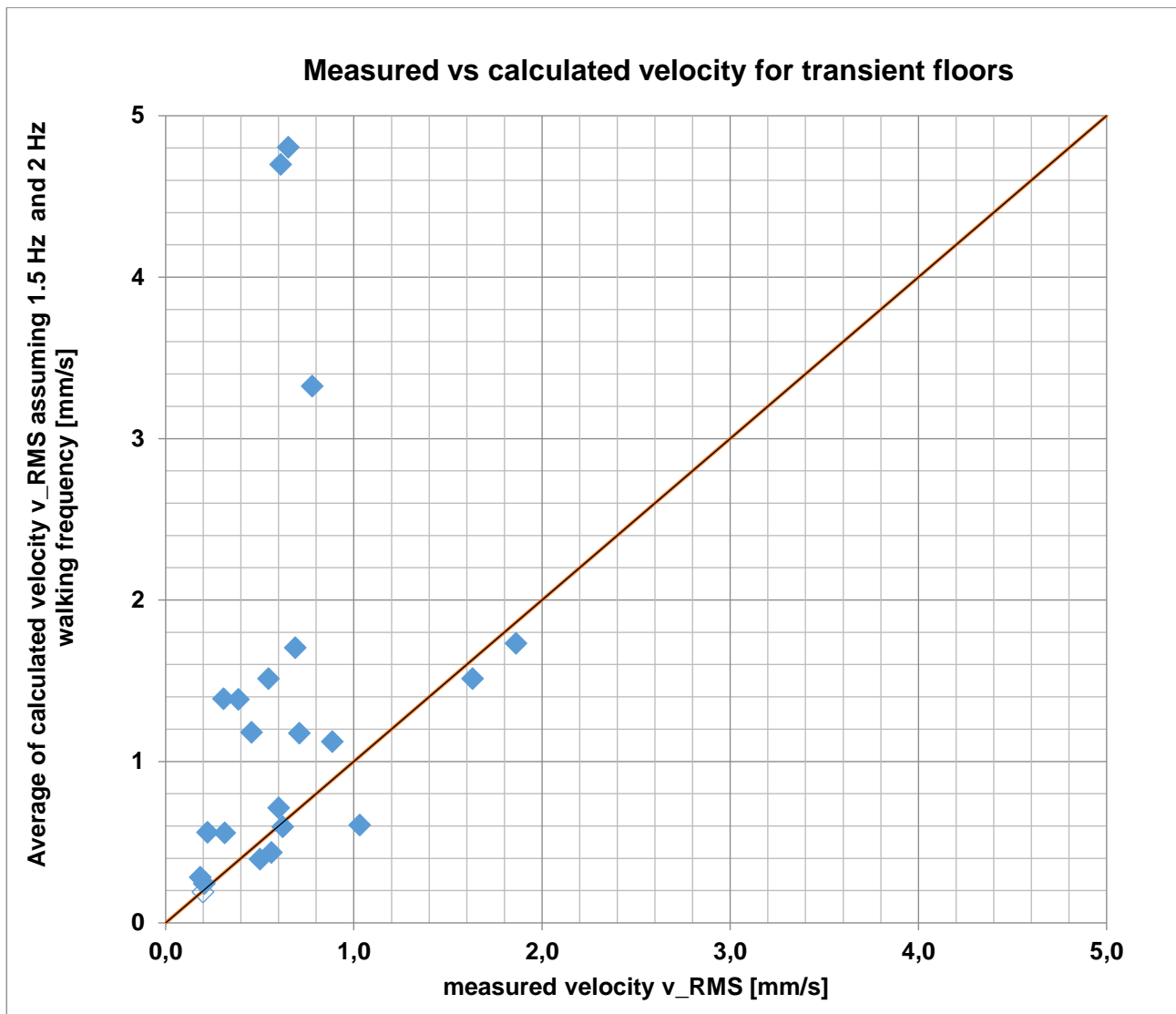


Fig. 3. Measured vs calculated V_{rms} values for single bay timber floors $f_1 < 8$ Hz.

Table 2: Measured transient response factors vs subjective evaluation (data from Patricia Hamm)

Measured response factor	Number of floors measured	Percentage of floors with subjectively evaluated acceptable performance
1 to 4	40	100
4 to 8	32	72
8 to 12	7	14
Greater than 12	5	0

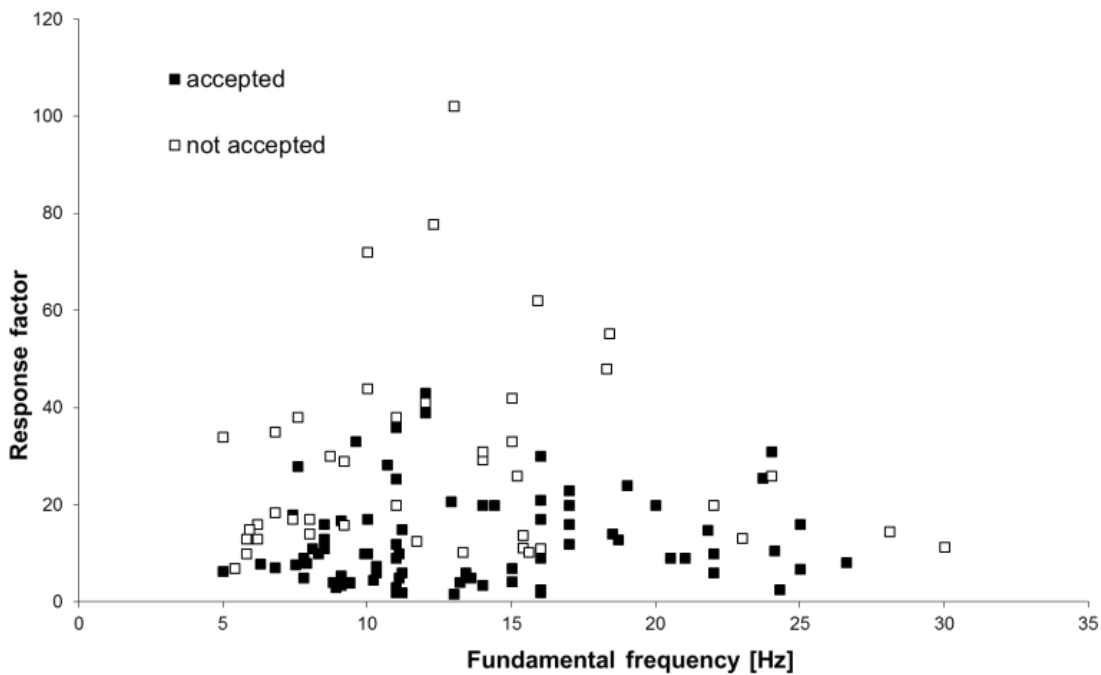


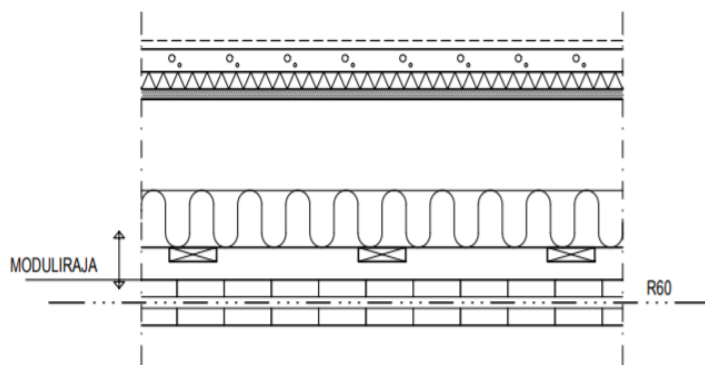
Fig. 4. Measured response factor vs frequency (Toratti et al)

There is limited test data for resonant timber floors. The resonant example given in section 9 shows a good match between the measured acceleration (500 mm/s²) and calculated using the method proposed in this paper (520 mm/s²).

9 Example calculation for joisted floors

The calculations below show how the methods presented in this paper applies to a typical transient and a typical resonant floor. These examples show how the method would be used in practice.

Transient Floor



Floor composition:

40 mm screed
 30 mm Impact sound insulation
 18 mm OSB panel
 260 mm Kerto-S span 5500 mm
 width 12000 mm, 51x260 K300 mm
 100 mm soft insulation and supporting boards 25x100 K400 mm (lower element CLT)

$$EI_L = 13800 \cdot 51 \cdot 260^4 / 12 = 1,03e12 \text{ [Nmm}^2 \text{ per beam]}$$

$E_{I_L} = 1,03e12/0,3 + 17000 * 1000*40^3/12 + 6780*1000*18^3/12 = 3,53e12$ [Nmm² per meter]

$E_{I_b} = 17000 * 1000*40^3/12 + 6780*1000*18^3/12 = 9.4e10$ [Nmm² per meter]

Floor mass = $2000 * 0,04 + 500*0,018 + 500*0,051*0,260/0,3+50 = 160$ kg/m²

Deflection from self weight

$w = 5/384*1,6*5500^4 / 3,53e12 = 4,29$ mm:

$f_1 = 8,7$ Hz

point load deflection [mm]

$b_{ef} = L/1,1 * (E_{I_b}/E_{I_L})^{0,25} = 2,019$ m

$w_{1KN} = 1000*5500^3/(48*E_{I_L}*2,019) = 0,486$ mm

Velocity calculation [m/s]

$I = 4,5$ (for 1,5 Hz walking frequency) and **$6,80$** (for 2 Hz walking frequency) [Ns]

Dynamic mass $m = 160 * 5,5*12/4 = 2640$

$V_{1,peak} = 0,0017$ (for 1,5 Hz walking frequency), **$0,0026$** (for 2 Hz walking frequency)

$K_{imp} = 1,19$

$V_{tot, peak} = 0,0020$ (for 1,5 Hz walking frequency); **$0,0031$** (for 2 Hz walking frequency)

$\beta = 0,380$

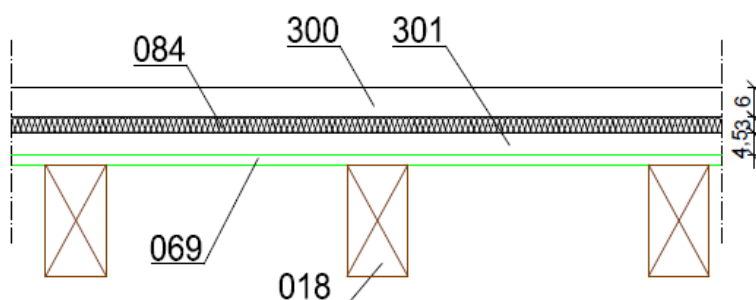
$V_{rms} = 0,0020*0,380 = 0,0077$ m/s (response factor $R = 7,7$) for 1,5 Hz walking frequency

$0,0031*0,380 = 0,0011$ m/s (response factor $R = 11,6$) for 2 Hz walking frequency

These values would correspond to floor performance levels II and III.

Resonant Floor

Example "Schneider2, 9.4.18, Event Nr. 8.



LEGENDE:	
018	- BSH.../... 12/22
069	- Profilbrett Fichte 18 mm
084	- EPS DES Trittschalldämmung
300	- Zementestrich
301	- gebundene Splittschüttung (Korngröße 6-8 mm)

Span: 4,6 m

Width: 5,0 m

Mass: $m = 247,5$ kg/m²

Damping: $\zeta = 0,03$ for joisted floors with a floating layer

Frequency: measured: 7,5 Hz

Frequency calculated:

$$f_1 = \frac{\pi}{2 \cdot l^2} \cdot \sqrt{\frac{EI}{m}} = \frac{\pi}{2 \cdot 4,6^2} \cdot \sqrt{\frac{2,32 \cdot 10^6}{247,5}} = 7,18 \text{ Hz}$$

$$EI = 11000 \cdot \frac{0,12 \cdot 0,22^3}{12} \cdot \frac{1}{0,625} + 25000 \cdot \frac{1 \cdot 0,06^3}{12} = 2,32 \frac{MNm^2}{m} \text{ including the stiffness of the floating screed.}$$

Measured acceleration was about $0,5 \text{ m/s}^2$ for a walking frequency of approximately 2.5 Hz.

Calculated acceleration:

$$a_{\text{rms}} = \frac{F_{\text{Dyn}}}{\sqrt{2} \cdot 2 \cdot \zeta \cdot M^*}$$

$$F_{\text{Dyn}} = \alpha \cdot \text{Walker weight}$$

$$\text{DLF} = e^{-0,4 \cdot 7,5} = 0,0498 \text{ as per the Austrian national annex}$$

$$\text{DLF} = 0,026 + 0,005(7,5) = 0,0635 \text{ as per Wilford et al}$$

$$\text{Walker weight} = 700\text{N}$$

$$M^* = \frac{247,5 \cdot 4,6 \cdot 5}{4} = 1423 \text{ kg}$$

$$a_{\text{rms}} = \frac{0,0498 \cdot 700}{\sqrt{2} \cdot 2 \cdot 0,03 \cdot 1423} = 0,288 \text{ m/s}^2$$

$$a_{\text{rms}} = \frac{0,0635 \cdot 700}{\sqrt{2} \cdot 2 \cdot 0,03 \cdot 1423} = 0,368 \text{ m/s}^2$$

To compare the measured and calculated value it is better to use the a_{max} value.

$$a_{\text{max}} = 0,288 \cdot \sqrt{2} = 0,407 \text{ m/s}^2 \text{ (DLF from Austrian National Annex)}$$

$$a_{\text{max}} = 0,368 \cdot \sqrt{2} = 0,520 \text{ m/s}^2 \text{ (DLF from Wilford et al)}$$

We can see that DLFs from both references give reasonably similar results. This is due to the fact the harmonic frequency that causes resonant floor response is in the range where DLFs from the both references match (see Figure 2)

10 Conclusions and ongoing work

The footfall induced vibration calculation method presented here is based on Willford et al (2006). This method is similar to the method presented in the JRC report (Sedlacek G. et al.: 2009).

More comparison calculations and measurements are needed to determine appropriate vibration criteria. This is underway in CEN TC250/SC5/WG3/subgroup floor vibrations.

It has been decided to keep the stiffness criterion. For very light floors less than 10 x the walker mass the loading models are no longer valid so it makes sense to keep the

point load deflection limit in place for these floors. The stiffness criterion allows for an approximate comparison of the proposed performance levels with existing national requirements. However further work is needed to ensure the stiffness criterion and the response factors correspond.

The dynamic response of floors is highly sensitive to the modal mass of the floor. A higher modal mass is very beneficial being directly proportional to the inverse of the response as long as its effect on the frequency is ignored. Therefore, if a realistic level of live load is included in the mass, it will have a beneficial effect on the calculated dynamic response. In the calculations presented in this paper live loads have not been included, but this is under discussion. It can also be seen that wide rectangular floors have a lower response than square floors of the same span and floor build up due to their increased modal mass.

Discussion is ongoing of what walking speed (frequency) is appropriate. It is clearly recognised that smaller floor areas result in lower walking frequencies as is considered in the Finnish national annex. The walking frequency has a direct impact on the dynamic load applied. A simple proposal being considered is that a 1,5 Hz walking frequency is used for residential spaces and a 2,0 Hz or greater frequency is used for offices and other uses. This may be oversimplified and one option would be to link walking frequency to the floor dimensions and walking patterns possible on longer stretches. For very long corridors etc walking speeds higher than 2Hz are possible.

Another point that is under discussion is that in order for floor vibrations to be perceived there needs to be both a walker producing the footfall and another person sensing the vibration, usually sitting on a chair. These people cannot be at the same point at midspan. Therefore, a reduction factor of about 0,7-0,9 has been discussed to account for this. In reality this factor is the mode shape value at the point of excitation by the walker multiplied by the mode shape value at the point of vibration perception by the person sitting on the chair.

Work is currently underway to evaluate suitable multi-span factors to account for the effect of floor being multi spanning when evaluating response. Multiple spans mean some increase in the modal mass and where spans are not of equal length an increase in the frequency of the floor. The two sets of factors being considered are those in the Austrian national annex based on beam theory assuming response in a single mode and those in Wilford et al based on plate theory whilst also accounting for multimodal response.

Overall it is believed that the method discussed in this paper offers a simple reliable way to check the vibration of rectangular timber floors on wall supports that can be

easily built into software and design tools. Work is ongoing to develop a similar method for floors on flexible beam supports.

11 References

- Eurocode 5 (2004): Design of timber structures - Part 1-1: General and rules for buildings. CEN. (EN 1995-1-1).
- Hamm P., Richter A., Winter S. (2010): Floor vibrations – new results. World conference of timber engineering 2010, Riva de Garda, Italy.
- Homb A., Terje Kolstad S (in publication): Evaluation of floor vibration properties using measurements and calculations. Engineering structures.
- ISO 10137 (2007): Bases for design of structures – Serviceability of buildings and walkways against vibrations.
- Järnerö K. (2014): Vibrations in timber floors – dynamic properties and human perception. Phd. thesis. Linnaeus University Sweden.
- Kreuzinger H., Mohr B.: Gebrauchstauglichkeit von Wohnungsdecken aus Holz; Abschlussbericht Januar 1999. TU München, Fachgebiet Holzbau. Forschungsvorhaben durchgeführt für die EGH in der DGfH.
- Sedlacek G. et al. (2009): Design of floor structures for human induced vibrations: JRC scientific and technical reports.
- Toratti T., Talja A. (2006): Classification of human induced floor vibrations. Building acoustics. Journal of Building Acoustics 2006 vol 13 no 3.
- Weckendorf J., Toratti T., Smith I., Tannert T. (2015): Vibration serviceability performance of timber floors. European Journal of Wood and Wood Products.
- Willford M., Young P. (2006): Design Guide for Footfall Induced Vibration of Structures - A tool for designers to engineer the footfall vibration characteristics of buildings or bridges (2006). ISBN 1-904482-29-5.
- Zhang B., Rasmussen B., Jorissen A., Harte A. (2013): Comparison of vibrational comfort assessment criteria for design of timber floors among the European countries. Eng Struct 52:592–607.
- Zimmer S, Augustin M. (2016): Vibrational behaviour of cross laminated timber floors. World conference of timber engineering 2016, Vienna Austria.

Discussion

The paper was presented by I Abeysekera

R Harris commented that it is important to measure acceptable floors to check against the criteria so that the design procedures are not too penalizing. I Abeysekera responded that a range of limits is set to allow different levels of performance to be accepted. K Crews commented that there is always a dilemma that the floor vibration design method being either un-conservative or too conservative. The different levels of performance approach is interesting.

U Kuhlmann stated that Europe attempted to apply a criterion for all materials. She suggested that may be flexible long span timber floor can be accepted by clients recognizing that such timber floors are more flexible compared to concrete floors. However this type of criterion should be material independent.

P Dietsch questioned whether it is desirable to standardize values in tables where floors are deemed unacceptable. I Abeysekera stated that this should not be a problem. Floors can be engineered and clients can choose their criteria based on the desired performance level.

S Winter commented that methods to evaluate floor performance are needed. However people in practice may not be too skilled to use these methods. There are other publications that can help fill the gap.

4 INTER Notes, Tallinn, Estonia 2018

Note 1 Criteria for Evaluating the Simplification of Design Values for Dowel
Type Fasteners - R Jockwer, T Uibel, M Kleiber

Criteria for evaluating the simplification of design rules for dowel-type fasteners

Robert Jockwer, ETH Zurich, Switzerland

Marion Kleiber, Harrer Ingenieure, Germany

Thomas Uibel, FH Aachen, Germany

Keywords: EYM, Johansen, Connections, Joints, Ease-of-use

1 Introduction

1.1 Task specifications of the project team

In the task specifications of Project Team SC5.T5 for drafting the chapter on connections in the revised version of Eurocode 5 it is asked for enhancing the ease of use of the design equations and regulations. This enhanced ease of use shall improve clarity, simplify routes through the Eurocode, avoid or remove rules of little practical use in design and avoiding additional and/or empirical rules for particular structure or structural-element types.

1.2 Requirements on EYM

One of the challenges for enhancing the ease of use the design regulations for connections concerns connections with dowel-type fasteners based on the European Yield Model (EYM). In addition to an enhanced ease of use different requirements for the design approaches can be defined:

- Calculation of characteristic values and compliance with the established system of partial safety factors and modification factors
- Conservatism of assumptions and simplifications
- Mechanical consistency, the simplifications have to be comprehensible
- Based on the same parameters as the EYM design equations (embedment strength, yield moment, diameter, timber member thickness)
- Recognition of EYM design rules

1.3 Demands from practice

Engineers in practice may have the following demands when applying the design regulations in EC5:

- Verification of connections with predefined configuration
- Conception of connections and optimization with regard to structural behaviour

Ease of use of design regulations can be achieved by the following strategies:

- Simplification of the equation
- Enhance the ease of navigation
- Give additional information

In general the simplification shall help the engineer to design good connection but avoid “Black Box” calculations. Different suggestions for simplification or enhanced ease of use of the EC5 design clauses for timber-to-timber connections with fasteners in double shear are presented in the following. It is focused on the load-carrying capacity of dowels and the contribution by the rope effect is not considered. It is focused on dowel type fasteners such as Dowels, Nails, Staples, Bolts and Screws.

2 Examples of simplified approaches

2.1 Empirical design equations

First empirically based equations for the load-carrying capacity of nailed connections were derived in the beginning of the 20th century. First simple design equations accounted for a quadratic impact of the nail diameter were established in design codes such as SIA 164:1953, CIB Structural Timber Design Code from 1980 or DIN 1052. More advanced design equations accounted for different indices of the nail diameter in the range of approx. 1.7 (SIA 164:1981).

2.2 Simplifications of the analytical equations

Rouger (1998) proposes simplified design equation of the EYM for timber-to-timber connections for fasteners in double shear. The failure modes with one plastic hinge in the fasteners or with inclination of the fastener (failure modes (g), (h) and (j) in EC5) are summarized to two simplified equations.

Applying relevant material property values and parameters for common configurations allows for developing simplified equations for the common applications in practice. Examples are e.g. the equations for nailed connection in SIA 265 (2012) or the simplifications proposed by Jorissen and Leijten. These approaches are strictly limited to the material, geometries and fastener types they were developed for.

2.3 Equations based on diagrams

Kangas and Kurkela (1996) proposed a simple design equation in which a parameter is taken from a diagram in dependency of the normalized fastener slenderness. Schatz (2009) developed additional diagrams in order to comply with the large diversity of possible configurations of connections. However, disadvantages of this method are the required large number of different diagrams the difficulty in reliably reading values from diagrams by the user.

2.4 Enhanced ease of navigation through selecting the relevant failure mode

The different failure modes according to EYM are relevant in dependency of the input parameters which can be represented by a normalised slenderness value. Möller

(1951) developed diagrams in order to pick the relevant failure mode in dependency of a normalized fastener slenderness. These diagrams were later further developed by Hilson (1995) in STEP Documentation.

2.5 Additional information supporting the engineer in design of connection

The EYM distinguishes failure modes of the connection in dependency of the relative slenderness of the fasteners. The required timber thickness (or relative slenderness) for achieving a failure mode with two plastic hinges in the fastener can be derived. Blaß and Ehlbeck (1998) proposed a simple approach based on this failure mode and a linear reduction of load-carrying capacity for smaller timber member thickness. This approach is successfully applied in DIN 1052 (2004) and SIA 265 (2003 and 2012).

3 Discussion

Simplifications of the EYM and the design procedures for dowel-type fasteners in EC5 should enable the engineer for a straightforward conception of connections. That requires information on which failure modes are most suitable for the respective demands. Information, such as illustrations of failure modes and optimal member thickness or fastener slenderness, has to be given to the engineer to assess the respective performance of the connection. The design equations and design recommendations in EC5 should help the engineer to design and optimize connections with regard to performance and efficiency.

4 References

- Blaß, H. J., Ehlbeck, J. (1998): Simplified design of connections with dowel type fasteners, In Proc. of CIB-W18 Meeting 31, CIB-W18/31-7-8. Savonlinna, Finland.
- DIN 1052 (2004): Design of timber structures – General rules and rules for buildings. DIN Deutsche Institut für Normung e.V., Beuth Verlag, Berlin, Germany.
- EN 1995-1-1 (2004) Eurocode 5: Design of timber structures - Part 1-1: General - Common rules and rules for buildings + A1. Bruxelles, Belgium: European Committee for Standardization CEN.
- Hilson B. O. (1995): Joints with dowel-type fasteners – theory. Timber Engineering STEP 1. First Edition, Centrum Hout, The Netherlands.
- Johansen K. W. (1949): Theory of timber connections. IABSE publications, 1949.
- Kangas, J. and J. Kurkela. 1996. A simple method for lateral load-carrying capacity of dowel type fasteners. In Proc. of the CIB-W18 Meeting 29. Bordeaux, France.
- Meyer, A. (1957): Die Tragfähigkeit von Nagelverbindungen bei statischer Belastung, Holz als Roh-Werkstoff 15(2), pp. 96-109.
- Möller, T. (1951): En ny metod för beräkning av spikförband, Report No. 117, Chalmers University of Technology, Gothenburg, Sweden.
- Rouger, F. (1998): A proposal for simplification of Johansen's formulae dealing with the design of dowelled type fasteners. In Proc. of CIB-W18 Meeting 31, CIB-W18/31-7-7. Savonlinna, Finland.
- Schatz, T. (2009): Diagramme zur Auswertung der Johansen-Formeln für einschnittige Holz- bzw. Holzwerkstoff-Verbindungen. Bautechnik, 86(4):206–210.
- SIA 265 (2012): Timber Structures. Zurich, Switzerland: SIA Swiss Society of Engineers and Architects.

5 Peer review of papers for the INTER Proceedings

Experts involved:

Members of the INTER group are a community of experts in the field of timber engineering.

Procedure of peer review

- Submission of manuscripts: all members of the INTER group attending the meeting receive the manuscripts of the papers at least four weeks before the meeting. Everyone is invited to read and review the manuscripts especially in their respective fields of competence and interest.
- Presentation of the paper during the meeting by the author
- Comments and recommendations of the experts, discussion of the paper
- Comments, discussion and recommendations of the experts are documented in the minutes of the meeting and are printed on the front page of each paper.
- Final acceptance of the paper for the proceedings with
 - no changes
 - minor changes
 - major changes
 - or reject
- Revised papers are to be sent to the editor of the proceedings and the chairman of the INTER group
- Editor and chairman check, whether the requested changes have been carried out.

6 Meetings and list of all CIB W18 and INTER Papers

CIB Meetings:

- 1 Princes Risborough, England; March 1973
- 2 Copenhagen, Denmark; October 1973
- 3 Delft, Netherlands; June 1974
- 4 Paris, France; February 1975
- 5 Karlsruhe, Federal Republic of Germany; October 1975
- 6 Aalborg, Denmark; June 1976
- 7 Stockholm, Sweden; February/March 1977
- 8 Brussels, Belgium; October 1977
- 9 Perth, Scotland; June 1978
- 10 Vancouver, Canada; August 1978
- 11 Vienna, Austria; March 1979
- 12 Bordeaux, France; October 1979
- 13 Otaniemi, Finland; June 1980
- 14 Warsaw, Poland; May 1981
- 15 Karlsruhe, Federal Republic of Germany; June 1982
- 16 Lillehammer, Norway; May/June 1983
- 17 Rapperswil, Switzerland; May 1984
- 18 Beit Oren, Israel; June 1985
- 19 Florence, Italy; September 1986
- 20 Dublin, Ireland; September 1987
- 21 Parksville, Canada; September 1988
- 22 Berlin, German Democratic Republic; September 1989
- 23 Lisbon, Portugal; September 1990
- 24 Oxford, United Kingdom; September 1991
- 25 Åhus, Sweden; August 1992
- 26 Athens, USA; August 1993
- 27 Sydney, Australia; July 1994
- 28 Copenhagen, Denmark; April 1995
- 29 Bordeaux, France; August 1996
- 30 Vancouver, Canada; August 1997
- 31 Savonlinna, Finland; August 1998
- 32 Graz, Austria; August 1999

- 33 Delft, The Netherlands; August 2000
- 34 Venice, Italy; August 2001
- 35 Kyoto, Japan; September 2002
- 36 Colorado, USA; August 2003
- 37 Edinburgh, Scotland; August 2004
- 38 Karlsruhe, Germany; August 2005
- 39 Florence, Italy; August 2006
- 40 Bled, Slovenia; August 2007
- 41 St. Andrews, Canada; August 2008
- 42 Dübendorf, Switzerland; August 2009
- 43 Nelson, New Zealand; August 2010
- 44 Alghero, Italy; August 2011
- 45 Växjö, Sweden; August 2012
- 46 Vancouver, Canada; August 2013

INTER Meetings:

- 47 Bath, United Kingdom; August 2014
- 48 Šibenik, Croatia; August 2015
- 49 Graz, Austria; August 2016
- 50 Kyoto, Japan; August 2017
- 51 Tallinn, August 2018

The titles of the CIB W 18 and INTER papers (starting from 2014) are included in the complete list of CIB/INTER papers: <http://holz.vaka.kit.edu/392.php>